uOttawa

L'Université canadienne
Canada's university

FACULTÉ DES ÉTUDES SUPÉRIEURES ET POSTOCTORALES

uOttawa

L'Université canadienne
Canada's university

FACULTY OF GRADUATE AND POSDOCTORAL STUDIES

Alexandre Zagorevski
AUTEUR DE LA THÈSE / AUTHOR OF THESIS

Ph.D. (Earth Sciences)
GRADE / DEGREE

Department of Earth Sciences
FACULTÉ, ÉCOLE, DÉPARTEMENT / FACULTY, SCHOOL, DEPARTMENT

Tectono-magmatic Evolution of Peri-Laurentian and Peri-Gondwanan Arc - Back Arc Complexes along the Red Indian Line, Central Newfounland Appalachians

TITRE DE LA THÈSE / TITLE OF THESIS

Cees van Staal
DIRECTEUR (DIRECTRICE) DE LA THÈSE / THESIS SUPERVISOR

CO-DIRECTEUR (CO-DIRECTRICE) DE LA THÈSE / THESIS CO-SUPERVISOR

EXAMINATEURS (EXAMINATRICES) DE LA THÈSE / THESIS EXAMINERS

Sandra Barr

Keith Benn

Sharon Carr

Mark Hannington

Keiko Hattori

Gary W. Slater
LE DOYEN DE LA FACULTÉ DES ÉTUDES SUPÉRIEURES ET POSTDOCTORALES /
DEAN OF THE FACULTY OF GRADUATE AND POSTDOCORAL STUDIES

TECTONO-MAGMATIC EVOLUTION OF PERI-LAURENTIAN AND PERI-GONDWANAN ARC – BACK ARC COMPLEXES ALONG THE RED INDIAN LINE, CENTRAL NEWFOUNDLAND APPALACHIANS

Alexandre Zagorevski

Thesis submitted to the
Faculty of Graduate and Postdoctoral Studies
in partial fulfillment of the requirements
for the Ph.D. degree in Earth Sciences

Department of Earth Sciences
University of Ottawa
and
Ottawa-Carleton Geoscience Centre

Your file Votre référence
ISBN: 978-0-494-15054-2
Our file Notre référence
ISBN: 978-0-494-15054-2

TABLE OF CONTENTS

LIST OF FIGURES

LIST OF TABLES

ABSTRACT

The Appalachian – Caledonian Orogen is a classic example of a Paleozoic accretionary orogen which turned into a collisional orogen. The Newfoundland Appalachians represent a critical element of the Appalachian – Caledonian Orogen to evaluate terrane linkages and tectonic models between the North American and European segments, especially those formed during the closure of Iapetus. This thesis presents new geochemical, geochronological, Sm/Nd isotope, structural and P/T data and proposes informal tectonostratigraphic framework for the central Newfoundland Appalachians. The data presented in this thesis are used to test tectonic models for closure of the Iapetus and thus have important implications for the interpretation of tectonic relationships in other parts of the northern Appalachians (e.g. New England) and the British Caledonides.

Central Newfoundland is underlain by the peri-Laurentian Annieopsquotch Accretionary Tract and peri-Gondwanan Victoria Lake Supergroup, separated by the Red Indian Line, the main Iapetan suture zone. Subduction in the Annieopsquotch Accretionary Tract initiated at c. 480 Ma. Subsequently two distinct continental arc – backarc terranes (c. 473 Ma Buchans and 465-460 Ma Red Indian Lake arcs) were formed over an approximately 15 Ma period. A refined tectonic model is proposed for the Annieopsquotch Accretionary Tract involving both thrust and strike-slip displacements. The data require rapid accretion of arc – backarc complexes to the Laurentian margin less than 10 Ma after their formation. This accretion forms part of the Taconic Orogeny and is associated with development of D_1 shear zones as early as c. 470 Ma.

The subduction in the Victoria Lake Supergroup initiated prior to 513 Ma. Subsequently two distinct arc complexes were formed (513-485 Ma Penobscot arc and 473-453 Victoria arc). The Penobscot arc has been previously interpreted as an intraoceanic arc, however Sm/Nd isotopes, zircon inheritance data and stratigraphic relationships indicate formation of the Penobscot arc on continental crust. This crust is similar to Ganderia, which is a postulated peri-Gondwanan microcontinent. The gap in arc magmatism between the Penobscot and Victoria arcs coincides with the obduction of ophiolites onto Ganderia (Penobscot Orogeny). The data presented herein support a new model for the tectonic evolution of the Penobscot arc above an east dipping subduction zone.

In this model the Penobscot ophiolites are obducted as a result of backarc basin inversion, possibly due to accretion of a seamount (Summerford Group) or ridge subduction. Following the Penobscot Orogeny, arc volcanism recommenced as the Victoria arc which rifted from the Ganderia margin opening a wide Exploits-Tetagouche backarc in its wake.

Coeval volcanism in the peri-Gondawanan and peri-Laurentian realms indicates that oceanic crust was subducted on both margins of the Iapetus, culminating in a Molluca sea-type arc-arc collision. The collision marks the end of the Taconic Orogeny and was associated with the development of an extensive south-southeast directed thrust belt. During the collision, the Victoria arc was partially subducted under the Annieopsquotch Accretionary Tract, leading to uplift and widespread angular unconformity in the Notre Dame Subzone, and subsidence and syn-tectonic marine sedimentation in the Exploits Subzone. Following the Taconic orogeny the subduction stepped back outboard of the composite Laurentian margin and initiated in the Exploits-Tetagouche backarc basin. This marks the start of the Salinic convergence of the composite Laurentian margin and Ganderia. The resulting collision culminated in the Salinic orogeny and development of south-southeast direct reverse fault and fold belt. Subsequently, the subduction stepped-back into outboard marginal basins resulting in the arrival of peri-Gondwanan micro-continent Avalonia, which was responsible for the Acadian orogeny and development of north-northwest directed thrust and fold belt in central Newfoundland.

ACKNOWLEDGEMENTS

First and foremost I wish to thank my supervisor, Cees R. van Staal, for introducing me to the world of tectonics in the last year of my undergraduate degree. His enthusiasm and wealth of knowledge continues to inspire me. This study greatly benefited from the encouragement and support of the Geological Survey of Canada Targeted Geoscience Initiative 3: Geology of the Iapetus Suture working group which included C. Johannes Lissenberg, Neil Rogers, Vicki McNicoll, Pablo Valverde-Vaquero, Joe Whalen and of course my supervisor. Extensive discussions with Johan, Neil, Cees and Vicki have greatly improved the scope and quality of this project while making the working environment stimulating and fun. The enthusiastic efforts of my field assistants, Gareth T. Smith and Steven Cain, are greatly appreciated, and their knack for destroying ATVs will never be forgotten. Michiel van Noorden and Sander Boutsma are thanked for assistance in mapping of the King George IV area.

The Ottawa-Carleton Radiogenic Isotope Group, specifically Brian Cousens and John Blenkinsop, are gratefully acknowledged for their training and support in obtaining the isotopic data for this thesis. Julie Peressini, Diane Bellerive, and Carole Lafontaine (Geochronology Laboratory, Geological Survey of Canada), Pat Hunt and Katherine Venance (EM, Geological Survey of Canada) are thanked for their assistance with the analytical work.

This project would not have been possible without the field work and analytical funding from Geological Survey of Canada Targeted Geoscience Initiative 3: Geology of the Iapetus Suture. Neither would it have been possible without the scholarships and supplements from the Natural Science and Engineering Research Council, Ontario Graduate Scholarship Program, Strategic Areas of Development Program, and Geological Survey of Canada.

At last, but not least, my gratitude goes to Angela Dumoulin for not only tolerating me during the time it took to complete this thesis, but for taking a keen interest in geology and being a willing companion even in the bogs of central Newfoundland. I can only hope that future will bring us as much joy as the last few years have.

STATEMENT OF CONTRIBUTION

The thesis is based on the original field data and samples collected by the author during 2001 amd 2002 mapping in central Newfoundland (Figure i.1). The author interpreted the tectono-stratigraphy within the study area, proposed several new tectono-stratigraphic units and correlated previously identifed tectono-stratigraphic units from the outside field area. As a direct result of the mapping the author made original contributions to five 1:50,000 map sheets (Lissenberg et al. 2005 b; Rogers et al. 2005a; van Staal et al. 2005 a, b, c).

The scope of the thesis has been expanded through collaboration with TGI3 (see Chapter 1) working group (J. Lissenber; V. McNicoll; N. Rogers; P. Valverde Vaquero; C.R. van Staal). Samples utilized in this study were collected by the author (VL01-A and VL02-A), C.J. Lissenberg (VL01-J and VL02-J). N. Rogers (RAX01 and RAX02), C.R. van Staal (VL01), and P. Valverde-Vaquero (RAX00). All geochemistry samples were processed and analyzed at commercial laboratories (see Appendix 4). Sm/Nd isotope analyses were carried by the author under supervision of B. Cousens and J. Blenkinsop (Geochemistry and Geochronology Research Institure, Ottawa-Carleton Geoscience Center, Ottawa, Canada) and commercially (see Appendix 4). Geochronological data was obtained at the Geochronology Laboratory (Geological Survey of Canada, Ottawa, Canada) under supervision of V. McNicoll. All geochronology samples were crushed and heavy minerals separated by Geochronology Laboratory staff. The author handpicked, grouped, and abraded fractions for VL01-A and VL02-A samples destined for TIMS analysis. The author hand picked zircons from VL01-A and VL02-A samples for SHRIMP analysis, and selected the targets in collaboration with V. McNicoll after they were mounted and imaged by the Geochronology Laboratory staff. All TIMS fractions were processed and analyzed by the Geochronology Laboratory staff. V. McNicoll analyzed all SHRIMP samples. Following the analysis, V. McNicoll processed and interpreted all geochronological data. Microprobe analysis of minerals selected by the author for P/T work was performed by Katherine Venance at the Geological Survey of Canada.

Chapters 2, 3 and 4 have been written by the author as stand-alone papers. Co-authorship in these papers reflects the contributions of data and ideas from the TGI3 working group. Chapter 2

is accepted for publication (A. Zagorevski, N. Rogers, C.R. van Staal, V. McNicoll, C.J. Lissenberg, P. Valverde-Vaquero, 2006), Chapter 3 (A. Zagorevski, C.R. van Staal, V. McNicoll, N. Rogers) has been submitted for publication (Sept. 2005) and Chapter 4 (A. Zagorevski, C.R. van Staal, V. McNicoll) is intended for publication. Original contributions by the author to these chapters are explained below.

The author carried out the mapping in southeast portion of the study area (Figure i.1). Four new tectonistratigraphic units were identified in and extended outside of the mapped area (Lloyds River Ophiolite Complex, Otter Pond Complex, Wigwam Brook Group, Pats Pond Group). The preliminary stratigraphy established in the northeast portion of the study area by N. Rogers (Rogers and van Staal, 2002) was extended by the author into the mapped area. The author interpreted the stratigraphy, tectonic relationships, and tectonic setting of the Lloyds River Complex, Otter Pond Complex, lower Red Indian Lake Group, Wigwam Brook Group and Pats Pond Group (Chapters 2 and 3). The author interpreted the affinity of the tectono-stratigraphic units and identified the position of the Red Indian Line. The author interpreted the structural history and tectonic significance of the boundaries of tectono-stratigraphic units and deciphered the tectonic architecture of the study area (Chapter 4). The proposed tectonic models benefited from contributions of C.J. Lissenberg and C.R. van Staal (Chapter 2) and from N. Rogers and C.R. van Staal (Chapter 3).

Three co-authored papers which have had significant contribution from the author have been included in the Appendix. Appendix 1 (Lissenberg et al. 2005 b) utilizes the data and samples collected by the author, thus improving the understanding of the relationships in the stratigraphically highest portions of the ophiolite. In addition, the tectonic model proposed by Lissenberg et al. (2005) utilizes the data and interpretations from Chapter 2. Appendix 2 (Rogers et al. in press) utilizes the Sm/Nd isotope data originally collected by the author to test the tectonic model proposed in Chapter 3. Finally, Appendix 3 (J. Lissenberg et al 2005 c) contains significant contributions from the author. These include sections and data relating to the Otter Brook Complex and Otter Brook shear zone which were interpreted and written by the author. The interpretation of the tectonic setting and architecture of the Annieopsquotch accretionary tract were strongly influenced by the work presented in Chapters 2 and 4.

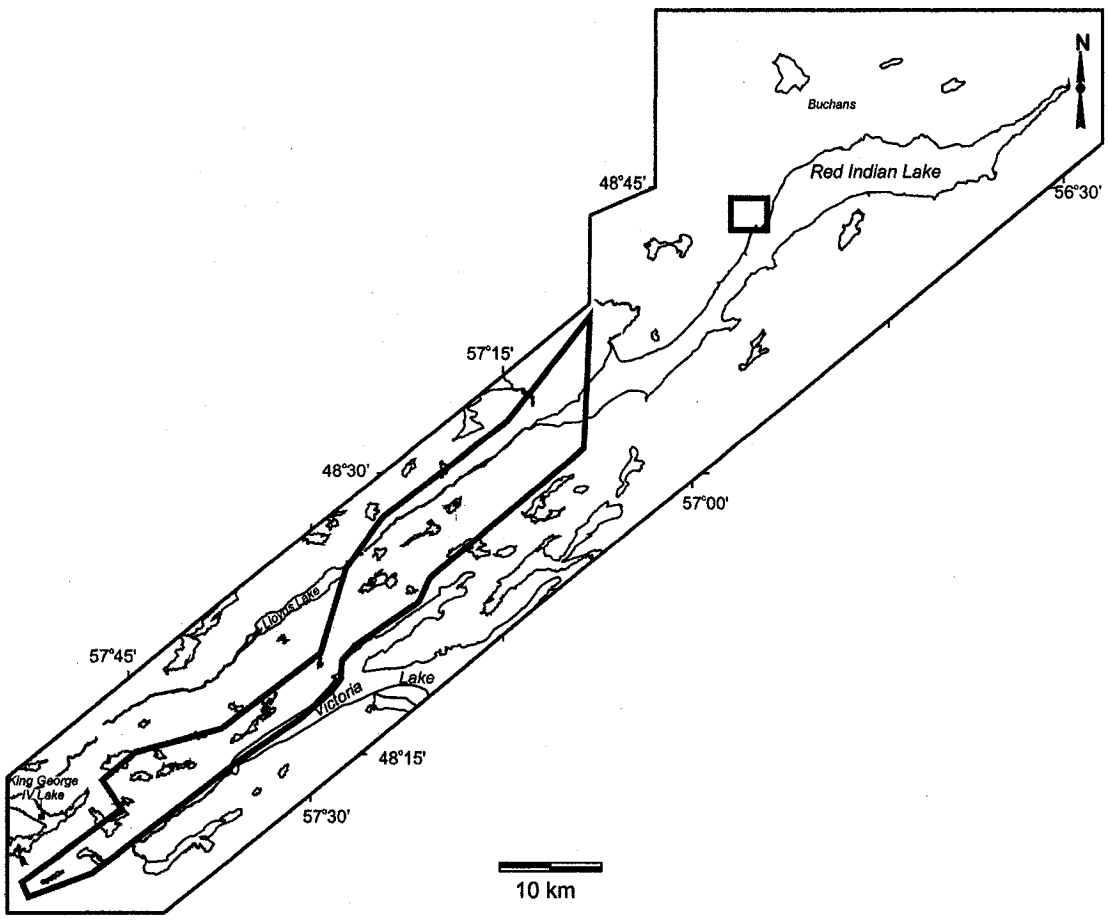

Figure i-1 Location of the areas mapped by the author

CHAPTER 1: INTRODUCTION

The Appalachian – Caledonian Orogen is an example of a long-lived accretionary orogen, which formed in response to the Palaeozoic closure of the Iapetus, Tornquist and Rheic oceans (Figure 1.1). Closure of these ocean basins that separated Laurentia, Gondwana and Baltica from each other (Figure 1.1; e.g. van Staal et al., 1998; Cocks and Torsvik, 2002) involved a diverse set of microcontinents, arcs and suprasubduction zone oceanic terranes that were accreted as single or composite entities to Laurentia in multiple stages forming a complex tectonic collage. Consequently, assessing the tectonic evolution of the Appalachians requires a good understanding of the provenance and tectonic processes involved in the accretion of the various terranes, including the role of trench-parallel translation and dispersion of terranes during and after accretion.

The Appalachian – Caledonian Orogen is a natural laboratory for studying the results of ancient plate tectonic processes as it is very accessible for study (see Williams 1995b). Indeed, since the advent of plate tectonics, the study of the Appalachians and Caledonides has lead to the concept of Wilson cycles (Wilson 1966) and to the acceptance of a proto-Atlantic ocean (Iapetus). The recognition of the Appalachians as an ancient collision zone (Wilson 1966) has quickly prompted development of tectonic models describing the opening and closure of Iapetus (Dewey 1969; Bird and Dewey 1970). Since then, numerous tectonic models have been developed for the New England and Canadian segments of the Appalachians as well as British Caledonides. Although many recent models agree in principle (e.g. Robinson et al. 1998; van Staal et al. 1998; Ryan and Dewey 2004; Lissenberg et al. 2005), there are differences in the timing of initiation (Ryan and Dewey, 2004; Lissenberg et al. 2005) and polarity of subduction (e.g., Karabinos et al. 1998; Moench and Aleinikoff 2000; Robinson et al. 1998). These differences may stem from a number of factors including tectonic excision, lack of along-strike continuity, poor exposure, or assignment of incorrect affinity to tectono-stratigraphic units or terranes.

The Newfoundland Appalachians represent a critical element of the Appalachian – Caledonian Orogen necessary to evaluate tectonic models and terrane linkages between the North American and European segments. This particularly applies to the terranes accreted during the Ordovician closure of Iapetus' main oceanic tract (van Staal 2005), because the zone of accreted

terranes is wide, relatively well exposed, generally of low metamorphic grade and there is a detailed integration of seismic reflection, geophysical and geological data (e.g., Thurlow et al. 1992; van der Velden et al. 2004). Hence, the data and interpretations presented herein may inspire a new look at the Ordovician tectonic evolution of the Appalachians and Caledonides.

GEOLOGICAL BACKGROUND

Williams (1978) subdivided the Canadian Appalachians into five lithotectonic belts or zones: Humber, Dunnage, Gander, Avalon and Meguma, the first four of which are exposed in Newfoundland (Fig. 1.2). The Humber zone represents the margin of North America (Laurentia). The Dunnage, Gander, Avalon and Meguma zones were subsequently recognized as suspect terranes (Williams and Hatcher 1983). The Dunnage Zone represents the vestiges of the Iapetus Ocean, while Gander, Avalon and Meguma zones represent micro-continents derived from Gondwanaland (see van Staal 2005 for review).

Investigations of the Dunnage zone have revealed significant structural, isotopic, faunal, stratigraphic, magnetic and gravity contrasts between the western and eastern Dunnage zone, leading to its subdivision into western Notre Dame Subzone and eastern Exploits Subzone and recognition of the Red Indian Line (Williams et al. 1988). The Red Indian Line has been now accepted as the main Iapetus suture zone, along which over 3000 km of ocean crust has been consumed during the Ordovician (e.g. van Staal 2005).

The Appalachian deformation along the Laurentian margin is generally described in terms of five orogenic episodes: the Early to Middle Ordovician Taconic, Early to Late Silurian Salinic, latest Silurian to Early Devonian Acadian, Middle Devonian to Early Carboniferous Neoacadian, and Carbonifeous to Permian Alleghenian orogenies (see van Staal 2005 for review). The Taconic, Salinic and Acadian orogenies are interpreted to reflect the successive arrival of the Dashwoods, Ganderian and Avalonian microcontinents at the Laurentian margin (see van Staal 2005 for review). Neoacadian and Alleghenian orogenies did not pervasively affect Newfoundland and are not going to be discussed any further. Another orogenic episode, the Penobscot orogeny, affected peri-Gondwanan crustal fragments prior to their juxtaposition with the Laurentian margin (Colman-Sadd

et al. 1992) is extremely important for understanding the development of the peri-Gondwanan Ganderia microcontinent.

The study area lies entirely within the Dunnage Zone along the Red Indian Line in central Newfoundland. The rocks of the Annieopsquotch Accretionary Tract (Figure 1.3; van Staal et al. 1998) lie to the west of the Red Indian Line while the rocks of the Victoria Lake Supergroup (Evans and Kean, 2002) lie to the east. The positions of the Annieopsquotch Accretionary Tract and Victoria Lake Supergroup on the opposite sides of the Red Indian Line reflect their peri-Laurentian and peri-Gondwanan provenance respectively.

Annieopsquotch Accretionary Tract

The Annieopsquotch Accretionary Tract is a tectonic collage of peri-Laurentian arc-backarc complexes that formed outboard of the Laurentian margin in Early to Late Ordovician (van Staal et al. 1998). Although it was defined in Newfoundland, correlatives of the Annieopsquotch Accretionary Tract have been proposed to occur in New England and British Caledonides (van Staal et al. 1998). Newfoundland Annieopsquotch Accretionary Tract spans from the Notre Dame Bay to central Newfoundland where it is cut out by the Victoria Lake shear zone (Figure 1.2; Valverde-Vaquero and van Staal 2001). The constituent units of the Annieopsquotch Accretionary Tract are juxtaposed along northwest dipping oblique reverse shear zones (Thurlow et al. 1992; van der Velden et al. 2004).

The Annieopsquotch Accretionary Tract includes the Annieopsquotch Ophiolite Belt (U/Pb zircon 477.5+2.6/-2, 481+4/-1.9 Ma: Dunning and Krogh 1985), volcano-sedimentary rocks of the Buchans Group – Roberts Arm Group (U/Pb zircon 473±2, 473+3/-2, 473±4 Ma: Dunning et al. 1987; Bostock 1988; Kean 1979a; Kerr and Dunning 2003; Swinden et al. 1997), undated Skidder ophiolite (Pickett 1987) and informally named volcano-sedimentary rocks along the shores of Red Indian Lake (See Chapter 2). All of these units have been accepted to have peri-Laurentian affinity (e.g. Nowlan and Thurlow 1984; Thurlow et al. 1992; van Staal et al. 1998). The Annieopsquotch Accretionary Tract is thought to have formed above a west-dipping subduction zone (Fig. 1.4; e.g. Swinden et al. 1997; van Staal et al. 1998) and the constituents units were accreted to the

Laurentian margin during the Taconic orogeny. However the complexity and span of this subduction zone and accretionary history has not yet been investigated in detail.

Victoria Lake Supergroup

The volcano-sedimentary rocks underlying the area to the east of the Red Indian Line were originally included in the peri-Gondwanan Victoria Lake Group, which contained two linear northeast trending litho-tectonic belts of regional extent, namely the Tulks Hill volcanics and Tally Pond volcanics (Kean, 1977; Kean and Jayasinghe, 1980). The Tulks Hill volcanics occupies the western portion of the Victoria Lake Supergroup, while the Tally Pond volcanics underlie the eastern portion. Subsequent studies have identified two non-coeval volcanic sequences in the western belt, the Tulks Hill volcanics (498+6/-4 Ma, 495±2 Ma: Evans et al. 1990) and the Victoria Mine Sequence (462+4/-2; Dunning et al. 1987). Recognition of several more distinct litho-tectonic sequences (e.g. Long Lake belt: c. 505 Ma, V. McNicoll and N. Rogers, personal communication) over time has lead to the expansion of the definition of the Victoria Lake Group to Victoria Lake Supergroup to reflect its composite nature (Evans and Kean 2002; also Rogers and van Staal 2002).

Despite the recognition of both arc and back arc-like volcano-sedimentary sequences throughout the Victoria Lake Supergroup (Dunning et al. 1987; Evans et al. 1990; Kean, 1977; Kean and Jayasinghe, 1980), the lack of consistent stratigraphic framework, detailed geochronology and/or geochemistry has precluded establishment of comprehensive tectonic models. However, tectonic models (Figure 1-4) have been proposed for the broadly correlative units in New Brunswick (e.g. Colman-Sadd et al. 1992; van Staal et al. 1998) and in the Notre Dame Bay (e.g. MacLachlan et al. 1998a; O'Brien et al. 1997).

The evolution of the Exploits Subzone have been generally described in terms of two distinct arc sequences (Figure 1.4; MacLachlan et al. 1998a, 1998b, 2001; van Staal et al. 1996; van Staal et al. 1998), the Middle Cambrian to Early Ordovician Penobscot arc and the Lower to Middle Ordovician Popelogan -Victoria arc (van Staal et al. 1998). The Penobscot arc was generated in an intraoceanic setting outboard of the margin of the Ganderia microcontinent (e.g. van Staal et al. 1996) above a west dipping subduction zone (MacLachlan et al. 1998a, 1998b,

2001; van Staal et al. 1996; van Staal et al. 1998). The closure of the basin between Ganderia and Penobscot arc culminated in the Penobscot orogeny (485-478 Ma) and obduction of ophiolitic rocks onto the Gander Zone of Newfoundland (Colman-Sadd et al. 1992), which were stitched to the Gander zone by 478 Ma (Tucker et al. 1994). Subsequently Popelogan-Victoria arc volcanism was established by c. 473 Ma (MacLachlan et al. 1998b) above the Penobscot arc basement requiring subduction zone flip and initiation of east-dipping subduction along the composite Ganderia margin (e.g. MacLachlan et al. 2001; van Staal et al. 1998).

PREVIOUS WORK

The first systematic geological mapping of the study area was conducted by Riley (1957) and Williams (1970), with subsequent investigations by Kean (1977; 1978; 1979a, b; 1982; 1983), Kean and Jayasinghe (1980; 1982), Herd and Dunning (1979), Dunning (1984), Evans et al. (1994a, b) and Evans et al. (1994). Additionally there have been numerous industry-led studies (e.g., Grimes-Graeme, 1934; MacKenzie et al., 1988; MacKenzie et al., 1990; 1993; Desnoyers, 1990a, b; Squires et al., 1990).

OBJECTIVES

This thesis forms a part of the Targeted Geoscience Initiative 1, a Canada-wide project established by the Geological Survey of Canada (2000-2003). The goal of Targeted Geoscience Initiative 1 was to turn resource potential into new social and economic benefits by increasing the level and effectiveness of private sector mineral exploration. The Newfoundland portion of the Targeted Geoscience Initiative was aimed at studying the collisional tectonics along the Red Indian Line suture zone in central Newfoundland. The primary objective of this thesis was to produce 1:50,000 scale maps and establish a consistent tectono-stratigraphic framework across the study area and investigate the continuity of the units outside of the study area. In addition four other objectives specific to this thesis were identified:

- To constrain the tectonic setting and provenance (i.e. peri-Laurentian vs. peri-Gondwanan) of the tectono-stratigraphic units utilizing stratigraphy, geochronology, geochemistry and Sm-Nd isotopes.

- To establish the exact location of the fundamental Iapetus suture zone (Red Indian Line) in the study area and test Williams' (1995) hypothesis of the structural and isotopic contrasts across it.
- To test existing tectonic models of the evolution of the peri-Laurentian and peri-Gondwanan crustal fragments.
- To understand the processes involved in the accretion of the tectono-stratigraphic units to the Laurentian margin leading to the growth of Laurentia and their subsequent dispersal during later tectonism.

THESIS ORGANIZATION

The thesis is divided into three main chapters and three appendices which have been written as stand-alone papers. As a result there is some overlap between them, especially in the introduction and geological background sections. In addition the geological maps of the study area are included as an Appendix. Chapters 2, 3 and Appendices 1, 2 deal with the development of the arc-backarc complexes in Iapetus while Chapter 4 and Appendix 3 focus on the juxtaposition of these with the Laurentian margin.

Chapter 2 and 3 present the stratigraphy as well as geochemical, Sm-Nd isotope and geochronological data on the peri-Laurentian and peri-Gondwanan tectono-stratigraphic units in the study area respectively. Based on these data the existing tectonic models of the peri-Laurentian and peri-Gondwanan arc-backarc complexes are tested and modified where appropriate. Appendix 1 supplements the data presented in Chapter 2 by providing geochemical data and interpreting the tectonic setting of the earliest igneous rocks in the Annieopsquotch Accretionary Tract. Chapter 3 is supplemented by Appendix 2 where geochemical and Sm-Nd isotope data on the peri-Gondwanan Proterozoic basement in central Newfoundland are presented. Understanding of the Proterozoic basement and its relationships to the arc – backarc complexes is critical to assessment of the evolution of the peri-Gondwanan tectonic elements and testing the model presented in Chapter 3.

Chapter 4 presents the structural analysis and P-T conditions of metamorphic rocks in the study area as well as geochronological data on Silurian plutonic rocks which constrain the timing of

deformation. The results of the structural analysis are compared to structural studies in the Notre Dame Bay area and to the well-established orogenic cycles of the Appalachians. Chapter 4 is supplemented by Appendix 3 which presents geochronological, isotopic and geochemical data on the intrusive rocks in the Annieopsquotch Accretionary Tract and utilizes these data to decipher the accretionary history of the Early to Middle Ordovician Laurentian margin. A summary of tectonic interpretations of the thesis is presented in Chapter 5 and implications for the continental growth in this portion of the Appalachians are discussed.

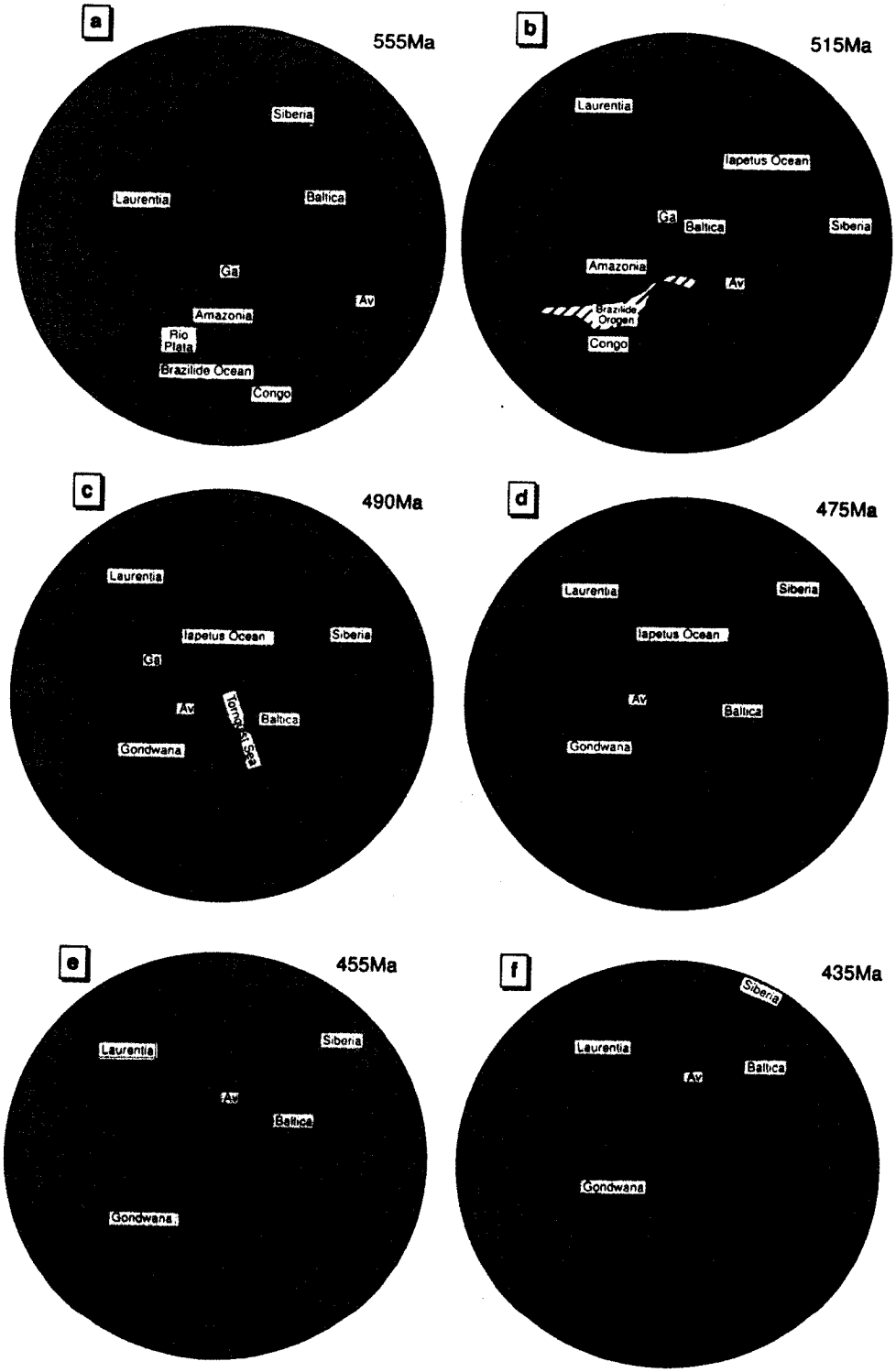

Figure 1-1 Late Neoproterozoic to Silurian paleogeographic/tectonic evolution of the Iapetus Ocean (modified from van Staal et al. 1998). Av - Avalonia, Ga - Gander

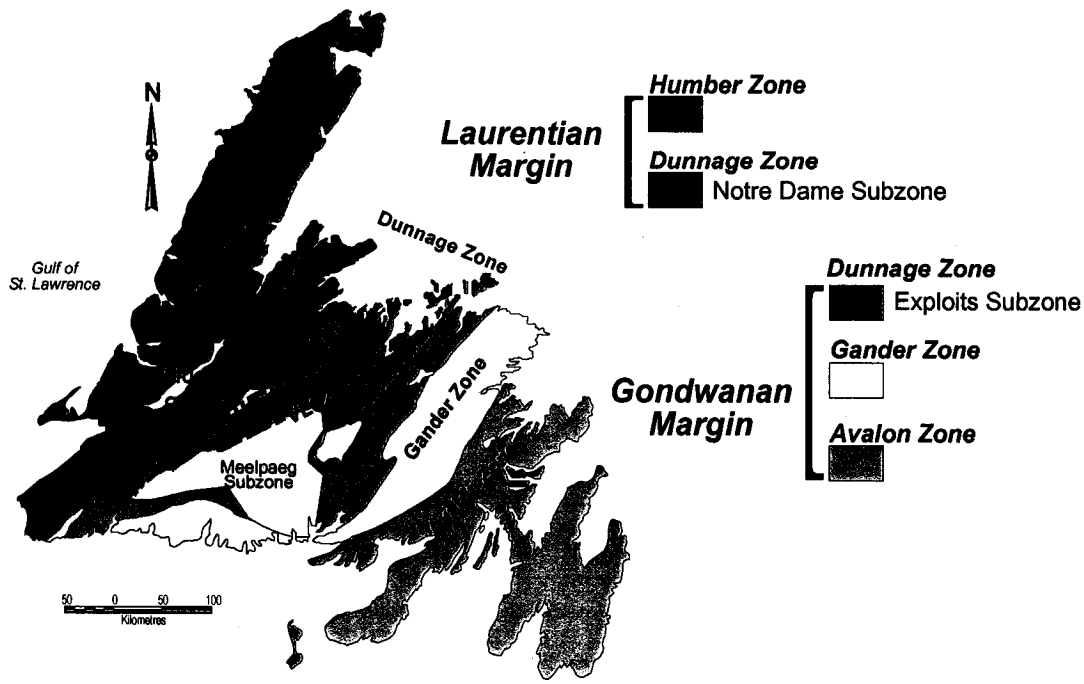

Figure 1-2 Lithostratigraphic subdivisions of Newfoundland (after Williams, 1995). RIL - Red Indian Line, VLSZ - Victoria Lake Shear Zone (Valverde-Vaquero and van Staal 2001).

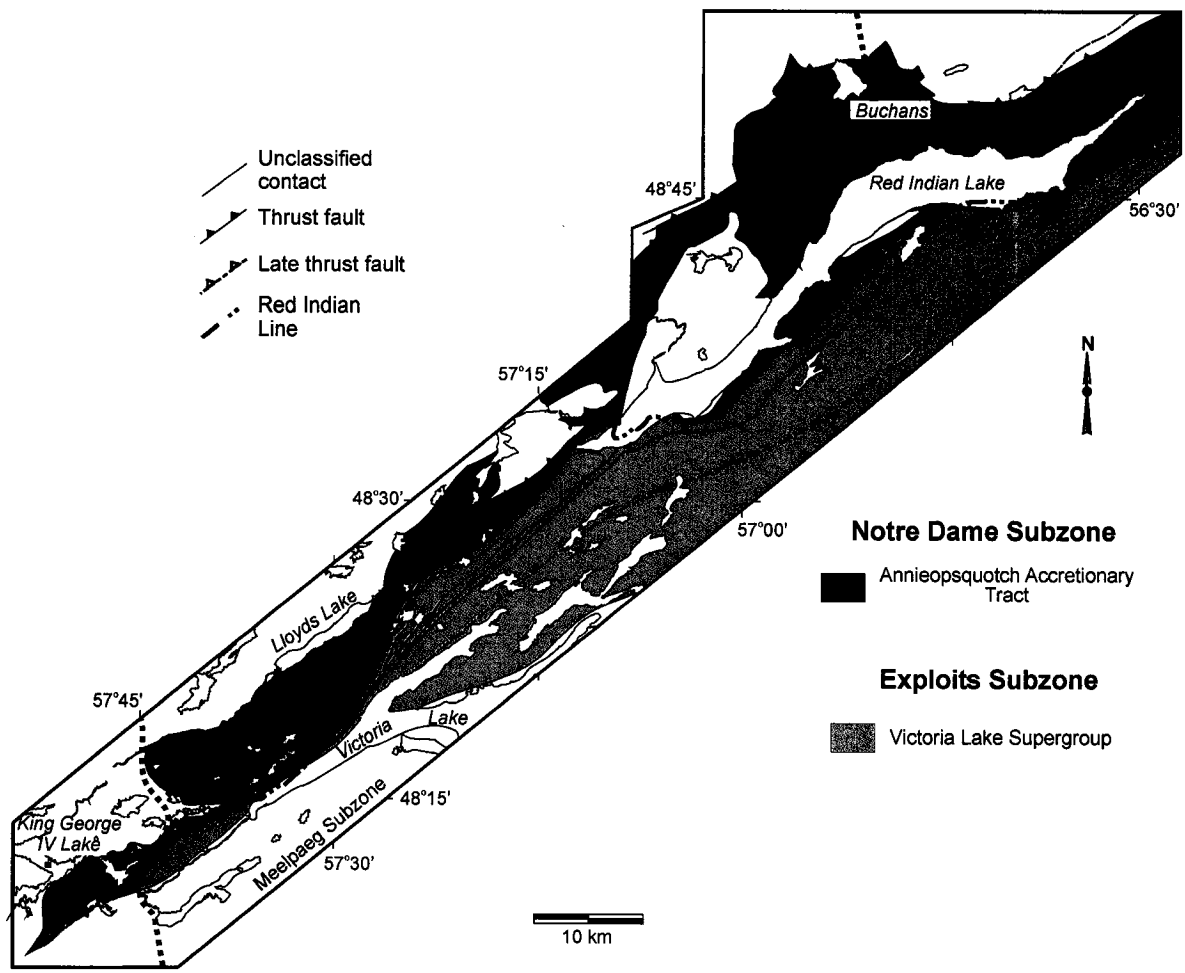

Figure 1-3 Locations of the Annieopsquotch Accretionary Tract and Victoria Lake Supergroup in the study area.

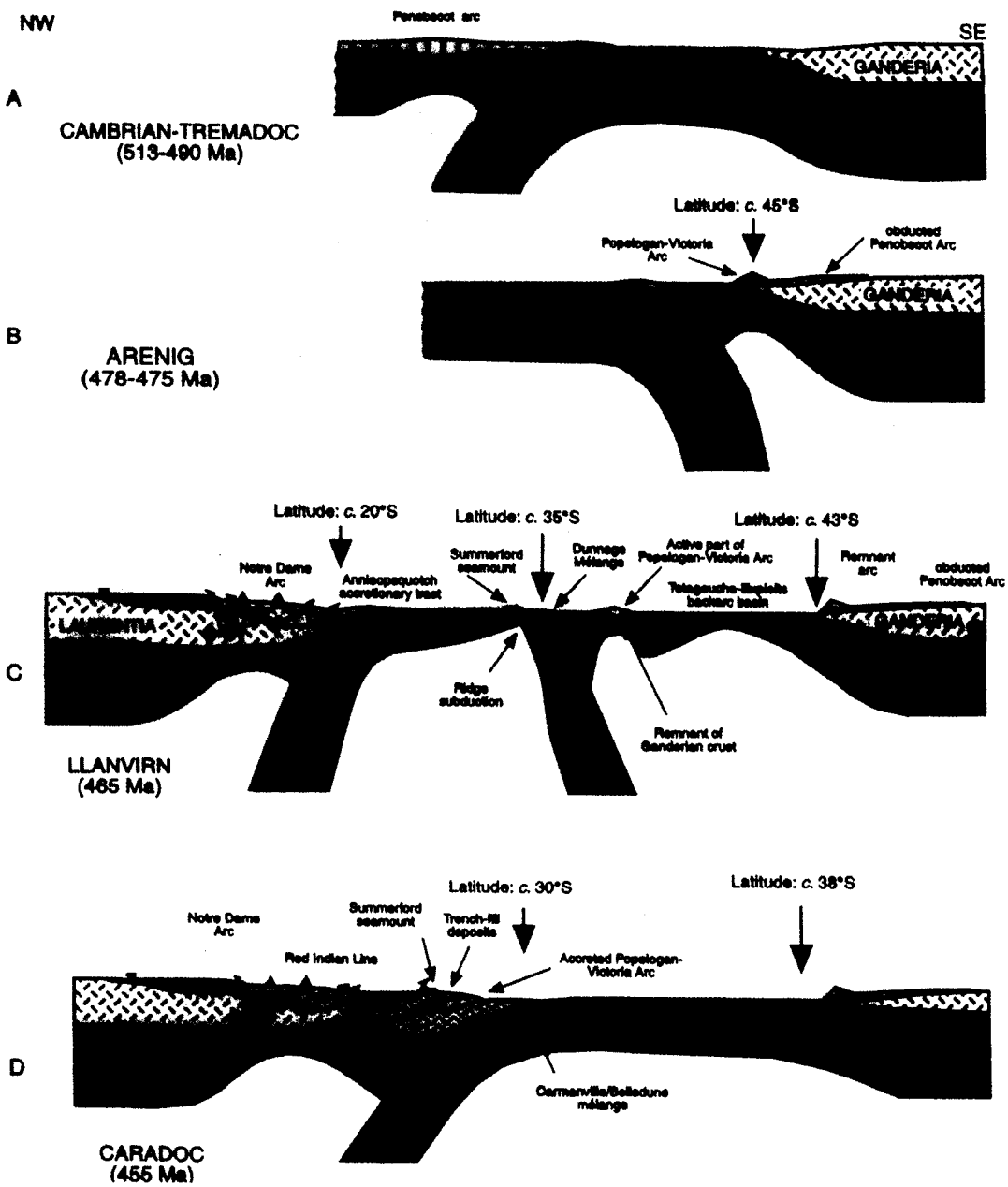

Figure 1-4 Cambrian to Caradoc tectonic evolution of the Gander margin and its convergence with the Annieopsquotch Accretionary Tract (from van Staal et al. 1998).

CHAPTER 2: LOWER TO MIDDLE ORDOVICIAN EVOLUTION OF PERI-LAURENTIAN ARC AND BACKARC COMPLEXES IN IAPETUS: CONSTRAINTS FROM THE ANNIEOPSQUOTCH ACCRETIONARY TRACT, CENTRAL NEWFOUNDLAND

ABSTRACT

The Annieopsquotch Accretionary Tract (AAT) in Newfoundland comprises a series of west-dipping structural panels, each containing remnants of ophiolitic and arc - backarc complexes of Laurentian affinity formed during the Ordovician closure of Iapetus. Panels were transferred from an upper plate to a lower plate setting during their Middle to Late Ordovician accretion to the Laurentian margin and become progressively younger eastward. Geochronological data indicate a complex and rapid history of generation and accretion of peri-Laurentian suprasubduction zone rocks. The rapid changes in tectonic environments and the complexity of the relationships are analogous to the complex arc – backarc relationships observed in the western Pacific today. The recognition of the peri-Laurentian provenance of these units based on stratigraphy, geochronology, isotopes and geochemistry defines the position of the Red Indian Line, the fundamental suture zone in the northern Appalachians, but more importantly enables the development of a realistic tectonic model for the AAT involving both thrust and sinistral transcurrent displacements.

The oldest and most inboard unit in the AAT is the Annieopsquotch Ophiolite Belt (c. 480 Ma), which marks the initiation of subduction outboard of the Laurentian margin. The Lloyds River Ophiolite Complex (LROC; c. 473 Ma) preserves a fragment of younger, more MORB-like backarc – oceanic crust than the adjacent, structurally overlying Annieopsquotch Ophiolite Belt. The LROC originated as a backarc to the Buchans Group (c. 473 Ma) ensialic bimodal calc-alkaline arc. The panels containing the Annieopsquotch Ophiolite Belt and LROC were stitched and overlain by ensialic arc rocks of the Otter Pond Complex (c. 468 Ma) immediately after their accretion to composite Laurentia together with the structurally underlying Buchans Group. The youngest, structurally lowest two panels, comprise the elements of the Red Indian Lake Group (465-460 Ma), which record opening of a backarc basin and subsequent establishment bimodal ensialic calc-alkaline arc sequence.

The observed relationships indicate that the AAT was generated above a single west-dipping subduction zone outboard of the Laurentian margin over approximately 20 Ma. Accretion mainly took place in two stages at c. 468 and 450 Ma, which correspond with the collision between Laurentia and the Dashwoods ribbon continent and the collision with peri-Gondwanan Victoria Arc along the Red Indian Line, respectively. Both collisions form part of the Taconic orogeny. The latter, Late Ordovician collision terminated the relatively rapid closure of the main Iapetan tract. The proposed model is similar to the correlative tracts in the British and Irish Caledonides, and may encourage a new look at the New England Appalachians.

INTRODUCTION

The Appalachian – Caledonian Orogen is an example of a long-lived accretionary orogen, which formed in response to the Palaeozoic closure of the Iapetus, Tornquist and Rheic oceans. Closure of these ocean basins that separated Laurentia, Gondwana and Baltica from each other (van Staal et al., 1998; Cocks and Torsvik, 2002) generated a diverse set of arc terranes, microcontinents and suprasubduction zone oceanic terranes that were accreted as single or composite terranes to Laurentia, in multiple stages, forming a complex tectonic collage. Consequently, assessing Laurentia's growth requires a good understanding of the provenance and tectonic processes involved in the accretion of the various terranes. Another important aspect is the role of trench-parallel translation and dispersion of terranes during and after accretion. Some workers have speculated that this process may have been important, because critical elements of tectonic systems (e.g., fore-arc basins) are missing in many places (van Staal et al., 1998).

The Newfoundland Appalachians represent a critical element of the Appalachian – Caledonian Orogen for evaluation of terrane linkages between the North American and European segments of the orogen. This particularly applies to the terranes accreted during the Ordovician closure of Iapetus' main oceanic tract (van Staal, 2005), because the zone of accreted terranes is wide, relatively well exposed, generally of low metamorphic grade and a detailed integration of seismic reflection and geological data has been done (e.g., Thurlow et al., 1992; van der Velden et al., 2004). This paper presents new data concerning the tectonic setting, age and structural architecture of the various igneous and sedimentary units that have been recognised in the

Annieopsquotch Accretionary Tract (AAT: van Staal et al., 1998; Zagorevski et al., 2003a, b) of Central Newfoundland, discusses the regional correlations with other known units in the AAT, and finally presents a model for the tectonic evolution of the AAT and its relationship to the Laurentian margin. It will be shown that the AAT comprises a series of Lower to Middle Ordovician peri-Laurentian oceanic and ensialic suprasubduction zone terranes that were assembled in west-dipping structural panels as a result of Ordovician sinistral-oblique accretion to Laurentia. Accretion terminated when the main Iapetan tract was closed and sutured with peri-Gondwanan elements along the Red Indian Line during the Late Ordovician (van Staal et al., 1998; van Staal, 2005).

The new interpretations of the AAT support previous correlations with the Northern Belt of the Southern Uplands accretionary system of the British Caledonides, although, as discussed below, in detail there appear to be differences in the tectonic setting of the accreted terranes and the time when west-directed subduction of Iapetus started (Ryan and Dewey, 2004; Lissenberg et al. in press a). Evidence of west-directed subduction in Newfoundland has ramifications for tectonic analyses of the northern Appalachians in New England and southern Quebec. Both the continuation of the AAT and the Red Indian Line, as well as the evidence for west-directed subduction in general are controversial themes in New England (e.g., Karabinos et al., 1998; Moench and Aleinikoff, 2000; Robinson et al., 1998), Hence, the data and interpretations presented herein may inspire a new look at the Ordovician tectonic evolution of the central part of the northern Appalachians in New England (e.g., Kim et al., 2002), where part of this history is masked by the extensive post-Ordovician cover sequences, largely absent in Newfoundland.

The tectonic architecture of the AAT was established by detailed geological mapping (i.e., Lissenberg et al., 2005c; Rogers et al., 2005a; van Staal et al., 2005 a, b, c), combined with high quality geochronology and geochemistry. This paper follows the stratigraphy developed during this mapping, which wherever possible took previously described units and expanded upon them so that they were categorised and ranked in a form that is compliant with the strictures of the North American Stratigraphic Code (i.e., the Skidder basalts become the Skidder Formation). Additionally, several new tectono-stratigraphic units (Lloyds River Ophiolite Complex, Mink Lake Formation and Red Indian Lake Group) that were identified for the first time during this mapping, and so cannot be

directly linked to any previously described entities, are described in detail in this paper. The unit names, rank and categories presented herein can be considered informal pending the release of the formalizing documentation for this region.

REGIONAL GEOLOGY

Williams (1979; 1995) originally subdivided the Northern Appalachians into the Humber, Dunnage, Gander, Avalon and Meguma zones, with the Humber Zone representing the remnants of the Laurentian passive margin and the Gander, Avalon and Meguma zones accreted peri-Gondwanan terranes (Fig. 2.1 inset). In this classification, the Dunnage Zone combines the vestiges of the Cambro-Ordovician peri-Laurentian (Notre Dame and Dashwoods subzone) and peri-Gondwanan (Exploits Subzone) continental and oceanic arc/backarc and ophiolitic complexes that formed within the Iapetus Ocean. The peri-Laurentian and peri-Gondwanan subzones are differentiated on the basis of marked contrasts in stratigraphy, structure, fauna and isotopic characteristics. The recognition of these differences over time led to the discovery of the Red Indian Line (Fig. 2.1; Williams et al., 1988), which was a major breakthrough in understanding Appalachian tectonics. The Red Indian Line represents a major crustal scale fault that is clearly visible in seismic surveys as a reflector extending to at least 20 km, at which point it is truncated by a Devonian, wedging-related structure (van der Velden et al., 2004).

This study discusses the sequences that occur immediately to the west of the Red Indian Line and which constitute the most outboard units of the peri-Laurentian Notre Dame Subzone (Fig. 2.1). The Notre Dame Subzone is dominated by Taconic deformed and metamorphosed Ordovician volcanic and plutonic rocks of the Notre Dame Arc (Whalen et al., 1997; van Staal et al., 1998) that are locally unconformably overlain by Silurian red beds. The Ordovician Notre Dame Arc was largely built upon the rocks of the Dashwoods Subzone. Dashwoods Subzone has been interpreted as a ribbon microcontinent interpreted to have rifted off Laurentia during the Early Cambrian (Waldron and van Staal, 2001).

ANNIEOPSQUOTCH ACCRETIONARY TRACT

The AAT is bounded to the west by the Lloyds River Fault/Hungry Mountain thrust system (Lissenberg and van Staal, 2002; Thurlow, 1981) and to the east by the Red Indian Line

(Zagorevski et al., 2003a, 2004). Internally, the constituent units of the AAT are juxtaposed along northwest dipping oblique reverse shear zones, which appear to become progressively younger to the southeast, suggesting progressive accretion to the Laurentian margin.

The structural relationships between the units of the AAT are well preserved in the Buchans area (Fig. 2.1), where an extensive south-southeast directed thrust duplex system was recognised with the Hungry Mountain thrust as the roof and the Red Indian Line as the floor thrusts (Fig. 2.1; e.g., Calon and Green, 1987; Thurlow et al., 1992). Structural relationships are more complicated southwest of Buchans where several phases of deformation have resulted in tight to isoclinal folding, steepening and reactivation of the thrusts as steep, southeast-directed sinistral oblique reverse faults (Zagorevski and van Staal, 2002). In the studied area, the thrusts are overprinted by open to tight moderately inclined folds and kinks related to Silurian to Devonian deformation, resulting in local overturning of the southeast-directed thrusts. Our interpretation of the original geometry of the AAT relies in part on the geometrical reconstruction of the thrust duplex in the Buchans area (Calon and Green, 1987; Thurlow et al., 1992).

The AAT contains the structural panels comprising the Annieopsquotch Ophiolite Belt (AOB; U/Pb zircon 477.5+2.6/-2, 481+4/-1.9 Ma: Dunning and Krogh, 1985), Lloyds River Ophiolite Complex (LROC; U/Pb zircon 473±3.7 Ma: see below), Otter Pond Complex (468±2 Ma: Appendix 3), Buchans Group (U/Pb zircon 473±1, 473±2, 473+3/-2, 473±4 Ma: Dunning et al., 1987; Bostock, 1988; Kean, 1979a; Kerr and Dunning, 2003; Swinden et al., 1997; see below) and the Red Indian Lake Group (U/Pb zircon 464.8±3.5, 462+2/-9, 465±2, 463±3 Ma: see below), which have a total structural thickness of 8 to 15 km (Fig. 2.1). The structural thickness of each panel individually varies significantly in the study area (0 to 5 km, ~2 km average) indicating partial to total excision of the lithostratigraphic units due to strike-slip related to transfer from upper plate to lower plate setting during accretion and subsequent deformation. The stratigraphy of each of these structural panels is described from the structurally highest (northwest) to the lowest (southeast), that is generally from old to young (Fig. 2.2). All units have been metamorphosed to (sub)-greenschist to amphibolite facies with the grade of metamorphism generally increasing towards the west.

Annieopsquotch Ophiolite Belt

The Annieopsquotch Ophiolite Belt (AOB) comprises several related supra-subduction zone ophiolite complexes (Fig. 2.1, 2.3, 2.4) that formed during the initiation of west-directed subduction outboard of the Dashwoods Subzone (Lissenberg et al., 2005a; Appendix 1). AOB preserves an early boninitic troctolite phase, along with later gabbro sill, sheeted dyke and pillow basalt zones (Dunning, 1984; Appendix 1). The gabbro-sheeted dyke-basalt sequence has a tholeiitic supra-subduction zone geochemical signature, although the stratigraphically highest basalts progressively develop more MORB-like compositions and are cut by enriched BAB-like sheeted dykes (Appendix 1). The AOB is separated from the structurally underlying Lloyds River Ophiolite and Otter Pond complexes by the Otter Brook – Boogie Lake Shear Zone (Fig. 2.3, 2.4).

Lloyds River Ophiolite Complex

The Lloyds River Ophiolite belt (LROC) is exposed as a c.1 km thick belt for over 100 km from Mink Lake to the town of Buchans. Previously it was recognized only as gabbro and mafic volcanic and included in the Victoria Lake Supergroup. LROC is defined as a series of geochemically distinct ophiolitic panels that are younger than the structurally overlying AOB (Figs. 2.1, 2.3 and 2.4). Spectacular exposures of this ophiolite complex occur along the Lloyds River (Fig. 2.3). The LROC contains rocks that were previously correlated with the Annieopsquotch Ophiolite Belt, as well locally with the Bay du Nord, Buchans and Victoria Lake groups (as defined by Kean, 1979b; 1982; 1983). LROC is intruded by felsic dykes typical of the Otter Pond Complex (Lissenberg et al., 2005b; Appendix 3; see below) and unconformably overlain by Upper Llandovery to Wenlock continental red beds and volcanic rocks (Dunning et al., 1990). The LROC is divided into two geochemically distinct suites that in the study area occur within distinct structural panels, but may occur together further to the north according to the geochemical database of Davenport et al. (1996; Table 2.1; Fig. 2.5).

Otter Brook Suite: The ophiolitic Otter Brook Suite, named after the exposure above the Otter Brook, (Fig. 2.3) comprises variably deformed gabbro, sheeted diabase (Fig. 2.4a) and pillow basalt. The basalt and locally diabase are vesicular and plagioclase phyric, whereas the gabbroic rocks display subophitic intergrowths between plagioclase and clinopyroxene. The clinopyroxene is

typically altered to hornblende and oxide assemblages. The Otter Brook Suite is separated from the AOB and the Otter Pond Complex by the Boogie Lake - Otter Brook Shear Zone (Fig. 2.3, 2.4).

Star Brook Suite: The ophiolitic Star Brook Suite comprises variably deformed gabbro, anorthosite, sheeted diabase and pillow basalt (Fig. 2.6b). The gabbro grades into anorthositic gabbro and anorthosite, defining a continuous, but fault-dissected, anorthosite-rich lens along the Lloyds River valley. The gabbro sequence is locally cut by plagioclase porphyritic diabase, similar to the dykes in the sheeted diabase zone. The sheeted dykes grade into a pillow lava sequence that is locally associated with thinly bedded limestone. The relationships between sheeted diabase and basalt are well preserved in the type locality along Star Brook. An additional reference section is designated for this suite immediately north of the south-western tip of Victoria Lake (UTM Zone 12 454600, 5344700 to 454600, 5345700; NAD 83). This area preserves a 0.75 km thick northwest younging sequence of layered and isotropic gabbro (c.500 m), diabase (c.50 m), and pillow basalt (c. 200 m).

Otter Pond Complex

The Otter Pond Complex (Fig. 2.1, 2.3, and 2.4; Appendix 3) occurs in a relatively thin (typically 10 - 200 m), highly deformed tectonite panel comprising rhyolite, amphibolite, metagabbro, mica and graphitic schist that are tentatively interpreted to represent a sequence of interlayered rhyolitic tuff (Fi g. 2.6c), basaltic flow and/or sill, pelite or altered felsic tuff and carbonaceous sedimentary rocks. This tectonite panel largely defines the Boogie Lake - Otter Brook Shear Zone along approximately 150 km of its length (Fig. 2.3, 2.4), which separates the LROC from the AOB. Northeast of Otter Pond, Silurian plutons intruded the Otter Pond Complex, which was transformed into interlayered biotite-muscovite-garnet, quartzo-feldspathic and migmatitic paragneiss by the accompanying metamorphism and coeval deformation (Fig. 2.6d; Chapter 4). Hornblende-phyric to oikiocrystic gabbro and diabase typical of the Otter Brook Complex intrude into the AOB. Chemistry of the Otter Pond Complex felsic and mafic rocks suggest formation in a calc-alkaline ensialic arc setting (ε_{Nd} –1 to –6.8; Appendix 3). Otter Pond Complex granodiorite intrudes along the Otter Brook – Boogie Lake Shear Zone and is interpreted to stitch the AOB, LROC, and Buchans Group (468±2 Ma; Appendix 3).

Buchans Group

The Buchans Group and correlative Roberts Arm Group comprise c. 473 Ma peri-Laurentian ensialic arc sequences that have an exposed combined strike length of approximately 200 km (Table 2.1, Fig. 2.5; Bostock, 1988; Dunning et al., 1987; Nowlan and Thurlow, 1984; Swinden et al., 1997; Thurlow and Swanson, 1987). The herein defined Mink Lake Formation is included in the Buchans Group based on its age, geochemistry, Sm-Nd isotope characteristics and similarity of structural position.

Mink Lake Formation: The Mink Lake Formation is restricted to an area southwest of Wood Lake and north of Mink Lake, which forms its type locality (Fig. 2.1, 2.4). The Boogie Lake and Wood Lake shear zones separate it from the AOB and LROC to the north and northeast, respectively, whereas the Mink Lake Shear Zone separates it from the Red Indian Lake Group to the southeast. The Mink Lake Formation is only gently folded and typically appears largely undeformed macroscopically. It is dominated by hematized pillow basalt and breccia (Fig. 2.6e) with some massive basalt flows, diabase, felsic tuff and jasper. Younging indicators suggest the felsic tuff occurs near the stratigraphically highest exposed level of the sequence, however, as neither the base nor the top of the formation are exposed its true position within the Buchans Group stratigraphy cannot be resolved at present.

Red Indian Lake Group

The herein defined Red Indian Lake Group (Figs. 2.1, 2.3, 2.4 and 2.7), predominantly exposed along the shores of Red Indian Lake, comprises rocks that were previously allocated to several informal units, such as the Healy Bay siltstone, Harbour Round basalt (Thurlow et al., 1992), Harbour Round formation (Kean and Jayasinghe, 1980) and Skidder basalt (Pickett, 1987). The definition of these informal units is herein expanded upon to reflect the lithological characteristics in the type localities and three revised units are proposed for the Red Indian Lake Group: Harbour Round, Healy Bay and Skidder formations. The Red Indian Lake Group is separated from the structurally overlying Buchans Group by the Tilley's Pond Fault (Thurlow et al., 1992) and correlative Mink Lake Shear Zone (Fig. 2.1, 2.4), the Wood Lake Shear Zone separates it from the structurally overlying LROC (Fig. 2.4), whereas the Red Indian Line separates it from the

structurally underlying peri-Gondwanan Victoria Lake Supergroup (Fig. 2.1; Evans and Kean, 2002). Internally within the Red Indian Lake Group the Clench Brook Fault juxtaposes the Skidder Formation with the structurally underlying Harbour Round and Healy Bay formations (Fig. 2.1). The Healy Bay Formation is stratigraphically inter-tongued with the more extensive Harbour Round Formation.

The Red Indian Lake Group is exposed in a 1-6 km wide, imbricated belt for at least 150 km from Wood Lake to Red Indian Lake (Fig. 2.1). Although the Red Indian Lake Group has yet to be recognised northeast of Red Indian Lake, correlatives may exist in the Roberts Arm – Chanceport belt (Table 2.1, Fig. 2.5)

Skidder Formation: The Skidder Formation, which is named after the previously defined Skidder basalt (Pickett, 1987), is a tholeiitic sequence of predominantly pillowed and massive amygdaloidal and variolitic basalt, and pillow breccia (Fig. 2.6f) that locally hosts significant VMS-style mineralization (Skidder Prospect; Pickett, 1987). These basaltic rocks are associated with interstitial jasper, interflow hematitic siltstone and jasper, and are intruded by gabbroic dykes and pods of chemically related trondhjemite (Davenport et al., 1996; Pickett, 1987). The Skidder Formation is well exposed in Skidder Brook, east of the Skidder Prospect, where pillow lava and breccia are cut by fine grained trondhjemitic dykes. The absence of calc-alkaline basalt and felsic tuff distinguishes the Skidder Formation from the upper basalt of the Harbour Round Formation. However, it may be in part correlative to chemically similar basalt in the lower member of the Harbour Round Formation (see below).

Harbour Round Formation: The Harbour Round Formation is informally subdivided into the lower and upper basalt members (Fig. 2.4, 2.6), with the lower basalt member dominating the southern portion of the formation's exposures and the upper basalt the northern part. All lithologies are inter-tongued with felsic tuff typical of the Healy Bay Formation. The central portion of the formation that occurs immediately north of Harbour Round, although structurally complex, preserves the stratigraphic relationships between these members, and as such forms the type locality. The lower basalt member comprises predominantly light green pillow basalt associated with hematitic red shale, interstitial limestone, diabase, gabbro, iron formation and felsic tuff.

The appearance of a polymictic volcanogenic conglomerate to breccia marks the base of the upper basalt member (Fig. 2.6g). The conglomerate ranges from clast to matrix supported, and thinly bedded to massive. The clasts comprise felsic volcanic, mafic volcanic and jasper. In the stratigraphically higher levels the conglomerate is associated with hematized pillow basalts, which are chemically distinct from the lower basalt member.

Healy Bay Formation: The Healy Bay Formation comprises mainly light grey to white, ash to crystal tuff locally associated with rhyolite, volcanoclastic sandstone and shale. All lithologies are locally interlayered with red shale and/or hematitic chert (Fig. 2.6h). Bedded red shale can locally be abundant with thickness exceeding several meters.

U-PB GEOCHRONOLOGY

Six new U-Pb zircon age determinations were conducted at the Geological Survey of Canada (Ottawa) utilizing as appropriate both Thermal Ionisation Mass Spectrometry (TIMS) and Sensitive High Resolution Ion Micro-Probe (SHRIMP II) methodologies. SHRIMP II analyses were conducted following the analytical procedures of Stern (1997), with standards and U-Pb calibration methods following Stern and Amelin (2003). The U-Pb TIMS analytical methods are outlined in Parrish et al. (1987), with treatment of analytical errors following Roddick (1987). U-Pb SHRIMP II and TIMS analyses are presented in Tables 2.2 and 2.3, respectively and are plotted on concordia diagrams with errors at the 2σ level (Fig. 2.8). Additional information on the analytical procedures is provided in Appendix A4.

Lloyds River Complex leucogabbro (VL02A178)

Sample VL02A178 consists of a white weathered leucogabbro that outcrops to the southeast of Lloyds River within the Star Brook Suite. This sample yielded a small amount of poor quality zircon grains and fragments. All of the grains preserve some euhedral faces and igneous zoning, however alteration patches are present in some grains. In total 9 grains were analysed with the SHRIMP II, producing a Concordia age calculated to be 473.0 ± 3.7 Ma (MSWD of concordance and equivalence = 1.5) (Table 2.2, Fig. 2.8a). This age is interpreted to be the crystallization age of the Star Brook Suite leuco-gabbro and therefore is also representative of the gabbro, sheeted dykes and pillow lavas of Star Brook Suite.

Mink Lake Formation felsic tuff (VL01A097)

Sample VL01A097 was obtained from a buff weathered, jasper chip bearing, bedded felsic tuff that directly overlies a basaltic flow. The sample yielded a small amount of variable quality zircon with several distinct morphologies including euhedral prisms, stubby prisms, and equant grains, as well as concoidal fragments derived from larger grains. Cores and inclusions were present in several grains. In addition, there were also presumably inherited slightly to strongly rounded prismatic to equant zircons and anhedral grains in the sample. Four fractions were selected for TIMS analysis (Table 2.3). Two fractions (E and F) are nearly concordant (0.2 %), and together define a Concordia age of 473.4 ± 1.2 Ma (MSWD of concordance and equivalence = 0.22) (Fig. 2.8b). Fraction C is 8.1% discordant and likely experienced recent Pb loss, whereas fraction B is interpreted to contain an inherited zircon component derived from an older crustal source. The age of 473.4 ± 1.2 Ma is interpreted to represent the crystallization age of the felsic tuff and the associated mafic volcanic rocks.

Skidder Formation trondhjemite (VL02A294)

Sample VL02A294 was collected from a small body of fine-grained trondhjemite that intrudes epidotized pillow breccia east of the Skidder Prospect. The trondhjemite was locally extensively quartz veined. This sample yielded a small amount of poor quality zircon grains and fragments. Most of the morphologies are interpreted to be magmatic in origin, with stubby prisms predominating. However, several rounded, presumably inherited zircons were also present. The dominant population of zircons from the trondhjemite, analysed on the SHRIMP, have a Concordia age calculated at 464.8 ± 3.5 Ma (MSWD of concordance and equivalence = 1.4, n=10) (Fig. 2.8c, Table 2.2). A second, younger population of zircons (n=6) had a calculated Concordia age of 424.2 ± 4.2 Ma (MSWD of concordance and equivalence = 1.1) (inset of Fig. 2.8c). Presence of two distinct zircon populations makes the interpretation of the age of the trondhjemite somewhat problematic. The trondhjemite could have crystallized at c. 424 Ma and inherited c. 465 Ma population; however, there is no documented Silurian oceanic crust in the AAT. The oceanic character of the Skidder Formation (Pickett, 1987; Swinden et al., 1997) is inconsistent with Silurian magmatism, which is predominantly ensialic calc-alkaline and alkaline (Whalen et al., 2003). The

Silurian age is best interpreted to either reflect hydrothermal zircon growth in microscopic quartz veins or possibly igneous growth in tonalitic veinlets related to the nearby, voluminous Silurian magmatism, that were collected along with the trondhjemite. The interpreted age of the trondhjemite, at 464.8 ± 3.5 Ma, also provides an age on the Skidder Formation basaltic volcanism.

Healy Bay Formation Tuff (RAX01-908; z7097)

Sample RAX01-908 (z7097) lies stratigraphically near the base of the Healy Bay Formation. This sample contains abundant euhedral prismatic zircons. Four multigrain zircon fractions were analysed by TIMS (Table 2.3). Three of these analyses are quite discordant (32-60%) and are interpreted to contain significant inherited components (Fig. 2.8d). Fraction A2 is nearly concordant; the $^{206}Pb/^{238}U$ age of this fraction is 462.3 ± 1.3 Ma. Zircons from this tuff sample were also placed on a grain mount and analysed by SHRIMP. SEM imaging revealed numerous zircons with core-rim relationships, as well as entirely magmatic grains with sharp oscillatory zoning. Thirteen analyses were collected from oscillatory zoned rims and grains interpreted to be magmatic in origin (Table 2.3). A Concordia age, calculated from these analyses, is 457.0 ± 3.7 Ma (MSWD of concordance and equivalence = 1.4) (Fig. 2.8e). SHRIMP analyses of zircon cores range in age from c. 935 to 1845 Ma (Table 2.2; not plotted), revealing contribution from older crustal sources. The best interpretation for the age of this tuff is taken to be 462 +2/-9 Ma, to take into account the age of nearly concordant fraction A2 and the Concordia age calculated from the SHRIMP analyses.

Healy Bay Formation Tuff (RAX00-903; z6679)

Sample RAX00-903 (z6679) occurs stratigraphically above RAX01-908. This sample contains abundant euhedral zircon ranging in morphology from equant grains to elongate crystals (Table 2.3). Six multigrain zircon fractions were analysed by TIMS. Fraction A1 is concordant and has a $^{206}Pb/^{238}U$ age of 465.1 ± 1.2 Ma (Fig. 2.8f, Table 2.3). Fractions E1 and C1 are discordant and contain inherited components. A linear regression including fractions C1, E1, and A1 has an upper intercept at ca. 2.3 Ga and a lower intercept at 465 ± 1 Ma (MSWD=0.02). Fraction B1, B2, and D1 are slightly discordant and may have undergone a minor amount of Pb loss. A weighted average of the $^{207}Pb/^{206}Pb$ ages of the most concordant analyses (A1, D1, B1) is 467.1 ± 2.9 Ma

(MSWD=0.19). The best interpretation for the age of the tuff is 465 ± 2 Ma and takes into account the error on all analysed fraction combinations.

Healy Bay Formation Felsic Tuff (RAX00-916; z6682)

Sample RAX00-916 (z6682) occurs in close association with the upper basalt member and is interpreted to occupy a similar stratigraphic position as the other geochronology samples in the Healy Bay Formation. The tuff contains a moderate amount of euhedral zircon with minor inclusions ranging in morphology from stubby prismatic grains to elongate crystals (Table 2.3). Four multigrain zircon fractions were analysed from this rock (Table 2.3). A linear regression utilizing all four TIMS analyses has an upper intercept of 1483 ± 15 Ma and a lower intercept of 463 ± 3 Ma (MSWD = 1.5) (Fig. 2.8g). Fractions Z2 and Z3A are quite discordant (33% and 35%, respectively) and are interpreted to contain inherited components. Fractions Z1A and Z1B are nearly concordant and their $^{206}Pb/^{238}U$ ages are within error of the lower intercept age. This date of 463 ± 3 Ma is interpreted to be the crystallization age of the tuff.

GEOCHEMISTRY

The analytical methods employed for determination of major, trace elements and isotopic ratios are described in Rogers (2004). The analyses are listed in Table 2.4 and Table 2.5. The compositional variation between groups is graphically presented in Figures 2.9 and 2.10. Numerous studies (see Pearce, 1996 for references) have shown that the pervasive sub-greenschist to amphibolite facies metamorphic and metasomatic conditions that the rocks in this study have experienced can result in some element mobility (e.g., Cs, Rb, Ba, K, Sr). Thus, the analysis of the data focuses on elements that are generally considered to be immobile under normal metamorphic conditions. Tholeiitic and calc-alkaline series are differentiated on the basis of trace element chemistry (Cabanis and Lecolle, 1989). FeO and Mg# were calculated assuming a Fe^{3+}/Fe^{2+} ratio of 0.1.

Lloyds River Ophiolite Complex

Otter Brook Suite

The Otter Brook Suite is dominated by high Ti tholeiitic basaltic rocks (TiO_2 1.3 to 3.1 wt%; FeO + MgO 16 to 20 wt%) that are characterized by enrichment in LREE (average La_n/Yb_n 2.6) and

Th (average La_n/Th_n 0.5), and slight a depletion in Nb (average La_n/Nb_n 1.7). The diabase and basalt members of this chemical grouping are moderately to strongly evolved, resulting in a Mg # of 35 to 60.

Star Brook Suite

The Star Brook Suite comprises three distinct geochemical types informally referred to herein as SB_1,SB_2 and SB_3. SB_1 consists of high Ti tholeiitic rocks that outcrop as gabbro, diabase and basalt with a notable homogeneous basaltic chemistry (TiO_2 1 to 2 wt%; FeO + MgO 13 to 21 wt%). This group is characterized by 0.8 to 2 times N-MORB trace element abundances, slight depletion to slight enrichment of LREE on N-MORB normalized spidergrams (La_n/Yb_n 1.2), slight but consistent depletion in Zr (Zr_n/Sm_n 0.9), slight enrichment of Th (La_n/Th_n 0.7), negligible depletion of Nb (La_n/Nb_n 1), and is primitive to moderately evolved (Mg# 49 to 66). A sample of basalt was analysed for Sm/Nd isotopes and yielded an $\varepsilon_{Nd(t=473)}$ value of +8.9.

SB_2 is also a high Ti tholeiite (TiO_2 1.33 to 1.72 wt%; FeO + MgO 10 to 18 wt%), but outcrops only as gabbro and diabase. This group is characterized by MORB-like trace element abundances, slight depletion to slight enrichment of LREE (La_n/Yb_n 1.3), depleted Zr (Zr_n/Sm_n 0.6), strong depletion in Th (La_n/Th_n 4.1), slight depletion to slight enrichment of Nb (La_n/Nb_n 1.1), and is moderately evolved (Mg# 58).

The SB_3 tholeiitic rocks (TiO_2 0.23 to 1.3 wt%; FeO + MgO 13 to 21 wt%) outcrop as gabbro, diabase and basalt. This group is heterogeneous, but has similar normalized profiles. The abundance of REE can be related to the fractionation index (Mg#). The group is characterized by strongly depleted LREE (La_n/Yb_n 0.5; HREE 0.4 to 1 times MORB), depleted Zr (Zr_n/Sm_n 0.6), slight enrichment in Th (La_n/Th_n 0.8), moderate depletion of Nb (La_n/Nb_n 2). The gabbro has a cumulate derived composition (Mg# 71 to 79), whereas the diabase and basalt are primitive to moderately evolved (Mg# 56 to 68).

Buchans Group

Mink Lake Formation

The Mink Lake Formation contains felsic and mafic volcanic rocks that are informally referred to herein as ML_1 and ML_2, respectively. ML_1 is represented by a single sample of bedded

rhyolitic tuff. This tuff is characterized by moderate LREE enrichment (La_n/Yb_n 3.8), strong Th enrichment (La_n/Th_n 0.2), and Nb depletion (La_n/Nb_n 2.9). This sample was analysed for Sm/Nd isotopes and yielded an ε_{Nd} value of -4.0.

ML_2 is represented by transitional calc-alkaline to tholeiitic pillow basalts (TiO_2 0.5 to 0.7 wt%; FeO + MgO 12 to 15 wt%), flows and rare dykes. This group is characterized by moderate LREE enrichment (La_n/Yb_n 3.3), Zr depletion (Zr_n/Sm_n 0.7), strong Th enrichment (La_n/Th_n= 0.3), and Nb depletion (La_n/Nb_n= 5.5). Samples are moderately evolved (Mg# 47 to 63). A sample of basalt was analysed for Sm/Nd isotopes and yielded an $\varepsilon_{Nd(t=473)}$ value of +0.9.

Red Indian Lake Group

Skidder Formation

The Skidder Formation contains two distinct basaltic units that are informally referred to herein as SK_1 and SK_2. SK_1 comprises tholeiitic basalt and pillow basalt (TiO_2 0.7 to1.1 wt%; FeO + MgO 10 to 19 wt%) characterized by slight LREE enrichment (La_n/Yb_n 2.1), Zr depletion (Zr_n/Sm_n 0.7), strong Th enrichment (La_n/Th_n 0.3), and Nb depletion (La_n/Nb_n 3.3). Samples are primitive to moderately evolved (Mg# 57 to 69). A sample of basalt was analysed for Sm/Nd isotopes and yielded an $\varepsilon_{Nd(t=464)}$ value of 4.3. Previously published analyses have the same geochemical and isotopic ($\varepsilon_{Nd(t=464)}$ value of +5.2) characteristics as this group (Fig. 2.9; Davenport et al., 1996; Swinden et al., 1997).

SK_2 is represented by two analyses of a basalt and andesite (TiO_2 1.2 to 1.6 wt%; FeO + MgO 9.4 to 20.8 wt%) and is characterized by moderate LREE enrichment (La_n/Yb_n 3.7), strong Th enrichment (La_n/Th_n 0.3), and slight Nb depletion (La_n/Nb_n 1.7). This group shares similar chemical characteristics to previously analyzed Skidder Formation trondhjemitic rocks (Davenport et al., 1996).

Harbour Round Formation

The Harbour Round Formation is divisible into five chemically distinct mafic volcanic units (informally referred to herein as HR_1 through HR_5). The HR_1 high Ti tholeiites comprise a generally homogeneous package of predominantly basalt with minor diabase and gabbro (TiO_2 0.8 to 2 wt%; FeO + MgO 12 to 19 wt%). This group is characterized by 0.5 to 2 times N-MORB trace element

abundances, slight depletion to slight enrichment of LREE on N-MORB normalized spidergrams (La_n/Yb_n 1.1), slight but consistent depletion in Zr (Zr_n/Sm_n 0.9), slight enrichment of Th (La_n/Th_n 0.7), negligible depletion of Nb (La_n/Nb_n 1.1), and is moderately evolved (Mg# 52 to 66).

HR_2 comprises tholeiitic basalt to andesite (TiO_2 1.3 to 1.9 wt%; FeO + MgO 15 to 17 wt%). This group is characterized by LREE enrichment (La_n/Yb_n 2.1), enrichment of Th (La_n/Th_n 0.5), slight depletion of Nb (La_n/Nb_n 1.2), and is moderately fractionated (Mg# 48 to 60). One sample has yielded an $\varepsilon_{Nd(t=464)}$ value of 7.7. HR_3 comprises several heterogeneous tholeiitic basalt analyses, which have chemistries similar to those of SB_2 Th-depleted tholeiite and SB_3 LREE depleted tholeiite.

HR_4 is comprised of tholeiitic basalt to andesite (TiO_2 0.6 to 0.8 wt%; FeO + MgO to 12 to 17 wt%). This group is characterized by LREE enrichment (La_n/Yb_n 2.9), depletion in Zr (Zr_n/Sm_n 0.6), strong enrichment of Th (La_n/Th_n 0.2), strong depletion of Nb (La_n/Nb_n 4.7), and is variably fractionated (Mg# 56 to 73).

HR_5 comprises transitional tholeiitic to calc-alkaline basalt to andesite (TiO_2 0.5 to 1.7 wt%; FeO + MgO 10 to 17 wt%). This group is characterized by strong LREE enrichment (La_n/Yb_n 8.9), slight enrichment to modest depletion in Zr (Zr_n/Sm_n 0.7), strong enrichment of Th (La_n/Th_n 0.2), strong depletion of Nb (La_n/Nb_n 4.2), and is variably fractionated (Mg# 43 to 72). One sample was analysed for Sm-Nd isotopic characteristic yielded an $\varepsilon_{Nd(t=464)}$ value of -2.0.

Healy Bay Formation

The volcanic rocks of the Healy Bay Formation consist predominantly of felsic lithic tuff, which is characterized by strong LREE enrichment (La_n/Yb_n 12.5), strong Th enrichment (La_n/Th_n 0.1), and Nb depletion (La_n/Nb_n 3.1). Analysis of Sm/Nd isotopes yielded distinctly negative $\varepsilon_{Nd(t=464)}$ values of between -6.4 and -7.7.

DISCUSSION

The data presented above allow for a detailed reconstruction of the tectono-magmatic processes in the Iapetus Ocean near Newfoundland's Laurentian margin during the Ordovician. Our data indicate the AAT is composed of several tectonic panels that have been accreted to the Dashwoods margin along northwest-dipping thrust faults (Figure 2.2). The revised top to bottom

tectono-stratigraphy of the AAT comprises the AOB (c. 480 Ma), LROC (c. 473 Ma), ensialic arc rocks of the Buchans Group including the Mink Lake Formation (c. 473 Ma), Otter Pond Complex (c. 468 Ma) and Red Indian Lake Group (c. 464 Ma). The general age progression of the rocks in the panels from the most inboard and oldest to the most outboard and youngest suggests accretion of progressively younger tectonic fragments that formed above a single west-dipping subduction zone. In the following sections the tectono-magmatic history for each tectonic panel will be discussed and a unified tectonic model presented.

Magmatism in the AAT

Lloyds River Ophiolite Complex

The ophiolitic LROC preserves the record of supra-subduction zone spreading with multiple source components. The Otter Brook Suite is characterized by prominent enrichment of LREE and Th and depletion of Nb, which suggests a contribution of both mantle and subduction components. The Star Brook Suite is dominated by mafic rocks that are MORB-like on the basis of their flat MORB-normalized trace element profiles and positive εNd valuesεNd values (SB_1). Although the tectonic setting of the SB_1 rocks are by themselves ambiguous (Fig. 2.10a), their association with the Th depleted MORB-like rocks SB_3 and LREE depleted with weak arc signature SB_2 rocks provides a more reliable interpretation. A number of studies (e.g., Fretzdorff et al., 2002; Hawkins and Allan, 1994; Leat et al., 2000; Pearce et al., 1995) have demonstrated associations of chemical groups comparable to LROC in modern backarcs, such as the Lau Basin and East Scotia Ridge backarc basin. Thus it is reasonable to conclude that the LROC formed in a backarc tectonic setting. Although the adjacent AOB is petrographically similar to the LROC, it does exhibit several important differences that distinguish it in regional studies. The chemical characteristics of the LROC mafic rocks are significantly different from those in the adjacent AOB (Fig. 2.9, 2.11). In addition, the LROC (473±3.7 Ma) is younger than the oldest age of the AOB (481 +4/-2 Ma: Dunning and Krogh, 1985). Despite the slight overlap of the 2σ errors, LROC is also statistically younger ($p<0.1$, one-sided t-test) than the youngest age obtained in the AOB on a late pegmatitic trondhjemite which may or may not be representative of the crystallization age of the bulk of the unit (478 +3/-2 Ma; Dunning and Krogh, 1985). The geochronological data thus supports the

petrological evidence that the AOB and LROC represent two different segments of Iapetan oceanic crust.

Buchans Group

Geochemistry, geochronology and isotopic characteristics of the Mink Lake Formation indicate eruption in a continentally influenced arc (Fig. 2.10a; Table 2.4). The depletion of Nb and Ti and enrichment of Th and LREE indicate an arc setting; whereas the low to negative ε_{Nd} values and zircon inheritance indicate significant contribution of mature continental crust to both its felsic and mafic rocks. Although the Sm/Nd isotopic characteristics cannot uniquely discriminate between continental basement and subduction of continentally derived sediment, a comparison to the modern arc systems (Swinden et al., 1997) supports the presence of continental basement, consistent with abundant zircon inheritance. The Mink Lake Formation is thus assigned an conitnental arc setting, identical to the interpretations made of the coeval peri-Laurentian (Nowlan and Thurlow, 1984) Buchans and Roberts Arm groups by Swinden et al. (1997). Since Mink Lake Formation occupies the same structural position in the Annieopsquotch Accretionary Tract as the coeval Buchans Group, it has been included in this group. Although the Mink Lake Formation does not appear to have any direct geochemical analogues in either the Buchans or Roberts Arm groups (Fig. 2.9; Davenport et al., 1996), it may correspond to the Ski Hill Formation in the Buchans area (Thurlow and Swanson, 1987).

Red Indian Lake Group

The presence of a strong Th/Nb anomaly and slight LREE enrichment in the Skidder Formation (SK_1) argues for a volcanic arc setting (Fig. 2.10b). The Sm/Nd isotopic data tend to suggest a source that is typical for an intra-oceanic arc, however, a continental setting with minimal upper crustal assimilation cannot be ruled out (Swinden et al., 1997). The SK_2 basalts exhibit enrichment in LREE and Th, but contain only a weak Th/Nb anomaly. This data suggests an enriched mantle source with a minor subduction component similar to that observed in the East Scotia Ridge backarc basin (Fretzdorff et al., 2002). The contemporaneous eruption of SK_1 and SK_2 lavas strongly indicates a transitional arc – backarc setting for the Skidder Formation.

The lower basalt member of the Harbour Round Formation is dominated by lavas that are similar to MORB and island arc tholeiite (Fig. 2.10b; $HR_{1,2,3}$). The association of these chemical groups is similar to that observed for the LROC and Eastern Lau Basin Spreading Centre (Fig. 2.9; Hawkins and Allan, 1994; Pearce et al., 1995) and suggests a juvenile/spreading-arc or backarc setting for the lower basalt member. However, the contemporaneous eruption of the island arc tholeiite-like, LREE and Th enriched, and Nb depleted HR_4 basalts point to a relatively immature arc setting for the lower basalt member. The transition to the upper basalt member of the Harbour Round Formation is defined by an intra-formational unconformity that is marked by a conglomeratic unit that is followed by the calc-alkaline HR_5 basalt (Fig. 2.10b). The prominent Th/Nb anomaly, LREE enrichment, and negative ε_{Nd} value of the HR_5 indicate eruption in a continental arc setting. The felsic tuffs of the Healy Bay Formation exhibit strong enrichment in Th and REE and depletion in Nb consistent with eruption in a volcanic arc setting (Fig. 2.10c), which together with the highly negative ε_{Nd} values and zircon inheritance confirms formation in an ensialic arc setting. Although the continental basement is nowhere exposed and there is no fossil control on the paleogeographic setting of the arc, the identification of inherited zircons in the c. 935-1845 Ma age range (Table 2.2) but not in the c. 500 to 800 Ma age range is more consistent peri-Laurentian provenance (e.g., Cawood and Nemchin, 2001) rather than peri-Gondwanan (e.g., van Staal et al., 1996). Thus the Red Indian Lake Group originated in a Llanvirn peri-Laurentian ensialic arc complex.

Implications for the position of the Red Indian Line

Prior to this study, the position of the Red Indian Line was only roughly defined in the map area, mainly drawn along the easternmost extent of the AOB and Buchans Group (Fig. 2.1; e.g., Evans and Kean, 2002; Williams et al., 1988). However, Thurlow et al. (1992) concluded that such a position was inconsistent with the observed relationships in this part of Newfoundland and the definition of the Red Indian Line. Instead they suggested a placement of the Red Indian Line further to the east, although they could not identify it. The peri-Laurentian provenance of the Red Indian Lake Group support their interpretation and the Red Indian Line is herein defined to lie immediately to the east of the peri-Laurentian Red Indian Lake Group (Fig. 2.1) where it is conveniently marked in several places by a highly tectonised black shale mélange along the eastern shore of Red Indian

Lake (Fig. 2.2d). Consequently, the LROC, Otter Pond Complex and Red Indian Lake Group lie to the west of the Red Indian Line and form part of the peri-Laurentian Notre Dame Subzone consistent with the original criteria that define the Red Indian Line, since they share the sub-Silurian unconformity and lack the Caradoc black shale cover typical of the Exploits Subzone (Williams et al., 1988).

Tectonic history of the AAT (480 to 468 Ma)

The age progression of the panels with progressively younger rocks occurring at the lower structural levels combined with a provenance immediately outboard of the peri-Laurentian Dashwoods ribbon continent with its Notre Dame arc suprastructure, is most simply related to intermittent generation of arc – backarc complexes above a single west-dipping subduction zone that was continuously retreating to the east (present coordinates) due to slab rollback. These relationships appear to hold along the entire segment of the AAT from central Newfoundland to Notre Dame Bay (Table 2.1, Fig. 2.5) and are generally supported by the correlatives of the AAT outside Newfoundland. Initiation of west-directed subduction in the Newfoundland AAT must have occurred shortly before c. 480 Ma, as is evidenced by the suprasubduction zone AOB (Appendix 1). Subsequently, a continental arc and oceanic backarc were generated further outboard above the same west-dipping subduction zone, represented by the c. 473 Ma Buchans Group and LROC, respectively (Fig. 2.12a).

The presence of peri-Laurentian continental arc magmatism outboard of the oceanic AOB where subduction initiated and the lack of a proto-Buchans remnant arc need to be explained in order for the rather simplified model presented above to be more widely applicable. The presence of the ensialic Buchans arc outboard of the intra-oceanic AOB requires either accretion of an independent microcontinental sliver to the AOB or the introduction of a continental crustal flake into the arc-trench gap through trench parallel strike-slip movements (fore-arc slivering). No direct evidence in the Newfoundland AAT, or correlative tracts, requires that the Buchans Group should be built on another distinct microcontinent. In addition, accretion of such a microcontinent would require the step-back or initiation of another phase of subduction shortly after the subduction initiation responsible for the AOB. Although this possibility cannot be completely ruled out, there is

ample evidence for sinistral oblique-slip southeast directed faulting throughout the Ordovician in the AAT (Lafrance and Williams, 1992; Lissenberg and van Staal, 2002; Thurlow, 1981; Zagorevski and van Staal, 2002), however it is frequently overprinted by Silurian and younger dextral transpression (e.g., Lafrance and Williams, 1992; Williams et al., 1993). The correlatives of the AAT outside Newfoundland, in the Northern Belt of the Southern Uplands terrane and South Connemara Group, have also experienced sinistral transpression in the Ordovician (e.g., Dewey and Shackleton, 1984; Elders, 1987; Ryan and Dewey, 2004), and fore-arc slivering accompanied by large trench-parallel movements have been invoked to explain the provenance of the conglomerates in the Northern Belt of the Southern Uplands terrane (Elders, 1987). Thus the position of the ensialic Buchans Arc outboard of the AOB and LROC is probably most simply explained by fore-arc slivering. This model can also explain the lack of an identifiable Buchans remnant arc, as the whole Buchans crustal block could have experienced trench-parallel transport outboard of active LROC magmatism (Fig. 2.12).

The evolution of the Newfoundland portion of the AAT is summarized in Fig. 2.12. West-dipping subduction initiated outboard of the Dashwoods, probably in a re-entrant prior to c. 480 Ma, with the Annieopsquotch spreading centre having formed due to rapid hinge retreat of the down-going slab (Appendix 1). Although, the exact timing of the sinistral strike-slip translation of the Buchans arc outboard of AOB and LROC is poorly constrained at present (pre c. 468 Ma), we infer that the subduction under the Dashwoods margin generated the Buchans arc on its leading edge approximately coeval with spreading responsible for the AOB and LROC along strike in the re-entrant. The propagation of the AOB/LROC spreading centre into the adjacent promontory on the active Dashwoods microcontinent isolated a sliver of Dashwoods with its Buchans suprastructure. Alternatively, a new spreading centre could have been initiated in a region far removed from the AOB that rifted the Buchans Arc from the leading edge of Dashwoods, with subsequent unrelated strike-slip faulting bringing this crustal fragment outboard of the AOB. A compressional event, potentially triggered by the Laurentia – Dashwoods collision to the west (Waldron and van Staal, 2001), may have initiated underthrusting of the AOB, LRC and the Buchans Group beneath the hot Notre Dame Arc along the Hungry Mountain Thrust system (Thurlow, 1981) prior to or

synchronously with the intrusion and eruption of the c. 468 Ma stitching Otter Pond Complex (Appendix 3).

Tectonic history of the AAT (< 468 Ma)

The close spatial association and peri-Laurentian provenance of the Buchans and Red Indian Lake groups suggest that they were generated above the same west-dipping subduction zone (Fig. 2.12). Following the c. 468 Ma event that led to the accretion of AOB, LROC and Buchans Group, the accreted Buchans Arc rifted due to renewed rollback of the west-dipping slab, leaving most of the exposed Buchans Group in a remnant arc position. Thus, the new Red Indian Lake ensialic arc and backarc basin were established by c. 464 Ma to the east of this remnant arc. Similar Llanvirn-Caradoc tectonic development of the peri-Laurentian margin has been inferred in the Caledonides as well, where an accretionary prism formed outboard of an active continental arc (e.g., Ryan and Dewey, 2004).

The main tract of the Iapetus Ocean was closed at c. 450 Ma resulting in a collision between peri-Laurentian Red Indian Lake and peri-Gondwanan Victoria Lake arcs (van Staal et al., 1998), and incorporation of the Red Indian Lake arc – backarc into the AAT. Caradoc closure of this portion of the Iapetus is consistent with along-strike correlatives in the peri-Laurentian portion of the Southern Uplands terrane, which start to contain characteristically peri-Gondwanan detritus during the Caradoc (Phillips et al., 2003).

During the collision, the Victoria Lake Arc was thrust beneath the AAT (van der Velden et al., 2004), forcing uplift and exhumation of the AAT (McNicoll et al., 2001) that led to a widespread sub-Silurian unconformity (e.g., Williams et al., 1988). Silurian continental red beds and volcanic rocks were subsequently deposited, forming an overlap sequence coeval with intrusion of consanguineous Silurian plutons into all units of the AAT.

Correlatives of AAT outside Newfoundland

The correlations of the AAT into the New England Appalachians and British Caledonides are somewhat controversial. In the New England Appalachians, extensive post-Ordovician cover has obscured many of the relationships between units leading to questions over their affinity (i.e. peri-Laurentian vs. peri-Gondwanan). The fact that both peri-Laurentian and peri-Gondwanan

terranes experienced coeval, but unrelated, arc-building events on opposite sides of the Iapetus Ocean this has lead to a variety of conflicting models (e.g., Karabinos et al., 1998; Moench and Aleinikoff, 2000; Robinson et al., 1998; van Staal et al., 1998). Van Staal et al. (1998) proposed that the AAT extends into New England and is represented by rocks of the Boil Mountain Complex, Jim Pond Formation (e.g., Coish and Rogers, 1987) and rocks in the Caucomgomoc inlier. This interpretation is consistent with the composite nature, age (477 ± 1, Kusky et al., 1997) and position of the Boil Mountain Complex and Jim Pond Formation outboard of the Chain Lakes Massif (Gerbi et al., 2005). The Chain Lakes Massif has been proposed to represent a portion of a Laurentian-derived microcontinent correlative to the Dashwoods in Newfoundland (Waldron and van Staal, 2001, Gerbi et al., 2005).

In the British Caledonides, van Staal et al. (1998) proposed a correlation of the AAT with the South Connemara Group in Ireland, which has recently been reinterpreted as a Middle to Late Ordovician accretionary complex that incorporated early-Ordovician seamounts above a north dipping subduction zone (Ryan and Dewey, 2004). The Northern Belt of the Southern Uplands terrane in Scotland is a direct correlative to the South Connemara Group (Ryan and Dewey, 2004; van Staal et al., 1998), it follows that these rocks should also be correlated to the AAT. Clasts in the South Connemara Group place it immediately outboard of the composite Laurentian margin (Grampian Highlands; Ryan and Dewey, 2004), whereas the provenance of clasts in conglomerates of the Northern Belt of the Scottish Southern Uplands terrane suggest large trench-parallel translations of fore-arc material (Elders, 1987). A direct correlation between members of the AAT and elements of the British Caledonides remains tenuous at present because the well-preserved sedimentary sequences of the Southern Uplands are largely absent in the northern Appalachians, a feature that may reflect strike-slip excision.

CONCLUSIONS AND TECTONIC IMPLICATIONS

Detailed mapping combined with geochronological, geochemical and isotopic studies of central Newfoundland AAT has allowed: i) the identification of the exact location of the Red Indian Line and the proposal of several new and previously unrecognised informal suprasubduction zone units of peri-Laurentian affinity, which has enabled the formulation of realistic reconstructions of the

development of the peri-Laurentian arc; ii) the understanding of their assembly into structural panels involving both thrusting and sinistral strike-slip translations; and iii) the understanding of the rate of growth of the Laurentian margin. Our data indicate that the various arc/backarc systems evolved very rapidly, with major tectonic changes occurring on the time scale of about five million years. The ensialic Buchans Arc was established at least seven million years after the initiation of subduction and was accreted to the Dashwoods margin less than five million years later, approximately coeval with calc-alkaline magmatism in the Otter Pond Complex. Subsequently, this accreted arc was rifted, with the development of the Red Indian Lake arc and backarc basin within approximately five million years. Although the rate of tectonic changes observed in the AAT is rapid and would have been impossible to resolve without very detailed and accurate geochronology, it is consistent with the timeframe of tectonic processes in recent arc systems such as those of the southwest Pacific (e.g., Hall, 2002)

The results of our work presented herein highlight the complexity of the tectonic processes that took place in the Ordovician immediately outboard of the Dashwoods microcontinent during and after its final docking to Laurentia. They involve a protracted (c. 20 m.y.) period of arc-trench migration that led to repetitive arc–rifting and backarc basin formation and rapid trench-parallel translation of fore-arc slivers in the Newfoundland Appalachians and British Caledonides. This complexity is probably also present elsewhere in the northern Appalachians and British Caledonides, but a complex post-Ordovician tectonic history, including deposition of thick Siluro-Devonian cover sequences may prevent its elucidation. In particular the identification of oblique accretion of complexes along the Laurentian margin may explain why parts of tectonic systems along the Laurentian margin appear to be missing in many places (van Staal et al., 1998). Accretion of large volumes of sedimentary rocks common to other Phanerozoic orogens (e.g., Alvarez-Marron et al., 2000; Sengor and Natal'in, 1996) do not appear to play a significant role in the development of the Newfoundland AAT. The Middle Ordovician growth of the Laurentian margin along this portion of the AAT appears to have been primarily accommodated by accretion of backarc crust and addition of juvenile material to the outboard ensialic magmatic arcs.

Figure 2-1 Simplified geology of the study area (modified from Kean, 1979b; Lissenberg et al., 2005c; Rogers et al., 2005a; van Staal et al., 2005 a, b, c). U/Pb ages compiled from Dunning and Krogh (1985), Dunning et al. (1987). Polygons A, B, and C indicate the location of detailed maps in Figures 2.3, 2.6, 2.7 respectively. Inset: Lithostratigraphic subdivisions of Newfoundland (after Williams, 1995). CBF – Clench Brook Fault, HMC – Hungry Mountain Complex, HMT – hungry Mountain Thrust, RIL – Red Indian Line, TPF – Tilley's Pond Fault.

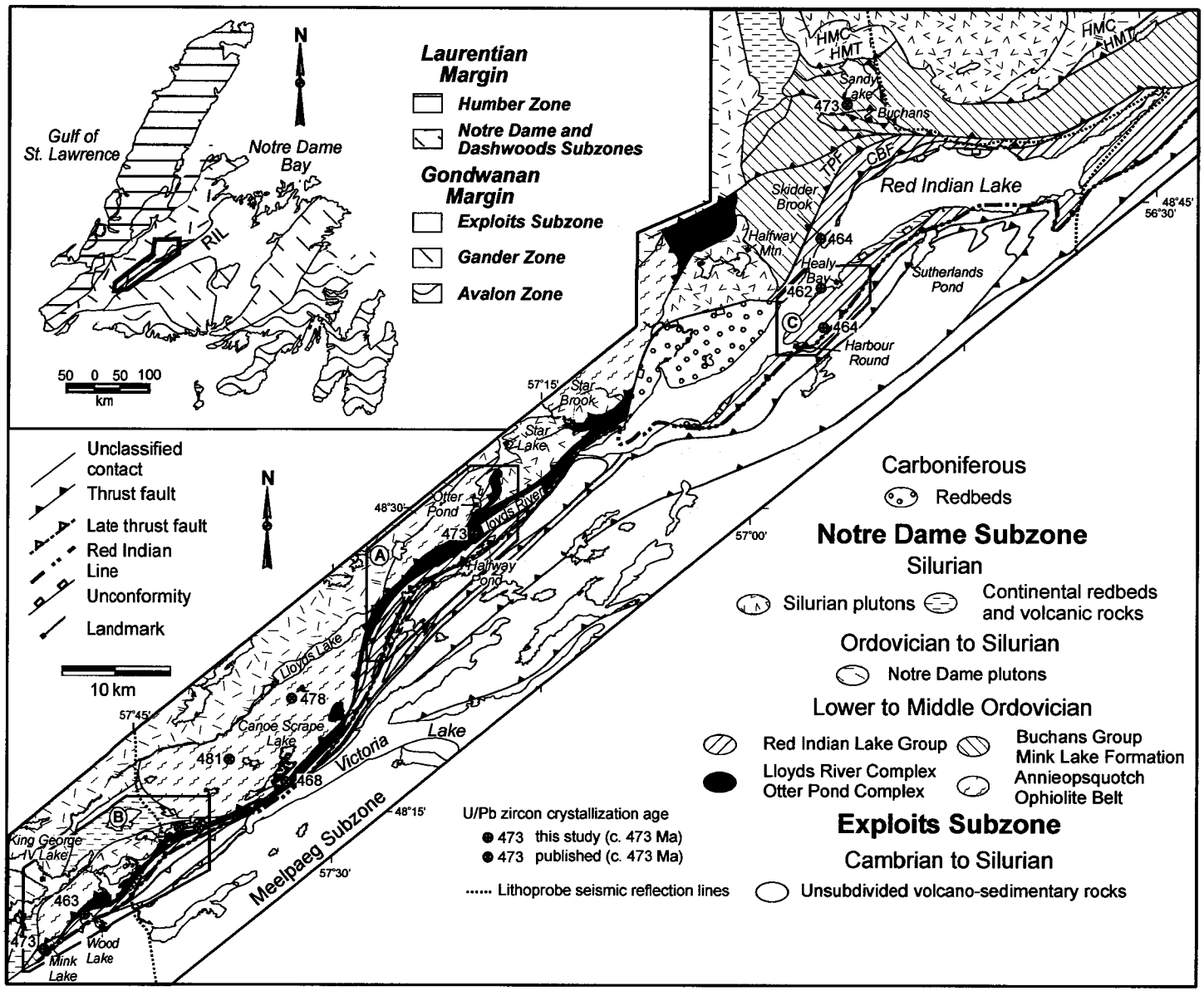
Laurentian Margin
Humber Zone
Notre Dame and Dashwoods Subzones
Gondwanan Margin
Exploits Subzone
Gander Zone
Avalon Zone
Gulf of St. Lawrence
Notre Dame Bay
RIL
N
50 0 50 100
km
Unclassified contact
Thrust fault
Late thrust fault
Red Indian Line
Unconformity
Landmark
10 km
HMC
HMT
Sandy Lake
473
Buchans
PL
CBF
Red Indian Lake
Skidder Brook
Halfway Mtn
464
Healy Bay
462
Sutherlands Pond
Harbour Round
48°45'
56°30'
57°15'
Star Brook
Star Lake
48°30'
Otter Pond
Lloyds River
473
Halfway Pond
57°00'
Lloyds Lake
478
57°45'
Canoe Scrape Lake
481
Victoria Lake
468
48°15'
Meelpaeg Subzone
57°30'
King George IV Lake
463
473
Mink Lake
Wood Lake
U/Pb zircon crystallization age
473 this study (c. 473 Ma)
473 published (c. 473 Ma)
Lithoprobe seismic reflection lines
Carboniferous
Redbeds
Notre Dame Subzone
Silurian
Silurian plutons
Continental redbeds and volcanic rocks
Ordovician to Silurian
Notre Dame plutons
Lower to Middle Ordovician
Red Indian Lake Group
Buchans Group
Mink Lake Formation
Lloyds River Complex
Otter Pond Complex
Annieopsquotch Ophiolite Belt
Exploits Subzone
Cambrian to Silurian
Unsubdivided volcano-sedimentary rocks

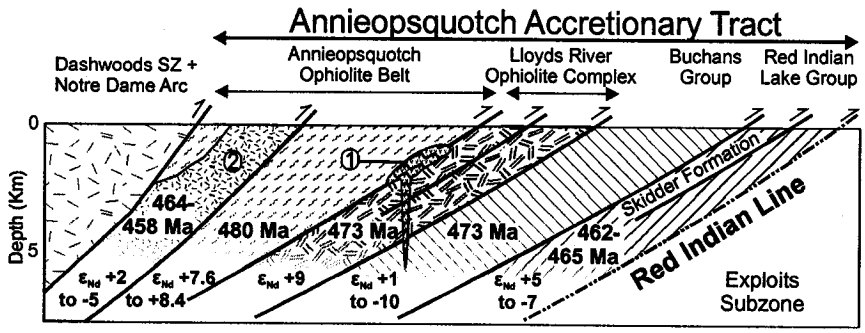

Figure 2-2 Schematic composite cross-section of the Annieopsquotch Accretionary Tract in central Newfoundland. (1) Otter Pond Complex (468±2 Ma; $\varepsilon Nd_{(468\,Ma)}$ 1 to 6.8); (2) Pierre's Pond Intrusive Suite (Appendix 3).

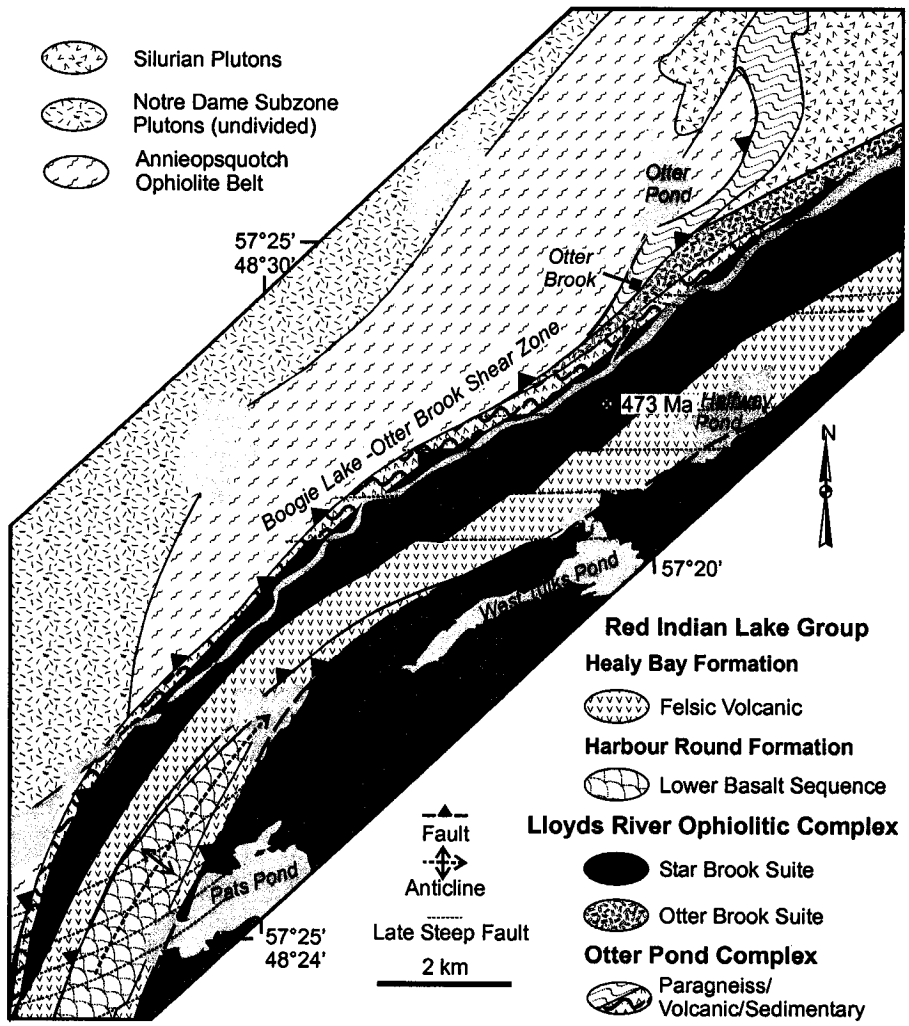

Figure 2-3 Detailed geology of the Otter Pond area demonstrating tectono-stratigraphic relationships between fault-bounded units and Silurian intrusive rocks. Location of the Lloyds River Ophiolite Complex leucogabbro U/Pb zircon sample is shown. WLSZ- Wood Lake Shear Zone

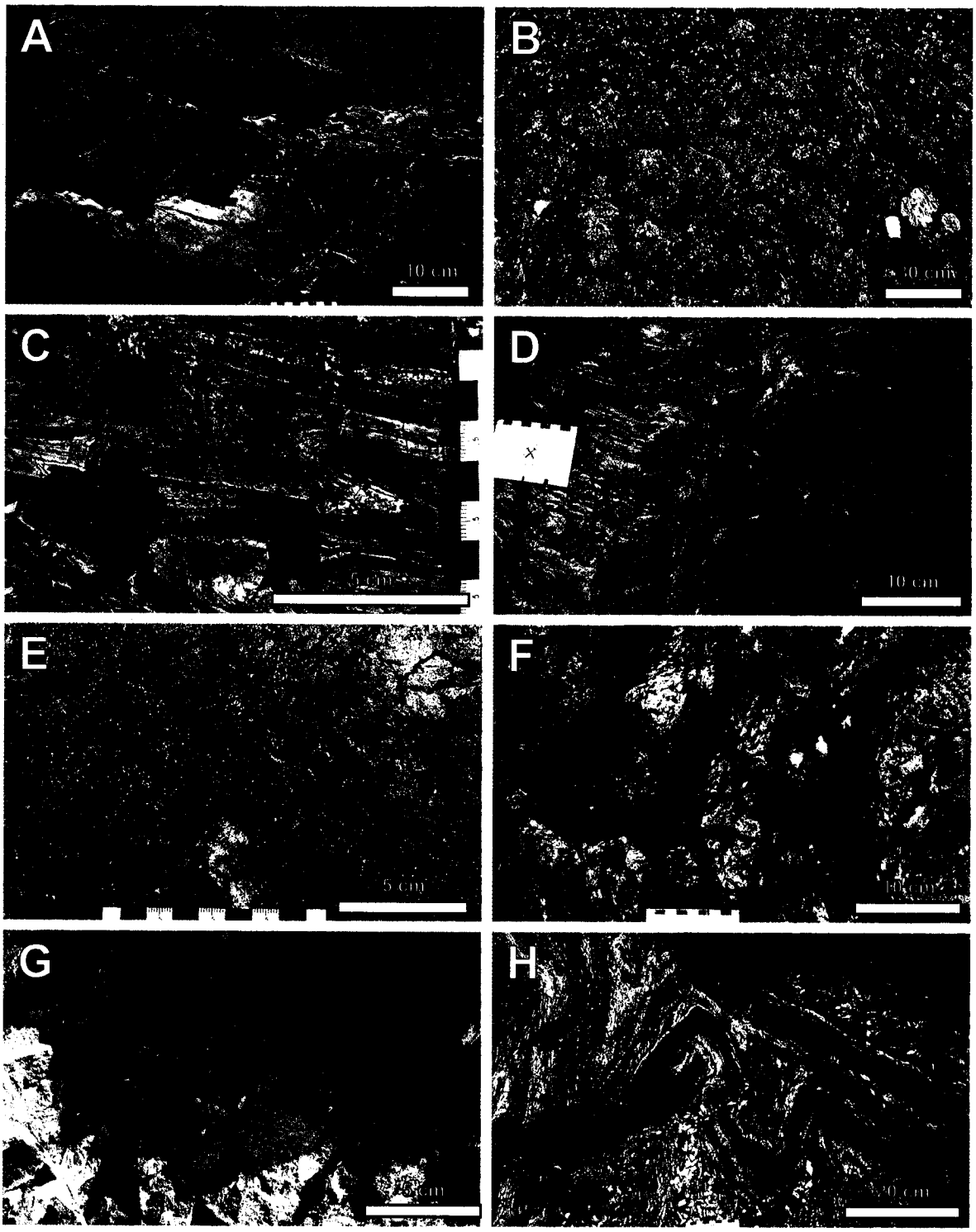

Figure 2-4 Representative photographs of the rocks in the Red Indian Lake Wood Lake area: (a) Angular vesicular mafic enclave in sheeted diabase zone of the Otter Brook Suite; (b) foliated Star Brook Suite pillow basalt; (c) folded Otter Pond Complex rhyolite; (d) folded Otter Pond Complex garnet-biotite-muscovite gneiss; (e) extremely well preserved basalt breccia immediately below the Mink Lake Formation dated felsic tuff; (f) epidotized Skidder Formation pillow basalt breccia immediately adjacent to the dated trondhjemite; (g) Harbour Round Formation conglomerate; (h) Healy Bay Formation complexly folded interbedded red shale, jasper and felsic tuff.

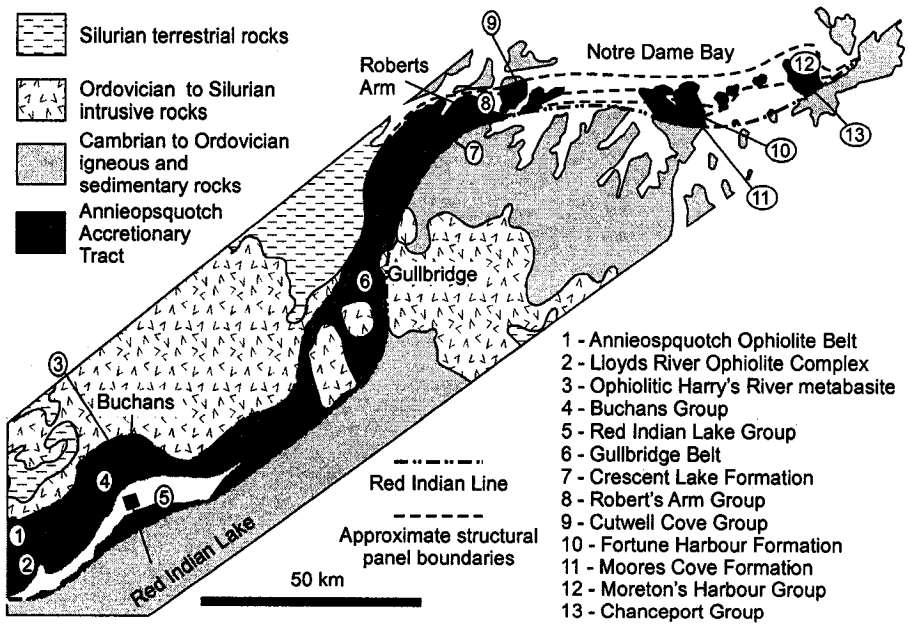

Figure 2-5 Correlation of the herein described tectono-stratigraphic units with those in the Notre Dame Bay area. For details see Table 2.1.

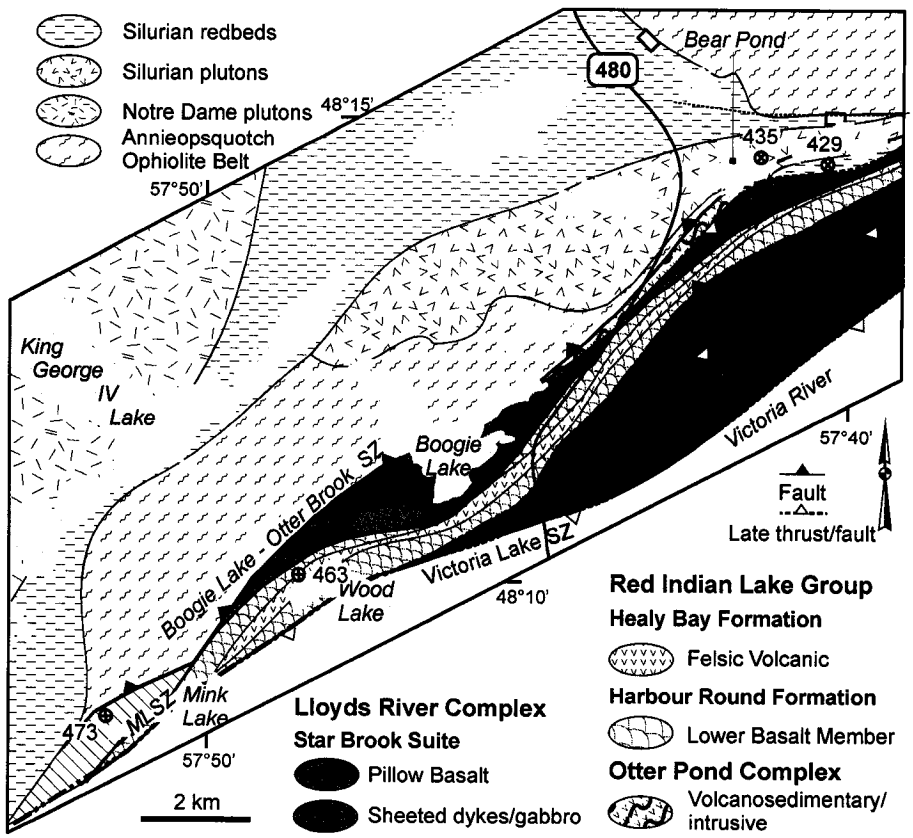

Figure 2-6 Detailed geology of the Wood Lake area demonstrating tectono-stratigraphic relationships between Annieopsquotch Ophiolite Belt, Mink Lake Formation and Red Indian Lake Group. Compiled U/Pb zircon ages from Dunning et al. (1990). For explanation of symbols see Figure 1.1. MLSZ-Mink Lake Shear Zone, WLSZ Wood Lake Shear Zone.

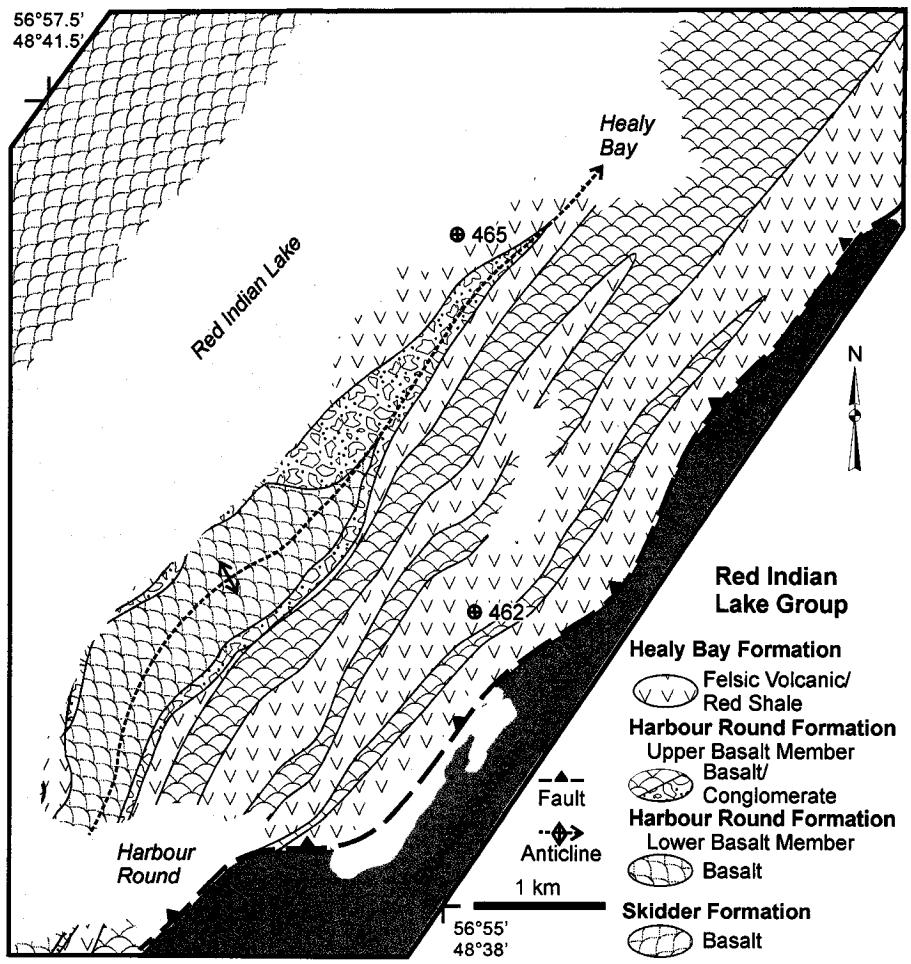

Figure 2-7 Detailed geology of the Harbour Round area demonstrating tectono-stratigraphic relationships between formations in the Red Indian Lake Group. For explanation of symbols see Figure 1.1.

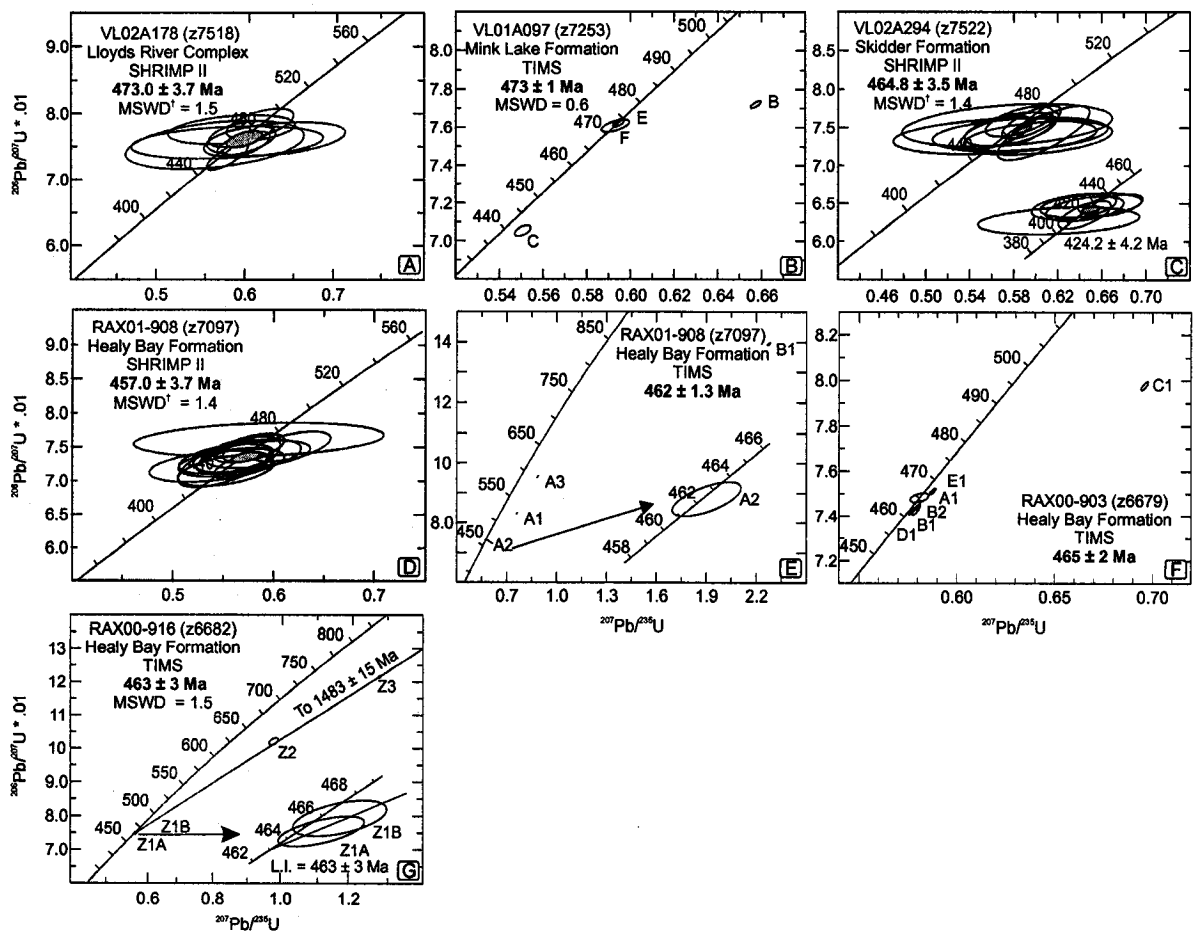

Figure 2-8 U/Pb SHRIMP II and TIMS Concordia diagrams (2ó, decay constants included). MSWD - Mean Square of Weighted Deviates. †MSWD of concordance and equivalence (Ludwig, 2001).

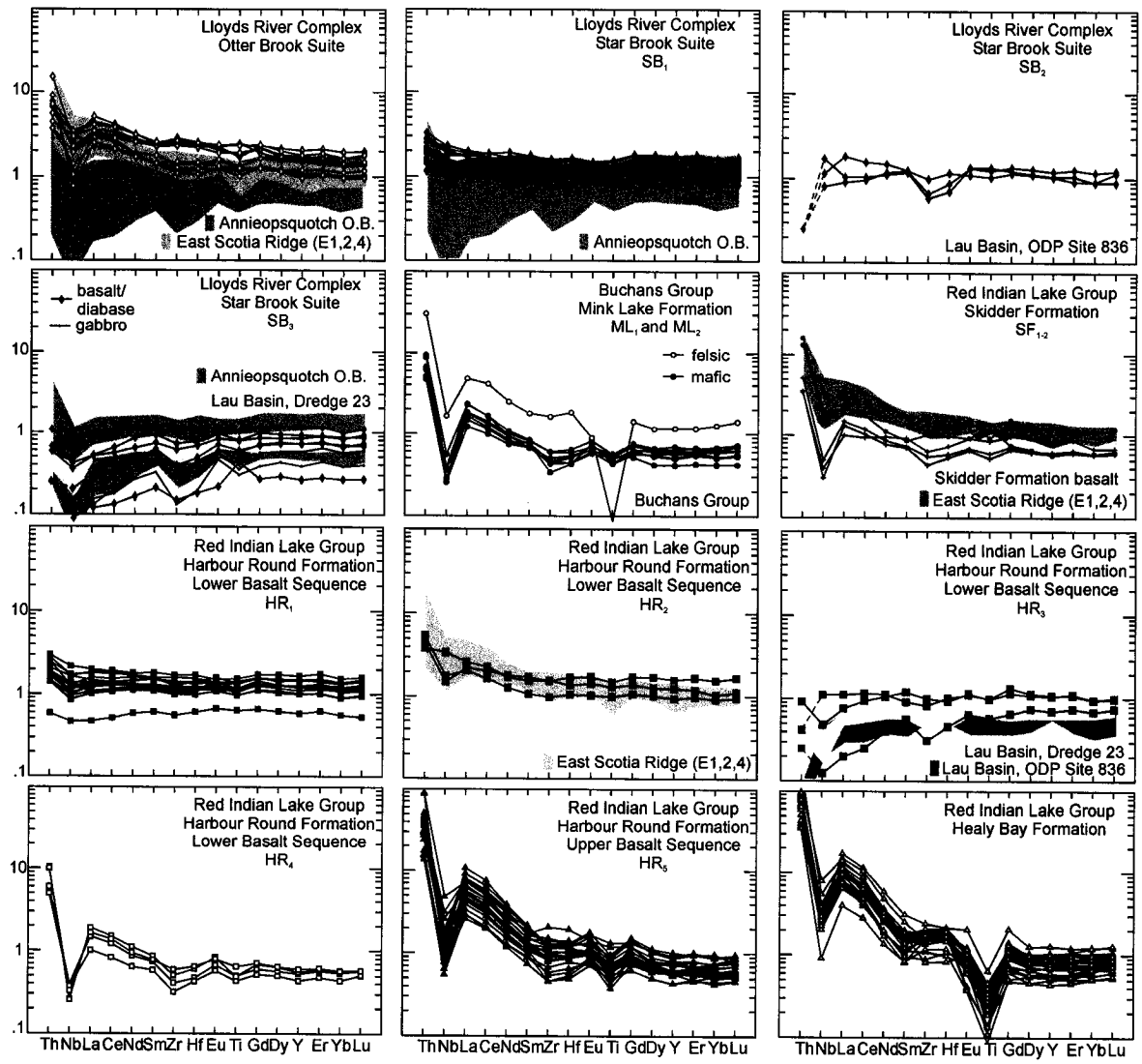

Figure 2-9 Extended REE spidergrams of the chemical groups defined in this study (N-MORB normalization values and order from Sun and McDonough, 1989; modified to exclude mobile trace elements). Shaded fields are basalt-sheeted dyke range from AOB; Skidder Formation and Buchans Group basalt (Davenport et al., 1996); selected samples from back-arc East Scotia Sea Ridge (Fretzdorff et al., 2002; Leat et al., 2000); selected samples from Lau Basin Dredge 23 (Pearce et al., 1995); selected samples from Site 836, ODP Leg 135 (Hawkins and Allan, 1994).

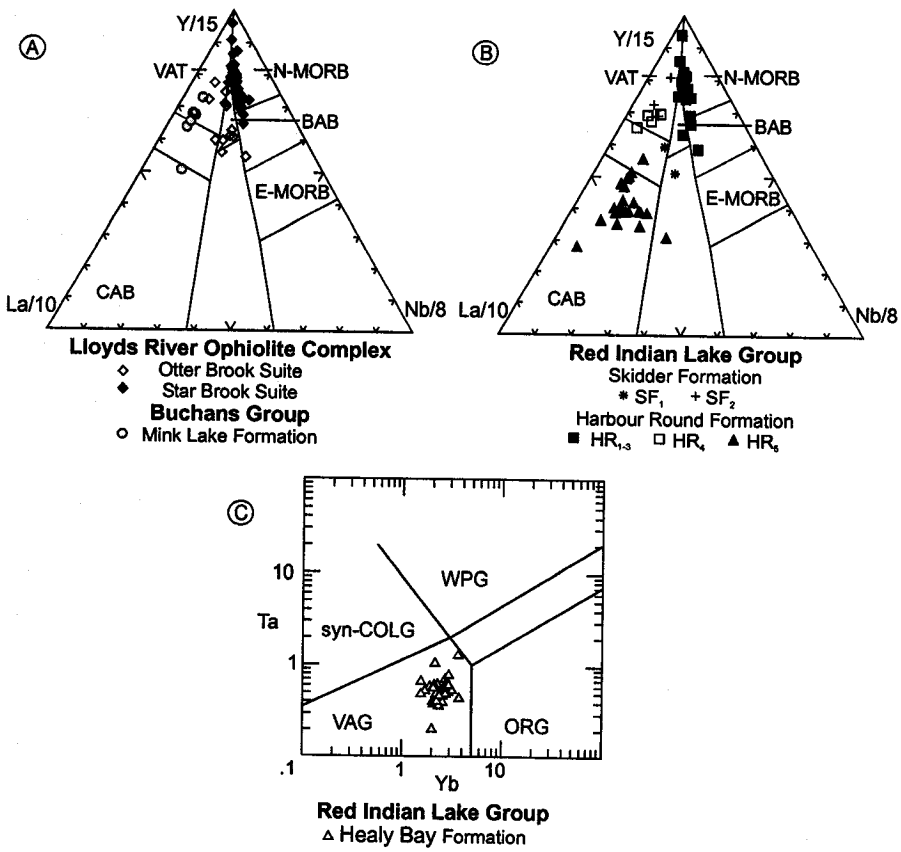

Figure 2-10 La/10-Y/15-Nb/8 tectonic setting discrimination diagrams for (a) Lloyds River Ophiolite Complex and Mink Lake Formation and (b) Red Indian Lake Group mafic volcanic, shallow intrusive and selected plutonic rocks (Cabanis and Lecolle, 1989); (c) Ta-Yb discrimination diagram for felsic volcanic rocks of the Healy Bay Formation (Pearce et al., 1994). BAB back-arc basalt, CAB calc-alkaline basalt, E-MORB enriched mid-ocean ridge basalt, N-MORB normal mid-ocean ridge basalt, ORG ocean ridge granite, syn-COLG syn-collisional granite, VAG volcanic arc granite, VAT volcanic arc tholeiite, WPG within plate granite.

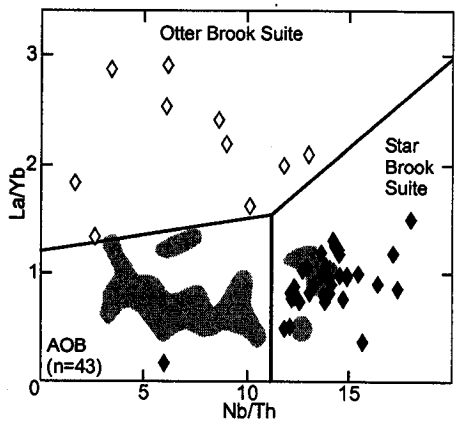

Figure 2-11 La/Yb vs. Nb/Th diagram comparing the chemical characteristics of the basalt and diabase of the Annieopsquotch Ophiolite Belt (shaded field; n=43) and Lloyds River Ophiolite Complex Otter Brook (open diamond) and Star Brook (filled diamond) suites. Annieopsquotch forms a very distinct field with only minor overlap with Star Brook Suite.

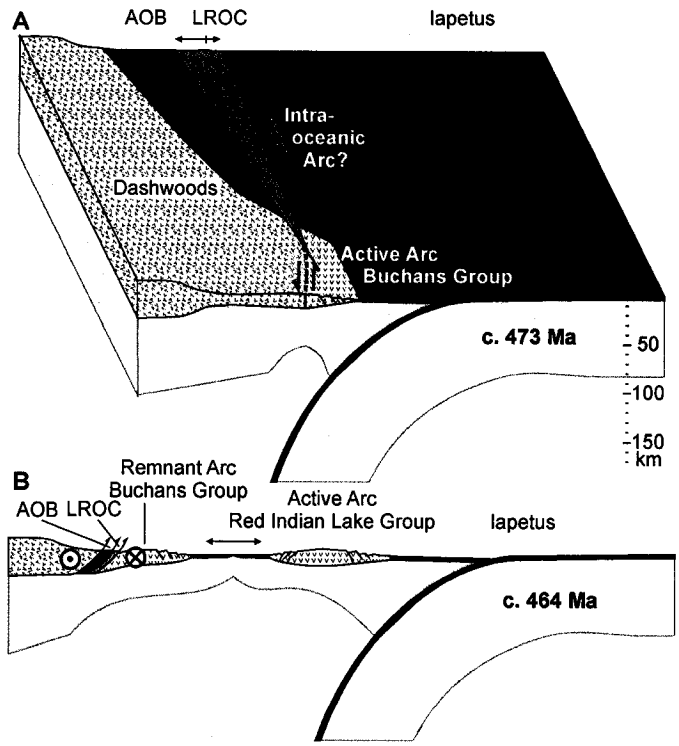

Figure 2-12 Tectonic evolution of the Annieopsquotch Accretionary Tract. A. Formation of Lloyds River Ophiolite Complex (LROC) outboard of the Dashwoods microcontinent is coeval with continentally influenced magmatism in the Buchans arc. An outline of a sinistral fault that juxtaposes Buchans Group and LROC is shown. B. Buchans arc rifts producing an intra-arc or small back-arc basin and new active Red Indian Lake arc. Annieopsquothc Ophiolite Belt (AOB) and LROC are faulted inboard of Buchans arc.

Table 2.1: Summary of correlatives of the tectono-stratigraphic units proposed herein in Newfoundland, and their tectono-magmatic affinity

Unit Name	Age	Characteristics	Tectonic Setting‡	Correlatives§
Red Indian Lake Group†	460 – 465 Ma	Healy Bay Formation†: Felsic volcanic and epiclastic rocks (tuff, rhyolite, sandstone) locally interlayered with red shale and/or red chert. Harbour Round Formation†: Tholeiitic to calc-alkaline pillow basalt, diabase, and andesite locally containing interpillow limestone and is interlayered with red chert and shale. Skidder Formation†: Tholeiitic pillow basalt and diabase locally associated with interpillow red chert and cut by fine-grained trondhjemite.	Continental arc and back-arc	Gullbridge area: No known correlatives Roberts Arm area: Crescent Lake Formation tholeiitic basalts and associated volcanic and epicalstic rocks (Bostock, 1988). Notre Dame Bay: Early Llanvirn (c. 465 Ma; G. Nolan personal communication in O'Brien, 2003) tholeiitic Mores Cove Formation of the Cottrell's Cove Group (Dec et al., 1997; O'Brien, 2003). Potentially Chanceport Group, as it lies in the same structural position as the Cottrell's Cove Group (Dec et al., 1997).
Otter Brook Complex†	c. 468 Ma	Banded rhyolite interlayered with graphitic schist, mica schist, and amphibolite	Continental arc	No known correlatives
Buchans Group	c. 473 Ma	Bimodal calc-alkaline volcanic rocks locally associated with epiclastic rocks and chert (Thurlow and Swanson, 1987; this study).	Continental arc	Gullbridge area: Tholeiitic volcanic rocks previously assigned to Roberts Arm Group from Great Gull Lake to Lake Bond (Swinden and Sacks, 1986; Pope et al., 1991) which despite atypical for Buchans Group (Davenport et al., 1996) have similar age (V. McNicoll, pers. comm.) Roberts Arm area: Roberts Arm Group excluding Crescent Lake Formation (c. 473 Ma; Bostock, 1988; Dunning et al., 1987) Notre Dame Bay: Potentially Fortune Harbour Formation of the Cottrell's Cove Group (Dec et al., 1997). Although an age of 484±2 Ma has been obtained (Dec et al., 1997), age is questionable due to multiple inheritance and lack of concordant analyses.
Lloyds River Ophiolite Complex†	c. 473 Ma	Star Brook and Otter Brook suites†: Tholeiitic pillow basalt, sheeted diabase, gabbro with minor anorthosite and trondhjemite. Interpillow red chert and limestone are locally present.	Back-arc	Buchans Area: Ophiolitic Harry's River Metabasite (Thurlow, 1991) equivalent to unit 2a of Lundberg Hill Formation (Calon and Green, 1987). Potentially portions of the upper Buchans Subgroup (Thurlow, 1981) Gullbridge and Roberts Arm areas: No known correlatives Notre Dame Bay: Potentially Cutwell Group on Pilley's and Triton islands and Moreton's Harbour Group (Swinden, 1996). These groups occupy an identical structural position above the Roberts Arm Belt, have similar tectonic setting (Swinden, 1996) although have not yet been reliably dated.

†Tectono-stratigraphic unit defined in this paper, ‡ Tectonic setting inferred herein from geochemical and geological characteristics, see text for discussion, § See Figure 7

Table 2.2: U/Pb SHRIMP analytical data

Spot name	U (ppm)	Th (ppm)	Th/U	Pb* (ppm)	^{204}Pb (ppb)	$^{204}Pb/^{206}Pb$	$\pm$ $^{204}Pb/^{206}Pb$	f(206)^{204}	$^{208}Pb/^{206}Pb$	$\pm$ $^{208}Pb/^{206}Pb$	$^{207}Pb/^{235}U$	$\pm$ $^{207}Pb/^{235}U$	$^{206}Pb/^{238}U$	$\pm$ $^{206}Pb/^{238}U$	Corr Coeff	$^{207}Pb/^{206}Pb$	$\pm$ $^{207}Pb/^{206}Pb$	Ages (Ma)† $^{206}Pb/^{238}U$	$\pm$ $^{206}Pb/^{238}U$	$^{207}Pb/^{206}Pb$	$\pm$ $^{207}Pb/^{206}Pb$	Ages (Ma)‡ $^{206}Pb/^{238}U$	$\pm$ $^{206}Pb/^{238}U$
VL02A178 (Z7518): Star Brook Suite leuco gabbro (UTM Zone 21 472808 5367792; NAD 8:																							
7518-10.1	265	173	0.675	21	0	0.000010	0.000010	0.0002	0.2114	0.0037	0.5770	0.0097	0.0736	0.0009	0.781	0.0569	0.0006	458	5	486	24	457	5
7518-9.1	323	438	1.397	32	1	0.000032	0.000054	0.0006	0.4450	0.0037	0.5949	0.0123	0.0753	0.0008	0.608	0.0573	0.0010	468	5	502	37	468	5
7518-18.1	211	239	1.167	20	5	0.000321	0.000164	0.0056	0.3524	0.0071	0.5814	0.0296	0.0776	0.0009	0.345	0.0544	0.0026	482	5	386	112	483	5
7518-19.1	56	101	1.870	6	2	0.000631	0.000254	0.0109	0.5907	0.0177	0.5764	0.0447	0.0756	0.0010	0.291	0.0553	0.0041	470	6	423	176	471	6
7518-20.1	66	63	0.988	6	3	0.000593	0.000219	0.0103	0.2993	0.0112	0.5627	0.0415	0.0753	0.0015	0.387	0.0542	0.0037	468	9	380	162	469	9
7518-4.1	77	60	0.801	7	1	0.000156	0.000173	0.0027	0.2648	0.0084	0.6320	0.0323	0.0762	0.0010	0.381	0.0602	0.0029	473	6	610	106	471	6
7518-5.1	478	501	1.088	45	3	0.000102	0.000073	0.0018	0.3337	0.0045	0.6137	0.0156	0.0784	0.0009	0.568	0.0568	0.0012	487	6	482	47	487	6
7518-7.1	275	401	1.505	28	3	0.000184	0.000069	0.0032	0.4665	0.0044	0.5918	0.0149	0.0769	0.0008	0.532	0.0558	0.0012	478	5	444	48	478	5
7518-2.1	260	456	1.815	28	4	0.000248	0.000067	0.0043	0.5700	0.0075	0.5910	0.0167	0.0759	0.0009	0.531	0.0565	0.0014	471	5	472	54	471	5
VL02A294 (Z7522): Skidder Formation trondjhemite (UTM Zone 21 506085 5397449; NAD 8:																							
7522-32.1	85	38	0.460	6	2	0.000399	0.000224	0.0069	0.1434	0.0115	0.4857	0.0382	0.0662	0.0009	0.297	0.0532	0.0040	413	6	339	181	414	5
7522-53.1	83	35	0.437	6	0	0.000010	0.000010	0.0002	0.1475	0.0035	0.5156	0.0125	0.0671	0.0009	0.670	0.0557	0.0010	419	6	440	41	419	6
7522-54.1	276	131	0.492	20	1	0.000037	0.000108	0.0007	0.1507	0.0046	0.5158	0.0185	0.0682	0.0008	0.454	0.0549	0.0018	425	5	408	74	425	5
7522-12.1	140	66	0.485	10	3	0.000339	0.000115	0.0059	0.1464	0.0051	0.5033	0.0200	0.0685	0.0009	0.431	0.0533	0.0019	427	5	340	84	428	5
7522-18.1	187	106	0.585	14	1	0.000079	0.000144	0.0014	0.1844	0.0060	0.5229	0.0240	0.0687	0.0008	0.375	0.0552	0.0024	428	5	420	99	429	5
7522-8.1	174	81	0.481	12	0	0.000010	0.000010	0.0002	0.1501	0.0024	0.5485	0.0141	0.0688	0.0008	0.530	0.0579	0.0013	429	5	525	49	427	5
7522-41.1	82	55	0.690	7	0	0.000043	0.000153	0.0007	0.2222	0.0070	0.6020	0.0276	0.0737	0.0009	0.379	0.0593	0.0025	458	5	577	96	457	5
7522-29.1	77	47	0.627	6	2	0.000383	0.000217	0.0066	0.1911	0.0091	0.5627	0.0379	0.0739	0.0010	0.310	0.0552	0.0036	460	6	422	151	460	5
7522-6.1	123	41	0.342	9	1	0.000077	0.000189	0.0013	0.1094	0.0074	0.5856	0.0326	0.0741	0.0009	0.338	0.0573	0.0030	461	5	503	121	460	5
7522-24.1	101	85	0.872	9	0	0.000010	0.000010	0.0002	0.2673	0.0048	0.6071	0.0171	0.0743	0.0014	0.769	0.0593	0.0011	462	9	577	40	460	9
7522-5.1	258	242	0.968	23	0	0.000016	0.000057	0.0003	0.3132	0.0035	0.5642	0.0132	0.0743	0.0009	0.610	0.0551	0.0010	462	5	414	42	463	5
7522-22.1	258	172	0.689	21	2	0.000099	0.000077	0.0017	0.2192	0.0048	0.5769	0.0169	0.0748	0.0009	0.520	0.0559	0.0014	465	5	450	57	465	5
7522-42.1	234	158	0.699	19	0	0.000010	0.000010	0.0002	0.2219	0.0025	0.5986	0.0092	0.0750	0.0008	0.793	0.0579	0.0005	466	5	526	21	465	5
7522-2.1	81	43	0.546	6	1	0.000266	0.000220	0.0046	0.1641	0.0095	0.5738	0.0391	0.0753	0.0011	0.340	0.0553	0.0036	468	7	423	151	469	7
7522-4.1	146	128	0.904	13	0	0.000010	0.000010	0.0002	0.2841	0.0048	0.5962	0.0109	0.0757	0.0009	0.719	0.0571	0.0007	470	5	496	29	470	5
7522-31.1	310	146	0.488	24	2	0.000099	0.000053	0.0017	0.1547	0.0028	0.5849	0.0125	0.0758	0.0008	0.602	0.0560	0.0010	471	5	452	39	471	5
RAX01-908 (z7097): Healy Bay Formation tuff (UTM Zone 21 506248 5392154; NAD 8:																							
7097-10.1	160	90	0.580	12	1	0.000115	0.000102	0.0020	0.1847	0.0056	0.5535	0.0195	0.0715	0.0010	0.485	0.0561	0.0018	445	6	457	71	445	6
7097-92.1	157	148	0.970	13	3	0.000295	0.000141	0.0051	0.3080	0.0069	0.5382	0.0252	0.0721	0.0010	0.399	0.0541	0.0023	449	6	376	100	450	6
7097-93.1	496	281	0.585	38	1	0.000041	0.000047	0.0007	0.1790	0.0024	0.5671	0.0108	0.0722	0.0008	0.654	0.0570	0.0008	449	5	491	32	449	5
7097-22.1	243	107	0.454	18	2	0.000105	0.000122	0.0018	0.1404	0.0052	0.5583	0.0216	0.0727	0.0009	0.417	0.0557	0.0020	452	5	441	81	452	5
7097-78.1	238	205	0.889	20	2	0.000102	0.000086	0.0018	0.2797	0.0077	0.5560	0.0210	0.0728	0.0015	0.658	0.0554	0.0016	453	9	428	65	453	9
7097-7.1	301	155	0.532	23	2	0.000093	0.000075	0.0016	0.1649	0.0035	0.5614	0.0154	0.0729	0.0008	0.504	0.0558	0.0013	454	5	446	54	454	5
7097-11.1	230	124	0.557	18	2	0.000137	0.000103	0.0024	0.1809	0.0045	0.5532	0.0193	0.0732	0.0009	0.461	0.0548	0.0017	456	5	404	71	456	6
7097-13.1	141	88	0.641	11	1	0.000079	0.000113	0.0014	0.2022	0.0056	0.5742	0.0220	0.0737	0.0010	0.469	0.0565	0.0019	458	6	473	77	458	6
7097-95.1	240	172	0.743	20	1	0.000096	0.000117	0.0017	0.2334	0.0051	0.5848	0.0213	0.0739	0.0008	0.424	0.0574	0.0019	460	5	506	75	459	5
7097-96.1	438	246	0.580	35	2	0.000084	0.000058	0.0015	0.1816	0.0027	0.5804	0.0127	0.0748	0.0008	0.602	0.0563	0.0010	465	5	463	39	465	5
7097-14.1	226	91	0.414	17	0	0.000029	0.000062	0.0005	0.1364	0.0040	0.5762	0.0142	0.0748	0.0009	0.581	0.0558	0.0011	465	5	446	46	465	5
7097-18.1	175	64	0.378	13	1	0.000082	0.000072	0.0014	0.1234	0.0035	0.6173	0.0163	0.0751	0.0009	0.561	0.0596	0.0013	467	5	590	49	465	6
7097-63.2	115	40	0.360	9	2	0.000288	0.000297	0.0050	0.1103	0.0121	0.5858	0.0509	0.0761	0.0010	0.276	0.0558	0.0047	473	6	446	199	473	7
7097-4.1	91	52	0.591	15	0	0.000028	0.000065	0.0005	0.2050	0.0038	1.5167	0.0360	0.1506	0.0020	0.648	0.0730	0.0013	904	11	1015	37		
7097-6.1	538	231	0.444	86	2	0.000022	0.000018	0.0004	0.1362	0.0012	1.4830	0.0213	0.1532	0.0017	0.830	0.0702	0.0006	919	9	935	17		
7097-31.1	54	34	0.645	9	0	0.000010	0.000010	0.0002	0.1984	0.0039	1.6083	0.0309	0.1576	0.0020	0.750	0.0740	0.0010	943	11	1042	26		
7097-28.1	273	119	0.451	48	0	0.000005	0.000056	0.0001	0.1393	0.0034	1.7115	0.0345	0.1698	0.0021	0.701	0.0731	0.0011	1011	12	1017	30		
7097-63.1	110	39	0.363	19	1	0.000084	0.000067	0.0015	0.1100	0.0032	1.7254	0.0409	0.1700	0.0023	0.669	0.0736	0.0013	1012	13	1031	36		
7097-30.1	41	28	0.710	8	1	0.000094	0.000177	0.0016	0.2208	0.0078	1.9094	0.0785	0.1770	0.0023	0.429	0.0782	0.0029	1051	13	1153	76		
7097-53.1	164	104	0.657	32	2	0.000095	0.000038	0.0017	0.1979	0.0024	1.8113	0.0371	0.1777	0.0024	0.733	0.0739	0.0010	1054	13	1040	29		
7097-3.1	121	99	0.847	35	2	0.000067	0.000048	0.0012	0.2606	0.0029	3.4639	0.0650	0.2441	0.0036	0.843	0.1029	0.0011	1408	18	1677	19		
7097-23.1	64	64	1.030	22	0	0.000010	0.000010	0.0002	0.3092	0.0070	3.9256	0.0763	0.2779	0.0045	0.886	0.1025	0.0009	1581	23	1669	17		
7097-45.1	49	17	0.366	17	4	0.000268	0.000097	0.0047	0.1020	0.0043	4.9982	0.1238	0.3214	0.0052	0.738	0.1128	0.0019	1797	25	1845	31		

Notes (see Stern, 1997):

Uncertainties reported at 1σ (absolute) and are calculated by numerical propagation of all known sources of error

f206^{204} refers to mole fraction of total ^{206}Pb that is due to common Pb, calculated using the ^{204}Pb-method; common Pb composition used is the surface blank

†204-corrected ages; ‡ 207-corrected ages (Stern 1997)

Table 2.3: U-Pb TIMS analytical data

Fract.†	Description‡	Wt.	U	Pb§	206Pb#	Pb††	Isotopic Ratios‡‡								Ages (Ma)##						
		ug	ppm	ppm	204Pb	pg	208Pb/206Pb	207Pb/235U	±1SE Abs	206Pb/238U	±1SE Abs	Corr.§§ Coeff.	207Pb/206Pb	±1SE Abs	206Pb/238U	±2SE	207Pb/235U	±2SE	207Pb/206Pb	±2SE	% Disc
VLA01-097 (Z7253): Mink Lake Formation felsic tuff (UTM Zone 21 436177 5332496; NAD 83)																					
B (30)	Co,Clr,Eq,Eu,fIn,fFr,M1°	7	483	38	5059	3	0.13	0.65738	0.00121	0.07721	0.00009	0.755	0.06175	0.00008	479.4	1.1	513.0	1.5	665.5	5.2	29.0
C (32)	pBr,Clr,Eu,St,rFr,M1°	7	264	19	1107	7	0.10	0.55070	0.00185	0.07054	0.00014	0.547	0.05662	0.00016	439.4	1.7	445.5	2.4	476.9	12.4	8.1
E (41)	pBr,Clr,Eu,St,fIn,M3°	14	297	23	2461	8	0.15	0.59456	0.00132	0.07623	0.00011	0.683	0.05656	0.00009	473.6	1.3	473.8	1.7	474.6	7.1	0.2
F (14)	Co,Clr,Frag,M3°	20	240	19	371	64	0.14	0.59307	0.00324	0.07608	0.00017	0.617	0.05653	0.00025	472.7	2.0	472.8	4.1	473.4	19.6	0.2
RAX00-903 (Z6679): Healy Bay Formation tuff (UTM Zone 21 515633 5394334; NAD 83)																					
A1 (20)	Co,Clr,Eu,El,fIn,NM5°	11	99	9	1310	4	0.28	0.58091	0.00237	0.07482	0.00010	0.446	0.05631	0.00021	465.1	1.2	465.0	3.0	464.5	16.2	-0.1
B1 (95)	Co,Clr,Eu,St,rIn,NM5°	30	245	20	6765	5	0.21	0.57675	0.00073	0.07421	0.00007	0.848	0.05636	0.00004	461.5	0.9	462.4	0.9	466.8	3.0	1.2
B2 (65)	Co,Clr,Eu,St,fIn,NM5°	17	246	19	4262	5	0.18	0.57932	0.00104	0.07429	0.00012	0.838	0.05655	0.00006	462.0	1.5	464.0	1.3	474.2	4.4	2.7
C1 (65)	Co,Clr,Eu,Eq,NM5°	15	306	26	12345	2	0.17	0.69595	0.00095	0.07977	0.00010	0.827	0.06328	0.00005	494.7	1.2	536.4	1.1	717.6	3.3	32.3
D1 (70)	Co,Clr,Eu,Pr,fIn,fFr,NM5°	16	321	26	1304	18	0.20	0.57914	0.00126	0.07446	0.00012	0.799	0.05641	0.00007	463.0	1.4	463.9	1.6	468.5	5.8	1.2
E1 (51)	Co,Clr,Eu,Pr,fIn,fFr,NM5°	14	374	30	3275	8	0.19	0.58769	0.00081	0.07510	0.00007	0.837	0.05676	0.00004	466.8	0.8	469.4	1.0	482.2	3.5	3.3
RAX00-916 (Z6682): Healy Bay Formation felsic tuff (UTM Zone 21 440098 5335591; NAD 83)																					
Z1A (1)	Co,Clr,Eu,St,fIn	10	157	13	576	13	0.25	0.58236	0.00193	0.07474	0.00011	0.623	0.05651	0.00015	464.7	1.3	466.0	2.5	472.5	11.8	1.7
Z2 (25)	Co,Clr,Eu,Pr,fIn	7	160	17	1537	2	0.18	0.97470	0.00663	0.10203	0.00051	0.503	0.06928	0.00042	626.3	6.0	690.9	6.8	907.2	24.9	32.5
Z3A (12)	Co,Clr,Eu,El,fIn	7	173	22	1219	8	0.17	1.27630	0.00244	0.12156	0.00018	0.707	0.07615	0.00010	739.5	2.1	835.2	2.2	1099.0	5.4	34.6
Z1B (2)	Co,Clr,Eu,St,fIn	19	146	12	863	15	0.23	0.58402	0.00211	0.07493	0.00013	0.508	0.05653	0.00018	465.8	1.6	467.0	2.7	473.1	13.7	1.6

Notes:

†All fractions are zircon and have been abraded following the method of Krogh (1982). Number in brackets refers to the number of grains in the analysis; ‡Zircon descriptions: Co=Colourless, pBr=Pale Brown, Clr=Clear, fFr=Few Fractures, rFr=Rare Fractures, fIn=Few Inclusions, rIn=Rare Inclusions, El=Elongate, Eq=Equant, Eu=Euhedral, Frag=Fragment, Pr=Prismatic, St=Stubby Prism, Dia=Diamagnetic, M1°=Magnetic @ 1.8A, 1°SS, M3°=Magnetic @ 1.8A, 3°SS, NM5°=Nonmagnetic @ 1.8A, 5°SS; §Radiogenic Pb; #Measured ratio, corrected for spike and fractionation; ††Total common Pb in analysis corrected for fractionation and spike; ‡‡Corrected for blank Pb and U and common Pb, errors quoted are 1 sigma absolute; procedural blank values for this study ranged from 0.1 0.3 pg for U and 2-5 pg for Pb; Pb blank isotopic composition is based on the analysis of procedural blanks; corrections for common Pb were made using Stacey-Kramers compositions; §§Correlation Coefficient; ##Corrected for blank and common Pb, errors quoted are 2 sigma in Ma.

Table 2.4: Annieopsquotch Accretionary Tract Sm/Nd isotopic data

Sample	Lithostratigraphic unit	Group	Age	Nd	Sm	$^{143}Nd/^{144}Nd$	$^{147}Sm/^{144}Nd$	$^{143}Nd/^{144}Nd_i$§	$\varepsilon Nd(t)$§
VL01A057	Star Brook Suite	SB_1	473	12.17	4.48	0.513173	0.2226	0.512483	8.87
VL01A097a	Mink Lake Formation	ML_2	473	7.68	2.17	0.512605	0.1706	0.512076	0.93
VL01A097b	Mink Lake Formation	ML_1	473	16.67	4.41	0.512319	0.1601	0.511823	-4.02
RAX01059	Skidder Formation	SK_1	464	9.46	3.44	0.512931	0.2201	0.512262	4.33
RAX01047	Harbour Round Fm.	HR_2	464	15.40	5.26	0.513064	0.2067	0.512436	7.73
RAX01049	Harbour Round Fm.	HRF_5	464	18.18	4.14	0.512357	0.1377	0.511939	-1.99
RAX01051	Healy Bay Formation		464	19.67	3.65	0.512054	0.1123	0.511713	-6.40
VL01A360	Healy Bay Formation		464	19.23	3.88	0.512074	0.1221	0.511703	-6.59
VL02A283	Healy Bay Formation		464	19.53	4.39	0.512059	0.1357	0.511646	-7.70
VL02A295	Healy Bay Formation		464	22.57	5.02	0.512101	0.1343	0.511693	-6.79

Sample location, lithology and geochemistry listed in Table 2.5; Concentration in ppm from isotope dilution; §Calculated at age of formation

Table 2.5: Geochemistry of peri-Laurentian arc - back-arc complexes in central Newfoundland

Sample	RAX00 705	RAX02 169	VL01 076	VL01 079	VL01A 071	VL01A 058	VL01A 277	VL01A 207b	VL01A 122a	VL01A 351	VL01A 352
UTMx†	440769	483605	442300	443650	449441	460378	461124	453940	447878	467183	467119
UTMy†	5336018	5376892	5337361	5338411	5342789	5350044	5350959	5345097	5342647	5363419	5363458
NTS map	12A/04	12A/11	12A/04	12A/04	12A/04	12A/05	12A/05	12A/05	12A/04	12A/06	12A/06
Unit	SB_1	SB_1	SB_1	SB_1	SB_1	SB_1	SB_1	SB_1	SB_1	SB_1	SB_1
Rock type‡	pbslt	bslt	diab	gabb	diab	bslt	bslt	bslt	bslt	gabb	diab
Laboratory§	1	4	5	5	5	5	5	5	5	6	3
SiO_2 (wt%)	48.70	47.96	48.92	50.80	49.50	47.83	49.64	49.99	46.09	45.88	47.78
TiO_2	1.22	1.57	1.08	1.46	1.30	1.37	1.40	1.27	1.35	1.42	1.11
Al_2O_3	20.20	14.38	16.34	16.36	15.60	14.77	13.95	14.22	17.60	14.23	16.04
Fe_2O_3 total	10.40	12.81	9.46	10.98	9.54	11.56	11.56	11.46	10.95	11.47	11.21
MnO	0.20	0.19	0.17	0.18	0.21	0.27	0.18	0.24	0.18	0.18	0.23
MgO	4.54	7.49	7.50	5.13	7.04	8.22	7.01	8.61	8.54	8.09	8.19
CaO	3.99	10.76	12.34	6.71	10.64	9.84	12.10	7.59	9.05	13.08	10.23
Na_2O	4.01	2.95	2.44	6.08	4.05	3.73	2.59	4.73	3.18	1.72	2.98
K_2O	2.15	0.06	0.33	0.14	0.12	0.05	0.08	0.04	0.28	0.57	0.49
P_2O_5	0.08	0.13	0.08	0.10	0.10	0.10	0.11	0.10	0.10	0.12	0.10
LOI	6.71	2.43	2.48	2.66	2.57	2.97	2.24	2.94	3.82	3.00	2.09
Total	99.00	100.81	101.12	100.60	100.66	100.70	100.85	101.17	101.15	99.81	100.53
Ba (ppm)	202	15.1	53.6	78.6	57.0	12.9	25.1	25.7	57.1	43.0	33.2
Cr	397	271	271	265	274	287	213	69	286	226	347
Cs	2.3	0.18	0.66	0.37	0.13	0.86	0.44	0.38	0.29	3.4	2.8
Hf	1.60	2.70	1.80	2.49	2.39	2.62	2.41	2.00	2.19	3.00	1.70
Nb	2.40	2.14	2.52	3.28	3.48	2.83	3.11	3.40	3.74	5.40	2.98
Ni	146	88	97	104	95	102	64	56	110	46	105
Pb	b.d.	1	13.46	4.15	2.52	0.25	0.36	1.68	0.97	1.3	6.3
Rb	50.0	0.47	9.55	2.9	1.49	0.82	1.2	0.44	6.44	35.2	25.7
Sc	41	47.2	43.4	42.9	39.1	43.5	39.4	43.6	43.2	43	52.5
Sr	143	140	134	209	401	119	184	137	166	196	204
Ta	0.23	0.26	b.d.	b.d.	b.d.	b.d.	b.d.	b.d.	b.d.	0.4	0.39
Th	0.14	0.17	0.18	0.22	0.24	0.23	0.22	0.22	0.27	0.3	0.23
U	0.11	0.06	0.06	0.08	0.08	0.07	0.07	0.08	0.08	b.d.	0.07
V	186	346	251	314	255	294	295	296	300	313	315
Y	35	41	24.86	31.06	29.79	34.1	32.76	29.32	30.75	32.2	26.6
Zr	52	91.5	58.7	81.1	84.7	87.5	82.4	69.7	77.3	74.6	65.7
La	3.80	3.02	2.70	3.21	3.58	2.96	3.14	2.92	3.42	4.90	2.90
Ce	9.60	9.60	7.40	9.55	10.46	9.20	9.51	8.46	9.79	12.70	7.97
Pr	1.90	1.81	1.31	1.64	1.82	1.69	1.70	1.49	1.66	2.04	1.41
Nd	10.00	10.36	7.32	9.03	9.64	9.20	8.89	7.93	8.63	9.80	7.59
Sm	3.40	3.72	2.52	3.14	3.32	3.48	3.26	2.89	2.96	3.40	2.58
Eu	1.30	1.44	1.10	1.32	1.42	1.21	1.28	1.15	1.24	1.10	0.99
Gd	4.90	5.95	3.84	4.68	4.50	4.90	4.55	3.96	4.24	4.48	3.71
Tb	0.94	1.04	0.66	0.82	0.77	0.88	0.86	0.74	0.82	0.75	0.67
Dy	5.70	6.89	4.36	5.55	5.00	5.95	5.66	4.84	5.22	5.37	4.51
Ho	1.20	1.54	0.99	1.22	1.10	1.29	1.29	1.10	1.19	1.09	0.97
Er	3.10	4.47	2.88	3.52	3.14	3.62	3.60	3.05	3.36	3.08	2.83
Tm	0.50	0.66	0.43	0.52	0.45	0.57	0.55	0.48	0.52	0.56	0.41
Yb	3.20	4.11	2.77	3.33	2.92	3.58	3.50	2.93	3.20	3.26	2.72
Lu	0.44	0.66	0.42	0.50	0.44	0.56	0.55	0.47	0.52	0.52	0.42
Mg#††	48.8	56.0	63.3	50.5	61.7	60.8	56.9	62.1	63.0	60.6	61.4
$(La/Th)n^{‡‡}$	1.3	0.9	0.7	0.7	0.7	0.6	0.7	0.6	0.6	0.8	0.6
$(La/Nb)n^{‡‡}$	1.5	1.3	1.0	0.9	1.0	1.0	0.9	0.8	0.9	0.8	0.9
$(Zr/Sm)n^{‡‡}$	0.54	0.67	0.63	0.92	0.91	0.89	0.90	0.86	0.93	0.78	0.91
$(La/Yb)n^{‡‡}$	1.4	0.9	1.2	1.2	1.5	1.0	1.1	1.2	1.3	1.8	1.3

† UTM zone 21 (NAD83); ‡ (p)bslt-(pillowed)basalt; (s)diab-(sheeted)diabase; gabb-gabbro; (f,l,m)tuff-(felsic,intermediate,mafic)tuff; gran -granodiorite; rhyo-rhyolite; fdyke-felsic dyke; (p)and-(pillowed)andesite; § Laboratory 1:GSC(2003); 2:OGS(2003); 3:McGill; OGS (2002); 4:McGill; OGS (2001); 5:OGS (2001); 6:Acme (2001); 7:XRAL Toronto; MUN (1992); 1 to 6: Rogers (2004); 7: Jenner et al., (1990); # b.d. - below detection; n.a. not applicable:†† Mg# = $Mg^{2+}/(Mg^{2+}+Fe^{2+})$, $Fe^{3+}/Fe^{2+}=0.1$; ‡‡ N-MORB normalized value (Sun and MacDonough, 1989)

Table 2.4: Annieopsquotch Accretionary Tract Sm/Nd isotopic data

Sample	Lithostratigraphic unit	Group	Age	Nd	Sm	$^{143}Nd/^{144}Nd$	$^{147}Sm/^{144}Nd$	$^{143}Nd/^{144}Nd_i$§	$\varepsilon Nd(t)$§
VL01A057	Star Brook Suite	SB_1	473	12.17	4.48	0.513173	0.2226	0.512483	8.87
VL01A097a	Mink Lake Formation	ML_2	473	7.68	2.17	0.512605	0.1706	0.512076	0.93
VL01A097b	Mink Lake Formation	ML_1	473	16.67	4.41	0.512319	0.1601	0.511823	-4.02
RAX01059	Skidder Formation	SK_1	464	9.46	3.44	0.512931	0.2201	0.512262	4.33
RAX01047	Harbour Round Fm.	HR_2	464	15.40	5.26	0.513064	0.2067	0.512436	7.73
RAX01049	Harbour Round Fm.	HRF_5	464	18.18	4.14	0.512357	0.1377	0.511939	-1.99
RAX01051	Healy Bay Formation		464	19.67	3.65	0.512054	0.1123	0.511713	-6.40
VL01A360	Healy Bay Formation		464	19.23	3.88	0.512074	0.1221	0.511703	-6.59
VL02A283	Healy Bay Formation		464	19.53	4.39	0.512059	0.1357	0.511646	-7.70
VL02A295	Healy Bay Formation		464	22.57	5.02	0.512101	0.1343	0.511693	-6.79

Sample location, lithology and geochemistry listed in Table 2.5; Concentration in ppm from isotope dilution; §Calculated at age of formation

Table 2.5 (continued)

VL02A 285	VL02A 214	VL02A 275a	VL02A 298b	VL02A 297	VL02A 291	VL01A 272	VL01J 107	VL02A 287	RAX02 170	VL01A 59	VL01J 063a	VL02A 225
480662	483699	484076	484922	484863	482863	459932	466735	481406	483690	460416	448841	477142
5373460	5376546	5377009	5378280	5378393	5375733	5349869	5362789	5374122	5376649	5350068	5344158	5371257
12A/11	12A/11	12A/11	12A/11	12A/11	12A/11	12A/05	12A/06	12A/11	12A/11	12A/05	12A/04	12A/06
SB_1	SB_1	SB_1	SB_1	SB_1	SB_1	SB_2	SB_2	SB_2	SB_3	SB_3	SB_3	SB_3
bslt	bslt	diab	bslt	diab	bslt	bslt	diab	sdiab	bslt	diab	diab	gabb
3	3	3	3	3	3	6	5	3	4	1	5	3
49.80	48.70	48.12	48.13	46.56	46.83	48.14	48.26	47.17	48.49	45.80	47.45	48.18
1.58	1.51	1.48	1.68	1.70	1.91	1.33	1.72	1.59	1.00	0.54	0.75	0.38
13.84	14.22	14.16	14.26	14.53	14.47	15.07	14.53	14.29	15.04	15.00	16.83	16.58
12.66	12.75	12.43	13.53	13.65	14.76	10.93	12.01	12.67	11.94	10.10	9.80	7.67
0.20	0.21	0.20	0.22	0.21	0.25	0.18	0.22	0.19	0.16	0.16	0.16	0.14
7.41	7.56	7.89	7.73	8.76	7.62	7.07	7.67	7.63	8.07	11.10	8.99	10.46
9.29	10.13	10.69	8.01	8.55	9.36	12.04	11.65	12.57	8.80	10.50	12.90	12.28
3.62	3.36	3.00	3.44	2.96	3.10	2.32	2.46	2.03	2.58	1.66	1.80	2.13
0.21	0.06	0.09	0.13	0.08	0.04	0.06	0.34	0.08	1.04	0.49	0.02	0.24
0.13	0.12	0.14	0.14	0.14	0.16	0.16	0.11	0.13	0.06	0.01	0.04	0.02
1.79	2.15	2.29	3.36	3.24	2.63	2.50	1.28	2.14	3.43	9.25	1.42	2.42
100.59	100.83	100.58	100.69	100.45	101.19	99.86	100.26	100.56	100.70	100.00	100.16	100.59
15.3	18.4	13.1	27.7	25.6	10.7	23.0	21.7	11.9	45.7	73.0	b.d.	14.0
178	213	364	209	211	152	267	216	284	420	194	434	410
0.50	0.14	0.13	0.15	0.19	0.12	0.30	2.1	0.17	0.38	0.62	0.23	0.63
2.70	2.50	2.40	2.70	2.90	3.40	2.40	1.46	1.80	1.40	0.37	0.99	0.40
2.43	2.34	4.94	2.49	2.44	3.23	2.70	4.02	1.89	0.97	0.33	0.47	0.20
74	78	107	77	73	72	39	82	89	99	79	157	167
2	1.3	1	0.8	b.d.	b.d.	0.7	3.15	1.3	b.d.	0.5	b.d.	1.1
4.39	0.23	0.18	1.46	1.25	0.24	0.25	23.2	0.52	20.4	14.0	0.28	8.82
48.9	49.6	44.2	45.5	49.1	52.5	35	46.8	43.8	48.3	53	37.1	40.8
177	200	217	129	73.9	81.4	126	174	119	135	82	68.3	123
0.31	0.3	0.41	0.31	0.28	0.33	0.2	b.d.	0.27	0.19	0.025	b.d.	0.14
0.2	0.19	0.34	0.18	0.2	0.23	b.d.	b.d.	b.d.	0.08	0.03	b.d.	b.d.
0.07	0.07	0.11	0.06	0.06	0.10	b.d.	0.02	0.01	0.08	b.d.	0.01	0.01
337	343	344	356	361	404	272	351	330	289	320	219	166
38.42	37.95	38.08	41.01	42.96	47.67	29.3	29.7	34	23.74	7.3	20.23	10.66
91	91	92	95.2	100	115	73.5	43.67	49.6	45.1	11	28.9	9.8
3.12	2.92	4.67	3.14	3.32	4.03	4.60	2.64	2.27	1.28	0.30	0.77	0.38
9.70	9.38	12.37	10.04	10.49	12.23	11.80	7.93	7.25	4.13	1.00	2.63	1.33
1.85	1.67	1.96	1.88	1.94	2.25	1.89	1.41	1.45	0.77	0.22	0.54	0.30
10.25	9.80	11.33	10.50	10.98	12.72	10.90	8.20	8.68	4.66	1.20	3.40	1.94
3.74	3.48	3.56	3.80	4.08	4.71	3.30	3.14	3.27	1.94	0.55	1.61	0.84
1.26	1.23	1.31	1.40	1.43	1.45	1.13	1.38	1.36	0.85	0.22	0.72	0.47
5.28	5.42	5.41	5.77	6.17	6.58	4.27	4.53	4.99	3.14	0.98	2.53	1.40
0.95	0.99	0.92	1.10	1.10	1.22	0.81	0.80	0.93	0.58	0.19	0.47	0.30
6.43	6.44	6.14	6.95	7.32	8.22	5.08	5.17	5.89	3.80	1.30	3.28	1.94
1.43	1.42	1.40	1.51	1.61	1.79	1.03	1.10	1.29	0.90	0.28	0.76	0.41
4.24	4.39	4.26	4.64	4.78	5.36	2.75	3.15	3.79	2.64	0.82	2.17	1.29
0.61	0.64	0.64	0.68	0.71	0.80	0.49	0.46	0.55	0.42	0.12	0.33	0.17
3.82	3.77	3.95	4.26	4.34	4.94	2.80	2.76	3.60	2.52	0.80	2.12	1.15
0.61	0.59	0.62	0.64	0.68	0.78	0.53	0.41	0.56	0.42	0.12	0.31	0.18
56.1	56.4	58.0	55.5	58.3	52.9	58.5	58.2	56.8	59.6	70.5	66.7	74.8
0.7	0.7	0.7	0.8	0.8	0.8	n.a.*	n.a.	n.a.	0.8	0.5	n.a.	n.a.
1.2	1.2	0.9	1.2	1.3	1.2	1.6	0.6	1.1	1.2	0.8	1.5	1.8
0.86	0.93	0.92	0.89	0.87	0.86	0.79	0.49	0.54	0.83	0.71	0.64	0.41
1.0	0.9	1.4	0.9	0.9	1.0	2.0	1.2	0.8	0.6	0.5	0.4	0.4

Table 2.5 (continued)

VL02A 223b	VL02A 233a	VL02A 206	VL02J 404	VL01A 283a	VL01J 151	VL01J 208a	VL01J 208b	VL02A 277	VL02A 255	VL02A 192a	VL02J 402	VL02J 403
477578	475514	484714	495564	465013	474143	495317	495317	483312	487807	474119	494496	494805
5371723	5370286	5378095	5398809	5357399	5370148	5397037	5397037	5376757	5383738	5369669	5398217	5398458
12A/06	12A/06	12A/11	12A/11	12A/06	12A/06	12A/11	12A/11	12A/11	12A/11	12A/06	12A/11	12A/11
SB_3	SB_3	SB_3	SB_3	OBS	OBS	OBS	OBS	OBS	OBS	OBS	OBS	OBS
gabb	bslt	diab	bslt	bslt	diab	bslt	bslt	sdiab	diab	diab	bslt	bslt
3	3	3	3	5	5	5	5	3	3	3	3	3
46.96	48.09	47.90	47.04	49.33	49.68	48.24	47.79	49.01	49.09	47.11	47.59	47.52
0.44	1.01	1.30	0.72	1.51	1.30	3.07	3.10	2.36	1.50	2.16	2.42	2.93
14.03	15.95	14.80	17.06	14.52	15.54	13.48	12.91	14.70	15.04	15.34	14.08	13.05
10.64	10.33	11.44	9.25	11.77	12.02	16.41	18.45	12.82	13.16	14.48	13.62	16.11
0.19	0.15	0.19	0.18	0.20	0.19	0.23	0.22	0.22	0.17	0.18	0.28	0.30
11.85	6.05	7.93	9.20	6.16	8.24	5.59	4.53	5.77	6.68	4.94	7.27	5.91
12.37	10.87	11.44	11.65	12.23	8.62	5.45	5.70	10.02	11.82	11.88	9.72	8.51
1.36	3.62	2.63	1.82	3.05	4.28	5.31	5.46	3.51	2.41	2.95	3.60	4.36
0.11	0.12	0.10	0.97	0.05	0.10	0.05	0.06	0.29	0.11	0.18	0.36	0.21
0.03	0.07	0.11	0.04	0.17	0.14	0.41	0.40	0.27	0.20	0.27	0.26	0.32
2.59	3.92	2.43	2.19	1.59	0.58	2.48	2.14	2.01	0.47	0.40	0.98	1.32
100.64	100.26	100.34	100.24	100.57	100.70	100.71	100.75	101.03	100.73	99.94	100.25	100.58
9.4	12.4	19.2	156	10.0	6.2	10.6	8.4	165	31.6	16.5	61.9	21.4
284	368	360	524	174	253	11	14	114	214	56	200	55
0.19	0.13	0.20	3.8	0.03	0.09	0.13	0.12	0.29	0.12	0.24	0.92	0.19
0.70	1.60	2.10	0.90	2.44	2.52	5.19	4.60	5.00	2.20	5.00	4.50	5.10
0.36	0.83	1.70	0.18	4.81	1.79	7.95	7.21	6.22	5.23	2.44	4.47	7.80
161	83	95	211	87	91	15	16	32	67	35	58	39
1.1	1	0.5	6.3	2.79	3.49	0.69	0.48	4.1	b.d.'	2	4.1	4.4
1.09	1.59	0.8	42.8	b.d.	0.75	0.21	b.d.	3.57	0.72	1.98	5.96	2.22
48.8	41.6	52.5	32.8	37.7	40.5	42.9	43.2	44.6	44.2	43.4	45.5	38.2
84.5	172	147	72.4	291	92.3	32.8	35.5	254	178	187	240	103
0.14	0.19	0.23	b.d.	b.d.	b.d.	0.48	0.47	0.57	0.41	0.28	0.3	0.59
b.d.	0.07	0.13	b.d.	0.79	1.08	0.92	0.8	1.82	0.85	0.93	0.44	0.66
0.02	0.03	0.04	b.d.	0.3	0.32	0.42	0.37	0.68	0.27	0.46	0.22	0.3
202	263	315	209	331	313	351	351	315	367	417	388	446
16.08	25.71	32.56	20.07	30.78	33.54	48.56	41.7	45.6	28.97	56.96	45.2	50.29
20.2	53.4	81.9	22.3	89.7	94.3	210	184	190	81.5	180	171	196
0.72	1.29	2.47	0.33	7.86	6.32	10.71	8.90	12.64	8.55	7.96	7.13	10.09
2.42	4.83	8.12	1.49	18.88	16.29	29.10	24.67	30.97	19.84	22.80	21.23	28.39
0.52	0.99	1.55	0.38	2.81	2.49	4.43	3.93	4.78	2.88	3.79	3.60	4.49
3.12	6.20	8.77	2.92	13.22	12.32	22.72	20.48	22.90	13.47	20.38	18.63	22.69
1.19	2.42	3.33	1.54	3.84	3.73	6.45	5.97	6.66	3.64	6.29	5.94	6.72
0.58	0.97	1.23	0.60	1.63	1.26	2.35	2.25	2.06	1.25	2.28	1.94	2.41
2.04	3.60	4.38	2.60	4.82	4.81	8.05	6.97	7.70	4.60	8.50	7.79	8.71
0.42	0.68	0.80	0.50	0.86	0.84	1.34	1.19	1.33	0.79	1.56	1.26	1.45
2.60	4.25	5.52	3.40	5.45	5.53	8.16	7.58	8.30	5.28	9.70	7.98	9.05
0.58	0.94	1.18	0.76	1.21	1.22	1.75	1.58	1.72	1.09	2.19	1.72	1.94
1.88	2.67	3.45	2.25	3.27	3.54	4.92	4.63	4.91	3.23	6.23	5.00	5.59
0.25	0.40	0.53	0.33	0.50	0.53	0.72	0.67	0.69	0.46	0.98	0.73	0.83
1.70	2.64	3.01	2.00	3.10	3.44	4.44	4.06	4.40	2.94	5.93	4.38	5.05
0.27	0.39	0.50	0.33	0.48	0.54	0.68	0.63	0.66	0.45	0.90	0.68	0.82
70.8	56.1	60.2	68.4	53.3	59.9	42.6	34.9	49.5	52.5	42.6	53.8	44.4
n.a.	0.9	0.9	n.a.	0.5	0.3	0.6	0.5	0.3	0.5	0.4	0.8	0.7
1.9	1.4	1.4	1.7	1.5	3.3	1.3	1.2	1.9	1.5	3.0	1.5	1.2
0.60	0.78	0.87	0.51	0.83	0.90	1.16	1.10	1.01	0.80	1.02	1.02	1.04
0.5	0.6	1.0	0.2	3.1	2.2	2.9	2.7	3.5	3.5	1.6	2.0	2.4

Table 2.5 (continued)

WXNF 173	VL01A 097b	VL01 050	VL01 083	VL01 082	VL01A 099	VL01A 098b	VL01A 097a	VL02A 015	VL02A 016a	RAX01 59	RAX02 158	VL02A 293
494350	436177	436019	435770	440850	435221	435139	436177	435952	435865	506714	506083	505825
5396260	5332496	5333068	5332411	5337211	5331405	5331286	5332496	5332145	5332372	5396042	5397449	5396324
12A/11	12A/04	12A/04	12A/04	12A/04	12A/04	12A/04	12A/04	12A/04	12A/04	12A/10	12A/10	12A/10
OBS	ML_1	ML_2	ML_2	ML_2	ML_2	ML_2	ML_2	ML_2	ML_2	SK_1	SK_1	SK_1
bslt	ftuff	pbslt	pbslt	pbslt	pbslt	pbslt	bslt	bslt	pbslt	pbslt	pbslt	bslt
7	5	5	5	5	3	3	3	3	3	2	4	3
48.2	72.76	54.95	50.27	47.12	49.57	51.95	52.78	47.58	49.51	50.90	51.52	46.47
1.59	0.11	0.65	0.61	0.55	0.63	0.70	0.71	0.54	0.65	1.08	0.75	0.66
14.65	11.83	14.97	16.94	15.34	14.71	14.66	16.48	14.59	17.47	16.06	15.07	15.99
12.05	4.25	9.83	9.97	9.80	9.83	9.72	11.77	9.09	12.17	11.73	12.31	9.49
0.21	0.05	0.12	0.16	0.20	0.16	0.20	0.20	0.17	0.19	0.14	0.44	0.17
6.32	1.70	5.06	7.13	7.50	5.97	5.99	4.94	4.55	4.92	7.25	8.85	9.75
8.81	4.10	8.00	6.88	9.03	6.33	6.35	6.90	15.96	7.63	5.22	3.47	12.21
3.15	0.43	2.92	4.98	2.53	1.15	4.44	2.37	0.18	2.42	5.47	1.30	1.35
0.34	2.84	0.04	0.24	1.05	2.87	0.07	1.33	0.07	2.09	0.07	0.31	1.23
0.2	0.02	0.07	0.08	0.07	0.06	0.10	0.10	0.10	0.08	0.11	0.12	0.08
3.1	2.56	4.11	4.07	6.98	8.89	6.27	2.73	7.25	3.52	3.25	5.88	2.93
98.62	100.64	100.71	101.32	100.18	100.20	100.48	100.35	100.11	100.69	101.27	100.06	100.46
113	147	14.0	31.9	209	207	37.4	290	10.3	329	41.0	27.3	193
190	3	26	89	56	50	32	37	5	21	21	165	573
b.d.	2.9	0.28	0.13	0.68	3.8	0.62	1.9	0.26	1.0	0.04	0.38	0.41
3.01	3.74	1.04	1.05	0.87	1.10	1.30	1.20	0.90	0.90	1.50	1.20	1.10
6.90	3.85	0.66	0.59	0.64	0.66	0.83	0.89	0.66	1.29	0.92	1.16	0.70
43	b.d.	22	43	37	30	19	19	27	3	21	48	196
b.d.	12.02	0.67	0.25	4.18	4.3	4.9	1.6	2.2	1.2	1.03	1.9	1.2
5	72.9	0.73	2.44	20.7	71.2	0.68	21.3	1.28	39.5	0.68	4.81	17.1
33	18.9	40.2	43.8	44.6	49.6	45.1	52.5	37	39.5	38.3	42.3	42.0
201	444	71.1	85.0	233	114	468	227	168	183	57.1	62.4	239
b.d.	b.d.	b.d.	b.d.	b.d.	0.22	0.24	0.24	0.22	0.12	b.d.	0.24	0.18
0.53	3.66	0.76	0.56	0.8	0.74	0.74	1.05	0.62	1.14	0.41	0.62	0.42
b.d.	0.83	0.23	0.53	0.33	0.13	0.22	0.27	0.34	0.27	0.23	0.17	0.11
341	14	234	236	294	315	315	324	315	376	283	248	267
27	32.7	16.58	15.36	13.85	14.11	17.58	19.38	15.99	11.44	22.96	17.12	16.33
111	119	34.4	32.3	24.9	36.8	43.9	44	31.5	33.2	46.9	40.7	32.1
6.23	12.12	4.37	3.06	4.41	3.72	4.58	5.65	4.12	5.78	2.49	3.72	3.31
15.76	30.82	10.02	7.40	9.89	8.53	10.45	12.32	8.99	12.22	7.05	8.94	7.74
2.48	4.23	1.45	1.10	1.44	1.27	1.53	1.73	1.25	1.62	1.24	1.32	1.11
12.4	18.01	6.77	5.41	6.67	5.73	7.26	7.84	6.13	6.86	7.00	6.30	5.66
3.77	4.66	1.97	1.76	1.94	1.79	2.14	2.18	1.78	1.75	2.43	1.93	1.85
1.36	0.91	0.72	0.65	0.76	0.64	0.84	0.70	0.61	0.58	0.94	0.70	0.66
4.58	5.20	2.60	2.31	2.23	2.15	2.64	2.78	2.06	1.88	3.56	2.64	2.45
0.78	0.86	0.46	0.42	0.36	0.38	0.46	0.46	0.38	0.31	0.62	0.48	0.46
5.25	5.24	2.82	2.72	2.40	2.44	2.93	3.00	2.50	1.88	4.26	2.89	2.79
1.1	1.17	0.63	0.58	0.54	0.54	0.67	0.68	0.57	0.41	0.92	0.64	0.62
3.13	3.45	1.82	1.78	1.61	1.70	2.00	1.92	1.76	1.26	2.59	1.91	1.80
0.45	0.56	0.29	0.28	0.24	0.25	0.32	0.31	0.25	0.19	0.35	0.26	0.29
2.97	3.85	1.88	1.78	1.56	1.53	1.92	2.07	1.57	1.27	2.07	1.78	1.76
0.44	0.64	0.28	0.28	0.24	0.25	0.31	0.33	0.24	0.19	0.31	0.29	0.27
53.4	46.6	52.9	60.9	62.5	57.0	57.3	47.8	52.2	46.8	57.4	61.0	69.1
0.6	0.2	0.3	0.3	0.3	0.2	0.3	0.3	0.3	0.2	0.3	0.3	0.4
0.8	2.9	6.2	4.8	6.4	5.3	5.1	5.9	5.8	4.2	2.5	3.0	4.4
1.05	0.91	0.62	0.65	0.46	0.73	0.73	0.72	0.63	0.67	0.69	0.75	0.62
2.6	3.8	2.8	2.1	3.4	3.0	2.9	3.3	3.2	5.6	1.5	2.5	2.3

Table 2.5 (continued)

RAX02 157	RAX02 156	RAX01 100	VL01 085	VL01A 125	VL01A 297	VL01A 303	VL01A 126	VL01A 131b	VL01A 299b	VL01A 078	VL01A 301b	VL01A 331b
507469	507598	501123	446650	447564	466268	466033	447772	446449	465979	445059	465984	467424
5398957	5399109	5383334	5340686	5341725	5359816	5357613	5341414	5340538	5358413	5338271	5358028	5360730
12A/10	12A/10	12A/10	12A/04	12A/04	12A/06	12A/06	12A/04	12A/04	12A/06	12A/04	12A/06	12A/06
SK_2	SK_2	HR_1	HR_1	HR_1	HR_1	HR_1	HR_1	HR_1	HR_1	HR_1	HR_1	HR_1
bslt	bslt	tuff	pbslt	bslt	bslt	bslt	pbslt	pbslt	bslt	diab	bslt	gabb
6	4	2	5	5	5	3	3	3	3	5	5	6
61.88	45.17	54.00	46.70	47.16	51.25	46.22	50.36	51.09	48.57	47.99	47.94	49.21
1.16	1.57	1.44	0.80	1.23	1.23	1.40	1.47	1.33	1.68	1.81	1.73	1.77
15.83	17.04	13.54	18.46	15.86	15.61	14.97	14.14	15.42	13.87	13.04	14.63	13.43
6.31	16.14	11.37	7.21	11.13	9.79	11.68	11.85	10.75	13.41	13.62	13.32	13.01
0.10	0.17	0.16	0.14	0.22	0.14	0.20	0.20	0.16	0.18	0.24	0.21	0.19
4.23	7.58	6.72	6.34	7.21	6.64	8.08	6.28	5.34	6.90	7.71	7.48	6.75
0.74	3.26	5.22	9.61	12.28	8.32	13.29	9.85	7.48	9.86	8.51	8.67	10.43
6.50	4.24	6.29	4.52	3.05	4.86	2.42	4.48	5.72	3.47	3.69	3.91	3.22
0.04	0.54	0.43	0.03	0.03	0.09	0.04	0.14	0.06	0.13	0.60	0.04	0.10
0.36	0.05	0.09	0.05	0.10	0.09	0.12	0.12	0.12	0.14	0.14	0.12	0.15
2.70	5.04	2.16	6.40	2.49	2.59	2.10	1.93	3.10	2.19	2.60	2.68	1.50
99.86	100.83	101.42	100.27	100.76	100.60	100.61	100.91	100.64	100.46	99.95	100.73	99.80
44.0	341	26.8	13.5	23.4	22.7	7.8	80.6	43.4	27.9	223	13.6	39.0
3	b.d.	154	371	264	221	420	366	274	178	103	154	151
b.d.	0.19	0.23	0.15	0.19	0.24	0.14	0.66	0.17	0.31	0.46	0.16	0.20
2.70	2.00	2.41	1.24	2.15	2.02	2.30	2.50	2.30	2.90	3.20	2.88	2.90
4.80	3.72	1.98	1.08	3.87	2.98	2.23	2.42	3.00	2.66	4.03	2.90	3.00
2	3	67	150	90	57	128	121	97	74	50	72	27
2.6	5	0.44	0.56	1.11	0.46	2	0.5	1.2	1.2	0.83	1.57	1.2
1.2	3.19	6.72	0.48	0.26	1.2	0.31	2.43	0.41	2.29	8.19	0.56	0.9
23	45.5	46.5	29.0	41.3	41.4	52.5	52.5	52.5	52.5	44.3	50.3	40
75.8	149	46.7	225	339	94.7	163	158	134	225	134	143	102
0.2	0.36	b.d.	b.d.	b.d.	b.d.	0.3	0.34	0.39	0.35	b.d.	b.d.	0.2
1.9	1.58	0.17	0.07	0.25	0.21	0.18	0.2	0.22	0.2	0.3	0.21	0.3
0.2	0.34	0.13	0.06	0.09	0.07	0.06	0.08	0.07	0.07	0.1	0.12	0.1
111	414	306	199	253	253	304	314	315	346	351	351	354
34.7	15.98	31.07	16.31	28.52	27.98	34.41	34.92	34.81	40.44	40.74	41.63	42.5
82.5	75.4	79.8	40.9	76.4	73.3	83.6	92.3	84.4	104	119	100	94
9.90	5.54	2.59	1.17	3.72	2.66	2.71	3.05	3.10	3.24	4.51	3.43	4.00
24.80	13.26	8.16	3.83	10.45	8.35	8.56	9.57	9.52	10.10	13.39	10.67	11.50
3.37	1.84	1.58	0.73	1.73	1.50	1.61	1.70	1.68	1.88	2.36	1.93	2.09
17.40	8.15	8.68	4.25	8.97	8.17	9.04	9.51	9.61	10.85	12.44	10.57	11.80
4.50	2.27	3.07	1.60	3.09	2.88	3.30	3.31	3.40	3.96	4.19	3.99	4.10
1.59	0.94	1.21	0.68	1.55	1.11	1.19	1.25	1.22	1.37	1.41	1.62	1.32
5.68	2.77	4.63	2.40	4.13	4.09	4.91	4.87	4.80	5.73	5.74	5.76	5.90
0.89	0.47	0.83	0.42	0.78	0.76	0.90	0.89	0.92	1.01	1.04	1.09	1.05
5.50	2.99	5.36	2.80	4.93	4.72	5.84	5.85	5.82	6.80	6.80	7.00	6.50
1.15	0.63	1.20	0.63	1.12	1.10	1.29	1.27	1.28	1.51	1.50	1.62	1.40
3.47	1.83	3.41	1.84	3.02	3.05	3.82	3.84	3.70	4.52	4.29	4.55	4.17
0.47	0.28	0.53	0.27	0.45	0.45	0.57	0.59	0.57	0.68	0.63	0.69	0.64
3.33	1.81	3.34	1.69	2.72	2.77	3.56	3.66	3.53	4.09	4.04	4.22	4.01
0.54	0.28	0.52	0.24	0.43	0.44	0.55	0.59	0.53	0.67	0.65	0.68	0.68
59.4	50.6	56.3	65.7	58.5	59.7	60.1	53.6	52.0	52.9	55.2	55.0	53.1
0.3	0.2	0.7	0.8	0.7	0.6	0.7	0.7	0.7	0.8	0.7	0.8	0.6
1.9	1.4	1.2	1.0	0.9	0.8	1.1	1.2	1.0	1.1	1.0	1.1	1.2
0.65	1.18	0.92	0.91	0.88	0.90	0.90	0.99	0.88	0.94	1.01	0.89	0.81
3.6	3.7	0.9	0.8	1.7	1.2	0.9	1.0	1.1	1.0	1.4	1.0	1.2

Table 2.5 (continued)

VL02A 021	VL02A 028	VL02A 080	VL02A 024	VL02A 274	RAX01 099	RAX01 047	VL02A 087	VL01A 133b	VL02A 197	VL02A 084	RAX01 048	RAX01 032
443604	464567	467364	447910	484804	501089	503114	467315	446907	480124	468133	503137	496519
5337182	5354343	5362844	5341643	5377692	5383217	5387085	5362451	5340466	5372628	5363329	5387255	5379867
12A/04	12A/06	12A/06	12A/04	12A/11	12A/10	12A/10	12A/06	12A/04	12A/11	12A/06	12A/10	12A/11
HR_1	HR_1	HR_1	HR_1	HR_1	HR_2	HR_2	HR_2	HR_3	HR_3	HR_3	HR_4	HR_4
bslt	pbslt	bslt	pbslt	bslt	mtuff	pbslt	bslt	mtuff	bslt	bslt	pbslt	mtuff
3	3	3	3	3	2	2	3	5	3	6	2	2
47.61	47.73	50.17	50.22	47.71	51.17	50.00	49.25	48.17	46.78	48.29	50.14	40.89
1.46	1.39	1.45	1.43	1.97	1.26	1.90	1.65	0.73	1.24	1.26	0.55	0.62
14.76	14.79	13.80	14.21	13.72	15.48	14.51	14.61	16.36	16.42	14.46	15.35	14.27
10.54	12.81	12.00	11.71	13.92	9.72	12.99	11.56	9.96	11.41	11.71	8.61	8.68
0.19	0.21	0.21	0.20	0.24	0.16	0.21	0.21	0.18	0.18	0.19	0.14	0.15
7.48	8.16	7.58	6.18	7.23	6.64	5.55	7.16	8.33	7.20	7.43	9.42	5.09
13.71	9.15	10.26	9.60	10.32	6.64	7.76	11.23	11.24	11.56	11.44	7.57	12.52
2.13	3.43	3.00	4.67	2.84	5.99	4.74	2.76	2.98	2.78	2.61	4.89	1.70
0.04	0.20	0.49	0.05	0.06	0.10	0.24	0.07	0.31	0.14	0.10	0.12	3.11
0.14	0.11	0.13	0.13	0.18	0.14	0.18	0.18	0.04	0.09	0.09	0.09	0.05
2.18	2.90	1.14	2.12	2.26	3.56	3.29	2.04	2.66	2.65	2.20	4.34	12.96
100.31	100.95	100.30	100.60	100.52	100.86	101.36	100.77	100.96	100.53	99.81	101.23	100.06
28.1	70.8	27.5	32.6	17.4	23.7	97.6	15.3	48.7	29.9	20.0	76.8	234
151	231	199	196	163	227	194	143	337	330	116	327	501
0.34	0.45	2.5	0.60	0.19	0.08	0.38	0.67	0.44	0.30	0.40	0.15	0.99
2.70	2.30	2.40	2.40	3.50	2.15	3.52	2.80	0.94	1.90	2.10	0.88	1.24
5.10	2.03	3.20	2.31	3.94	4.11	3.53	7.93	0.29	1.12	2.60	0.86	0.60
69	107	84	77	70	83	102	65	131	115	35	143	195
0.5	0.9	4.6	0.6	1.9	2.04	1.6	2.5	0.6	3.7	0.2	1.14	1.18
0.42	2.68	29.4	0.46	0.36	1.37	3.5	0.74	7.58	2.46	2.1	1.41	45.1
38	43	40	45	46.6	43	34.1	47.0	37.3	44.2	39	35.7	32.5
300	91.4	125	167	117	159	140	277	83.8	312	162	115	229
0.48	0.31	0.34	0.34	0.38	b.d.	b.d.	0.67	b.d.	0.18	b.d.	b.d.	b.d.
0.36	0.17	0.23	0.18	0.34	0.65	0.53	0.46	b.d.	0.11	b.d.	0.6	1.25
0.11	0.05	0.08	0.07	0.10	0.54	0.16	0.18	0.01	0.03	b.d.	0.23	0.39
235	281	303	314	406	316	514	298	225	286	307	212	223
33.41	35.51	33.66	35.14	46.87	26.35	44.58	34.87	19.79	29.85	30.7	12.22	15.46
106	78.8	91.1	89.7	126	72.7	114	116	23.3	74.3	61	23.6	37.4
5.00	2.54	3.51	3.16	4.61	5.15	5.54	6.58	0.50	1.90	2.80	2.52	4.75
14.09	8.06	10.56	9.50	14.41	12.36	15.41	17.18	1.89	7.01	8.70	6.18	11.23
2.26	1.48	1.75	1.71	2.47	1.89	2.58	2.54	0.44	1.38	1.40	0.95	1.72
12.10	8.29	9.68	9.47	13.12	9.28	13.28	12.58	2.95	7.76	8.30	4.68	8.09
3.99	3.19	3.37	3.43	4.80	2.81	4.54	4.08	1.48	3.17	2.40	1.54	2.26
1.46	1.15	1.21	1.30	1.54	1.05	1.78	1.47	0.66	1.18	1.14	0.59	0.85
5.38	4.87	4.67	4.97	6.40	3.92	6.40	5.12	2.41	4.27	4.95	1.91	2.52
0.90	0.89	0.85	0.93	1.20	0.70	1.16	0.88	0.48	0.76	0.79	0.36	0.47
5.83	5.74	5.82	5.76	7.89	4.61	7.83	5.76	3.40	5.00	5.24	2.27	2.88
1.25	1.29	1.22	1.32	1.71	1.00	1.72	1.21	0.78	1.10	1.06	0.49	0.62
3.76	3.74	3.53	3.93	5.27	2.89	5.00	3.56	2.22	3.35	3.22	1.42	1.75
0.53	0.55	0.48	0.54	0.75	0.45	0.76	0.52	0.34	0.50	0.49	0.22	0.26
3.20	3.76	3.60	3.62	4.74	2.80	4.76	3.17	2.11	2.93	2.90	1.33	1.64
0.50	0.53	0.53	0.59	0.73	0.43	0.76	0.51	0.34	0.46	0.45	0.23	0.26
60.7	58.1	57.9	53.5	53.1	59.8	48.2	57.4	64.6	57.9	58.0	70.5	56.1
0.7	0.7	0.7	0.8	0.7	0.4	0.5	0.7	n.a.	0.8	n.a.	0.2	0.2
0.9	1.2	1.0	1.3	1.1	1.2	1.5	0.8	1.6	1.6	1.0	2.7	7.4
0.94	0.88	0.96	0.93	0.94	0.92	0.89	1.01	0.56	0.83	0.90	0.54	0.59
1.9	0.8	1.2	1.1	1.2	2.2	1.4	2.5	0.3	0.8	1.2	2.3	3.5

Table 2.5 (continued)

RAX01 033	VL01A 080a	RAX00 709	RAX00 706	RAX00 707	RAX01 054	RAX01 062	RAX01 061	RAX01 060	RAX01 067	RAX01 076	RAX01 064	RAX01 035
497088	446204	443569	440819	440869	488958	534506	533826	532918	529249	508414	530989	510647
5379494	5340308	5336518	5336018	5336018	5379606	5407801	5407267	5406265	5401639	5394308	5406069	5395316
12A/11	12A/04	12A/04	12A/04	12A/04	12A/11	12A/15	12A/15	12A/15	12A/15	12A/10	12A/15	12A/10
HR_4	HR_4	HR_5	HR_5	HR_5	HR_5	HR_5	HR_5	HR_5	HR_5	HR_5	HR_5	HR_5
pbslt	bslt	bslt	pbslt	pbslt	and	pbslt	pbslt	pand	pbslt	mtuff	pbslt	bslt
2	5	1	1	1	2	2	2	2	2	2	2	2
44.35	52.66	57.40	47.20	44.40	56.89	49.97	41.80	58.61	48.46	50.37	49.73	48.74
0.82	0.63	0.64	0.48	0.54	0.73	1.51	0.80	0.62	0.74	0.95	0.71	0.91
17.81	16.14	17.30	16.00	18.20	17.20	16.24	14.30	11.56	14.56	14.85	13.80	15.47
10.16	7.95	8.07	6.68	9.10	8.62	8.93	7.86	10.06	8.92	8.09	7.04	8.76
0.25	0.10	0.13	0.18	0.23	0.17	0.14	0.13	0.50	0.15	0.17	0.18	0.15
6.84	9.93	4.39	11.00	9.80	3.25	5.97	5.87	7.95	7.80	4.33	5.28	8.94
6.66	3.07	2.59	7.08	8.16	6.60	5.24	12.55	4.70	10.00	8.22	10.28	5.84
3.92	4.82	3.57	2.43	1.91	2.44	5.27	3.74	0.12	3.82	4.13	4.37	3.61
2.01	0.04	1.34	0.07	0.39	1.69	0.46	0.16	0.19	1.37	0.46	0.22	0.42
0.09	0.09	0.09	0.24	0.27	0.24	0.26	0.18	0.09	0.27	0.24	0.14	0.20
8.55	5.53	7.21	12.64	11.91	3.23	7.26	13.72	5.45	5.30	9.40	9.19	8.30
101.46	100.96	99.00	98.20	99.30	101.07	101.25	101.11	99.85	101.39	101.20	100.93	101.35
152	77.4	337	95.0	102	251	348	67.1	706	504	140	229	92.7
75	64	19	1160	1040	5	81	323	35	303	55	208	289
1.4	0.37	1.3	0.12	0.36	1.6	0.96	0.77	0.96	0.38	2.0	0.11	0.83
1.33	0.96	2.50	1.10	1.20	2.77	3.97	2.32	1.01	2.14	2.89	1.34	1.91
0.76	0.92	2.40	1.80	2.00	2.47	7.38	3.43	1.29	4.35	6.07	1.50	3.87
39	60	b.d.	388	341	b.d.	8	156	40	81	36	92	132
1.06	5.43	2	7	13	4.4	2.7	0.99	6.68	2.1	5.14	0.95	2.42
44.1	0.53	26.0	1.2	9.1	59.9	9.33	3.2	5.45	32.3	14.7	4.05	11.9
39.7	34	22	31	36	17.7	19.7	31.7	24.9	37.6	26.1	36	31.3
93.3	166	112	343	498	451	205	169	121	165	153	157	188
b.d.	b.d.	0.2	0.16	0.15	b.d.	0.4	b.d.	b.d.	b.d.	b.d.	b.d.	b.d.
1.2	0.72	4.2	1.9	2.1	10.39	4.42	3.6	1.82	5.08	5.62	1.64	3.26
0.44	0.29	1.3	0.74	0.68	3.51	1.4	1.19	0.49	2.56	0.98	0.54	0.58
343	278	153	254	434	168	179	223	231	242	244	257	266
16.81	14.83	22	16	18	17.31	22.3	16.29	12.08	16.18	20.4	12.07	15.05
44.0	30.3	88	34	40	94.5	154	87.6	34.4	74.4	103	43.9	66.6
4.09	3.70	11.00	8.50	9.90	26.98	19.28	13.00	7.27	11.79	14.42	7.34	10.92
10.32	9.16	23.00	18.00	21.00	56.65	42.97	28.60	15.16	26.24	31.99	15.60	25.08
1.53	1.38	2.90	2.50	2.80	7.16	5.59	3.78	1.99	3.66	4.35	2.15	3.38
6.91	6.34	12.00	11.00	12.00	28.48	22.46	15.57	8.64	16.45	18.88	9.20	13.78
2.04	1.94	2.60	2.60	2.90	5.53	4.52	3.39	1.96	3.54	3.93	2.31	3.32
0.81	0.69	0.94	0.83	0.90	1.68	1.46	0.98	0.73	1.00	1.22	0.78	1.06
2.62	2.21	2.90	2.70	3.10	4.47	4.40	3.09	2.30	3.16	3.79	2.30	2.96
0.45	0.38	0.54	0.46	0.51	0.63	0.68	0.50	0.36	0.48	0.59	0.37	0.50
2.91	2.58	3.20	2.70	3.00	3.46	4.05	2.92	2.27	3.02	3.72	2.26	2.97
0.64	0.56	0.70	0.55	0.60	0.72	0.86	0.61	0.50	0.60	0.81	0.48	0.62
1.82	1.70	1.90	1.40	1.60	1.99	2.40	1.91	1.44	1.71	2.33	1.38	1.78
0.27	0.25	0.33	0.23	0.26	0.30	0.37	0.27	0.21	0.25	0.35	0.21	0.27
1.74	1.64	2.30	1.60	1.70	1.98	2.22	1.78	1.29	1.49	2.27	1.38	1.69
0.26	0.26	0.39	0.23	0.28	0.32	0.35	0.29	0.21	0.24	0.36	0.21	0.27
59.5	73.1	54.2	78.2	70.1	45.1	59.3	61.9	63.3	65.6	53.8	62.0	69.0
0.2	0.2	0.1	0.2	0.2	0.1	0.2	0.2	0.2	0.1	0.1	0.2	0.2
5.0	3.7	4.3	4.4	4.6	10.2	2.4	3.5	5.3	2.5	2.2	4.6	2.6
0.77	0.55	1.20	0.46	0.49	0.61	1.21	0.92	0.62	0.75	0.93	0.68	0.71
2.9	2.8	5.8	6.5	7.1	16.6	10.6	8.9	6.9	9.7	7.7	6.5	7.9

Table 2.5 (continued)

RAX01 056	RAX01 049	RAX01 031	RAX01 063	RAX01 058	RAX01 065	RAX02 129	RAX02 103	RAX02 153	RAX02 154	RAX02 102	RAX02 101	VL02A 014
502988	501727	500049	535078	503298	524147	537110	514047	513134	509807	513531	513126	440325
5387700	5386376	5384112	5409320	5388722	5404056	5410490	5397396	5403769	5402136	5396921	5396703	5335838
12A/10	12A/10	12A/10	12A/15	12A/10	12A/15	12A/16	12A/10	12A/15	12A/15	12A/10	12A/10	12A/04
HR_5	HR_5	HR_5	HR_5	HR_5	HR_5	HR_5	HR_5	HR_5	HR_5	HR_5	HR_5	HR_5
mtuff	mtuff	bslt	pbslt	diab	gabb	pbslt	bslt	bslt	pbslt	bslt	bslt	bslt
2	2	2	2	2	2	4	4	4	4	4	6	6
51.25	51.10	49.36	48.26	51.83	49.64	52.48	49.98	52.73	48.13	50.65	55.84	48.21
0.75	0.89	0.78	0.79	0.83	1.69	0.69	1.08	0.72	0.87	1.16	1.21	1.03
16.28	16.51	16.69	16.54	14.92	15.71	14.10	19.12	16.64	18.69	16.49	14.86	16.41
8.14	9.46	8.33	10.06	11.90	13.46	7.68	12.18	9.61	9.88	12.18	11.22	7.45
0.23	0.24	0.08	0.16	0.17	0.23	0.14	0.13	0.18	0.24	0.20	0.12	0.12
8.29	7.29	9.58	5.94	7.34	5.42	5.04	4.02	3.73	9.10	6.87	3.92	5.64
4.84	6.41	5.18	8.48	2.58	6.11	10.42	2.41	9.28	3.18	4.13	5.63	8.83
4.83	4.96	1.44	5.28	3.96	4.67	2.73	5.78	1.77	4.66	4.15	3.29	4.88
1.73	0.46	5.34	0.09	1.57	1.32	1.28	2.31	2.32	0.71	0.80	0.44	0.45
0.16	0.16	0.13	0.17	0.20	0.22	0.22	0.26	0.15	0.16	0.27	0.29	0.36
4.74	3.76	4.53	5.50	5.80	2.91	5.12	3.56	3.55	5.14	3.92	2.90	6.40
101.25	101.25	101.46	101.27	101.10	101.40	99.98	100.86	100.72	100.81	100.86	99.75	99.85
359	129	464	79.1	253	462	726	409	507	497	300	169	233
59	109	223	38	21	5	420	54	53	152	21	27	157
1.0	0.62	2.5	0.06	1.0	0.14	0.41	2.5	0.81	0.50	0.27	1.0	0.50
1.91	1.80	1.80	1.76	1.62	2.61	2.30	2.40	1.90	2.10	2.50	2.70	2.70
3.40	2.87	3.25	3.08	1.81	2.74	4.53	4.13	2.43	2.87	4.50	4.30	11.30
50	55	88	36	22	7	132	18	24	59	19	10	104
1.73	3.09	1.26	5.03	1.82	4.01	16	5.4	9.5	4.3	7.6	2.9	1.3
33.0	7.24	124	1.59	19.4	31.2	37.0	60.8	55.6	11.6	9.7	19.2	11.5
36.2	33.3	40.8	31.1	17.1	38.1	28.0	40.2	38.9	52.5	42.3	31	27
173	236	191	122	137	275	592	76.7	312	396	154	382	184
b.d.	b.d.	b.d.	b.d.	b.d.	b.d.	0.33	0.38	0.22	0.37	0.42	0.3	0.5
3.75	3.57	2.86	3.52	1.64	3.69	6.12	4.66	4.77	3.44	4.9	5.3	10.8
0.75	0.69	0.54	1.02	0.72	0.78	0.91	0.37	1.03	0.84	0.88	1.1	2.1
316	319	320	463	553	751	218	229	315	315	357	383	256
15.58	16.4	15.97	16.48	16.29	25.97	20.14	26.04	16.82	17.04	24.21	28.3	21.4
66.3	58.5	61.6	61.2	50.22	92.61	89.8	85.5	72.5	77.2	91.2	87.1	112
12.12	13.98	10.87	13.69	6.52	15.73	19.34	18.48	16.89	13.05	20.14	23.00	18.10
25.84	28.98	22.75	27.02	14.87	34.32	38.03	38.22	34.19	27.64	43.44	49.20	41.30
3.48	3.62	3.02	3.43	2.06	4.72	4.79	5.44	4.35	3.59	6.00	6.25	5.49
14.51	15.21	12.62	14.39	9.39	20.10	19.08	22.65	16.95	14.39	25.24	27.30	24.20
3.08	3.48	2.87	3.24	2.37	4.93	4.02	5.33	3.60	3.18	5.50	5.70	4.30
1.07	1.18	0.98	1.08	0.73	1.72	1.08	1.59	1.08	1.01	1.37	1.83	1.33
3.07	3.53	2.86	3.41	2.65	4.91	3.89	5.17	3.53	3.34	5.30	5.61	4.37
0.48	0.55	0.48	0.50	0.43	0.79	0.56	0.81	0.51	0.53	0.81	0.74	0.55
3.01	3.30	2.86	2.98	2.87	4.84	3.49	4.76	2.86	3.12	4.66	5.12	3.60
0.64	0.68	0.63	0.64	0.62	1.01	0.72	1.08	0.60	0.61	1.01	1.03	0.72
1.82	1.83	1.62	1.86	1.83	2.97	2.06	2.98	1.73	1.89	2.84	2.83	2.09
0.27	0.28	0.27	0.27	0.27	0.42	0.31	0.47	0.25	0.26	0.44	0.44	0.27
1.69	1.71	1.61	1.89	1.68	2.70	2.05	2.73	1.56	1.66	2.66	2.95	2.21
0.27	0.27	0.26	0.27	0.25	0.40	0.32	0.43	0.25	0.27	0.43	0.35	0.36
68.9	62.7	71.5	56.3	57.3	46.7	58.9	41.8	45.8	66.8	55.1	43.2	62.3
0.2	0.2	0.2	0.2	0.2	0.2	0.2	0.2	0.2	0.2	0.2	0.2	0.1
3.3	4.5	3.1	4.1	3.4	5.4	4.0	4.2	6.5	4.2	4.2	5.0	1.5
0.76	0.60	0.76	0.67	0.75	0.67	0.79	0.57	0.72	0.86	0.59	0.54	0.92
8.7	10.0	8.2	8.8	4.7	7.1	11.5	8.3	13.2	9.6	9.2	9.5	10.0

Table 2.5 (continued)

RAX00	RAX01	RAX01	RAX01	RAX01	RAX01	RAX01	RAX01	RAX01	RAX01	RAX01	RAX02	RAX02
710	057	910	051	011	030	055	908	009	081	909	155	144
443569	503226	502989	500800	506205	503767	503672	506248	506539	505297	503520	509807	529723
5336518	5388500	5387699	5385042	5388840	5386729	5387478	5392154	5391273	5387579	5389050	5402136	5401170
12A/04	12A/10	12A/10	12A/10	12A/10	12A/10	12A/10	12A/10	12A/10	12A/10	12A/10	12A/15	12A/15
HBF	HBF	HBF	HBF	HBF	HBF	HBF	HBF	HBF	HBF	HBF	HBF	HBF
ltuff	ftuff	ftuff	ftuff	ftuff	ftuff	ftuff	ftuff	ftuff	ftuff	ftuff	fdyke	rhyo
1	2	2	2	2	2	2	2	2	2	2	6	4
65.60	77.21	76.04	79.38	74.23	67.48	68.93	69.28	65.21	63.96	63.75	81.42	77.60
0.43	0.14	0.18	0.26	0.30	0.44	0.45	0.50	0.49	0.50	0.58	0.11	0.24
15.10	12.48	12.60	11.33	13.65	15.88	15.87	14.52	17.11	18.45	16.25	9.87	10.82
6.34	1.45	1.27	2.15	2.60	4.54	4.42	5.03	5.68	5.74	7.00	1.52	2.58
0.14	0.05	0.18	0.46	0.06	0.08	0.07	0.09	0.09	0.10	0.10	0.03	0.07
2.91	1.55	1.69	0.33	1.35	1.85	1.82	2.04	2.62	2.41	3.10	0.65	1.41
1.74	0.20	0.32	0.03	1.49	0.37	0.56	1.35	1.02	0.30	1.37	0.78	1.53
4.96	1.16	1.17	2.76	2.77	3.89	3.22	2.47	3.56	3.08	3.28	4.09	4.70
0.45	4.70	4.74	2.59	2.56	2.77	2.97	2.60	2.45	3.47	2.61	0.62	0.29
0.06	0.03	0.04	0.04	0.04	0.08	0.10	0.12	0.12	0.19	0.11	0.02	0.05
4.51	2.30	2.37	1.58	1.85	2.56	2.47	2.79	2.87	3.14	2.95	0.70	0.85
99.80	101.28	100.62	100.92	100.91	99.94	100.88	100.79	101.21	101.36	101.09	99.87	100.16
162	241	635	697	796	591	588	710	533	684	644	540	339
15	b.d.	b.d.	2	13	17	17	42	33	26	57	27	46
0.40	2.0	1.7	1.8	2.9	2.6	3.0	2.4	2.9	3.2	2.0	b.d.	0.12
2.40	3.70	4.18	3.36	3.42	4.02	4.03	3.88	4.01	3.84	3.72	2.20	3.30
2.10	9.59	9.36	6.70	12.82	8.13	8.23	6.59	8.85	8.73	7.42	6.10	5.25
b.d.	b.d.	b.d.	b.d.	7	9	9	15	14	13	25	5	8
8	1.18	13.71	9.19	4.13	7.15	4.74	13.49	27.59	114.03	11.94	7.4	3.8
6.4	85.5	69.3	82.2	71.7	88.9	92.4	78.3	81.9	113	76.2	14.0	4.57
15	6.68	b.d.	5.95	7.77	15.05	14.5	13.8	18.5	18.9	20.6	4	10.4
184	2.5	8.22	58.9	257	42.8	88.7	164	148	47.6	156	172	133
0.2	0.6	0.66	0.42	1.04	0.46	0.48	0.36	0.61	0.53	0.39	0.6	0.48
4.2	8.44	8.38	10.12	22.59	10.29	10.85	9.24	11.24	10.77	9.63	8.1	6.21
1.2	2.06	2.17	2.57	5.36	2.32	2.57	2.17	2.67	2.63	2.06	1.4	1.56
90	9	9	32	35	75	78	90	93	94	108	8	46
17	27.91	12.26	19.16	15.27	22.6	20.53	21.95	23.3	26.44	22.86	14.9	19.85
87	108	133	111	109	138	138	146	132	120	132	65.9	123
10.00	23.86	17.06	26.57	32.63	28.27	22.99	25.40	23.38	23.41	26.26	18.80	16.16
21.00	50.17	34.28	46.44	66.63	43.28	40.16	49.16	55.54	49.05	53.98	36.30	32.48
2.50	6.16	4.05	5.63	6.18	6.07	5.44	6.08	5.58	6.07	6.36	3.81	3.62
9.90	22.97	14.17	20.10	18.73	21.91	20.52	22.60	20.08	22.39	24.08	14.40	13.63
2.20	4.66	2.60	3.67	3.17	4.08	4.17	4.39	4.15	4.79	4.76	2.50	2.79
0.69	0.72	0.42	0.85	0.66	1.02	1.04	1.23	1.02	1.07	1.25	0.38	0.61
2.50	4.42	2.30	3.36	2.38	3.82	3.88	4.12	3.90	4.52	4.31	1.88	2.74
0.43	0.72	0.36	0.54	0.41	0.63	0.64	0.63	0.71	0.77	0.67	0.28	0.48
2.60	4.69	2.10	3.20	2.54	3.94	3.75	3.80	4.06	4.71	4.07	2.50	3.00
0.57	1.03	0.45	0.68	0.55	0.84	0.83	0.81	0.88	1.04	0.87	0.49	0.71
1.60	2.96	1.35	1.98	1.76	2.48	2.56	2.28	2.62	3.07	2.53	1.63	2.14
0.27	0.46	0.22	0.32	0.30	0.40	0.41	0.34	0.42	0.47	0.38	0.21	0.35
2.00	2.77	1.55	2.17	2.14	2.55	2.73	2.34	2.76	3.16	2.56	2.11	2.20
0.33	0.43	0.24	0.36	0.33	0.41	0.45	0.37	0.42	0.49	0.38	0.30	0.38
50.0	70.0	74.4	31.8	53.1	47.0	47.3	46.9	50.1	47.8	49.1	48.2	54.4
0.1	0.1	0.1	0.1	0.1	0.1	0.1	0.1	0.1	0.1	0.1	0.1	0.1
4.4	2.3	1.7	3.7	2.4	3.2	2.6	3.6	2.5	2.5	3.3	2.9	2.9
1.41	0.82	1.82	1.07	1.22	1.20	1.18	1.19	1.13	0.89	0.98	0.94	1.57
6.1	10.5	13.4	14.9	18.6	13.5	10.3	13.2	10.3	9.0	12.5	10.9	9.0

Table 2.5 (continued)

RAX02 143	RAX02 152	VL01A 308	VL01A 229	VL01A 292b	VL01A 309	VL01A 360	VL01A 133a	VL01A 313	VL02A 173	VL02A 283	VL02A 013b	VL02A 158
529793	513700	466576	446955	465233	466970	440098	446907	467207	474579	481058	440098	470197
5401149	5404021	5358915	5340646	5359136	5359300	5335591	5340466	5359806	5368625	5373193	5335591	5365831
12A/15	12A/15	12A/06	12A/04	12A/06	12A/06	12A/04	12A/04	12A/06	12A/06	12A/11	12A/04	12A/06
HBF	HBF	HBF	HBF	HBF	HBF	HBF	HBF	HBF	HBF	HBF	HBF	HBF
gran	ftuff	ftuff	ftuff	ftuff	ftuff	ftuff	ftuff	ftuff	gran	ftuff	ftuff	ftuff
4	4	5	5	5	6	5	3	3	3	3	6	3
69.36	63.52	73.89	73.53	75.56	74.80	70.43	74.16	75.05	75.43	76.19	75.13	70.56
0.39	0.81	0.18	0.30	0.28	0.33	0.34	0.26	0.33	0.28	0.35	0.33	0.34
14.78	16.23	13.60	12.96	11.93	12.24	14.78	13.26	11.87	12.79	8.28	11.81	15.53
3.95	4.95	2.11	2.42	2.23	3.34	2.97	2.44	3.22	2.09	7.06	3.48	2.98
0.08	0.08	0.14	0.08	0.07	0.05	0.07	0.19	0.07	0.12	0.60	0.06	0.05
1.83	2.71	2.93	0.63	1.57	1.15	1.74	0.96	1.17	0.54	1.16	1.12	1.07
1.99	1.46	0.26	1.40	1.12	0.86	0.31	1.14	1.45	1.50	0.82	0.59	0.67
4.65	6.78	0.82	4.04	2.07	3.63	2.58	4.68	2.48	4.81	1.95	2.58	3.08
1.30	0.71	3.83	2.63	2.30	1.55	4.09	1.84	2.57	1.72	2.58	2.53	3.80
0.08	0.23	0.03	0.05	0.07	0.05	0.06	0.06	0.06	0.04	0.07	0.05	0.07
1.80	2.59	2.71	1.83	3.06	1.80	2.54	1.09	1.82	0.57	0.68	2.10	1.66
100.23	100.09	100.49	99.87	100.25	99.86	99.92	100.09	100.11	99.90	99.76	99.86	99.82
280	268	1036	806	643	470	877	396	912	821	305	647	846
37	20	2	1	2	3	8	47	46	35	72	7	32
0.84	0.74	1.8	1.6	1.4	0.90	3.1	0.90	2.1	2.4	11.9	1.7	3.9
3.00	4.40	3.57	3.07	3.50	3.10	4.24	3.50	3.40	3.40	1.70	4.10	3.70
5.70	6.06	7.77	9.73	6.14	6.70	9.16	7.57	6.80	7.54	6.82	7.30	9.39
8	6	b.d.	b.d.	b.d.	3	b.d.	8	7	5	31	6	8
8	20.6	4.2	31.54	3.04	4.4	17.75	23.7	29	20	5.4	8.5	42
37.4	20.0	91.0	70.9	66.2	46.1	123	52.5	72.0	63.8	167	75.5	136
13.5	21.9	3.63	9.55	9.56	8	12.3	16.3	15.1	9.97	11.8	8	15.2
207	143	32.1	186	136	89.2	48.8	93.6	145	168	101	60.3	104
0.48	0.43	0.58	0.58	0.38	0.4	0.57	0.7	0.61	0.46	0.56	0.4	0.6
4.49	10.81	11.73	10.05	7.15	9.1	9.73	8.05	7.96	9.26	5.25	7.7	11.46
1.16	2.39	1.58	3.14	1.76	1.9	2.54	1.86	1.93	1.88	2.47	1.9	2.84
65	66	24	28	30	44	45	46	73	25	47	49	56
16.01	35.74	14.11	26.39	19.03	21.9	25.45	25.46	21.41	22.69	21.46	16.2	29.19
122.7	178	114.96	101.02	127.98	111	154.16	129.5	131.8	119.4	60.5	134.6	126.9
18.51	42.88	18.75	27.11	20.09	28.20	26.52	24.15	24.66	29.80	23.54	26.10	34.49
30.05	85.37	38.54	52.33	40.92	48.50	51.32	46.80	46.90	58.16	54.39	48.10	65.29
3.85	11.17	3.89	6.45	4.92	5.59	6.33	5.56	5.70	6.85	5.49	5.38	7.63
14.12	43.26	12.25	22.64	18.01	21.40	22.08	20.43	20.63	25.27	21.55	20.80	26.93
2.75	8.14	2.13	4.58	3.67	3.90	4.48	4.03	3.88	4.60	4.63	3.60	5.23
0.82	2.07	0.40	0.98	0.87	0.89	1.03	0.77	0.93	1.19	1.01	0.72	1.04
2.63	7.52	1.77	4.24	3.31	3.31	4.09	4.02	3.59	3.98	5.01	2.62	4.69
0.41	1.05	0.32	0.72	0.55	0.51	0.67	0.64	0.57	0.61	0.76	0.49	0.78
2.46	5.75	2.10	4.36	3.27	3.70	4.19	4.12	3.48	3.66	4.46	3.00	4.61
0.52	1.25	0.49	0.95	0.72	0.67	0.92	0.85	0.74	0.74	0.78	0.62	1.05
1.49	3.58	1.53	2.70	2.08	2.15	2.61	2.65	2.25	2.28	2.26	1.54	3.07
0.23	0.55	0.28	0.41	0.33	0.38	0.42	0.44	0.35	0.35	0.36	0.30	0.42
1.55	3.74	1.90	2.67	2.08	2.04	2.70	2.72	2.27	2.37	2.06	2.23	2.94
0.25	0.56	0.34	0.44	0.35	0.30	0.46	0.44	0.38	0.39	0.33	0.42	0.49
50.2	54.4	75.2	36.2	60.5	42.9	56.1	46.2	44.2	36.0	26.4	41.2	43.9
0.2	0.2	0.1	0.1	0.1	0.1	0.1	0.1	0.1	0.2	0.2	0.2	0.1
3.0	6.6	2.2	2.6	3.0	3.9	2.7	3.0	3.4	3.7	3.2	3.3	3.4
1.59	0.78	1.92	0.78	1.24	1.01	1.22	1.14	1.21	0.92	0.46	1.33	0.86
14.6	14.0	12.0	12.4	11.8	16.9	12.0	10.8	13.3	15.3	13.9	14.3	14.3

Table 2.5 (continued)

VL02A 022b	VL02A 295a	VL02A 012	VL02A 081
446730	484785	439962	468746
5340544	5377776	5335514	5364078
12A/04 HBF ftuff 6	12A/11 HBF ftuff 3	12A/04 HBF ftuff 3	12A/06 HBF ftuff 3
74.28	70.28	77.43	64.45
0.37	0.39	0.17	0.37
12.05	14.99	12.78	15.55
3.82	3.79	1.02	5.80
0.06	0.08	0.05	0.10
1.10	1.41	0.56	2.60
0.70	0.58	0.34	2.76
2.53	3.21	4.21	5.82
2.97	3.11	2.26	0.48
0.04	0.08	0.03	0.07
1.90	1.89	1.18	2.09
99.90	99.81	100.04	100.10
619	763	521	206
7	34	29	26
2.1	3.4	1.4	0.67
3.00	3.90	4.40	2.00
7.40	8.88	18.52	4.74
5	11	6	11
4.5	19.9	4.7	11.1
89.6	117	81.6	10.5
9	18.1	5	23.1
50.7	146	132	283
0.5	0.77	1.27	0.52
7.7	9.28	14.11	4.79
2.5	2.21	3.24	1.24
61	71	109	139
22.9	27.98	27.6	16.12
135.6	126	113.5	80.8
26.90	27.83	37.08	16.22
50.20	52.75	78.29	32.20
5.87	6.44	9.50	3.61
21.40	23.61	35.39	13.69
3.50	4.87	6.61	2.96
0.86	1.03	1.15	0.77
3.51	4.76	5.17	2.61
0.49	0.73	0.71	0.41
4.18	4.43	4.44	2.54
0.69	1.01	1.00	0.54
2.30	2.88	3.21	1.71
0.33	0.44	0.53	0.26
2.89	2.95	3.65	1.70
0.36	0.44	0.58	0.28
38.6	44.8	54.5	49.4
0.2	0.1	0.1	0.2
3.4	2.9	1.9	3.2
1.38	0.92	0.61	0.97
11.4	11.5	12.4	11.6

CHAPTER 3: UPPER CAMBRIAN TO UPPER ORDOVICIAN PERI-GONDWANAN ISLAND ARC ACTIVITY IN THE VICTORIA LAKE SUPERGROUP, CENTRAL NEWFOUNDLAND: TECTONIC DEVELOPMENT OF THE GANDERIAN MARGIN

ABSTRACT

The Exploits Subzone of the Newfoundland Appalachians comprises remnants of Cambro-Ordovician peri-Gondwanan arc and backarc complexes that formed within the Iapetus Ocean. The Exploits Subzone experienced at least two accretionary events as a result of the rapid closure of the main portion of the Iapetus tract: the Penobscot orogeny (c. 480 Ma), which juxtaposed the Penobscot Arc (c. 513-486 Ma) with the Gander margin, and c. 450 Ma collision of the Victoria Arc (c. 473-454 Ma) with the Annieopsquotch Accretionary Tract that juxtaposed the peri-Laurentian and peri-Gondwanan elements along the Red Indian Line.

The newly recognised Pats Pond Group forms a temporal equivalent to other Tremadocian intra-oceanic complexes of the Penobscot Arc. The Pats Pond Group (c. 487 Ma) has a geochemical stratigraphy that is consistent with rifting of a volcanic arc. An ensialic setting is indicated by low εNd values (εNd 0.3 to -0.5) near the stratigraphic base and its abundant zircon inheritance (c. 560 Ma and 0.9-1.2 Ga). The spatial distribution of Tremadocian arc – backarc complexes indicates that the Penobscot arc is best explained in terms of a single east-dipping subduction zone that although differing from previous west-dipping subduction models, does explain the obduction of backarc Penobscot ophiolites onto the Gander Margin due to an outboard compressional event.

The newly recognised Wigwam Brook Group (c. 454 Ma) disconformably overlies the Pats Pond Group and records the youngest known phase of ensialic arc volcanism (εNd –4.1) in the Victoria Arc, which is also related to east-dipping subduction. Thus the Penobscot and the overlying Victoria Arc are reinterpreted in terms of a single, relatively long-lived east-dipping subduction zone beneath the peri-Gondwanan microcontinent of Ganderia. The cessation of arc volcanism towards the top of the Wigwam Brook Group and the subsequent syn-tectonic sedimentation in the Badger Group constrain the arrival of the leading edge of Ganderia with the ensialic arc complexes to the Laurentian margin to c. 454 Ma.

INTRODUCTION

The Penobscot and Victoria arc systems of the Exploits Subzone formed during the complex Cambro-Ordovician closure of the Iapetus Ocean in proximity to Ganderia, postulated to be a ribbon-like microcontinent outboard of Gondwana (van Staal et al. 1998). Following the Upper Ordovician arc-arc collision with the Red Indian Lake Arc they were emplaced under the Annieopsquotch Accretionary Tract (Fig. 1.4; e.g., van Staal et al. 1998; van der Velden et al. 2004; Chapter 2) along the Red Indian Line (Williams 1995) closing the main tract of Iapetus. This paper examines the last stages of evolution of the Ordovician Victoria and Cambro-Ordovician Penobscot arcs.Two previously unrecognized volcano-sedimentary units are described, namely the Pats Pond and Wigwam Brook groups, based on detailed and regional mapping in central Newfoundland (Lissenberg et al., in press; Rogers et al., 2005a; van Staal et al., in press a, b, c) combined with high quality geochronology and geochemistry.

The Lower Ordovician Pats Pond Group was generated during the last stages of Penobscot Arc development. It forms a temporal equivalent to the previously defined lower Wild Bight, lower Exploits and lower Bay du Nord groups (MacLachlan and Dunning 1998a; O'Brien 1992; O'Brien et al. 1997; Tucker et al. 1994) and places important constraints on the tectonic setting of the Tremadoc Penobscot Arc including the polarity of subduction and involvement of continental crust. The Upper Ordovician Wigwam Brook Group disconformably overlies the Pats Pond Group. The Wigwam Brook Group contains the youngest known arc volcanic rocks in the Victoria Arc and records the cessation of arc volcanism in the upper portions of its stratigraphy. The age and stratigraphic relationships in the Wigwam Brook Group place new time constraints on the Red Indian Lake – Victoria arc collision. The identification of the position of the Red Indian Line based on the peri-Gondwanan affinity of the Pats Pond Group and Wigwam Brook Group and peri-Laurentian affinity of the adjacent Annieopsquotch Accretionary Tract (Chapter 2) requires revision of the north-western boundary of the peri-Gondwanan Victoria Lake Supergroup (Evans and Kean 2002), and thus enables a tectonic model for this portion of the Newfoundland Appalachians to be developed.

REGIONAL GEOLOGY

The Dunnage Zone of Newfoundland Appalachians contains the vestiges of the Cambro-Ordovician continental and intra-oceanic arc – backarc and ophiolitic complexes that formed within the Iapetus Ocean (Fig. 3.1 inset; Williams 1995). The Dunnage Zone is subdivided into the peri-Laurentian Notre Dame and Dashwoods subzones and the peri-Gondwanan Exploits Subzone (Williams 1995). The peri-Laurentian and peri-Gondwanan subzones are differentiated on the basis of stratigraphic, structural, faunal and isotopic contrasts that are marked by the Red Indian Line, the fundamental suture zone of the Newfoundland Appalachians (Fig. 3.1; Williams 1995), which was subsequently imaged by Lithoprobe seismic reflection surveys as a major crustal scale fault (van der Velden, et al. 2004) which has the surface expression of black shale melange in the Red Indian Lake area.

To the west of the Red Indian Line, the peri-Laurentian Notre Dame Subzone is in part represented by the Annieopsquotch Accretionary Tract, a tectonic collage of arc and backarc complexes that formed outboard of the Laurentian margin (van Staal et al. 1998; Chapter 2). To the east of the Red Indian Line, the peri-Gondwanan Exploits Subzone is dominated by volcanic and sedimentary rocks, which display a generally continuous Upper Ordovician-Silurian stratigraphy, contain lower-Ordovician insular (Celtic) faunas, and relatively radiogenic lead in mineral deposits (Williams 1995). The Exploits Subzone of Newfoundland and its correlatives in New Brunswick have been interpreted to mainly represent the remnants of the Cambrian- Early Ordovician Penobscot and Early to Middle Ordovician Popelogan-Victoria arcs that formed outboard of the Gander margin (e.g., van Staal 1994; van Staal et al. 1998).

STRATIGRAPHY

The rocks underlying the study area were previously included in the Tulks Hill volcanics of the Victoria Lake Supergroup (e.g., Kean and Jayasinghe 1980). However, recent mapping in association with detailed geochronology have required that the area be subdivided into several distinct tectono-stratigraphic units (Lissenberg et al., in press; Rogers et al., 2005a; van Staal et al., in press a, b, c), and that the stratigraphy be revised. Two new fault-bounded tectono-stratigraphic

units are proposed herein, namely the Pats Pond and Wigwam Brook groups, which together form the western most portion of the Victoria Lake Supergroup.

The Pats Pond and Wigwam Brook groups are metamorphosed to dominantly sub- to greenschist facies conditions and have experienced multiple phases of deformation, the intensity of which varies significantly across the study area. Shear zone-truncated synform-antiform pairs characterize the macroscopic structural style in the study area. Shear zones, interpreted to represent mainly steepened thrust faults, are marked by high strain phyllonites (Fig. 3.4), mélange and broken formation. The effects of folding, faulting and thrust repetition, in association with ubiquitous poor exposure preclude any realistic estimations of the thickness of stratigraphic units.

The Pats Pond Group is exposed along the Burgeo Highway and in the Pats Pond area (Fig. 3.1, 3.3). In the Pats Pond – Red Indian Lake (Fig. 3.3a) area the Lower Ordovician upward facing Pats Pond Group and disconformably overlying Upper Ordovician Wigwam Brook Group are exposed in a doubly plunging anticline. The Wigwam Brook Group is bound to the northwest by the Red Indian Line (Fig. 3.4a), and to the southeast by the Barren Pond Shear Zone (Fig. 3.3a, 3.4b). Near the Burgeo Highway, the Pats Pond Group forms a southeast facing fault-bounded structural panel that is cut out to the southeast by the Victoria Lake Shear Zone (Fig. 3.3b; Valverde-Vaquero and van Staal 2002) and to the northwest by the Red Indian Line.

Pats Pond Group

The Pats Pond Group comprises mainly interdigitating mafic and intermediate tuffs. The sections in the Burgeo and Pats Pond areas were correlated on the basis of the characteristics of their volcanic rocks (e.g., quartz-phyric andesite) and distinctive geochemical and Sm-Nd isotopic characteristics (e.g., calc-alkaline basalt; Fig. 3.5). Calc-alkaline pillow basalt forms a distinct unit with limited exposure at the lowest exposed stratigraphic level of Pats Pond Group. The basalt is brown weathered and almost always sparsely to abundantly amygdaloidal. The amygdales are commonly radial with respect to the centre of the pillow and are more abundant towards the top. Although the basalt appears aphyric in outcrop, most thin sections contain small to coarse euhedral colourless pyroxene phenocrysts and glomeroporhyrocrysts (Fig. 3.6a) locally rimmed by colourless actinolite. Fragments of this basalt occur in the overlying tuff breccia in the Burgeo Highway area.

Feldspar and/or quartz porphyritic ash tuff, lapilli tuff and tuff breccia are abundant and represent a characteristic unit of the Pats Pond Group. Breccia is commonly bimodal, and contains mafic and intermediate to felsic fragments in a finer-grained feldspar porphyritic mafic to intermediate groundmass. Feldspar comprises 5 to 45% of the rock by volume with crystal or glomeroporphyrocryst diameters ranging from <1 mm to >1 cm, although the average is around 3 to 4 mm. In general, quartz is subordinate and comprises less than 5% of the rock by volume, with crystal diameters from <1 mm to 1 cm. Locally, both mafic and felsic fragments contain small colourless microscopic phenocrysts of pyroxene (Fig. 3.6b). Bimodal tuff grades into and is interlayered with light green to buff coloured quartz (± feldspar) porphyritic andesitic tuff, lapilli tuff, tuff breccia, flows and related subvolcanic intrusions. Quartz phenocrysts may comprise as much as 40% by volume of the rock, with diameters ranging from 2 mm to 1 cm. Andesitic tuffs are overlain by bimodal mafic- aphyric felsic tuff breccia and aphyric rhyolite, which form the last distinctive horizon in the Pats Pond Group. These rocks are in turn overlain by basaltic to andesitic tuff breccia, lapilli tuff and grey rhyolitic tuff, which form the highest observed stratigraphic horizon in the Pats Pond Group.

Wigwam Brook Group

The Wigwam Brook is a volcano-sedimentary package of rocks exposed on the periphery of the doubly plunging Pats Pond-Red Indian Lake anticline and continues further northeast as a fault bounded sliver (Fig. 3.3). The contact with the Pats Pond Group is poorly exposed, but is interpreted to be an unconformity, because of the apparent hiatus between the two groups (see below). The Wigwam Brook Group is subdivided into three lithologically distinct formations, namely the Dragon Pond, Halfway Pond, and Perriers Pond formations (Fig. 3.5).

The Dragon Pond Formation dominantly comprises an overall coarsening-up sequence of felsic volcanic and volcaniclastic rocks. The base of the Dragon Pond Formation comprises a tuffaceous turbiditic sandstone and siltstone that is locally associated with dark shale, felsic tuff and tuff breccia, flow-banded rhyolite and felsic dykes. The tuffaceous turbidite becomes interlayered and grades into a volcano-sedimentary breccia (Fig. 3.6c) and conglomerate over a 20 m interval. The latter rocks have a predominantly local provenance, as indicated by the abundance of angular

clasts, similar to the underlying beds (Fig. 3.6c). However the presence of a few well-rounded granitoid cobbles suggests a minor contribution from a distal source. The breccia horizon is overlain by felsic tuff, lapilli tuff and tuff breccia containing fragments of turbidite and black shale. The uppermost portions of the Dragon Pond Formation contain gabbro sills, massive to pillowed basalt flows and mafic tuff.

The Halfway Pond Formation conformably overlies the Dragon Pond Formation and is mainly comprised of sedimentary rocks. The transition from the Dragon Pond Formation to the Halfway Pond Formation is gradational, and is marked by an increase in siltstone and shale and a decrease of the volcanic and epiclastic components. Unlike the Dragon Pond Formation where the sandstones are predominantly epiclastic, the wackes of the Halfway Pond Formation contain abundant smoky quartz and black shale fragments. A marked increase in abundance of black shale versus grey shale marks the transition from the Halfway Pond to the Perriers Pond Formation. The Perriers Pond Formation comprises abundant, locally calcareous, black shale with minor volcanogenic siltstone and sandstone and is most readily identifiable in the northeastern portion of the mapped area, where it is commonly transformed into broken formation and mélange.

U-PB GEOCHRONOLOGY

Analytical Techniques

SHRIMP II analyses were conducted at the Geological Survey of Canada (GSC) using analytical procedures described by Stern (1997), with standards and U-Pb calibration methods following Stern and Amelin (2003). Isoplot v. 2.49 (Ludwig 2001) was used to generate concordia plots and calculate Concordia ages. The data are presented in Table 1 and plotted in concordia diagrams with errors at the 2σ level (Fig. 3.7). Additional information on the analytical techniques and data treatment is in the Appendix 4.

Pats Pond Group VL01A-067 (z7252)

A sample of rusty weathering intermediate to bimodal breccia (VL01A-067) that overlies the lower calc-alkaline basalt was collected in the Burgeo Highway area (Fig. 3.1, 3.3, 3.5), and is thought to represent some of the oldest rocks present in the Pats Pond Group. The sample yielded sparse, fair quality zircon (n = 57). Angular fragments, with smaller amounts of prism fragments,

prisms and rounded zircons, comprise the zircon population. Most of the zircons are euhedral and SEM study revealed oscillatory zoning in the majority of the zircon grains (n = 41), suggesting magmatic derivation. Some of these contained distinct, presumably inherited cores (n = 9). The rest of the grains (n = 16) were either not zoned or irregularly zoned and lacked crystal faces suggesting partial resorbtion. SHRIMP analysis yielded three distinct age populations of zircon: c. 488 Ma (n = 12), c. 553 Ma (n = 1), and c. 0.9-1.2 Ga (n = 5; Fig. 3.7a, Table 3.1). A Concordia age, calculated from the SHRIMP analyses of the youngest population, is 488 ± 3 Ma (MSWD of concordance and equivalence = 1.1, n=12). All zircons in this population displayed oscillatory zoning. This age of 488 ± 3 Ma is interpreted to represent the eruption age of the tuff breccia. Two analyses on a single un-zoned partially resorbed zircon are c. 553 Ma which is interpreted to be a xenocryst. The c. 0.9-1.2 Ga population is represented by slightly to moderately discordant xenocrystic zircons that were not zoned or irregularly zoned and partially resorbed.

Wigwam Brook Group VL01A-314 (z7630)

A sample of beige weathering, quartz- and feldspar-rich tuff (VL01A-314) immediately overlying the breccia-conglomerate horizon in the Dragon Pond Formation was collected in the Pats Pond area. The sample yielded abundant zircon with several distinct morphologies including: euhedral needles, prisms, equant multifaceted zircons, angular fragments, slightly to moderately rounded prisms, and very well rounded zircon grains. Most of the zircons were colourless to slightly yellow, however some of the very well rounded zircons were distinctly purple. SEM imaging of 87 zircons revealed mostly igneous oscillatory zoning and at least euhedral faces on many zircons. Some zircons contained distinct cores (n = 3). Several rounded zircons with irregular or no zoning (purple zircon) were also observed (n = 4). SHRIMP analyses have yielded two age populations of zircon. A Concordia age, calculated from the dominant age population, is 453 ± 4 Ma (MSWD of concordance and equivalence = 1.7, n = 22) (Fig. 3.7b, Table 3.1). These analyses are from both rounded and euhedral morphologies with oscillatory zoning. This age of 453 ± 4 Ma is interpreted to represent the eruption age of the tuff. One purple, un-zoned and rounded zircon was analyzed and yielded a discordant age of c. 2.7 Ga (Table 1, not plotted).

GEOCHEMISTRY

The majority of the volcanic units have been sampled for geochemistry during this study and analysed for major and trace elements using XRF and ICP-MS techniques (Table 3.2). Samples are separated into groups based on stratigraphic position and chemical characteristics on extended spidergrams. Selected samples were analysed for Sm-Nd isotopic composition (Table 3.3). Complete analytical results, methods and errors are presented in Rogers (2004). Several ratios were calculated to ease the discussion of data, including La_n/Th_n, La_n/Nb_n, Zr_n/Sm_n, La_n/Sm_n and Gd_n/Lu_n (N-MORB normalization factors, Sun and McDonough 1989). These represent the intensity of the Th, Nb and Zr anomalies, and the slope of LREE and HREE. Cs, Rb, Ba, K, Pb and Sr are considered to be mobile under the metamorphic and metasomatic conditions experienced by the rocks in this study (Cann 1970). Only immobile elements are plotted on the extended trace element spidergrams presented in Fig. 3.8 (N-MORB normalized; Sun and McDonough 1989). FeO and Mg# were calculated assuming a Fe^{3+}/Fe^{2+} ratio of 0.1.

Pats Pond Group

Pats Pond Group comprises six geochemical types that occur at distinct stratigraphic levels. In ascending order, they are informally referred herein as PP_1-PP_6 , such that type PP_1 comprises the lowest exposed stratigraphic unit and type PP_6 occurs near the stratigraphic top. PP_1 (n = 4) consists of transitional calc-alkaline basaltic andesite to island arc tholeiite. (Fig. 3.8, 3.9a). The samples exhibit consistently strong Th enrichment (average La_n/Th_n 0.2), strong Nb depletion (La_n/Nb_n 8.1), slight Ti depletion, negative Zr and Hf anomalies (Zr_n/Sm_n 0.5), strong enrichment of LREE (La_n/Sm_n 2.9) and slight enrichment of MREE (Gd_n/Lu_n 1.4). The samples are primitive to moderately evolved (Mg# 70.5 to 58.7). Sm-Nd isotope composition analyses of two samples yielded ε_{Nd487} values of -0.54 and +0.34 (Table 3).

PP_2 (n = 2) comprises calc-alkaline basalt and mafic tuff and is locally intercalated with PP_{3-4} andesite (Fig. 3.8, 3.9a). The samples have very similar trace element profiles as PP_1 on extended spidergrams; however, they have overall lower absolute abundances of trace elements (Fig. 3.8). Similar to PP_1, the samples exhibit consistently strong Th enrichment (La_n/Th_n 0.2), strong Nb depletion (La_n/Nb_n 5.7) and negative Zr and Hf anomalies (Zr_n/Sm_n 0.5). However, this

group appears to lack Ti depletion, has stronger enrichment of LREE (La_n/Sm_n 3.9) and has flat HREE (Gd_n/Lu_n 1.1). PP_2 samples are primitive to moderately evolved (Mg# 70.5 to 58.7).

PP_3 and PP_4 (n = 12) comprise calc-alkaline arc andesite to rhyolite (SiO_2 49 to 73 wt%; Fig. 3.8, 3.9a). The types were separated on the basis of field characteristics, however, PP_3 and PP_4 have similar geochemical characteristics. PP_3 comprises feldspar (± quartz) volcanic rocks that generally occur in the lower portion of the stratigraphy, whereas PP_4 comprises quartz (± feldspar) volcanic rocks that occur higher in the stratigraphy. PP_3 and PP_4 have very similar trace and major element characteristics. Samples exhibit consistently strong Th enrichment (La_n/Th_n 0.2), strong Nb depletion (La_n/Nb_n 4.4) and generally prominent Ti depletion. Zr and Hf anomalies range from un-depleted to moderately depleted (Zr_n/Sm_n 0.8). There is strong enrichment of LREE (La_n/Sm_n 2.4) and moderate depletion of MREE (Gd_n/Lu_n 0.75) resulting in characteristic concave-up profile for these samples on N-MORB normalized spidergrams (Figure 3.8). The two types may be differentiated geochemically on the basis of the slope of HREE (Gd_n/Lu_n 2.6 (PP_3); 2.1 (PP_4)). PP_3 and PP_4 samples are moderately to strongly evolved (Mg# 47 to 56 (PP_3), 42 to 51 (PP_4)). Sm-Nd isotope composition analysis of two PP4 samples yielded ε_{Nd487} values of +4.7 and +5.5 (Table 3.3). The rocks of this suite plot in the volcanic arc field on a Yb – Ta plot (Fig. 3.9a; Pearce et al. 1984).

PP_5 is represented by a single moderately evolved (Mg# 57) sample of IAT that exhibits strong Th enrichment and prominent Nb depletion. There is slight enrichment of LREE (La_n/Sm_n 1.4) and slight depletion of MREE (Gd_n/Lu_n .85). This sample plots on the intersection of MORB – BAB – VAB fields La/10-Y/15-Nb plot (Fig. 3.9a; Cabanis and Lecolle 1989).

PP_6 (n = 2) comprises high silica trondhjemitic rhyolite (SiO_2 80 to 83 wt%; O'Connor 1965). Samples exhibit strong Th enrichment (La_n/Th_n 0.1), prominent Nb depletion (La_n/Nb_n 2.3), and strong Eu and Ti depletion. There are prominent positive Zr and Hf anomalies (Zr_n/Sm_n 1.4), strong enrichment of LREE (La_n/Sm_n 3.2) and prominent depletion of MREE (Gd_n/Lu_n 0.66). The samples are strongly evolved (Mg# 34 to 43). Sm-Nd isotope composition analysis of one sample yielded an ε_{Nd487} value of +3.89 (Table 3). The rocks of this suite plot on the boundary of arc and ocean ridge granite fields on the Yb – Ta plot (Fig. 3.9a; Pearce et al. 1984).

Wigwam Brook

The Dragon Pond Formation of the Wigwam Brook Group comprises five distinct geochemical types of volcanic rocks, referred to herein as WB_1 to WB_5. WB_1 is a high silica rhyolite (n = 2; SiO_2 76 to 84 wt%) and occurs near the base of the Dragon Pond Formation (Fig. 3.8, 3.9b). The samples exhibit strong Th (La_n/Th_n 0.2), Nb (La_n/Nb_n 0.5) and LREE (La_n/Sm_n 2.9) enrichment. Ti is strongly depleted, as is Eu in one sample. Sm-Nd isotope analysis of one sample yielded an ε_{Nd454} value of +6.0 (Table 3). The samples plot in within-plate field on granitoid discrimination plots (Fig. 3.9; Pearce et al. 1984).

WB_2 is andesitic (n=3; SiO_2 60 to 64 wt%) and occurs throughout the Dragon Pond Formation interlayered with group WB_3 rhyodacite (Fig. 3.8, 3.9b). The samples exhibit consistently strong Th enrichment (La_n/Th_n 0.2), strong Nb (La_n/Nb_n 5.9) and Ti depletion, prominent negative Zr and Hf anomalies (Zr_n/Sm_n 0.70) and strong enrichment of LREE (La_n/Sm_n 3.7) and flat HREE profile (Gd_n/Lu_n 1.1). The andesite is moderately evolved (Mg# 46 to 51). WB_2 samples plot on the boundary of the volcanic arc and ocean ridge/within plate granite field on granitoid discrimination plots (Fig. 3.9b; Pearce et al. 1984).

WB_3 andesite to rhyodacite (n = 7; SiO_2 58 to 74 wt%) exhibit consistently strong Th enrichment (La_n/Th_n 0.2), strong Nb depletion (La_n/Nb_n 4.3), strong Ti depletion, slight negative Zr and Hf anomalies (Zr_n/Sm_n 0.9) and strong enrichment of LREE (La_n/Sm_n 6.7) and slight enrichment of MREE (Gd_n/Lu_n 1.3). This geochemical type is strongly evolved (Mg# 16 to 50). The sample analysed for its Sm-Nd isotope composition was collected immediately above the breccia horizon and yielded an ε_{Nd454} –4.0 (Table 3). A second sample, which was collected stratigraphically below the breccia horizon, yielded an ε_{Nd454} –4.1. Although the geochemistry of this sample was not determined, the measured Sm-Nd ratio of <0.2 is consistent with other samples in this group (>0.2 in WB_2). WB_3 samples plot in the volcanic arc granite field on granitoid discrimination plots (Fig. 3.9b; Pearce et al. 1984).

WB_4 type comprises dacitic tuff (n = 2; SiO_2 67 to 69 wt%). The samples occupy an uncertain stratigraphic position in the northeastern part of the Wigwam Brook Group and are associated with rocks typical of the Dragon Pond Formation (Fig. 3.8, 3.9b). WB_4 is characterized

by strong Th enrichment (La_n/Th_n 0.2), strong Nb depletion (La_n/Nb_n 6.0), strong Ti depletion, slight negative Zr and Hf anomalies (average (Zr_n/Sm_n 0.7) and strong enrichment of LREE (La_n/Sm_n 3.1) and slight enrichment of HREE (Gd_n/Lu_n 0.8). WB_4 samples are strongly evolved (Mg# 33 to 42). They plot in the volcanic arc granite field on granitoid discrimination plots (Fig. 3.9b; Pearce et al. 1984).

WB_5 comprises several analyses of tholeiitic basalt (n = 4) and gabbro (n = 1; Fig. 3.8, 3.9b). The samples exhibit Th enrichment (La_n/Th_n 0.2 to 0.5), strong Nb depletion (La_n/Nb_n 4.2 to 6.9), negative Zr and Hf anomalies (Zr_n/Sm_n 0.6 to 0.8), prominent enrichment of LREE (La_n/Sm_n 1.2 to 2.6), slight enrichment to slight depletion of HREE (Gd_n/Lu_n 0.9 to 1.3). The samples plot in the field transitional between calc-alkaline basalt and island arc tholeiite on the La-Y-Nb discrimination plot (Fig. 3.9b; Cabanis and Lecolle 1989).

DISCUSSION

The Pats Pond and Wigwam Brook groups form the western most portion of the peri-Gondwanan Victoria Lake Supergroup. The adjacent rocks of the Red Indian Lake Group to the west display peri-Laurentian affinities (Zagorevski et al., in press; Chapter 2) and thus the Red Indian Line can be precisely defined to lie between the Wigwam Brook and Red Indian Lake groups (Fig. 3.1) where it is conveniently marked by black shale melange. In the following sections the tectonic settings and correlatives of the Pats Pond and Wigwam Brooks groups will be discussed and they will be placed into a regional tectonic framework. This enables a realistic tectonic model to be proposed for the Victoria Lake Supergroup and related tectonic elements in Newfoundland that is directly applicable to the correlative belts in New Brunswick and Maine.

Pats Pond Group and Correlatives

The c. 487 Ma age of the Pats Pond Group is distinctly younger than the adjacent rocks of the Cambrian Victoria Lake Supergroup (Fig. 3.1; c. 513-494 Ma; Dunning et al. 1991; Evans et al. 1990; Evans and Kean 2002) and is consistent with the interpretation that it does indeed form a distinct fault-bounded unit. The Pats Pond Group preserves a chemical stratigraphy that is entirely consistent with a supra-subduction zone origin. The transitional tholeiitic to calc-alkaline basalt (PP_1, PP_2) in the lower and middle Pats Pond Group has a strong arc signature as indicated by Th

and LREE enrichment and Nb depletion. Intermediate and felsic rocks higher in the stratigraphy (PP_3, PP_4) display similar characteristics indicative of an arc volcanic setting. The stratigraphically highest IAT (PP_5) and trondhjemitic rhyolite (PP_6) on the other hand have weak arc signatures, suggesting a transitional setting between an arc and backarc environment (Fig. 3.8, 3.9a). The upward transition from arc to backarc in the Pats Pond Group is interpreted to represent the progressive rifting of a dominantly extensional calc-alkaline arc.

Temporal equivalents to the Pats Pond Group occur in north-central Newfoundland and include the Exploits Group (c. 486 Ma, O'Brien et al. 1997), Wild Bight Group and South Lake Igneous complex (c. 489-486 Ma, MacLachlan and Dunning 1998a; O'Brien 1992), and New Bay Pond sequence (Jenner and Swinden 1992). These record transitions from arc tholeiite to trondhjemitic rhyolite to refractory backarc tholeiite (O'Brien et al. 1997), refractory arc tholeiite to boninite to non-arc tholeiite (MacLachlan and Dunning 1998a), and refractory arc tholeiite to non-arc tholeiite (Jenner and Swinden 1992), respectively. Eruption of refractory arc tholeiite and boninite in modern settings is generally associated with the propagation of a backarc spreading centre into an active arc (e.g., Tonga: Falloon and Crawford 1991; New Hebrides: Monzier et al. 1993). The tectonic setting of the Pats Pond Group and its temporally correlative sequences strongly suggests active rifting of a Tremadoc arc, generally referred to as the Penobscot Arc (van Staal et al. 1998).

This arc was generally accepted to be an ensimatic arc system in the Newfoundland Appalachians (e.g., Jenner and Swinden 1993; MacLachlan and Dunning 1998a; O'Brien et al. 1997). However, geochronology of the Pats Pond Group has revealed significant Proterozoic zircon inheritance. Presence of inherited zircon, in the c. 560 Ma and c. 0.9-1.2 Ga age range, is consistent with the presence of Gander-like crust in the source (e.g., Rogers et al. 2003; McNicoll et al. 2001; McNicoll et al. 2003; van Staal et al. 1996).

The age of the youngest inherited zircon is identical to the nearby, continentally contaminated Crippleback Igneous Suite and related Sandy Brook Group (Fig. 3.2; Evans et al. 1990; Kerr et al. 1995; Appendix 2) suggesting a magmatic link. Although no zircon inheritance has been identified in the Crippleback Igneous Suite, the Sm-Nd isotopic data indicate c. 1.1-1.3 Ga T_{DM}

ages (Kerr et al. 1995) consistent with presence of Mesoproterozoic crust in the source region similar to the older inherited population of zircon in the Pats Pond Group. We thus interpret the Pats Pond group to have erupted in an ensialic arc setting above attenuated Cripplebeck basement. Cripplebeck Igneous Suite has been recently proposed to form a remnant of Ganderian basement in central Newfoundland (Appendix 2).

Low ε_{Nd} values (-0.5 to +0.3) in the Pats Pond mafic volcanic rocks (PP_1) likewise support the interaction of magma with mature continental crust. The role of continental material in the genesis of the Pats Pond Group can qualitatively investigated using the Sm-Nd isochron diagram to illustrate possible mixing/partial melting relationships (Fig. 3.10). Three hypothetical sources are used in the discussion of the isotopic data: depleted mantle (DM), subducted continental material (SCM), and exposed continental material (ECM). The DM field for the Tremadocian mantle follow Jenner and Swinden (1993) and is in excellent agreement with the composition of Ordovician ophiolitic rocks in Newfoundland. The SCM field represents the range of Gander Zone meta-sedimentary rocks that could have been subducted in the Tremadoc and is also representative of the Gander Zone continental basement (compiled from D'Lemos and Holdsworth 1995; Kerr et al. 1995; c.f. Jenner and Swinden 1993). The ECM field is derived from the exposed Proterozoic igneous and volcanic rocks (Fig. 3.2; Cripplebeck Intrusive Suite and Sandy Brook Group: Appendix 2; Kerr et al. 1995) that may represent portions of the basement to the Penobscot Arc (Appendix 2). The ECM is similar to the SCM, however it has a lower $^{147}Sm/^{144}Nd$ ratio and higher ε_{Nd} values.

The PP_1 calc-alkaline basalt plots within a mixing field between DM and SCM/ECM sources. A simple mixing relationship is consistent with the high Mg# (66.5 and 70.5) indicating that the basalts likely represent relatively unfractionated liquids. PP_4 felsic rocks have lower $^{147}Sm/^{144}Nd$ than would be expected if a simple mixing model of the DM and SCM source components were assumed. An addition of a third component, such as a low-degree partial melt of either DM or SCM (similar to ECM), could easily explain the observed data.

Similar to Pats Pond Group, Sm-Nd isotope data of the Wild Bight Group (MacLachlan and Dunning 1998a; Swinden et al. 1990) indicate influence of continental material in the source area of the magmatic rocks of the Penobscot Arc. In the absence of clear zircon inheritance, this has been

interpreted to represent contamination of the magma source region by subduction of continentally–derived sedimentary material. An entirely ensimatic setting for the Wild Bight and Exploits groups would require a transition from continental to oceanic arc substrate along strike of the Penobscot Arc, and trench parallel transport of arc and basement-derived sediment from areas of ensialic magmatism (see below). Such transition would generally reflect major irregularities in the Gander continental margin relative to the strike of the arc (e.g., Kermadec Arc: Gamble et al. 1995) and can be explained by local transgression of the Penobscot Arc onto oceanic crust adjacent to such irregularities in the margin during arc-trench migration. Alternatively, the Wild Bight Group could represent advanced stages of rifting of an ensialic magmatic arc.

Evolution of the Penobscot Arc

The Cambrian to Lower Ordovician portions of the Victoria Lake Supergroup, which include Pats Pond Group, form part of the extensive Penobscot Arc system that extends from Newfoundland to Maine (van Staal et al. 1998). Improved understanding of the provenance and significance of the Victoria Lake Supergroup and the adjacent units in Newfoundland allows us to evaluate the tectonic models of the Penobscot Arc system.

In the Victoria Lake Supergroup, the arc complexes become progressively younger towards the Red Indian Line. From east to west these include Tally Pond (c. 513 Ma: Dunning et al. 1991; Appendix 2), Long Lake (c. 505 Ma: McNicoll, unpublished data; van Staal et al., in press c), Tulks (c. 498 Ma: Evans et al. 1990) and Pats Pond groups (c. 487 Ma; see above). Similarly, the Wild Bight and Exploits groups (c. 486-489 Ma) are also located along the Red Indian Line in north-central Newfoundland. Although such a distribution could be due to a complicated deformation history, it more likely reflects the original relative positioning of these magmatic phases. Hence, since the Tremadoc phase of an extensional Penobscot Arc should be situated trench-ward from the Cambrian phases, the trench should lie to the west (Fig. 3.2, 3.11a). The Penobscot ophiolites (c. 494 Ma: Dunning and Krogh 1985) interpreted to have formed in a backarc tectonic setting (Jenner and Swinden 1996) are currently positioned to the east of the Cambro-Ordovician Penobscot Arc, consistent with the proposed trench location to the west.

The current distribution of the arc-backarc complexes indicates that the Penobscot Arc was formed above an east dipping (present coordinates) subduction zone. The earliest known supra-subduction zone magmatism was occurring by c. 513 Ma (Tally Pond Group in Newfoundland; Dunning et al. 1991, Appendix 2; Mosquito Lake Formation in New Brunswick: McLeod et al. 2003; Johnson and McLeod 1996), along an attenuated or perhaps irregular Gander margin (Fig. 3.11a'). The presence of Gander margin is indicated by basement-cover relationships (Appendix 2; van Staal et al., 2004; Johnson and McLeod 1996), zircon inheritance data (Squires and Moore 2004) and Sm-Nd isotopic characteristics (Fig. 3.12; Appendix 2). Ensialic arc volcanism (e.g., Rogers 2004) was occurring until c. 494 Ma, when the Penobscot backarc basin was formed (Jenner and Swinden 1993) separating the ensialic Penobscot Arc from its parent (Ganderian) microcontinent. Similar to the ensialic portions of the Penobscot Arc, the Penobscot backarc basin ophiolites show evidence of contamination by crustal material (Jenner and Swinden 1993) suggesting rifting of an ensialic basement. Following the rifting event, calc-alkaline ensialic arc volcanism was re-established by c. 490 Ma (Pats Pond Group) while portions of the Penobscot arc were still undergoing active extension (e.g., Wild Bight Group: MacLachlan and Dunning 1998a; Swinden et al. 1990; Exploits Group: O'Brien et al. 1997).

A prominent magmatic gap in the arc-magmatism in the Exploits Subzone (c. 485-480 Ma; van Staal et al. 1998) coincides with the obduction of the Penobscot backarc basin ophiolites onto the Gander passive margin prior to c. 478 Ma (Colman-Sadd et al. 1992; Tucker et al. 1994) and an unconformity on the Gander Zone in Newfoundland and east-central Maine (Boone et al. 1989). Previously this has been interpreted to mark the arc-continent collision with the west-dipping subduction attached to the Gander Margin (Fig. 3.11a; MacLachlan et al. 1998; van Staal et al. 1994), however this is inconsistent with an east-dipping subduction zone model proposed above where Gander margin is never subducted.

The reason for the inversion of the Penobscot backarc basin in incompletely understood at present, although evidence for an outboard collision event may be preserved in the Notre Dame Bay area of Newfoundland. The Summerford Group basalts (at least Tremadoc: Kay 1967) have been interpreted as remnants of a seamount(s) (Jakobi and Wasowski 1985). The tectonic position

of the Summerford seamount in the Dunnage melange and along the Red Indian Line suggests that it was accreted to the Penobscot Arc starting in Tremadoc (van Staal et al. 1998). During the accretion of the Summerford Seamounts the Penobscot backarc basin was still young (~10 m.y.). Investigations of the structure of young ensialic backarc basins indicate that they develop a strong asymmetry with the spreading concentrated near the magmatic front, where the lithosphere is the weakest (e.g., Barker et al. 2003). This inherent asymmetry favours the obduction of backarc crust onto the continental margin if the ensialic arc and young backarc are placed under compression (e.g., Rocas Verdes: Dalziel 1986; Barker et al. 2003). Accretion of the outboard Summerford Seamounts may thus certainly be a viable cause for the Penobscot Orogeny and accompanying magmatic gap. Following the obduction of the Penobscot ophiolites, felsic arc-related plutons intruded the Gander margin and stitched the Penobscot ophiolites by 478-474 Ma (e.g., Colman-Sadd et al. 1992; Tucker et al. 1994), placing an upper age constraint on the age of the Penobscot Orogeny in Newfoundland.

Tectonic setting of the Wigwam Brook Group

The Wigwam Brook Group is the youngest known tectono-stratigraphic unit in the Victoria Lake Supergroup. The Wigwam Brook Group unconformably overlies the Pats Pond Group indicating deposition above Penobscot Arc basement. Chemistry of the volcanic rocks indicates that there are two distinct tectonic settings preserved in the basal Dragon Pond Formation. High silica rhyolite (WB_1) near the base of the Dragon Pond Formation lacks arc signature and plots in part in the within-plate field on granitoid tectonic discrimination diagram (Pearce et al. 1984), and could have erupted in a tectonic setting such as a rifting ensialic arc. The age of eruption of WB_1 rhyolite is poorly constrained at present and it may be significantly older that the overlying volcanic rocks (454-485 Ma). The proposed extensional setting is consistent with the dominantly extensional evolution of the Victoria Arc in the Middle Ordovician (e.g., MacLachlan and Dunning 1998b; O'Brien et al. 1997; van Staal et al. 1998). Alternatively, this unusual chemistry may be related to ridge subduction inferred for the broadly correlative portions of the Bathurst Supergroup of New Brunswick (Rogers et al. 2003; van Staal et al. 2003).

Felsic volcanic rocks that are geochemically different were deposited above the WB_1 rhyolite and associated volcanoclastic sediments. WB_{2-4} andesitic and dacitic rocks exhibit LREE enrichment and Nb depletion consistent with derivation in a volcanic arc setting. The low ε_{Nd} values (-4.0) in WB3 dacite indicate strong influence of mature continental crust in the source (T_{DM} ~1370 Ma). The associated mafic volcanic rocks near the top of the Dragon Pond Formation also indicate eruption in a volcanic arc setting. The predominantly felsic volcanic activity combined with very low ε_{Nd} values, zircon inheritance and basement-cover relationships indicate eruption of the Dragon Pond Formation in a mature ensialic arc setting above composite Penobscot and Gander basement.

The upper portions of the Dragon Pond Formation record waning of volcanic activity, suggesting a significant change in tectonic environment. The overlying Halfway Pond and Perrier's Pond Formations are predominantly sedimentary. Shale and immature wacke comprise the Halfway Pond Formation while shale and black shale dominate the Perrier's Pond Formation. The transition from Dragon Pond Formation to Halfway Pond and Perrier's Pond formations is interpreted to represent the shut off of ensialic arc volcanism. Volcanism shut off is well documented elsewhere in the Exploits Subzone. The predominantly volcanic Victoria Lake Supergroup is (un-) conformably overlain by marine black shale and turbidite sequence of the Caradoc to Llandovery Badger Group (Williams et al. 1993).

Evolution of the Victoria Arc

Following the Penobscot Orogeny, Middle to Upper Ordovician rocks of the Victoria Lake Supergroup were deposited on the composite Penobscot - Gander basement. Volcanic rocks of the Victoria Lake Supergroup were erupted in various arc-related settings related to the Victoria Arc magmatism in central Newfoundland (e.g., Evans and Kean 2002). The oldest dated felsic ensialic arc volcanic rocks in the Victoria Lake Supergroup are contained in a structural panel immediately to the east of the Wigwam Brook Group (c. 453 Ma), within the c. 462 Ma (Dunning et al. 1987) Sutherlands Pond Group (Rogers et al., 2005a), which contains E-MORB-like basalt (Upper Basalts: Evans and Kean 2002). Coeval calc-alkaline arc felsic and E-MORB mafic magmatism suggests the presence of an immature backarc basin to the east of the Wigwam Brook arc

volcanics. Further to the east, the Middle Ordovician Diversion Lake Group (Kean and Mercer 1981) basalts and Harpoon Gabbro intrusive suite (465±2: Pollock et al. 2002; 2004) have enriched within plate characteristics with tholeiitic and calc-alkaline affinities (Evans and Kean 2002; Pollock and Wilton 2001), suggestive of rifting of ensialic basement. Similar to the older portions of the Victoria Lake Supergroup, this configuration most simply reflects the location of the trench to the west of the arc – backarc along or underneath the Red Indian Line.

Correlative arc sequences to the Victoria Arc include the Wild Bight-Exploits Arc and backarc in the north-central Newfoundland (MacLachlan et al. 2001) and Popelogan Arc – Tetagouche backarc in New Brunswick (van Staal et al. 1998). The oldest supra-crustal rocks in Newfoundland include the Upper Wild Bight Group (Fig. 3.2; c. 473 Ma: MacLachlan et al. 1998b) and Upper Exploits Group (Fig. 3.2; Arenig: O'Brien et al. 1997). The Wild Bight Group records the establishment of ensialic calc-alkaline arc magmatism above composite Gander and Penobscot basement and subsequent rifting of this arc (MacLachlan et al. 1998). The stratigraphy of the adjacent Exploits Group also indicates opening of a backarc in which the sedimentation was active until at least the Caradoc (O'Brien et al. 1997). Similarly, calc-alkaline magmatism was established in the Popelogan Arc in New Brunswick by c. 474 Ma (e.g., Rogers et al. 2003) followed by the opening of the Tetagouche backarc basin (e.g., Staal et al., 1991; Rogers and van Staal 2003; van Staal et al. 1998).

The distribution of the Popelogan – Victoria Arc and Exploits – Tetagouche backarc complexes indicates east-dipping subduction underneath the Gander margin, which culminated in the opening of the wide Japan Sea-like Exploits – Tetagouche backarc basin (e.g., van Staal, 1994; Rogers and van Staal 2003; MacLachlan et al. 2001; O'Brien et al. 1997; van Staal et al. 1998). Volcanism and sedimentation in the Victoria – Popelogan Arc and Exploits – Tetagouche backarc were active until the Caradoc, followed by a general cessation of arc volcanism (Victoria Arc: see above, Williams et al. 1993; Popelogan Arc: van Staal et al. 1991), syn-tectonic sedimentation (Badger Group: Williams et al. 1993), and the unroofing of the peri-Gondwanan (van Staal et al. 1991) and peri-Laurentian (e.g., Bostock 1978; Dunning et al. 1987; Kean 1983) arc complexes. Subsequently deposited syn-tectonic sedimentary rocks in the Exploits Subzone contain detrital

contribution from both the Notre Dame Arc and Laurentian basement (Badger Group: McNicoll et al. 2001; Nelson 1981). This evidence suggests Upper Caradoc collision of the peri-Gondwanan Victoria – Popelogan arc and the peri-Laurentian Annieopsquotch Accretionary Tract along the Red Indian Line and closure of the main tract of Iapetus (van Staal et al. 1998; Chapter 2).

CONCLUSIONS

Two new peri-Gondwanan tectono-stratigraphic units, the Tremadoc Pats Pond Group and unconformably overlying Caradoc Wigwam Brook Group, have been identified through detailed mapping and high-resolution geochemistry and geochronology in the Victoria Lake Supergroup in Newfoundland. The Pats Pond and Wigwam Brook groups define the western-most extent of the Victoria Lake Supergroup and the position of the Red Indian Line. They also preserve the last stages of volcanism and sedimentation of the Penobscot and Victoria arcs and provide constraints on the evolution of these two arc systems. The tectonic model for the Penobscot Arc presented herein differs from the previously proposed models with the ensialic Penobscot Arc built above an east-dipping (present coordinates) subduction zone along the Gander margin. Ensialic Penobscot arc volcanism was active from 513 to 485 Ma, and at least in part was accompanied by opening of an oceanic backarc basin. Obduction of the backarc ophiolites onto the Gander Margin at 485-480 Ma and the local formation of unconformities on the Gander margin mark the Penobscot Orogeny, which formed in response to closing the back arc basin and resulted in an arc magmatic gap. Calc-alkalic arc magmatism was re-established above an east-dipping subduction zone by at least c. 473 Ma (Fig. 3.11b; e.g., MacLachlan and Dunning 1998b; Rogers et al. 2003). The Popelogan – Victoria Arc formed in a generally extensional setting, as indicated by the eruption of coeval non-arc volcanic rocks, and the formation of the wide Japan Sea-like Exploits – Tetagouche backarc basin (Fig. 3.11b; van Staal, 1994; O'Brien et al. 1992; MacLachlan and Dunning 1998b; Rogers and van Staal. 2003; van Staal et al. 1998). Magmatism and sedimentation in the Victoria – Popelogan Arc and Tetagouche-Exploits backarc continued until the Caradoc collision with the Peri-Laurentian Red Indian Lake Arc (e.g., Rogers and van Staal 2003; O'Brien et al. 1992; Dunning et al. 1987; van Staal et al. 1998), marking the closure of the main portion of Iapetus and the arrival of the leading edge of Ganderia to the Laurentian margin. Subsequently, subduction stepped back into the

Tetagouche – Exploits backarc basin, closing the remainder of the Iapetus by the end Early Silurian (Fig. 3.11b; e.g., van Staal et al. 1998), which led to the Salinic Orogeny.

Figure 3-1 Simplified geology of the study area (modified from Kean, 1979b; Lissenberg et al., 2005c; Rogers et al., 2005a; van Staal et al., 2005 a, b, c). U/Pb ages compiled from Dunning and Krogh (1985), Dunning et al. (1987), Evans et al. (1990), Zagorevski et al. (2006). Polygons A and B indicate the location of detailed maps in Figures 3.3a and 3.3b respectively. Inset: Lithostratigraphic subdivisions of Newfoundland (after Williams, 1995). RIL – Red Indian Line

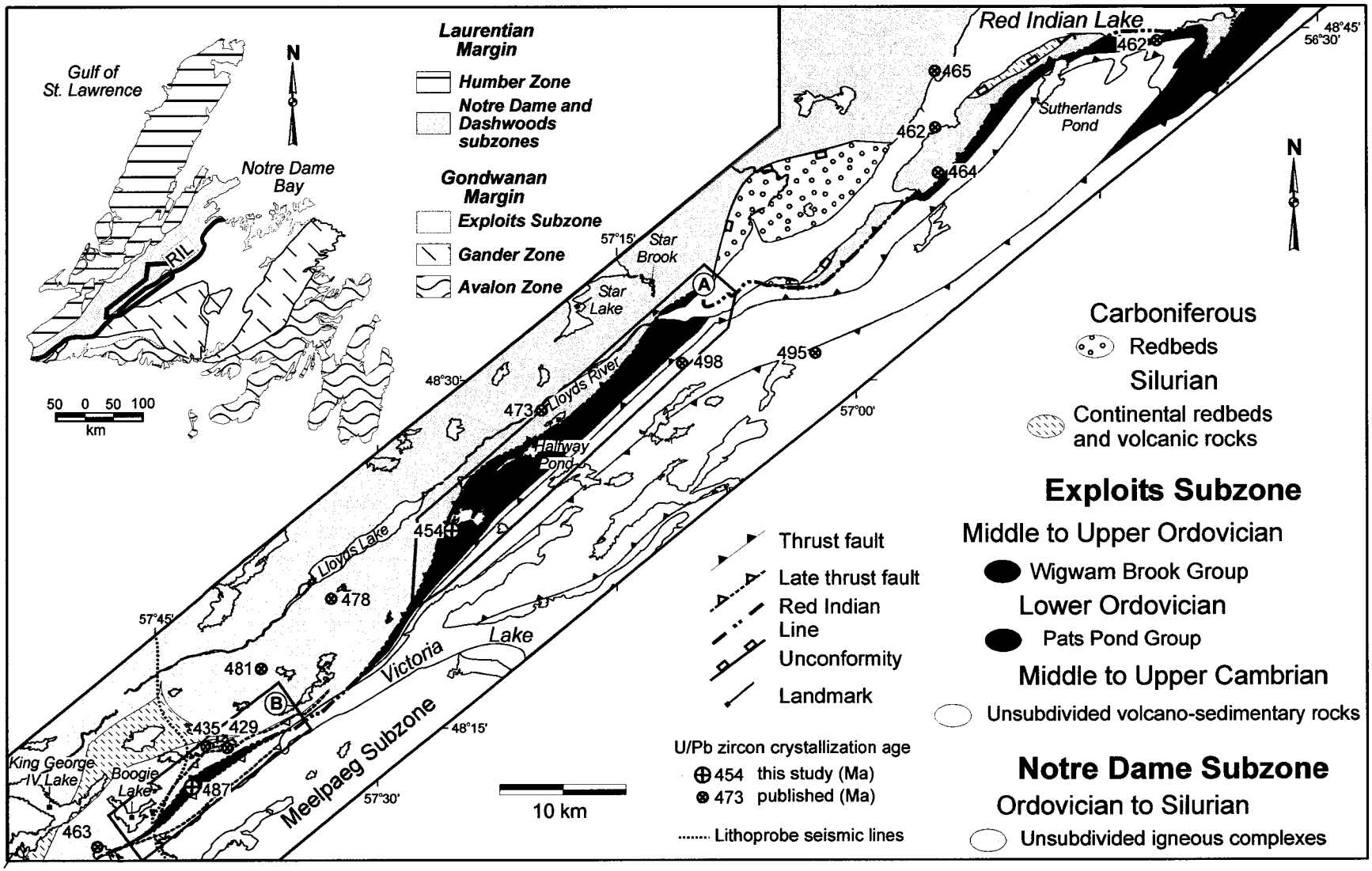
Gulf of St. Lawrence
Notre Dame Bay
RIL
N
50 0 50 100
km
Laurentian Margin
Humber Zone
Notre Dame and Dashwoods subzones
Gondwanan Margin
Exploits Subzone
Gander Zone
Avalon Zone
Red Indian Lake
Sutherlands Pond
Star Brook
Star Lake
Lloyds River
Lloyds Lake
Victoria Lake
Meelpaeg Subzone
Boogie Lake
King George IV Lake
48°45'
56°30'
48°30'
57°15'
57°00'
57°45'
48°15'
57°30'
462
465
464
498
495
473
454
478
481
435
429
487
463
10 km
Thrust fault
Late thrust fault
Red Indian Line
Unconformity
Landmark
U/Pb zircon crystallization age
454 this study (Ma)
473 published (Ma)
Lithoprobe seismic lines
Carboniferous
Redbeds
Silurian
Continental redbeds and volcanic rocks
Exploits Subzone
Middle to Upper Ordovician
Wigwam Brook Group
Lower Ordovician
Pats Pond Group
Middle to Upper Cambrian
Unsubdivided volcano-sedimentary rocks
Notre Dame Subzone
Ordovician to Silurian
Unsubdivided igneous complexes

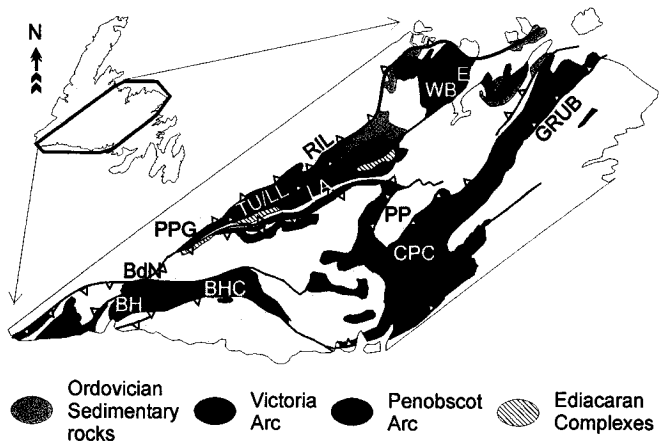

Figure 3-2 Distribution of Ediacaran Suites, Cambro-Ordovician Popelogan arc, and Ordovician Victoria arc complexes in Newfoundland (modified from van Staal et al. 1998). BdN - Bay du Nord Group; BH - Baggs Hill Granite; BHC - Blue Hills of Couteau ophiolite Complex; CPC - Coy Pond Complex; E - Exploits Group; GRUB - Gander River Ultrabasic Belt; PP - Pipestone Pond Complex; PPG - Pats Pond Group; RIL - Red Indian Line; TP - Tally Pond Group; TU - Tulks; WB - Wild Bight Group.

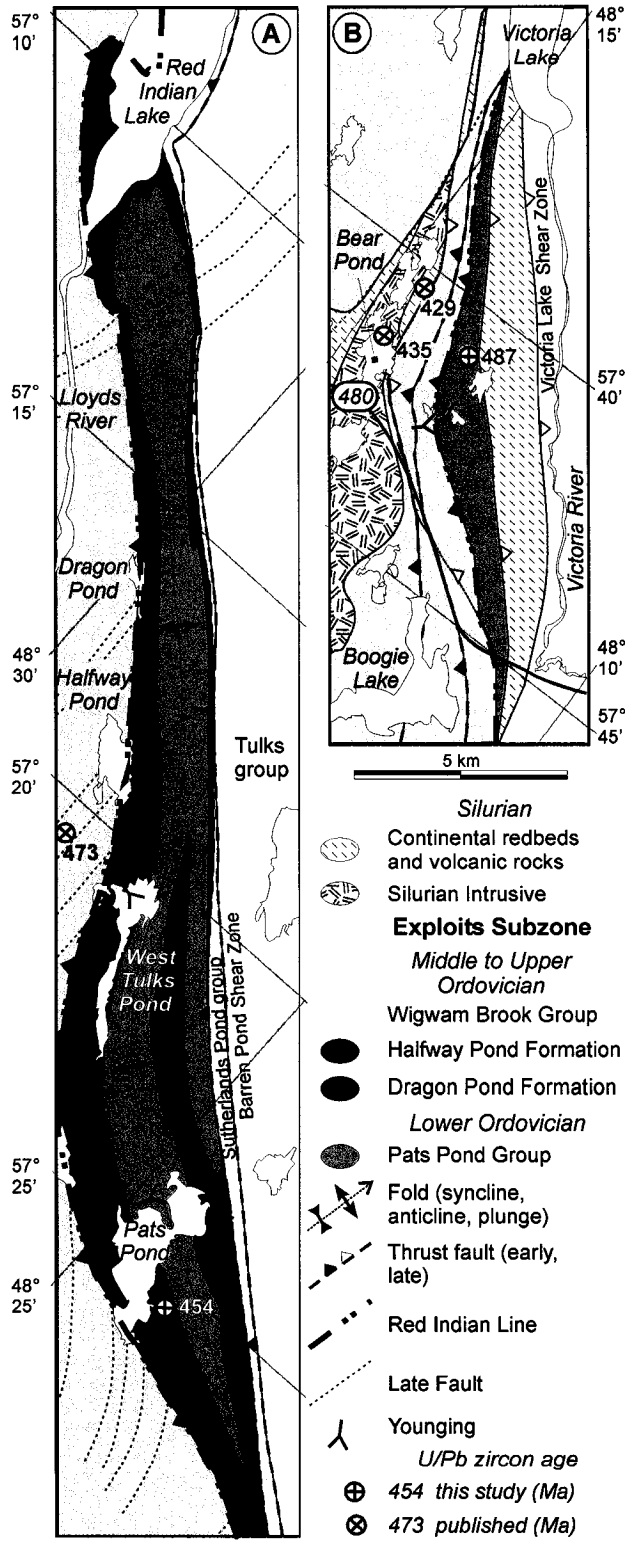

Figure 3-3 Detailed geology of Pats Pond - Red Indian Lake area and Route 480 area. Compiled U/Pb zircon age from Zagorevski et al. (2006).

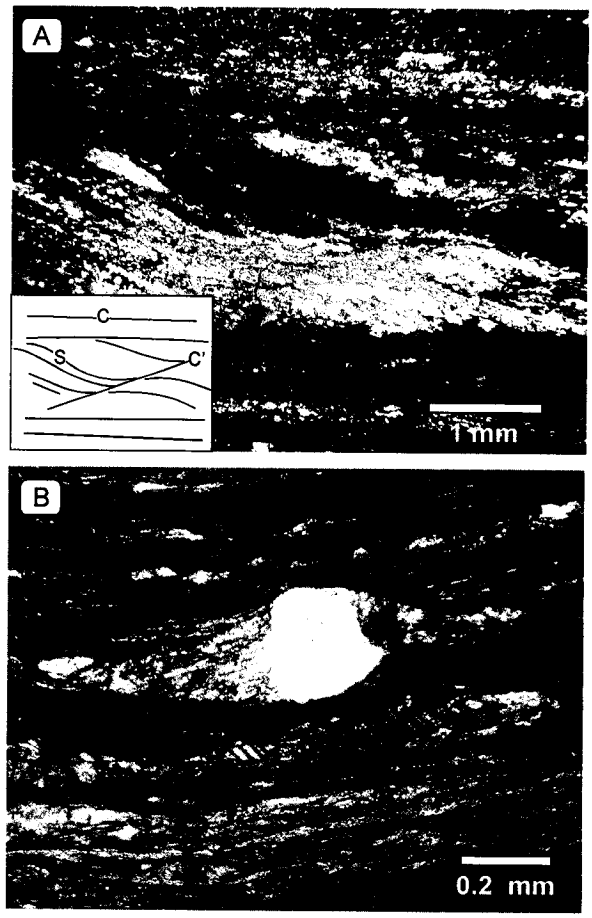

Figure 3-4 Photomicrographs of tectonites bounding the Pats Pond and Wigwam Brook groups. (a) Horizontal thin section of highly deformed Halfway Pond Formation meta-sedimentary rock marking the Red Indian Line displaying well-developed S-C-C' fabric indicating sinistral transcurrent shear; parallel to lineation, perpendicular to foliation, CPL; (b) Quartz porphyroclast with carbonate-rich strain shadow in the Barren Pond shear zone phyllonite, PPL.

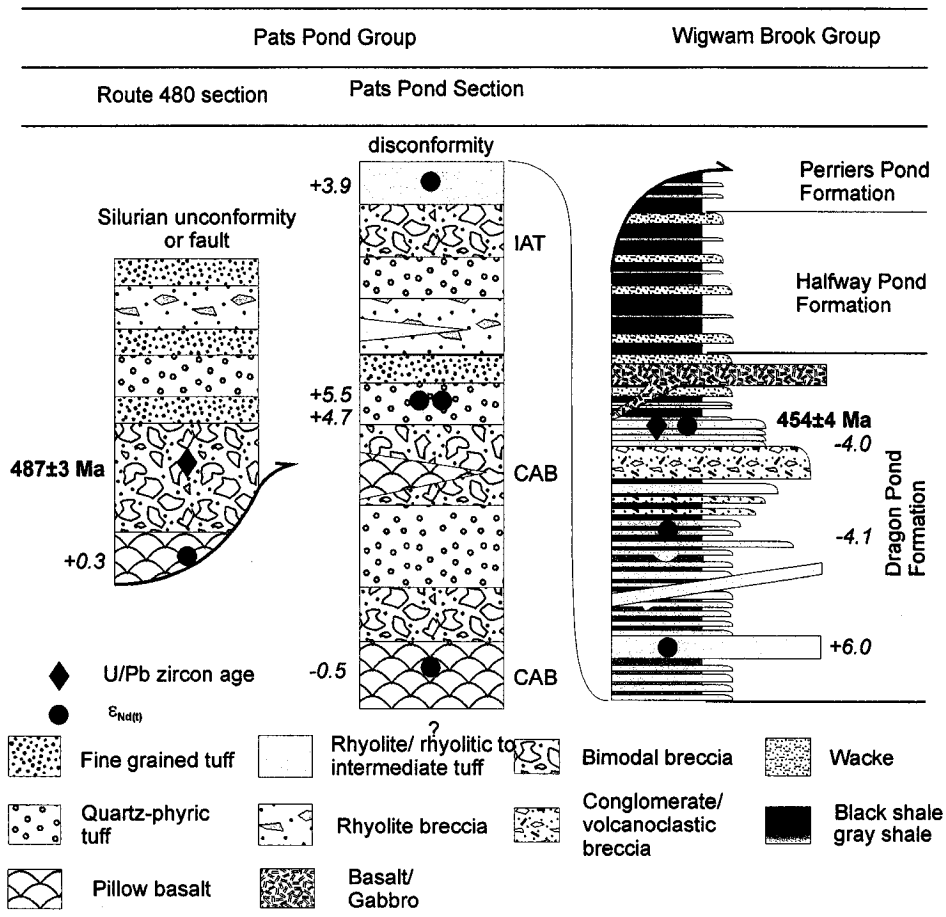

Figure 3-5 Schematic stratigraphy of Tremadocian Pats Pond and upper Ordovician Wigwam Brook groups.

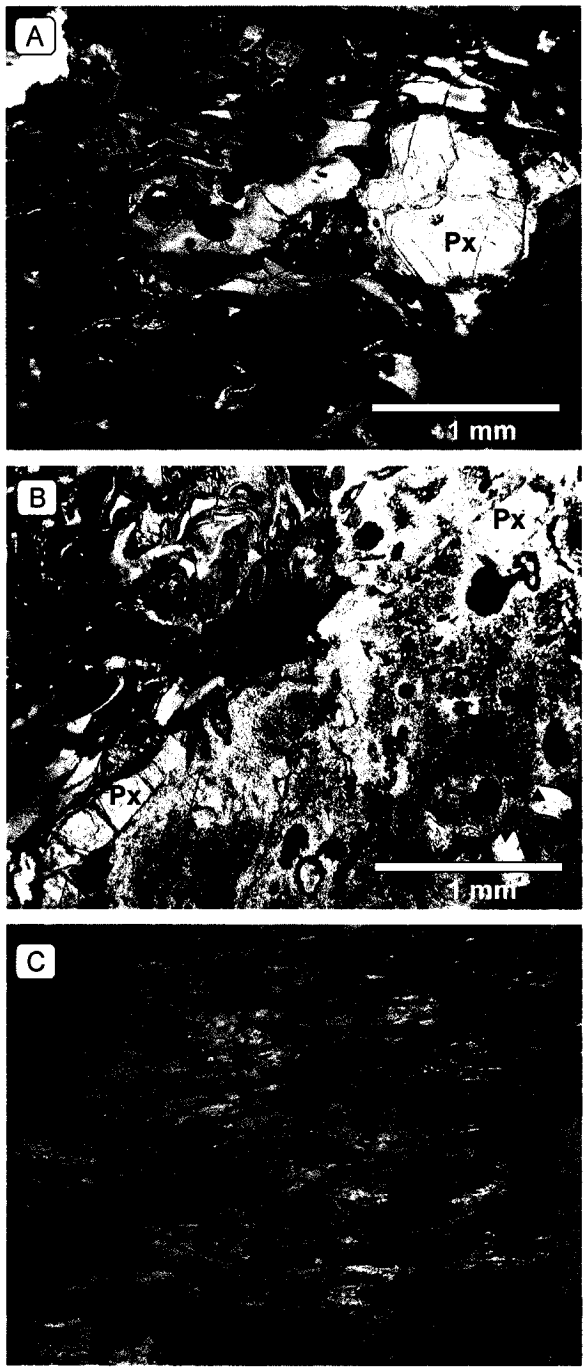

Figure 3-6 Pats Pond Group bimodal tuff breccia unit; Photomicrocgraphs (PPL) of (a) pyroxene glomeroporphyritic mafic tuff matrix, (b) intermediate, pyroxene porphyritic lapilli in mafic tuff matrix (top left). (c) Tuff breccia unit at the dated locality of Wigwam Brook Formation containing accidental fragments of underlying epiclastic tuff, shale and dark shale (arrows), which were locally folded during subsequent deformation.

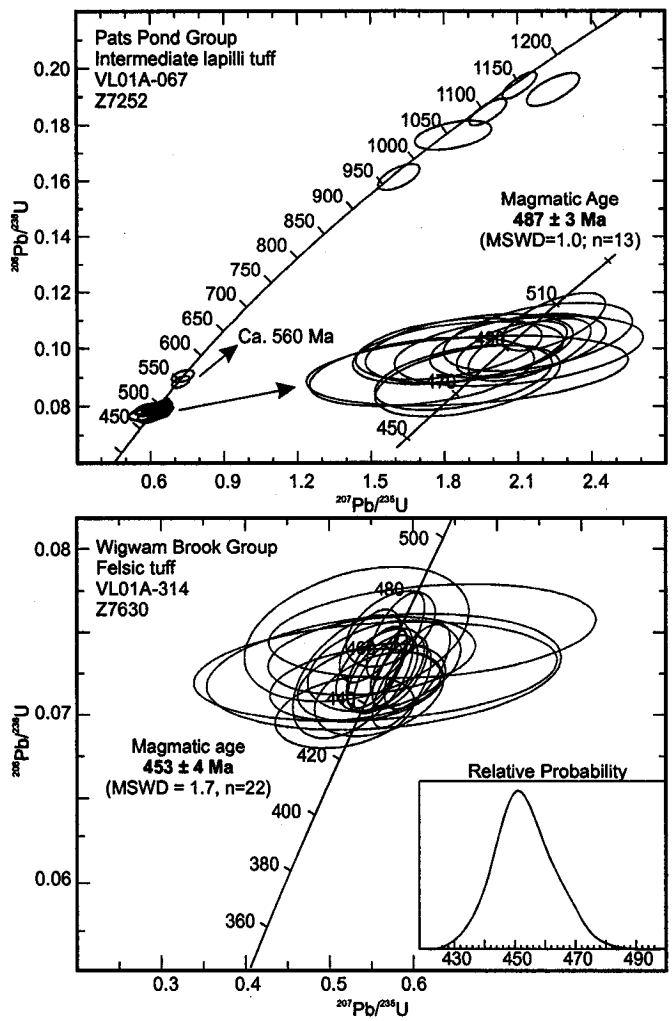

Figure 3-7 U/Pb concordia diagrams for the Pats Pond (a) and Wigwam Brook (b) groups. MSWD - Mean Square of Weighted Deviates of concordance and equivalence (Ludwig, 2001)

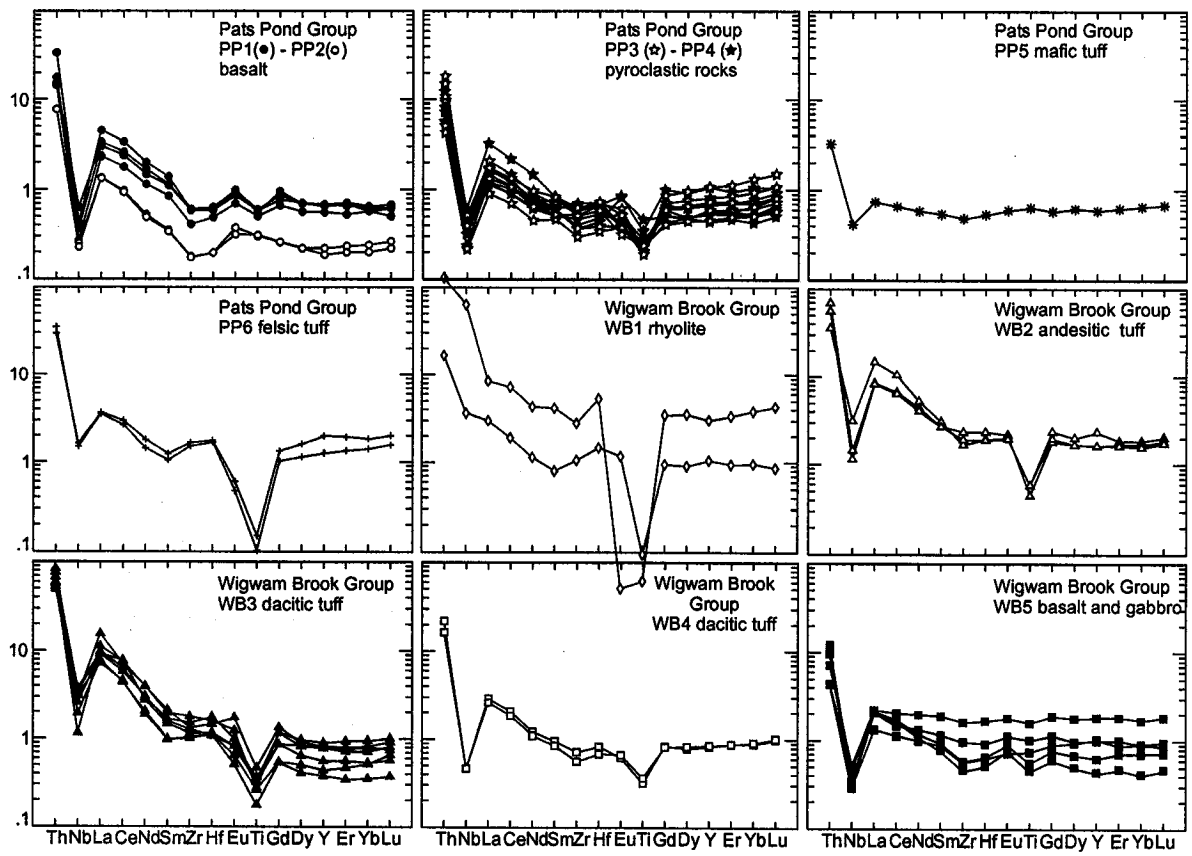

Figure 3-8 Chemical characteristics of the Pats Pond and Wigwam Brook groups (N-MORB normalized, Sun and McDonough, 1989).

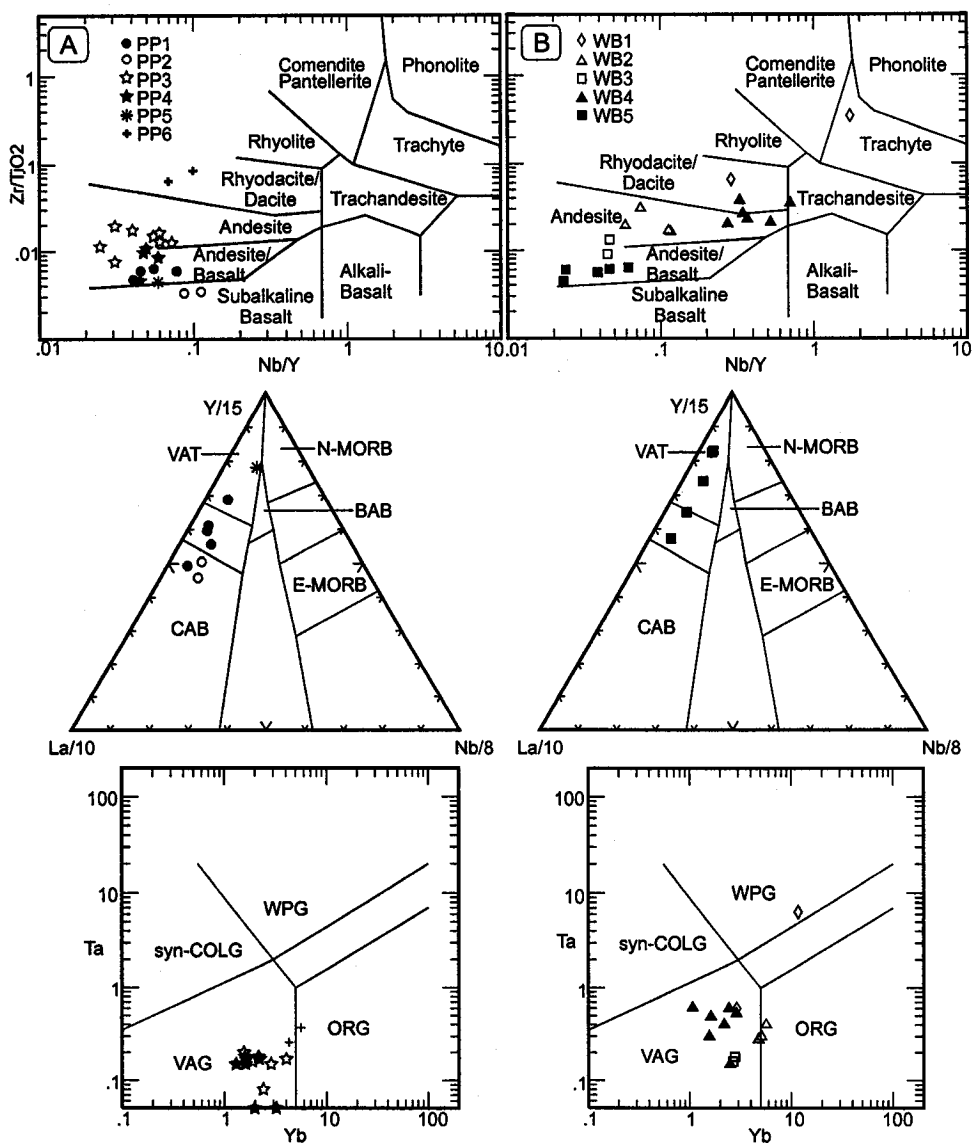

Figure 3-9 Nb/Y vs. Zr/TiO2 rock type classification (Winchester and Floyd, 1977), La/10-Y/15-Nb/8 (Cabanis and Lecolle, 1989) and Yb vs. Ta (Pearce et al. 1984) tectonic discrimination diagrams for Pats Pond and Wigwam Brook Groups.

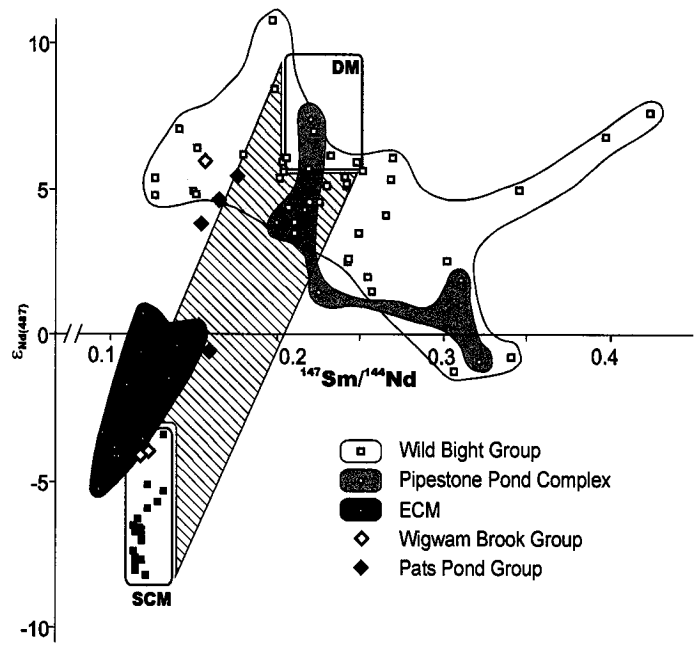

Figure 3-10 Sm-Nd diagram demonstrating the range of values in the Lower Ordovician Pats Pond and Upper Ordovician Wigwam Brook groups. The range of values in Lower Ordovician Wild Bight Group (MacLachlan and Dunning, 1998a; Swinden et al. 1990), Upper Cambrian Pipestone Pond Complex (Jenner and Swinden, 1993) is plotted for reference. Field with diagonal lines illustrates mixing trend between SCM and DM. ECM (exposed continental material), SCM (subducted continental material), DM (depleted mantle); see text for discussion.

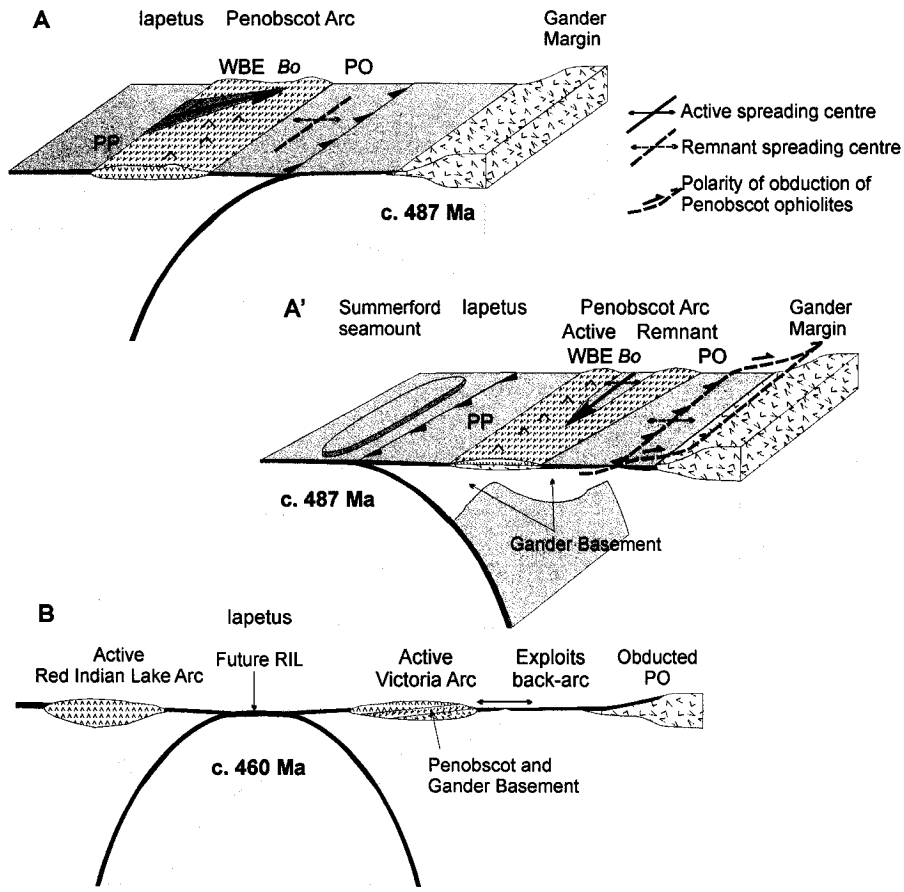

Figure 3-11 Upper Cambrian tectonic evolution of the Penobscot arc (A-A') and its convergence with the Gander margin; and Upper Ordovician tectonic evolution of the Victoria Lake arc (B) and its convergence with the peri-Laurentian Red Indian Lake arc and Annieopsquotch Accretionary Tract. (A) and (A') represent alternate models for obduction of Penobscot ophiolites onto the Gander margin. Bo - boninite; PO - Penobscot Ophiolites; PP - Pats Pond Group; WBE - Wild Bight and Exploits groups.

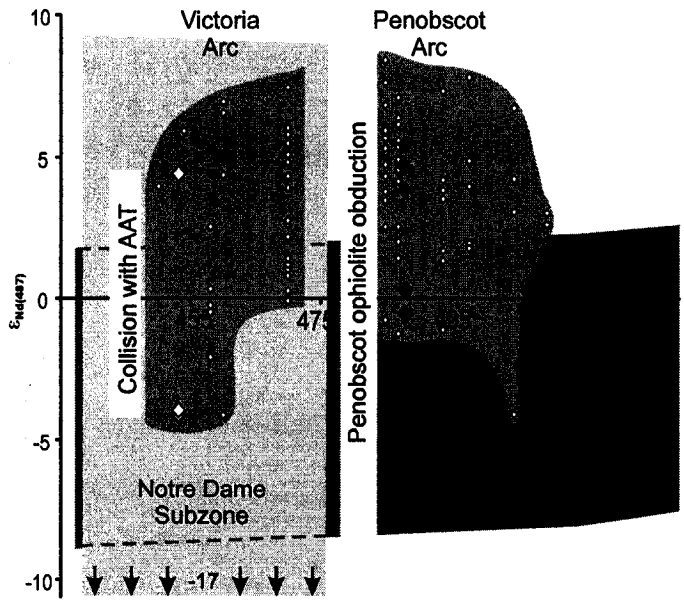

Figure 3-12 Nd isotope evolution diagram of the arc and back-arc complexes of the Penobscot and Victoria Lake arcs showing initial εNd plotted vs. age. Large diamonds - this study, small diamonds and fields - compiled from Jenner and Swinden (1993), Kerr et al. (1995), MacLachlan and Dunning (1998 a, b), Rogers (2004), Swinden et al. (1990, 1997), Whalen et al. (1997).

Table 3-1: U/Pb SHRIMP analytical data

Spot name	U (ppm)	Th (ppm)	Th/U	Pb* (ppm)	^{204}Pb (ppb)	^{204}Pb/^{206}Pb	±^{204}Pb/^{206}Pb	f(206)^{204}	^{206}Pb/^{205}Pb	±^{206}Pb/^{205}Pb	^{207}Pb/^{235}U	±^{207}Pb/^{235}U	^{206}Pb/^{238}U	±^{206}Pb/^{238}U	Corr Coeff	^{207}Pb/^{206}Pb	±^{207}Pb/^{206}Pb	Ages (Ma)[1] ^{206}Pb/^{238}U	±^{206}Pb/^{238}U	^{207}Pb/^{206}Pb	±^{207}Pb/^{206}Pb	Ages (Ma)[2] ^{206}Pb/^{238}U	±^{206}Pb/^{238}U
VLA01-067 (Z7252)																							
7252-18.1	116	64	0.569	9	3	0.000446	0.000117	0.0077	0.1846	0.0087	0.5962	0.0240	0.0766	0.0011	0.461	0.0565	0.0020	476	6	472	82	475	6
7252-25.1	157	79	0.519	13	3	0.000316	0.000114	0.0055	0.1562	0.0051	0.5936	0.0231	0.0768	0.0010	0.444	0.0561	0.0020	477	6	454	80	477	6
7252-2.1	91	44	0.494	7	2	0.000328	0.000155	0.0057	0.1477	0.0069	0.5672	0.0292	0.0772	0.0011	0.381	0.0533	0.0026	480	6	340	113	481	6
7252-54.1	101	50	0.509	8	4	0.000534	0.000232	0.0093	0.1650	0.0096	0.5960	0.0418	0.0773	0.0011	0.316	0.0559	0.0038	480	6	449	156	480	6
7252-43.1	135	76	0.581	11	3	0.000290	0.000107	0.0050	0.1811	0.0072	0.5902	0.0274	0.0787	0.0010	0.383	0.0544	0.0024	488	6	389	100	489	6
7252-49.1	106	32	0.315	8	3	0.000373	0.000160	0.0065	0.0969	0.0066	0.6288	0.0322	0.0788	0.0011	0.383	0.0579	0.0028	489	6	525	108	488	6
7252-26.1	187	120	0.661	16	2	0.000139	0.000066	0.0024	0.2145	0.0037	0.6358	0.0159	0.0789	0.0010	0.590	0.0584	0.0012	490	6	546	45	489	6
7252-23.1	120	49	0.421	10	3	0.000383	0.000123	0.0063	0.1365	0.0053	0.5843	0.0242	0.0790	0.0010	0.406	0.0537	0.0021	490	6	357	88	492	6
7252-48.1	214	142	0.686	19	2	0.000119	0.000059	0.0021	0.2188	0.0035	0.6244	0.0143	0.0790	0.0009	0.573	0.0573	0.0011	490	5	505	42	490	5
7252-37.1	122	68	0.576	10	3	0.000350	0.000136	0.0061	0.1801	0.0060	0.5974	0.0270	0.0790	0.0011	0.413	0.0548	0.0023	490	6	406	96	491	6
7252-6.1	119	69	0.595	10	0	0.000058	0.000111	0.0010	0.1914	0.0052	0.6283	0.0229	0.0792	0.0010	0.455	0.0575	0.0019	491	6	512	73	491	6
7252-27.1	130	68	0.540	11	2	0.000181	0.000118	0.0031	0.1782	0.0055	0.6410	0.0245	0.0799	0.0011	0.458	0.0582	0.0020	495	6	538	77	495	6
7252-52.1	256	211	0.851	24	2	0.000111	0.000050	0.0019	0.2730	0.0054	0.6509	0.0134	0.0810	0.0009	0.635	0.0583	0.0009	502	5	541	36	501	5
7252-57.2	195	16	0.085	16	1	0.000088	0.000073	0.0015	0.0295	0.0029	0.7244	0.0187	0.0885	0.0010	0.549	0.0593	0.0013	547	6	579	48	546	6
7252-57.1	269	22	0.084	23	2	0.000107	0.000102	0.0019	0.0277	0.0039	0.7321	0.0232	0.0905	0.0010	0.465	0.0587	0.0017	559	6	555	63	559	6
7252-56.1	100	134	1.382	21	4	0.000316	0.000085	0.0055	0.4326	0.0059	1.6157	0.0431	0.1613	0.0023	0.626	0.0726	0.0015	964	13	1004	43		
7252-42.1	45	15	0.356	8	4	0.000590	0.000172	0.0102	0.1054	0.0070	1.8379	0.0786	0.1763	0.0026	0.458	0.0756	0.0029	1047	14	1084	79		
7252-53.1	155	78	0.522	30	7	0.000272	0.000049	0.0047	0.1619	0.0026	1.9795	0.0383	0.1846	0.0024	0.747	0.0778	0.0010	1092	13	1141	26		
7252-55.1	40	20	0.515	8	0	0.000010	0.000010	0.0002	0.1817	0.0066	2.2457	0.0542	0.1926	0.0029	0.703	0.0846	0.0015	1135	15	1306	34		
7252-38.1	148	90	0.625	31	2	0.000093	0.000039	0.0016	0.1922	0.0025	2.1090	0.0355	0.1940	0.0023	0.790	0.0789	0.0008	1143	13	1169	21		
VLA01-314 (Z7630)																							
7630-22.1	322	123	0.396	23	7	0.000359	0.000197	0.0062	0.1151	0.0081	0.5194	0.0338	0.0701	0.0009	0.313	0.0537	0.0034	437	5	360	147	438	5
7630-30.1	185	117	0.653	14	2	0.000166	0.000177	0.0029	0.2063	0.0090	0.5606	0.0314	0.0712	0.0010	0.378	0.0571	0.0030	443	6	496	119	443	6
7630-19.1	169	135	0.822	14	0	0.000010	0.000010	0.0002	0.2580	0.0209	0.5876	0.0144	0.0717	0.0010	0.670	0.0595	0.0011	446	6	585	40	444	6
7630-7.1	325	185	0.588	25	4	0.000201	0.000236	0.0035	0.1903	0.0098	0.5325	0.0416	0.0718	0.0009	0.280	0.0538	0.0041	447	5	363	180	448	5
7630-56.1	248	137	0.570	19	4	0.000242	0.000205	0.0042	0.1694	0.0090	0.5514	0.0359	0.0719	0.0010	0.326	0.0556	0.0035	448	6	438	144	448	6
7630-6.1	405	103	0.263	29	0	0.000010	0.000010	0.0002	0.0855	0.0025	0.5589	0.0117	0.0722	0.0009	0.673	0.0561	0.0009	450	5	457	35	449	5
7630-9.1	245	132	0.557	19	1	0.000086	0.000135	0.0015	0.1724	0.0074	0.5294	0.0292	0.0723	0.0015	0.493	0.0531	0.0026	450	9	335	113	451	9
7630-55.1	556	522	0.970	47	0	0.000012	0.000060	0.0002	0.2946	0.0061	0.5646	0.0169	0.0724	0.0010	0.552	0.0566	0.0014	451	6	474	57	450	6
7630-5.1	236	149	0.653	19	0	0.000010	0.000010	0.0002	0.2100	0.0066	0.5853	0.0134	0.0726	0.0009	0.630	0.0585	0.0011	452	5	549	40	450	5
7630-20.1	95	54	0.590	7	1	0.000230	0.000529	0.0040	0.1985	0.0213	0.5662	0.0860	0.0726	0.0014	0.253	0.0566	0.0084	452	9	476	366	451	8
7630-46.1	103	54	0.545	8	3	0.000406	0.000544	0.0070	0.1846	0.0216	0.5560	0.0881	0.0726	0.0012	0.230	0.0556	0.0086	452	7	435	390	452	6
7630-12.1	376	240	0.660	29	3	0.000113	0.000111	0.0020	0.1973	0.0064	0.5615	0.0215	0.0727	0.0010	0.477	0.0560	0.0019	452	6	453	77	452	6
7630-50.1	649	457	0.728	52	0	0.000002	0.000053	0.0000	0.2204	0.0042	0.5575	0.0147	0.0728	0.0010	0.624	0.0555	0.0012	453	6	434	47	453	6
7630-11.1	168	152	0.930	14	0	0.000010	0.000010	0.0002	0.3037	0.0078	0.6057	0.0159	0.0729	0.0011	0.651	0.0603	0.0012	454	6	613	44	451	6
7630-40.1	274	255	0.961	24	1	0.000075	0.000196	0.0013	0.3133	0.0105	0.5666	0.0372	0.0729	0.0011	0.355	0.0564	0.0035	454	7	466	143	454	7
7630-41.1	523	300	0.592	41	0	0.000010	0.000010	0.0002	0.1919	0.0029	0.5721	0.0089	0.0731	0.0008	0.775	0.0567	0.0006	455	5	482	22	455	5
7630-48.1	230	98	0.443	17	4	0.000246	0.000298	0.0043	0.1397	0.0119	0.5516	0.0502	0.0735	0.0010	0.266	0.0544	0.0048	457	6	388	212	458	5
7630-18.1	377	227	0.620	30	4	0.000163	0.000060	0.0028	0.1871	0.0048	0.5493	0.0149	0.0741	0.0009	0.552	0.0538	0.0012	461	5	360	52	462	5
7630-64.1	198	145	0.754	16	0	0.000010	0.000010	0.0002	0.2287	0.0117	0.5800	0.0142	0.0747	0.0011	0.677	0.0563	0.0010	465	6	464	41	465	6
7630-17.1	94	53	0.584	7	3	0.000490	0.000301	0.0085	0.1682	0.0145	0.5340	0.0545	0.0748	0.0017	0.338	0.0518	0.0050	465	10	275	238	468	10
7630-2.1	119	107	0.927	10	2	0.000294	0.000473	0.0051	0.2940	0.0227	0.6235	0.0793	0.0750	0.0012	0.245	0.0603	0.0075	466	7	613	294	464	6
7630-49.1	221	106	0.496	17	2	0.000170	0.000098	0.0030	0.1493	0.0084	0.5743	0.0217	0.0752	0.0009	0.444	0.0554	0.0019	467	6	429	78	468	6
7630-3.1	106	73	0.707	61	0	0.000010	0.000010	0.0002	0.1856	0.0029	12.2733	0.1982	0.4829	0.0069	0.926	0.1843	0.0011	2540	30	2692	10		

Notes (see Stern, 1997):

Uncertainties reported at 1σ (absolute) and are calculated by numerical propagation of all known sources of error

f206^{204} refers to mole fraction of total ^{206}Pb that is due to common Pb, calculated using the ^{204}Pb-method; common Pb composition used is the surface blank

[1] 204-corrected ages; [2] 207-corrected ages (Stern 1997)

Table 3.2: Geochemistry of peri-Gondwanan Penobscot and Victoria arc complexes

Sample	VL02A 026	VL02A 202	VL02A 204	VL02A 205	VL01A 341b	VL02A 150	VL01A 021	VL01A 067	VL01A 344	VL02A 121
UTMx†	448003	484514	484361	484179	469183	470046	453123	449594	470315	477638
UTMy†	5341400	5376241	5376134	5375787	5360797	5362877	5344015	5341669	5360839	5367582
NTS map	12A/04	12A/11	12A/11	12A/11	12A/06	12A/06	12A/04	12A/04	12A/06	12A/06
Type	PP_1	PP_1	PP_1	PP_1	PP_2	PP_2	PP_3	PP_3	PP_3	PP_3
Rock type‡	pbslt	pbslt	bslt	bslt	mtuff (fp)	mtuff	ituff (fqp)	ituff (fp)	ituff (fp)	ituff (fqp)
Laboratory§	1	1	1	1	2	1	2	2	3	1
SiO_2 (wt%)	46.65	50.39	56.02	50.66	48.36	46.48	59.5	49.41	67.79	54.26
TiO_2	0.745	0.642	0.731	0.699	0.38	0.385	0.32	0.59	0.44	0.354
Al_2O_3	16.29	15.37	14.18	15.19	16.17	18.11	15.46	18.8	13.05	17.16
MnO	0.12	0.159	0.155	0.19	0.09	0.201	0.12	0.16	0.03	0.15
MgO	9.59	8.88	6	9.4	8.26	6.97	3.02	5.44	1.81	5.51
CaO	8.57	7.46	6.09	5.32	9.86	11.83	6.23	8.57	6.9	6.59
Na_2O	3.1	4.21	5.93	4.97	1.34	0.83	2.11	1.38	2.92	3.67
K_2O	0.99	0.09	0.22	0.05	0.13	0.02	2.47	0.01	0.02	0.68
P_2O_5	0.134	0.098	0.114	0.145	0.02	0.048	0.04	0.04	0.24	0.031
LOI	5.05	3.06	1.58	3.58	4.39	3.79	5.56	3.94	2.2	2.5
Fe_2O_3 total	8.73	9.75	9.21	9.89	12.2	11.62	5.95	12.88	4.48	9.48
Total	100.07	100.2	100.27	100.23	101.21	100.33	100.78	101.22	99.89	100.41
Ba (ppm)	72.04	48.9	129.15	23.19	96.47	11.77	145.59	10.83	39	646.74
Cr	387.57	420	82.33	582	55.78	95.79	57.09	58.8	27.368	34.88
Cs	0.863	0.145	0.278	0.136	0.08	0.076	1.84	0.08	b.d.	0.435
Hf	1.3	1	1.2	1.2	0.4	0.4	1.1	0.9	1.4	1
Nb	1.48	0.63	0.86	1	0.58	0.53	0.74	0.55	1.4	0.9
Ni	144.12	135.26	31.18	174.32	24.97	31.55	16.86	16.89	4.4	12.5
Pb	2.2	2.2	1.8	3.3	6.2	6.4	3.6	5.91	9.5	2.3
Rb	18.45	0.64	2.56	0.45	2.13	0.14	57.72	b.d.	b.d.	12.04
Sc	39	44.31	41.71	52.5	48.46	48.77	31.68	49.1	16	36.74
Sr	284	157.1	119.3	234	223.36	323	118.89	366.56	196.5	176.9
Ta	0.22	0.16	0.17	0.18	b.d.	0.15	b.d.	b.d.	b.d.	0.18
Th	1.82	1.72	2.12	4.06	0.93	0.92	0.98	0.87	1.8	0.68
U	0.572	0.455	0.499	1.009	0.43	0.717	0.44	0.52	1.2	0.308
V	255.74	315	315	315	314.63	315	189.69	351	53	210.38
Y	19.14	15.56	19.05	18.21	5.22	6.14	15.05	12.26	29.7	15.29
Zr	44.4	30.2	43.2	44.4	13.05	12.9	34.64	27.02	42.7	29.7
La	8.33	5.8	7.5	11.18	3.38	3.34	2.85	3.01	8.1	2.97
Ce	19.43	13.32	17.8	25.28	7.23	7.03	6.8	7.66	16.4	6.83
Pr	2.634	1.845	2.405	3.374	0.92	0.876	0.92	1.13	2.15	0.987
Nd	12.22	8.33	10.75	14.49	3.82	3.58	4.48	5.4	10.8	4.76
Sm	3.02	2.23	2.92	3.64	0.92	0.89	1.34	1.62	2.2	1.54
Eu	0.997	0.714	0.878	0.973	0.38	0.318	0.46	0.84	0.87	0.542
Gd	3.176	2.433	2.842	3.502	0.94	0.945	1.84	1.86	3.68	1.864
Tb	0.557	0.438	0.507	0.572	0.16	0.161	0.34	0.34	0.64	0.37
Dy	3.186	2.565	3.207	3.172	0.99	1	2.23	2.19	4.16	2.203
Ho	0.71	0.571	0.645	0.691	0.22	0.226	0.5	0.51	1.02	0.562
Er	2.123	1.573	1.952	2.048	0.59	0.691	1.55	1.39	2.82	1.696
Tm	0.309	0.243	0.311	0.291	0.1	0.115	0.24	0.2	0.52	0.29
Yb	1.98	1.75	1.9	1.75	0.61	0.73	1.6	1.3	3.21	1.59
Lu	0.314	0.232	0.278	0.284	0.1	0.123	0.283	0.225	0.47	0.295
Mg#	70.5	66.5	58.7	67.4	59.6	56.7	52.5	47.9	46.8	55.9
(La/Th)n	0.2	0.2	0.2	0.1	0.2	0.2	0.1	0.2	0.2	0.2
(La/Nb)n	5.2	8.6	8.1	10.4	5.4	5.9	3.6	5.1	5.4	3.1
(Zr/Sm)n	0.52	0.48	0.53	0.43	0.5	0.52	0.92	0.59	0.69	0.69
(La/Sm)n	2.9	2.74	2.7	3.23	3.86	3.95	2.24	1.95	3.87	2.03
(Gd/Lu)n	1.27	1.31	1.25	1.55	1.16	0.98	0.81	1	0.97	0.77

UTM zone 21 (NAD83); (p)bslt-(pillowed)basalt; (s)diab-(sheeted)diabase; gabb-gabbro; (f,I,m)tuff - (felsic,intermediate,mafic) tuff; gran-granodiorite; rhyo-rhyolite; fdyke-felsic dyke; (p)and-(pillowed)andesite; (q,fp-(quartz,feldspar) porphyritic; § 1:McGill (XRF); Ontario Geological Survey (OGS; ICPMS; 2001), 2:OGS (2001), 3:Acme (2001), 4:GSC (2003), 5:OGS (2002), 6:McGill; OGS (2003); see Rogers (2004); # b.d. - below detection; n.a. not applicable: Mg# =Mg2+/(Mg2++Fe2+), Fe3+/Fe2+=0.1; N-MORB normalized value (Sun and MacDonough, 1989)

Table 3.2 (ctn'd)

VL02A 134b	VL01A 335	VL01A 336	VL02A 128	VL02A 135	VL02A 199	VL02A 200b	VL02A 221	VL02A 104	VL02A 122a	VL02A 246b	VL02A 140b
475491	470759	470187	473877	475697	480957	483707	486013	468948	477869	478760	475721
5366640	5361846	5361777	5365750	5366577	5371665	5373650	5375420	5358950	5367612	5368443	5367161
12A/06	12A/06	12A/06	12A/06	12A/06	12A/06	12A/11	12A/11	12A/06	12A/06	12A/06	12A/06
PP_3	PP_4	PP_4	PP_4	PP_4	PP_4	PP_4	PP_4	PP_5	PP_6	PP_6	WB_1
ituff (fqp)	ftuff (qfp)	ftuff	ftuff	ftuff	ftuff (qp)	ftuff (qp)	ftuff (qfp)	ituff	ftuff	ftuff (qp)	rhyolite
1	4	2	1	1	3	1	1	1	1	1	3
61.15	64	72.69	65.63	65.54	61.46	67.81	67.83	49.26	83.46	79.89	84.41
0.3	0.32	0.26	0.287	0.24	0.29	0.24	0.301	0.805	0.125	0.19	0.12
14.59	14.4	12.89	13.42	13.92	14.68	14.19	12.34	18.59	9.4	11.47	8.24
0.087	0.1	0.02	0.101	0.093	0.11	0.026	0.079	0.123	0.012	0.009	0.01
3.59	3	1.7	2.25	2.12	4.11	2.65	3.02	5.46	0.26	0.31	0.1
5.94	1.46	1.9	6.19	6.17	3.02	3.17	4.19	5.43	0.23	0.09	0.65
2.61	5.25	5.26	3.06	3.31	2.47	3.26	2.1	3.93	5.36	6.09	3.79
0.04	0.17	0.3	0.63	0.12	1.62	0.61	0.34	1.46	0.03	0.33	0.53
0.055	0.05	0.06	0.069	0.049	0.03	0.053	0.037	0.024	0.024	0.042	0.03
3.04	7.01	1.35	2.15	2.25	3.4	2.3	2.32	5.8	0.24	0.42	1
8.68	8	3.85	6.17	6.35	8.72	5.58	7.44	9.04	0.75	1.3	0.96
100.11	99.8	100.29	99.98	100.18	99.95	99.9	100.02	99.95	99.9	100.15	99.89
24.24	102	25.33	43.43	10.92	259	48.33	52.67	81.32	13.44	69.56	476
37.77	23	0.5	35.27	34.97	20.526	21.42	41.05	31.2	17.46	13.91	6.842
0.114	0.1	0.08	0.192	0.122	0.3	0.205	0.209	0.687	0.077	0.125	0.1
1.3	1.5	1.42	0.7	0.8	1.4	1.5	1.2	1.1	3.4	3.6	3
1.04	1.2	0.92	0.5	0.51	1	0.93	0.92	0.97	3.46	3.79	8.5
10.44	5	b.d.	11.7	9.52	7	5.1	12.06	12.96	2.96	3	2.6
4.3	2	2.96	4.1	4	3.3	6	7.2	1.4	3	1.9	4.4
0.4	2.7	3.34	6.06	1.86	13.2	4.38	4.54	17.76	0.24	4.07	10.3
38.81	31	20.61	37.05	37.3	33	26.95	35.2	32.07	7.5	10.39	2
76.4	87	69.97	142.5	156.4	176.9	100.9	85.1	151.2	32.3	34.9	96.5
0.18	b.d.	b.d.	0.16	0.17	b.d.	0.17	0.2	0.19	0.26	0.37	0.6
1.47	1.8	1.11	0.51	0.61	2.2	1.17	1.28	0.39	4.18	3.5	2
0.589	0.62	0.6	0.567	0.346	1	0.662	0.964	0.158	1.22	1.107	0.5
214.1	136	58.32	198.98	184.02	220	88.8	231.5	315	3.83	10.12	9
18.97	20	22.96	16.22	20.65	16.6	30.12	12.75	16.52	34.95	55.27	29.4
44.9	52	45.42	21.9	27.3	37.8	46.6	38	35.9	110.7	122.1	78.3
4.22	5.2	4.15	2.26	3.63	4.3	4.35	3.33	1.86	8.8	9.08	7.5
9.46	11	9.1	5.26	8.29	9.4	10.04	8.04	4.96	19.88	22.26	14.3
1.253	1.4	1.26	0.699	1.077	1.07	1.387	1.067	0.746	2.463	2.908	1.91
5.61	6.6	5.78	3.32	5.14	5.1	7.07	4.71	4.28	10.37	13.1	8.3
1.7	1.8	1.9	1.23	1.55	2.1	2.19	1.39	1.43	2.76	3.23	2.1
0.4	0.4	0.62	0.388	0.4	0.38	0.53	0.318	0.614	0.483	0.611	1.19
2.22	2.4	2.62	1.58	2.353	2.17	3.194	1.501	2.138	3.753	4.866	3.48
0.439	0.43	0.51	0.318	0.461	0.36	0.599	0.337	0.415	0.717	1.029	0.61
2.836	2.9	3.48	2.234	2.992	2.21	4.391	2.027	2.819	5.182	7.244	4.12
0.685	0.67	0.86	0.54	0.687	0.54	1.072	0.463	0.603	1.184	1.755	0.85
2.1	2.1	2.55	1.791	2.151	1.7	3.333	1.48	1.854	3.969	5.707	2.8
0.349	0.35	0.43	0.315	0.366	0.29	0.557	0.24	0.304	0.613	0.862	0.44
2.16	2.4	2.86	1.88	2.21	1.98	4.03	1.55	2	4.29	5.59	2.91
0.383	0.42	0.49	0.329	0.368	0.37	0.678	0.26	0.309	0.706	0.905	0.39
47.4	45	49	44.3	42.1	50.7	50.9	46.9	56.8	43	34.2	18.5
0.1	0.1	0.2	0.2	0.3	0.1	0.2	0.1	0.2	0.1	0.1	0.2
3.8	4	4.2	4.2	6.6	4	4.4	3.4	1.8	2.4	2.2	0.8
0.94	1.03	0.85	0.63	0.63	0.64	0.76	0.97	0.89	1.43	1.34	1.33
2.61	3.04	2.3	1.93	2.46	2.15	2.09	2.52	1.37	3.35	2.96	3.76
0.72	0.71	0.66	0.59	0.79	0.73	0.58	0.71	0.85	0.65	0.66	1.1

Table 3.2 (ctn'd)

VL02A 186	VL01A 347	VL02A 218b	VL02A 262b	RAX01 034	RAX01 082	RAX01 914	RAX02 117	VL01A 325	VL01A 327b	VL02A 209b	RAX02 123
471462	468280	485985	486138	506207	505319	523396	527100	467791	468324	485544	541568
5365230	5360643	5377340	5377671	5387828	5387227	5399306	5395447	5359382	5361335	5378179	5408696
12A/06	12A/06	12A/11	12A/11	12A/10	12A/10	12A/10	12A/10	12A/06	12A/06	12A/11	12A/16
WB_1	WB_2	WB_2	WB_2	WB_3	WB_3	WB_3	WB_3	WB_3	WB_3	WB_3	WB_4
rhyolite	rhyolite	fluff	fluff	atuff	fluff	fluff	fluff	fluff	rhyolite	fluff	fluff
1	3	1	1	5	5	5	3	3	2	1	6
76.23	63.73	61.48	60.24	58.48	67.52	74.33	75.9	69.67	73.11	72.24	69.45
0.062	0.74	0.571	0.735	0.59	0.42	0.22	0.33	0.46	0.4	0.354	0.396
12.82	14.47	18	17.14	18.44	16.43	13.79	11.63	12.9	10.72	14.17	13.49
0.02	0.12	0.096	0.062	0.18	0.18	0.09	0.11	0.07	0.21	0.141	0.146
1.97	2.8	2.86	2.06	1.68	1.68	2.01	0.19	2.29	1.94	0.96	1.31
0.41	2.46	2.19	3.55	5.17	0.28	0.66	0.2	1.79	0.83	0.93	2.59
1.13	3.64	4.45	3.42	3.42	3.83	4.76	3.05	2.78	3.32	4.44	2.77
3.26	1.29	1.79	2.93	2.85	2.81	1.8	1.34	1.93	0.35	2.1	2.2
0.012	0.6	0.183	0.227	0.27	0.06	0.07	0.05	0.09	0.07	0.098	0.102
2.42	2.4	2.67	4.83	3.55	2.55	1.72	2	2.8	2.12	1.69	2.3
1.5	7.57	5.92	5.25	6.28	5.07	2.14	3.87	4.99	7.18	3.09	5.8
99.84	99.85	100.21	100.46	100.89	101.07	99.76	99.84	99.84	100.26	100.22	100.57
167.9	216	248.45	354.23	539.16	617.05	396.05	281	481	113.17	797.58	589.04
13.15	6.842	9.01	21.18	3.04	15.49	b.d.	54.736	54.736	40.87	32.28	29.15
2.454	0.6	1.791	1.887	1.88	2.24	1.13	2	1.4	0.3	2.876	2.238
10.9	4	4.8	3.9	2.94	3.58	2.25	2.3	2.2	2.36	3.2	1.7
147.3	7.4	3.36	2.68	2.66	8.68	7.41	4.5	6	8.15	7.19	1.08
3.34	13.1	1.72	8.33	b.d.	8.61	b.d	16.4	25.1	23.43	7.66	3.37
12.9	8.1	4.3	2.4	2.41	18.68	4.54	4.8	18.4	26.41	9.6	10.1
85.32	30.4	45.83	73.44	75.22	88.49	58.93	44.4	61.8	11.76	79.74	39.59
1.55	21	16.79	22.12	10.86	18.48	3.96	9	14	9.49	12.45	27.14
71.3	247.3	258.3	167.5	435.68	49	152.31	88.7	180.3	177.95	183	190.5
6.36	0.4	0.3	0.28	b.d.	0.53	0.61	0.3	0.4	0.49	0.6	0.16
15.36	4.3	8.3	6.72	8.05	9.17	5.93	6.3	6.8	7.11	10.05	2.63
4.909	2.6	2.72	1.813	2.3	2.07	1.02	1	1.7	1.46	2.433	1.439
3.6	85	18.7	66.27	88.29	70.64	22.02	66	100	50.2	68.37	71.01
85.25	65.5	45.34	45.52	22.9	25.15	10.56	12.2	21.9	15.57	21.83	23.21
208.6	124	173.3	142.1	96.74	110.56	76.37	74.9	92.3	83.81	130.6	53.1
21.26	37.2	21.32	20.77	27.98	24.34	18.09	19.3	23.1	22.92	38.66	7.25
54.42	78.9	50.28	48.16	56.88	48.08	34.19	33.1	43.7	58.15	53.89	15.46
7.629	8.61	7.34	6.566	7.31	5.79	4.02	3.65	5.28	5.53	8.003	1.973
31.41	38.5	32.55	29.81	28.55	21.26	13.65	14.9	22.2	20.08	28.96	8.78
10.93	8.2	7.14	7.12	5.56	4.36	2.56	2.6	4.1	3.81	5.1	2.51
0.037	2.05	2.227	1.994	1.75	1.01	0.52	0.66	0.84	0.84	1.251	0.626
12.797	8.7	6.6	7.229	4.9	4.24	1.96	2.01	3.16	3.16	4.231	3.08
2.561	1.39	1.216	1.194	0.71	0.72	0.32	0.33	0.58	0.51	0.588	0.563
16.11	9.14	7.61	7.58	4.08	4.38	1.86	2.28	3.78	2.92	3.708	3.581
3.27	2.03	1.635	1.566	0.86	0.94	0.35	0.41	0.71	0.61	0.734	0.847
10.021	5.51	4.993	4.816	2.36	2.78	1.02	1.39	2.12	1.65	2.274	2.631
1.695	0.99	0.798	0.784	0.37	0.43	0.15	0.21	0.33	0.26	0.352	0.419
11.72	5.67	5.1	4.77	2.5	2.89	1.07	1.56	2.19	1.62	2.44	2.69
1.945	0.93	0.844	0.785	0.422	0.46	0.166	0.3	0.37	0.256	0.338	0.449
74.1	44.6	51.3	46.1	36.8	46.4	16.2	43.9	50	37.1	40.4	33
0.1	0.4	0.1	0.1	0.2	0.1	0.1	0.1	0.2	0.2	0.2	0.1
0.1	4.7	5.9	7.2	9.8	2.6	2.3	4	3.6	2.6	5	6.3
0.68	0.54	0.86	0.71	0.62	0.9	1.06	1.02	0.8	0.78	0.91	0.75
2.05	4.77	3.14	3.07	5.29	5.87	7.43	7.81	5.93	6.33	7.97	3.04
0.81	1.16	0.97	1.13	1.44	1.14	1.43	0.83	1.06	1.5	1.54	0.85

Table 3.2 (ctn'd)

RAX02	RAX01	RAX01	VL01A	VL02A	VL02A
124	008	053	326a	093	137b
540962	507160	486738	468783	468913	475442
5408352	5388689	5378303	5361759	5363345	5367675
12A/16	12A/10	12A/11	12A/06	12A/06	12A/06
WB_4	WB_5	WB_5	WB_5	WB_5	WB_5
fluff	pbslt	pbslt	gabbro	bslt	bslt
6	5	5	4	1	1
67.58	45.86	47.51	48.3	47.26	50.8
0.461	0.71	0.57	0.95	1.289	1.989
13.35	17.28	11.02	15.1	15.95	14.01
0.176	0.12	0.16	0.17	0.172	0.202
2.22	6.48	7.33	8.61	7.9	5.51
1.76	6.96	12.63	7.39	8.72	7.82
4.19	1.12	4.73	3.41	3.87	4.53
1.06	2.87	0.78	0.28	0.25	0.24
0.13	0.12	0.08	0.07	0.122	0.165
2.39	9.28	9.26	6.24	3.62	1.83
6.8	9.72	6.59	12	11.37	13.11
100.13	100.53	100.65	99.1	100.61	100.25
541.67	226.65	160.02	44	57.73	30.92
19.97	251.97	338.47	199	316.32	31.74
1.64	2.83	3.18	0.19	0.165	1.216
1.4	1.34	1.05	1.3	1.9	3.4
1.08	0.82	0.68	0.67	1.09	1.22
2.99	90.08	152.7	73	117.54	24.16
15	2.12	1.31	b.d.	1.7	2.6
25.15	53.79	21.34	3.4	3.13	9.23
28.9	35.2	28.17	45	52.5	41.18
533.7	145.35	224.39	115	120.4	155
0.18	0.15	0.15	b.d.	0.22	0.22
1.96	1.46	1.17	0.52	0.53	0.86
1.004	1.04	0.47	0.14	0.547	0.221
83.36	312.28	225.46	344	360	424
23.99	17.67	12.07	29	28.11	50.99
41.6	43.05	33.81	42	71.8	118.5
6.52	5.31	5.02	3.3	5.18	5.5
13.78	12.87	12.11	8.5	10.85	15.29
1.8	1.86	1.78	1.3	1.877	2.56
7.98	8.57	7.99	7.3	9.62	14.34
2.23	2.46	2.02	2.3	3.03	4.96
0.676	0.91	0.78	0.74	1.143	1.817
3.017	2.81	2.19	3.3	4.209	6.897
0.556	0.46	0.36	0.66	0.717	1.299
3.776	3.11	2.24	4.3	4.471	8.065
0.878	0.71	0.48	0.94	1.003	1.916
2.607	2.12	1.4	2.6	3.007	5.416
0.437	0.31	0.23	0.43	0.421	0.856
2.79	2.18	1.25	2.8	2.76	5.12
0.456	0.33	0.208	0.44	0.392	0.831
41.6	59.2	70.8	61	60.2	47.8
0.2	0.2	0.2	0.3	0.5	0.3
5.6	6	6.9	4.6	4.4	4.2
0.66	0.62	0.59	0.65	0.84	0.85
3.08	2.27	2.61	1.51	1.8	1.17
0.81	1.05	1.29	0.93	1.33	1.03

Table 3.3: Sm/Nd isotope data

Sample	Stratigraphic unit	Type	Age	Nd	Sm	$^{143}Nd/^{144}Nd$		$^{147}Sm/^{144}Nd$	$^{143}Nd/^{144}Nd^{\S}$	$\varepsilon Nd(t)^{\S}$
VL01A325	Dragon Pond Fm.	WB_3	454	19.32	3.94	0.512217	(16)	0.1234	0.511850	-3.98
VL01A315#	Dragon Pond Fm.	WB_3	454	17.72	3.45	0.512194	(13)	0.1178	0.511844	-4.08
VL02A140b	Dragon Pond Fm.	WB_1	454	7.21	1.87	0.512824	(14)	0.1570	0.512357	5.93
VL02A246b	Pats Pond Group	PP_6	487	11.22	2.87	0.512701	(15)	0.1546	0.512208	3.85
VL02A221	Pats Pond Group	PP_4	487	3.12	0.85	0.512777	(14)	0.1655	0.512249	4.67
VL02A128	Pats Pond Group	PP_4	487	2.17	0.63	0.512854	(6)	0.1766	0.512291	5.48
VL02A202	Pats Pond Group	PP_1	487	10.14	2.68	0.512493	(12)	0.1598	0.511983	-0.54
VL02A026	Pats Pond Group	PP_1	487	13.04	3.30	0.512515	(15)	0.1530	0.512026	0.31

Lithology, location and geochemistry listed in Table 3.2; Concentration in ppm from isotope dilution; § Calculated at age of formation; # felsic tuff, no geochemical analysis, NAD83, UTM Zone 21 468729 5360774

CHAPTER 4: DISTINCT TACONIC, SALINIC AND ACADIAN DEFORMATION ALONG THE IAPETUS SUTURE ZONE, NEWFOUNDLAND APPALACHIANS

ABSTRACT

The understanding of the tectonic history of Newfoundland Appalachians has important implications for the entire Appalachian – Caledonian Orogen as the Newfoundland Appalachians provide a critical geological link between the Northern Appalachians and British Caledonides. The Newfoundland Appalachians also have good exposure relative to the rest of Northern Appalachians and in addition have a long history of high quality mapping, geochemistry and geochronology which can be integrated with shallow level and crustal scale seismic reflection studies.

Structural mapping in central Newfoundland has identified seven distinct phases of deformation (D_1 to D_7), the most significant of which are D_1, D_2, and D_4. D_1 involved the formation of an Ordovician south-southeast directed thrust belt and concominant development of mylonites and phyllonites. The arc – backarc complexes exposed in central Newfoundland are predominantly juxtaposed along D_1 shear zones, which include the Red Indian Line. Late Ordovician to early Silurian D_2 reverse fold and fault belt overprints D_1 mylonites and is the most distinctive deformation event in the study area. Late Silurian to Devonian D_4 is associated with folds and north-northwest directed dextral thrust and reverse faults which overprint D_1 to D_3 structures. The extension of Noel Paul's Line in central Newfoundland, the Victoria Lake shear zone, is attributed to the D_4. Identification of multiple deformation events and evidence for reactivation of structures has important implications for the interpretation of terrane boundaries in Newfoundland. Our data indicate that D_1 terrane boundaries may have protracted deformation histories spanning several deformation events. Depending on the intensity of overprinting or reactivation, D_1 terrane boundaries may be interpreted as D_2 or D_4 shear zones.

The deformation history proposed in this paper closely corresponds to the established Appalachians orogenic cycles. D_1 is correlated with Taconic orogeny and involved accretion of arc – backarc complexes to the Laurentian margin. D_2 and D_3 are correlated with the Salinic and Acadian orogenies which involved the accretion of the Ganderia and Avalon microcontinents to the Laurentian margin respectively.

INTRODUCTION

The Appalachians – Caledonides are a classic example of a long-lived (c. 200 Ma) Paleozoic accretionary orogen formed as a result of the closure of Iapetus, Tornquist, and Rheic oceans (van Staal 2005; van Staal et al., 1998; Williams and Hatcher, 1983). The Appalachian deformation along the Laurentian margin can be described in terms of five orogenic episodes: the Early to Middle Ordovician Taconic, Early to Late Silurian Salinic, latest Silurian to Early Devonian Acadian, Middle Devonian to Early Carboniferous Neoacadian, and Carbonifeous to Permian Alleghenian orogenies (van Staal 2005). These orogenies resulted from the successive arrival of the Dashwoods, Ganderia, Avalonia and Meguma microcontinents and Gondwana continent respectively at the Laurentian margin.

The Newfoundland Appalachians provide the critical geological link between the northern Appalachians and British Caledonides. Most importantly, the central Newfoundland Appalachians are unique in that they allow the integration of high quality field investigations, geochronology, geochemistry, and both shallow and crustal-scale seismic reflection surveys. The understanding of structures associated with the Appalachian orogenic episodes and their kinematic significance in central Newfoundland is thus an integral step in understanding the assembly and dispersal of terranes along the Laurentian margin.

Deformation in the central mobile belt (Notre Dame and Exploits subzones: Fig. 4.1 inset) of Newfoundland has been traditionally interpreted as Taconic or Acadian (e.g. Dean and Strong 1977; Hibbard, 1983; Kean and Jayasinghe 1980; Kean 1983; Karlstrom et al. 1983). The majority of the tectonic studies have presented evidence for both Silurian and Devonian deformation phases (e.g. Arnott et al. 1985; Dunning et al. 1990; Elliot et al. 1991; van der Pluijm 1986; Lafrance and Williams 1992; Karlstrom et al. 1983; O'Brien 2003; Williams et al. 1993), which were all initially ascribed to the Acadian orogeny. However this makes the Acadian orogeny very long (>40 My) and it does not adhere to the original definition of the strictly Latest Silurian to Early Devonian Acadian orogeny related to the docking of Avalonia (Bradley, 1983; Robinson et al. 1998; van Staal, 2005). To rectify this problem Dunning et al. (1990) proposed a correlation of the Early to Late Silurian orogenesis with the Salinic disturbance recognised by Boucot (1962) in New England. The Salinic

orogeny involved the development of a northwest-directed thrust and fold belt in the Humber zone (Fig. 4.1; e.g. Cawood et al. 1994) and a southeast-directed thrust and fold belt in the eastern Notre Dame Subzone and Exploits Subzone (Dean and Strong 1977; Lafrance and Williams 1992; O'Brien 2003; Szybinski 1995).

Regional investigations of the Early to Middle Ordovician Taconic deformation in the Dunnage zone are rare (e.g. Dean and Strong, 1977; Hibbard, 1983; Szybinski 1995) or restricted to mine scale (e.g. Calon and Green 1987). Most of these do not take into account the new data that has since been collected, although significant progress in the regional understanding of the Taconic deformation has been recently made using geochronology (Lissenberg et al. 2005b) and seismic reflection (Thurlow et al. 1992; van der Velden et al. 2004). In addition, regional field investigations (i.e. Lissenberg et al. 2005c; Rogers et al. 2005a; van Staal et al. 2005a, b, c) in conjunction with high quality geochronological analysis has lead to reinterpretation of the tectono-stratigraphic relationships in central Newfoundland (Chapter 2, 3; Appendix 3; van Staal et al. in press; Whalen et al. in press).

In this study, we investigate the structural history of the Annieopsquotch Accretionary Tract and Victoria Lake Supergroup along the Red Indian Line, the main Iapetus suture zone. Three major ductile phases and three brittle-ductile phases of deformation have been identified in this study. The generations of structures were primarily recognized by overprinting relationships whenever possible, otherwise structures were characterized by style, orientation, and metamorphic assemblages. Despite the complexity of the structural history the kinematic significance and age of the different generations of structures have been discerned.

The deformation history proposed herein has significant implications for the regional tectonic framework. Specifically, the apparent disparity between the structural history inferred from the seismic studies (Thurlow et al. 1992; van der Velden et al. 2004) and surface mapping (e.g. Kerr 1996) can now be addressed. The confirmation of an Ordovician southeast-directed accretionary tract and Silurian southeast-directed fold and thrust belt has important implications for the assembly of terranes along the composite Laurentian margin. Significantly, the identification of significant thrust and strike-slip related deformation in the Ordovician and Silurian, as hypothesised

by Elders (1987) for example, may explain the excision of many tectono-stratigraphic units and juxtaposition of unrelated terranes. The proposed deformation history can be correlated with the well-established orogenic cycles in the Appalachians, specifically the Taconic, Salinic and Acadian orogenies (van Staal 2005), and highlights the importance of the frequently neglected Middle to Late Ordovician Taconic orogeny.

REGIONAL GEOLOGY

The complexity of the closure of Iapetus is reflected in the zonal division of the northern Appalachians, where five zones have been defined: Humber, Dunnage, Gander, Avalon and Meguma (Fig. 4.1; Williams 1995). The Humber Zone represents the Cambro-Ordovician Laurentian margin. The Dunnage zone lies outboard of the Humber zone and contains allochtonous ensialic and ensimatic arc-backarc complexes that formed within the realm of the Iapetus Ocean. Further outboard, the Gander, Avalon and Meguma zones represent microcontinents derived from Gondwana (see van Staal 2005 for review).

The Dunnage Zone was originally subdivided into the peri-Laurentian Notre Dame and the peri-Gondwanan Exploits subzones (Williams et al., 1988). Other subsequent subdivisions (Williams, 1995) reflect minor regional differences internal to these two subzones that have no tectonic significance for this paper. The Notre Dame subzone comprises the remnants of Cambrian to Middle Ordovician ophiolitic rocks that were for most part invaded by plutons of an Early to Middle Ordovician Notre Dame arc built upon a ribbon microcontinent referred to as Dashwoods (Waldron and van Staal 2001). The Exploits Subzone contains peri-Gondwanan ensialic and ensimatic arc-backarc complexes. The identification of faunal, paleomagnetic, isotopic, and structural contrasts, between the Notre Dame and Exploits subzones has lead to recognition of the Red Indian Line (Williams et al. 1988), which is the fundamental suture zone in northern Appalachians. More than 3000 km of Iapetus oceanic lithosphere has been consumed along it (van Staal 2005). The Red Indian Line was originally defined along the northern coast of Newfoundland, however, its exact position and characteristics were recently investigated in central Newfoundland (Zagorevski et al. 2006; Chapter 3). This research led to new tectonic models for the formation of the tectono-stratigraphic units in central Newfoundland (Chapter 2, 3).

Cambrian and Ordovician Rocks

A large number of tectono-stratigraphic units have been proposed or had their definitions expanded during recent geological investigations in central Newfoundland (i.e. Lissenberg et al. 2005c; Rogers et al. 2005a; van Staal et al. 2005 a, b, c). The detailed stratigraphy, geochemistry and geochronology of most of these units have already been described (Chapter 2, 3; Appendix 1, 2) and are briefly summarized here (Fig. 4.1, 4.2, 4.3). Immediately to the west of the Red Indian Line, the peri-Laurentian Annieopsquotch Accretionary Tract (van Staal et al. 1998) is represented, from west to east, by the Annieopsquotch Ophiolite Belt (c. 480 Ma; Dunning 1984; Dunning and Krogh 1985), Lloyds River Ophiolite Complex (c. 473 Ma; Chapter 2), Buchans Group (c. 473 Ma; Chapter 2; Dunning et al. 1987; Thurlow and Swanson 1987), Otter Pond Complex (c. 468 Ma; Appendix 3), and Red Indian Lake Group (c. 464 Ma; Chapter 2). The eastern extent of the Red Indian Lake Group defines the Red Indian Line in the study area (Fig. 4.1, 4.2, 4.3) and marks the transition to the peri-Gondwanan Victoria Lake Supergroup (Evans and Kean 2000), which comprises, from west to east, Pats Pond (c. 487 Ma) and Wigwam Brook (c. 453 Ma: Chapter 3) groups, Sutherlands Pond Group (c. 460 Ma: Rogers et al. 2005a) and Tulks Group (c. 498 Ma: Evans et al. 1990; Rogers et al. 2005a).

The Annieopsquotch Ophiolite Belt comprises several partially dismembered ophiolitic massifs with typical ophiolitic sequence (cumulates, gabbro, sheeted diabase, basalt) with supra-subduction zone geochemistry (Appendix 1). The Annieopsquotch Ophiolite Belt is juxtaposed with the Lloyds River Ophiolite Complex along the Otter Brook shear zone (Appendix 3). The Lloyds River Ophiolite Complex comprises a narrow (1-2 km) linear belt of predomninantly gabbro, sheeted diabase and pillow basalt formed in a back arc setting (Chapter 2). The Mink Lake shear zone separates the Lloyds River Ophiolite Complex from coeval ensialic Buchans Group (c. 473 Ma) calc-alkaline basalt, felsic volcanic rocks and related intrusive rocks that locally host significant VMS mineralization (Dunning et al. 1990; Thurlow 1981; Chapter 2). The Otter Pond Complex (c. 468 Ma: Appendix 3) comprises rhyolite, granodiorite, mica schist, graphitic schist, amphibolite and gabbro, which occur along and generally mark the Otter Brook – Boogie Lake shear zone. Otter Pond Complex plutonic rocks intrude both the Annieopsquotch Ophiolite Belt and the Lloyds River

Ophiolite Complex (Appendix 3). The Wood Lake shear zone separates the structurally overlying Buchans Group from the Red Indian Lake Group. The Red Indian Lake Group comprises pillow basalt, felsic volcanic rocks, and red shale and chert deposited in an ensialic arc – backarc environment.

The Red Indian Lake Group is structurally juxtaposed with the nearly coeval Wigwam Brook Group of the Victoria Lake Supergroup (Evans and Kean 2002) along the Red Indian Line (Fig. 4.1, 4.2, 4.3). Wigwam Brook Group comprises a sequence of ensialic arc-related felsic volcanic, epiclastic and sedimentary rocks that unconformably overly the bimodal tuffaceous ensialic arc rocks and pillow basalts of the Lower Ordovician Pats Pond Group. The Victoria Delta Fault (Thurlow et al. 1992) marks the western boundary of the Sutherlands Pond Group (Victoria Lake Supergroup), which comprises sedimentary, felsic volcanic and mafic volcanic rocks deposited in a backarc setting (Rogers et al. 2005a; Evans and Kean 2002). Tulks Group is bounded to the west by the Barren Pond Fault and comprises felsic, intermediate and mafic volcanic rocks erupted in an arc setting. Regionally the Ashgill to Wenlock marine turbidites of the Badger Group (Williams 1993) overlie all units of the Victoria Lake Supergroup. These represent forearc siliciclastic rocks deposited during the closure of the Tetagouche-Exploits backarc basin (Valverde-Vaquero et al. in press; van Staal et al. 1994, 1998)

Silurian

The Silurian is marked by extensive plutonism in the Notre Dame Subzone (Fig. 4.3; 440 Ma to 427 Ma: Whalen et al. in press). In the study area, the Boogie Lake (435 Ma: Dunning et al. 1990) and Puddle Pond (430-427 Ma: Whalen et al. in press) intrusive suites cross-cut the regionally significant Otter Pond shear zone (Fig. 4.3). The Boogie Lake intrusive suite (King George IV area) contains a full range of compositions from gabbro to monzonite. The main pluton is generally unfoliated to weakly foliated, however, satellite dykes are locally folded. The slightly younger Puddle Pond Suite comprises diorite and tonalite. Both diorite and tonalite are locally interlayered and strongly deformed along the southeastern tectonic contact (Otter Brook shear zone) between the Annieopsquotch Ophiolite Belt and Lloyds River Ophiolite Complex at Star Brook. Felsic dykes related to this phase of Notre Dame Subzone plutonism (van Staal et al. in

press; Whalen et al. in press) locally crosscut the earliest fabrics in the rocks situated along the Victoria Delta Fault.

Silurian plutonism was in part coeval with subaerial volcanism and deposition of continental red-beds (c. 430-427 Ma: Chandler et al. 1987; Dunning et al. 1990). Regionally, the red-beds unconformably overlie the Notre Dame Subzone and portions of the Exploits Subzone (Fig. 4.3; Williams 1993). In the study area, red-beds unconformably overlie all of the Ordovician rocks of the Annieopsquotch Accretionary Tract as well as the Boogie Lake Intrusive Suite (Kean 1980). In the King George IV area, red-beds are generally tilted, locally to vertical attitudes, and contain little or no cleavage development. Along the southeast margin of the Annieopsquotch Ophiolite Belt in the King George IV area (Fig. 4.3), red-beds unconformably overlying the Lloyds River Ophiolite Complex are exposed in a well-cleaved tight overturned synclinal belt in the footwall of the Otter Brook shear zone. In the Red Indian Lake area (Fig. 4.3) the red-beds are strongly deformed.

The youngest Silurian unit in the study area, the Rogersons Lake conglomerate, is exposed along the Victoria Lake shear zone to the southeast of the Victoria Lake Supergroup (King George IV area; Fig. 4.3),. The conglomerate contains rounded clasts of felsic, intermediate and mafic volcanic rocks, jasper, siltstone, shale, red sandstone and granite. It grades into coarse sand and locally contains thin lenses of carbonate. The locally intense deformation has resulted in flattening and stretching of clasts (Valverde-Vaquero and van Staal, 2001). Although no original stratigraphic relationships are preserved due to faulting, the clast provenance, including previously foliated sedimentary, felsic and mafic volcanic and plutonic rocks, suggests derivation from the Notre Dame arc, Annieopsquotch Accretionary Tract, and Victoria Lake Supergroup. Presence of red-sandstone clasts suggests that Rogersons Lake conglomerate is at least in part younger than the adjacent red-beds.

DEFORMATION HISTORY

The Annieopsquotch Accretionary Tract displays a relatively simple macroscopic structure with internally folded structural panels bounded by curvilinear shear zones (Fig. 4.3). The total structural thickness of the Annieopsquotch Accretionary Tract varies from 8 to 15 km. The thickness of individual structural panels varies between 0 and 5 km, indicating partial to total excision of

tecono-stratigraphic units along strike. Detailed observations indicate that the macroscopic simplicity is deceptive and the rocks have experienced multiple phases of deformation. Four major ductile (D_1 to D_4) and three brittle-ductile phases of deformation (D_5 to D_7) have been recognized in the mapped area based on overprinting relationships as well as available age and stratigraphic constrains. The study area has been subdivided into four structural domains (King George IV, Pats Pond, Tulks Valley, Red Indian Lake: Fig. 4.3) for ease of discussion.

D_1 deformation

The earliest deformation (D_1) recorded in Cambro-Ordovician rocks is represented by schistosity, cleavage or differentiated layering (S_1) which was subsequently folded by upright open to isoclinal F_2 folds (Fig. 4.4, 4.5, 4.6; see below). Consequently, the orientation of the D_1 fabrics is mainly dependent on the nature and intensity of D_2 deformation. As a result of D_2 transposition the regional penetrative foliation is commonly an $S_1 - S_2$ composite foliation. Nevertheless, the presence of D_1 strain can generally be ascertained and separated from the D_2 overprint.

In areas of low D_1 strain, S_1 is at shallow angle or (sub)-parallel to compositional layering (S_0; Fig. 4.5a,b,c). Rarely, S_1 is axial-planar to very tight or isoclinal recumbent F_1 folds of S_0 and quartz veins (Fig. 4.7a). In general, D_1 strain is heterogeneous and localised into high strain zones. In shale-rich formations, D_1 strain was strongly partitioned into shale resulting in boudinage and dismemberment of more competent sandstone or tuff layers within the incompetent shale matrix and development of broken formation or mélange (e.g. Victoria Delta Fault see Fig. 12 Thurlow et al. 1992). High strain zones in the competent ophiolitic gabbro-diabase-pillow basalt complexes frequently contain metabasite boudins enveloped by S_1 mylonite (Fig. 4.6b). Along high strain zones S_1 frequently contains a strongly developed elongation lineation (L_1) defined by elongated minerals, lapilli, and pebbles, dismembered porphyroclasts, and dismembered veins.

D_1 strain becomes most intense along the boundaries of the structural panels containing the fault-bounded tectono-stratigraphic units discussed above (Fig. 4.3, 4.6). From west to east regionally significant boundaries are: Otter Brook shear zone, Wood Lake shear zone, Red Indian Line, Victoria Delta Fault and Barren Pond Fault (Fig. 4.2, 4.3, 4.6). Although these zones generally contain the composite S_{1-2} fabric, the predominance of mylonitc S_1 combined with overprinting by F_2

folds on small (Fig. 4.5d,e, 4.6) and regional scale indicate that these boundaries are principally D_1 shear zones which were reoriented and reactivated during D_2 rather than D_2 shear zones (see below).

Metamorphic mineral assemblages defining S_1 vary significantly in the study area. Along Lloyds River (Fig. 4.1), S_1 in metabasic tectonites is defined by actinolite to magnesiohornblende – plagioclase ± epidote ± chlorite ± phengite (Fig. 4.7), while felsic tectonites comprise muscovite – plagioclase ± biotite ± garnet. Mylonites derived from tschermakite oikiocrystic to porphyritic gabbro (Otter Pond Complex: Appendix 3) display partial to complete recrystallization of the porphyroclasts to magnesiohornblende with development of euhedral low-strain magnesiohornblende mantles parallel to S_1. The mineral assemblages and strain-induced recrystallization of magnesiohornblende indicate that amphibolite facies metamorphism was achieved during D_1 along this portion of the Otter Brook shear zone. To the southeast of the Otter Pond shear zone, S_1 is defined by greenschist facies metamorphic assemblages (chlorite-epidote-albite-calcite±actinolite, chlorite-muscovite±garnet±biotite).

D_2 deformation

In Ordovician rocks D_2 structures are characterized by well-developed NE-trending steeply dipping spaced S_2 crenulation cleavage or schistosity (Fig. 4.5, 4.6d, 4.7, 4.8). S_2 is axial-planar to open to isoclinal, shallowly to moderately plunging upright F_2 folds of S_0 and S_1 (Fig. 4.5, 4.6, 4.7). F_2 folds of the D_1 shear zones are non-cylindrical on the regional scale (Fig. 4.3, 4.8). For example, F_2 in the rocks straddling the Red Indian Line plunge moderately to the southwest in the Pats Pond domain and moderately to the northwest in the northeast portion of the Red Indian Lake domain (Fig. 4.4, 4.8; van Staal et al. 2005; Lissenberg et al. in press). Regionally, F_2 folds of S_1 tectonites are asymmetric and overturned to the southeast with the northwest dipping limbs longer than the southeast dipping limbs.

Along northwest dipping sections of D_1 shear zones, transposition of S_1 into S_2 is commonly indicated by the presence of isoclinal to rootless intrafolial F_2 folds of S_1 and boudins containing S_1 differentiated layering (Fig. 4.5e, 4.6d). This is accompanied by development of S-C fabrics which suggest sinistral oblique reverse shear with the northwest side up. D_2 strain was therefore localized

along portions of D_1 shear zones which were reactivated as steep southeast-directed sinistral oblique reverse faults. Boudinage and segmentation of epidote veins and porphyroclasts suggests that the rocks in the composite D_{1-2} shear zones generally accommodated large extensions (>100%).

Along portions of the Otter Pond shear zone, the development of S_2 foliation was accompanied by growth of greenschist to amphibolite facies minerals (see below). In metabasites, S_2 is defined by magnesiohornblende mantles around syn-D_1 amphiboles and locally accompanied by neocrystallization of magnesiohornblende parallel to S_2. In quartzo-feldspathic rocks the development of S_2 was accompanied by dynamic recrystallization and neocrystallization of phyllosilicates and feldspar. Mimetic growth (Passchier and Trouw, 1998) of strain free micas around F_2 folds suggests that the metamorphism outlasted deformation at least locally. To the southeast of the Otter Brook shear zone, dynamic recrystallization associated with D_2 is generally restricted to septae of fine grained muscovite and chlorite while the predominant deformation mechanisms were solution transfer and crystalplastic deformation evidenced by development of monocrystalline quartz ribbons, undulose feldspars and quartz, and kinking of biotite porphyroblasts.

D_2 fabrics in the Ordovician tectonites are continuous with the fabric in the unconformably overlying Silurian supra-crustal rocks and consanguineous plutons (Fig. 4.3). The S_2 foliation is the first fabric that is developed in the Silurian rocks, although it is not regionally penetrative in all of the Silurian rocks. Silurian redbeds and volcanic rocks around King George IV Lake, for example, generally lack any macroscopic cleavage development, although they are tilted into steep attitudes in many places. In the King George IV domain, a thin sliver (0-20 m) of folded steeply dipping red-beds that unconformably overlie the Lloyds River Ophiolite Complex is intimately associated with the footwall of the Otter Brook shear zone (Zagorevski and van Staal 2002). The bedding in the red-beds is (sub)-parallel to the S_{1-2} composite fabric in the Otter Brook Shear zone suggesting that they were overthrust by the Annieopsquotch Ophiolite Belt and folded into steep attitude during D_2. Although D_2 deformation has resulted in utilization of the Otter Brook shear zone as a D_2 thrust, this shear zone has clearly experienced an earlier phase of deformation. This is indicated by the

presence of S_1 mylonites and phyllonitesthat are folded by F_2 (Fig. 4.5c, 4.6d) and geochronological constraints (Appendix 3). Therefore Otter Brook shear zone is probably best described as a composite D_{1-2} shear zone.

The best developed D_2 fabrics in the Silurian rocks occur in the Puddle Pond Intrusive Suite in the Star Brook area (Tulks Domain: Fig. 4.3). Along the Otter Pond shear zone, the Puddle Pond Intrusive Suite has attained a very strong northeast trending S_2 compositional layering and foliation (Fig. 4.8). S_2 compositional layering is locally manifested on a meter-scale as inter-layering between tonalite and diorite sheets (Fig. 4.9a). On microscopic scale S_2 is a differentiated layering with quartz rich and feldspar-rich layers transected by C and C' shearbands (Fig. 4.9a inset). S_2 is associated with a down-dip to northerly raking L_2 mineral lineation (Fig. 4.8). S_2 composite foliation is defined by quartz-feldspar-biotite-hornblende±epidote±titanite in the diorite indicating amphibolite facies deformation in the hanging wall of the Otter Brook shear zone. S_2 in a consanguineous tonalite to the southeast is defined by a greenschist facies assemblage of quartz-feldspar-biotite-epidote-sericite, suggesting an inverted metamorphic sequence in this area. The attitude of the S-C fabrics and pitch of the lineations suggest sinistral oblique west side up motion along this portion of the Otter Pond shear zone during D_2.

Evidence for D_2 reactivation of D_1 shear zones has been presented for the Otter Pond shear zone, however, the Wood Lake shear zone, Red Indian Line, Victoria Delta fault, and Barren Pond Fault also localised D_2 strain with the sinistral-oblique reverse movement. Significantly, the melange belt that marks the Victoria Delta fault contains a suite of Silurian (see below) inter-tectonic to syn-D_2 dykes which cross-cut S_1 but are dismembered in the melange zone (see Fig. 12 Thurlow et al. 1992) indicating Silurian reactivation of the Victoria Delta Fault, probably during D_2.

D_3 deformation

In the footwall of the Otter Brook Shear zone in the Star Brook area, a shallow to moderately northwest-dipping spaced zonal crenulation cleavage is locally developed in the Ordovician rocks (Fig. 4.5b,c, 4.8). This crenulation cleavage is sub-parallel to the S_2 in the adjacent Puddle Pond Intrusive Suite (Fig. 4.8); however it clearly cuts across the composite S_{1-2} in this area and is thus designated as S_3. The geometry and asymmetry of the F_3 mesoscopic and

microscopic open crenulations (Fig. 4.5b) suggest that this cleavage can be interpreted as shear bands related to southeast directed shear along the composite S_{1-2}. Similarly oriented shallowly dipping shear bands or crenulation cleavages, and related open folds of composite S_{1-2} occur throughout the Cambro-Ordovician rocks although they are particularly well developed in the mechanically weak phyllonites associated with shear zones. Since these are folded by F_4 folds on the regional scale (Fig. 4.8), they are tentatively correlated with S_3. The angular relationship of S_3 with the composite S_{1-2} and the asymmetry of F_3 folds preclude their interpretation as shear bands formed during F_2-related flexural shear.

D_4 deformation

D_4 deformation is most noticeable in the King George IV domain (Fig. 4.3). Small-scale folds of composite S_{1-2} fabrics (Fig. 4.5e) and steep to moderately southeast dipping crenulation cleavage (Fig. 4.10) is attributed to D_4. The orientation of the F_4 folds is highly variably and is controlled by the orientation of composite S_{1-2} structures. Discrimination between S_4 and composite S_{1-2} can be tenuous as both of the fabrics are steep and have sub-parallel strike, however this generally can be accomplished by establishing overprinting relationships. In addition, S_4 is predominantly southeast dipping (Fig. 4.10) whereas S_{1-2} generally has a northwest-dip (Fig. 4.8).

The Otter Brook shear zone (King George IV domain) is folded by small-scale F_4 folds that generally have shallow plunges. These folds are asymmetric and overturned to the northwest, resulting in generally southeast dipping composite D_{1-2} fabrics. The red-beds in the footwall of the Otter Pond shear zone (Zagorevski and van Staal 2002) are also folded by F_4 folds and contain a steeply to moderately southwest dipping S_4 cleavage (Fig. 4.11). In the hanging wall of the Otter Pond shear zone, red-beds and volcanic rocks (S_0) are folded on the regional scale without significant cleavage development. Limited data on these structures suggests that these folds are shallowly plunging and slightly overturned to the northwest, consistent with F_4 folding (Fig. 4.10).

Southeast of the Otter Pond shear zone, the Rogersons Lake Conglomerate (Fig. 4.3; Kean and Jayasinghe 1980) contains well developed S_4 spaced composite cleavage and a strong down-dip to northeast-plunging L_4 elongation lineation (Fig. 4.10) defined by stretched pebbles and cobbles. Presence of S-C fabric, asymmetric strain shadows around pebbles and cobbles (Fig.

4.9b), and northeast plunging L_4 indicate northwest directed dextral reverse shear in the Rogersons Lake Conglomerate. D_4 shear fabrics in the Rogersons Lake Conglomerate are parallel to and have the same kinematic significance as the fabric along the Victoria Lake shear zone (Valverde-Vaquero and van Staal, 2001), which is thus interpreted as a D_4 shear zone. This interpretation is consistent with the observed map pattern (Valverde-Vaquero and van Staal, 2002; van Staal et al. 2005), where the Victoria Lake shear zone truncates all of the D_{1-2} shear zones in the King George IV domain.

The effects of D_4 deformation are less noticeable outside of King George IV domain and development of S_4 cleavage was not pervasive. S_4 is largely manifested as a late steep crenulation cleavage that crosscuts composite S_{1-2} and is associated with variably plunging F_4 asymmetric folds. The small angle between the composite S_{1-2} and S_4 structures has locally resulted in the reactivation of S_{1-2} surfaces during D_4 (Fig. 4.5b). In these cases, the presence of F_4 folds of shallowly dipping S_3 definitively indicates D_4 deformation. In the Pats Pond and Tulks Valley domains, presence of S_4 is locally indicated by dextral boudinage of quartz veins in D_{1-2} shear zones under low-grade conditions, suggesting local reactivation of D_{1-2} shear zones as steep dextral faults.

D_{5-7} deformation

$D_1 - D_4$ structures are all overprinted by an inhomogenously developed northwest-striking steeply to moderately dipping S_5 crenulation cleavage and moderately to steeply plunging F_5 folds of S_1 to S_4. In areas of high D_5 strain, S_5 crenulation cleavage is readily distinguishable from the earlier formed foliations by its high angle to the pre-existing structures and overprinting relationships (Fig. 4.10). Development of S_5 is most intense in the area at the boundary of Pats Pond and King George IV domains, where S_5 finely spaced and axial planar to steeply plunging F_5 folds of composite S_{1-2}. In the Tulks Valley area, S_5 is spaced on a meter scale and is manifested as northwest striking sinistral kink bands. The orientation of the S_5 structures indicates a period of northeast southwest shortening at high angle to the strike of pre-existing structures.

D_6 strucutures are almost ubiquitously developed in all units and lithologies although the intensity decreases towards the northwest. They include shallowly plunging recumbent F_6

crenulations and box folds with locally developed axial planar spaced S_6 crenulation cleavage and conjugate kink bands. The establishment of conclusive overprinting relationships with S_5 has proven to be difficult due to heterogeneous development of S_5 and S_6, however, several outcrops suggest that S_5 is folded by F_6. Therefore S_6 is probably the younger fabric. The orientation of S_6 indicates that vertical shortening was accommodated during D_6 potentially as a result of $D_{3\text{-}5}$ thickening.

The latest phase of deformation (D_7) in the study area is represented by late brittle faults with apparent dextral displacement on the surface up to 700 m (Lissenberg et al. 2005c; Rogers et al. 2005a; van Staal et al. 2005 a, b, c). These faults cut across much of the study area and are especially apparent on geophysical compilations of Oneschuck et al. (2001, 2002). Although no outcrops of the faults have been observed, they have a locally very pronounced topographic influence. Along the Lloyds River gorge (Fig. 4.1), surface trace of the faults closely coincides with topographic breaks in the steep slope that suggest that these faults are steeply dipping. In the King George IV area, east-west trending fault juxtaposes the Annieopsquotch Ophiolite Belt and Silurian red-beds suggesting south side down. Unfortunately since the faults are not exposed and no small-scale structures have been positively related to them, their kinematic significance is ambiguous at this time.

GEOCHRONOLOGY

In order to constrain the timing of deformation, two U-Pb geochronology determinations were conducted at the Geological Survey of Canada (Ottawa) utilizing Thermal Ionisation Mass Spectrometry (TIMS). U-Pb TIMS analytical methods utilized in this study are outlined in Parrish et al. (1987). Heavy mineral concentrates were prepared using standard crushing, grinding, Wilfley™ table, and heavy liquid techniques. Mineral separates were sorted by magnetic susceptibility using a Frantz™ isodynamic separator. Multigrain zircon fractions were very strongly air abraded and titanite multigrain fractions were lightly air abraded following the method of Krogh (1982). Treatment of analytical errors follows Roddick (1987), with errors on the ages reported at the 2σ level (Table 4.1). A Concordia age (Ludwig 1998) is calculated for the samples presented in this paper. A Concordia age incorporates errors on the decay constants and includes both an evaluation of concordance and equivalence of the data (how well the data fit the assumption that they are

repeated measurements of the same point). The calculated Concordia ages and errors quoted in the text are at 2σ with decay constant errors included. U-Pb TIMS concordia diagrams are presented in Fig. 4.12. Additional information on the analytical procedures is provided in Appendix A4.

Puddle Pond Intrusive Suite (VL02A-241)

At Star Brook (Fig. 4.3), Puddle Pond Suite Diorite (431.6±4 Ma, $^{40}Ar/^{39}Ar$ hbl: Whalen et al. in press) is interlayered on meter scale with Puddle Pond Suite tonalite (427±1 Ma zircon: Whalen et al. in press) and intruded into the trace of the Otter Pond Boogie Lake shear zone. Both the diorite and tonalite are strongly sheared (Fig. 4.7a). Shear-sense indicators indicate south-southeast directed reverse shear at amphibolite facies metamorphic conditions that is progressively overprinted by greenschist facies metamorphic assemblages to the east (footwall). Puddle Pond Intrusive Suite diorite was sampled to constrain the age of amphibolite facies deformation and cooling to greenschist facies. The sample yielded abundant clear, uniformly light brown-orange fragments of euhedral titanite crystals (average 310 by 220 μm) with rare fractures and opaque inclusions. Three multi-grain titanite fractions were analyzed and all three analyses overlap each other and the concordia curve(Fig. 4.12). A Concordia age calculated using all three analyses is 426.0 ± 1.4 Ma (MSWD of concordance and equivalence=0.29, probability=0.92). Since the closure temperature of titanite is >500°C (Frost et al. 2000), this date is interpreted to represent the cooling of the diorite below amphibolite facies conditions, and thus places a upper limit on the time of amphibolite-facies deformation (D_2) at Star Lake Dam. Therefore D_2 deformation overlaps with the Salinic orogenic episode (Dunning et al. 1990).

Felsic dyke (RAX00-902)

A suite of feldspar porphyritc felsic dykes intruded black shale melange and broken formation of the Victoria River Delta fault (Thurlow et al. 1992), a few hundred meters south of the Red Indian Line that is here hidden beneath Red Indian Lake (Fig. 4.3). These dykes cut the scaly fabric (S_1) but are also contained as blocks in the melange zone indicating syn-tectonic (D_2) or inter-tectonic emplacement (see Fig. 4.12 of Thurlow et al., 1992). The dyke sample contained a moderate amount of zircon and four multi-grain fractions were analyzed (Fig. 4.12). Two fractions

(C1 and E1) overlap each other and concordia. A Concordia age using these 2 analyses is calculated to be 432.4 ± 0.8 Ma (MSWD of concordance and equivalence=0.19, probability=0.90). Fraction B1 is interpreted to have undergone minor Pb loss and fraction C2 contains an inherited component, probably of Ordovician age. The age of 432±1.4 Ma is interpreted to be the crystallization age of the felsic dyke.

METAMORPHISM

The generally low grade of metamorphism and multiple deformation events complicate the interpretation of equilibrium textures in tectonites, making it difficult to obtain precise temperature and pressure conditions. In addition, mafic tectonites, which form the predominant lithology, lack pressure sensitive mineral assemblages. Despite these complications several samples were useful in constraining the metamorphic conditions during deformation. Analytical procedures and mineral data are presented in Appendix 4 and Tables 4.2-4.6, respectively.

VL02-A193 Otter Pond Complex epidote amphibolite

A sample of epidote amphibolite was collected along the Otter Pond shear zone. S_1 wraps around large (up to 0.5 cm) recrystallized amphibole porphyroclasts and is folded by F_2 folds with no obvious mineral growth parallel to S_2. The matrix is heterogeneous and locally comprises an amphibolite-facies assemblage of hornblende-plagioclase, but more commonly an epidote amphibolite-facies assemblage of clinozoisite - amphibole -phengite ± plagioclase ± Mg-chlorite. The disappearance of chlorite in the hornblende-plagioclase domains suggests that the P-T conditions lie very close to the chlorite-out isograd (~550°C: Apted and Liou, 1983; Liou 1973, Liou et al. 1974). Based on the petrogenetic relationships determined by Ernst and Liu (1998), the persistence of epidote at the chlorite-out isograd suggests P > 0.3 GPa.

Compositions of plagioclase and amphibole were analyzed from both amphibolite and epidote amphibolite domains. Amphibole has a compositional range from magnesiohornblende, tschermakite to pargasite. Plagioclase is zoned and generally exhibits albite rich cores (An_{36}) and anorthite rich rims (An_{44}). Selected rim compositions of amphibole and plagioclase yield a narrow range of temperature (580-660°C assuming 0.4 GPa; Fig. 4.13a) on equilibrium mineral pairs utilizing the thermometer of Holland and Blundy (1994). The obtained temperature is in excellent

agreement with the inferred temperature near the chlorite-out isograd and is consistent with the T ~ 575-650°C (TiO_2 in amphibole) obtained from a semi-quantitative amphibole thermometer of Ernst and Liu (1998).

Massone and Schreyer (1987) have proposed a semi-quantitative phengite geobarometer that is based on the Si content of phengite in a limiting assemblage of phlogopite – K-feldspar – quartz. However, they have suggested that this geobarometer may be applied to non-limiting assemblages as long as there is a Fe-Mg silicate present, in which case minimum pressures may be derived. Massone and Szpurka (1997) have subsequently improved the phengite geobarometer.

Phengite is present in the clinozoisite ± amphibole ± plagioclase ± Mg-chlorite domains and is absent in the amphibole-plagioclase domains. This suggests that phengite is stable with amphibole, epidote and chlorite only up to ~550°C, the minimum temperature obtained on the amphibole-plagioclase assemblage. Two distinct populations of phengite have been identified in this sample (~3.23 Si pfu and ~3.1 Si pfu). Utilizing phengite barometer of Massone and Szpurka (1997) at 550°C in a non-limiting assemblage suggests minimum pressure of ~0.6 GPa. However owing to the lack of equilibration observed in natural phengites (Massone and Schreyer, 1987), this population may have formed under significantly lower temperatures which would have the effect of lowering the minimum pressure. The second population of phengite is restricted to smaller grains and phengite in contact with amphibole. Application of the barometer to these phengites suggests a lower minimum pressure of ~0.35 GPa. Examined lines of evidence indicate that metamorphism that accompanied D_1 deformation was characterized by intermediate temperature and pressure (P>0.3 GPa and T>550°C).

VL02-A192 Otter Pond Complex muscovite-garnet-biotite schist

A sample of muscovite schist was collected along the Otter Pond shear zone. S_1 foliation is defined by biotite-muscovite-garnet and feldspar-quartz rich domains. S_1 is transposed into a S_2 crenulation schistosity by tight to isoclinal F_2 folding, S_2 is defined by new large muscovite porphyroblasts and small biotite crystals which grew parallel to the F_2 axial plane. Formation of S_2 foliation is associated with neocrystalization of fine grained garnets in the mica-rich domains. Composite S_{1-2} foliation is subsequently folded by F_3 or F_4 kink bands accompanied by

retrogression of the S_2 mineral assemblages to fine grained aggregates of muscovite and chlorite. In S_2 cleavage domains, garnet, biotite, muscovite, plagioclase (An_{14-17}) and K-feldspar display a very narrow range of compositions. Core and rim analyses yield a narrow temperature (440-460°C) and pressure (0.29-0.35 GPa) range during D_2 based on garnet biotite-thermometer and garnet-biotite-muscovite-anorthite thermobarometer (Fig. 4.13b; Berman 1988).

VL02-A261 garnet-biotite-muscovite schist

A sample of Otter Pond Complex garnet-biotite-muscovite schist was collected along the Otter Brook shear zone. The orientation of the foliation is parallel to the local S_{1-2} composite fabric and it is interpreted to be S_2. S_2 is a compositional banding defined by alternating quartz and mica rich layers. Mica rich layers contain garnet-biotite-muscovite-plagioclase-quartz equilibrium mineral assemblage. Plagioclase has a very narrow compositional range from An_{23} to An_{25}, with the more albite-rich compositions occurring in proximity to garnet. Garnet displays consistent zoning with Mg and Fe-rich cores and Ca-rich rims. Muscovite is enriched in Fe and Mg towards the rim while biotite has a very narrow compositional range. The garnet-biotite thermometer indicates maximum temperature of ~540°C for the core and ~450°C for the rim compositions. P-T conditions calculated on basis of the garnet-biotite-muscovite-anorthite assemblage are almost identical for both core and rim compositions suggesting lack of equilibration during cooling from core to rim (Fig. 4.13c). Thus the best constraint on the pressure is the intersection of this reaction with garnet-biotite thermometer at the highest temperature which is equivalent to ~2 kbar.

Phengite geobarometer

Chlorite-muscovite assemblages are common in many felsic volcanic and epiclastic rocks as well as in greenschist – epidote amphibolite facies metabasites. In addition, as muscovite typically crystallizes parallel to foliations, the growth of muscovite relative to formation of fabric can be easily established. Application of the semi-quantitative phengite geobarometer (Massone and Schreyer 1987) can yield minimum pressure in non-limiting mineral assemblages as long as an Fe-Mg silicate phase is present. As chlorite is present in textural equilibrium with muscovite in all of the felsic volcanic and epiclastic rocks, and in some metabasites, the phengite barometer can be

utilized as a qualitative guide to decipher the tectonic history. The compositional range of phengite is summarized in Figure 4.14.

As the Si isopleths are not horizontal, the temperature needs to be specified in order to place any meaningful constraint on the minimum pressure. Although it is difficult to obtain temperature constraints in many of the rocks, the maximum temperature which has been obtained during the course of this study occurs along the Otter Pond shear zone (~650°C). However, other samples yielded lower temperature (460-550°C). Thus for samples along Otter Pond shear zone, an average temperature of 550° is used unless other constraints are available. The temperature appears to decrease to the southeast of the Otter Pond shear zone. Conodonts (CAI 5+, Nowlan 2004) recovered along the Victoria Delta Fault in the Tulks Valley domain (Fig. 4.3) suggest maximum T = 440°C (Rejebian et al. 1987). This is taken as typical maximum temperature achieved by rocks southeast of the Otter Brook shear zone.

D_1 phengites consistently contain 3.2 to 3.3 Si pfu (Table 4.7). Utilizing the phengite barometer of Massone and Szpurka (1997), D_1 phengite yields P = 0.45 to 0.6 GPa at T = 440 to 550°C. Although the majority of these estimates are minimum pressure estimates in non-limiting assemblages, two samples of the D_1 phengites do contain the limiting assemblage and suggest moderate pressure (~0.55-0.6 GPa). D_2 phengite contains ~3.11 Si pfu (Table 4.7), suggesting lower P ~ 0.2 to 0.35 GPa at T ~ 440 to 550°C during D_2 deformation. The pressure range for the D_2 obtained by phengite barometry is in agreement with the pressure obtained by garnet-biotite-muscovite-plagiolase thermobarometer for syn D_2 assemblages (see above). Utilizing the phengite geobarometer in combination with quantitative thermobarometry (see above) suggests that P recorded by syn-D_1 mineral assemblages was the highest (>0.3 G.Pa), while syn- to post-D_2 mineral assemblages record lower pressures (0.2-0.3 GPa).

Amphibole chemistry

Lloyds River Ophiolite Complex metabasites (VL02A232, VL02A236, VL02A240, VL02A257, VL02A275) are utilized for studying metamorphism – deformation relationships in proximity to the Otter Pond shear zone along the Lloyds River gorge. The fine grain size, local lack of equilibrium, presence of assemblages which are poorly constrained by thermodynamic data as

well as commonly complex mineral zoning preclude precise P-T condition determination from these samples. The analysis of the amphibole and plagioclase compositions can nonetheless be informative qualitatively, especially considering the uniform chemical composition of the samples (Zagorevski et al. 2006). The compositional range of amphiboles is summarized in Figure 4.15.

Three distinct generations of amphibole ($A_1 - A_3$) growth have been observed in this suite. A_1 amphiboles generally occur as mantled cores or porphyroclasts and typically display extensive recrystallization and exsolution of fine-grained xenomorphic titanite. At least locally, A_1 amphiboles have a preferred orientation defining S_1 and are folded by F_2 folds, thus they are interpreted to have grown during D_1 deformation (Fig. 4.7). A_1 amphiboles are Al poor and generally have actinolite to magnesiohornblende compositions.

Transition from A_1 cores to Al-rich A_2 rims is abrupt in some samples, while others have a complete compositional range or patchy replacement of A_1 actinolite to A_2 magnesiohornblende. A_2 amphiboles show both pre- and syn-S_2 growth. Syn-D_2 hornblende-plagioclase pairs yield a range of temperatures from 466 to 640°C (assuming 3 kbar; Holland and Blundy, 1994). Core-rim relationships in the plagioclase and amphibole indicate increasing temperature during D_2 deformation along this portion of the Otter Brook shear zone. Syn-D_2 amphiboles are locally crosscut by A_3 pargasite indicating that the metamorphism outlasted D_2.

Further away from the Otter Brook shear zone the different phases of amphibole growth can still be differentiated (A_1-A_3), however all of these amphibole phases have a much more restricted range of compositions from actinolite to Al-poor magnesiohornblende (VLA02-275). This suggests that only the samples in the immediate vicinity of the Otter Pond shear zone experienced the elevated temperatures during and after D_2.

DISCUSSION

The central Newfoundland Appalachians preserve a complex collage of tectono-stratigraphic units that were formed and structurally juxtaposed during the closure of the Iapetus Ocean. We have identified four episodes of ductile deformation (D_{1-4}) that were followed by several minor brittle-ductile episodes (D_{5-7}). Significantly, the less complex structural history of the patchy Silurian cover and relatively low intensity overprint of by D_{2-7} structures has allowed the

identification of a distinct phase of Ordovician deformation (D_1) and elucidation of its kinematic significance, which allows us to address long-standing issues in the assembly of the Dunnage Zone, principally involving the timing of accretion and the vergence of D_1 structures. To this end, we will begin with reconstructing of D_1 tectonostratigraphy and constraining the age of structures. A schematic block diagram depicting D_1-D_4 evolution is presented in Figure 4.16.

D_1 tectono-stratigraphy

Despite the locally strong transposition of S_1 into S_2 and the reactivation of the D_1 shear zones as D_2 south-southeast directed reverse-faults sufficient evidence is preserved to reconstruct the D_1 tectono-stratigraphy. S_1 fabrics range from weak within the tectonic panels to mylonitic along the boundary zones. Local preservation of shallow dipping mylonitic S_1 in the hinges of upright F_2 (Fig. 4.5d) suggests that S_1 was originally shallowly dipping. The enveloping surface of asymmetric upright F_2 folds of S_1 is moderately north to northwest dipping. Although this geometry could indicate location on the northwest-dipping limb of a regional scale upright fold, the lack of repetition of tectono-stratigraphic units to the southeast strongly suggests that this is not the case. More likely the original orientation of the enveloping surface of S_1 controlled subsequent asymmetry of upright F_2 folds, such that its enveloping surface also had a northwest dip (Fig. 4.16).

Localization of the D_2 strain along the D_1 shear zones and local reactivation complicates the interpretation of the direction of transport during D_1. In the Tulks Valley domain for example, L_1 extension lineations in the Barren Pond Fault are commonly reutilized as F_2 fold axes, whereas other kinematic indicators such as S-C fabrics are likely to have formed during D_2, making reconstruction of D_1 transport difficult if not impossible. The D_1 shear sense indicators must then be looked for in areas where the F_2 fold axes are not coincident with L_1 and where D_2 strain is low. In the Pats Pond domain the upright F_2 folds plunge to the southwest and S_2 is oblique to the very well developed shallowly south plunging L_1 stretching lineation. Development of asymmetric strain shadows around volcanic fragments suggests sinistral shear along the Red Indian Line. If the effects of F_2 folding are removed and the surface is reconstructed to a northwest dip, L_1 lineation would plunge to the north and have a moderate rake suggesting south-southeast-directed thrusting.

The consistent northwest younging of the structural panels, (sub)-parallelism of the S_1 fabrics with S_0 compositional layering, and map scale low angle cut-offs of tectono-stratigraphic units are best explained by originally shallow northwest-dipping D_1 shear zones. Combining this evidence with the consistent old over young relationships across D_1 shear zones suggests that D_1 shear zones most likely represent southeast-directed thrusts.

Age of D_1 deformation and local correlations

Despite D_2 folding and reactivation of D_1 shear zones, the kinematic significance of D_1 has been ascertained. Thrust related deformation and intermediate pressure (0.45 to 7 Gpa: see above) during D_1 suggest the development of D_1 structures during the accretion of the elements of the Annieopsquotch Accretionary Tract to the Laurentian margin. Geochronological, isotopic and stratigraphic data indicate that D_1 thrusting was not a single short lived accretionary episode but was progressive and protracted.

The early D_1 thrusts juxtaposed Annieopsquotch Ophiolite Belt, Lloyds River Ophiolite Complex and Buchans Group. Portions of the Otter Brook shear zone are marked by syn-tectonic Otter Pond Complex (468±2 Ma: Appendix 3) intrusive phases of which stitch the contact between the Annieopsquotch Ophiolite Belt and Lloyds River Ophiolite Complex. Despite intrusion into ophiolitic rocks, the Otter Pond Complex shows high degree of a crustal contamination (ε_{Nd} –1 to –6: Appendix 3) and contains zircon inheritance that is identical in age to the structurally underlying Buchans Group (Chapter 2; Dunning et al. 1987). This suggests that Annieopsquotch Ophiolite Belt and Lloyds River Ophiolite were also juxtaposed with the Buchans Group prior to c. 468 Ma.

Shear zones that share the age and characteristics with the early D_1 thrusts described herein have been previously identified outside of the immediate study area (Fig. 4.3; Hungry Mountain Thrust: Calon and Green, 1987; Thurlow, 1981; Lloyds River Fault: Lissenberg et al. 2005b). The Lloyds River Fault forms the boundary between the Annieopsquotch Ophiolite Belt to the southeast and Dahswoods Subzone to the northwest. Lloyds River Fault accommodated sinistral south-southeast directed underthrusting of the Annieopsquotch Ophiolite Belt from 470 to 458 Ma (Fig. 4.3; Lissenberg et al. 2005b) under intermediate pressure amphibolite facies (800°C and at 0.6 GPa: Lissenberg et al. 2005).

In the Buchans area, early D_1 thrusting is exemplified by the Hungry Mountain thrust (Fig. 4.3; Thurlow, 1981; Calon and Green 1987), a probable correlative of the Otter Brook shear zone. The Hungry Mountain Thrust juxtaposes the Hungry Mountain Complex (463±4; 467±8: 469±1 Ma: van Staal et al. in press; Whalen et al. 1997) with the structurally underlying greenschist to amphibolite facies ophiolite (Harry's River metabasite; e.g. Calon and Green 1987) and sub-greenschist facies Buchans Group (Calon and Green 1987; Thurlow 1981; Thurlow and Swanson 1987). The inverted metamorphic gradient below the Hungry Mountain thrust (Thurlow 1981) indicates that the emplacement took place while the Hungry Mountain complex was still hot, thus the thrusting must have occurred prior to the cooling of the youngest pluton (466±2 Ma: Whalen et al. 1997). The development of the Buchans thrust stack is thought to have occurred synchronously with the Hungry Mountain Thrust (e.g. Airport Thrust: Calon and Green, 1987; Thurlow and Swanson, 1987; Thurlow et al. 1992) and hence, thought to have formed during D_1.

The Wood Lake shear zone, Red Indian Line, Victoria Delta Fault, and Barren Pond shear zone juxtaposed the accreted tectono-stratigraphic units with the Red Indian Lake Group (465-460 Ma: Chapter 2), Wigwam Brook Group (c. 453 Ma: Chapter 3), Sutherlands Pond Group (c. 464 Ma: Dunning et al. 1987) and Tulks Group (498-495 Ma: Evans et al. 1990). These shear zones could not have been involved in the early D_1 thrusting as they juxtapose units that are too young, and hence they are collectively interpreted to be late D_1 thrusts.

Almost ubiquitous presence of Caradocian black shale mélange along segments of late D_1 thrusts (e.g. Victoria Delta Fault: Thurlow et al., 1992; Red Indian Line: Rogers and van Staal, 2002) and involvement of tectono-stratigraphic units as young as 453±4 Ma (Wigwam Brook Group: Chapter 3) suggest that the juxtaposition of the Annieopsquotch Accretionary Tract and Victoria Lake Supergroup along the Red Indian Line occurred in Late Caradoc, consistent with the lack of involvement of any identifiable Ashgill-age rocks in these D_1 shear zones. Correlatives of the late D_1 shear zones can be readily identified in the Buchans area and include the Willey's River Fault, Powerline Fault, and Tilley's Pond Fault (Fig. 4.3). The Powerline Fault terminates the early D_1 Buchans thrust stack and juxtaposes portions of the Buchans Group with the structurally underlying Red Indian Lake Group. Geophysical compilation (Davenport et al. 1996) suggests that the

Powerline Fault is continuous with the Willey's River Fault, which is locally marked by black shale melange (Thurlow et al. 1992). The Tilley Pond Fault juxtaposes the Skidder Formation of the Red Indian Lake Group with the Buchans Group (Fig. 4.3).

The upper limit on the D_1 deformation is provided by the unconformably overlying Silurian strata and cross-cutting plutons that intrude along the D_1 shear zones. Unconformable Silurian conglomerate locally contains previously foliated clasts (Kean 1983; Kean and Jayasinghe 1980) indicating erosion of D_1 tectonites. Silurian plutons occasionally contain xenoliths of D_1 tectonites (e.g. Boogie Lake: Zagorevski and van Staal 2002; Lloyds River Granite: Lissenberg 2005) or have a map pattern of stitching plutons (e.g. Halfway Mountain Granodiorite: Whalen et al. 1987). Dykes of the Silurian Topsails Suite cut across the D_1 thrust in the Buchans area (Thurlow 1981). These relationships suggest that the D_1 deformation was finished by c. 435+6/-3 Ma, the age of the oldest crosscutting pluton in the study area (Boogie Lake Intrusive Suite: Dunning et al. 1990).

Age of D_2 deformation

The Boogie Lake Intrusive Suite also provides a lower constraint on the D_2 deformation. This suite is locally weakly foliated (S_2) and satellite dykes are folded by F_2, suggesting pre- to syn-D_2 emplacement and cooling. Similarly Puddle Pond Suite felsic dykes (432.4±0.8 Ma: see above), which intrude along the Victoria River delta fault near the Red Indian Line, crosscut the existing scaly mélange fabric, which is parallel to the composite S_{1-2} foliation in the adjacent volcanic and sedimentary rocks. The felsic dyke is dismembered within the mélange zone and some parts contain a weak foliation parallel to S_{1-2}. These relationships suggest syn-D_2 or inter-tectonic (D_1 to D_2) emplacement of the dyke into the fault zone. These dykes and the Boogie Lake Intrusive suite thus indicate that D_2 started prior to or at c. 430 Ma.

Puddle Pond Suite at Star Brook provides additional constraints on the duration of the D_2 deformation although upper constraints of D_2 could not be obtained in the study area. The Puddle Pond Intrusive Suite diorite and tonalite (431±4 Ma $^{40}Ar/^{39}Ar$ and 427±1: Whalen et al. in press) are deformed at amphibolite facies. The cooling of titanite below its closure temperature (>500°C: Frost et al. 2000) at 426±1 Ma (U/Pb titanite: see above) indicates that the suite cooled below amphibolite

facies. However, greenschist-facies deformation in the suite, including formation of mylonite indicates that D_2 continued after 426±1 Ma.

The plutonic rocks in the study area constrain D_2 deformation to have started at least by c. 435 Ma and finished sometime after c. 426 Ma. This age range of deformation implies that all of the Silurian supra-crustal rocks (c. 430-427 Ma: Chandler et al. 1987; Dunning et al. 1990) have been deposited syn-tectonically. In the study area, Silurian red-beds (c. 429 Ma: Dunning et al. 1990) are intimately associated with the footwall of the D_2 reactivated Otter Brook shear zone, suggesting the red-beds were probably deposited syn-tectonically at the toe of the southeast vergent thrust stack. If correct, the latter implies that at least part of the thrust stack had breached sea level during the Early Silurian and was being eroded.

Ages of D_{3-7} deformation

There are no direct constraints on the timing of the D_3 deformation. S_3 clearly post-dates F_2 upright folding. However, in the Star Brook area, S_3 shear bands are nearly parallel with S_2 in the adjacent Puddle Pond Suite Pluton suggesting that S_3 may be in part coeval with D_2, potentially forming late during D_2 during south-southeast directed shear. The D_3 deformation is thus best constrained as syn- to post 426±1 Ma.

Similar to D_3, the age of D_4 is poorly constrained at present. Since F_4 clearly overprint composite S_{1-2} fabric the start of D_4 postdates 426±1 Ma (see above). To the southeast of the study area, the age of D_4 deformation is constrained by the Meelpaeg Subzone syn-kinematic migmatite (417±2Ma: Currie et al. 1991), which predates the final post-peak metamorphism juxtaposition of the Meelpaeg Subzone amphibolite-facies tectonites with the Exploits Subzone greenschist-facies tectonites along the Victoria Lake shear zone (Valverde-Vaquero and van Staal 2001). There are no further time constrains available to constrain the duration of D_4 or the timing of D_{5-7}.

REGIONAL IMPLICATIONS

The proposed structural history (Fig. 4.16) is consistent with the available stratigraphic and structural evidence from central Newfoundland and regional tectono-stratigraphic framework (e.g. van Staal et al. 1998), although application of this model outside of the study area is difficult because comparable stratigraphic, geochronological, isotopic and structural controls are rare or

absent. We have demonstrated that the Ordovician D_1 terrane boundaries in central Newfoundland have been reactivated during Early to Middle Silurian D_2 and locally during Late Silurian to Early Devonian D_4 (see above). Thus the D_1 terrane boundaries could have accomodated Middle Ordovician to late Silurian south-southeast directed thrusting and folding (D_1, D_2, D_3), or latest Silurian -Early Devonian northwest-directed dextral oblique thrusting and folding (D_4) depending of the intensity of the overprinting deformation (Fig. 4.11). This sequence of events may shed some light on the controversy surrounding the age and kinematic significance of the terrane boundaries elsewhere in Newfoundland, as they may be products of multiple episodes of shear zone reactivation.

The proposed deformation history can be tested in the correlative tracts in the Notre Dame Bay area, where the interpretation of structures has been controversial (e.g. Arnott et al. 1985; Dean and Strong 1977; Dec et al. 1995; Dec and Swinden 1994; Elliot et al. 1991; Kerr 1996; van der Pluijm 1986; Lafrance and Williams 1992; Szybinski 1995). Complex deformation in the Notre Dame Bay has resulted in various interpretations of the significance of the terrane boundaries ranging from north-directed thrusts, south-directed thrusts, strike-slip faults of regional significance to relatively minor faults (see Dean and Strong (1977) for discussion, also Arnott et al. 1985; Dec and Swinden 1994; Kerr 1996; Lafrance and Williams 1992).

Our structural history is most consistent with the model of Szybinski (1995) who proposed Middle Ordovician deformation (465±2.5 Ma: U/Pb zircon on syn-kinematic Coopers Cove Pluton), followed by Silurian southeast-directed thrusting and folding (c.f. Lafrance and Williams 1992). Despite identification of Middle Ordovician deformation (equivalent to early D_1), no shear zones have been identified related to either early or late D_1, and the terrane boundaries in the Notre Dame Bay are generally interpreted as wholly Silurian structures (Szybinski 1995; Lafrance and Williams 1992) inconsistent with Ordovician terrane boundaries in our model. These seemingly contradictory interpretations may be reconciled by multiple reactivation of shear zones. For example, the Lobster Cove – Chanceport fault, a terrane boundary in the Notre Dame Bay, has been interpreted to be a Silurian thrust based on the presence of the Silurian Springdale group in the footwall (e.g. Dean and Strong 1978; Lafrance and Williams 1992; Szybinski 1995). The Lobster Cove fault occurs above

the Buchans – Roberts Arm and is a likely correlative of the Otter Brook shear zone. Similar to the Otter Brook shear zone, the Lobster Cove fault records a period Silurian south-southeast-directed thrusting, however based on our work, we predict that the Lobster Cove Fault was reactivated during the Silurian (equivalent to D_2) and has an earlier Ordovician history.

Correlation of the D_2 structures with the structures in the Notre Dame Bay area has important implications for the timing of D_2 in the study area. In the Notre Dame Bay, the maximum age of correlated D_2 deformation is provided by the predominantly Llandovery to Wenlock Botwood Group (Williams 1993). Crosscutting Ludlow felsic dikes (422±2 Ma: Elliot et al. 1991) and the unconformably overlying Stony lake volcanic rocks (423+3/-2 Ma: Dunning et al. 1990) indicate that the Botwood Group was deformed before the Late Silurian.

Subsequent deformation in Notre Dame Bay was accommodated by a northwest-directed thrust and fold belt (Szybinski 1995) and dextral shear zones and folds (Lafrance and Williams 1992). The maximum age of the deformation is constrained by crosscutting dykes of the Loon Bay Suite (408±2 Ma: Elliot et al. 1991). The age and vergence of the structures suggests that this phase of deformation is correlative to D_4 and is most simply related to the Acadian arrival of Avalonia. Application of the structural model developed for central Newfoundland to the Notre Dame Bay region yields significant promise for establishing a regionally consistent sructural framework. Salinic and Acadian deformation is easily comparable between the two areas; however the identification of Taconic structures in the Notre Dame Bay is difficult at present. Future studies should concentrate on the identification of the Ordovician structures as these constrain the first order architecture of the Dunnage Zone and control the distribution of tectono-stratigraphic units including those hosting significant mineralization.

TECTONIC SIGNIFICANCE

D_1 has been herein constrained by geochronology and tectono-stratigraphic relationships to involve several discrete or continuous thrusting events starting at c. 470 and lasting as late as 435 Ma. Early D_1 involved the Lloyds River Fault (Lissenberg 2005) Otter Brook shear zone, and Hungry Mountain Thrust (Thurlow, 1982). The late D_1 involved the Mink Lake shear zone, Wood Lake shear zone, Powerline, Willey's River, and Tilley's Pond faults (Thurlow et al. 1992), Red Indian Line,

Victoria Delta Fault (Thurlow et al. 1992) and Barren Pond Fault (Fig. 4.3). The shallow north-westerly dip of the enveloping surface of asymmetrical F_2 folds combined with old-over-young relationships indicate that the juxtaposition of the tectono-stratigraphic units occurred along shallow northwest-dipping reverse shear zones (Fig. 4.16). Both shallow (4.5 km: Thurlow et al. 1992) and the trans island Lithoprobe seismic reflection surveys (Fig. 4.17; van der Velden et al. 2004) support our interpretation of the original orientation and kinematic significance of the D_1 thrusts. Thurlow et al. (1992) have identified many of the D_1 thrusts in the Buchans area, where they dip between 0 and 45° degrees to the northwest. Crustal scale reflectors that correspond to the surface trace of the Lloyds River Fault, Otter Brook shear zone and the Red Indian Line dip approximately 45-55° to the northwest on the re-interpreted seismic reflection profiles of van der Velden et al. (2004). D_1 thrusts are continuous along the entire length of the mapping area (~150 km) and likely continue to the northeast through the Gullbridge belt (Pope et al. 1991) to the Roberts Arm Group (Bostock 1978).

The regional (>150 km strike length) and crustal scale continuity (>25 km depth, van der Velden et al. 2004) of the D_1 structures and moderate pressure metamorphism (<400 to 650°C, 4.5 to 8 kbar: see above; Lissenberg 2005) indicate that D_1 structures formed during assembly of the Annieopsquotch Accretionary tract. As already discussed, the development of D_1 thrusts and movement along them occurred from Middle Ordovician to Lower Silurian. The early development of the southeast-directed D_1 thrust stack (Fig. 4.16, 4.17) is probably related to stresses generated during the closure of the Humber Seaway (Waldron and van Staal 2001) and the Laurentia-Notre Dame arc collision (van Staal et al. submitted) This phase of deformation involves strictly peri-Laurentian tectonic elements and is therefore Taconic (van Staal 2005). The Taconic D_1 lasted at least until c. 460 Ma, the age of the syn-tectonic Pierres Pond Intrusive Suite (Appendix 3).

The late Caradoc arrival of the peri-Gondwanan Victoria Arc at the Laurentian margin closed the main tract of the Iapetus in a Molluca sea-type collision (van Staal et al. 1998) and juxtaposed the peri-Laurentian and peri-Gondwanan terranes along the Red Indian Line (late D_1), marking the end of the strictly peri-Laurentian Taconic orogeny (Fig. 4.17). This late phase of D_1 resulted in continuation of development of a south-southeast-directed thrust belt and movement along the early D_1 thrusts. During this event, the Victoria Arc was thrust beneath the Notre Dame

Arc and Annieopsquotch Accretionary Tract (Fig. 4.17; van der Velden et al. 2004). This was accompanied by uplift in the Notre Dame Subzone and syn-tectonic Late Ordovician to Early Silurian marine sedimentation in the Exploits Subzone (lower part of Badger Group, Williams et al., 1993). Immediately after the Late Caradoc collision between the Laurentian margin and the Victoria arc, subduction stepped back into the Exploits-Tetagouche backarc basin (Fig. 4.17; van Staal et al. 1998).

The presence of the Silurian overlap sequence in the Notre Dame and western part of the Exploits subzones indicates that this portion of the Newfoundland Appalachians was assembled prior to the Silurian. Development of a Silurian-age south-southeast-directed thrust and fold belt, intrusion of syn-tectonic plutons (see above; Dunning et al. 1990), local mélange formation (e.g. Joey's Cove Melange; Lafrance and Williams 1992), Silurian unconformities (Williams 1995) and reactivation of D_1 shear zones (e.g. Red Indian Line: see above) represent documented products of the Salinic Orogeny (D_{2-3}). D_2 (>432 to <426 Ma: see above), which is also responsible for formation of the main regional transposition foliation (S_2) and accompanying lower pressure metamorphism (<440 to 650 °C and 0.2 to 0.35 GPa: see above) in the Annieopsquotch Accretionary Tract. Associated folds (F_2) steepened and reactivated the D_1 shear zones as south-southeast-directed sinistral oblique reverse faults and thrusts (Fig. 4.16). The development of the southeast-directed fold and thrust belt during the Salinic orogeny is ascribed to the Ashgill – Wenlock closure of the Exploits-Tetagouche backarc basin (Fig. 4.17; van Staal et al., 1998; Valverde Vaquero et al., in press), which finally sutured along the Dog Bay Line (Williams 1993) and led to the accretion of Ganderia to the composite Laurentian margin (e.g. Dunning et al. 1990; van Staal et al. 1998; van Staal 2005; Williams 1993). During the collision the Gander margin (van Staal 1994) was partially subducted under the composite Laurentian margin (e.g. van der Velden et al. 2004). The end of the Salinic orogeny is marked by the eruption of the apparently undeformed, c. 423 Ma Stony Lake Rhyolite, which lies on an angular unconformity above the cleaved and generally steeply dipping Botwood Group (e.g. Dunning et al. 1990).

Subsequent to the Salinic accretion of Ganderia, subduction stepped back outboard into the narrow seaway between Ganderia and Avalonia (van Staal, 2005; Appendix 2; Valverde Vaquero et

al. in press). The latest Silurian accretion of Avalonia is responsible for the start of the Acadian Orogeny (D_4) and marks the last significant phase of regional ductile deformation in the study area (Fig. 4.16). Northwest directed, dextral oblique Victoria Lake shear zone forms the most notable D_4 structure in the study area and accommodated the northwest dextral oblique emplacement of the Gander zone amphibolites (Meelpaeg allochton) over the Exploits Subzone (e.g. van der Velden et al. 2004). Elsewhere, Acadian D_3 resulted in reactivation of D_{1-2} shear zones as dextral faults and formation of F_3 northwest directed folds and brittle-ductile faults.

Figure 4-1 Simplified geology of the study area (modified from Kean, 1979b; Lissenberg et al., 2005c; Rogers et al., 2005a; van Staal et al., 2005 a, b, c). U/Pb ages compiled from Dunning and Krogh (1985), Dunning et al. (1987), Zagorevski et al. (2006). Inset: Lithostratigraphic subdivisions of Newfoundland (after Williams 1995). CBF – Clench Brook Fault, HMC – Hungry Mountain Complex, HMT – Hungry Mountain Thrust, RIL – Red Indian Line, TPF – Tilley's Pond Fault.

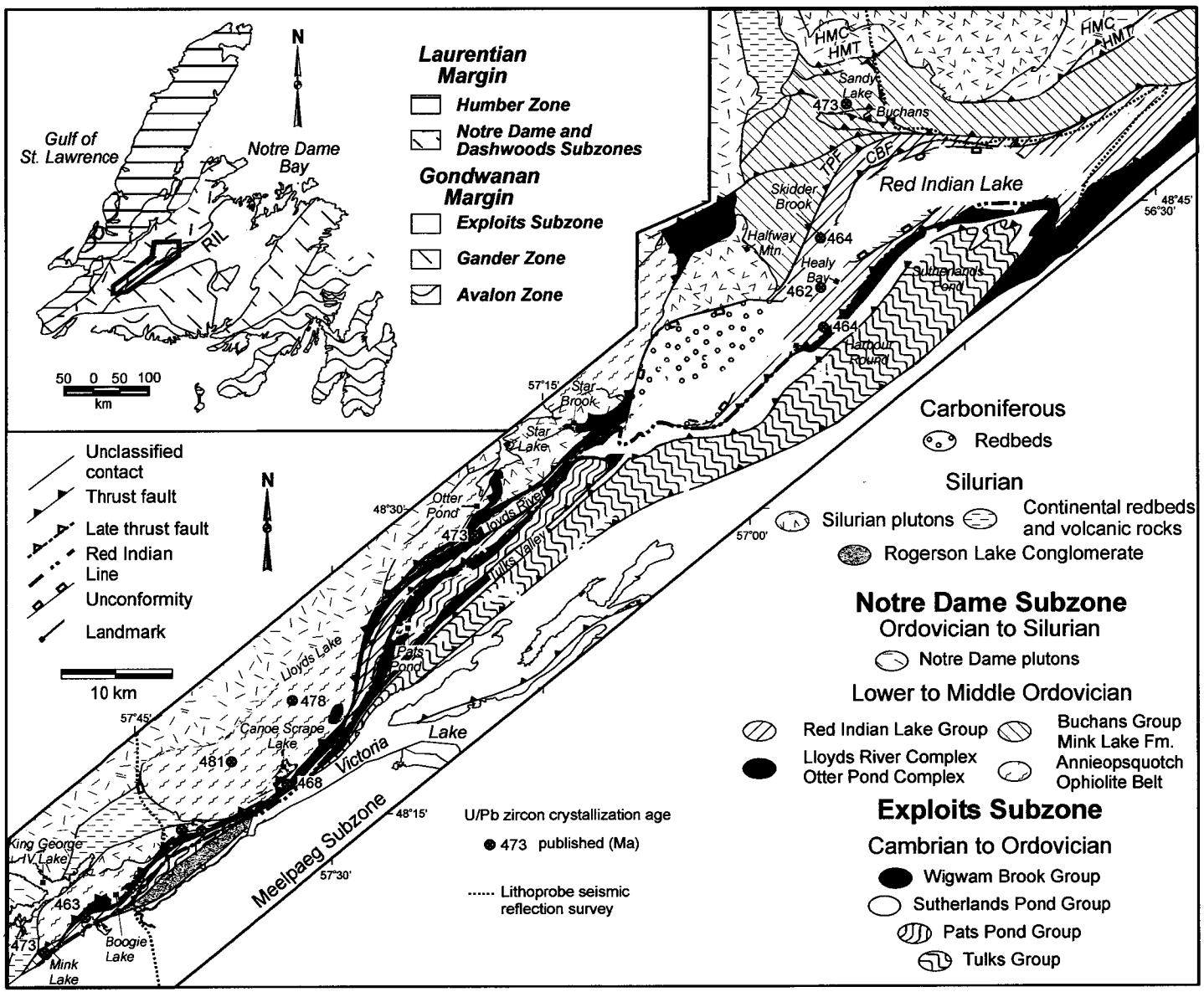
Laurentian Margin
Humber Zone
Notre Dame and Dashwoods Subzones
Gondwanan Margin
Exploits Subzone
Gander Zone
Avalon Zone
Gulf of St. Lawrence
Notre Dame Bay
RIL
50 0 50 100
km
N
Unclassified contact
Thrust fault
Late thrust fault
Red Indian Line
Unconformity
Landmark
10 km
HMC
HMT
Sandy Lake
473
Buchans
TPF
CBF
Red Indian Lake
Skidder Brook
Halfway Mtn.
464
Healy Bay
462
Sutherlands Pond
Harbour Round
48°45'
56°30'
57°15'
Star Brook
Star Lake
48°30'
Otter Pond
473
Lloyds River
Tulks Valley
57°00'
Lloyds Lake
Pats Pond
478
57°45'
Canoe Scrape Lake
481
468
Victoria Lake
48°15'
Meelpaeg Subzone
57°30'
King George IV Lake
463
473
Mink Lake
Boogie Lake
U/Pb zircon crystallization age
473 published (Ma)
Lithoprobe seismic reflection survey
Carboniferous
Redbeds
Silurian
Silurian plutons
Continental redbeds and volcanic rocks
Rogerson Lake Conglomerate
Notre Dame Subzone
Ordovician to Silurian
Notre Dame plutons
Lower to Middle Ordovician
Red Indian Lake Group
Lloyds River Complex
Otter Pond Complex
Buchans Group
Mink Lake Fm.
Annieopsquotch Ophiolite Belt
Exploits Subzone
Cambrian to Ordovician
Wigwam Brook Group
Sutherlands Pond Group
Pats Pond Group
Tulks Group

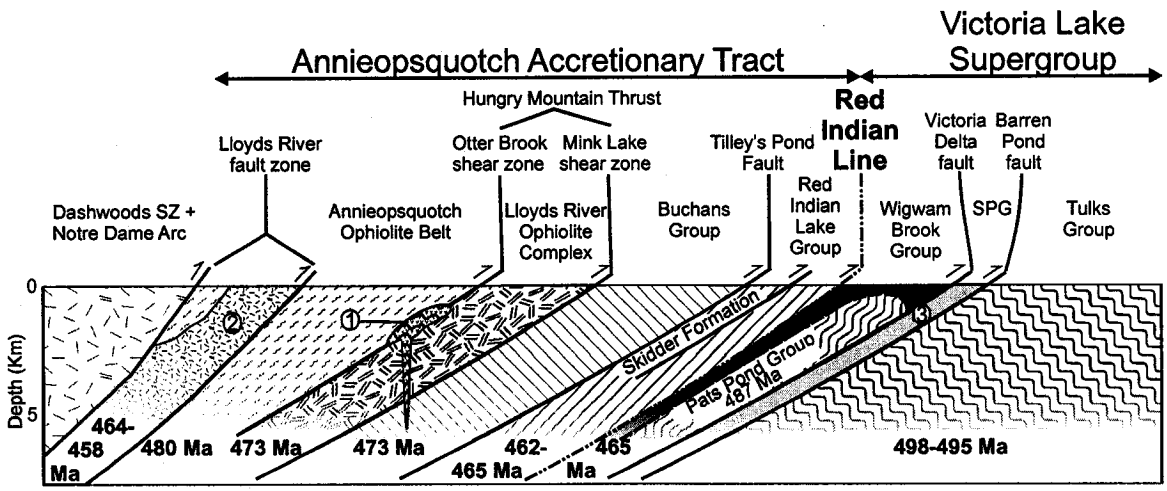

Figure 4-2 Schematic tectono-stratigraphy of the study area. SPG - Sutherlands Pond Group (c. 462 Ma: Dunning et al. 1987; Rogers and van Staal 2002). Age dates from Dunning and Krogh (1985), Evans et al. (1990), Lissenberg et al. (2005b), Zagorevski et al. (submitted), Zagorevski et al. (2006).

Figure 4-3 Location of the major shear zones and structural domains.

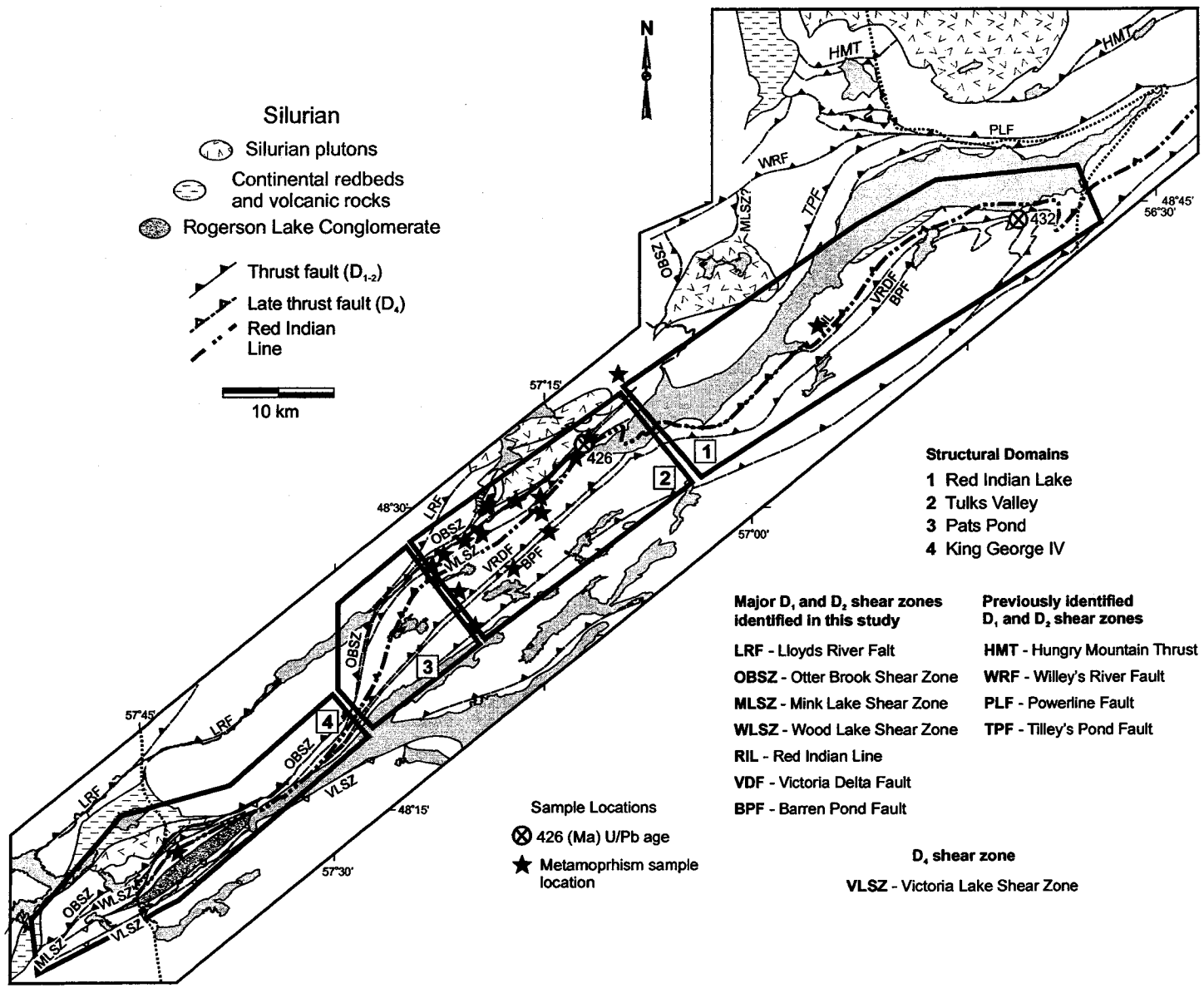
Silurian
Silurian plutons
Continental redbeds and volcanic rocks
Rogerson Lake Conglomerate
Thrust fault (D_{1-2})
Late thrust fault (D_4)
Red Indian Line
10 km
N
HMT
PLF
WRF
TPF
MLSZ?
OBSZ
RIL
VRDF
BPF
LRF
WLSZ
VLSZ
426
432
1
2
3
4
57°15'
57°00'
48°30'
48°45'
56°30'
57°45'
48°15'
57°30'
Structural Domains
1 Red Indian Lake
2 Tulks Valley
3 Pats Pond
4 King George IV
Major D_1 and D_2 shear zones identified in this study
LRF - Lloyds River Falt
OBSZ - Otter Brook Shear Zone
MLSZ - Mink Lake Shear Zone
WLSZ - Wood Lake Shear Zone
RIL - Red Indian Line
VDF - Victoria Delta Fault
BPF - Barren Pond Fault
Previously identified D_1 and D_2 shear zones
HMT - Hungry Mountain Thrust
WRF - Willey's River Fault
PLF - Powerline Fault
TPF - Tilley's Pond Fault
D_4 shear zone
VLSZ - Victoria Lake Shear Zone
Sample Locations
426 (Ma) U/Pb age
Metamoprhism sample location

Figure 4-4 Equal area lower hemisphere projections of bedding in Ordovician rocks (S_0) and first generation structures (S_1, L_1; N = number of points; see text for discussion).

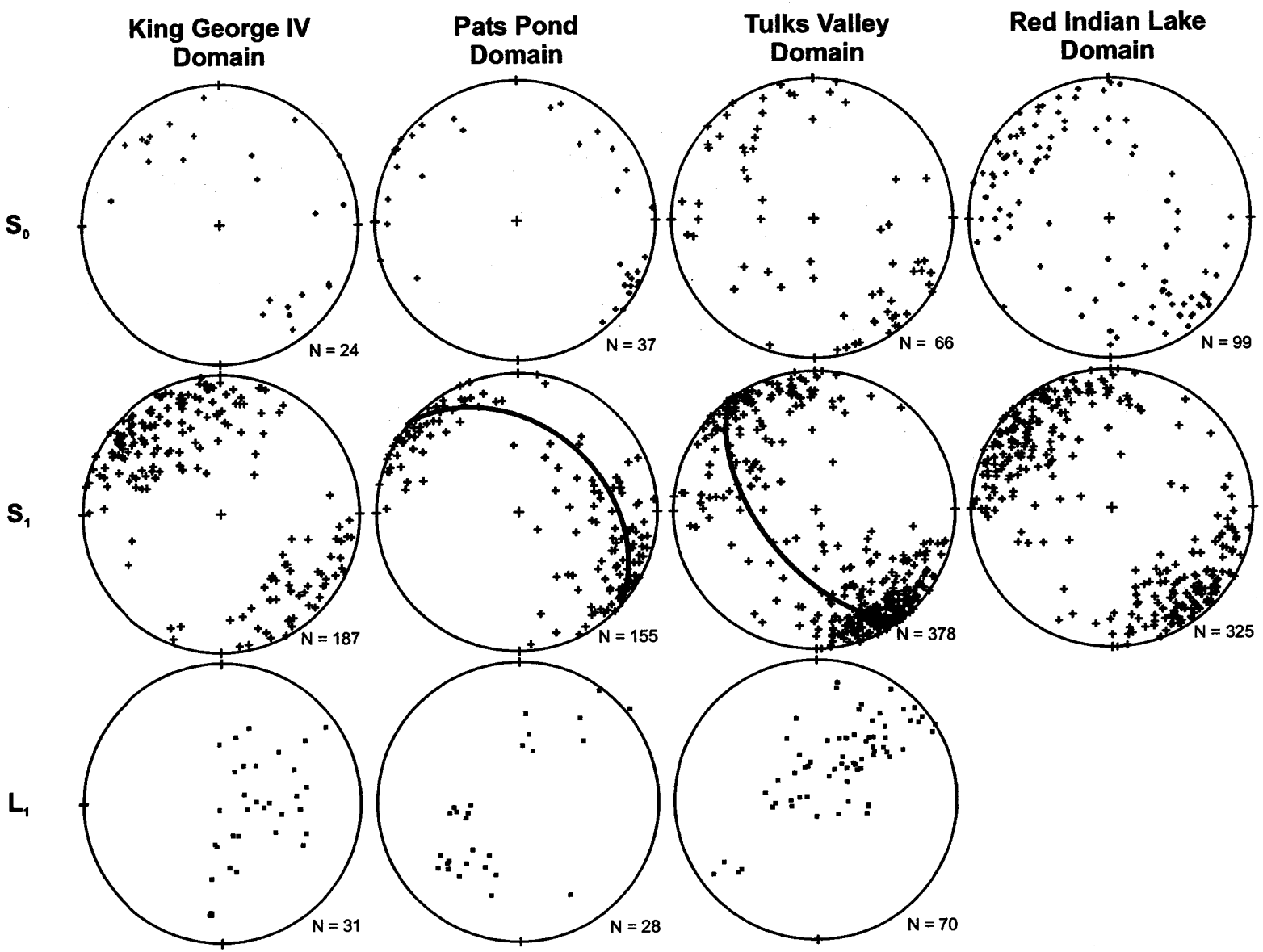
King George IV Domain
Pats Pond Domain
Tulks Valley Domain
Red Indian Lake Domain
S0
S1
L1
N = 24
N = 37
N = 66
N = 99
N = 187
N = 155
N = 378
N = 325
N = 31
N = 28
N = 70

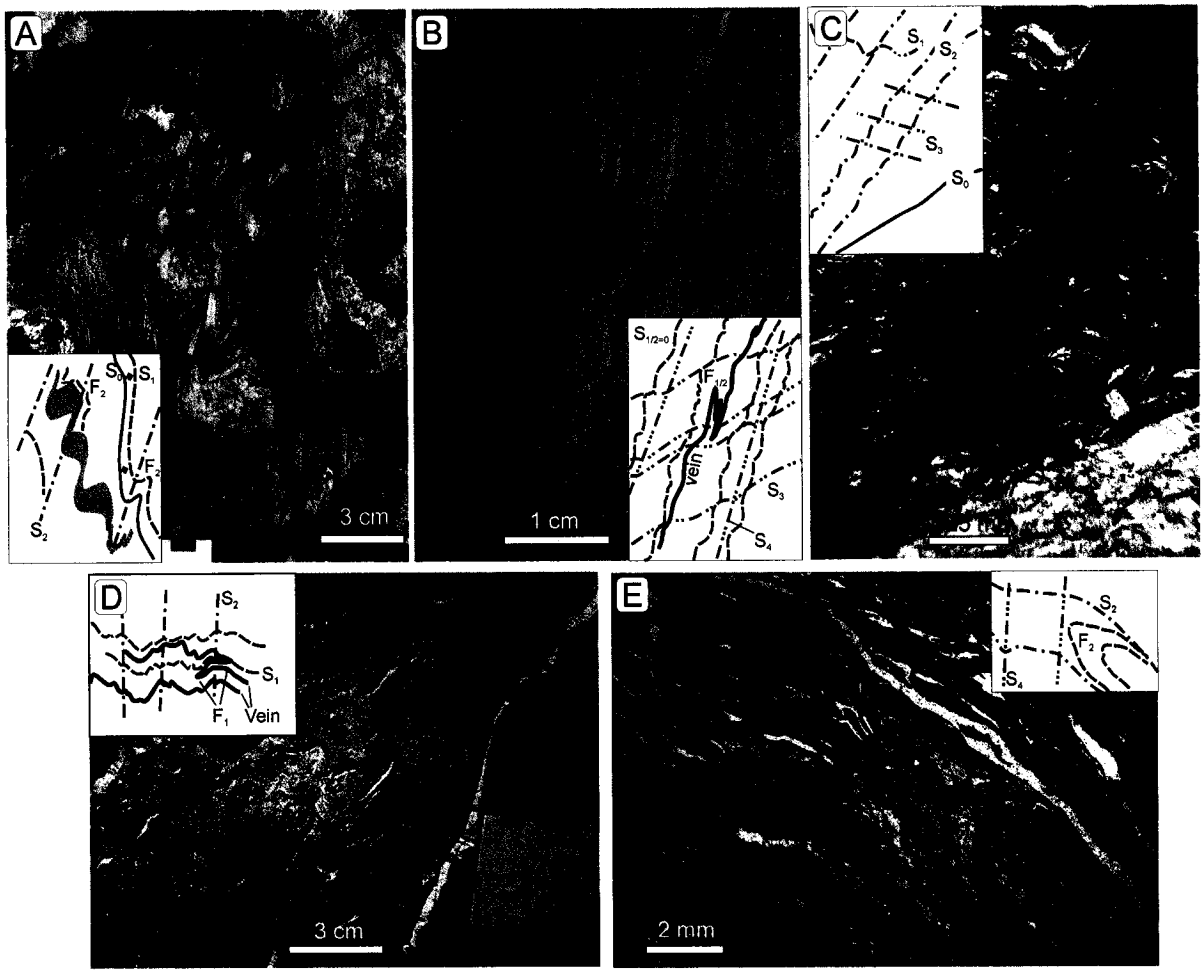

Figure 4-5 Fabric relationships. A. Ramp-folded (F_2) quartz veins aligned parallel to S_0=S_1 in Red Indian Lake Group felsic tuff (Pats Pond Domain), horizontal outcrop. B. Strong bedding parallel slaty cleavage is axial planar to SE vergent $F_{1/2}$ folds of veins in Red Indian Lake Group siltstone. S_1 is overprinted by SE vergent S_3 shear-band cleavage, which in turn is folded by F_4 folds. Vertical section facing NE. C. Zonal crenulation cleavage (S_2) deforming bedding (sub)-parallel slaty cleavage (S_1). S_2 is crenulated by F_3. Vertical section facing SW. D. Upright F_2 folds of F_1 folded quartz veins in mylonitic felsic volcanic of the Red Indian Lake Group. Vertical outcrop facing SW. E. Upright F_4 of composite S_{1-2} foliation in the Otter Brook shear zone, King George IV domain.

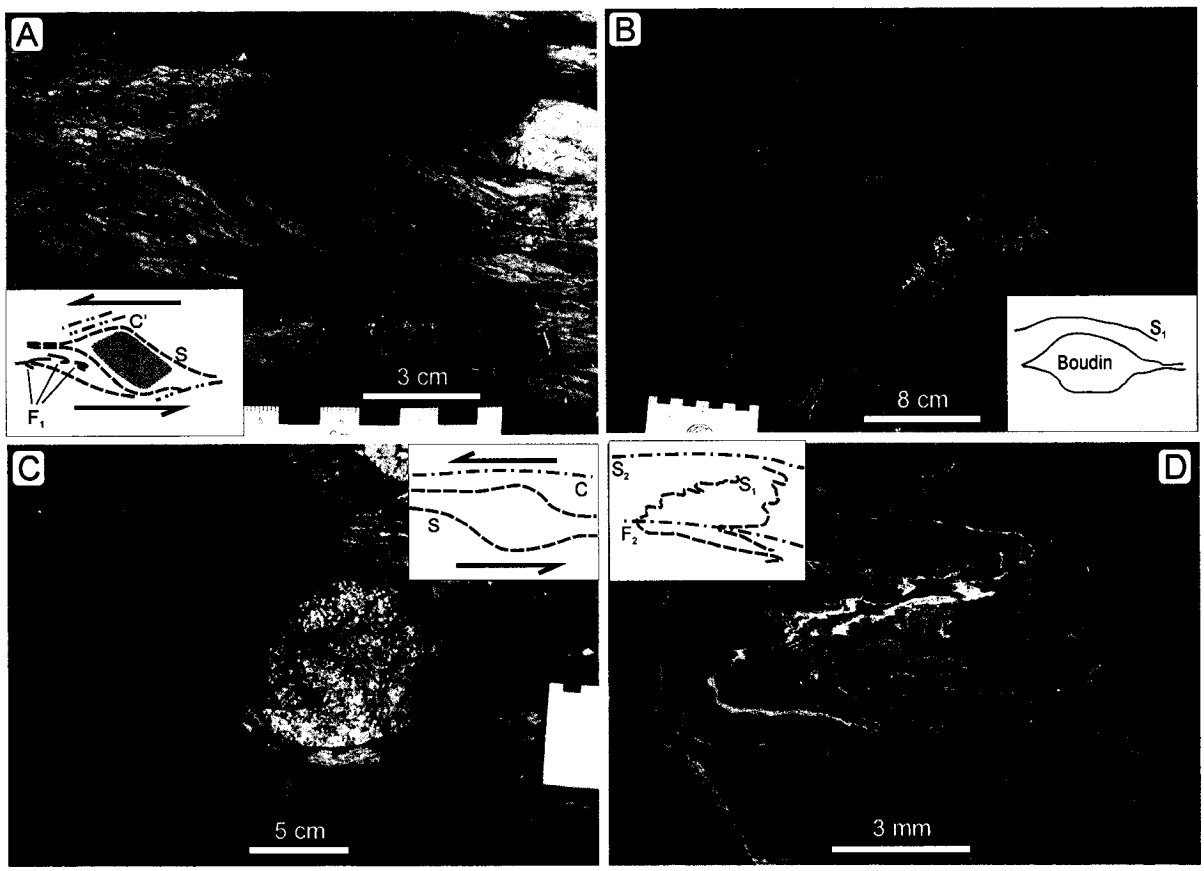

Figure 4-6 Shear zone fabrics. A. Sinistral shear in Red Indian Lake Group mafic phyllonites. Epidosite boudin has σ asymmetry with tight interfolial F_1 folds developed parallel to S. C'-type shear bands transect the outcrop. Horizontal outcrop Pats Pond domain. B. Boudinage of metabasite in Otter Brook shear zone. Horizontal outcrop, Pats Pond domain. C. Sinistral shear in conglomerate of the Wigwam Brook Group near the Red Indian Line. Horizontal outcrop Pats Pond domain. D. F_2 folded mylonitic S_1 in the Otter Brook shear zone, Pats Pond domain.

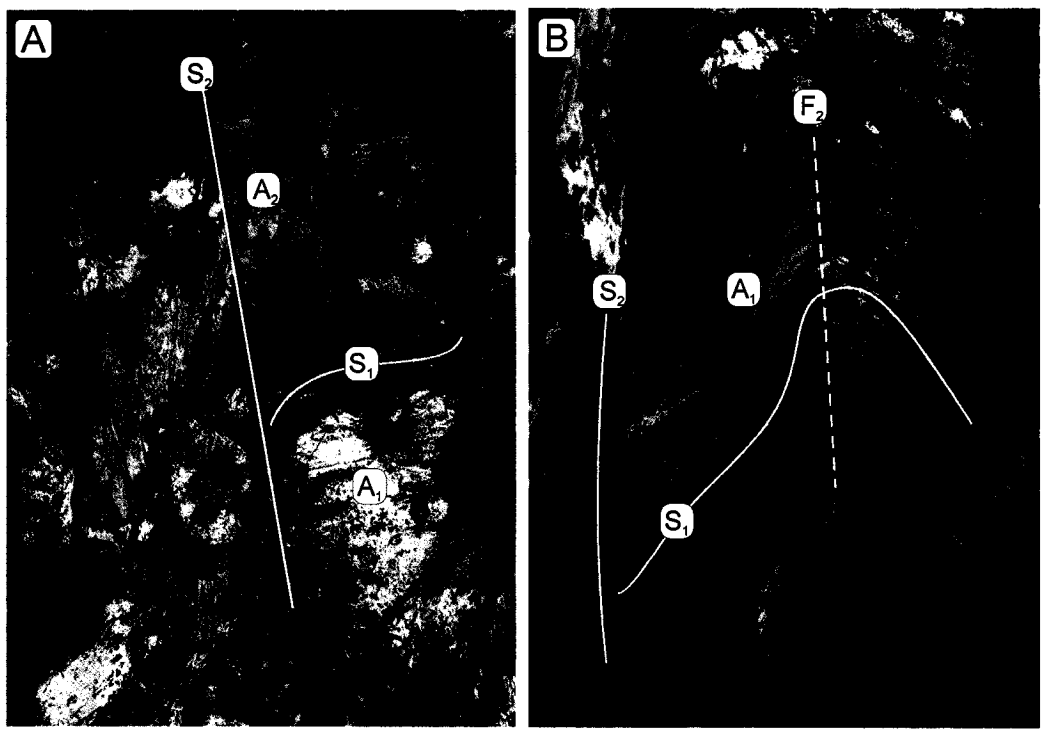

Figure 4-7 Tectono-metamorphic relationships along Otter Brook shear zone. A. First generation amphibole (A_1) parallel to S_1 is truncated by S_2 cleavage. Second generation amphibole A_2 grows parallel to S_2. B. F_2 folded S_1-parallel A_1 amphibole is truncated by S_2.

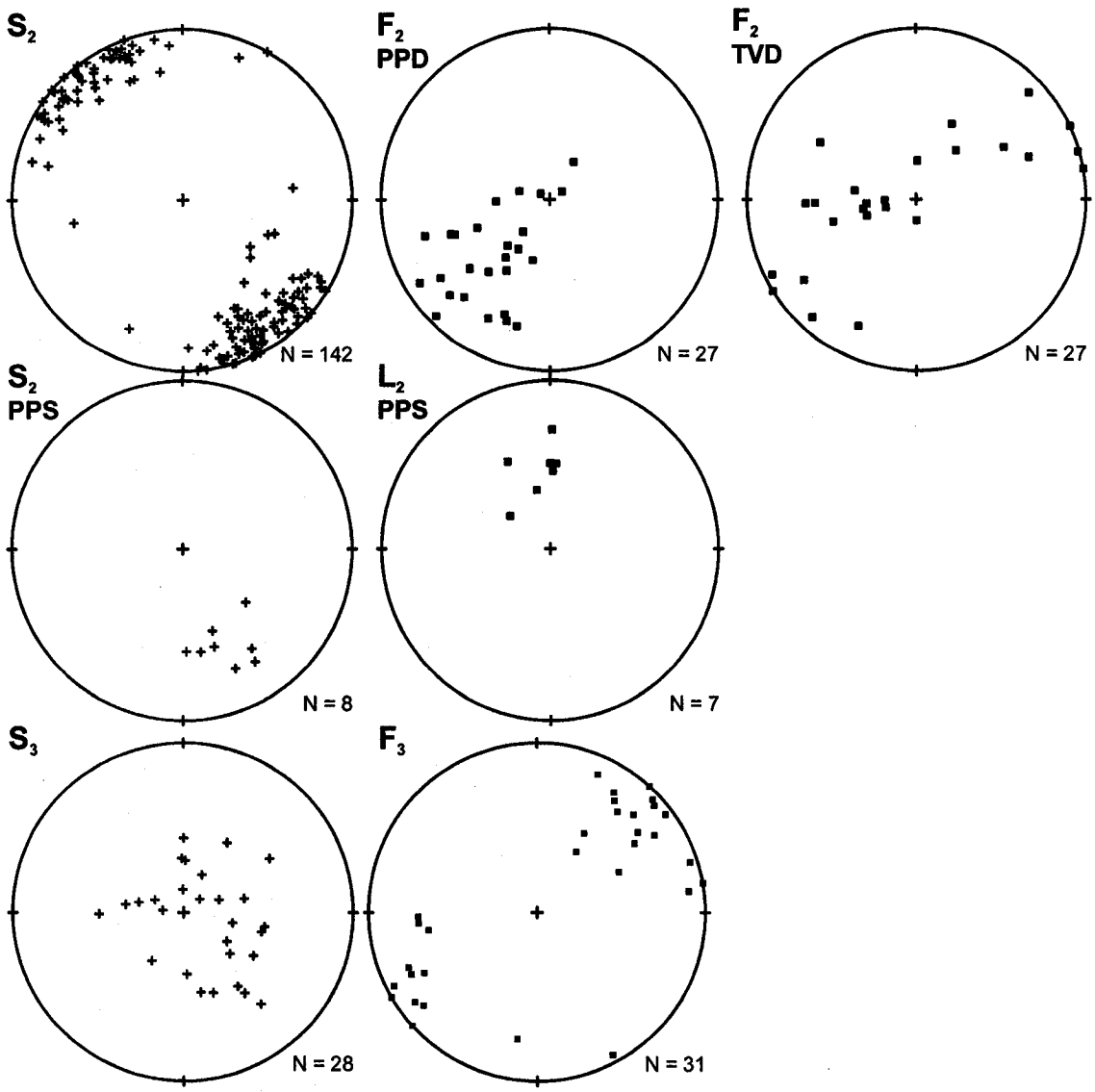

Figure 4-8 Equal area lower hemisphere projections of second generation structures (S_2, F_2, L_2, S_3, F_3). PPD - Pats Pond Domain, TVL - Tulks Valley Domain, PPS - Silurian Puddle Pond Suite.

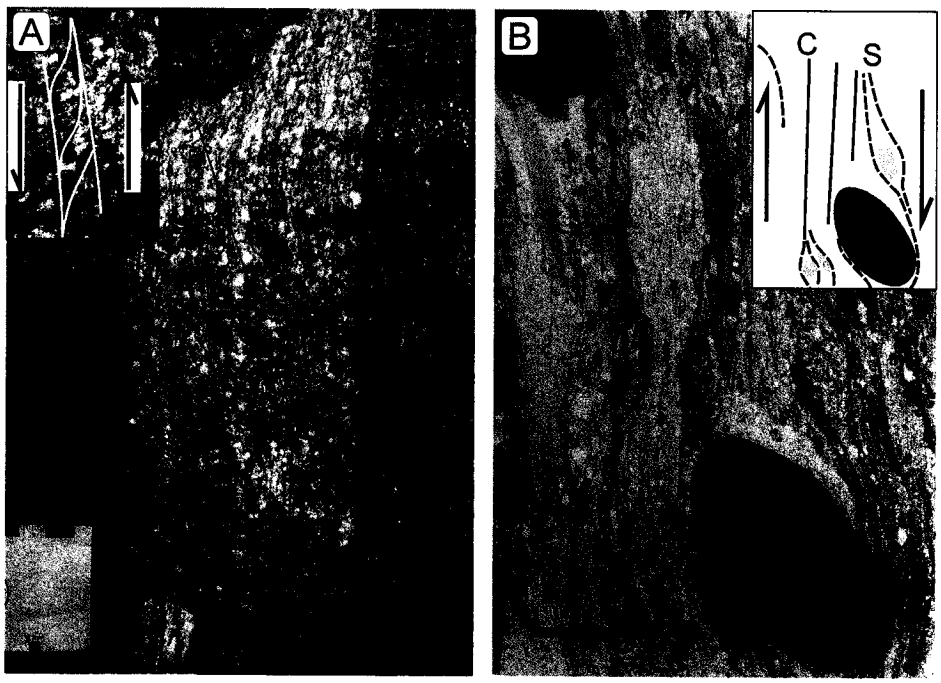

Figure 4-9 Second and fourth generation shearing. A. Interlayered tonalite and diorite of the Puddle Pond Suite with strongly developed S_2. S-C fabric (inset) indicates west side up. Vertical section facing SW. B. Strongly deformed (S_4) Rogersons Lake Conglomerate displaying σ-type asymmetry around pebbles, indicating SE side up. Vertical section facing SW.

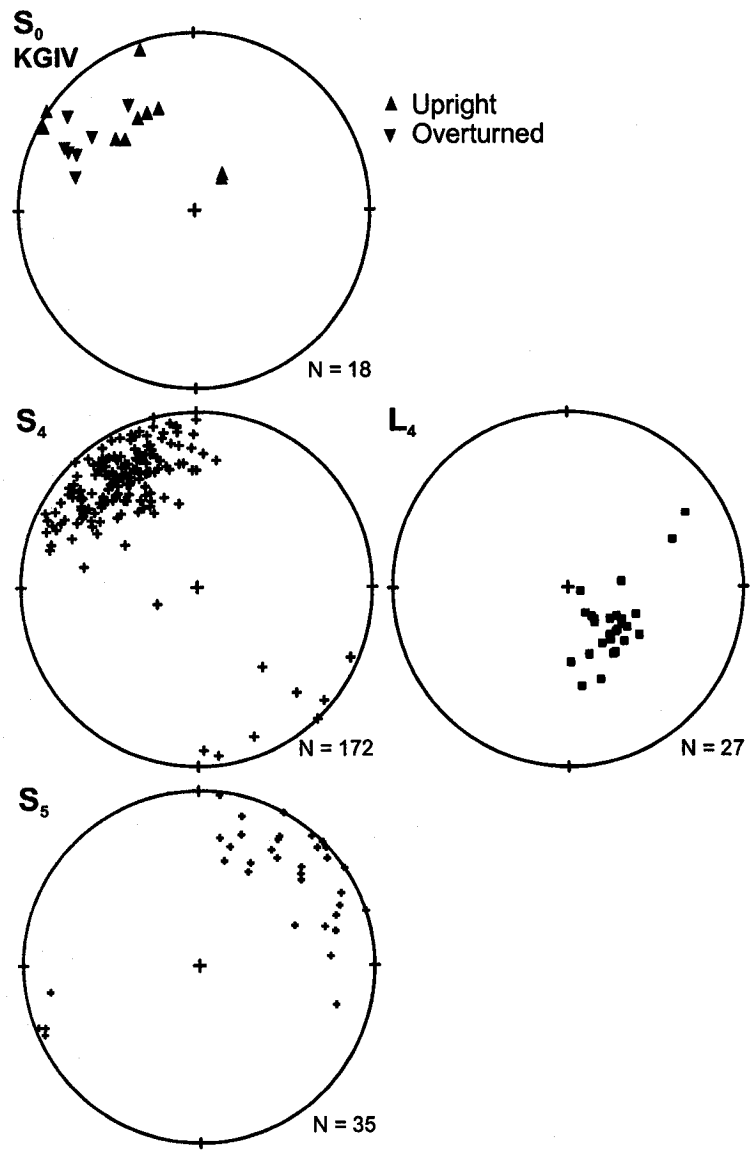

Figure 4-10 Equal area lower hemisphere projections of bedding (S_0) in Silurian sedimentary rocks in King George IV domain (KGIV) as well as fourth (S_4, L_4) and fifth (S_5) generation structures.

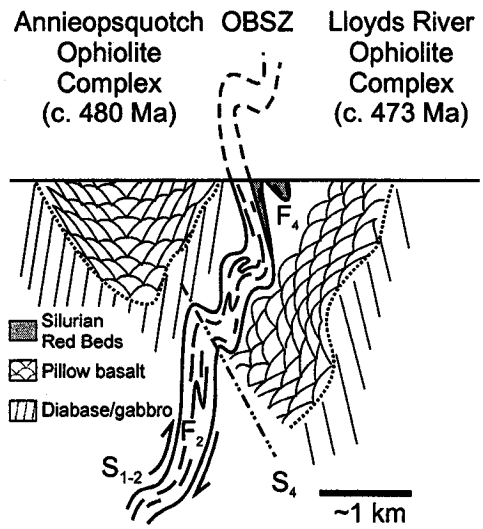

Figure 4-11 Schematic sketch of structural relationships along the Otter Brook shear zone in King George IV domain.

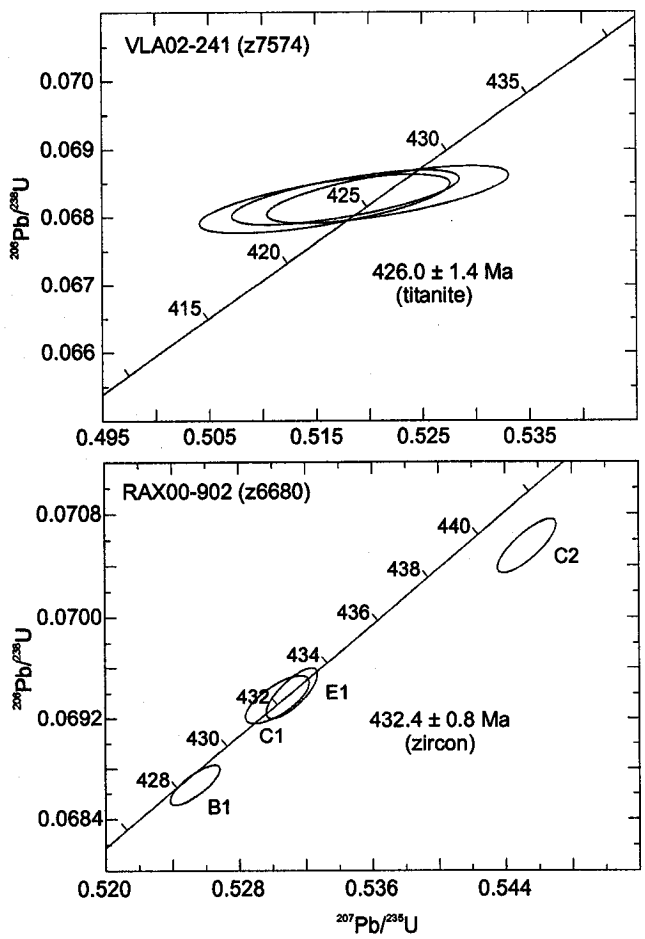

Figure 4-12 U/Pb TIMS concordia diagrams (2σ, decay constants included). See text for discussion.

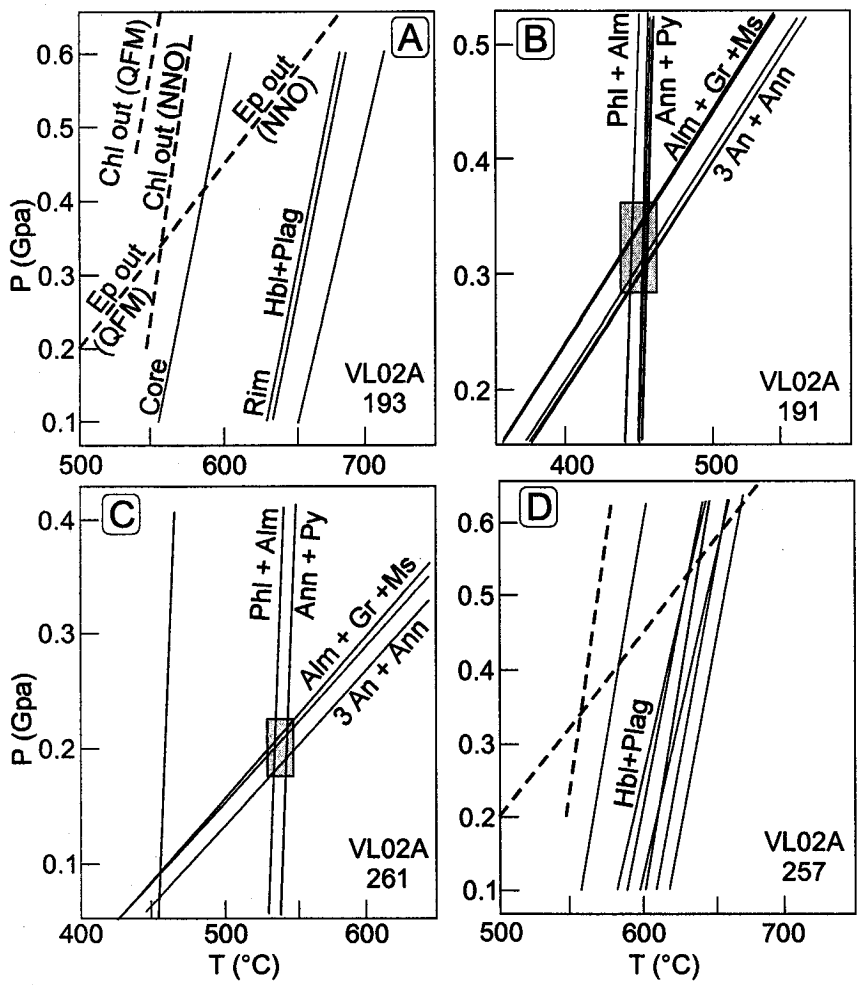

Figure 4-13 P-T constraints on metamorphism along the Otter Pond shear zone. Chlorite-out and epidote-out curves from Apted and Liou (1983), Liou et al. (1974) and Liou (1973).

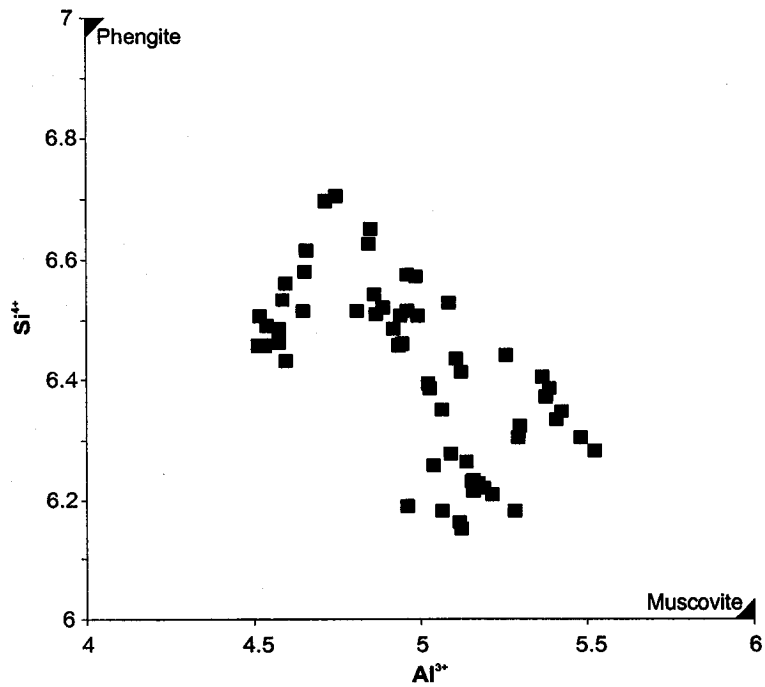

Figure 4-14 Compositional spectrum of phengitic mica plotted on Si^{4+} - Al^{3+} molecular proportion diagram. Mica composition calculated on the basis of 22 oxygens.

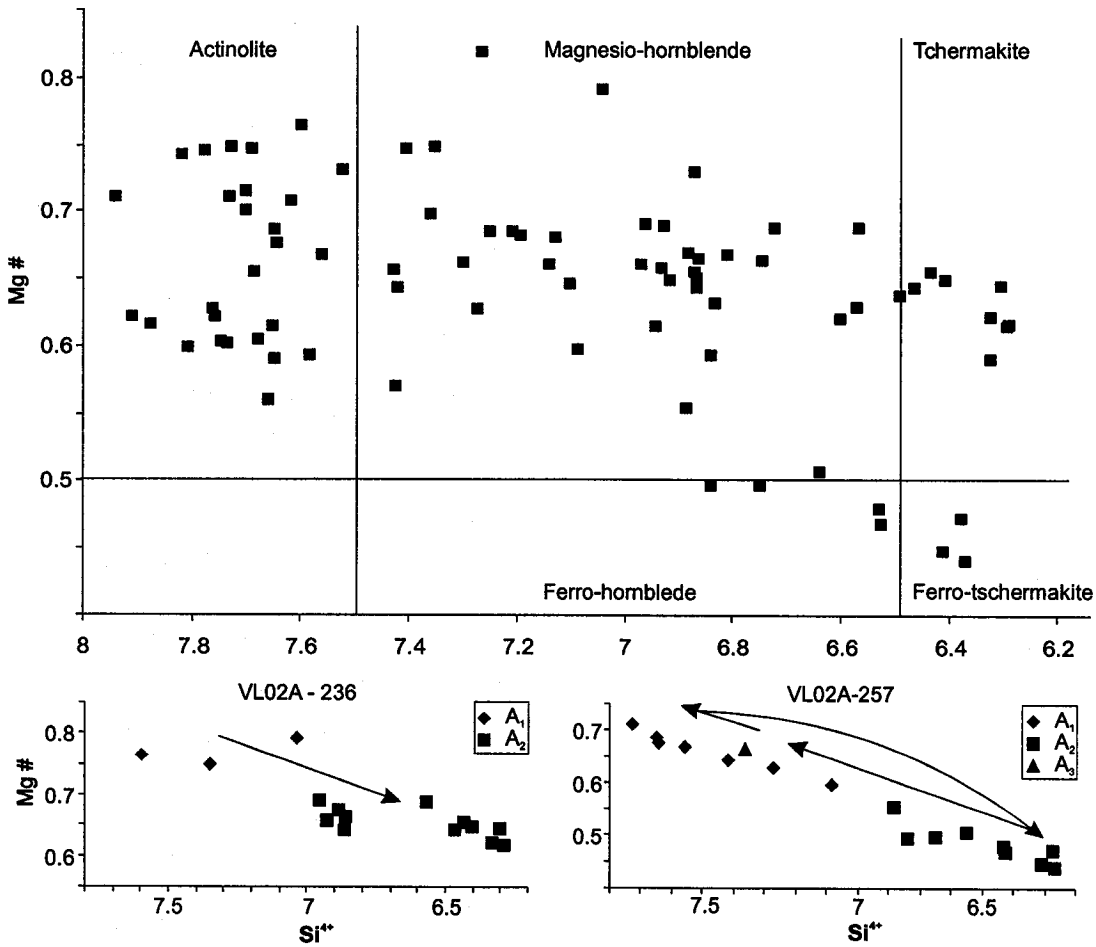

Figure 4-15 Compositional spectrum of amphiboles plotted on calcic amphibole classification diagram of Leake et al. (1997). Amphibole composition calculated following Leake et al. (1997). B and C. Compositional paths of the first, second and third generation amphiboles (A_1 to A_3) along Otter Brook shear zone.

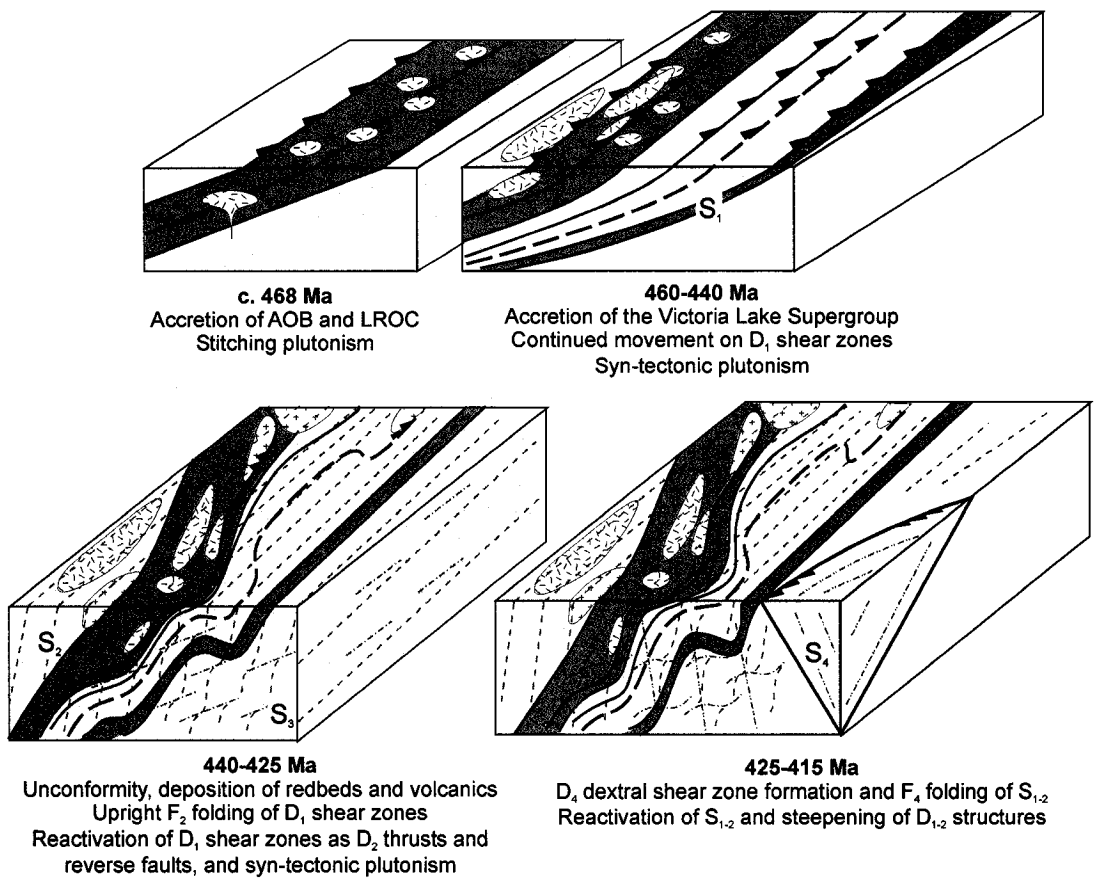

Figure 4-16 Schematic block diagram depicting the D_1 to D_4 structural evolution of the central Newfoundland Appalachians.

Figure 4-17 Early Ordovician to late Silurian tectonic evolution of the central Newfoundland Appalachians (A-E). F. Interpretation of migrated seismic reflection data from northern Lithoprobe profile (see Fig. 4.3 for location; from van der Velden et al. 2004). AAT – Annieopsquotch Accretionary Tract; AOB – Annieopsquotch Ophiolite Belt; LRC – Lloyds River Ophiolite Complex; PO – Penobscot ophiolites; RIL – Red Indian Line; SG – Summerford Group

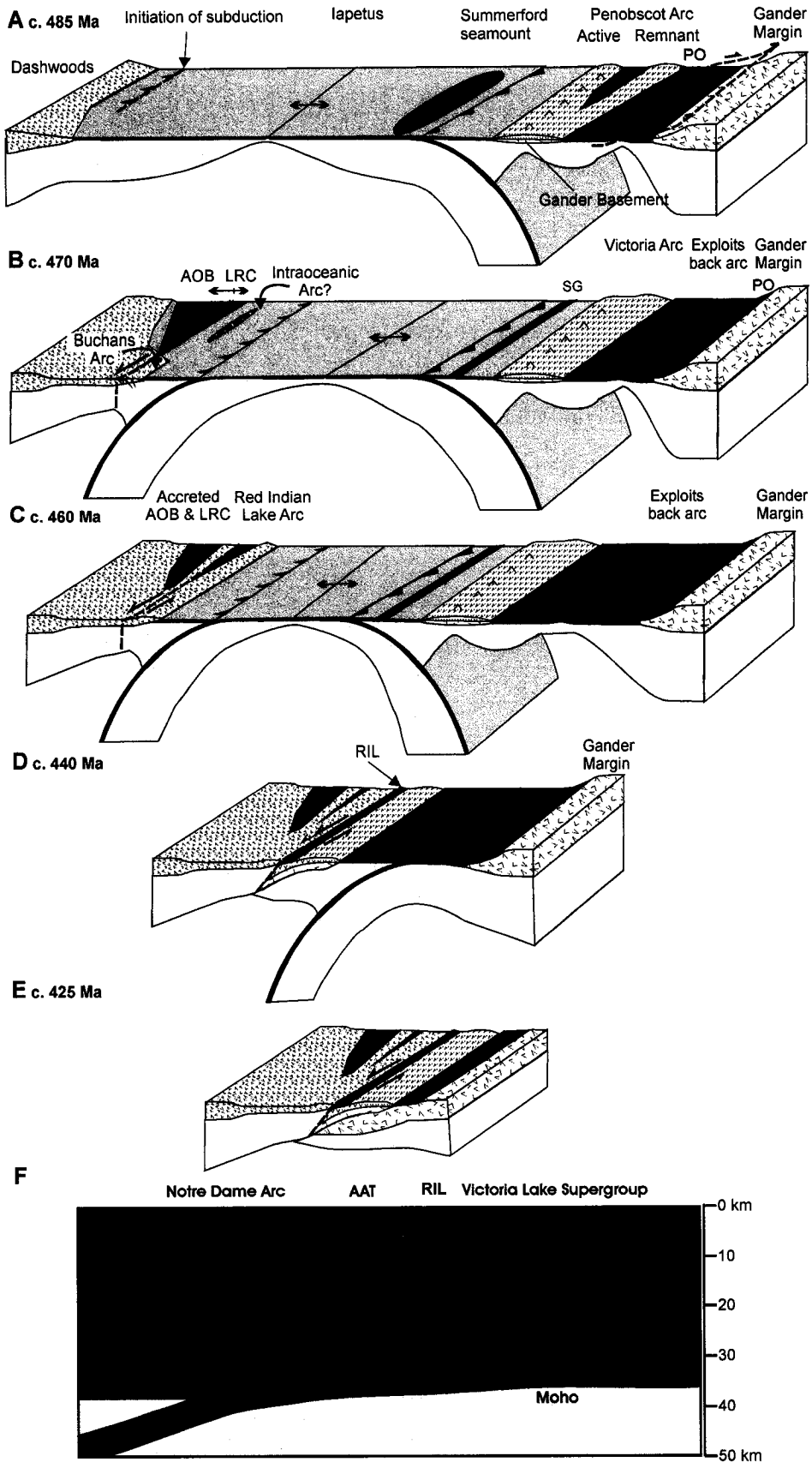
A c. 485 Ma
Initiation of subduction
Iapetus
Summerford seamount
Penobscot Arc
Active Remnant
Gander Margin
Dashwoods
PO
Gander Basement
B c. 470 Ma
Victoria Arc Exploits back arc
Gander Margin
AOB LRC
Intraoceanic Arc?
SG
PO
Buchans Arc
C c. 460 Ma
Accreted AOB & LRC
Red Indian Lake Arc
Exploits back arc
Gander Margin
D c. 440 Ma
RIL
Gander Margin
E c. 425 Ma
F
Notre Dame Arc
AAT
RIL
Victoria Lake Supergroup
0 km
10
20
30
40
50 km
Moho

Table 4.1: U-Pb TIMS analytical data

Fract.[1]	Description[2]	Wt. ug	U ppm	Pb[3] ppm	206Pb[4] 204Pb	Pb[5] pg	Isotopic Ratios[6] 208Pb 206Pb	207Pb 235U	±1SE Abs	206Pb 238U	±1SE Abs	Corr.[7] Coeff.	207Pb 206Pb	±1SE Abs	Ages (Ma)[8] 206Pb 238U	±2SE	207Pb 235U	±2SE	207Pb 206Pb	±2SE	% Disc
RAX00-902 (Z6680)																					
B1 (Z; 47)	Co,Clr,Pr,nIn,NM5°	15	365	26	4849	2	0.14	0.52535	0.00075	0.06867	0.00008	0.7988	0.05549	0.00005	428.1	0.9	428.7	1.0	432.0	3.8	0.9
C1 (Z; 18)	Co,Clr,St,rIn,NM5°	31	110	8	4613	1	0.12	0.53030	0.00096	0.06935	0.00010	0.7207	0.05546	0.00007	432.3	1.1	432.0	1.3	430.6	5.6	-0.4
C2 (Z; 24)	Co,Clr,St,fIn,NM5°	19	173	12	6322	1	0.12	0.54531	0.00088	0.07055	0.00010	0.808	0.05606	0.00005	439.5	1.3	441.9	1.2	454.6	4.3	3.4
E1 (Z; 40)	Co,Clr,Pr,fIn,rFr,NM5°	14	387	27	8296	3	0.13	0.53117	0.00077	0.06940	0.00010	0.7715	0.05551	0.00005	432.6	1.2	432.6	1.0	432.7	4.4	0.0
VLA02-241 (Z7574)																					
TA (T; 21)	Br,Clr,fFr,fIn,Frag	336	94	10	184	805	0.73	0.52177	0.00568	0.06833	0.00021	0.6909	0.05538	0.00050	426.1	2.5	426.3	7.6	427.5	39.8	0.3
TB (T; 21)	Br,Clr,fFr,fIn,Frag	359	92	10	181	856	0.82	0.51587	0.00589	0.06820	0.00022	0.6841	0.05486	0.00052	425.3	2.6	422.4	7.9	406.7	42.0	-4.7
TC (T; 23)	Br,Clr,fFr,nIn,Frag	334	102	10	197	810	0.65	0.51781	0.00535	0.06829	0.00020	0.6947	0.05499	0.00047	425.9	2.4	423.7	7.2	411.9	37.8	-3.5

Notes:
1 Z=zircon; T=titanite. All zircon fractions are abraded following the method of Krogh (1982); titanite fractions also lightly air abraded. Number in brackets refers to number of grains in analysis. 2Fraction descriptions: Co=Colourless, Br=Light Brown, Clr=Clear, fFr=Few Fractures, fIn=Few Inclusions, nIn=Numerous Inclusions, rIn=Rare Inclusions, Eu=Euhedral, Frag=Fragment, Pr=Prismatic, St=Stubby Prism, NM5°=Nonmagnetic @ 1.8A, 5°SS. 3Radiogenic Pb. 4Measured ratio, corrected for spike and fractionation. 5Total common Pb in analysis corrected for fractionation and spike. 6Corrected for blank Pb and U and common Pb, errors quoted are 1 sigma absolute; procedural blank values for this study ranged from 0.1 pg U and 2-3 pg Pb for zircon analyses and 2 pg U and 7 pg Pb for titanite analyses; Pb blank isotopic composition is based on the analysis of procedural blanks; corrections for common Pb were made using Stacey-Kramers compositions. 7Correlation Coefficient. 8Corrected for blank and common Pb, errors quoted are 2 sigma in Ma.

Table 4.2 Amphibole compositions

Sample	VL02-A193				VL02-A232						VL02-A236					
	core		rim (syn-S_1)		cores (A_1)		pre to syn-S_2 (A_2)		syn - S_2 (A_2)		syn-S_1 (A_1)		syn - S_2 (A_2)		late to post S_2 (A_3)	
	μ	S.D.	μ	S.D.	μ	S.D.	μ	S.D.	μ	S.D.	μ	S.D.	μ	S.D.	μ	S.D.
Na_2O	0.79	0.11	1.47	0.16	0.17	0.03	1.16	0.15	0.84	0.31	0.72	0.23	1.29	0.08	1.89	0.12
K_2O	0.24	0.07	0.51	0.08	0.04	0.03	0.18	0.04	0.12	0.03	0.09	0.03	0.15	0.02	0.36	0.02
FeO	13.50	0.69	15.50	0.83	11.39	0.35	13.82	0.86	12.35	0.51	10.39	0.93	13.17	0.22	12.56	0.22
MgO	12.78	1.09	9.97	0.56	16.35	0.47	12.93	0.75	14.65	0.85	15.79	1.03	12.71	0.18	11.27	0.17
Al_2O_3	7.76	1.67	12.57	0.92	1.31	0.40	8.29	1.09	5.30	1.82	6.19	2.09	10.15	0.13	14.95	0.52
SiO_2	49.08	1.84	43.53	1.24	55.22	0.26	48.04	1.19	52.00	1.00	51.79	2.09	47.57	0.53	43.07	0.21
CaO	12.42	0.10	12.03	0.14	12.87	0.02	12.42	0.34	12.71	0.14	12.58	0.49	12.51	0.24	12.55	0.16
TiO_2	0.38	0.14	0.70	0.08	0.03	0.02	0.21	0.16	0.12	0.08	0.17	0.11	0.29	0.05	0.11	0.05
Cr_2O_3	0.13	0.03	0.03	0.04	0.00	0.00	0.12	0.07	0.04	0.04	0.05	0.04	0.01	0.01	0.04	0.03
MnO	0.27	0.05	0.28	0.05	0.36	0.03	0.36	0.04	0.36	0.08	0.24	0.07	0.19	0.05	0.25	0.04
NiO	0.03	0.03	0.02	0.03	0.06	0.02	0.03	0.03	0.03	0.02	0.04	0.02	0.07	0.04	0.02	0.03
F	0.06	0.10	0.04	0.08	0	0	0.01	0.02	0	0	0.05	0.09	0.16	0.14	0.03	0.05
Cl	0.02	0.01	0.02	0.02	0.01	0.01	0.01	0.01	0.01	0.01	0.02	0.02	0.01	0.03	0.01	0.02
BaO	0.05	0.05	0.01	0.01	0.04	0.06	0.03	0.03	0.06	0.03	0.03	0.05	0.00	0.00	0.06	0.08
ZnO	0.02	0.03	0.03	0.05	0.04	0.04	0.05	0.05	0.02	0.02	0.00	0.00	0.03	0.03	0.01	0.03
V_2O_3	0.02	0.04	0.05	0.03	0.07	0.01	0.06	0.04	0.11	0.04	0.06	0.05	0.07	0.07	0.04	0.03
P_2O_5	0.01	0.02	0.03	0.06	0.06	0.08	0.04	0.07	0.05	0.06	0.00	0.00	0.05	0.05	0.06	0.09
Total	97.54	0.46	96.79	0.62	98.02	0.20	97.75	0.43	98.78	0.78	98.22	0.51	98.44	0.58	97.28	0.61
	Mg-hornblende n = 5		Mg-hornblende n = 4		Actinolite n = 2		Mg-hornblende n = 10		Mg-hornblende n = 3		Mg-hornblende n = 3		Mg-hornblende n = 3		Pargasite n = 3	

Table 4.2 continued

VL02-A240						VL02A-257					VL02-A275	
cores (A_1)		pre to syn-S_2 (A_2)		syn - S_2 (A_2)		cores (A_1)		pre to syn-S_2 (A_2)		syn - S_2 (A_2)	pre to syn-S_2 (A_{1-2})	
μ	S.D.	μ	S.D.	μ	S.D.	μ	S.D.	μ	S.D.		μ	S.D.
0.31	0.06	0.82	0.30	1.43	0.29	0.57	0.27	1.38	0.14	0.60	0.29	0.16
0.04	0.02	0.07	0.03	0.08	0.04	0.06	0.03	0.27	0.06	0.06	0.04	0.02
10.87	0.74	12.67	0.47	14.32	0.54	14.13	1.44	18.73	0.64	15.40	16.26	1.07
16.12	0.50	14.06	1.13	11.44	0.67	14.10	1.59	8.66	0.98	13.94	13.12	0.78
2.73	0.32	6.54	1.98	10.94	1.31	4.25	1.96	11.95	1.54	4.42	2.18	0.82
53.79	0.45	50.22	2.52	45.70	1.43	51.86	2.39	43.85	1.53	51.06	52.68	1.21
12.69	0.11	12.46	0.28	12.02	0.21	12.37	0.54	12.04	0.16	12.09	12.58	0.73
0.06	0.05	0.24	0.19	0.35	0.05	0.57	0.40	0.23	0.09	0.14	0.15	0.23
0.03	0.03	0.14	0.06	0.06	0.07	0.03	0.03	0.06	0.06	0.11	0.11	0.11
0.29	0.05	0.29	0.04	0.28	0.04	0.27	0.05	0.26	0.03	0.29	0.39	0.07
0.05	0.04	0.02	0.01	0.02	0.02	0.01	0.01	0.02	0.03	0.05	0.03	0.03
0.08	0.15	0.25	0.16	0.06	0.08	0.05	0.06	0.10	0.11	0.00	0.13	0.16
0.01	0.02	0.02	0.01	0.02	0.02	0.07	0.05	0.15	0.06	0.00	0.01	0.01
0.04	0.02	0.02	0.02	0.03	0.03	0.04	0.04	0.06	0.04	0.02	0.03	0.04
0.02	0.03	0.02	0.03	0.03	0.03	0.05	0.05	0.02	0.02	0.00	0.03	0.04
0.06	0.04	0.10	0.01	0.05	0.06	0.05	0.04	0.04	0.04	0.05	0.05	0.04
0.05	0.03	0.05	0.04	0.04	0.06	0.03	0.04	0.04	0.07	0.13	0.06	0.08
97.26	0.36	98.00	1.18	96.87	0.59	98.49	0.42	97.85	0.33	98.35	98.14	0.72
Actinolite		Mg-hornblende		Mg-hornblende		Mg-hornblende		Fe-hornblende		Mg-hornblende	actinolite	
n = 5		n = 4		n = 5		n = 5		n = 5		n =1	n = 15	

Table 4.3 Feldspar compositions

Sample	VL02-193					VL02-A232		VL02-A236		VL02-A257		VL02-A192				VL02-A261			
	rim		middle		core	matrix		matrix		matrix / porphyroclasts		core	rim			a		b	
	μ	S.D.	μ	S.D.		μ	S.D.	μ	S.D.	μ	S.D.		μ	S.D.		μ	S.D.	μ	S.D.
Na_2O	4.91	0.07	5.46	0.18	7.32	10.99	0.13	7.84	0.09	11.58	0.25	9.92	9.73	0.11	0.07	8.79	0.24	8.77	0.15
K_2O	0.05	0.01	0.05	0.01	0.05	0.06	0.02	0.05	0.02	0.03	0.02	0.11	0.13	0.05	15.98	0.16	0.03	0.16	0.06
CaO	11.23	0.16	10.44	0.24	7.26	1.43	0.38	6.99	0.14	0.23	0.24	3.06	3.30	0.09	0.01	4.68	0.25	4.76	0.17
FeO	0.18	0.04	0.15	0.04	0.15	0.19	0.04	0.05	0.03	0.23	0.16	0.08	0.14	0.04	0.16	0.15	0.08	0.11	0.06
SrO	0.22	0.05	0.23	0.06	0.18	0.01	0.02	0.04	0.04	0.01	0.02	0.01	0.01	0.02	0.00	0.02	0.03	0.03	0.03
BaO	0.01	0.02	0.04	0.02	0.05	0.05	0.03	0.01	0.03	0.03	0.04	0.00	0.03	0.03	0.07	0.04	0.06	0.04	0.04
SiO_2	53.70	0.10	54.74	0.47	58.66	66.36	0.13	58.05	0.66	68.61	0.47	63.07	63.16	0.26	65.00	61.31	0.64	62.27	0.32
Al_2O_3	29.05	0.16	28.14	0.19	24.97	21.18	0.33	26.21	0.33	19.82	0.27	22.47	22.73	0.24	18.46	23.61	0.36	23.50	0.19
Total	99.35	0.34	99.24	0.40	98.64	100.27	0.51	99.23	0.39	100.54	0.36	98.71	99.23	0.25	99.75	98.75	0.44	99.65	0.37
	An_{55}		An_{51}		An_{35}	An_{07}		An_{33}		An_{03}		An_{14}	An_{15}		Or_{99}	An_{22}		An_{23}	
	n = 2		n = 7		n = 1	n = 4		n = 5		n = 15		n = 1	n = 4		n = 1	n = 11		n = 12	

Table 4.4 Mica compositions

Sample	VL02A-027		VL02A-049		VL02A-070		VL02A-105		VL02A-115		VL02A-192				VL02A-193			
	Muscovite		Muscovite		Muscovite		Muscovite		Muscovite		Muscovite		Biotite		Muscovite(rx)		Muscovite	
	μ	S.D.	μ	S.D.	μ	S.D.	μ	S.D.	μ	S.D.	μ	S.D.	μ	S.D.	μ	S.D.	μ	S.D.
Na_2O	0.11	0.05	0.16	0.04	0.75	0.09	0.25	0.04	0.57	0.09	0.71	0.05	0.07	0.02	0.20	0.05	0.13	0.02
K_2O	9.32	0.26	10.44	0.26	9.02	0.00	10.42	0.11	9.91	0.44	10.25	0.12	9.62	0.14	10.75	0.26	10.98	0.08
FeO	2.74	0.31	5.54	0.25	1.17	0.17	1.39	0.13	4.49	0.90	2.96	0.08	14.34	0.21	2.08	0.49	1.51	0.43
MgO	1.68	0.37	2.06	0.19	2.23	0.09	2.19	0.13	1.21	0.47	1.04	0.10	14.00	0.12	1.93	1.09	2.05	0.42
Al_2O_3	32.35	0.61	27.50	0.19	30.58	0.53	31.03	0.34	31.47	0.69	32.42	0.21	16.87	0.09	32.25	1.33	31.09	1.07
SiO_2	52.14	0.76	46.06	0.23	47.87	0.04	47.07	0.49	44.91	0.51	45.62	0.28	36.83	0.10	46.18	0.50	47.59	0.31
CaO	0.01	0.01	0.01	0.02	0.03	0.00	0.00	0.00	0.01	0.01	0.00	0.00	0.01	0.01	0.06	0.03	0.02	0.02
TiO_2	0.03	0.03	0.51	0.05	0.02	0.01	0.33	0.07	0.31	0.05	0.46	0.05	1.42	0.20	0.10	0.06	0.04	0.05
Cr_2O_3	0.02	0.02	0.04	0.06	0.04	0.01	0.02	0.01	0.05	0.03	0.02	0.03	0.02	0.03	0.06	0.04	0.02	0.01
MnO	0.19	0.05	0.05	0.03	0.05	0.04	0.02	0.03	0.06	0.03	0.06	0.07	0.64	0.08	0.02	0.00	0.03	0.03
NiO	0.00	0.00	0.02	0.03	0.02	0.03	0.02	0.01	0.00	0.00	0.04	0.03	0.01	0.01	0.02	0.03	0.01	0.02
F	0.21	0.30	0.17	0.16	0.22	0.02	0.05	0.12	0.20	0.17	0.11	0.12	0.33	0.26	0.00	0.00	0.10	0.14
Cl	0.00	0.00	0.01	0.01	0.02	0.02	0.01	0.01	0.01	0.01	0.01	0.02	0.03	0.02	0.03	0.01	0.01	0.02
BaO	0.12	0.05	0.45	0.06	0.73	0.03	0.77	0.11	0.39	0.07	0.25	0.07	0.06	0.05	0.29	0.21	0.06	0.05
ZnO	0.03	0.04	0.03	0.05	0.03	0.04	0.03	0.03	0.00	0.00	0.02	0.04	0.03	0.06	0.02	0.03	0.05	0.04
V_2O_3	0.03	0.03	0.16	0.08	0.08	0.04	0.03	0.03	0.12	0.03	0.02	0.03	0.05	0.06	0.00	0.00	0.04	0.03
P_2O_5	0.00	0.00	0.01	0.02	0.06	0.09	0.00	0.01	0.05	0.05	0.05	0.06	0.02	0.03	0.06	0.08	0.01	0.01
Total	98.99	0.72	93.21	0.53	92.91	0.29	93.65	0.31	93.76	0.48	94.05	0.28	94.35	0.17	94.06	0.06	93.76	0.15
	n = 3		n = 7		n = 2		n = 6		n = 7		n = 8		n = 6		n = 2		n = 3	

Table 4.4 continued

VL02A-242		VL02A-262a				VL02A-262b				VL02A-280		VL02A-049	
Muscovite		Muscovite		Biotite		Muscovite		Biotite		Muscovite		Muscovite	
μ	S.D.	μ	S.D.	μ	S.D.	μ	S.D.	μ	S.D.	μ	S.D.	μ	S.D.
0.38	0.06	0.46	0.06	0.10	0.06	0.47	0.02	0.08	0.02	0.17	0.10	0.23	0.21
10.67	0.08	10.68	0.12	9.54	0.11	10.60	0.20	9.64	0.18	8.70	0.51	10.90	0.20
4.44	0.61	1.20	0.22	20.66	0.47	1.36	0.13	20.72	0.10	1.20	0.23	2.20	0.36
0.96	0.09	0.59	0.10	8.27	0.13	0.68	0.05	7.97	0.17	3.20	0.28	2.55	0.62
31.89	0.65	35.00	0.25	18.53	0.11	34.41	0.37	18.46	0.23	31.06	1.17	29.65	1.09
45.20	0.38	45.17	0.17	34.89	0.42	45.73	0.73	35.17	0.19	51.20	1.23	48.28	0.50
0.01	0.01	0.01	0.01	0.01	0.01	0.01	0.01	0.00	0.01	0.03	0.02	0.05	0.04
0.46	0.38	0.33	0.08	1.83	0.24	0.42	0.05	2.36	0.06	0.05	0.05	0.11	0.13
0.02	0.03	0.03	0.04	0.02	0.02	0.02	0.03	0.06	0.06	0.44	0.51	0.01	0.02
0.04	0.04	0.03	0.03	0.45	0.04	0.05	0.04	0.47	0.04	0.01	0.02	0.05	0.04
0.02	0.03	0.03	0.02	0.03	0.03	0.03	0.05	0.06	0.02	0.00	0.01	0.00	0.00
0.12	0.18	0.13	0.18	0.32	0.14	0.10	0.07	0.27	0.12	0.08	0.09	0.07	0.10
0.01	0.01	0.01	0.01	0.03	0.02	0.01	0.01	0.02	0.01	0.03	0.01	0.02	0.01
0.54	0.17	0.37	0.12	0.21	0.03	0.35	0.08	0.16	0.03	0.14	0.02	0.16	0.05
0.01	0.01	0.00	0.00	0.09	0.07	0.01	0.01	0.03	0.03	0.02	0.01	0.03	0.04
0.03	0.03	0.03	0.04	0.03	0.03	0.07	0.07	0.03	0.06	0.02	0.02	0.02	0.05
0.05	0.08	0.04	0.05	0.03	0.04	0.04	0.07	0.00	0.01	0.04	0.04	0.04	0.06
94.85	0.63	94.12	0.20	95.05	0.36	94.36	0.60	95.53	0.25	96.38	2.40	94.37	0.51
n = 6		n = 5		n = 4		n = 6		n = 5		n = 4		n = 5	

Table 4.5 Garnet compositions

Sample	VL02-A192				VL02-A261(a)				VL02-A261(b)			
	core (poikilitic)		rim (clear; partially resorbed or euhedral)		core		rim		core		rim	
	μ	S.D.	μ	S.D.	μ	S.D.	μ	S.D.	μ	S.D.	μ	S.D.
FeO	16.22	0.34	16.02	0.12	27.28	0.44	26.21	0.76	27.37	0.42	25.97	0.40
MgO	1.86	0.09	1.89	0.09	1.92	0.38	1.41	0.15	1.91	0.13	1.55	0.08
Al_2O_3	19.74	0.23	20.66	0.44	21.25	0.29	20.84	0.10	21.23	0.17	21.11	0.10
SiO_2	36.67	0.22	36.84	0.22	36.33	0.57	36.09	0.52	36.68	0.35	36.57	0.32
CaO	2.20	0.13	1.64	0.37	0.92	0.06	0.98	0.02	0.88	0.06	1.45	0.34
TiO_2	0.21	0.05	0.08	0.06	0.03	0.02	0.02	0.03	0.03	0.03	0.04	0.03
Cr_2O_3	0.05	0.04	0.03	0.03	0.05	0.05	0.08	0.05	0.01	0.01	0.01	0.01
MnO	22.36	0.26	22.54	0.37	12.12	0.46	13.89	0.57	12.13	0.42	13.17	0.17
Total	99.32	0.32	99.69	0.56	99.90	0.94	99.52	0.46	100.23	0.35	99.85	0.47
	n = 4		n = 8		n = 10		n = 3		n = 6		n = 4	

Table 4.6 Location of samples

Sample	UTM Zone 12 (NAD83)	
	E	N
AZ02-027	448169	5341148
AZ02-049	475115	5361762
AZ02-070	473581	5365008
AZ02-105	478453	5367068
AZ02-115	481595	5370270
AZ02-192	474119	5369669
AZ02-193	481027	5372105
AZ02-232	475530	5370224
AZ02-236	471197	5367341
AZ02-240	472097	5368237
AZ02-242	484991	5378768
AZ02-257	487880	5384754
AZ02-261	476140	5372330
AZ02-275	484076	5377009
AZ02-280	478735	5373139
AZ02-284	480860	5373484
NR01-037	506044	5389197

Table 4.7 Summary of semi-quantitative phengite geobarometry

Sample	Mineral Assemblage	Phengite Si pfu	Limiting Assemblage	Pressure$_{(T)}$ GPa	Fabric relationships
RAX01-010 felsic tuff	Albite-chlorite-muscovite	3.27 (n=2) 3.13±0.02 (n=3)	N	$P_{440°}$ = 0.45 $P_{440°}$ = 0.2	Syn D_1 Recrystallized
VL02A-027 intermediate tuff	Chlorite-muscovite-albite-k-feldspar-calcite	3.32±0.03 (n=3)	Y	$P_{440°}$ = 0.55	Pre-D_2
VL02A-049 felsic tuff	Chlorite-muscovite-quartz-albite	3.23±0.01 (n=7)	N	$P_{440°}$ = 0.4	Syn D_1
VL02A-070 felsic tuff	Chlorite-muscovite-albite-quartz	3.26 (n=2)	N	$P_{440°}$ = 0.45	Syn D_1
VL02A-105 felsic tuff	Chlorite-muscovite-albite-quartz	3.21±0.03 (n=6)	N	$P_{440°}$= 0.4	Syn D_1
VL02A-115 intermediate tuff	Chlorite-epidote-muscovite-albite-quartz-calcite	3.11±0.02 (n=7)	N	$P_{440°}$= 0.15	Syn to post D_2
VLA02-193 gabbro	Epidote-pargasite-phengite-plagioclase-titanite±biotite	3.23±0.03 (n=4) 3.14 (n=2)	N	$P_{<550°}$= 0.6 $P_{550°}$= 0.35	Syn D_1 Recrystallized
VLA02-242 xenolith in tonalite	Biotite-muscovite-feldspar-quartz-epidote	3.10±0.02 (n=6)	N	$P_{550°}$= 0.35	Syn D_2
VLA02-280 felsic tuff	Biotite-muscovite-plagioclase-k-feldspar-quartz	3.27±0.02 (n=5)	Y	$P_{500°}$= 0.6	Syn D_1
VLA02-284 Pillow basalt	Actinolite-epidote-chlorite-albite-phengite-calcite	3.27±0.02 (n=5)	N	$P_{500°}$= 0.6	Syn D_1

CHAPTER 5: SUMMARY AND CONCLUSIONS

Williams et al. (1988) proposed to subdivide the Dunnage zone into peri-Laurentian Notre Dame and peri-Gondwanan Exploits subzones based on faunal, lead isotope, structural, and stratigraphic contrasts apparent across the Red Indian Line. Subsequently Williams (1995) made more subdivisions (e.g. Dashwoods Subzone), but these represent minor subdivisions that do not distract from the principal twofold subdivision. As a result, the Red Indian Line became recognized as the fundamental Iapetan suture zone in the northern Appalachians along which the largest portion of the Iapetus was consumed (van Staal et al. 1998). However, many of the contrasts that define the Red Indian Line are difficult to obtain at every section. Particularly, the provenance of sparsely preserved fauna is commonly equivocal; the style, diachroneity and heterogeneity of deformation may result in a range of ages of the unconformities; and the stratigraphic relationships may be controlled by local basin architecture. To date the single most reliable criteria has been the lead isotopic characteristics of the syngenetic massive sulphide deposits.

ADDITIONAL CRITERIA FOR THE SUBDIVISION OF THE DUNNAGE ZONE

The contrasts intrinsic to the definition of the Red Indian Line have all been confirmed during this study in central Newfoundland (except faunal due to the lack of suitable rocks). Additionally, we have identified two supplementary criteria that can be utilized to differentiate the two subzones: zircon inheritance and Sm/Nd isotopic characteristics. The lowest ε_{Nd} values recorded in the Exploits Subzone occur in the youngest rocks (Wigwam Brook Group: ε_{Nd} –4), while the majority of the rocks have generally maintained positive to slightly negative ε_{Nd} values (ε_{Nd} +8 to –1) with T_{DM} ages generally in the 1.30 to 0.6 Ga range (Fig. 5.1; Chapter 2). In contrast to the Exploits Subzone, volcanic rocks of the Notre Dame Subzone display consistently lower ε_{Nd} values, with ε_{Nd} in felsic volcanic rocks commonly in the -3 to -10 range, indicating greater contribution of continental crust and/or more mature continental crust (Fig. 5.1; Chapter 2; Appendix 3). The difference in the Sm/Nd isotopic characteristics reflects the fundamental differences in the nature of the Gondwanaland-derived and Laurentia-derived basement in the Exploits (ε_{Nd} +8 to –1) and Notre Dame (ε_{Nd} –3 to –10) subzones respectively.

An effective way of studying the nature of the basement is through zircon inheritance studies in igneous rocks. Zircon inheritance indicates that the volcanic rocks of the Exploits Subzone have been deposited on continental basement that experienced tectono-magmatic events at c. 560 Ma and c. 900-1200 Ma (Chapter 3) similar to the Proterozoic Cripplebback Igneous Suite and Sandy Lake Group (c. 560 Ma, T_{DM} ~1300: Appendix 2; Kerr et al. 1995), which stratigraphically underlie the oldest portions of the Penobscot arc (Appendix 2; Johnson and McLeod 1996). This basement likely represents a fragment of Ganderia (Appendix 2), a Gondwana-derived microcontinent, which is typified by zircon provenance in the 0.54-0.55, 0.6-0.8, 1.0-1.55, and 2.5-2.7 Ga age ranges (van Staal et al. 1996), ε_{Nd} values greater than –4 and T_{DM} ages of igneous rocks spanning from 0.9 to 1.35 Ga in the Late Precambrian rocks (Appendix 2; Kerr et al. 1994).

The ensialic plutonic and volcanic rocks of the Annieopsquotch Accretionary Tract have abundant inheritance in the 935 to 1845 Ma age range (Chapter 2; Dec et al. 1997), consistent with the presence of Laurentian basement at depth (e.g. Cawood et al., 1995; Cawood et al. 2001; Cawood and Nemchin, 2001). The presence of inheritance in the 1.0-1.55 Ma age ranges is common to both subzones and is thus not a reliable differentiation tool. However, zircon inheritance in the 1.7-1.9 Ga age range is characteristic of the Laurentian margin (Cawood and Nemchin 2001). In addition, zircon inheritance in the 540-565 Ma age range appears to be restricted to the peri-Gondwanan terranes in the Dunnage zone, owing to the extensive magmatism of this age in the Gander zone (Evans et al. 1990; Dunning and O'Brien 1989; Appendix 2). Although c. 750 Ma to 550 Ma magmatism (e.g. Sept Isle Intrusion and Skinner Cove Pluton) related to the opening of Iapetus (Cawood et al. 2001 and references therein) and subsequent separation of the Dashwoods microcontinent from the Laurentian margin (Waldron and van Staal, 2001) is present in Laurentia (Cawood et al. 2001), it primarily affected the Humber zone and does not appear to have had any effect on the Ordovician rocks of the Notre Dame Subzone.

Sm/Nd isotopic signatures and presence of specific age range of zircon inheritance have great potential in characterizing and distinguishing the Notre Dame and Exploits subzones (Fig. 4.17). They indicate the contribution of continental basement to both subzones; however, the

contrasts that were observed in this study indicate that the nature of the basement is fundamentally different between peri-Laurentian and peri-Gondwanan terranes.

TECTONIC DEVELOPMENT OF THE ARC-BACK ARC COMPLEXES

The identification of the Red Indian Line in central Newfoundland (Chapter 2, 3) based on the criteria discussed above has facilitated the development of more realistic tectonic models for the Ordovician peri-Laurentian and Cambro-Ordovician peri-Gondwanan arc-back arc complexes that were present in the main tract of the Iapetus Ocean prior to (Chapter 2, 3) and following their juxtaposition with the Laurentian margin in the Caradoc (Chapter 4).

Annieopsquotch Accretionary Tract

The formation of the Annieopsquotch Accretionary Tract commenced at approximately the same time as the collision of the Dashwoods Microcontinent with the Humber margin of the Laurentia. During the collision, the far-field stresses were probably transferred outboard of the Dashwoods microcontinent into the Iapetus Ocean basin, initiating west-dipping subduction and generating the supra-subduction zone Annieopsquotch Ophiolite Belt (Fig. 4.17; Lissenberg et al., 2005b) at c. 480 Ma. According to the model of Stern and Bloomer (1992) the magmatic front should have stabilized c. 10 Ma after the initiation of subduction, consistent with the observations in the Annieopsquotch Accretionary Tract, where the oldest arc rocks occur in the continental Buchans arc (Fig. 4.17; c. 473 Ma; Chapter 2) and accompanying back arc (Lloyds River Ophiolite Complex: Chapter 2).

The required movement of the continental Buchans arc outboard of the juvenile Annieopsquotch Ophiolite Belt was likely accomplished by trench parallel translation of the Buchans arc (fore-arc sliver, Chapter 2). This culminated in the accretion of the Annieopsquotch Ophiolite Belt and Buchans arc to the Dashwoods margin by c. 468 Ma, the age of stitching Otter Pond Complex (Appendix 3). The age of accretion and involvement of strictly peri-Laurentian terranes indicate that this episode forms part of the Taconic orogeny. Sinistral oblique underthrusting of the accreted rocks beneath the Dashwoods margin was accommodated by northwest-dipping D_1 thrust faults. Subsequent to accretion of the above rocks, arc magmatism rejuvenated outboard of

Dashwoods forming the continental Red Indian Lake arc and related backarc basin (Fig. 4.17). This arc-backarc system lasted until at least c. 460 Ma (Chapter 2).

Penobscot and Victoria arcs

In contrast to previous models (e.g. van Staal et al. 1996; van Staal et al. 1998), we have demonstrated that the Penobscot arc in Newfoundland was at least in part built on Gander-like basement (Chapter 2, Appendix 2). This is corroborated by data from New Brunswick (Johnson and McLeod, 1996). The spatial relationships of the Penobscot arc back arc system (Chapter 3) strongly suggest that subduction was east-directed, rather than west-directed as has been proposed in previous models (e.g. van Staal et al. 1998). The Penobscot arc is herein interpreted to have formed in a dominantly extensional setting along the Gander margin (Fig. 4.17).

Shut off of arc magmatism and obduction of the Penobscot backarc ophiolites onto the Gander margin represent the start of the Penobscot orogeny (c. 485-480 Ma; van Staal et al. 1998). The onset of orogenesis is best explained by a collision of the Penobscot arc with an outboard plateau or seamount, such as preserved in the Summerford Group (Jakobi and Wasowski, 1985). Following the Penobscot Orogeny: a new arc (Victoria arc) was established above an east-dipping subduction zone by c. 473 Ma (e.g. van Staal et al., 1998). The Victoria Arc was extensional and was accompanied by opening of the wide Japan Sea-type Tetagouche – Exploits marginal basin (Fig. 4.17; e.g. Rogers et al. 2003). Victoria Arc was active until c. 453 Ma, the time of the inferred collision with the Red Indian Lake Arc (Chapter 3).

ASSEMBLY OF THE DUNNAGE ZONE

Both the peri-Laurentian Red Indian Lake arc (465-460 Ma: Chapter 2) and peri-Gondwanan Victoria arc (473-453 Ma: Chapter 3; McLachlan et al. 2001) were active contemporaneously outboard of Laurentia and Gondwana respectively (Fig. 4.17). Contemporaneous subduction on both sides of Iapetus requires the closure of the main Iapetus basin to have terminated in a Molucca Sea (e.g. Pubellier et al. 1999) or Solomon Sea (Abbot et al. 1994; Whitmore et al. 1999) style arc-arc collision and the accretion of the two arc systems to the Laurentian margin. During the collision the peri-Gondwanan Victoria Arc was partially subducted underneath the Annieopsquotch Accretionary Tract. This is supported by the reprocessed seismic

reflection data (van der Velden et al. 2004) and small-scale structures (Chapter 4), which indicate underthrusting of the Exploits Subzone beneath the Notre Dame Subzone during D_1 deformation. As a result of the underthrusting of the Victoria Arc, the Notre Dame Subzone was uplifted, which led to a sub-Silurian unconformity. A syn-tectonic Ordovician to Silurian sedimentary basin (e.g. McNicoll et al. 2001; Williams et al., 1993) was formed above the unsubducted part of the Victoria arc. The arc-arc collision resulted in a development of a south-southeast-directed thrust belt in the Annieopsquotch Accretionary Tract and western Exploits Subzone.

Following this collision, subduction stepped back into the Tetagouche-Exploits back arc basin, closing this portion of Iapetus along the Dog Bay Line (Williams et al. 1993) by Early to Middle Silurian due to arrival of the main part of the Ganderian microcontinent (Fig. 4.17). Docking of Ganderia led to the Salinic Orogeny. The Salinic orogeny also resulted in formation of a south-southeast-directed thrust and fold belt (D_2), which is the predominant structural phase in the study area, although its architecture appears to be controlled by the earlier formed Taconic structures. The Salinic orogeny commonly masks the nature of the earlier Taconic tectonism. Subsequent Acadian Orogeny resulted from the collision of the Avalonian microcontinent with the expanding composite Laurentian margin. Acadian structures (D_4), unlike Taconic and Salinic, are typified by northwest-directed transport and are generally dextral.

DEVELOPMENT OF THE LAURENTIAN MARGIN

The development of continental margins and the relative roles of various accretionary processes are of fundamental importance to the question of crustal growth through time. The Dunnage zone of Newfoundland provides a unique opportunity to study accretionary processes as this part of the orogen is relatively well exposed and constrained by both seismic reflection and surface studies. Abundant accreted sediments that commonly complicate the interpretation of history of other accretionary orogens are lacking in this segment of the Appalachians, allowing detailed reconstruction of original relationships between various tectono-stratigraphic units.

In most accretionary orogens the role of forearc accretion is thought to be the dominant process of adding juvenile material to the continental margins (e.g. Sengor and Natal'n, 1996). However, lack of preservation of any sizable Ordovician accretionary prisms indicates that sediment

accretion of supracrustal rocks probably played a minor role. Notable exceptions are the Summerford Group and Dunnage Melange (Jakobi and Wasowski, 1985). The majority of accreted juvenile material appears to be preserved in the ophiolitic rocks that have either formed during the initiation of subduction (Annieopsquotch Ophiolite Belt) or in a back arc setting (Lloyds River Ophiolite Complex, Skidder Formation, Harbour Round Formation, Pipestone Pond Complex). Thus, the majority of accreted juvenile material was derived from the inversion of marginal basins.

Based on an integration of seismic reflection studies and surface exposures, ophiolitic rocks in the Annieopsquotch Accretionary Tract have been subducted to at least 25 km depth prior to being scraped off and are exposed as 1 to 5 km thick belts over entire length of the study area (c. 150 km). The volume of accreted ophiolitic rocks in the study area alone is c. 18000 km^3, with accretion occurring over a time span of c. 20 Ma. The rate of accretion of ophiolitic material is thus at least 0.001 km^3/a. This estimate takes into account only one subduction zone in the Iapetus and strike length of only ~200 km, the extrapolation of this result to multiple subduction zones and several thousand kilometre strike length of the Appalachian orogen, then the rate of accretion of ophiolitic material through marginal basin inversion alone should be at least an order of magnitude higher (not counting arc magmatism or forearc accretion). When compared to the estimated global crustal growth rate of c. 0.025 km^3/a (Sengor and Natal'n, 1996), inversion of marginal basins and accretion of mafic complexes (archipelago model: Hsu et al. 1995) can be an extremely efficient process representing a significant portion of the crustal growth budget.

FUTURE AVENUES FOR RESEARCH

The identification of a well-developed peri-Laurentian accretionary tract and establishment of new tectonic models for central Newfoundland in Chapter 2 raises a number of research opportunities in the northern Appalachians and Caledonides. Preliminary correlations with tectono-stratigraphic units along strike in Newfoundland were proposed in Chapter 2; however, many of the proposed correlative units are poorly understood and lack detailed geochronology or isotopic studies. An important step in understanding the tectonic evolution of the AAT would be to confirm the continuation of these tectono-stratigraphic units along strike or to explain the lack of continuity in terms of primary stratigraphic relations (i.e. variation in the depositional rates between volcanic

centers), structural excision (thrust vs. strike-slip, Chapter 4), or subduction geometry (i.e. several kinematically unrelated subduction zones vs. one subduction zone).

The complexity and the extent of the Penobscot arc in Newfoundland revealed in Chapter 3 allowed the proposal of a new tectonic model for the evolution of the peri-Gondwanan continental fragments. This model accounts for the distribution of the arc-backarc complexes in Newfoundland however it has not yet been tested in the correlative tracts in Northern Appalachians and Caledonides.

The data presented herein allow the refinement of the tectonic model of van Staal et al. (1998) for the peri-Laurentian tectonic elements and propose an alternate model for the peri-Gondwanan tectonic elements. The lack of equivalent detailed data outside of Newfoundland prevents direct correlation of many of the elements of the Annieopsquotch Accretionary Tract and Victoria Lake Supergroup outside of Newfoundland. As a result, it is difficult to test the presented tectonic models in the correlative tracts in Northern Appalachians and Caledonides. However, the proposed modifications to the existing tectonic models should be tested outside of Newfoundland to confirm their validity.

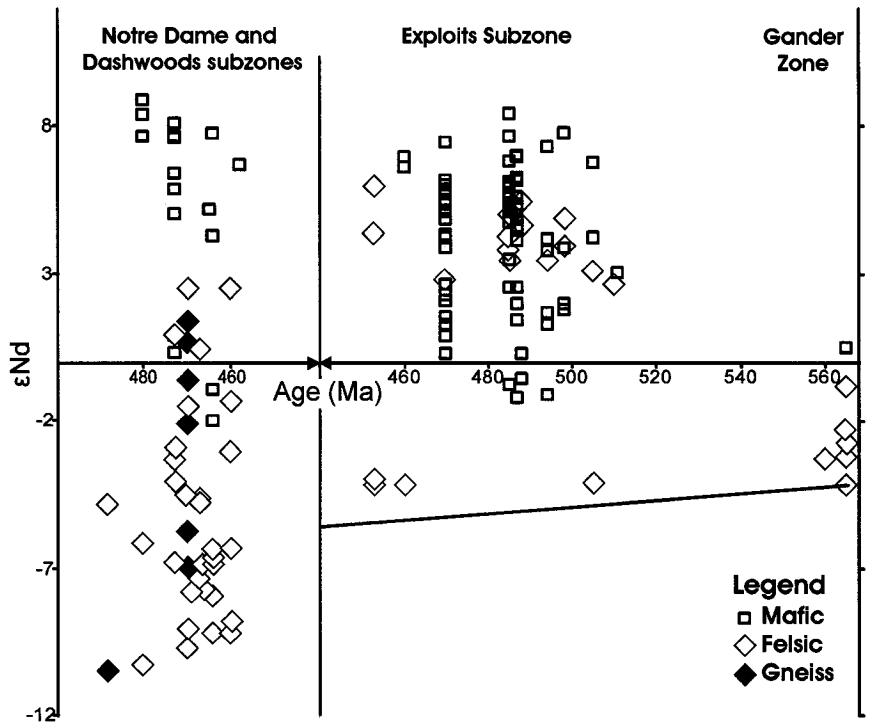

Figure 5-1 Sm/Nd isotopic evolution of the Notre Dame and Exploits subzones. Compiled from Jenner and Swinden (1993), Kerr et al. (1995), Lissenberg et al. (2005b), MacLachlan and Dunning (1998 a, b), Rogers (2004), Rogers et al. (2006), Swinden et al. (1990, 1997), Whalen et al. (1997), Zagorevski et al. (2006), Zagorevski et al. (submitted).

APPENDIX 1: GEOCHEMICAL CONSTRAINTS ON THE ORIGIN OF THE ANNIEOPSQUOTCH OPHIOLITE BELT, NEWFOUNDLAND APPALACHIANS

Lissenberg, C.J., van Staal, C.R., Bedard, J.H., and Zagorevski, A.

Geological Society of America Bulletin, Volume 117 (11/12) p. 1413-1426

ABSTRACT

The Early Ordovician Annieopsquotch ophiolite belt occurs immediately west of the main Iapetus suture zone, and imposes important constraints on the tectonic processes associated with closure of the peri-Laurentian portion of Iapetus. The Annieopsquotch ophiolite, the most prominent ophiolite within the Annieopsquotch ophiolite belt, exposes a 5.5-km-thick section of gabbros, sheeted dikes, and pillow basalts, in which three magmatic episodes have been recognized based on field and geochemical data. The first phase is composed of layered troctolites, which are preserved as enclaves within the gabbro zone. Trace element modeling suggests the troctolites crystallized from boninitic melts. The troctolite substrate was intruded by the dominant, second, tholeiitic magmatic phase, which formed a gabbro-sheeted dike-basalt sequence. All tholeiites have suprasubduction zone chemical characteristics, but the suprasubduction zone signature decreases toward the top of the basalt sequence. The third magmatic episode is composed of primitive dikes, which are interpreted as off-axis intrusions. Other ophiolites within the Annieopsquotch ophiolite belt have comparable geochemical signatures, suggesting they may have constituted a single piece of oceanic lithosphere. Based on geochemical and regional tectonic constraints, the Annieopsquotch ophiolite belt is interpreted to have formed during initiation of west-directed subduction. Fast rollback of the subducting slab would have induced volatile-fluxed decompression melting of previously depleted mantle, yielding boninitic melts. The suprasubduction zone tholeiite sequence would have formed from ascending fertile mantle fluxed with sub-duction-related fluids as rollback continued. This suggests that the Annieopsquotch ophiolite belt does not represent the remnants of normal oceanic crust or backarc basin crust, as previously thought. Our model constrains the initiation and early evolution of a west-dipping peri-Laurentian subduction zone that was responsible for formation of several arc-backarc complexes currently preserved in the Annieopsquotch Accretionary Tract.

INTRODUCTION

Ophiolites are relics of oceanic lithosphere that commonly delineate suture zones between former oceanic or continental terranes. Their origin and tectonic evolution thus impose important constraints on tectonic reconstructions of orogens. The Appalachian-Caledonian orogen results from the Paleozoic closure of Iapetus Ocean, which led to the assembly of Laurentia with a number of intra-oceanic and continental arcs, basins, and microcontinents (Williams, 1979; van Staal et al., 1998). The Annieopsquotch ophiolite belt occupies a key position in the Newfoundland Appalachians because it is situated close to the main Iapetus suture zone. It is the largest and structurally highest belt in a series of accreted ophiolites and arc-back arc complexes termed the Annieopsquotch Accretionary Tract (Fig. A1.1; van Staal et al., 1998; Chapter 2). This accretionary tract marks an important episode of generation and accretion of intra-oceanic complexes to the Laurentian margin, and represents a period of major ocean closure and continental growth. However, its tectonic evolution has hitherto been poorly constrained due to limited field, geochemical, and geochronological data.

Recent reevaluation of the Annieopsquotch Accretionary Tract has shown that the units within the Annieopsquotch Accretionary Tract become progressively younger to the east, indicating they formed above a retreating west-dipping subduction zone (Zagorevski et al., 2003b; Chapter 2). The Annieopsquotch ophiolite belt holds the key to the early evolution of this subduction zone as it is the oldest and structurally highest component of the Annieopsquotch Accretionary Tract.

Previous geochemical results appeared to indicate that lavas and dykes from the Annieopsquotch ophiolite belt had normal mid-ocean ridge basalt (NMORB) chemistry (Dunning, 1987; Swinden et al., 1997). Consequently, van Staal et al. (1998) suggested the Annieopsquotch ophiolite belt represented pieces of Iapetus oceanic lithosphere scraped-off during west-directed subduction underneath the Laurentian margin. This chapter presents new geochemical and regional tectonic data that result from a comprehensive study of the Annieopsquotch ophiolite belt, and provides more rigorous constraints on its origin. We argue that the Annieopsquotch ophiolite belt formed during the initiation of west-directed subduction near Laurentia prior to 480 Ma, and records a complex history of supra-subduction zone (SSZ) opening and closure prior to accretion to the

Laurentian margin. This constrains the age of formation and the early evolution of a west-dipping peri-Laurentian subduction zone, providing an important step in understanding the evolution of the Annieopsquotch Accretionary Tract and the peri-Laurentian portion of Iapetus.

GEOLOGICAL FRAMEWORK

The Newfoundland Appalachians have been subdivided in several tectonostratigraphic zones (Williams, 1979; Fig. A1.1), that represent, from west to east, Laurentian Grenville basement and passive margin cover (Humber Zone), rocks formed in the oceanic realm of Iapetus (Dunnage Zone), and peri-Gondwanan continental blocks (Gander and Avalon zones). Peri-Laurentian rocks in the Dunnage Zone define the Notre Dame and Dashwoods subzones, and are separated from peri-Gondwanan rocks of the Exploits Subzone by the fundamental suture zone of the Newfoundland Appalachians, the Red Indian Line (Williams et al., 1988; Williams, 1995).

On the Laurentian side of the Red Indian Line is a series of east-vergent thrust slices containing 480-464 Ma ophiolites and arc-back arc complexes (Annieopsquotch ophiolite belt, Dunning and Chorlton, 1985; Lloyds River complex, Buchans Group and Red Indian Lake Group, Zagorevski et al., 2003; Fig. A1.1). The structural collage of the complexes display the characteristic architecture of an accretionary complex, and are collectively referred to as the Annieopsquotch Accretionary Tract (van Staal et al., 1998; Chapter 2, Appendix 3). Recent work has shown that these complexes young eastwards (480-464 Ma; Dunning and Krogh, 1985; Zagorevski et al., 2003), suggestive of formation above a west-dipping subduction zone (Zagorevski et al., 2003; Chapter 2, Appendix 3).

In southwest Newfoundland the Annieopsquotch Accretionary Tract is bounded to the northwest by the Lloyds River Fault Zone, which comprises three shear zones (Fig. A1.1; the southeastern, central, and northwestern shear zones). This fault system separates the Annieopsquotch Accretionary Tract to the east from a peri-Laurentian microcontinent called Dashwoods, which was separated from Laurentia by an oceanic basin termed the Humber Seaway during the Cambrian-Early Ordovician (Waldron and van Staal, 2001). The earliest record of orogenic activity in the Dashwoods microcontinent is the Upper Cambrian (<501 Ma; Szybinski, 1995; Swinden et al., 1997) obduction of the Lower to Middle Cambrian Lushs Bight oceanic tract

(508-501 Ma; Elliott et al., 1991; Szybinski, 1995; Kurth et al., 1998). The Lushs Bight oceanic tract was emplaced by attempted subduction of Dashwoods in an east-dipping subduction zone (van Staal et al., 1998). Obduction was followed by closure of the Humber Seaway by east-directed subduction underneath the Dashwoods microcontinent, and led to (1) formation of the SSZ the Baie Verte oceanic tract at 489-484 Ma (Dunning and Krogh, 1985; Cawood et al., 1996; Kurth et al., 1998); (2) formation of a continental arc (the Notre Dame Arc) on the Dashwoods microcontinent (Whalen et al., 1997; van Staal et al., 2003a); (3) collision between the Dashwoods microcontinent and Laurentia by at least 475 Ma and the obduction of the Baie Verte oceanic tract onto the Laurentian margin (Waldron and van Staal, 2001).

The Annieopsquotch ophiolite belt contrasts with the Lushs Bight and Baie Verte ophiolite belts; it is younger (481-478 Ma; Dunning and Krogh, 1985), and was thrust underneath the Dashwoods microcontinent, rather than obducted onto Dashwoods or the Laurentian margin (van Staal et al., 1998; Lissenberg 2005). The Annieopsquotch ophiolite belt comprises three main ophiolitic massifs, the Annieopsquotch, Star Lake, and King George IV ophiolites (Fig. A1.1). The ophiolite massifs are nearly continuous, and are separated by gabbroic to granitic plutons that contain ophiolitic enclaves. The Long Range ophiolitic complex, which occurs 70 km southwest of the King George IV ophiolite, was originally included in the Annieopsquotch ophiolite belt by Dunning and Chorlton (1985). However, the Long Range complex is older than the Annieopsquotch ophiolite belt and was obducted onto the Dashwoods microcontinent prior to intrusion of the Cape Ray granodiorite (488 Ma; Dubé et al., 1998), suggesting a closer link with the Lushs Bight oceanic tract. In addition, ultramafic and several layered gabbroic bodies within the northern Dashwoods Subzone have been considered to form part of the Annieopsquotch ophiolite belt (Dunning and Chorlton, 1985). We have examined these bodies, and, based on geochronological, lithological, and structural data, concluded that the majority are unrelated to the Annieopsquotch ophiolite belt. Several mafic- and ultramafic fragments that occur along strike of the Annieopsquotch ophiolite belt to the northeast (e.g., Hall Hill complex; Bostock, 1988; Hungry Mountain complex; Whalen et al., 1997) have a similar tectonic setting and age of (479 Ma for the Hall Hill complex; Dunning et al., 1987), and are considered to be part of the Annieopsquotch ophiolite belt. The Annieopsquotch

ophiolite belt thus extends for c. 200 km from southwest Newfoundland to Notre Dame Bay on Newfoundland's north coast (Fig. A1.1).

Structural and geochronological data imply that the Annieopsquotch ophiolite belt was thrust northwestward underneath the Dashwoods microcontinent and its Notre Dame Arc prior to 470 Ma along the sinistral oblique Lloyds River Fault Zone (Lissenberg 2005). This is consistent with seismic reflection data, which suggests the Annieopsquotch ophiolite belt forms a thrust slice that extends to at least 15 km depth and structurally underlies the Dashwoods microcontinent (van der Velden et al., 2004). Similar kinematic histories have also been documented along the northeastern extension of the Lloyds River Fault Zone, the Hungry Mountain thrust (Calon and Green, 1987; Thurlow et al., 1992; Fig. A1.1). Underthrusting was accompanied by amphibolite-facies metamorphism along the Lloyds River Fault Zone, but the interior of the ophiolite massifs generally retained most of their original igneous mineralogy (Dunning, 1987; Lissenberg 2005). The Annieopsquotch ophiolite belt is separated from younger units of the Annieopsquotch Accretionary Tract to the east by the Otter Brook Shear Zone. The change in orientation of the ophiolite pseudostratigraphy from the King George IV ophiolite, through Annieopsquotch to the Star Lake ophiolite, suggests that the Annieopsquotch ophiolite belt was deformed into large doubly-plunging folds prior to the final movement accommodated by the Lloyds River Fault Zone and the Otter Brook Shear Zone (Fig. A1.1).

In current tectonic models for the Newfoundland Appalachians, the Annieopsquotch ophiolite belt is regarded either as relic of normal Iapetus oceanic crust scraped off during west-directed subduction underneath the composite Laurentian margin (van Staal et al., 1998), or as having formed in a back-arc basin behind the continental Buchans arc or its oceanic extension (Swinden et al., 1997). In this chapter we present field and geochemical data that bear on this topic.

THE ANNIEOPSQUOTCH OPHIOLITE BELT

The Annieopsquotch ophiolite is the biggest (25 x 8 km) and best-exposed ophiolite of the Annieopsquotch ophiolite belt, and will be used as a template for the entire belt. It preserves a steeply southeast-dipping (c. 70°), fault-bounded section through 5.5 km of oceanic crust, with 3-3.5 km of gabbroic rocks (olivine gabbros and gabbros), 1.5-2 km of sheeted dykes and at least 500 m

of pillow basalts. Pegmatitic pods and trondhjemitic bodies occur locally throughout the gabbroic zone. Hydrothermal metamorphism increases in intensity up-section. Narrow, greenschist-facies mylonitic zones occur locally, but do not appear to have seriously disrupted the ophiolite pseudostratigraphy. The base of the ophiolite is faulted and intruded by numerous Ordovician mafic-intermediate and Silurian felsic plutonic rocks, and the lowermost crust and mantle are not exposed except for a few isolated ultramafic enclaves in the Middle Ordovician tonalites that intruded the Annieopsquotch ophiolite belt.

The gabbro zone of the Annieopsquotch ophiolite is subdivided into 3 parts (Lissenberg 2005). The lowermost 500 m of the exposed section comprises coarse-grained gabbros, olivine gabbros, and subordinate Fe-rich pyroxenites that contain abundant decimeter- to decameter-sized enclaves of layered troctolite, olivine gabbro, and subordinate anorthosite (Fig. A1.2a). Layering in the troctolites is locally isoclinally folded and anorthositic layers are commonly boudinaged, suggesting high-temperature deformation. Modal grading is commonly preserved, however, and layer thicknesses vary from a few cm to 1 m. The dips of layering and foliation in the troctolites are dominantly paleo-vertical, sub-parallel to the strike and dip of the sheeted dykes (Dunning, 1987). The troctolite enclaves are extensively veined and replaced by the gabbroic rocks (Fig. A1.2b). The veins show no evidence of a penetrative high-temperature deformation event, and the surrounding gabbros are generally massive and lack fabrics. These field relationships imply that an early troctolite-forming phase was deformed, and then intruded by a second gabbro-forming magmatic phase. Fine-grained dykes that crosscut both the troctolites and gabbros form a minor component (<5%) of this subzone.

Troctolites have variable proportions of plagioclase (20-90%), but rocks with around 60% plagioclase (An_{80}- An_{90}) and 40% Ol (Fo_{82} - Fo_{84}) are particularly abundant. Olivine is 0.5 - 3 mm, sub- to euhedral, and variably serpentinized. Plagioclase is subhedral, 1 - 6 mm sized, and is locally recrystallized into polygonal aggregates. In rocks thought to be free from superimposed metasomatic effects (see below), clinopyroxene is rare (0-10%), occurring as sub- euhedral ca. 2 - 7 mm sized oikocrysts and 0.5 – 1 mm sized crystals interstitial to plagioclase. Troctolites have adcumulate textures, and commonly exhibit well-defined, layer-parallel shape-preferred orientations

defined by plagioclase laths and, locally, elongated olivines. Olivine is variably serpentinized, and is locally surrounded by coronas of pale green amphibole. Plagioclase is partly sericitized.

Clinopyroxene modes generally increase towards the host gabbros, elevated olivine contents occur in the gabbros immediately surrounding the enclaves, and pyroxenites develop at some troctolite-gabbro contacts. In addition, the gabbros immediately surrounding the troctolites contain up to 20% orthopyroxene and are rich in Fe-Ti oxides. These relationships suggest that the troctolites reacted with the magmas from which the gabbros crystallized. In these transitional samples, clinopyroxene occurs in a diversity of habits, including anhedral to subhedral grains, oikocrysts, and perfectly euhedral prisms (generally 5 mm, up to12 mm). Orthopyroxene occurs as 2-3 mm sized subhedral crystals, as rims and exsolutions on and within clinopyroxene.

Host gabbros of the troctolitic enclaves are generally massive, and have variable olivine contents (0-20%). They are characterized by subhedral 1-5 mm sized plagioclase laths and 2-7 mm sized an- to subhedral clinopyroxene with sub-ophitic to ophitic textures. Olivine occurs as 0.5-2 mm sized anhedral grains. Domains characterized by weak hydrothermal overprints still show partial to complete serpentinization of olivine. In more altered zones, clinopyroxene and rims of plagioclase are replaced by aggregates of fine-grained green amphibole.

Overlying the troctolite-bearing level is 1.5 km of gabbros and olivine gabbros that make up 5-30 m thick sills. These rocks are described in detail in Lissenberg (2005). The gabbroic sills are generally medium- to coarse-grained, but commonly have fine-gained upper and lower margins. Sill contacts are locally marked by downward growing dendritic plagioclase and clinopyroxene up to 10 cm in length. The gabbros are massive to layered, with layering defined by subtle variations in modal content of olivine, plagioclase, and clinopyroxene on a centimeter to decameter scale. Crosscutting fine-grained diabase dykes, locally with chilled margins, are rare at this level (5%). The gabbros are cumulates dominated by plagioclase (An_{55} – An_{74}) and clinopyroxene (En_{41-50} Wo_{38-46} Fs_{8-24}), with minor olivine (Fo_{64} – Fo_{68}), and rarely have a shape-preferred orientation. Ophitic and sub-ophitic textures are common, and crescumulate textures have been observed locally. Brown amphibole and oxides fill interstices. Trace element modeling results suggest that many of these gabbros contain high fractions of trapped melt (15-25%; Lissenberg 2005). Hydrothermal

metamorphic overprints are variably developed, and are commonly related to veins and cracks. In general, alteration becomes more pervasive up-section. It is characterized by extensive replacement of clinopyroxene by green amphibole, and growth of small amphibole grains along grain boundaries and cracks in plagioclase. Sericitization of plagioclase and formation of epidote occur only in the most altered samples.

The upper 500 m of the gabbroic zone is composed of texturally heterogeneous gabbros with liquid-like compositions (Lissenberg 2005). These gabbros generally have a higher content of Fe-Ti oxides than is typical of underlying gabbros. Pegmatitic gabbro pods, some of which grade into hornblende gabbro, occur locally (Dunning, 1987). In some locations, gabbro pods grade into diabase, suggesting this level is the root zone of the sheeted dykes (Dunning, 1987). These relationships, and data presented in Lissenberg 2005, suggest that this level is essentially composed of frozen melts, and preserves relics of the axial melt lens of the spreading ridge. Within this level, the proportion of crosscutting dykes increases upwards as the sheeted dyke complex is approached. The gabbros are characterized by subhedral 2-5 mm sized plagioclase laths and 0.5-7 mm sized anhedral clinopyroxene with subophitic textures. Locally, clinopyroxene occurs interstitially between plagioclase. Fe-Ti oxides occur as irregularly shaped grains that appear to have overgrown and partly replaced plagioclase and clinopyroxene. Clinopyroxene is completely replaced by aggregates of small green amphibole. These aggregates also replace plagioclase along grain boundaries and cracks, but plagioclase otherwise remains relatively unaffected by hydrothermal metamorphism. Epidote-filled cracks dissect the gabbros.

Trondhjemite bodies form about 1% of the gabbro zone, and are concentrated near its top. They generally occur as intrusion breccia matrices, although locally they form the cores of pegmatitic gabbro pods (Dunning, 1987). In many cases, the trondhjemites are spatially associated with putative paleo-normal faults (Dunning, 1984). These faults are represented by poorly exposed narrow zones of cataclasites and mylonitic rocks.

The sheeted dyke complex consists of subparallel diabasic dykes with widths typically 1-10 m at its base, and 0.5-3 m higher up in the section (Dunning, 1987). Dykes range from aphanitic to medium grained, and may have subophitic to diabasic textures, with nearly equal amounts of

clinopyroxene and plagioclase. Oxides may be abundant (up to 20%). Dykes are commonly plagioclase-phyric (generally <5%, locally 10%), rarely plagioclase + clinopyroxene-phyric. Pillow lavas (0.2-1 m) are commonly aphyric, but may contain a few percent plagioclase phenocrysts (Dunning, 1987). The lavas are cut by abundant dykes, and locally contain interpillow jasper. Dykes and basalts are generally pervasively altered, with complete replacement of clinopyroxene by amphibole and partial replacement of plagioclase by sericite, chlorite, and epidote.

The 25 x 7 km sized Star Lake ophiolite massif exposes a shallowly north to northeast-dipping, tectonically bounded section through gabbros and sheeted dykes (Fig. A1.1). Basalts are present to the northeast of the sheeted dykes, and were considered to be part of the ophiolite by Whalen (1993). However, recent mapping and geochemical data suggest they form part of the structurally underlying Lloyds River Complex, which comprises a 473 Ma arc-back arc sequence (Chapter 2). The thickness of the Star Lake ophiolite units is uncertain. The lowermost part of the gabbro zone of Star Lake, like Annieopsquotch, also contains abundant troctolitic enclaves, suggesting it preserves a similar section. The fault-bounded, 12 x 5 km, King George IV ophiolite comprises similar gabbros, sheeted dykes, and basalts of uncertain thickness. The ophiolite pseudostratigraphy and pillow tops indicate that the King George IV ophiolite youngs towards the west with a dip of >60°.

The Hungry Mountain complex of the Notre Dame Arc is dominated by diorite and tonalite that contain abundant mafic-ultramafic fragments, which were interpreted by Whalen et al. (1997) to be correlative to the Annieopsquotch ophiolite. The Hall Hill complex was described in detail by Bostock (1988), and comprises a 25 x 5 km sized fault-bounded block of variably metamorphosed gabbros, plagiogranite, and basalts, cut by diabase dykes (Bostock, 1988). It is situated on the north coast of Newfoundland immediately southeast of the Lobster Cove fault (Fig. A1.1).

WHOLE-ROCK GEOCHEMISTRY

Sampling and analytical techniques

We analyzed major and trace elements for 78 samples of troctolites, gabbros, sheeted dykes, and lavas from the Annieopsquotch ophiolite, 15 samples from the Star Lake ophiolite, and 4 from the King George IV ophiolite. Data are listed in Table A1.1, with the exception of data of

gabbros and some of the crosscutting dykes of the Annieopsquotch ophiolite, which are given in Lissenberg (2005; Table 4.1). Details on the different procedures an be found in Appendix 4 and Rogers (2004).

Element mobility

Hydrothermal ocean floor metamorphism and subsequent accretion-related metamorphism has affected the Annieopsquotch ophiolite belt to various degrees. The distribution of hydrous assemblages is thought to predominantly reflect ocean floor processes, but mineral equilibria were probably partly reset during the amphibolite-facies metamorphism which accompanied accretion of the Annieopsquotch ophiolite belt to the Dashwoods microcontinent. The effect of these metamorphic episodes on the geochemistry of the samples is evaluated by plotting various elements against the immobile incompatible element zirconium, which is also an index of fractionation. The sheeted dykes show good correlations against Zr for all elements but Rb and Cs; Ba, Pb, Sr, and K (with the exception of two samples) also show reasonable correlations. The dominantly magmatic abundance patterns are consistent with the low LOI (average 1.2%). Basalts show greater element mobility than dykes, concurrent with an increase in LOI (average 2.1%). Some basalts have increased contents of SiO_2 and Na_2O, while some CaO has been removed. Sr, Ba, and Cs were mobile in most samples. Abundances of K_2O and Rb are low (<0.1% and 0.1-2 ppm, respectively) in almost all samples, likely indicating removal of these elements. Al_2O_3 shows a broad correlation with Zr, suggesting limited mobility, and Pb correlates well with Zr for all but the most altered samples. Nonetheless, despite the relatively consistent behaviour of the LILE, we mostly use immobile trace elements (REE, HFSE) for the paleo-tectonic interpretation of the gabbros, sheeted dykes, and basalts. Element abundances in troctolites are inferred to be almost entirely magmatic in origin.

Troctolites, Annieopsquotch ophiolite

The troctolites have high Mg# = 0.81-0.85 (Mg# = $Mg/(Mg+Fe^{2+})$, assuming $Fe^{3+}/Fe^{2+} = 0.1$) and show major element chemical patterns dominated by accumulation of plagioclase and olivine. Incompatible trace element abundances are low (e.g., chondrite normalized Yb_N = 0.4-0.8; normalization values of Sun and McDonough, 1989), whereas compatible elements such as Ni are

high (Table A1.1). They also have strong positive Eu anomalies (Eu/Eu* = 3.31-4.19), reflecting their plagioclase-cumulate nature. The REE patterns are flat, LILE (Cs, Rb, K, Sr, Pb) are strongly enriched, and HFSE contents are low (mostly below detection limit; Fig. A1.3a,b).

In order to evaluate the origin of the troctolite substrate, compositions of the magmas that generated the Annieopsquotch troctolites were calculated using the method of Bédard (1994). This method calculates the liquid in equilibrium with a given cumulus assemblage by combining whole rock geochemical analyses with an updated, parameterized partition coefficient dataset (Bédard, pers. comm). Trapped melt was modeled as a phase with D=1 for all elements under the assumption that was in equilibrium with the cumulus phases, and calculations were repeated with different amounts of trapped melt. The modes of the samples were estimated from thin section, augmented by CIPW modes, but have little effect on the calculated melt composition (Bédard, 1994). Partition coefficients were calculated for each phase in each sample based on mineral compositions determined by electron microprobe. The use of a trapped melt fraction in equilibrium with the cumulus crystals assumes that (see also Bédard, 1994) (1) the trapped melt remained in contact with the main melt resevoir during growth of the cumulus crystals and their adcumulus overgrowths (see Wager et al., 1960), and (2) that no late-stage percolation of trapped melt (more evolved or more primitive than the equilibrium trapped melt) occurred. Equilibrium between the trapped melt and cumulus crystals is supported by the absence of prominent compositional zoning in the Annieopsquotch cumulates, which would be expected had more primitive or more evolved melt percolated the cumulate pile.

The composition of the model melts for different amounts of assumed trapped melt are listed in Table A1.2 and illustrated in Figure 4. The melts that generated the troctolites were clearly more depleted in incompatible elements than NMORB, with flat REE patterns, and U-shaped extended-REE plots with enrichment in LILE. Assuming 10% trapped melt, the TiO_2 contents of the model liquids are low (c. 0.3%), whereas Cr and Ni contents are high (c. 600 ppm and c.100-300 ppm, respectively). The low REE and HFSE contents and high compatible element contents signal melting of a refractory source, which is typical of boninites (e.g., Crawford et al., 1989). The model liquids correspond reasonably well with boninites from the Betts Cove ophiolite (Fig. A1.4; Bédard,

1999), suggesting that the troctolite substrate formed from boninite-like magmas. The plagioclase-rich nature of the troctolites is enigmatic, but may indicate that the parental magmas, if indeed boninitic, were of the high-calcium type, which is the least depleted of the boninitic subtypes (Crawford et al., 1989). The Mg# of the parental melt was 61-58, as calculated from olivine analyses using an olivine-liquid partition coefficient of 0.3 (Roeder and Emslie, 1970), and neglecting the trapped melt effect (Barnes, 1986). This is in the lower range of typical boninites (e.g., Crawford et al., 1989), suggesting that the parental magmas were evolved, which may in part account for the abundance of plagioclase. Plagioclase phenocrysts have been described in similarly evolved high-calcium boninites from Tonga (Mg# 57-63; Falloon and Crawford, 1991), the New Hebrides arc (Mg# 60-70; Monzier et al., 1993), and the Izu-Bonin-Mariana fore-arc (Mg# 55; Meyer, 1980; Hickey and Frey, 1982). In these suites, plagioclase phenocrysts are associated with clinopyroxene, orthopyroxene and olivine.

We note that the high Cs content of the model liquids (3.2-10.5 ppm assuming 10% trapped melt; Fig. A1.4), which reflects the high Cs content of the whole rock analyses (0.39-1.32 ppm) probably does not reflect the original magmatic abundance of this element. Its concentration far exceeds that in any Tertiary-recent boninite. The same may hold for Rb and K in samples VL01J035b and VL02J310A and P in samples VL02J309B and VL02J310a. Unrealistically high Cs (and locally Ba, K, and P) contents in some troctolites suggest that (1) the trapped melt was evolved, having concentrations of these elements that exceed concentrations in equilibrium with the cumulus phases, or (2) LILE were introduced by an external agent, possibly a melt or hydrous fluid associated with the intrusion and crystallization of the gabbros, or a post-magmatic hydrous fluid responsible for serpentinization.

The gabbro-sheeted dyke-basalt sequence, Annieopsquotch ophiolite

The basaltic sheeted dykes and pillow lavas of the Annieopsquotch ophiolite belt define a typical tholeiitic differentation trend with increasing Fe-content during differentiation, consistent with low-pressure fractionation of olivine, plagioclase, and clinopyroxene. The basaltic Annieopsquotch ophiolite belt dykes and lavas have a wide compositional range, with MgO 4.45-9.55 %, SiO_2 45.3-53.3%, Mg# 0.42-0.72, and TiO_2 0.36-1.95%. Three chemical groups have been recognized based

primarily on the degree of LREE depletion (La/Sm) and the extent of Nb depletion (Fig. A1.5). Differences between these groups are also reflected in contrasting Mg# and TiO_2 contents (Table A1.1).

The first group comprises nearly all of the sheeted dykes and basaltic lavas, as well as some dykes that crosscut the gabbro zone, and is characterized by LREE depletion slightly stronger than NMORB (NMORB normalized La/Sm = 0.59–1.35, av. = 0.81) and low Nb contents (Fig. A1.5). It has average SiO_2 and TiO_2 contents of 49.2% and 1.25%, respectively, and an average Mg# of 0.56. Trace element patterns resemble MORB overall, but negative anomalies for Nb, Zr, and Ti are apparent, and dykes show enrichment in K, Ba, and, in some samples, Pb and Sr (Fig. A1.3c-d). These features are ubiquitous in intraoceanic arcs, which result from melting of a mantle source triggered by the release of hydrous fluids from the subducting slab and/or metasomatized mantle (e.g., Tatsumi et al., 1986). Trace element and isotopic evidence indicates that, in primitive island arc tholeiites, the depleted mantle wedge imparts the LREE depletion signature, while the slab-derived fluids carry LILE (Cs, Ba, Rb, K, Pb, Sr) into the sub-arc mantle, enriching the arc source in these components (e.g., Pearce, 1983; Tatsumi et al., 1986; Saunders et al., 1991; Hawkesworth et al., 1991; Class et al., 2000). Depletion in HFSE (Ti, Nb, Zr, Ta) may result from residual phases within the mantle source and/or subducting slab (rutile, titanite: e.g., Saunders et al., 1991; Brenan et al., 1994), a solubility effect in the fluids released from the slab (e.g., Keppler, 1996), or interaction of rising magmas with the mantle (Kelemen et al., 1990). The HFSE depletion and enrichment in LILE of the Annieopsquotch tholeiites thus suggest that the spreading center at which the ophiolites formed was situated near a subduction zone, or tapped a source previously enriched by subduction zone processes. A suprasubduction zone (SSZ) setting is consistent with the similarity between the Annieopsquotch tholeiites and basalts from the Lau back arc basin (Fig. A1.3c-d), which have been interpreted to be melts of a depleted MORB-like mantle, but with a distinct subduction zone component (low HFSE and enriched LILE) derived from the associated Lau remnant arc and active Tofua arc (Hawkins and Allan, 1994).

The second group is found only among the basaltic lavas, and is particularly abundant near the stratigraphic top of the extrusive section. It has higher average SiO_2 (50.5%) and TiO_2 (1.43%)

contents and lower average Mg# (0.52) than Group 1, and shows NMORB-like LREE depletion and Nb contents (Fig. A1.5). These basalts exhibit only small Nb, Zr, and Ti anomalies (Fig. A1.3e-f), suggesting they have a NMORB-like source, with only a minor SSZ signature.

The third group comprises dykes that crosscut the gabbros, lavas, and sheeted dykes. They are characterized by strong LREE depletion relative to NMORB (average La/Sm_N = 0.45), low incompatible element contents (average TiO_2 = 0.98%; average Nb_N =0.18) and high Mg# (0.53-0.72, average 0.63). Their trace element patterns show variable Nb, Ti, and Zr anomalies (Fig. A1.3g-h), and the samples have variable HREE contents for a given Mg#. The low but variable incompatible element contents and strong LREE depletion suggest these dykes are generated by variable degrees of partial melting of a depleted source, and the preservation of dykes with Mg# of 0.72 suggest some of them have experienced little fractionation since leaving their mantle source. Based on their occurrence throughout the ophiolite pseudostratigraphy, their primitive nature, low incompatible element contents and the magnitude of geochemical variation, we interpret these dykes to be off-axis intrusions that sampled the last, most depleted increments of melt from the melting column. This interpretation is supported by the fact that most of these dykes are markedly fresher than their host rocks. It is also consistent with off-axis lava compositions from the East Pacific Rise, which are more primitive than NMORB, and have lower incompatible element contents (Reynolds and Langmuir, 2000).

Annieopsquotch gabbros have high Mg# (0.53-0.81, average 0.71) and low TiO_2 contents (average 0.49%). The low incompatible element contents indicate that most are cumulates, with the exception of sample VL02J341A, which comes from the uppermost part of the gabbro zone. Their trace element patterns show marked negative Nb, Ti and Zr anomalies, as well as enrichment in Pb, suggesting they may have crystallized from melts similar to Group 1 basalts (Fig. A1.3i-j). The parental magmas of gabbroic cumulates, modeled in a similar fashion as for the troctolites, have compositions indistinguishable from Group 1 dykes and basalts, suggesting these gabbros, dykes and basaltic lavas are consanguineous (Lissenberg 2005). Two samples (VL02J326b and VL01J339a) have negligible Zr and Ti anomalies, and a small Nb anomaly, and may have crystallized from melts with Group 2-like compositions.

The Star Lake and King George IV ophiolites

In order to evaluate the along-strike variety in magma compositions in the Annieopsquotch ophiolite belt, We compare the chemistry of the Annieopsquotch ophiolite, presented above, with the chemistry of the other major components of the belt (Star Lake, King George IV).

The majority of samples from the Star Lake and King George IV ophiolites follow trends very similar to Group 1 of the Annieopsquotch ophiolite. Dykes and basalts from King George IV and Star Lake are indistinguishable from the Annieopsquotch dykes and basaltic lavas (Figs. A1.6a-b, g-h); they too are MORB-like, LREE depleted, and characterized by HFSE depletion, and so are interpreted also to have formed in a SSZ setting. Star Lake ophiolite gabbros are generally depleted in LREE, Zr and Ti, and enriched in LILE. They have the same composition as gabbros from the Annieopsquotch ophiolite (Fig. A1.6c-d), which are cumulates complementary to the melt compositions preserved in the sheeted dykes and basaltic lavas. Like those from Annieopsquotch, troctolites from the Star Lake ophiolite show strong REE-HFSE depletion, and enrichment in Cs, Ba, K, Sr and Pb (Fig. A1.6c,d). In contrast, the Fo content of olivine in Star Lake troctolites (average 81.8) is slightly lower than that in Annieopsquotch troctolites (83.1), whereas absolute REE contents are slightly higher (Fig. A1.6c-d). These data are compatible with three hypotheses, which are not mutually exclusive. The Star Lake ophiolite troctolites may have: 1) accumulated from a slightly more differentiated version of the same melt which generated the troctolites in the Annieopsquotch ophiolite; 2) formed from a somewhat less depleted source; 3) retained a larger fraction of trapped melt. These data suggest the majority of the Star Lake and King George IV ophiolites formed from magmas very similar, if not identical, to those from which the Annieopsquotch ophiolite formed.

A group of five gabbroic samples that occur in the upper level of the gabbro zone of the main Star Lake massif, as well as in a smaller ophiolitic body just to the west of it (Fig. A1.1), have trace element patterns that deviate from the MORB-like patterns of the Annieopsquotch gabbros. The age relationships between these anomalous gabbros and the tholeiitic gabbros are unclear. The anomalous gabbros are dominated by clinopyroxene and plagioclase, with, in two samples, olivine (15%) and orthopyroxene (5%). These rocks have a mesocumulate texture, with

intercumulus amphibole, suggesting the magma was hydrous. They have SiO_2 44.9-48.5%, TiO_2 0.12-0.15%, Mg# 0.77-0.80 and positive Eu anomalies (1.4-2.1), reflecting their cumulate nature. One of these anomalous gabbros (VL02J380a) has lower SiO_2 (41%), and high FeO and TiO_2 contents (16.3% and 1.24%, respectively), suggesting accumulation of Fe-Ti oxides. Trace element patterns are characterized by low HREE abundances, significantly lower than the gabbros from the Annieopsquotch ophiolite, and enrichment in LREE (i.e. high La/Nd), which is not observed anywhere within the Annieopsquotch ophiolite (Fig. A1.6e-f). The Mg# of the parental melt was 0.45, as calculated from olivine and orthopyroxene compositions using Fe/Mg partition coefficients of 0.30 and 0.27, respectively, and neglecting the trapped melt effect (Barnes, 1986). The relatively low Mg# of the parental melt and accumulation of Fe-Ti oxides in sample VL02J380A, suggest the melt was quite evolved. The presence of orthopyroxene as a cumulus phase suggests the parental melt was SiO_2 saturated. For reasonable assumed trapped melt fractions, estimated from the change in LREE slope and LILE contents during modeling, calculated parental melts of the olivine gabbros are markedly more depleted than Annieopsquotch sheeted dykes and basalts with similar Mg# (Table A1.2; Fig. A1.7); and calculated melt TiO_2 contents (around 0.5%) are much lower than would be expected from evolved MORB-like magmas. Thus despite their fractionated nature, incompatible element abundances of the model parental melts are very low, suggesting the melts from which they evolved were extremely depleted, and may have been similar to the boninitic magmas that generated the troctolites. A boninitic parent is consistent with the observed enrichment in LREE, with the SiO_2 saturation indicated by the presence of orthopyroxene, and with the hydrous nature of the melt suggested by the presence of intercumulus amphibole. The similarity in degree of depletion, measured by the HREE content, between the calculated melt and evolved boninites from the Tonga ridge (Mg# 47; Falloon and Crawford, 1991) supports this interpretation (Fig. A1.7). Interestingly, the evolved boninite from Tonga is olivine-plagioclase-orthopyroxene-clinopyroxene phyric (Falloon and Crawford, 1991), which corresponds to the cumulus phases in the modeled Star Lake olivine gabbro. If the Star Lake olivine gabbros were indeed generated from a boninitic melt, this suggests a genetic link with the troctolites that occur within the lowermost part of the Annieopsquotch and Star Lake gabbro zone, although a stronger enrichment in LREE and

steeper slope in the MREE indicates the melts which generated the olivine gabbros were different from those that generated the troctolites. Possibly, these rocks represent a higher-level relict of a boninitic substrate that formed the basement to the SSZ sequence?

DISCUSSION

The geochemical similarity of the tholeiitic sequences of the Annieopsquotch, Star Lake and King George IV ophiolites, as well as the occurrence of troctolite enclaves in the lower part of the gabbro zone of both the Star Lake and Annieopsquotch ophiolites, supports previous interpretations that the Annieopsquotch ophiolite belt represents a single piece of oceanic lithosphere (Dunning and Chorlton, 1985; Dunning, 1987). Data presented herein show that the Annieopsquotch ophiolite belt comprised three distinct magma series. The first phase encompassed the formation of a boninitic substrate or basement, represented by the troctolitic enclaves in the gabbros of the Annieopsquotch and Star Lake ophiolites. The Star Lake gabbros that appear to have crystallized from an evolved boninitic melt may also have formed during this phase, although relationships are not clear from field evidence. The boninitic phase was followed by tholeiitic gabbros, sheeted dykes, and lavas, which dominate the Annieopsquotch, Star Lake, and King George IV ophiolites. The tholeiitic magmas initially had a strong SSZ geochemical signature (Group 1), which became less pronounced with time (Group 2). The age-gap between the boninitic and tholeiitic series is not constrained. Finally, depleted tholeiitic off-axis dykes cut the entire sequence.

Model for Generation of the Annieopsquotch ophiolite belt

Any model for generation of the Annieopsquotch ophiolite belt has to account for the following: 1) an early phase of boninitic magmatism; 2) a main phase of rapid seafloor-spreading tapping mantle enriched by subduction zone processes; 3) accretion to the Dashwoods microcontinent within 10 Ma after formation of the tholeiite sequence; 4) a lower-plate setting during accretion to the Dashwoods microcontinent. An additional constraint is provided by the fact that the Annieopsquotch ophiolite belt is the oldest unit preserved within the Annieopsquotch Accretionary Tract, and is juxtaposed with the Dashwoods microcontinent. Thus there is no record of preexisting intra-oceanic units within the peri-Laurentian portion of Iapetus that may have contributed to formation of (part of) the Annieopsquotch ophiolite belt.

The depleted nature of boninites (high MgO, Ni, Cr, low Al_2O_3, TiO_2, HREE) is widely interpreted to result from melting of a refractory mantle wedge, from which melts had previously been extracted. This source is enriched by a LILE-rich hydrous fluid, and possibly by a LREE rich melt, commonly interpreted to be derived from the subducting slab and/or overlying sediments (e.g., Crawford et al., 1989; Sobolev and Danyushevsky, 1994; Bédard, 1999). The temperatures required for melting refractory mantle to produce boninites (1100° - 1550°C: Crawford et al., 1989; Sobolev and Danyushevsky, 1994) are higher than those expected in a typical sub-arc mantle wedge, and three end-member processes have been proposed to explain the elevated mantle temperatures. The first involves introduction of a heat source into "normal" sub-arc mantle wedge, by subduction of a spreading ridge (Crawford et al., 1989) or propagation of a spreading center into an arc or fore-arc (e.g., Tonga: Falloon and Crawford, 1991; New Hebrides: Monzier et al., 1993). The second process invokes rapid upwelling of mantle in response to extension induced by arc or fore-arc rifting rifting (Crawford et al., 1981; Hickey and Frey, 1982; Bédard et al., 1998) or the initiation of subduction (e.g., Izu-Bonin-Mariana fore-arc; Stern and Bloomer, 1992; Pearce et al., 1992). The third process involves a high geothermal gradient caused by the presence of a mantle plume (Macpherson and Hall, 2001).

Whereas we cannot rule out the possibility that there was influence of a mantle plume, no evidence exists within the Annieopsquotch ophiolite belt of an OIB-like geochemical signature. We therefore infer a plume was not the primary cause of boninite generation in the Annieopsquotch ophiolite belt. In addition, as mentioned above, there is no record of an intra-oceanic arc of the appropriate age and structural position associated with the Annieopsquotch ophiolite belt. The absence of an associated intra-oceanic arc indicates the boninitic magmas did not form by arc or fore-arc rifting or propagation of a spreading center into an arc.

The Annieopsquotch ophiolite belt is bounded by the Early Ordovician (488-480 Ma; van Staal et al., 2003) continental Notre Dame Arc and its Dashwoods basement on the northwestern side and the younger Lloyds River complex and Buchans arc (473 Ma; Dunning et al., 1987; Zagorevski et al., 2003) on the southeastern. The Buchans arc is built on attenuated continental crust (Zagorevski et al., 2003), suggesting that the Buchans arc, like the Notre Dame Arc, was built

on a rifted piece of Laurentian crust. This raises the possibility that the Annieopsquotch ophiolite belt may have been generated in a peri-continental intra-arc rift basin separating the Buchans and Notre Dame arcs (cf. Swinden et al., 1997). In such a scenario the boninites could have been generated in the early stages of arc rifting by decompression melting of a mantle source that was already depleted in HFSE and HREE and enriched in LILE and LREE due to the generation of Notre Dame Arc magmas. The tholeiites could then have formed by subsequent upwelling of less depleted mantle as the extension proceeded, with the magma supply increasing to the point where it kept pace with the rate of opening. However, three lines of arguments indicate this scenario is unlikely. First, boninites have not been observed in young oceanic basins that formed by rifting of continental arcs, such as the Japan Sea, the Bransfield Strait, the Gulf of California and the Sarmiento complex. The earliest magmas formed in these basins are typically tholeiitic basalts with suprasubduction zone signatures, which are quickly followed by MORB-like lavas (e.g., Saunders et al., 1982; Keller et al., 2002). Second, there is a remarkable scarcity of clastic sedimentary rocks within the Annieopsquotch Accretionary Tract, and the Annieopsquotch ophiolite belt in particular, contrary to what would be expected within an immature rift separating two continental blocks (e.g., Gulf of California; Saunders et al., 1982). Third, Nd isotopic data for the Annieopsquotch ophiolite belt suggest it is very juvenile (ε_{Nd}=7.6-8.3; Swinden et al., 1997), inconsistent with a crustal contribution.

The only remaining possibility to explain the absence of an associated intra-oceanic arc is a scenario in which the Annieopsquotch ophiolite belt formed during initiation of subduction. This is similar to the Izu-Bonin-Mariana fore-arc, where the early stage of subduction was characterized by widespread boninitic magmatism (200 km wide) in a strongly extensional environment interpreted to result from rollback of the old Pacific plate in the early stages of subduction (Stern and Bloomer, 1992). Hall et al. (2003) showed that after a finite amount of convergence (100 km), the buoyancy-related force of the sinking slab leads to a period of rapid rollback, with extension rates in the overriding plate of 10 cm/yr. Rapid extension allows for the ascent of mantle to shallow levels, leading to the high geothermal gradient required for boninite genesis. In this scenario,

decompression melting of the mantle, as well as contact melting of the overlying depleted mantle, aided by slab-derived fluids, would have yielded the boninites.

Using the Izu-Bonin-Mariana forearc as an analogy, the following evolution of the Annieopsquotch ophiolite belt is envisaged (Fig. A1.8). Subduction would have initiated outboard of the Dashwoods microcontinent, perhaps as a result of a plate reorganization following initial collision between Laurentian promontories and the Dashwoods microcontinent. Sedimentological evidence suggests the collision was underway at least by the Middle Arenig (475 Ma; see Waldron and van Staal, 2001), which coincides with a marked gap in arc magmatism in the Dashwoods microcontinent (van Staal et al., 2003). Subduction likely initiated along a preexisting weak zone in the crust. Little is known about the spreading history of Iapetus, although the presence of peri-Laurentian microcontinents (e.g., Dashwoods) suggests the presence of abandoned spreading centers and associated transform faults near the Laurentian margin (Müller et al., 2001). Such zones of weakness may have been reactivated during subduction initiation. Given that Laurentia separated from west Gondwana at 570 Ma (Cawood et al., 2001), the oceanic lithosphere immediately outboard of the Dashwoods microcontinent was likely rather cool at the time of subduction initiation, with a lithospheric thickness approaching 95 km (Richardson et al., 1995). The lithospheric mantle was probably already depleted after the extraction of Iapetus oceanic crust from it.

Subduction initiation caused early extension in the overriding plate, leading to stretching and eventual break-up (Fig. A1.8). Melt production during stretching and initial break-up was probably minor, due to a low geothermal gradient and absence of fluids derived from the subducting slab. Once started, rollback proceeds extremely fast, leading to very quick influx of hot mantle from below (Hall et al., 2003). After 60 km of subduction of the downgoing plate, the more fertile asthenospheric mantle would have ascended to 50 km depth, assuming the amount of upwelling is more or less equal with the amount of mantle displaced by rollback. At this stage, boninitic magmas would have formed when the depleted mantle reached a level where it was fluxed with fluids derived from the subducted slab (Fig. A1.8b). These magmas generated crust now preserved as the Annieopsquotch and Star Lake troctolites, and some gabbros. Associated volcanic rocks have

not been observed; We speculate that they have been tectonically removed during rollback-induced extension of the boninitic substrate, possibly by low-angle detachment faulting similar to that occurring along mid-ocean ridges (e.g., Karson, 1999). Subduction initiation and boninite genesis must have occurred prior to 480 Ma, the age of the tholeiitic sequence (Dunning and Krogh, 1985), but the time interval between the boninitic and tholeiitic phases is uncertain.

As extension proceeds, fertile mantle may decompress enough to initiate melting (e.g., Pearce & Parkinson, 1993), an effect that would be amplified if the rising fertile mantle enters the region of the mantle wedge that is fluxed by fluids expelled from the subducting slab (Fig. A1.8c). In the Annieopsquotch ophiolite belt, this process may have yielded tholeiitic SSZ magmas at 481-478 Ma, which generated the dominant gabbro-sheeted dyke-basaltic lava sequence. Rapid extension was accompanied by a robust supply of magma and led to seafloor spreading. Extension may have contributed to break-up of the boninitic substrate, producing the current configuration of isolated troctolitic enclaves within the gabbros. Continued spreading may have removed the spreading axis from the vicinity of the subducting slab and its derived fluids, leading to more MORB-like compositions at the top of the extrusive section. This is analogous to the rapid transition from SSZ to MORB-like compositions during formation of back arcs (e.g., Ewart et al., 1994).

As the convergence rate and subduction angle stabilize, a true magmatic arc may form after 15 Ma (Stern and Bloomer, 1992). In contrast, the absence of andesites and dacites suggests that the Annieopsquotch ophiolite belt never reached the stage of a true magmatic arc. Instead, arc magmatism was localized outboard of the Annieopsquotch ophiolite belt forming the Buchans arc on a piece of Dashwoods basement which is interpreted to have been emplaced by trench-parallel transport (Chapter 2; Zagorevski et al., 2003; Fig. A1.8d).

Implications for tectonic evolution of the Newfoundland Appalachians

Structural relationships in the Lloyds River Fault Zone, which separates the Annieopsquotch ophiolite belt from the remnants of the Dashwoods microcontinent, suggest the Annieopsquotch ophiolite belt was thrust underneath Dashwoods (Fig. A1.1; Lissenberg 2005). The fact that similar structural relationships occur in related segments along strike for at least 200 km (Dean and Strong, 1977; Calon and Green, 1987; Thurlow et al., 1992), and that the Lloyds River

Fault zone extends to 15 km depth (van der Velden et al., 2004), together indicate the Annieopsquotch ophiolite belt occupied a lower plate setting during accretion to the Dashwoods microcontinent. Thus after its formation the Annieopsquotch ophiolite belt was transferred from an upper to a lower plate setting (Fig. A1.8). Moreover, age data indicate arc-back arc complexes of the Annieopsquotch Accretionary Tract, to the southeast of the Annieopsquotch ophiolite belt, become progressively younger to the east (Zagorevski et al., 2003). These relationships suggest that the subduction zone in which the Annieopsquotch ophiolite belt was formed dipped to the west. After generation of the Annieopsquotch ophiolite belt during initiation of subduction, west-directed subduction thus continued, with the overlying arc remaining in extension during most of its history. This episode was marked by important strike-slip movements, leading to trench-parallel transport of the basement to the Buchans arc (Zagorevski et al., 2003). In addition, accretion of the various units of the Annieopsquotch Accretionary Tract to the Dashwoods microcontinent involved a sinistral strike-slip component (Lissenberg 2005). This suggests that both subduction and subsequent accretion were oblique. We note, however, that strike slip processes cannot have been responsible for the occurrence of the two distinct units (boninites and tholeiites) within the Annieopsquotch ophiolite belt, e.g. by initiating spreading in a previously generated boninitic crust formed by arc-related processes (arc rifting, propagation of a spreading center into an arc), as such older units do not exist.

CONCLUSIONS

Field and geochemical data from the Annieopsquotch ophiolitic belt show that the different massifs have similar compositions and record similar magmatic histories, and likely constitute a single accreted oceanic terrane. Field relationships imply that the Annieopsquotch ophiolite belt was generated in three phases. The first phase, of unknown age, encompasses troctolites and olivine gabbros formed from boninitic melts. The absence of an associated coeval intra-oceanic arc suggests the boninites were generated during initiation of subduction outboard of the Dashwoods microcontinent by shallow melting of a previously depleted mantle source. Subduction likely initiated in response to the collision between the Dashwoods microcontinent and the Laurentian margin. The second magmatic phase comprises the tholeiitic SSZ gabbro-sheeted dyke-basalt sequence formed

at 480 Ma, followed by the final magmatic episode represented by off-axis dykes that cut the entire ophiolite. This model differs significantly from existing tectonic models for the Newfoundland Appalachians, where the Annieopsquotch ophiolite belt is interpreted as scraped-off NMORB Iapetus oceanic crust (van Staal et al., 1998), or as back-arc basin crust (Swinden et al., 1997). These data constrain the timing of initiation of west-directed subduction outboard of the composite Laurentian margin. This subduction zone was responsible for formation of the entire Annieopsquotch Accretionary Tract, and thus played a significant role in Early Ordovician Appalachian orogenesis.

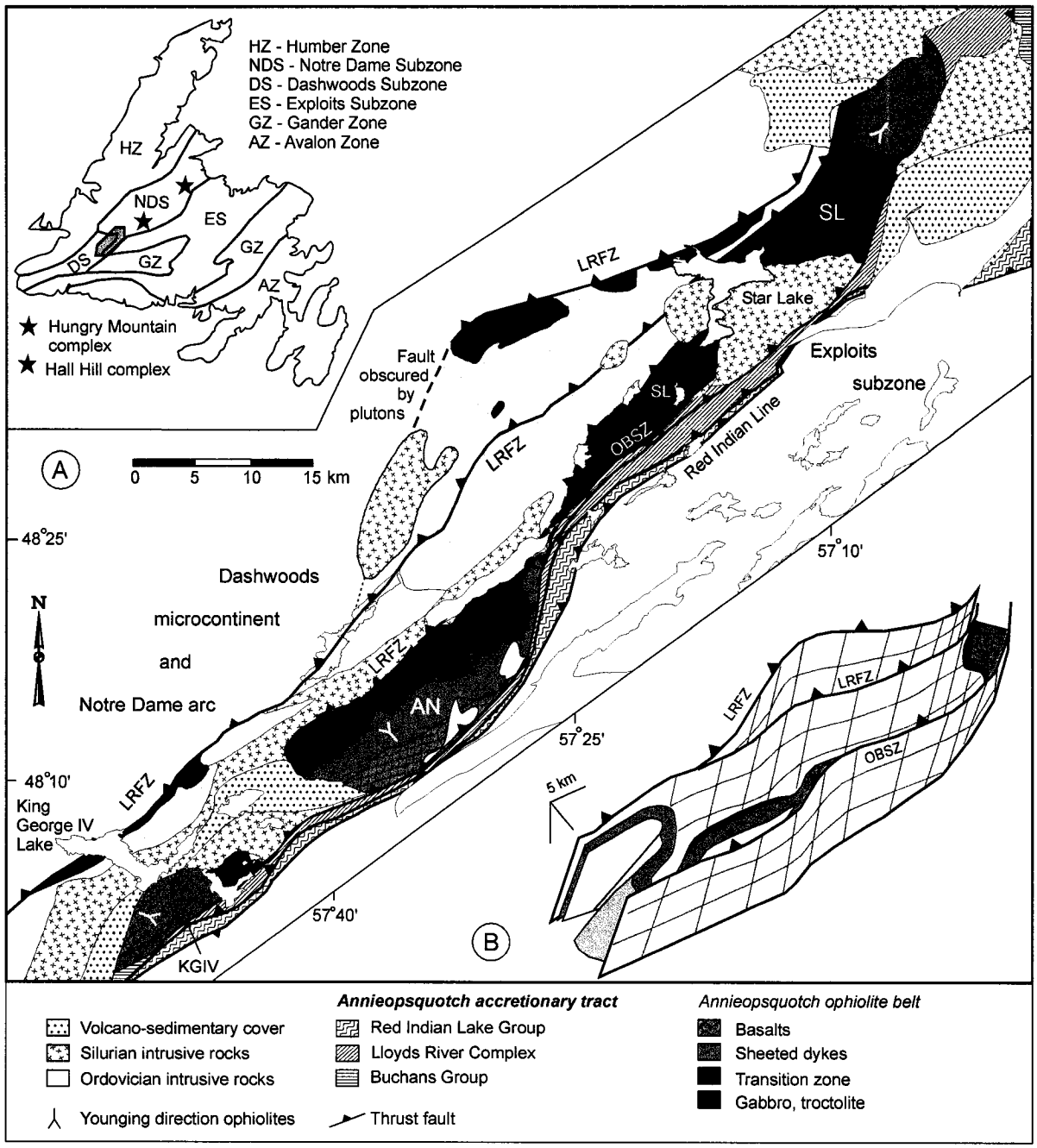

Figure A1.1: (a) Geological map of the Annieopsquotch Accretionary Tract, showing the regional relationships and stratigraphic units of the Annieopsquotch (AN), Star Lake (SL) and King George IV (KGIV) ophiolites. Inset shows location, tectonostratigraphic zones of the Newfoundland Appalachians, as well as the locations of the Hungry Mountain and Hall Hill complexes. OBSZ=Otter Brook Shear Zone. Modified from Lissenberg et al. (in press) and van Staal et al. (in press a,b,c). (b) Schematic block diagram illustrating the structure of the main components of the Annieopsquotch ophiolite belt, ignoring Middle Ordovician-Silurian intrusions and cover sequences. Plunge of folds is estimated from dip of ophiolite pseudostratigraphy. Contacts between gabbro zone and transition zone, transition zone and sheeted dykes, and sheeted dykes and basalts are dark grey, grey and light grey, respectively.

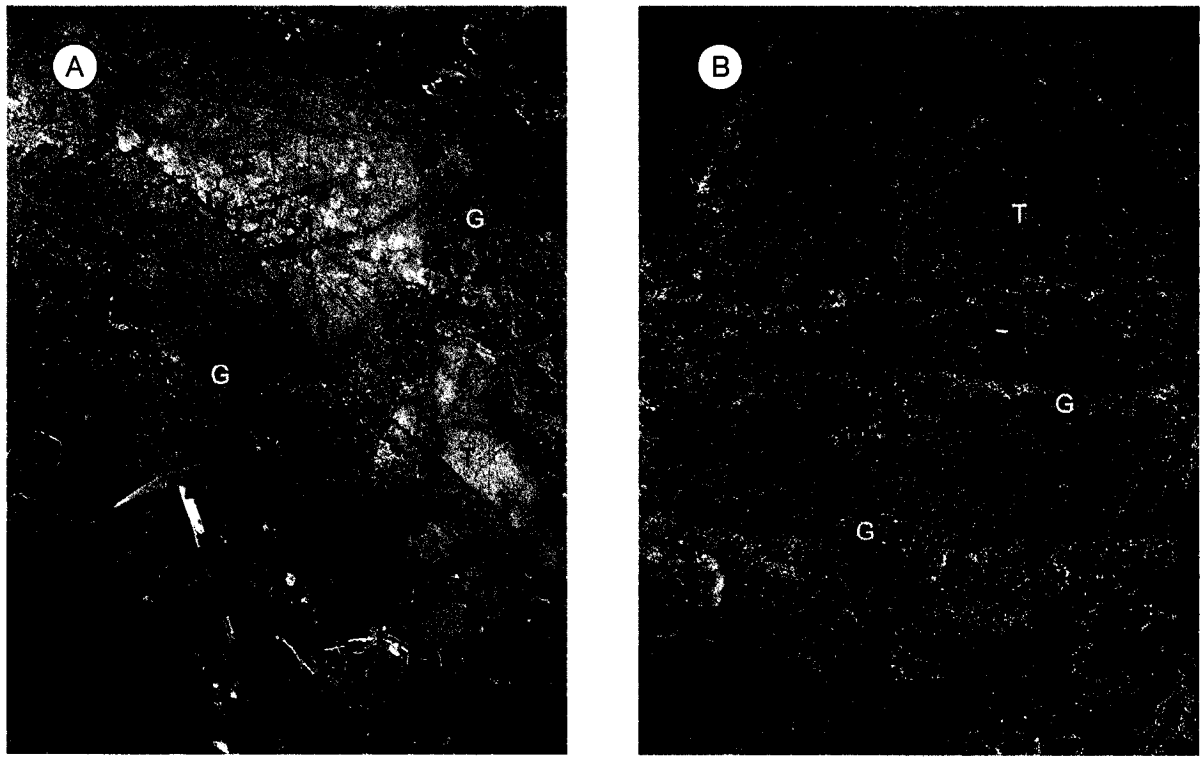

Figure A1.2: Field relationships between troctolites and gabbros in the Annieopsquotch ophiolite. (a) Fine-grained troctolite (T) forms decameter-sized enclaves within invading medium-grained gabbro (G). Hammer for scale is 30 cm long. (b) Medium-grained, layered troctolite enclave (T) is cut by numerous medium- to coarse-grained olivine gabbro and gabbro veins (G; vertical and horizontal in photo). Pen for scale (15 cm long) is parallel to layering in troctolite.

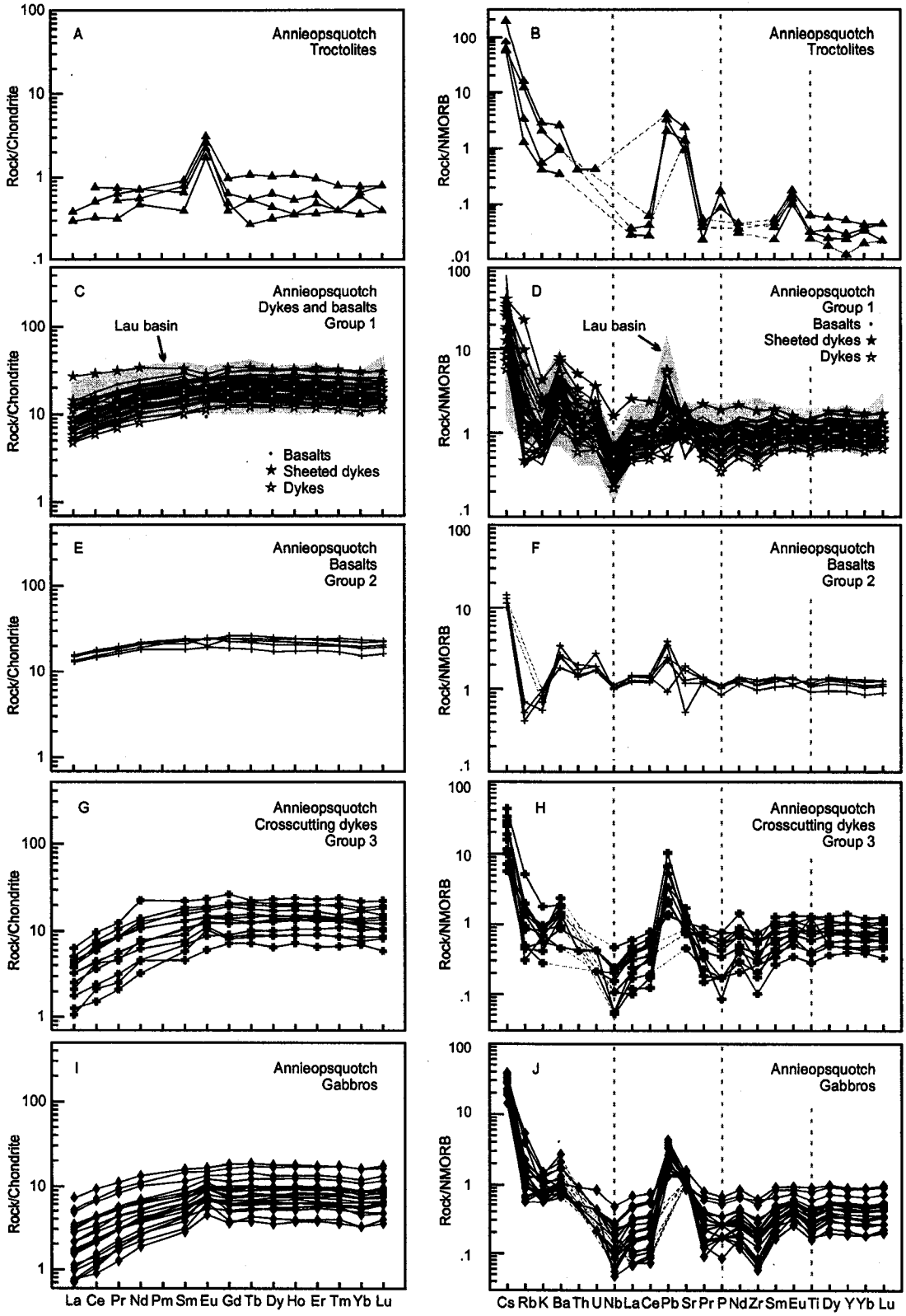

Figure A1.3: Whole rock geochemical data of the Annieopsquotch ophiolite. (a-b) troctolites; (c-d) sheeted dykes and basalts (Group 1); (e-f) basalts (Group 2); (g-h) Crosscutting dykes (Group 3); (i-j) gabbros. Note the very depleted nature of the troctolites, and relative depletion in Nb, Ti and Zr of sheeted dykes and basalts. Grey fields outline the composition of basalts from the Lau basin (Hergt et al., 1994 a, b). Normalizing values from Sun and McDonough (1989).

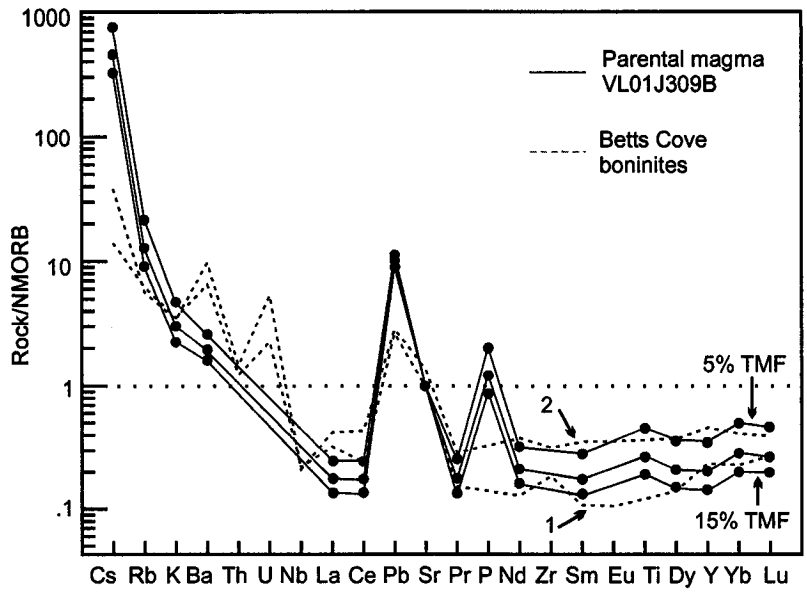

Figure A1.4: Modeled composition of the parental magma of troctolite VL01J309B for different assumed trapped melt fractions (5, 10 and 15%). Dashed lines are average compositions of low-Ti (1) and intermediate-Ti (2) boninites from the Betts Cove ophiolite (Bédard et al., 2000b). Note the similarity between the model composition and the boninites. Normalizing values from Sun and McDonough (1989).

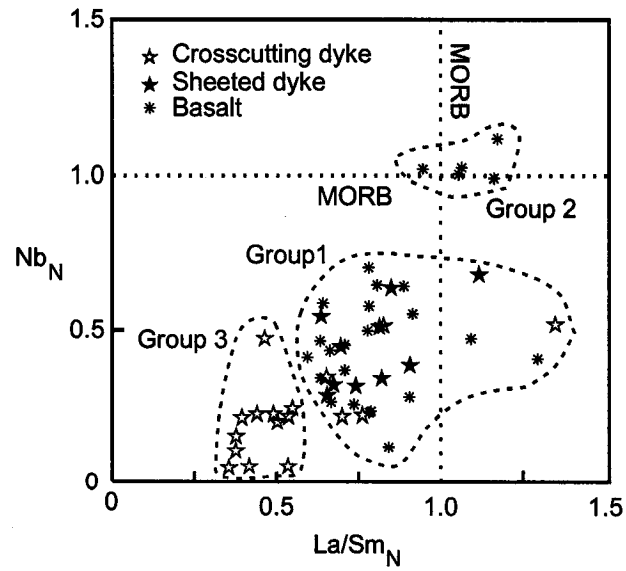

Figure A1.5: La/Sm_N vs. Nb_N of Annieopsquotch sheeted dykes, basalts and dykes crosscutting the ophiolite pseudostratigraphy. Annieopsquotch rocks can be subdivided into 3 chemically distinct groups based on the degree of LREE- and Nb depletion.

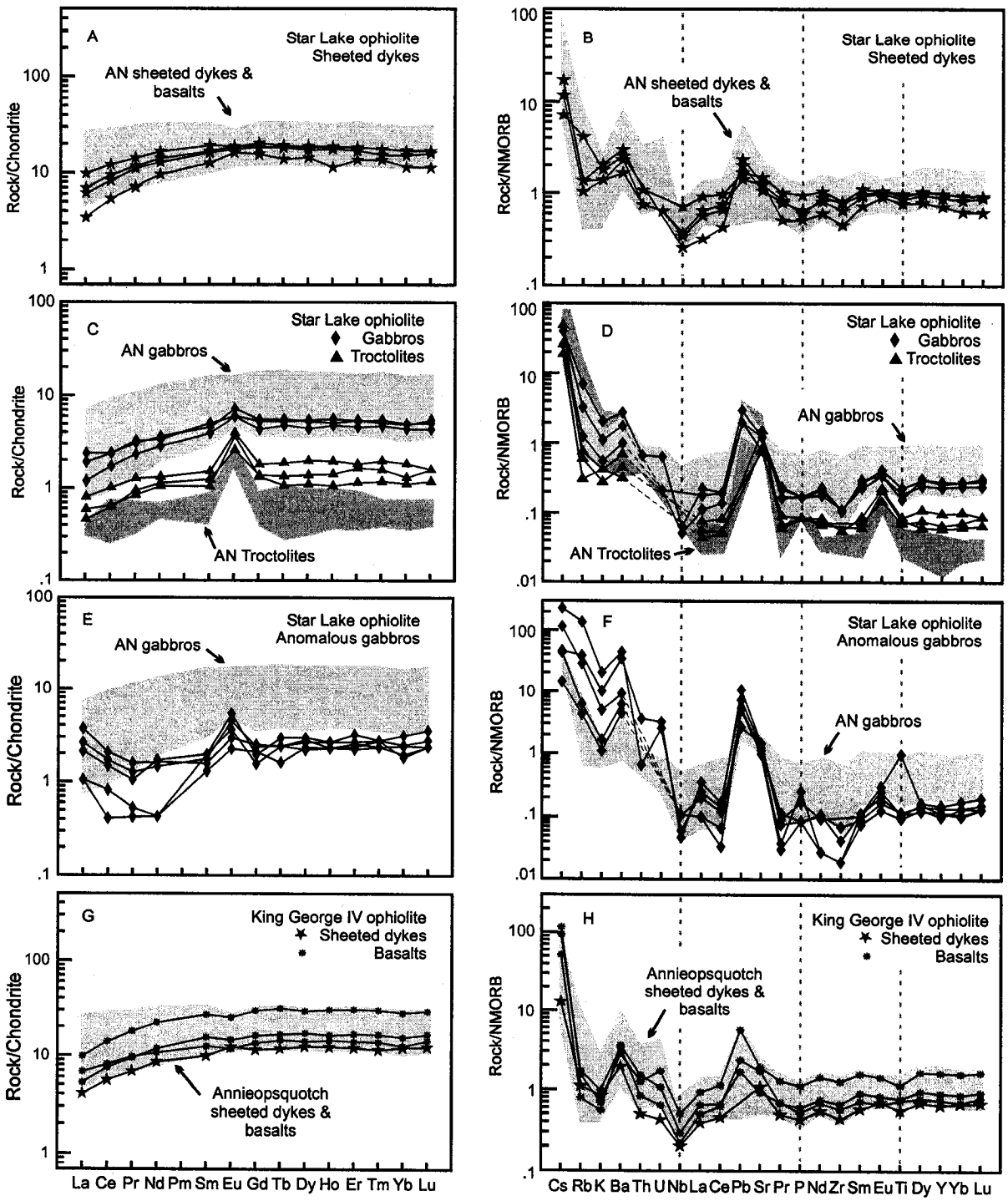

Figure A1.6: Comparison between trace element patterns of the Annnieopsquotch, Star Lake and King George IV ophiolites. (a-b) Sheeted dykes from the Star Lake ophiolite; (c-d) Gabbros and troctolites from the Star Lake ophiolite; (e-f) Anomalous gabbros from from the Star Lake ophiolite; (g-h) Sheeted dykes and basalts from the King George IV ophiolite. Normalizing values from Sun and McDonough (1989).

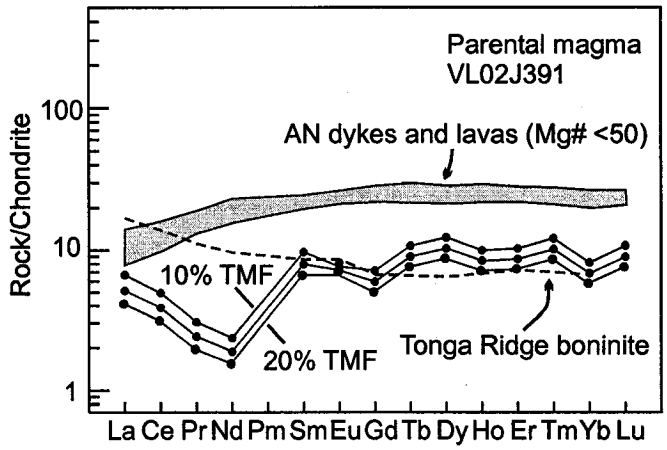

Figure A1.7: Modeled parental magmas of anomalous olivine gabbro VL02J391 from the Star Lake ophiolite for 10%, 15% and 20% trapped melt (see text for details), compared with evolved boninitic rocks from the Tonga Ridge (Mg# 47; Falloon and Crawford, 1991). Note the similarity in degree of depletion (i.e. HREE contents) between the SL parental magmas and the evolved boninites. Normalizing values from Sun and McDonough (1989).

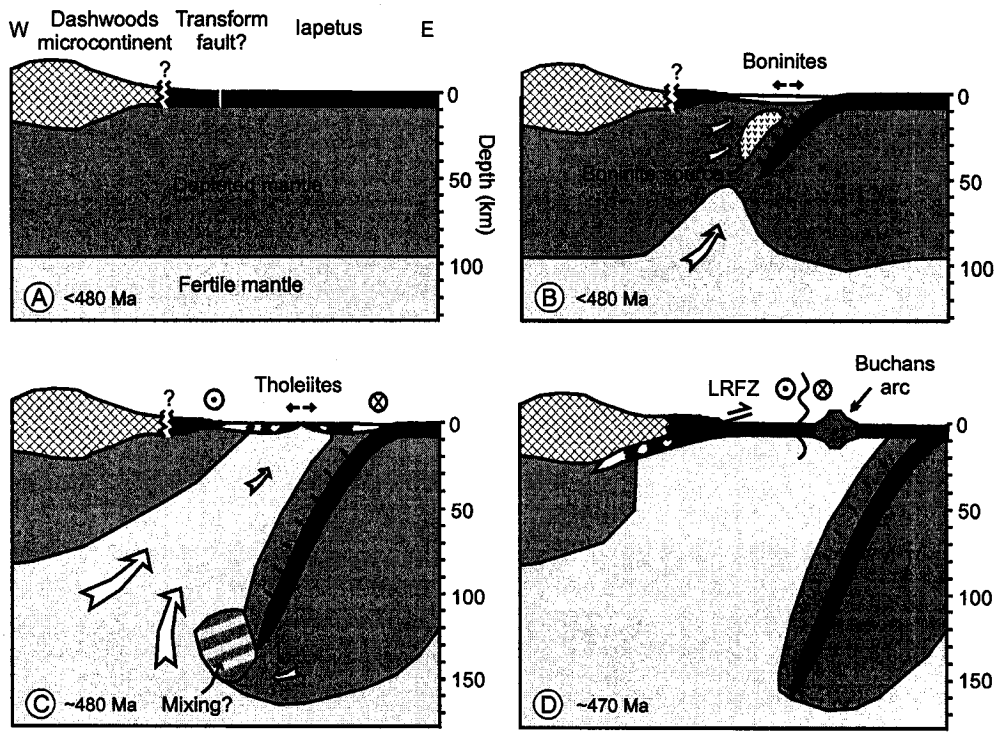

Figure A1.8: Model for generation of the Annieopsquotch ophiolite belt. Initiation of west-dipping subduction outboard of the Dashwoods microcontinent leads to extension in the upper plate, and upwelling of mantle already depleted by the generation of oceanic crust. Aided by fluids expelled from the downgoing plate, the depleted mantle melts at shallow levels yielding boninites. Continuing rollback causes upwelling of a fertile mantle diapir, which, in the presence of slab-derived fluids, melts to yield SSZ tholeiites. These form the gabbro-sheeted dyke-basalt sequence as a spreading center rifts the boninitic substrate. Finally, the Annieopsquotch ophiolite belt is thrust beneath the Dashwoods microcontinent. LRFZ=Lloyds River Fault Zone.

Table A1.1: Whole-rock geochemical data of the Annieopsquotch ophiolite belt

sample[1]	1J035b	1J35c	2J309b	2J310a	1J177b	1J181a	1J188	1J189	1J190	1J191	1J192	1J193
Ophiolite	AN	AN	AN	AN	AN	AN	AN	AN	AN	AN	AN	AN
Lithology	Troctolite	Troctolite	Troctolite	Troctolite	Sheeted dyke	Sheeted dyke	Sheeted dyke	Sheeted dyke	Sheeted dyke	Sheeted dyke	Sheeted dyke	Sheeted dyke
UTM x[2]	447956	447956	447871	447899	464470	459907	456008	456411	456345	456158	456034	455871
UTM y	5348318	5348318	5348194	5348092	5359115	5358064	5349897	5349630	5349588	5349364	5349225	5349006
SiO_2	43.01	41.28	40.63	45.19	50.10	48.51	49.06	48.43	51.82	53.29	49.13	48.04
TiO_2	0.03	0.04	0.04	0.08	1.65	1.20	1.01	0.90	1.12	1.81	1.46	1.14
Al_2O_3	28.32	19.58	15.99	25.64	14.95	16.73	15.99	17.05	15.52	15.17	15.43	15.90
Fe_2O_3*	2.44	5.30	8.53	3.96	14.11	10.40	10.90	10.33	11.34	13.13	13.03	11.06
MnO	0.04	0.09	0.12	0.06	0.19	0.19	0.19	0.17	0.18	0.15	0.22	0.19
MgO	5.39	16.01	21.60	7.70	5.61	8.12	8.08	7.66	6.06	4.45	7.10	7.34
CaO	16.17	11.36	8.36	13.94	9.73	11.42	11.89	13.02	9.98	8.39	11.36	11.52
Na_2O	1.41	0.91	0.66	1.65	3.36	2.54	2.13	1.79	3.67	3.28	2.29	2.39
K_2O	0.21	0.04	0.03	0.15	0.09	0.19	0.07	0.04	0.09	0.31	0.07	0.08
P_2O_5	b.d.	b.d.	0.02	0.01	0.12	0.09	0.07	0.05	0.11	0.22	0.09	0.08
LOI	2.66	3.94	4.39	1.62	0.56	0.74	0.94	0.78	0.96	0.39	0.77	1.25
Total	99.68	98.55	100.48	100.06	100.48	100.14	100.34	100.22	100.85	100.58	100.96	98.99
Trace elements (ppm)												
Ba	16.5	5.9	2.2	6.6	25.8	23.2	14.9	6.7	45.2	50.3	14.9	19.5
Cr	56	268	310	220	69	401	329	330	>500	41	190	306
Cs	1.32	0.56	0.39	0.41	0.06	0.25	0.09	0.07	0.23	0.29	0.12	0.13
Hf	b.d.	b.d.	b.d.	b.d.	2.44	2.01	1.49	1.30	2.32	3.81	2.17	1.95
Nb	b.d.	b.d.	b.d.	b.d.	1.49	1.19	0.90	0.75	1.59	3.74	1.27	0.67
Ni	158	516	665	244	41	158	120	100	35	32	77	105
Pb	1.23	0.62	1.00	b.d.	0.24	0.68	0.24	0.29	0.64	0.68	0.75	0.27
Rb	8.84	1.9	0.73	6.78	0.47	5.54	0.99	0.47	1.24	12.86	0.63	1.51
Sc	2.2	7.7	4.6	5.6	41.4	34.9	39.0	40.1	41.5	35.1	42.1	39.8
Sr	218	127	84	125	109	97	101	73	164	146	94	100
Th	0.05	b.d.	b.d.	b.d.	0.26	0.16	0.20	0.09	0.40	0.61	0.10	0.11
U	0.02	b.d.	b.d.	b.d.	0.08	0.07	0.05	0.03	0.11	0.17	0.04	0.03
V	9	22	20	35	530	261	286	261	335	322	394	306
Y	0.34	0.8	0.65	1.42	39.98	30.00	25.09	22.27	30.50	51.52	34.34	27.96
Zr	b.d.	b.d.	b.d.	b.d.	83.10	65.87	51.24	36.75	73.60	135.95	69.02	59.02
La	b.d.	b.d.	0.07	0.09	2.94	2.16	1.88	1.23	3.42	6.38	1.85	1.61
Ce	b.d.	0.46	0.20	0.31	9.01	6.80	5.84	4.12	9.42	17.75	6.48	5.52
Pr	0.05	0.07	0.03	0.06	1.67	1.25	1.04	0.78	1.57	2.94	1.31	1.10
Nd	0.26	0.33	0.22	0.33	9.52	7.52	6.08	4.72	8.67	15.74	8.00	6.59
Sm	0.12	0.1	0.06	0.14	3.64	2.79	2.18	1.92	3.22	5.05	3.06	2.59
Eu	0.15	0.13	0.10	0.18	1.45	1.12	0.94	0.83	1.17	1.65	1.22	1.10
Gd	0.10	0.13	0.08	0.20	5.15	4.16	3.55	2.98	4.31	6.90	4.63	3.84
Tb	0.01	0.02	0.02	0.04	0.95	0.71	0.62	0.54	0.77	1.27	0.86	0.73
Dy	0.08	0.16	0.11	0.26	6.39	4.91	4.07	3.63	4.99	8.20	5.75	4.84
Ho	0.02	0.03	0.02	0.06	1.46	1.08	0.92	0.83	1.12	1.83	1.32	1.07
Er	0.06	0.1	0.08	0.16	4.35	3.18	2.72	2.47	3.37	5.54	3.91	3.27
Tm	0.01	0.01	0.01	0.02	0.66	0.46	0.38	0.37	0.50	0.82	0.58	0.50
Yb	0.06	0.11	0.10	0.13	4.06	2.94	2.48	2.41	3.33	5.16	3.68	3.22
Lu	0.01	0.02	0.01	0.02	0.61	0.46	0.39	0.35	0.50	0.77	0.57	0.50
Mg#[3]	0.83	0.84	0.85	0.81	0.46	0.63	0.62	0.62	0.54	0.42	0.54	0.59

[1]Prefix VL0 has been omitted from all samples; [2]UTM in NAD83, zone 21; [3]Mg# = $Mg/(Mg+Fe^{2+})$ assuming $Fe^{3+}/Fe^{2+}=0.1$;
b.d. = below detection limit

Table A1.1 (continued)

sample	1J194	1J196b	1J177a	2A228b	1J195	1J196a	1J199a	1J205a	1A167b	*1A260*	1A105b	*1A048*	1A211
Ophiolite	AN	AN	AN	AN	AN	AN	AN	AN	AN	AN	AN	AN	AN
Lithology	Sheeted dyke	Sheeted dyke	Sheeted dyke	SSZ Basalt	SSZ Basalt	SSZ Basalt	SSZ Basalt	SSZ Basalt	SSZ Basalt	SSZ Basalt	SSZ Basalt	SSZ Basalt	SSZ Basalt
UTM x	455599	455619	464470	463483	455720	455619	454388	455164	450771	458836	455174	462974	453255
UTM y	5348700	5348407	5359115	5359321	5348477	5348407	5347672	5347338	5344879	5348483	5347352	5352999	5345045
SiO_2	48.38	47.45	49.47	50.52	49.29	49.25	49.60	48.81	49.03	47.59	48.79	48.30	49.52
TiO_2	0.98	1.05	1.44	1.61	0.93	0.73	1.04	1.37	1.70	1.16	1.34	1.27	0.93
Al_2O_3	16.00	15.88	15.26	14.57	17.16	17.14	17.26	14.28	14.66	14.91	13.75	13.64	15.04
Fe_2O_3*	11.04	11.53	12.63	13.43	11.51	10.52	10.85	11.91	14.42	11.19	15.57	13.58	9.44
MnO	0.20	0.21	0.20	0.16	0.18	0.19	0.19	0.21	0.32	0.17	0.28	0.18	0.16
MgO	8.34	8.60	6.85	5.70	5.77	5.98	6.10	6.15	6.44	6.54	6.78	6.91	6.96
CaO	11.53	10.65	10.94	9.95	11.52	12.08	10.53	9.82	7.47	12.55	9.51	11.32	8.68
Na_2O	2.00	2.56	2.72	3.38	3.04	3.06	3.48	4.43	4.46	2.85	3.29	2.42	5.35
K_2O	0.07	0.04	0.16	0.13	0.08	0.07	0.05	0.04	0.04	0.04	0.05	0.10	0.07
P_2O_5	0.06	0.07	0.07	0.14	0.06	0.05	0.07	0.09	0.11	0.08	0.09	0.08	0.08
LOI	2.06	2.64	1.03	0.72	1.19	1.37	1.47	3.56	2.45	2.70	2.02	2.00	4.40
Total	100.66	100.68	100.77	100.37	100.73	100.44	100.62	100.66	101.09	99.84	101.47	99.84	100.63
Trace elements (ppm)													
Ba	20.6	20.3	26.1	30.4	25.1	26.3	15.4	16.4	11.0	23.0	22.7	35.0	25.4
Cr	311	259	206	99	188	209	201	257	19	260	200	171	357
Cs	0.18	0.07	0.20	0.14	0.14	0.05	0.06	0.09	0.08	0.05	0.14	0.40	0.19
Hf	1.46	1.56	2.18	2.50	1.50	1.14	1.64	2.20	2.71	2.20	1.99	1.10	1.41
Nb	0.74	0.80	1.04	1.50	0.62	0.54	1.16	1.08	1.51	1.10	1.01	0.60	0.95
Ni	125	113	66	45	64	79	65	95	30	42	83	22	142
Pb	0.34	0.73	0.61	0.40	0.24	0.28	0.38	0.28	0.88	0.50	0.73	0.20	0.49
Rb	1.36	0.26	3.50	1.16	1.48	1.10	0.68	0.24	b.d.	0.25	b.d.	2.30	0.65
Sc	40.1	45.2	42.2	42.2	37.7	34.4	37.9	40.8	44.3	36.0	37.0	37.0	35.4
Sr	102	153	98	108	210	178	170	122	130	184	140	85	94
Th	0.13	0.16	0.15	0.27	0.09	0.09	0.12	0.12	0.20	0.20	0.10	0.10	0.28
U	0.04	0.05	0.05	0.07	0.19	0.06	0.04	0.05	0.08	0.05	0.05	0.05	0.07
V	290	295	474	358	283	243	268	320	441	282	286	342	244
Y	21.68	25.08	34.92	39.72	26.08	19.85	25.48	33.75	40.54	27.10	33.20	30.30	20.67
Zr	44.43	51.17	65.72	79.60	46.34	37.47	53.54	68.71	88.19	47.80	63.23	49.40	49.21
La	1.53	1.81	2.13	3.08	1.52	1.19	1.76	1.86	2.86	2.70	1.84	1.40	2.67
Ce	4.88	5.77	7.02	9.50	5.02	3.98	5.64	6.47	9.27	8.70	6.05	4.00	7.21
Pr	0.94	1.07	1.36	1.76	0.94	0.74	1.04	1.31	1.74	1.26	1.23	0.86	1.22
Nd	5.53	6.01	7.99	10.24	5.52	4.32	5.90	7.96	9.91	7.90	7.25	5.80	6.28
Sm	2.17	2.32	3.22	3.65	2.40	1.60	2.38	3.09	3.73	2.60	2.92	2.00	2.17
Eu	0.88	0.81	1.17	1.47	1.10	0.70	1.01	1.24	1.50	1.00	1.25	0.82	0.91
Gd	3.09	3.45	4.57	5.61	3.29	2.63	3.41	4.86	5.52	3.87	4.48	3.50	2.94
Tb	0.57	0.62	0.87	1.03	0.62	0.48	0.65	0.87	1.05	0.71	0.81	0.68	0.55
Dy	3.76	4.08	5.75	6.86	4.11	3.20	4.21	5.48	7.00	4.29	5.46	4.69	3.46
Ho	0.84	0.90	1.29	1.48	0.97	0.73	0.93	1.25	1.60	0.93	1.22	1.05	0.81
Er	2.41	2.67	3.72	4.54	2.82	2.10	2.75	3.78	4.44	2.74	3.60	3.02	2.18
Tm	0.37	0.41	0.58	0.67	0.43	0.32	0.41	0.55	0.68	0.42	0.53	0.53	0.34
Yb	2.29	2.53	3.60	4.37	2.68	2.01	2.53	3.66	4.17	2.97	3.31	3.30	2.08
Lu	0.38	0.39	0.57	0.66	0.42	0.31	0.38	0.56	0.67	0.43	0.53	0.60	0.34
Mg#	0.62	0.62	0.54	0.48	0.52	0.55	0.55	0.53	0.49	0.56	0.49	0.53	0.62

Table A1.1 (continued)

sample	1A164b	1A100	1J203	1A238	1A197	1A266	1J198	2A031b	1J200a	1A103	1A104	1J201
Ophiolite	AN	AN	AN	AN	AN	AN	AN	AN	AN	AN	AN	AN
Lithology	SSZ Basalt	SSZ Basalt	SSZ Basalt	SSZ Basalt	SSZ Basalt	SSZ Basalt	SSZ Basalt	SSZ Basalt	SSZ Basalt	SSZ Basalt	MORB-like Basalt	MORB-like Basalt
UTM x	451523	455767	454757	456264	453750	459545	454822	464245	454456	455496	455211	454583
UTM y	5345001	5347572	5347733	5346557	5345885	5349781	5347768	5354895	5347738	5347546	5347393	5347865
SiO_2	50.98	50.07	48.19	48.42	50.49	48.70	47.75	48.28	47.46	48.90	48.68	49.94
TiO_2	1.95	1.92	1.61	1.31	1.29	1.43	1.29	0.97	0.80	1.34	1.68	1.50
Al_2O_3	13.60	14.11	14.50	15.22	13.98	15.05	16.08	15.45	18.49	14.77	13.69	14.51
$Fe_2O_3^*$	13.72	15.33	13.03	12.14	13.33	13.17	12.34	10.64	10.25	13.99	15.25	13.46
MnO	0.24	0.32	0.19	0.20	0.26	0.22	0.23	0.19	0.20	0.27	0.22	0.20
MgO	7.05	7.13	7.21	7.26	7.32	7.37	7.47	7.49	7.90	8.02	6.64	6.31
CaO	5.97	7.11	10.58	11.17	5.65	11.67	11.18	11.33	10.88	6.64	6.64	8.90
Na_2O	5.22	4.18	3.25	2.43	4.82	2.24	2.20	3.60	2.42	4.13	4.55	4.05
K_2O	0.04	0.05	0.07	0.13	0.05	0.06	0.03	0.05	0.04	0.04	0.07	0.07
P_2O_5	0.13	0.13	0.09	0.08	0.09	0.09	0.09	0.08	0.05	0.09	0.13	0.13
LOI	2.34	0.98	2.08	2.55	3.68	0.85	1.58	2.36	2.18	2.95	2.26	1.26
Total	101.23	101.36	100.80	100.91	100.95	100.84	100.26	100.52	100.69	101.14	99.81	100.31
Trace elements (ppm)												
Ba	6.8	16.1	12.4	41.0	14.0	14.6	8.7	27.9	8.1	16.2	11.5	16.7
Cr	144	32	142	211	23	181	207	207	269	247	180	162
Cs	0.56	0.13	0.13	0.16	0.25	0.10	0.10	0.09	0.09	0.10	0.09	0.10
Hf	3.15	3.30	2.46	1.77	1.91	2.12	2.09	1.40	1.32	2.68	2.72	2.83
Nb	1.37	1.64	0.96	0.80	0.86	1.05	1.35	0.66	0.55	1.29	2.38	2.34
Ni	59	29	74	80	37	76	90	105	94	116	72	55
Pb	0.91	0.29	0.58	1.14	0.64	0.31	0.22	0.70	0.14	0.65	1.04	1.17
Rb	0.25	0.22	0.30	2.90	0.26	0.84	0.32	0.31	0.37	0.34	b.d.	0.29
Sc	48.8	42.8	42.8	43.0	39.2	42.6	42.3	39.0	38.9	40.9	40.3	38.8
Sr	45	107	109	96	47	87	89	160	159	131	47	117
Th	0.21	0.26	0.12	0.09	0.16	0.13	0.14	0.14	0.10	0.17	0.18	0.24
U	0.09	0.08	0.04	0.03	0.10	0.04	0.04	0.07	0.09	0.06	0.08	0.09
V	430	475	416	323	308	339	322	281	238	280	298	311
Y	44.51	45.92	36.88	30.54	30.42	33.18	33.10	24.89	20.91	36.88	35.85	37.01
Zr	99.73	103.65	74.04	55.93	60.02	66.64	68.59	50.10	39.80	86.63	91.02	95.37
La	2.51	3.31	1.93	1.61	1.85	1.98	2.20	1.84	1.37	3.01	3.20	3.71
Ce	8.87	10.91	6.76	5.71	6.17	6.78	7.19	5.54	4.40	8.02	9.41	10.96
Pr	1.73	2.08	1.34	1.14	1.19	1.30	1.35	0.95	0.82	1.63	1.65	1.87
Nd	10.01	11.40	8.47	6.62	6.90	7.57	8.08	5.70	4.86	8.87	9.01	10.29
Sm	4.11	4.46	3.42	2.67	2.75	2.94	2.96	2.14	1.83	3.46	3.56	3.70
Eu	0.92	1.44	1.39	1.10	1.07	1.25	1.15	0.92	0.82	1.01	1.17	1.36
Gd	6.09	6.23	5.30	4.08	4.05	4.48	4.44	3.28	2.81	5.04	5.02	5.41
Tb	1.18	1.20	0.97	0.78	0.78	0.86	0.82	0.61	0.53	0.91	0.91	0.98
Dy	7.97	7.87	6.30	5.07	5.21	5.63	5.41	4.07	3.44	6.02	6.04	6.36
Ho	1.82	1.81	1.44	1.19	1.19	1.30	1.21	0.90	0.76	1.32	1.36	1.37
Er	5.20	4.97	4.30	3.28	3.29	3.64	3.55	2.76	2.26	3.84	3.87	3.98
Tm	0.80	0.80	0.64	0.50	0.51	0.56	0.52	0.36	0.36	0.58	0.58	0.62
Yb	4.97	4.95	4.24	3.13	3.24	3.55	3.33	2.72	2.17	3.70	3.73	3.98
Lu	0.81	0.80	0.66	0.50	0.53	0.56	0.50	0.38	0.34	0.59	0.57	0.58
Mg#	0.53	0.50	0.55	0.57	0.54	0.55	0.57	0.61	0.63	0.56	0.49	0.51

Table A1.1 (continued)

sample	1J204a	1J204b	1J205b	1J054b	1J056d	1J063a	1J065c	1J199b	1J200b	1J202	*2J308*	2J315c
Ophiolite	AN	AN	AN	AN	AN	AN	AN	AN	AN	AN	AN	AN
Lithology	MORB-like Basalt	MORB-like Basalt	MORB-like Basalt	Cross-cutting dyke	Cross-cutting dyke	Cross-cutting dyke	Cross-cutting dyke	Cross-cutting dyke	Cross-cutting dyke	Cross-cutting dyke	Cross-cutting dyke	Cross-cutting dyke
UTM x	454951	454951	455164	456398	456621	448841	448583	454388	454456	454692	447970	447440
UTM y	5347446	5347446	5347338	5354259	5357789	5344158	5345186	5347672	5347738	5347724	5348189	5345777
SiO_2	51.02	52.09	50.89	45.28	48.88	47.45	47.41	47.71	48.12	51.89	48.08	47.68
TiO_2	1.18	1.42	1.36	1.62	0.91	0.75	0.76	1.20	0.52	0.48	0.36	1.59
Al_2O_3	13.25	13.51	14.15	14.56	15.86	16.83	16.61	15.63	15.77	14.64	16.71	13.73
Fe_2O_3*	12.85	12.39	12.03	14.46	10.48	9.80	9.80	11.67	9.70	9.38	7.92	14.84
MnO	0.19	0.16	0.20	0.19	0.18	0.16	0.16	0.19	0.17	0.16	0.14	0.22
MgO	6.71	6.33	5.94	8.57	9.05	8.99	8.90	8.30	9.55	7.35	9.25	7.81
CaO	9.18	9.04	9.79	13.84	12.40	12.90	12.89	11.80	12.98	11.86	14.94	11.57
Na_2O	4.09	4.52	4.36	1.65	2.12	1.80	1.82	1.97	1.49	3.66	1.28	2.59
K_2O	0.05	0.06	0.04	0.05	0.07	0.02	0.04	0.04	0.05	0.05	0.13	0.06
P_2O_5	0.10	0.12	0.12	b.d.	0.05	0.04	0.04	0.07	0.02	0.02	0.02	0.09
LOI	1.45	1.12	2.08	0.79	0.82	1.42	1.42	1.90	1.81	1.74	1.10	0.70
Total	100.07	100.76	100.96	101.01	100.81	100.16	99.84	100.49	100.18	101.22	99.99	100.92
Trace elements (ppm)												
Ba	15.8	16.3	21.7	8.6	9.2	b.d.	5.5	b.d.	b.d.	14.9	12.0	11.1
Cr	248	225	239	104	279	434	439	248	429	341	322	93
Cs	0.07	0.08	0.10	0.19	0.04	0.23	0.20	0.07	0.17	0.08	0.30	0.11
Hf	2.00	2.40	2.32	0.26	1.37	0.99	0.98	1.91	0.60	0.71	0.25	0.90
Nb	2.31	2.39	2.60	0.12	0.51	0.47	0.53	0.53	0.13	0.13	0.25	0.36
Nl	76	86	86	79	116	157	151	148	153	124	18	55
Pb	0.68	0.28	0.74	1.02	0.42	b.d.	b.d.	0.66	b.d.	1.02	1.60	3.10
Rb	b.d.	0.23	0.39	1.12	0.87	0.28	0.78	0.26	1.10	0.53	2.90	0.47
Sc	37.2	37.4	37.2	55.8	42.1	37.1	36.2	39.4	38.7	31.1	39.0	>50
Sr	106	175	153	88	90	68	66	69	41	156	113	119
Th	0.18	0.17	0.21	b.d.	0.05	b.d.	b.d.	0.05	b.d.	b.d.	b.d.	b.d.
U	0.13	0.08	0.09	b.d.	0.02	0.01	0.02	0.02	0.01	0.02	b.d.	0.01
V	274	319	319	734	241	219	225	291	233	190	177	396
Y	26.38	33.49	31.20	13.08	22.85	20.23	20.22	29.34	16.25	13.08	11.10	28.88
Zr	71.72	82.95	81.96	b.d.	45.14	28.89	29.31	56.02	15.16	21.85	7.60	21.20
La	3.07	3.55	3.60	0.30	1.02	0.77	0.77	1.20	0.42	0.60	0.25	0.94
Ce	9.00	10.56	10.38	0.93	3.99	2.63	2.71	4.73	1.46	2.21	1.30	3.63
Pr	1.54	1.81	1.76	0.20	0.82	0.54	0.53	1.01	0.30	0.46	0.24	0.81
Nd	8.43	10.22	9.77	1.51	5.04	3.40	3.46	6.52	2.14	2.91	2.10	5.53
Sm	2.78	3.51	3.23	0.89	2.00	1.61	1.65	2.86	1.06	1.18	0.70	2.62
Eu	1.12	1.43	1.44	0.60	0.85	0.72	0.74	1.12	0.51	0.65	0.35	1.07
Gd	3.85	4.98	4.62	1.67	2.90	2.53	2.52	4.20	1.86	1.76	1.48	4.29
Tb	0.68	0.86	0.82	0.32	0.55	0.47	0.48	0.75	0.38	0.34	0.27	0.81
Dy	4.34	5.76	5.23	2.27	3.83	3.28	3.36	4.97	2.56	2.24	1.65	5.27
Ho	0.98	1.24	1.17	0.51	0.84	0.76	0.77	1.10	0.60	0.51	0.41	1.17
Er	2.91	3.55	3.34	1.49	2.34	2.17	2.23	3.34	1.75	1.52	1.09	3.35
Tm	0.43	0.52	0.51	0.22	0.36	0.33	0.34	0.52	0.28	0.22	0.17	0.49
Yb	2.59	3.34	3.16	1.30	2.22	2.12	2.10	3.16	1.75	1.46	1.18	2.89
Lu	0.41	0.52	0.49	0.21	0.35	0.31	0.31	0.50	0.27	0.22	0.15	0.47
Mg#	0.53	0.53	0.52	0.56	0.65	0.67	0.66	0.61	0.68	0.63	0.72	0.53

Table A1.1 (continued)

sample	*2J318*	*2J319*	*2J326c*	2J341c	2J335a	2J375a	2J375b	2J370b	2J335d	2J373	2J334c
Ophiolite	AN	AN	AN	AN	SL	SL	SL	SL	SL	SL	SL
Lithology	Cross-cutting dyke	Cross-cutting dyke	Cross-cutting dyke	Cross-cutting dyke	Troctolite	Troctolite	Troctolite	Gabbro	Gabbro	Gabbro	Gabbro
UTM x	447510	447239	448207	447964	483907	484014	484014	485169	485742	483907	459859
UTM y	5346085	5345849	5346760	5345489	5383239	5384685	5384685	5385153	5384684	5383239	5376247
SiO_2	48.37	48.50	48.46	48.61	44.90	43.35	46.18	47.08	47.33	47.97	48.51
TiO_2	0.97	1.05	1.65	0.90	0.11	0.09	0.10	0.24	0.20	0.29	0.15
Al_2O_3	15.65	15.00	14.12	16.18	19.40	17.63	28.84	19.22	16.97	17.22	16.17
Fe_2O_3*	10.78	11.34	13.74	9.97	6.65	7.44	2.12	5.7	6.07	7.55	6.79
MnO	0.16	0.18	0.21	0.16	0.10	0.11	0.04	0.11	0.11	0.13	0.14
MgO	8.66	8.41	7.01	8.66	15.50	17.06	3.52	9.32	10.99	9.58	11.03
CaO	12.48	12.76	11.41	13.13	11.51	11.31	16.25	15.05	15.34	13.71	13.66
Na_2O	1.86	1.89	2.28	1.72	1.30	1.07	1.72	1.47	1.1	1.77	1.16
K_2O	0.06	0.06	0.03	0.05	0.02	0.03	0.03	0.08	0.04	0.15	0.73
P_2O_5	0.06	0.01	0.09	0.06	0.01	0.01	0.01	0.02	0.02	0.02	0.01
LOI	0.70	0.70	0.80	0.70	0.83	2.38	1.16	1.75	1.66	1.71	1.77
Total	99.82	99.95	99.84	100.22	100.44	100.65	100.06	100.11	99.9	100.19	100.17
Trace elements (ppm)											
Ba	9.0	6.0	8.0	2.9	2.8	2.0	4.4	11.2	6.3	17.5	213.4
Cr	328	226	123	382	312	680	489	310	279	465	227
Cs	0.05	0.05	0.05	0.13	0.34	0.13	0.18	0.28	0.18	0.28	0.32
Hf	1.00	0.80	1.70	1.20	0.10	0.10	b.d.	0.30	0.30	0.30	0.20
Nb	0.50	0.25	1.10	0.57	b.d.	b.d.	b.d.	0.12	b.d.	0.15	0.11
Ni	59	45	30	124	538	598	122	133	137	143	89
Pb	0.60	2.00	0.40	b.d.	b.d.	b.d.	b.d.	0.60	0.60	0.90	2.20
Rb	0.80	1.10	0.25	0.17	0.33	0.17	0.42	1.84	0.70	3.93	21.54
Sc	35.0	41.0	40.0	31.6	12.6	15.0	9.2	32.2	39.5	33.7	48.5
Sr	73	92	96	78	68	75	137	110	71	111	114
Th	b.d.	b.d.	b.d.	b.d.	b.d.	b.d.	b.d.	b.d.	b.d.	0.08	0.43
U	b.d.	b.d.	b.d.	0.02	b.d.	b.d.	b.d.	0.01	0.01	0.03	0.15
V	297	347	392	246	57	56	37	122	124	138	151
Y	28.80	21.00	39.20	22.09	2.75	1.85	1.66	6.51	7.38	7.77	3.83
Zr	39.40	13.00	41.10	39.90	4.10	b.d.	b.d.	8.30	7.90	8.00	5.20
La	0.90	0.50	1.50	1.06	0.19	0.11	0.14	0.28	0.45	0.56	0.88
Ce	4.30	2.60	5.90	3.80	0.62	0.38	0.40	1.05	1.45	1.46	1.26
Pr	0.83	0.43	1.18	0.80	0.12	0.09	0.08	0.22	0.31	0.29	0.15
Nd	6.10	3.70	10.60	4.97	0.61	0.53	0.49	1.32	1.56	1.69	0.76
Sm	2.40	1.40	3.40	2.03	0.23	0.19	0.16	0.60	0.78	0.70	0.24
Eu	1.00	0.83	1.37	0.86	0.23	0.15	0.21	0.35	0.35	0.42	0.17
Gd	3.98	2.82	5.49	3.13	0.37	0.28	0.27	0.89	1.10	1.14	0.51
Tb	0.67	0.47	0.84	0.59	0.07	0.05	0.04	0.18	0.20	0.21	0.09
Dy	4.34	3.51	5.92	3.79	0.50	0.35	0.28	1.12	1.40	1.35	0.67
Ho	0.99	0.81	1.36	0.85	0.11	0.08	0.06	0.27	0.32	0.29	0.15
Er	2.77	2.42	3.84	2.50	0.30	0.27	0.19	0.76	0.89	0.91	0.44
Tm	0.39	0.34	0.61	0.36	0.05	0.04	0.03	0.12	0.14	0.13	0.07
Yb	2.90	1.95	3.75	2.38	0.31	0.22	0.19	0.74	0.85	0.83	0.42
Lu	0.39	0.26	0.57	0.37	0.04	0.04	0.03	0.11	0.13	0.14	0.07
Mg#	0.64	0.62	0.53	0.65	0.84	0.83	0.78	0.78	0.80	0.73	0.78

Table A1.1 (continued)

sample	*2J380a*	2J387	*2J391*	*2J392*	1J209a	*2J393*	2J411a	2J411b	1A112b	2A010b	2A019	10081
Ophiolite	SL	SL	SL	SL	SL	SL	SL	SL	KGIV	KGIV	KGIV	KGIV
Lithology	Gabbro	Gabbro	Gabbro	Gabbro	Sheeted dyke	Sheeted dyke	Sheeted dyke	Sheeted dyke	Basalt	Basalt	Basalt	Sheeted dyke
UTM x	488056	487361	489099	489240	492722	489991	492426	492426	437696	439662	437979	440800
UTM y	5390420	5386304	5389582	5389567	5394620	5389428	5394801	5394801	5334147	5336422	5333899	5337911
SiO_2	40.80	44.90	46.68	46.35	48.57	47.25	48.16	47.94	50.30	48.82	49.39	48.08
TiO_2	1.24	0.14	0.14	0.12	1.16	0.97	1.24	1.079	0.93	0.98	1.43	0.70
Al_2O_3	15.35	21.25	15.41	14.29	15.86	16.58	16.24	16.13	14.92	15.64	15.66	19.01
Fe_2O_3*	19.97	5.91	7.67	8.34	11.77	10.38	11.14	10.56	11.63	10.16	11.51	8.63
MnO	0.20	0.10	0.13	0.14	0.20	0.17	0.19	0.177	0.21	0.18	0.16	0.14
MgO	7.20	10.65	11.61	12.46	8.35	9.22	8.37	8.73	8.95	8.63	6.52	7.90
CaO	12.32	11.61	16.15	15.97	11.78	12.14	11.40	11.93	5.67	11.63	8.74	13.28
Na_2O	0.79	1.12	0.54	0.49	2.36	1.89	2.65	2.32	5.19	2.68	3.65	1.82
K_2O	0.36	1.46	0.12	0.08	0.10	0.13	0.15	0.1	0.04	0.07	0.05	0.06
P_2O_5	0.01	0.02	0.03	0.01	0.07	0.06	0.11	0.076	0.06	0.07	0.13	0.05
LOI	1.60	3.07	1.30	1.50	0.76	1.10	1.06	1.2	3.38	1.73	3.20	1.16
Total	99.85	100.31	99.88	99.87	100.97	99.96	100.78	100.33	101.28	100.67	100.52	100.83
Trace elements (ppm)												
Ba	58.0	276.1	39.0	28.0	10.4	16.0	18.9	14.5	22.6	21.2	17.6	12.2
Cr	7	364	547	650	304	294	290	347	369	366	250	308
Cs	0.80	1.61	0.30	0.10	0.12	0.05	0.12	0.082	0.36	0.66	0.82	0.09
Hf	0.25	0.10	0.25	0.25	1.78	1.40	1.80	1.6	1.36	1.50	2.90	1.06
Nb	0.25	0.14	0.25	0.25	0.87	0.60	1.66	0.8	0.68	0.51	1.17	0.47
Ni	0	292	95	163	118	53	133	144	170	143	106	128
Pb	0.80	3.20	1.60	1.50	0.42	0.70	0.50	0.60	0.50	0.70	1.70	n.d.
Rb	15.70	76.28	3.50	2.40	0.76	2.30	0.76	0.58	0.44	0.95	0.84	0.62
Sc	49.0	18.0	45.0	48.0	43.2	35.0	42.7	39.8	40.8	41.7	41.8	32.1
Sr	130	131	102	89	111	116	134	95	83	153	172	98
Th	b.d.	0.08	b.d.	b.d.	0.09	b.d.	0.13	0.09	0.18	0.10	0.15	0.06
U	b.d.	0.12	b.d.	b.d.	0.03	b.d.	b.d.	0.03	0.05	0.03	0.08	0.02
V	893	64	164	147	305	252	315	270	272	282	315	208
Y	4.20	3.26	3.20	2.80	27.40	19.80	27.36	24.64	20.68	25.08	44.94	17.87
Zr	3.10	b.d.	1.40	1.40	58.30	33.40	59.70	47.9	41.98	49.40	93.00	32.30
La	0.50	0.62	0.25	0.25	1.61	0.80	2.28	1.42	1.62	1.24	2.32	0.96
Ce	0.90	1.04	0.50	0.25	5.67	3.20	7.28	4.94	4.95	4.60	8.50	3.39
Pr	0.10	0.12	0.05	0.04	1.09	0.67	1.33	1.03	0.92	0.89	1.69	0.65
Nd	0.80	0.68	0.20	0.20	6.50	4.40	7.62	5.89	4.98	5.48	10.35	3.99
Sm	0.30	0.27	0.30	0.20	2.51	1.90	2.90	2.43	1.90	2.37	4.10	1.51
Eu	0.31	0.26	0.21	0.13	1.08	0.92	1.07	1.01	0.68	0.84	1.45	0.71
Gd	0.40	0.49	0.32	0.43	3.73	3.14	4.08	3.7	2.77	3.31	6.08	2.35
Tb	0.11	0.09	0.09	0.06	0.68	0.51	0.71	0.67	0.54	0.62	1.17	0.44
Dy	0.75	0.56	0.71	0.59	4.73	3.59	4.60	4.31	3.55	4.33	7.43	3.13
Ho	0.15	0.13	0.13	0.13	1.04	0.63	1.02	0.98	0.81	0.92	1.71	0.69
Er	0.53	0.37	0.39	0.42	2.98	2.21	2.99	2.75	2.30	2.76	5.03	1.98
Tm	0.07	0.06	0.07	0.06	0.44	0.34	0.44	0.38	0.35	0.42	0.76	0.29
Yb	0.53	0.33	0.31	0.41	2.80	1.90	2.84	2.53	2.12	2.62	4.75	2.05
Lu	0.09	0.06	0.06	0.06	0.42	0.28	0.42	0.40	0.36	0.42	0.74	0.31
Mg#	0.44	0.80	0.77	0.77	0.61	0.66	0.62	0.62	0.63	0.65	0.55	0.67

Table A1.2: Modeled trace element compositions (ppm) of parental magmas of troctolites from the Annieopsquotch ophiolite and anomalous gabbros from the Star Lake ophiolite

Sample	VL01J35c			VL01J35b			VL02J310a			VL02J309b			VL02J391			VL02J392		
Unit	Troctolite AN			Troctolite AN			Troctolite AN			Troctolite AN			Gabbro SL			Gabbro SL		
TMF[1] (%)	5	10	15	5	10	15	15	10	5	15	10	5	10	15	20	10	15	20
K	3918	2490	1825	17579	11800	8880	6339	8379	12354	1344	1811	2776	7783	5649	4434	5061	3676	2894
P	b.d.	b.d.	b.d.	b.d.	b.d.	b.d.	336	459	722	455	633	1042	995	728	574	169	123	97
Ti	2976	1945	1445	1982	1349	1022	2895	4064	6819	1457	2052	3465	3756	3146	2706	3326	2797	2403
Ba	44	33	26	98	77	63	25	31	39	10	12	16	256	196	158	184	140	113
Co	59	57	55	50	48	46	41	39	37	50	48	47	53	54	55	42	41	40
Cr	467	572	739	92	113	145	737	819	920	645	686	733	174	181	188	214	227	239
Cs	8.2	4.8	3.4	17.4	10.5	7.6	2.31	3.20	5.21	2.27	3.18	5.30	2.5	1.8	1.4	0.8	0.6	0.4
Cu	247	235	224	70	67	65	87	90	94	86	90	94	186	177	169	213	202	192
Ga	7.6	7.6	7.6	7.7	7.7	7.7	8.87	8.80	8.73	6.28	6.22	6.16	9.3	9.3	9.3	10.1	10.2	10.2
Hf	b.d.	b.d.	b.d.	b.d.	b.d.	b.d.	b.d.	b.d.	b.d.	b.d.	b.d.	b.d.	1.55	1.20	0.98	1.58	1.22	1.00
Nb	b.d.	b.d.	b.d.	b.d.	b.d.	b.d.	b.d.	b.d.	b.d.	b.d.	b.d.	b.d.	2.40	1.62	1.23	2.39	1.62	1.23
Ni	327	306	288	298	276	260	126	113	102	152	144	137	37	39	41	39	38	38
Pb	2.2	1.9	1.7	3.2	2.9	2.7	b.d.	b.d.	b.d.	2.7	3.0	3.4	6.1	5.2	4.6	6.0	5.1	4.5
Rb	34	18	12	152	82	56	43	62	113	5	7	12	32	22	17	21	14	11
Sc	16	22	35	3	4	6	27	35	48	19	23	30	15	16	16	18	18	19
Sr	138	136	134	170	168	167	98	98	98	88	88	89	151	146	142	147	142	137
Ta	2.70	1.42	0.97	2.66	1.41	0.96	0.70	1.01	1.84	0.74	1.07	1.89	0.45	0.31	0.24	0.42	0.30	0.23
Th	b.d.	b.d.	b.d.	0.92	0.48	0.33	b.d.	b.d.	b.d.	b.d.	b.d.	b.d.	b.d.	b.d.	b.d.	b.d.	b.d.	b.d.
U	b.d.	b.d.	b.d.	0.33	0.18	0.13	b.d.	b.d.	b.d.	b.d.	b.d.	b.d.	b.d.	b.d.	b.d.	b.d.	b.d.	b.d.
V	88	95	103	31	33	36	184	242	353	93	119	163	120	121	123	117	119	122
Y	10.36	6.71	4.96	3.91	2.64	1.99	8.66	12.38	21.65	3.97	5.67	9.92	13.97	11.76	10.15	12.82	10.73	9.22
Zn	78	70	63	79	64	54	55	58	62	67	69	71	28	26	24	26	25	24
Zr	b.d.	b.d.	b.d.	b.d.	b.d.	b.d.	b.d.	b.d.	b.d.	b.d.	b.d.	b.d.	11.2	8.1	6.3	11.0	7.9	6.2
La	b.d.	b.d.	b.d.	b.d.	b.d.	b.d.	0.39	0.49	0.66	0.34	0.44	0.62	1.58	1.22	0.99	1.66	1.26	1.02
Ce	4.17	2.94	2.27	b.d.	b.d.	b.d.	1.39	1.75	2.39	0.99	1.29	1.84	3.03	2.36	1.94	1.59	1.23	1.00
Pr	0.66	0.46	0.36	0.39	0.29	0.23	0.28	0.36	0.50	0.17	0.23	0.33	0.29	0.23	0.19	0.24	0.19	0.16
Nd	3.30	2.28	1.74	2.15	1.57	1.23	1.61	2.09	2.99	1.16	1.54	2.32	1.10	0.88	0.73	1.16	0.91	0.76
Sm	1.11	0.75	0.56	1.12	0.80	0.62	0.75	1.00	1.53	0.34	0.46	0.74	1.49	1.22	1.03	1.05	0.85	0.71
Eu	1.00	0.86	0.75	0.89	0.79	0.71	0.27	0.29	0.30	0.18	0.20	0.21	0.44	0.42	0.39	0.30	0.28	0.27
Gd	1.57	1.03	0.77	1.03	0.72	0.55	1.13	1.56	2.55	0.47	0.66	1.11	1.47	1.22	1.05	2.08	1.72	1.47
Tb	0.25	0.16	0.12	0.11	0.07	0.06	0.25	0.35	0.58	0.11	0.15	0.26	0.40	0.34	0.29	0.28	0.23	0.20
Dy	2.04	1.33	0.99	0.90	0.61	0.46	1.54	2.18	3.77	0.67	0.95	1.66	3.12	2.62	2.26	2.72	2.27	1.95
Ho	0.39	0.25	0.19	0.23	0.16	0.12	0.34	0.48	0.85	0.15	0.21	0.37	0.57	0.48	0.41	0.59	0.50	0.43
Er	1.32	0.85	0.63	0.72	0.48	0.36	0.97	1.39	2.49	0.49	0.70	1.24	1.71	1.44	1.24	1.92	1.61	1.38
Tm	0.13	0.09	0.06	0.12	0.08	0.06	0.15	0.22	0.39	0.08	0.11	0.20	0.31	0.26	0.22	0.28	0.23	0.20
Yb	1.48	0.94	0.69	0.76	0.49	0.37	0.82	1.18	2.14	0.61	0.87	1.53	1.39	1.16	1.00	1.90	1.59	1.36
Lu	0.20	0.13	0.09	0.13	0.08	0.06	0.15	0.22	0.40	0.09	0.12	0.21	0.27	0.23	0.20	0.28	0.23	0.20

[1]TMF = trapped melt fraction used in modeling; b.d.= below detection limit; AN=Annieopsquotch; SL=Star Lake

APPENDIX 2: NEOPROTEROZOIC AND CAMBRIAN ARC MAGMATISM ALONG THE EASTERN MARGIN OF THE VICTORIA LAKE SUPERGROUP: A REMNANT OF GANDERIAN BASEMENT IN CENTRAL NEWFOUNDLAND?

Rogers, N., van Staal, C.R., McNicoll, V., Pollock, J, Zagorevski, A., and Whalen, J.

Precambrian Research, 2006 (in press)

ABSTRACT

The eastern margin of the composite and structurally complex Victoria Lake Supergroup has previously been mapped where the Silurian Rogerson Lake conglomeratic rocks unconformably overlie Cambrian Tally Pond volcanic rocks. However, the recognition that the form of this contact changes between an unconformity and a brittle-ductile fault, in conjunction with the Neoproterozoic age of the Cripplebeck Intrusive Suite, dictate that the above interpretation of the nature of this margin requires revision. These discrepancies are resolved by the recognition of a Neoproterozoic, largely bimodal volcanic sequence (Sandy Brook Group), which is unconformably overlain by Rogerson Lake rocks to the east, with these combined units in fault contact with the Tally Pond Group to the west.

The Sandy Brook Group and Cripplebeck Intrusive Suite form a terrane of circa 563 Ma rocks with continental arc-like geochemical signatures. The distinctly negative $\varepsilon_{Nd,563}$ values for the felsic rocks (mean –3) of this terrane imply derivation from a crystalline basement older than the largely Pan-African crust that underlies contemporaneous volcanic rocks in West Avalonia, but similar to that inferred for the Gander Zone. Thus this terrane is likely to be the leading edge of the peri-Gondwanan microcontinent Ganderia.

The circa 511 Ma Tally Pond Group arc magmatism represent some of the oldest products of Iapetean subduction in Newfoundland. Although the Tally Pond Group are only observed to be in fault contact with the circa 50 million year older Sandy Brook Group, the high proportion of felsic volcanic rocks, Sandy Brook/Cripplebeck age inherited zircons and Pb isotopic data all support the inference that the Tally Pond Group was formed on Sandy Brook/Cripplebeck continental crust.

INTRODUCTION

The Victoria Lake Supergroup of central Newfoundland has long been known to be a composite and structurally complex amalgamation of arc-related terranes (e.g., Kean and Evans, 1988a, b; Evans et al., 1990; Dunning et al., 1991; Evans and Kean, 2002; Rogers and van Staal, 2002). However, the true diversity of these terranes, their ages and structural relationships are only now coming to light following detailed mapping combined with whole-rock geochemical, Nd-isotopic and U/Pb zircon geochronological studies. This paper focuses on the Neoproterozoic and Cambrian magmatic rocks observed along the eastern margin of the Victoria Lake Supergroup, as this area contains the Duck Pond and Boundary volcanic massive sulphide deposits, which have proven and probable reserves of 5.48 million tonnes of ore grading 3.3% Cu, 5.8% Zn, 0.9% Pb, 59 g/t Ag and 0.8 g/t Au (Moore, 2003) and are expected to go into production in 2006 (Aur Resouces Inc., press release, 2004). Although the deposits themselves are well documented by Moore (2003) and Squires and Moore (2004), and many of the age relationships have been known for sometime (e.g., Evans et al., 1990; Dunning et al., 1991) the regional tectonostratigraphy has not previously been presented in a form that is internally consistent, categorises all the known units and is compliant with the naming hierarchy of the North American Stratigraphic Code. This paper rectifies this by following the stratigraphy used in Rogers et al. (2005a, b), however the unit names presented herein can still be considered to be informal pending the release formalizing documentation.

The Victoria Lake Supergroup had traditionally been separated into two major volcanic belts, the Tulks Hill volcanics along the western margin and the Tally Pond volcanics along the eastern margin (Kean and Jayasinghe, 1980; Kean et al., 1981; Kean, 1985). Kean and Evans (1988a, b) and Dunning et al. (1991) recognised that these belts were composite units. In the Tally Pond volcanics Dunning et al. (1991) determined three distinct volcanic units: i) bimodal volcanic rocks termed therein the Lake Ambrose volcanic belt; ii) a fault-bounded suite of mafic and felsic volcanic rocks called therein the Sandy Lake sequence, which were provisionally related to the Lake Ambrose volcanic rocks; and iii) the chemically distinct pillow basalts of the Diversion Lake Group (interpreted as Upper Ordovician in age). Subsequent Neoproterozoic U/Pb zircon ages obtained for the Crippleback Lake and Valentine Lake plutons (Evans et al., 1990) complicated

geological interpretations for this area as these bodies had originally been interpreted as intrusive into and thus co-magmatic with or younger than the Lake Ambrose volcanic belt rocks (Kean and Evans, 1988b).

In this paper we present a model for the Neoproterozoic to Cambrian tectonic evolution of the eastern margin of the Victoria Lake Supergroup that is consistent with all the existing data and then place the formation of these rocks into an orogen-scale context.

GEOLOGICAL BACKGROUND

Riley (1957) and Williams (1970) conducted the first major regional scale geological mapping of the Red Indian Lake area, with subsequent more detailed mapping by Kean (1977; 1978; 1979a, b; 1982; 1983), Kean and Jayasinghe (1980; 1982), Herd and Dunning (1979), Dunning (1984), Evans et al. (1994a, b) and Evans et al. (1994). Additionally there have been numerous industry-led studies (e.g., Grimes-Graeme, 1934; MacKenzie et al., 1988; MacKenzie et al., 1990; 1993; Desnoyers, 1990a, b; Squires et al., 1990) due to the high potential for volcanogenic massive sulphide (VMS) and gold mineralization.

The Victoria Lake Supergroup (originally defined by Kean (1977) as the Victoria Lake Group) constitutes part of the Exploits Subzone of the Dunnage Zone (Williams et al., 1988; Figs. A2.1 and A2.2). Kean (1977) proposed that this "group" include all the pre-Caradocian volcanic and sedimentary rocks that occur between Red Indian Lake and the Silurian Rogerson Lake conglomerate. Kean and Jayasinghe (1980; 1982) informally divided the volcanic rocks of the Victoria Lake Group into two major regional units; namely the Tulks Hill and Tally Pond volcanics, which were separated from each other by a predominantly sedimentary sequence that was believed to be laterally equivalent to and largely derived from the volcanic rocks. Although Kean and Jayasinghe (1980; 1982) originally mapped the Cripplebeck Lake Pluton as being intrusive into the volcanic rocks adjacent to it, Evans and Kean (2002) reinterpreted the contact as a fault as it had been found to be Neoproterozoic (565 +4/-3 Ma; Evans et al., 1990), whereas the Tally Pond volcanics were interpreted as wholly Upper Cambrian in age. In addition to these rocks Evans and Kean (2002) proposed a "southern terrane" for the Victoria Lake Supergroup that comprised the Ordovician volcanic sequence extending east of the Rogerson Lake conglomerate to the Noel

Paul's Line. However, Valverde-Vaquero et al. (in press) have shown that these rocks are a distinct tectonostratigraphic package (therein named the Red Cross Group) and thus should not be included within the definition of the Victoria Lake Supergroup.

Rogers and van Staal (2002) developed a revised framework for the Victoria Lake Supergroup, consisting of several distinct blocks that were separated from each other by major faults, interpreted as thrusts, mainly based on the interpretations of nearby, and probably kinematically related faults on basis of seismic evidence (Thurlow et al., 1992). Each of these blocks was distinguished by a petrographically and chronologically distinct, Upper Cambrian, dominantly volcanic assemblage that is overlain by an Ordovician, largely sedimentary, sequence. As the rank and association of various units were at that time unresolved, they were classified by the informal and non-specific term of assemblages. This stratigraphy was further developed and the various units given a category/rank compliant with the strictures of the North American Stratigraphic Code for a series of 1:50,000 scale maps (Rogers and van Staal, 2005; Rogers et al., 2005a, b; van Staal et al., 2005). It should be noted that wherever possible previously existing informal stratigraphic names were used as a basis for this new stratigraphy (i.e., the Tally Pond volcanics became the Tally Pond Group). On these maps the Victoria Lake Supergroup is designated as consisting of the predominantly volcanic Tally Pond (circa 511 Ma – Dunning et al., 1991; Squires and Moore, 2004, see below), Long Lake (circa 505 Ma – Rogers et al., 2003 and unpublished data), Tulks (circa 498 Ma – Evans et al., 1990), Pats Pond (circa 488 Ma – Zagorevski et al., 2004) and Sutherlands Pond (circa 460 Ma – Dunning et al., 1987; Rogers et al., 2003 and unpublished data) groups and the late Arenig to Caradoc, largely sedimentary, Noel Paul's Brook and Wigwam Brook groups.

Previous lithogeochemical studies (e.g., Swinden et al., 1989; Dunning et al., 1991; Pollock and Wilton, 2001; Evans and Kean, 2002) have not defined chemically distinctive stratigraphic divisions for the Tally Pond volcanic rocks. However, they did demonstrate arc-like- affinities for these rocks, with the basaltic volcanic rocks ranging from island-arc tholeiite to calc-alkalic in composition.

STRATIGRAPHY AND REGIONAL LITHOLOGIES

The following stratigraphy follows the outline presented in Rogers et al. (2005a, b) for the Neoproterozoic to Cambrian sequences present within the study area (Figs. A2.2 and A2.3). The designation and regional distribution of units is in part based on data presented in the subsequent four sections. In particular, some volcanic dominated units in poorly exposed parts of the study area could not be correlated without geochemistry and/or geochronology.

Sandy Brook Group

The Neoproterozoic Sandy Brook Group (circa 563 Ma; see below) represents the oldest known supracrustal sequence within the region (Fig. A2.2). A brittle fault zone (Frigid Pond Fault) with an unknown magnitude of motion defines its western margin and separates it from the remainder of the Victoria Lake Supergroup. To the east the Sandy Brook Group is unconformably overlain by the Silurian (circa 428 Ma – Pollock et al., 2002) red, polymict conglomerate and sandstone of the Rogerson Lake Formation of the Botwood Group (Rogers et al., 2005b). The name for this unit is derived from the previously described Sandy Lake sequence volcanic rocks (Dunning et al, 1991) that make up a substantial portion of this group in the vicinity of the Cripplebeck Lake Pluton. However, the unit was named after Sandy Brook as opposed to Sandy Lake (from which Sandy Brook flows), as there is a more complete section along this watercourse and it avoids confusion with the Sandy Lake Formation of the Buchans Group.

The internal stratigraphy of the Sandy Brook Group has not yet been defined, mainly due to limited access and extremely poor exposure. The group consists primarily of volcanic rocks, which are associated with minor siliciclastic sedimentary rocks that locally include black shale. The volcanic rocks include pillowed and massive basalts, mafic tuffs, cryptocrystalline andesite flows and cherty, quartz-phyric, high-silica rhyolite. The relative proportions of the various lithologies is undetermined, although the mafic volcanic rocks seem to dominate in the vicinity of Sandy Brook.

Cripplebeck Intrusive Suite

The Cripplebeck Intrusive Suite consists of the Neoproterozoic (circa 563 Ma – Evans et al., 1990) Cripplebeck Lake, Valentine Lake and Lemottes Lake plutons (Fig. A2.2). These rocks

intrude the penecontemporaneous Sandy Brook Group with which they are probably co-magmatic. Together these two sequences form the eastern section of the study area.

The Valentine Lake Pluton, which defines the southeastern extent of the study area (Fig. A2.2), ranges in composition from pyroxenite via gabbro and diorite to tonalite and/or trondhjemite (Evans and Kean, 2002). The gabbro and diorites are typically equigranular, holocrystaline and medium to coarse grained, whereas the more felsic rocks are quartz-phyric. The pyroxenite phase only represents a minor proportion of the pluton, occurring as a small, isolated body near Valentine Lake (Evans and Kean, 2002). The western margin of the Valentine Lake Pluton is unexposed, but is interpreted to be truncated by the Frigid Pond Fault, based on the map pattern and shearing of adjacent units (Evans and Kean, 2002). It is unconformably overlain to the east by the Silurian Rogerson Lake Formation that is in part derived from it.

The Crippleback Lake Pluton forms a northeasterly trending body between Noel Paul's Brook and West Lake (Fig. A2.2). It is basically bimodal in composition with a mafic phase to the north consisting of gabbro and diorite and a felsic phase consisting largely of quartz monzonite with minor granodiorite in the central and southern portion of the pluton. The mafic phase is typified by massive, equigranular, grey to dark grey, medium-grained rocks that frequently contain disseminated sulphide. The felsic rocks are mainly medium-grained, equigranular and unfoliated, with a light grey colour although the quartz monzonite often has a reddish hue. The Crippleback Lake Pluton's northern margin is truncated by the Frigid Pond Fault, which in the vicinity of Noel Paul's Brook is represented by a brittle fault zone in excess of 150 m wide. To the south these rocks are in assumed intrusive contact with Sandy Brook Group rocks.

The definition of the Lemotte's Lake Pluton has been extended from a wholly granitic body (Kean and Mercer, 1981; Evans and Kean, 2002) to include adjacent gabbroic rocks. Although originally interpreted as Silurian or younger (Kean and Mercer, 1981), it has subsequently been reinterpreted as Neoproterozoic based on its petrographic similarity and spatial association to the Crippleback Lake Pluton (e.g., Evans and Kean; 2002). This assertion is supported by an unpublished laser ablation zircon age (D.H.C. Wilton, personal communication, 2003).

Tally Pond Group

The Upper Cambrian (circa 511 Ma) Tally Pond Group (Figs. A2.2 and A2.3), which were previously called the Tally Pond volcanics (e.g., Evans and Kean, 2002), is divided into the predominantly felsic volcanic rocks and minor subvolcanic intrusive and sedimentary rocks of the Bindons Pond Formation (this is a new name as these rocks have only previously been classified lithologically and not as a stratigraphic unit) and the mafic volcanic rocks of the Lake Ambrose Formation (unit name derived from the previously described Lake Ambrose basalts of Dunning et al, 1991). Although at least in part coeval, the gross map distribution and regional structure suggest that the Lake Ambrose Formation occurs mostly stratigraphically below the Bindons Pond Formation, whose rocks become more prevalent towards the top of the Tally Pond Group (Fig. A2.3). This stratigraphic interpretation is consistent with detailed sections based on drillhole compilations through the Duck Pond and Boundary deposits (e.g., Squires et al., 2001; Moore, 2003). It should be noted that in this section the unmineralized, dominantly mafic (i.e., largely Lake Ambrose Formation) "Upper Block" is interpreted to be thrust over the younger, dominantly felsic (i.e., largely Bindons Pond Formation) "Mineralized Block" along the Duck Pond Thrust.

The Lake Ambrose Formation consists of typically vesicular and/or amygdaloidal, dark green to grey, massive or, locally, pillowed tholeiitic basaltic lavas, in association with minor tuff, pillow breccia, volcanic breccia and andesitic flows. The felsic volcanic rocks of the Bindons Pond Formation comprise aphyric, massive to flow-banded dacite and rhyolite, quartz-phyric and/or feldspar-phyric rhyolite, volcaniclastic and epiclastic tuff, crystal tuff, volcanic breccia and subvolcanic quartz porphyry. Due to the poor exposure throughout the Tally Pond Group, the relative distribution of these various felsic volcanic lithologies is unclear. In addition to felsic volcanic rocks the Bindons Pond Formation also includes minor clastic sedimentary rocks and massive sulphide (e.g., the Duck Pond deposit).

The Tally Pond Group is primarily exposed in a largely anticlinal structure that is truncated to the south and east by the Frigid Pond Fault. It is interpreted that prior to truncation by the west-directed Frigid Pond Fault, the Tally Pond Group outlined a north-eastward (current coordinates) plunging fold (Figs. A2.2 and A2.3). The northern and eastern margins of the Tally Pond Group are

overlain apparently unconformably by sedimentary rocks of the Noel Paul's Brook Group (see below). Two additional antiformal inliers, each consisting mostly of Bindons Pond Formation felsic volcanic rocks, occur within Noel Paul's Brook Group rocks (Fig. A2.3).

WHOLE-ROCK GEOCHEMISTRY AND ND ISOTOPE DATA

For this study, 16 new, high-quality whole-rock geochemical analyses were obtained, and combined with 16 previously published analyses from the study area that are of similar analytical quality (Evans and Kean, 2002). All of these analyses were sampled with the intention of resolving petrogenetic, tectonic and structural problems, rather than alteration and/or mineralization issues. Samples were selected so that they did not exhibit any anomalous alteration characteristics, were free of veins and were relatively unaffected by mineralization (both syn- and post-volcanic in origin). Trace element data for both the previously published and newly acquired analyses were determined by X-Ray florescence (XRF) and inductively coupled plasma mass spectrometry (ICP-MS) or emission spectrometry (ICP-ES), with the rare earth elements (REE) analysed by ICP-MS. Details of the analytical procedures for the previously published samples is presented in Evans and Kean (2002). Details of the analytical procedures and elemental accuracies for the newly acquired data are given in Rogers (2004). The mean and standard deviation for each of the units discussed herein are presented in Tables A2.1 to A2.2.

In addition to the whole-rock chemical data, 8 Nd isotopic analyses were also obtained for selected samples in order to help constrain the tectonic evolution of the study area. The details of these Nd isotopic analyses including interpreted crystallization age, ε_{Nd} and, where appropriate, modal age (T_{DM} calculated after DePaolo, 1981) are given in Table A2.3. The complete data tables, locations and details of the analytical procedures for these analyses are presented in Rogers (2004).

Sandy Brook Group

Although the Sandy Brook Group has not, as yet, been formally subdivided into formations, it is clear from both major and trace element systematics that the volcanic rocks within this group can be subdivided by rock type (Fig. A2.4; Table A2.1). Thus, this group's volcanic rocks are split into units with rhyolitic, andesitic and basaltic compositions, with the basaltic rocks further

subdivided chemically into two distinct units (referred to herein as basalt I and basalt II). It should be noted that although unit basalt II is compositionally a basaltic andesite, it is considered as a basalt herein, as it is macroscopically indistinguishable from unit basalt I rocks.

In general, the Sandy Brook Group felsic volcanic rocks have higher SiO_2, K_2O, Pb, Rb, Sb, Th, Tl, U, V and light rare earth (LREE), and lower Fe_2O_3t, MnO, MgO, CaO, Na_2O, Sc, Sr, Y and heavy rare earth (HREE) compositions than the rhyolitic rocks of the Tally Pond Group. On a chondrite normalised REE profile these rocks show a steeply negatively dipping slope for the LREE, whereas the heavy rare earth (HREE) profile is relatively flat. They also differ from the other rhyolitic rocks in the study in not exhibiting an Eu anomaly (Fig. A2.5a). On a MORB normalised multi-element spidergram these rocks exhibit the most negative overall slope in comparison to the other rhyolitic rocks in the study and also exhibit very pronounced Nb and Ti negative anomalies (Fig. A2.5b). Three Nd isotopic analyses were obtained for Sandy Brook Group rhyolitic rocks that give $\varepsilon_{Nd,563}$ values of –0.67, -3.21 and –5.18, and T_{DM} ages of 1153, 1260 and 1337 Ma, respectively (Table A2.3).

The Sandy Brook Group andesitic volcanic rocks tend to have the higher SiO_2, Al_2O_3, K_2O, Ba, Pb, Rb and LREE, and lower Fe_2O_3t, MgO, CaO, Na_2O, Cu, Sc, Sr and V contents than the intermediate composition rocks in of the Tally Pond Group. These rocks exhibit moderate, negatively inclined chondrite normalised REE and multi-element spidergram profiles (Fig. A2.6), with a prominent negative Nb trough in the latter.

The two basaltic units within the Sandy Brook Group have distinctly different compositions as demonstrated by their respective chondrite normalised REE and multi-element spidergram profiles (Fig. A2.7). Basalt I typically has higher Fe_2O_3t, Sc and V and lower TiO_2, CaO, K_2O, Ba, Hf, Nb, Rb, Th, U, Y, Zr and REE contents than the other basaltic volcanic rocks within the study, whereas basalt II rocks tend to have the highest SiO_2, Ba, Hf, Nb, Sr, Ta, Th, U, Y, Zr and LREE, and lowest Fe_2O_3t, Sc and V contents. The chondrite normalised REE profile of basalt I is relatively flat (Fig. A2.7a), as is its multi-element spidergram profile, with the notable exceptions of moderate Nb and slight Hf troughs and relatively large Th peak. In contrast basalt II exhibits a higher and strongly negative sloping chondrite normalised REE profile (Fig. A2.7a). It is notable that that basalt

II also has a significantly higher LREE content than the Sandy Brook Group andesites, and so the variance in REE profiles between the various basalt units cannot be directly related to the more siliceous nature of the basalt II rocks. The multi-element spidergram profile from basalt II also has a strongly negative slope, along with moderate Nb and small Ti troughs. On multiple standard tectonic discrimination plots the two basaltic units from the Sandy Brook Group invariably fall within the fields for arc volcanism (Fig. A2.8). However, Figures A2.8b, c and d clearly demonstrate a significant difference between the two basaltic units with basalt I plotting within the island arc tholeiite/depleted arc fields and basalt II as mature and/or continental arc-like calc-alkaline basalt.

Crippleback Intrusive Suite

Although the Crippleback Intrusive Suite ranges in composition from pyroxenite and gabbro to granodiorite, the only the whole-rock chemistry of the quartz-monzonitic portion of the Crippleback Lake Pluton was analysed for this study. The major and trace element systematics of this unit is consistent with quartz monzonite or granodiorite. Compared to the spatially associated, consanguineous (see below) rhyolites of the Sandy Brook Group, the Crippleback quartz monzonite are distinctly less siliceous and consequently enriched in all the other major elements (Table A2.1). However, in respect to their trace element compositions the two rock types are effectively indistinguishable, as is illustrated by their respective MORB normalised multi-element spidergram profiles (Fig. A2.9).

Neodymium isotopic analysis provides $\varepsilon_{Nd,563}$ values of –3.90 and –4.60 for these samples, with model ages of 1261 and 1354 Ma, respectively (Table A2.3). These values are broadly similar to previously published Nd isotopic analyses for the Crippleback Intrusive Suite (Kerr et al., 1995) that produced an $\varepsilon_{Nd,563}$ value of –2.91 and T_{DM} of 1237 Ma for a quartz monzonite sample from the Crippleback Lake Pluton and from the Valentine Lake Pluton an $\varepsilon_{Nd,563}$ value of –0.88 and T_{DM} of 1310 Ma for a granodioritic sample, along with an $\varepsilon_{Nd,563}$ value of 0.48 for a gabbroic sample.

Tally Pond Group

The volcanic rocks of the Tally Pond Group are subdivided between the Bindons Pond and Lake Ambrose formations (Table A2.2). The Bindons Pond Formation comprises the felsic volcanic rocks of the Tally Pond Group. Chemically these rocks consist of dacite to rhyolite (Fig. A2.4; Table

A2.2). The chondrite normalised REE profile for the Bindons Pond Formation felsic volcanic rocks exhibit the flattest overall slope, but largest Eu trough of all of the volcanic rocks in this study (Fig. A2.5a). On a MORB normalised multi-element spidergram these rocks display very prominent Nb and Ti troughs (Fig. A2.5b). Two samples of Bindons Pond Formation felsic volcanic rocks were also analysed for Nd isotopes producing $\varepsilon_{Nd,511}$ values of 1.77 and 2.64 (Table A2.3).

Although the mafic volcanic rocks of the Lake Ambrose Formation form, at least macroscopically, a petrographically indistinguishable suite of rocks, chemically, in particular with reference to their major element compositions, they are divisible into basalt, basaltic andesite and andesite subsets (Fig. A2.4; Table A2.2). In contrast to the significant major element variations between these three subsets, the trace element characteristics are remarkably consistent (Figs. A2.6 and A2.7). All of the Lake Ambrose Formation volcanic rocks have a fairly straight and slightly negatively dipping chondrite normalised REE profile, and a MORB normalised multi-element profile that, except for its enriched Th and clear Nb trough, is relatively flat at approximately unity, but is distinctive from all the other mafic volcanic rocks within the study in having a small negative Zr trough. Compared to the andesitic rocks of the Sandy Brook Group the andesitic rocks of the Lake Ambrose Formation have lower concentrations of SiO_2, Al_2O_3, K_2O, Rb, Zr and LREE and higher Fe_2O_3t, MgO, CaO, NaO and Sc contents (Tables A2.1 and A.2). The basaltic rocks of the Lake Ambrose Formation are the most MnO, CaO and K_2O rich, and SiO_2, Al_2O_3, Na_2O, Sr, Ta and HREE poor of all of the basalts in this study (Table A.2). One sample of Lake Ambrose Formation basalt also underwent Nd isotopic analysis giving an $\varepsilon_{Nd,511}$ value of 3.06 (Table A2.3). On standard tectonic discrimination plots the Lake Ambrose Formation basaltic volcanic rocks occur in the fields for island arc tholeiite basalt (Fig. A2.8), although they are distinctly less depleted than the island arc tholeiite-like basalts from the Sandy Brook Group (Figs. A2.8c, d).

GEOCHRONOLOGY

The following two U/Pb zircon analyses were conducted at the Geochronology Laboratory of the Geological Survey of Canada following the U-Pb isotope dilution analytical methods (Thermal Ionization Mass Spectrometry - TIMS) outlined in Parrish et al. (1987). Standard crushing, grinding, Wilfley™ table, and heavy liquid techniques prepared heavy mineral concentrates. Mineral

separates were sorted by magnetic susceptibility using a Frantz™ isodynamic separator. Zircon fractions analyzed were very strongly air abraded following the method of Krogh (1982). Treatment of analytical errors follows Roddick et al. (1987). Analytical results are reported in Table A2.4, where errors on the ages are presented at the 2σ level, and displayed in the concordia plots (Fig. A2.10). Sample locations are presented in Table A2.4 with approximate distribution shown in Figures A2.2 and A2.3.

Sample RAX02921 – Sandy Brook Group

Sample RAX-02-921, a light greyish brown, quartz-phyric, felsic volcanic rock of the Sandy Brook Group, contains abundant clear, euhedral zircon ranging in morphology from elongate to stubby prisms. Four-multigrain zircon fractions were analyzed from this rock (Table A2.4; Fig. A2.10a). A linear regression of all 4 analyses with a fixed lower intercept at the origin has an upper intercept of 563 ± 2 Ma (MSWD = 1.2). This Neoproterozoic age of 563 ± 2 Ma is interpreted to be the crystallization age of the rock.

Sample JP-01-GC1 – Bindons Pond Formation, Tally Pond Group

Sample JP-01-GC1 represents a quartz-phyric, felsic ash tuff that was collected approximately 2.5 km northeast of Tally Pond from diamond-drillcore at a depth of approximately 20 m. The unit is interpreted to conformably overly the Boundary volcanogenic massive sulphide deposit. The tuff is light grey-green and fine-grained with quartz and minor feldspar crystals; it permeated by a network of quartz and calcite veins and minor (1 to 2%) disseminated pyrite. The intimate stratigraphic and spatial association of the tuffaceous volcanic rocks with laminated and banded sulphides and the pervasive sericite and chlorite alteration contained within these rocks suggests that this volcanic event is genetically related to massive sulphide mineralization.

The sample yielded numerous (>100) zircons which were separated into three multi-grain fractions (Table A2.4; Fig. A2.10b: A1) colourless, euhedral, stubby prisms; B1) small, colourless, well faceted crystal tips; and B2) clear to pale brown zircon fragments with numerous inclusions. All of the zircons contain numerous internal and surficial fractures with growth zoning evident in several grains; there are however, no visible cores. All three fractions have varying uranium contents, from small amounts in fraction A1 (89 ppm) to more moderate amounts in fractions Z3 (132 ppm) and Z2

(231 ppm). Two fractions (A1 and B1) overlap concordia, with similar 207Pb/206Pb ages of 510 and 509 Ma respectively. The third fraction (Z3) lies slightly beneath concordia and gives a 207Pb/206Pb age of 514 Ma, which could reflect slight Pb-loss or incomplete zircon dissolution. With more weight given to the more precise analyses (fractions Z1 and Z2) a late Cambrian date of 509 ±1 Ma is interpreted as the age of igneous crystallization.

DISCUSSION

The Neoproterozoic to Cambrian tectonic evolution of the eastern margin of the Victoria Lake Supergroup

The Neoproterozoic and Cambrian rocks along the eastern margin of the Victoria Lake Supergroup record two distinct phases of magmatic activity, separated from one another by an apparent hiatus of approximately 50 million years. The first of these phases is represented by the Neoproterozoic (circa 563 Ma) Sandy Brook Group volcanic rocks and consanguineous plutonic rocks of the Cripplebback Intrusive Suite. These rocks form a distinct narrow, elongate block that is separated from the Lower to Middle Cambrian and younger rocks to the west by the mainly brittle Frigid Pond Fault and an unconformity, defined by the Silurian, predominantly terrestrial to shallow marine Botwood Group, to the east (Fig. A2.2). Whole-rock geochemistry and Nd isotopes suggest that these units are co-magmatic, with the Cripplebback Intrusive Suite representing the subvolcanic equivalent to the Sandy Brook Group volcanic rocks. The presence of calc-alkaline basalts and strongly negative ε_{Nd} values are consistent with these rocks having evolved in a continental arc setting.

All Neoproterozoic arc magmatism in Newfoundland, and the Northern Appalachians in general, has historically been related to the peri-Gondwanan microcontinent of Avalonia (Nance and Murphy, 1994; Nance et al., 2002), or as it was previously described, the Avalon Zone (Williams, 1979). If correct, this would suggest that the Upper Neoproterozoic Sandy Brook Group – Cripplebback Intrusive Suite (SB-C) is part of the Avalon Zone, implying that Avalonian crustal basement extends from Newfoundland's east coast beneath the Gander Zone (Fig. A2.1) and the adjacent Exploits Subzone at least as far as the Red Indian Line in central Newfoundland (Fig. A2.1). Geological studies (e.g., Williams and Piasecki, 1990; van Staal and Fyffe, 1991; Colman-

Sadd et al., 1992) have indicated that the Gander Zone represents the structural and stratigraphical basement to the Exploits subzone. This basement has been imaged seismically as a distinct crustal block, referred to either as the central lower crustal block (Hall et al., 1998) or Ganderian basement (van der Velden et al., 2004); from herein the latter term will be used. Van Staal et al. (1998) proposed that this Ganderian basement and its Lower Palaeozoic cover represent a distinct microcontinent called Ganderia.

In northeastern Newfoundland the Ganderian basement is clearly separated from Avalonian basement by the subvertical, Moho-cutting Dover Fault (Keen et al., 1986), but its separation is less obvious in southeastern Newfoundland. Nevertheless, van der Velden et al. (2004) interpreted the boundary as a listric northwest-dipping fault. Also, correlation between SB-C and Avalonia is not supported by geochronology or isotopic data. Arc magmatism in, at least, the Newfoundland portion of Avalonia had largely ceased by 585 Ma (Krogh et al., 1988; O'Brien et al., 1996; Nance et al., 2002) to be replaced by rift and/or wrench basin volcanism (Nance et al., 2002). Furthermore, the typical ε_{Nd} values for West Avalonian Neoproterozoic arc magmatism are positive (generally ranging between 0.5 and 3 (e.g., Murphy and Nance, 2002)), as opposed to the distinctly negative ε_{Nd} values observed for the SB-C rocks. Similarly, the T_{DM} ages for West Avalonia range from circa 1200 Ma to circa 600 Ma, whereas the SB-C rocks typically have a T_{DM} of circa 1250 Ma. Also, the Cambro-Ordovician history of the overlying Victoria Lake Supergroup differs greatly from that of Avalon Zone (e.g., O' Brien et al., 1996; Barr et al., 1998). All told, the SB-C correlates much better with the nearby coeval igneous rocks in the Hermitage Flexure in southern Newfoundland and related rocks in Maritime Canada, which have previously been proposed as representing exposed Ganderian basement (Dunning and O'Brien,1989; van Staal et al., 1996; Barr et al., 1998). In the Hermitage Flexure, arc magmatic rocks with ages ranging between 585 and 560 Ma and ε_{Nd} values between –0.3 and –1.6 (Kerr et al., 1995) are followed by Cambrian tectonomagmatism (Dunning and O'Brien, 1989; Dubé et al., 1998), thus showing a comparable geological evolution to that preserved in the SB-C at a time when the Avalon zone was characterised by rift and/or wrench basin volcanism and platformal sedimentation.

The Nd isotopic data for the SB-C implies that it was derived from crystalline basement that at least in part consists of rocks that are older than the typical circa 1000 Ma, juvenile crust of Avalonia (Mallard and Rogers, 1997; Murphy and Nance, 2002). The implied basement to the SB-C is consistent with what isotopic studies on Palaeozoic granitoids have indicated for the Gander Zone of Newfoundland (Kerr et al., 1995; Schofield and D'Lemos, 2000) and elsewhere (e.g., van Staal et al., 1996; Barr and Kerr, 1997). Although a clear basement-cover relationship between Neoproterozoic rocks and the Palaeozoic rocks of the Gander Zone is not known in Newfoundland, it does occur in southern New Brunswick where uppermost Lower Cambrian to Lower Ordovician Gander Zone arenites of the Matthews Lake Formation, New River belt (van Staal et al., 2004) disconformably overlie Neoproterozoic and Lower Cambrian arc-like volcanic and plutonic rocks (Johnson and McLeod, 1996; Johnson, 2001), which also have moderately negative ε_{Nd} values (Barr et al., 2003) and a complicated Early Palaeozoic tectonomagmatic history. Hence, it is reasonable to assume that although the SB-C terrane occurs within the Exploits Subzone, it can also be considered to represent a portion of exposed Ganderian basement. Late Neoproterozoic to Early Cambrian arc magmatic rocks also occur in the Exploits Subzone of northern New Brunswick (van Staal et al., 1996), which according to palaeomagnetic (Liss et al., 1993) and faunal (Williams et al., 1995) evidence formed at high southerly latitudes, collectively supporting the interpretation that Ganderia is a large peri-Gondwanan crustal block in the northern Appalachians that was tectonically distinct from Avalonia during at least the Early Palaeozoic (e.g., O'Brien et al., 1996; van Staal et al., 2004).

At circa 511 Ma the Tally Pond Group volcanic rocks are amongst the oldest known products of Iapetean subduction in Ganderia (van Staal et al., 1998). Dunning et al. (1991) speculated that the significant volume of felsic volcanic rocks in the Tally Pond Group indicated that the group formed on thickened arc crust (i.e., by circa 511 Ma the arc was firmly established and mature) and/or it was built on continental crust. Although the Frigid Pond Fault wholly separates the Tally Pond Group from the SB-C terrane (Fig. A2.2) the lack of any significant deformation zone indicates that it is unlikely that this fault represents any major movement. Thus it is highly probable that the Tally Pond Group formed on SB-C crust. With the recognition inherited zircons of SB-C age

within Tally Pond Group felsic volcanic rocks (V. McNicoll, unpublished data, reported in Squires and Moore, 2004) this hypothesis is largely proven. Furthermore, the Pb-isotopic data for the Duck Pond massive sulphide deposit of the Tally Pond Group (Swinden and Thorpe, 1984; Pollock and Wilton, 2001) is indicative of an evolved crustal input, which is consistent with a SB-C-like basement to the Tally Pond Group.

The ε_{Nd} values for the Tally Pond Group are approximately 2 for the felsic volcanic rocks and 3 for the mafic volcanic ones (Table A2.3; Fig. A2.11). Assuming that the ε_{Nd} values observed for the SB-C are largely representative of the basement to the Tally Pond Group, then, given the Nd isotopic evolution curve (Fig. A2.11), the Tally Pond volcanic rocks could be formed by the fractionation of approximately 60 % depleted mantle and 40 % assimilated crust. Even though the Tally Pond Group is effectively bimodal, the fractionation model for the felsic volcanic rocks, as determined from the isotopic data, is realistic as the first formed felsic melt is expected to produce a density barrier that inhibits the eruption of mafic to intermediate composition volcanic rocks. The exact proportion of crustal assimilation is likely to be slightly higher than 40 %, as the contribution of a mafic basement component cannot be reliably incorporated into the modelling. This is because the proportion of mafic basement, as represented by the gabbroic/dioritic phase of the Crippleback Intrusive Suite and basaltic volcanism of the Sandy Brook Group, is unknown. Also high-quality whole-rock chemical analyses of the gabbros and diorites of the Crippleback Intrusive Suite are not available. Kerr et al. (1995) did obtain a Nd-isotopic analysis for a gabbro sample from within the Valentine Lake Pluton that had an ε_{Nd} value of 0.48. However, this sample was obtained as part of a regional reconnaissance study and subsequent mapping has determined that the Valentine Lake Pluton contains multiple phases of mafic intrusive rocks, at least some of which are probably Silurian or younger based on cross-cutting relationships with the unconformably overlying Rogerson Lake Formation (P. Valverde-Vaquero, personal communication, 2003; Rogers, 2004). Hence, a more focused study is required before a reliable Nd isotopic composition can be applied to the mafic portion of the Crippleback Intrusive Suite.

In addition to the Tally Pond Group, the Victoria Lake Supergroup also includes (in chronological order) the Long Lake, Tulks and Pats Pond groups (Rogers et al., 2005a; van Staal et

al., 2005) that along with the circa 486 Ma Wild Bight Group of north-central Newfoundland (O'Brien et al., 1997; MacLachlan and Dunning, 1998) and Lower Cambrian to Tremadoc volcanic rocks of southern New Brunswick and Maine (Johnson and McLeod, 1996) collectively form the Penobscot Arc (van Staal, 1994; van Staal et al., 1998). Contrary to the model presented by van Staal et al. (1998) and MacLachlan and Dunning (1998), this study shows that the Penobscot Arc was likely formed on Ganderian basement as opposed to having been accreted to it in the early Arenig.

Neoproterozoic and Cambrian tectonic reconstructions for Ganderia

Continental arc volcanic and plutonic rocks that are coeval with and have similar Nd isotopic characteristics to the SB-C and the related Ganderian basement rocks elsewhere in the Canadian Appalachians, occur in the Carolina terrane (for review see Hibbard et al., 2002) and the British Isles (see below), thus presenting an indication of the extent of Ganderia within the Appalachian – Calidonide Orogen. Ingle et al. (2003) have identified via SHRIMP geochronolgy 552 ± 19 and 553 ± 20 Ma arc-like felsic volcanic rocks in the Uwharrie Formation and Albemarle Group, respectively, of the Carolina Terrane. Both of these units have, at least in part, distinctly negative ε_{Nd} values (Mueller et al., 1996; Ingle et al. 2003), which are interpreted as indicting a relatively old component to their source (i.e., these rocks are not solely derived from circa 1000 Ma, juvenile crust). Ingle et al. (2003) postulated that the Carolina terrane had a close affinity with the Amazon craton and consists of Orinoquian-like crust (possibly mixed with Tocantins-like crust). This isotopic correlation with the Amazon craton for the Carolina terrane coincides with van Staal et al's (1996; 1998) interpreted Amazonian provenance for Ganderia, which is consistent with palaeomagnetism (Liss et al., 1993), faunas (Williams et al., 1995) and black shale compositions (Fyffe and Pickerill, 1993).

In the British Isles van Staal et al. (1998) interpreted that Ganderian basement stretched from southeast Ireland (Rosslare-Leinster terranes), through the Isle of Man and the Lake District of England (Lakesman Terrane), up to the Northern Belt Median Fault within the Southern Uplands of Scotland. Although van Staal et al. (1996) postulated that Ganderian basement in the British Isles outcropped in the Rosslare and Coedana complexes in Ireland and Anglesey, respectively, neither of these area is necessarily directly comparable to the SB-C terrane, as they are both too old at

circa 615 Ma (Max and Roddick, 1989; Tucker and Pharaoh, 1991) to be unequivocally related, although rocks of approximately this age also occur in Ganderian basement exposed in New Brunswick (Barr and White, 1996; Barr et al., 2003). However, isotopic data, their association with Lower Palaeozoic marine siliciclastic rocks typical of the Gander Zone, and their Early Palaeozoic tectonic history (Max et al., 1990; Gibbons and Horak, 1996) resemble those of Ganderian rocks in North America. Ganderia may also extend into central England. Recent SHRIMP geochronology of the supposedly arc-related Bardon Hill Complex within the Charnwood Forest inlier of central England has provided an age of 566 ± 3.1 Ma (Compston et al., 2002), which is identical within error for the ages obtained for the SB-C terrane. Furthermore, this unit also has negative ε_{Nd} values (Thorogood, 1990) similar to those of the SB-C rocks and a different Cambrian history than the other Avalonian terranes exposed in England and Wales (Compston et al., 2002). There are also indicators for this age of magmatism from detrital zircons in sedimentary rocks from the Southern Uplands of Scotland (Phillips et al., 2003.), possibly derived from the now buried Novantia terrane (Armstrong and Owen, 2001), which may have rifted off Ganderia (see below). However, as this data cannot be combined with whole-rock chemistry and Nd isotopic analysis, it is impossible to test whether they are related to Ganderian arc magmatism

Although currently unproven, we postulate that at circa 540 Ma (see below) the Neoproterozoic arc magmatism that formed the Sandy Brook Group and Crippleback Intrusive Suite stopped in response to the replacement of subduction by transform faulting following ridge – trench collision (Nance et al., 2002). In addition to ending arc magmatism, this change to a transform margin helps accommodate the relative anticlockwise rotation of Gondwana and its associated peri-Gondwanan terranes such that it caused Ganderia to move from the Ran Sea, which in the Neoproterozoic separated it from Baltica (Hartz and Torsvik, 2002), into Iapetus.

The above is represented on a global tectonic reconstruction map (Fig. A2.12) based on the palaeomagnetic constraints and geological correlations outlined in Nance and Murphy (1994), van Staal et al. (1998), Cocks and Torsvik (2002), Hartz and Torsvik (2002), Nance et al. (2002) and Stampfli and Borel (2002). The 560 Ma reconstruction shows the Ganderian microcontinent as a ribbon-like entity outboard of the "South American" portion of Gondwana, whereas Avalonia is

positioned relatively far removed within the Pan-African deformation belt adjacent to palaeo North Africa. It is suspected that at this time Gondwana had not completely amalgamated, but was in the midst of accretion related to the Brazilide Orogen, and thus the separation between Avalonia and Ganderia was potentially quite large at this time, depending on exactly how and when the various parts of Gondwana were joined together. The main constraint on the distance between Avalonia and Ganderia in the Neoproterozoic comes from palaeomagnetic data that has Ganderia at low southerly latitudes, whilst central Avalonia was at a mid southerly latitude. In our reconstruction the Carolina Terrane is shown as part of Ganderia, however it could alternatively be a separate, but spatially associated microcontinent. At this time, subduction of the Ran Sea was continuing beneath Ganderia, in contrast to Avalonia where it had ceased circa 25 million years earlier following subduction of the spreading ridge transforming the margin into a strike – slip regime. This strike – slip motion, along with the relative anti-clockwise rotation and southward motion of palaeo North Africa, with which it was a fellow traveller, was progressively bringing Avalonia along the southern margin of the Ran Sea closer towards Ganderia. However, it is likely that the strike – slip margin propagated to the south of Ganderia, in the process creating the oceanic seaway whose subsequent closure during the Silurian was responsible for the Acadian Orogeny (van Staal, 2005; van Staal et al., 2004).

We postulate that subduction of the Ran Sea beneath Ganderia continued until circa 540 Ma, at which time ridge – trench collision resulted in a tectonothermal event as is suggested by high temperature structures (van Staal et al., 1996) and metamorphism (O'Brien et al., 1991; Barr and White, 1996). The relative timing of this event throughout Ganderia dictates that the collision was at a relatively high angle. Following this collision, the ocean facing margin of Ganderia went into a strike – slip regime, in the same way that Avalonia had done at circa 585 Ma. This process, in association with the ongoing anti-clockwise rotation of Gondwana, resulted in Ganderia moving out of the Ran Sea where it faced Baltica and into Iapetus.

In the 510 Ma tectonic reconstruction (Fig. A2.12) Ganderia is shown having obtained its position within the southern Iapetus Ocean facing Laurentia. With this change of position, the ocean facing margin of Ganderia has reverted to subduction. Avalonia by this stage was partially situated

en-echelon south of Ganderia, and subsequently also started to experience subduction beneath the portion of it that now occurs within the British Isles, as is shown by the Tremedocian magmatism at Rhobell Fawr (Kokelaar, 1986).

SUMMARY

The recognition of distinct arc-related magmatic events expressed in the rocks along the eastern margin of the Victoria Lake Supergroup provides a window into the Neoproterozoic to Cambrian tectonic evolution of the northern Appalachians and beyond. The identification of the Neoproterozoic Sandy Brook Group and Crippleback Intrusive Suite as the immediate basement to the subsequent Iapetean-related volcanism helps constrain the tectonic model as it links the Exploits Subzone throughout its tectonic evolution with the peri-Gondwanan microcontinent of Ganderia. Furthermore, comparison with coeval and isotopically similar magmatism elsewhere provides possible linkages to the Uwharrie Formation and Albemarle Group of the Carolina Terrane and the Charnwood Forest Pre-Cambrian inlier of the English Midlands. Whether this swathe of the Appalachian – Calidonide Orogen from the Carolina Terrane to the British Isles was wholly Ganderia or represents two (or more) related peri-Gondwanan microcontinents is beyond the scope of this study. However it is evident that each of these regions is built on isotopically similar crust probably derived from the South American cratonic rocks that were affected by Pan-African events and that they all experienced arc magmatism in the Latest Neoproterozoic in response to subduction prior to the inception of the Iapetus Ocean.

Geochronology confirms that the circa 511 Ma Tally Pond Group volcanic rocks as the oldest known evidence for subduction along the peri-Gondwanan side of Iapetus. In contrast to earlier studies, this work proves that the Tally Pond Group was not the product of subduction in an oceanic setting, but was built on the Ganderian microcontinent. Thus it provides a constraint on the tectonic setting/development of the Middle Cambrian to Tremadoc Penobscot Arc throughout the northern Appalachians.

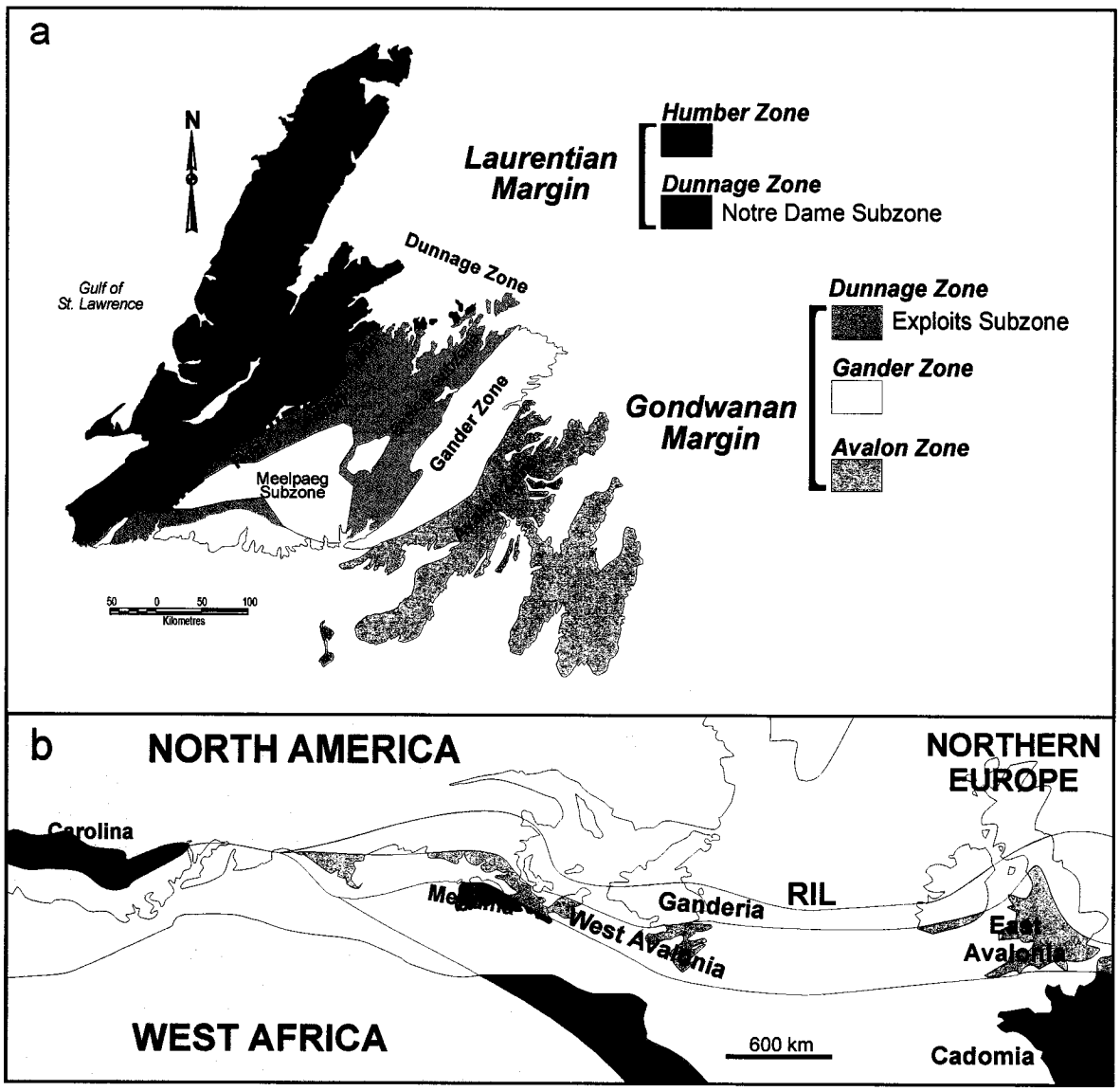

Figure A2-1 a) Lithotectonic zones of the Newfoundland Appalachians (modified after Williams et al., 1988). Highlighted region indicates the regional extent of the Sandy Brook and Tally Pond Groups. b) Early Mesozoic reconstruction of the North Atlantic showing the location of Ganderia and Avalonia, along with related peri-Gondwanan terranes (modified after Nance and Murphy, 1994; Nance et al., 2002).

Figure A2-2 Bedrock geological map of the Tally Pond Group, Victoria Lake Supergroup and adjacent sequences in central Newfoundland (modified after Rogers and van Staal (2005), Rogers et al. (2005a, b), van Staal et al. (2005) and references therein). Selected mineral deposits:- B – Boundary; Bo – Bobby's Pond; BP – Burnt Pond; Da – Daniel's Pond; DP – Duck Pond; JP – Jack's Pond; L – Lemarchant; LL – Long Lake; TE – Tulks East; VM – Victoria Mine.

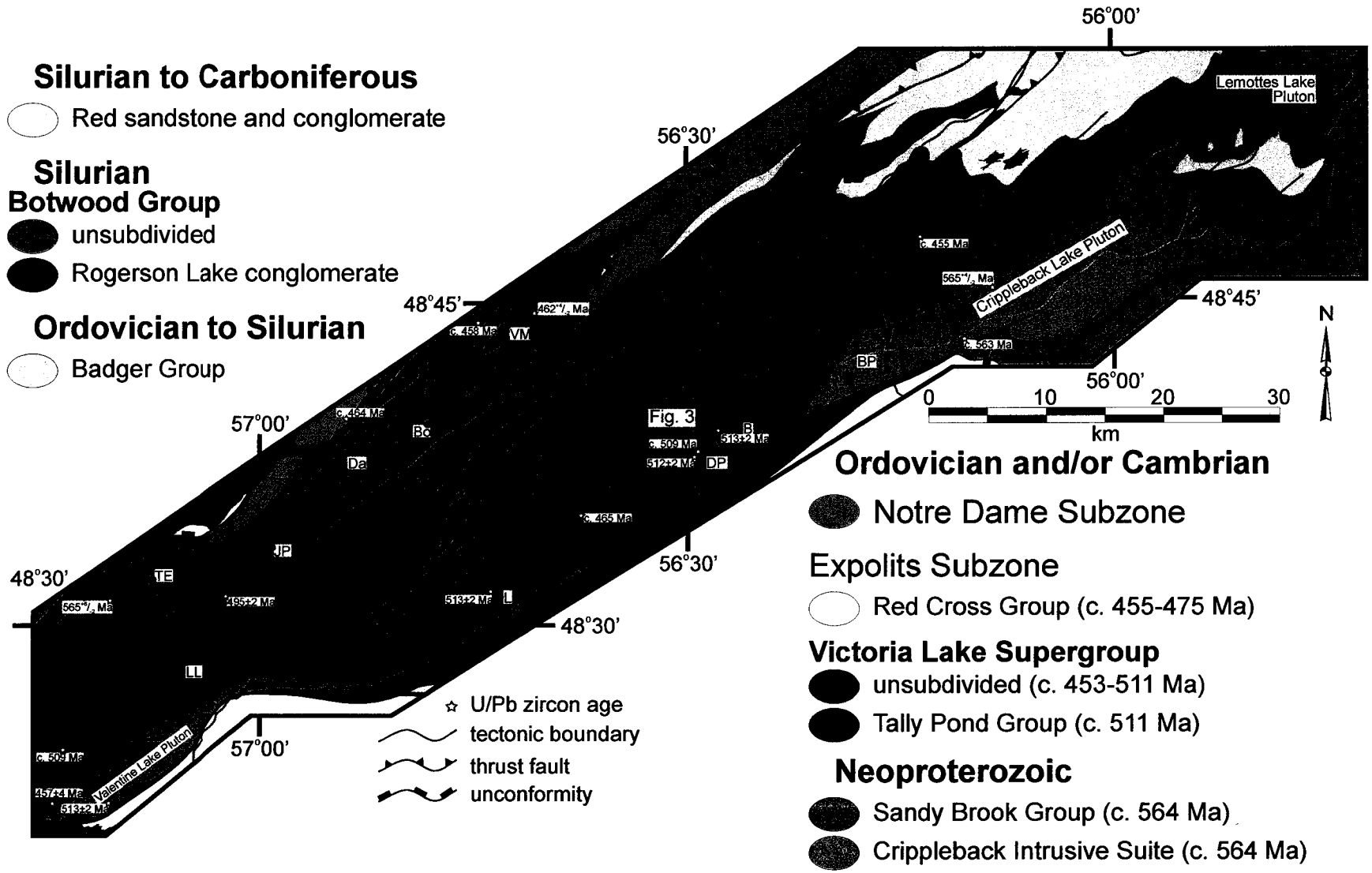
Silurian to Carboniferous
Red sandstone and conglomerate
Silurian
Botwood Group
unsubdivided
Rogerson Lake conglomerate
Ordovician to Silurian
Badger Group
Ordovician and/or Cambrian
Notre Dame Subzone
Expolits Subzone
Red Cross Group (c. 455-475 Ma)
Victoria Lake Supergroup
unsubdivided (c. 453-511 Ma)
Tally Pond Group (c. 511 Ma)
Neoproterozoic
Sandy Brook Group (c. 564 Ma)
Cripplebeck Intrusive Suite (c. 564 Ma)
U/Pb zircon age
tectonic boundary
thrust fault
unconformity
56°00'
56°30'
57°00'
48°45'
48°30'
Lemottes Lake Pluton
Cripplebeck Lake Pluton
Valentine Lake Pluton
Fig. 3
VM
BP
Bo
Da
DP
JP
TE
LL
L
B
N
0 10 20 30
km

Figure A2-3 Detailed bedrock geology of the Tally Pond Group (modified after Rogers and van Staal (2005), Rogers et al. (2005a, b), van Staal et al. (2005) and references therein). Extent of the map area is shown on Figure A2.2. Selected mineral deposits:- B – Boundary; BP – Burnt Pond; DP – Duck Pond; L – Lemarchant.

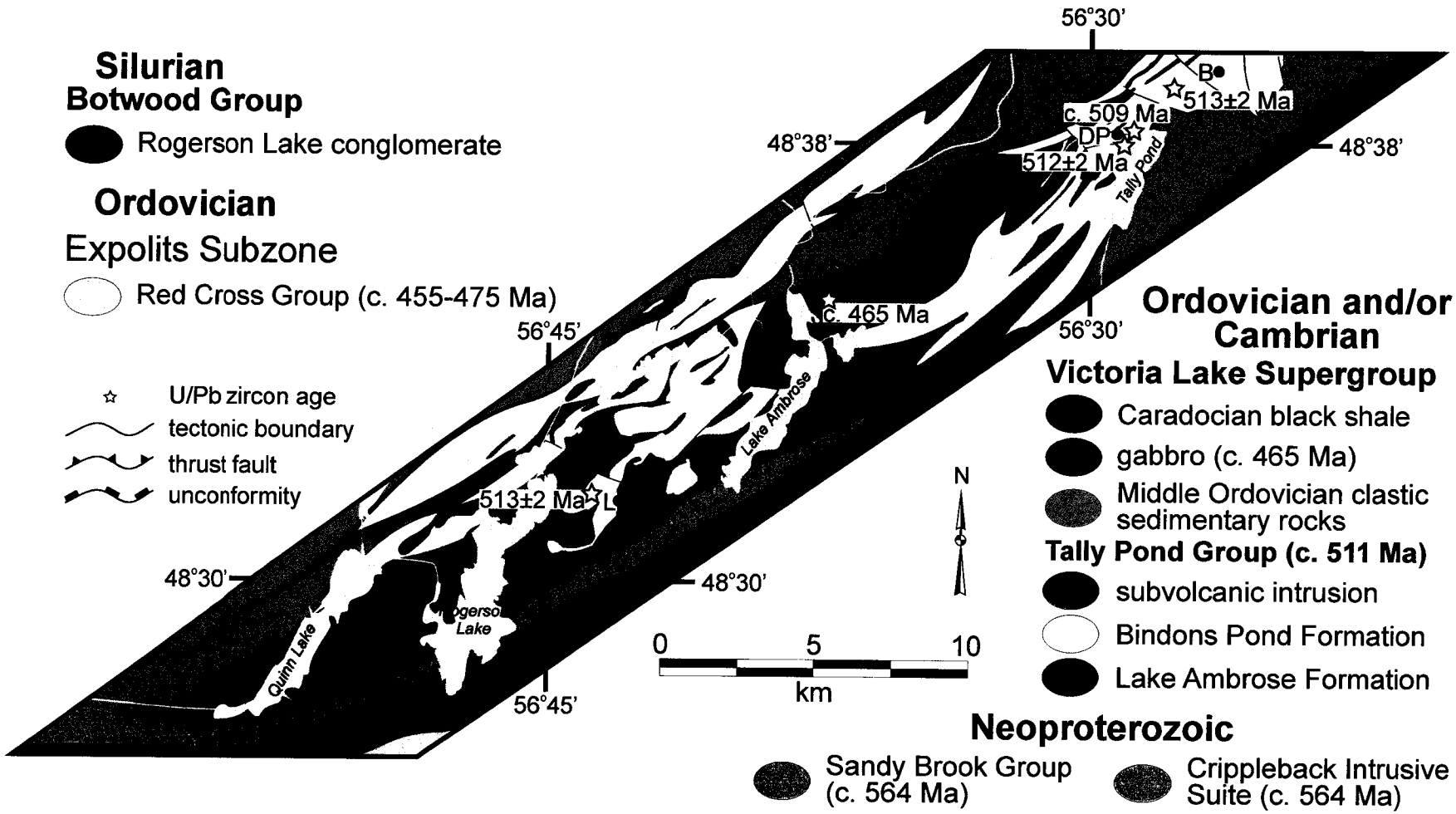
Silurian
Botwood Group
Rogerson Lake conglomerate
Ordovician
Expolits Subzone
Red Cross Group (c. 455-475 Ma)
U/Pb zircon age
tectonic boundary
thrust fault
unconformity
56°30'
56°45'
48°38'
48°30'
513±2 Ma
c. 509 Ma
512±2 Ma
c. 465 Ma
Tally Pond
Lake Ambrose
Quinn Lake
Lake
N
0
5
10
km
Ordovician and/or Cambrian
Victoria Lake Supergroup
Caradocian black shale
gabbro (c. 465 Ma)
Middle Ordovician clastic sedimentary rocks
Tally Pond Group (c. 511 Ma)
subvolcanic intrusion
Bindons Pond Formation
Lake Ambrose Formation
Neoproterozoic
Sandy Brook Group (c. 564 Ma)
Crippleback Intrusive Suite (c. 564 Ma)

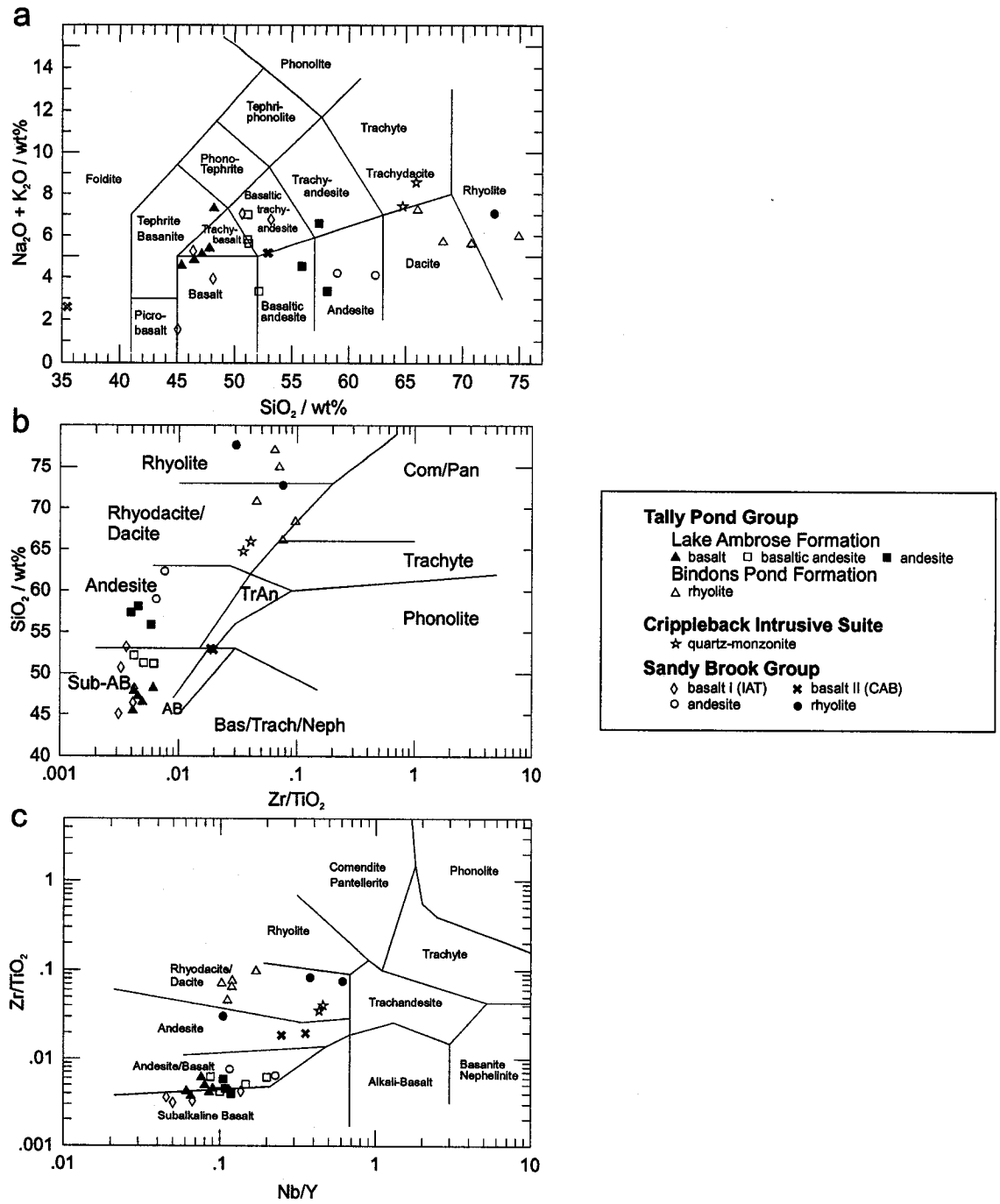

Figure A2-4 Lithological discrimination plots: a) SiO2 Na2O + K20 (LeBas et al., 1986); b) Zr/TiO2 SiO2 (Winchester and Floyd, 1977); c) Nb/Y Zr/TiO2 (Winchester and Floyd, 1977)

.

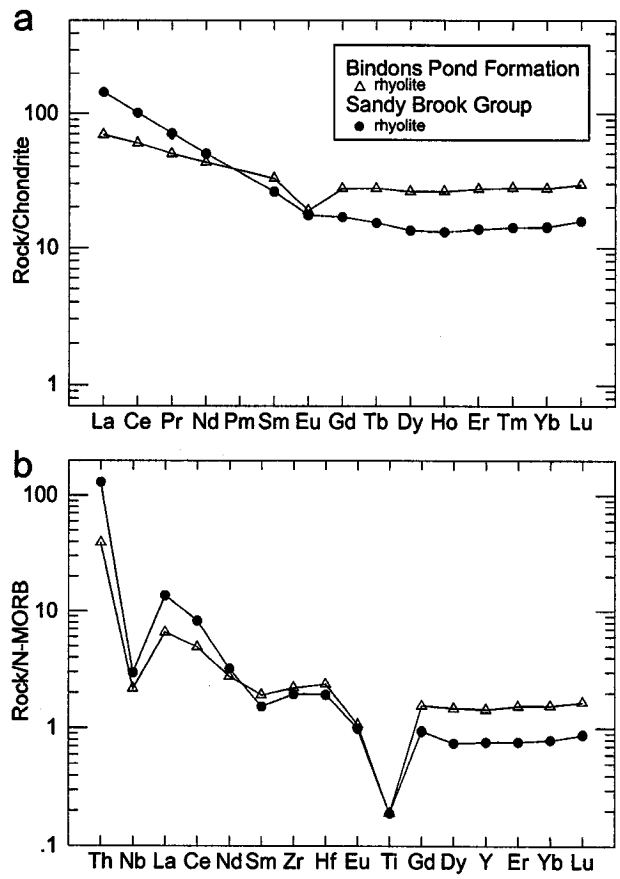

Figure A2-5 a) Mean, chondrite normalised REE profile for the rhyolitic rocks within this study (normalisation factors after Sun and McDonough, 1989). b) Mean, MORB normalised multi-element spidergram for the rhyolitic rocks within this study (normalisation factors after Sun and McDonough, 1989).

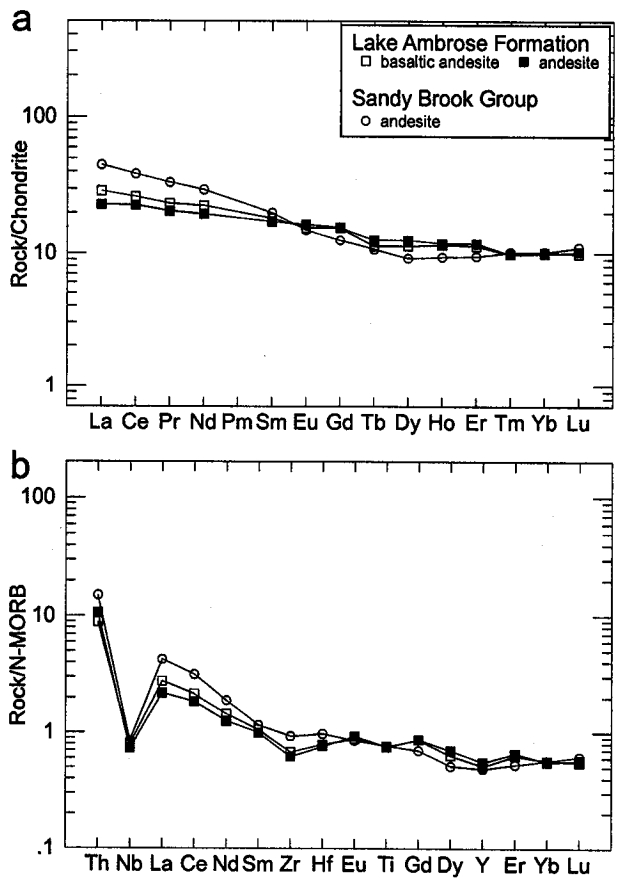

Figure A2-6 a) Mean, chondrite normalised REE profile for the andesitic rocks within this study (normalisation factors after Sun and McDonough, 1989). b) Mean, MORB normalised multi-element spidergram for the andesitic rocks within this study (normalisation factors after Sun and McDonough, 1989).

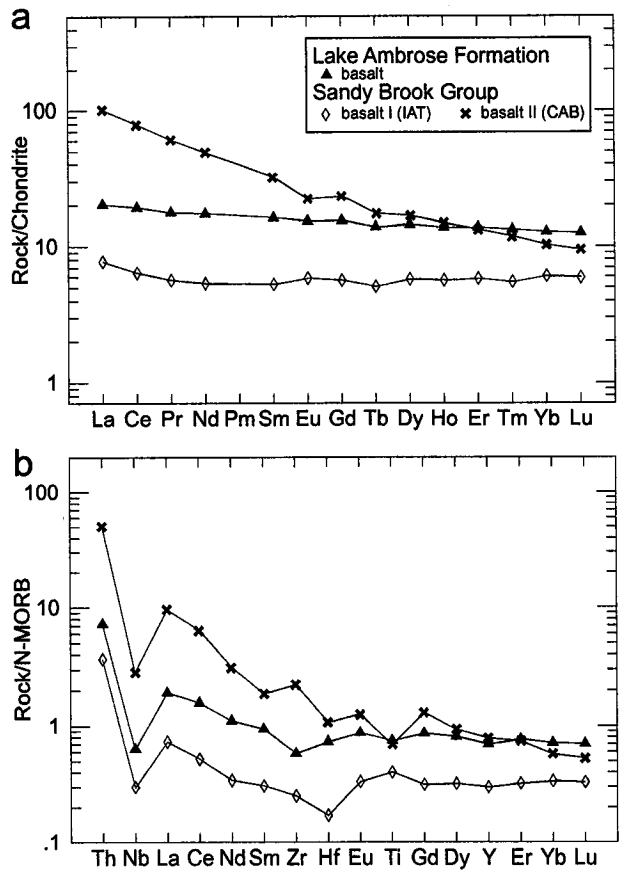

Figure A2-7 a) Mean, chondrite normalised REE profile for the basaltic rocks within this study (normalisation factors after Sun and McDonough, 1989). b) Mean, MORB normalised multi-element spidergram for the basaltic rocks within this study (normalisation factors after Sun and McDonough, 1989).

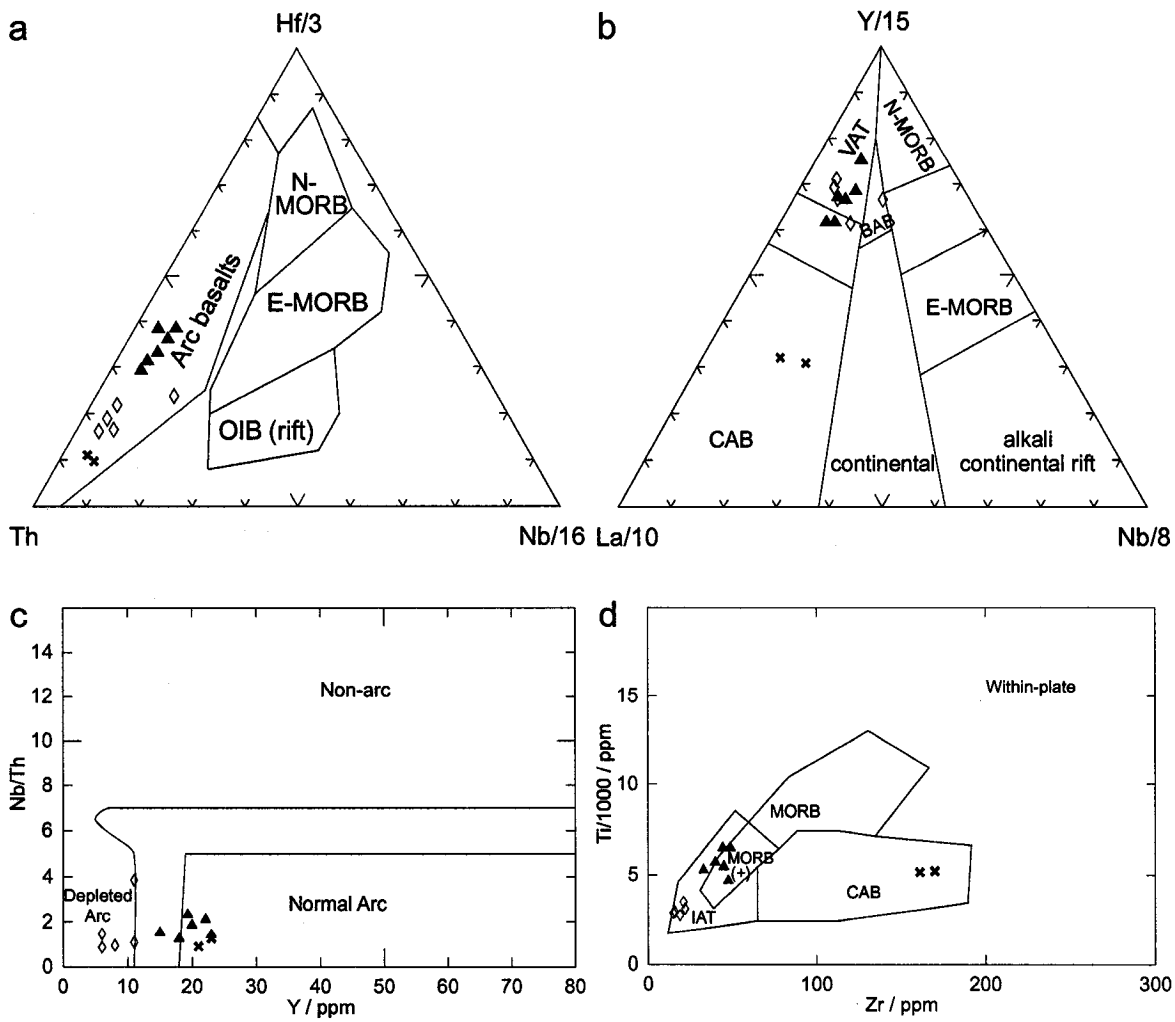

Figure A2-8 Mafic volcanic tectonic discrimination plots: a) Th Hf/3 Nb/16 (Wood, 1980); b) La/10 Y/15 Nb/8 (Cabanis and Lecolle, 1989); c) Y Nb/Th (Swinden et al., 1989); d) Zr Ti/1000 (modified after Pearce and Cann, 1973, and Pearce, 1982).

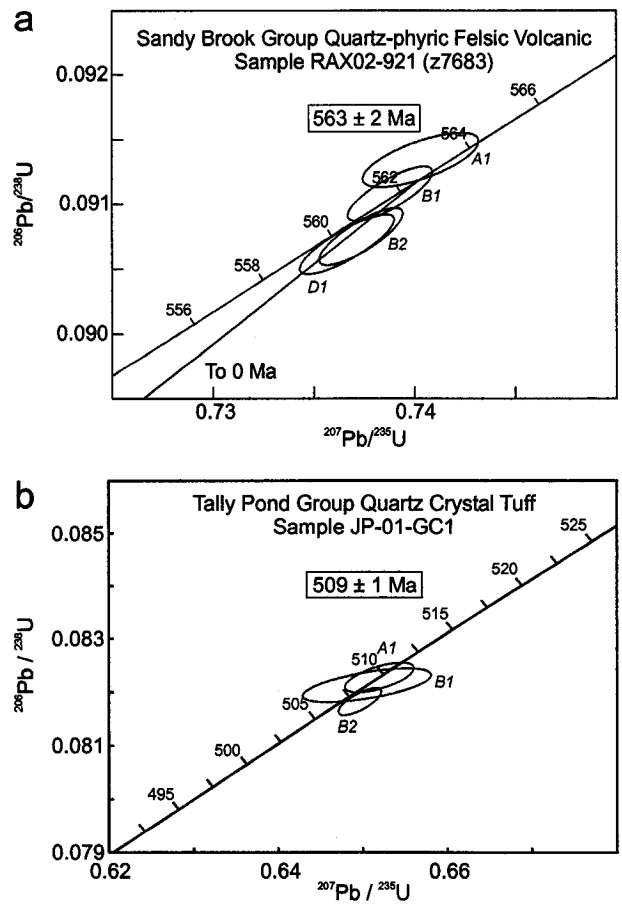

Figure A2-10 U/Pb zircon concordia plots for the dated samples.

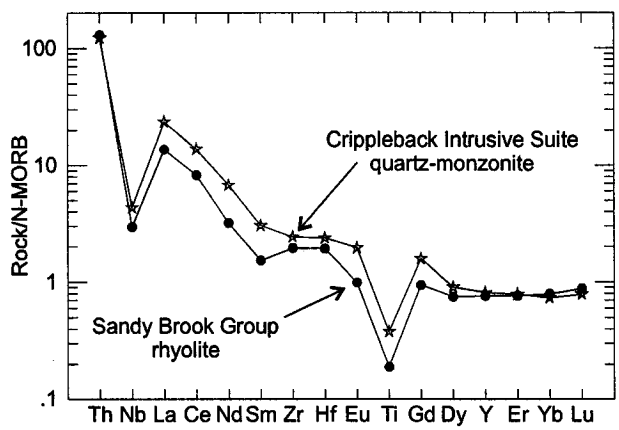

Figure A2-9 Comparison on a MORB normalised multi-element spidergram of mean whole-rock chemical analyses for Sandy Brook Group rhyolitic rocks and quartz-monzonite from the Crippleback Intrusive Suite. Normalisation factors after Sun and McDonough (1989).

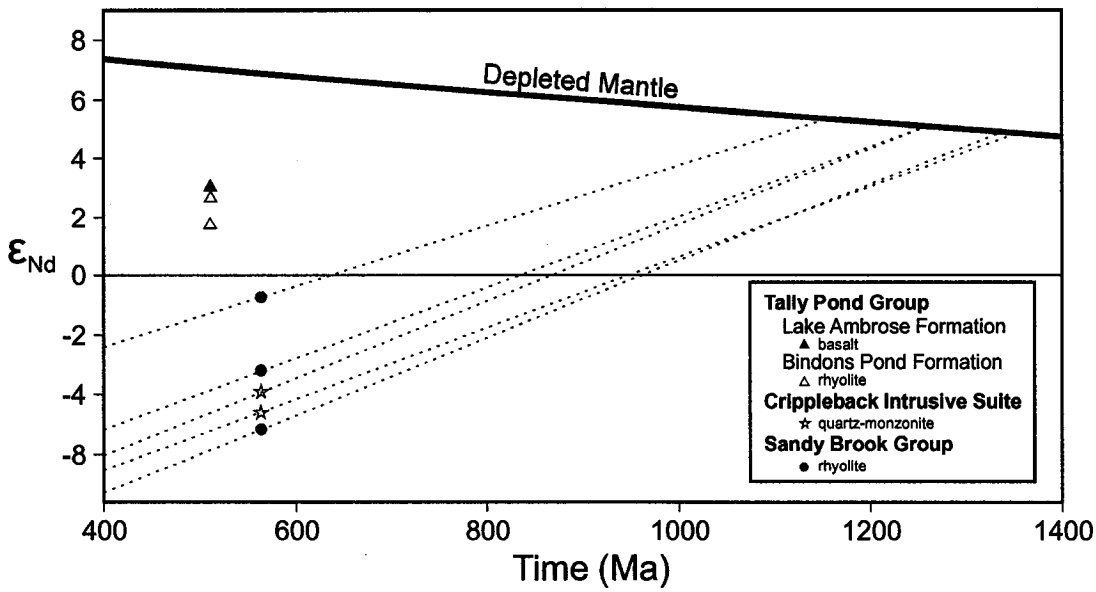

Figure A2-11 ε_{Nd} time plot showing the Nd isotopic evolution curves for the Crippleback Intrusive Suite quartz-monzonite and Sandy Brook Group rhyolitic rocks. Depleted mantle evolutionary curve based on DePaolo (1981).

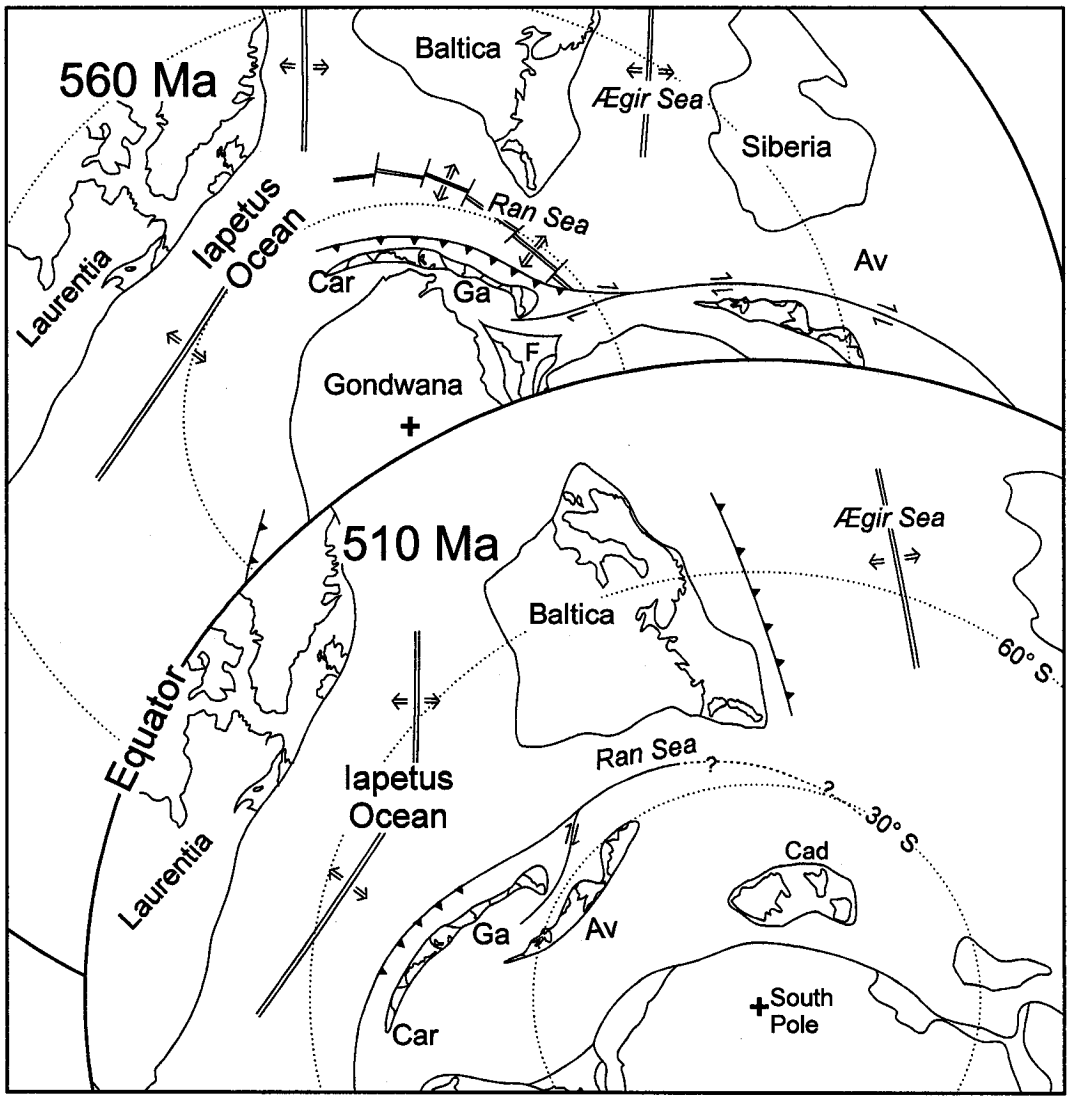

Figure A2-12 Tectonic reconstructions of the distribution of the continental landmasses within the southern hemisphere at 560 and 510 Ma. Nomenclature for the oceanic terranes follows Hartz and Torsvik (2002). The reconstruction is primarily based on palaeomagnetic data and geological correlations outlined in Nance and Murphy (1994), van Staal et al. (1998), Cocks and Torsvik (2002), Hartz and Torsvik (2002), Nance et al. (2002) and Stampfli and Borel (2002) and references therein. With the exception of Avalonia and Ganderia, detailed analysis of the merits of the various orientations of the continetal blocks as presented in the aforementioned publications is beyond the scope of this study, and thus their positions should not be considered definitive. The position of the spreading centres and active margins are largely representational and not necessarily exhaustive (i.e., in the 510 Ma reconstruction the active margin outboard of Ganderia and Avalonia may extend past Cadomia cf. Stampfli and Borel, 2002). A = Avalonia; Cad = Cadomia; Car = Carolina Terrane; F = Florida; Ga = Ganderia.

Table A2.1: Representative whole-rock chemical compositions for Neoproterozoic igneous rocks within the study area.

		Cripplebeck Intrusive Suite		**Sandy Brook Group**							
		quartz-monzonite		rhyolite		andesite		basalt I (IAT)		basalt II (CAB)	
		σ	S.D.	σ	S.D.	σ	S.D.	σ	S.D.	σ	S.D.
SiO_2	wt%	65.33	0.83	77.36	4.41	60.66	2.36	48.69	3.27	52.9	0.08
TiO_2	wt%	0.48	0.04	0.24	0.05	0.97	0.24	0.51	0.05	0.87	0.01
Al_2O_3	wt%	16.45	0.57	13.58	2.12	21.66	1.1	18.87	1.42	18.27	0.15
Fe_2O_3t	wt%	4.32	0.76	1.44	0.26	8.21	1.72	12.27	1.51	8.42	0.08
MnO	wt%	0.12	0.07	0.01	0.01	0.09	0.03	0.22	0.06	0.19	0
MgO	wt%	1.81	0.64	0.19	0.21	0.88	0.44	6.14	1.73	5.91	0.09
CaO	wt%	1.08	0.11	0.14	0.15	0.31	0.05	4.76	3.24	5.63	0.03
Na_2O	wt%	3.64	1.53	1.67	1.9	1	0.25	4.57	2.08	4.45	0.01
K_2O	wt%	4.34	0.71	3.3	0.13	3.17	0.31	0.34	0.44	0.7	0.01
P_2O_5	wt%	0.19	0.06	0.06	0.02	0.25	0.01	0.03	0.01	0.2	0.01
LOI	wt%	2.2	0.56	1.89	0.23	3.42	0.33	5.09	1.37	3.45	0
Total	wt%	99.94	0.01	99.87	0.19	100.62	0.16	100.26	0.13	100.13	0.01
Ba	ppm	1470	0	976.97	453.26	543.34	237.72	137.2	58.57	492	2.83
Cr	ppm	14.24	7.06	10.66	5.81	9.37	0.33	---	---	---	---
Cs	ppm	3.39	1.88	1.69	0.31	1.48	0.27	1.61	2.24	1.06	0.03
Hf	ppm	4.85	0.21	3.93	1.1	2	0.71	0.35	0.07	2.21	0
Nb	ppm	10.1	0.4	6.89	3.82	1.98	0.46	0.7	0.46	6.65	2.05
Ni	ppm	4.9	3.11	2.03	1.63	10.89	2.54	---	---	---	---
Pb	ppm	10.95	9.97	24.43	8.17	20.2	10.75	---	---	---	---
Rb	ppm	156.05	48.35	118.61	20.15	72.19	13	10	14.18	16	0
Sc	ppm	5.67	4.14	4.35	1.72	23	2.84	44.4	7.6	23	1.41
Sr	ppm	331.85	142.06	57.9	47.1	59.75	20.72	211.4	76.76	712.5	14.85
Ta	ppm	0.72	0.13	0.57	0.45	0.12	0.05	0.17	0.19	0.44	0.04
Th	ppm	14.7	5.62	15.59	12.04	1.81	1.01	0.44	0.04	6.05	0.49
U	ppm	3.46	1.17	3.45	1.95	0.83	0.19	0.11	0.05	1.66	0.13
V	ppm	82.46	42.09	28.49	10.64	234.99	64.62	506.4	61.78	231	5.66
Y	ppm	22.66	0.04	21.36	5.53	13.61	8.94	8.4	2.51	22	1.41
Zr	ppm	178.8	4.53	143.87	53.25	69	24.75	18.6	3.05	165.5	6.36
La	ppm	58.87	11.74	34.29	14.94	10.61	0.86	1.84	0.33	23.96	0.73
Ce	ppm	103.67	15.94	62	24.4	23.54	2.79	3.93	0.67	48.3	1.7
Pr	ppm	13.21	2.88	6.74	2.28	3.17	0.47	0.54	0.12	5.8	0.19
Nd	ppm	49.39	12.03	23.35	5.74	13.8	1.73	2.51	0.58	22.99	0.57
Sm	ppm	7.99	1.56	4	0.32	3.05	0.04	0.81	0.19	4.93	0.08
Eu	ppm	1.98	0.41	1.01	0.07	0.87	0.03	0.34	0.09	1.29	0.01
Gd	ppm	5.77	0.81	3.47	0.27	2.57	0.59	1.16	0.34	4.78	0.1
Tb	ppm	0.83	0.1	0.57	0.1	0.4	0.22	0.19	0.06	0.65	0.04
Dy	ppm	4.11	0.37	3.41	0.9	2.33	1.39	1.46	0.43	4.25	0.34
Ho	ppm	0.78	0.04	0.74	0.24	0.53	0.35	0.32	0.09	0.84	0.08
Er	ppm	2.33	0.04	2.27	0.64	1.57	1.09	0.96	0.28	2.21	0.3
Tm	ppm	0.37	0.03	0.36	0.08	0.26	0.17	0.14	0.05	0.3	0.04
Yb	ppm	2.25	0.01	2.42	0.64	1.73	1.22	1.03	0.31	1.74	0.13
Lu	ppm	0.36	0.01	0.4	0.11	0.28	0.18	0.15	0.04	0.24	0.03
		n = 2		n = 3		n = 2		n = 5		n = 2	

Table A2.2: Representative whole-rock chemical compositions for the Tally Pond Group volcanic rocks

		Tally Pond Group							
		Lake Ambrose Formation						Bindons Pond Formation	
		basalt		basaltic andesite		andesite		rhyolite	
		σ	S.D.	σ	S.D.	σ	S.D.	σ	S.D.
SiO_2	wt%	44.59	6.01	51.42	0.49	57.13	1.14	71.42	4.56
TiO_2	wt%	0.95	0.12	0.96	0.36	0.95	0.32	0.24	0.04
Al_2O_3	wt%	15.43	2.04	18.75	2.39	15.4	1.13	13.36	1.81
Fe_2O_3t	wt%	10.48	2.21	10.51	1.16	11.35	1.11	3.01	0.92
MnO	wt%	2.19	3.11	0.14	0.08	0.1	0.03	0.38	0.71
MgO	wt%	5.78	4.36	5.9	1.44	3.67	1.78	1.13	1.11
CaO	wt%	8.6	7.34	2.86	2.64	3.47	0.28	1.62	1.21
Na_2O	wt%	3.3	0.96	4.63	0.95	3.99	1.62	3.64	0.84
K_2O	wt%	1.6	1	0.81	0.92	0.82	0.62	2.23	1.47
P_2O_5	wt%	0.12	0.04	0.2	0.12	0.07	0.09	0.05	0.01
LOI	wt%	8.39	4.13	5.02	0.73	4.16	1.84	2.76	1.48
Total	wt%	100.67	0.81	100.38	0.23	100.41	0.47	99.85	0.37
Ba	ppm	301.97	122.72	283.09	295.94	96.47	80.59	309.63	182.9
Cr	ppm	71.63	83.36	26.41	---	4	---	14.62	6.12
Cs	ppm	0.45	0.43	0.49	0.4	1.15	1.12	0.99	0.51
Hf	ppm	1.51	0.2	1.62	0.54	1.56	0.7	4.84	0.75
Nb	ppm	1.49	0.28	1.84	0.53	1.7	0.51	5.03	1.51
Ni	ppm	36.46	15.88	10.48	---	16.42	---	3.77	2.23
Pb	ppm	2.99	0.92	7.5	---	4.1	---	4.52	1.79
Rb	ppm	17.35	13.89	20.17	17.76	20.08	14.64	34.42	10.39
Sc	ppm	36.7	7.53	34.42	7.78	31.08	3.88	10.76	3.42
Sr	ppm	172.49	51.45	229.8	293.85	97.13	84.13	101.47	18.22
Ta	ppm	0.12	0.03	0.11	0.05	0.19	0.1	0.37	0.16
Th	ppm	0.87	0.13	1.07	0.23	1.28	0.55	4.7	2.23
U	ppm	0.48	0.24	0.85	0.68	0.91	0.84	1.58	0.58
V	ppm	333.03	73.4	369.25	65.15	330.24	43.69	15.71	14.6
Y	ppm	19.58	2.89	14.32	3.54	15.42	4.58	40.12	5.67
Zr	ppm	43.18	5.87	50.18	15.72	45.63	20.06	162.85	16.5
La	ppm	4.79	1.73	6.85	1.82	5.44	1.94	16.36	6.41
Ce	ppm	11.77	3.39	16.04	4	13.87	5.13	36.64	12.9
Pr	ppm	1.68	0.4	2.22	0.44	1.95	0.69	4.73	1.47
Nd	ppm	8.1	1.62	10.5	1.68	9.14	3.38	20.08	5.99
Sm	ppm	2.48	0.48	2.79	0.6	2.63	1.04	5.01	1.02
Eu	ppm	0.89	0.17	0.9	0.09	0.95	0.44	1.09	0.23
Gd	ppm	3.18	0.47	3.19	0.7	3.2	1.32	5.65	1.18
Tb	ppm	0.52	0.1	0.42	0.08	0.47	0.15	1.03	0.21
Dy	ppm	3.68	0.58	2.87	0.77	3.18	1.25	6.65	1.11
Ho	ppm	0.78	0.12	0.65	0.17	0.67	0.22	1.49	0.2
Er	ppm	2.28	0.37	1.86	0.57	1.95	0.67	4.53	0.39
Tm	ppm	0.34	0.04	0.25	0.06	0.25	0.06	0.71	0.06
Yb	ppm	2.18	0.31	1.72	0.31	1.69	0.48	4.69	0.34
Lu	ppm	0.32	0.05	0.25	0.06	0.26	0.05	0.75	0.04
		n = 6		n = 4		n = 3		n = 5	

Table A2.3: Nd isotopic data for selected samples within the study area. Age determinations are by U/Pb zircon geochronology and regional correlation. Model ages (T_{DM}) are calculated after DePaulo (1981).

Sample	Unit	Nd ppm	Sm ppm	Measured $^{143}Nd/^{144}Nd$	Measured $^{147}Sm/^{144}Nd$	Age Ma	Epsilon Nd(t)	DePaulo T_{DM} / Ma
RAX01002	Lake Ambrose Formation basalt	4.64	1.82	0.512929	0.2368	511	**3.06**	
RAX02189	Bindons Pond Formation rhyolite	25.38	5.92	0.512587	0.1409	511	**2.64**	
RAX02214	Bindons Pond Formation rhyolite	11.48	2.94	0.512588	0.1547	511	**1.77**	
RAX02210	Crippleback quartz-monzonite	46.6	7.35	0.512064	0.0954	563	**-3.9**	1261
RAX02212	Crippleback quartz-monzonite	35.59	6.04	0.512056	0.1026	563	**-4.6**	1354
RAX02174	Sandy Brook Group rhyolite	14.74	2.84	0.512308	0.1164	563	**-0.67**	1153
RAX02176	Sandy Brook Group rhyolite	22.72	3.87	0.512128	0.103	563	**-3.21**	1260
RAX02921	Sandy Brook Group rhyolite	25.5	3.98	0.511995	0.0943	563	**-5.18**	1337

Table A2.4: U-Pb TIMS analytical data

Fraction[1]	Wt. (mg)	U (ppm)	Pb[2] (ppm)	$^{206}Pb/^{204}Pb$[3]	Pbc[4] (pg)	$^{208}Pb/^{206}Pb$	Isotopic Ratios[5] $^{206}Pb/^{238}U$	$^{207}Pb/^{235}U$	$^{207}Pb/^{206}Pb$	Ages[6] (Ma) $^{206}Pb/^{238}U$	$^{207}Pb/^{235}U$	$^{207}Pb/^{206}Pb$
RAX02-921 (Z7683): Sandy Brook Group - felsic volcanic (NAD83, UTM zone 21, 560464E - 5396564N)												
A1 (13): c,cl,rin,el,eu	18	334	34	1452	24	0.242	0.09134±0.0010	0.74031±0.00145	0.05878±0.00008	563.5 ± 1.2	562.6 ± 1.7	559 ± 6.2
B1 (18): c,cl,rin,eu,st	20	337	34	10144	4	0.241	0.09108±0.0010	0.73879±0.00106	0.05883±0.00005	561.9 ± 1.2	561.7 ± 1.2	560.8 ± 3.7
B2 (6): c,cl,eu,st	18	405	41	4103	10	0.229	0.09075±0.0011	0.73735±0.00104	0.05893±0.00005	560 ± 1.3	560.9 ± 1.2	564.4 ± 3.6
D1 (21): c,cl,rin,eu,st	20	393	40	2320	19	0.232	0.09069±0.0011	0.73665±0.00118	0.05891±0.00005	559.6 ± 1.3	560.5 ± 1.4	563.8 ± 3.9
JP-01-GC1 (Z7038): Tally Pond Group - quartz crystal tuff (NAD83, UTM zone 21, 541103E - 5389364N)												
A1 (32): st,f,c,in	16	89	8	741	10	0.162	0.08227±0.0017	0.6520±0.0031	0.05748±0.00024	510 ± 2	510 ± 3	510 ± 11
B1 (31): ti,f,c,cl	29	231	20	318	115	0.164	0.08212±0.0019	0.6505±0.0059	0.05745±0.00049	509 ± 2	507 ± 5	509 ± 22
B2 (43): ti,f,c,in	17	132	11	1817	6	0.166	0.08182±0.0016	0.6497±0.0020	0.05759±0.00013	507 ± 2	508 ± 2	514 ± 6

Notes:[1]Number in brackets is the number of grains in the analysis; morphologies: st=stubby prisms, ti=tips, f=well faceted, c=colourless to pale brown, cl=clear, in=numerous inclusions, rin=rare inclusions, el=elongate, eu=euhedral;[2]radiogenic Pb; [3]measured ratio, corrected for spike and fractionation; [4]total common Pb in picograms in analysis corrected for fractionation and spike; [5]corrected for blank Pb and U and common Pb, errors quoted are one sigma in percent;[6]corrected for blank and common Pb, errors quoted are two sigma.

APPENDIX 3: ASSEMBLY OF THE ANNIEOPSQUOTCH ACCRETIONARY TRACT, NEWFOUNDLAND APPALACHIANS: AGE- AND GEODYNAMIC CONSTRAINTS FROM SYN-KINEMATIC INTRUSIONS

Lissenberg, C.J., Zagorevski, A., McNicoll, V.J., van Staal, C.R., and Whalen, J.B.

The Journal of Geology, 2005, volume 113, p. 553-570

ABSTRACT

The Annieopsquotch Accretionary Tract (AAT) comprises several ophiolites and arc-back-arc igneous complexes that were accreted to the Dashwoods microcontinent during the Ordovician Taconic orogeny. The Lloyds River Fault Zone, which separates the AAT from the Dashwoods microcontinent, yielded $^{40}Ar/^{39}Ar$ hornblende ages of ca. 470 Ma. The fault zone was intruded syn-kinematically by the shoshonitic Portage Lake monzogabbro and the Pierre's Pond suite, which gave U/Pb zircon ages of 462 ± 2 Ma plus 464 ± 2 Ma and 459 ± 3 Ma, respectively. The Otter Pond granodiorite intruded syn-kinematically into the Otter Brook Shear Zone, which separates the Annieopsquotch ophiolite belt from the structurally underlying ophiolitic Lloyds River Complex. It yielded a U/Pb zircon age of 468 ± 2 Ma. The Buchans arc and its continental basement were accreted to the Lloyds River Complex prior to 468 Ma. Syn-kinematic plutons have arc affinity, with ε_{Nd} ranging between -0.9 and -6.8, and are coeval with the adjacent Notre Dame Arc. Our data thus suggest the majority of the AAT was accreted to the Dashwoods microcontinent by 468 Ma, when consanguineous, dominantly arclike plutons intruded within the AAT and adjacent Notre Dame Arc. The Portage Lake monzogabbro and Otter Pond mafic suite are more mafic than Notre Dame Arc plutons of similar age because of their intrusion into the thin, mafic crust of the AAT and ascent along shear zones. Our data indicate the formation and subsequent accretion of ophiolites and arc-back-arc complexes occurred within a very short time span (5 to10 Ma). The sources of AAT syn-orogenic magmatism are diverse and include melting of subarc mantle during slab breakoff, lithospheric mantle, and lower crust. The Ordovician Appalachian margin of Laurentia grew by the accretion of oceanic terranes and intrusion of mantle-derived magma. Recycling of continental crust by rifting and subsequent collision played an important part of the tectonic evolution of the AAT.

INTRODUCTION

The Annieopsquotch Accretionary Tract is a well-preserved Ordovician accretionary complex that occurs along the fundamental suture formed by the Ordovician-Silurian closure of the Iapetus Ocean, the Red Indian Line (Williams et al., 1988; van Staal et al., 1998). It comprises several fault-bounded, west-dipping slices of dominantly mafic arc-back arc complexes and ophiolites that formed in the upper plate above a west-dipping subducting slab and have been transferred from their original intra-oceanic setting to the peri-Laurentian Dashwoods microcontinent by underplating. Detailed mapping, in combination with extensive geochemistry and high-precision U-Pb and $^{40}Ar/^{39}Ar$ geochronology, have provided a tightly constrained geological framework for the Annieopsquotch Accretionary Tract, making it one of the best-documented examples of an Early Paleozoic accretionary complex. The Annieopsquotch Accretionary Tract thus provides a unique opportunity to study the processes involved in accretionary tectonics, and to evaluate the differences and similarities between Paleozoic and Mesozoic-Cenozoic accretionary orogeny. Of particular interest are the relative contributions of oceanic material and recycled continental crust and the sources involved in magmatism in accretionary tracts. These issues remain a subject of intense research and debate, particularly because of the role accretionary complexes play in continental growth (e.g., Sengör and Natal'in, 1996; Xiao et al., 2003).

In this appendix, we describe the results of $^{40}Ar/^{39}Ar$ geochronology of the shear zones that separate different units of the Annieopsquotch Accretionary Tract, and U/Pb geochronology and geochemistry of the plutons that intrude these shear zones. These data provide age constraints on juxtaposition of the different components of the Annieopsquotch Accretionary Tract, and constrain the geodynamic evolution of the Annieopsquotch Accretionary Tract. Linking the tectonic and magmatic events of the Annieopsquotch Accretionary Tract with those that took place in the adjacent Dashwoods microcontinent provides constraints on the overall tectonic evolution of the peri-Laurentian portion of the Newfoundland Appalachians during the Early to Late Ordovician Taconic orogeny (Williams and Hatcher 1983). We will demonstrate that: (1) the majority of the Annieopsquotch Accretionary Tract was accreted to Dashwoods by 468 Ma, indicating that accretion occurred within 5-10 Ma after formation of the units; (2) the Annieopsquotch Accretionary

Tract comprises an important component of recycled continental crust in addition to accreted oceanic crust, and sediments are notably absent; (3) plutons intruding the Annieopsquotch Accretionary Tract tapped variable sources (sub-arc mantle, lithospheric mantle, crust); (4) magmatism in the Annieopsquotch Accretionary Tract is related to the adjacent Notre Dame Arc, but is chemically more primitive owing to intrusion into thin, predominantly mafic crust of the Annieopsquotch Accretionary Tract and ascent along shear zones.

REGIONAL GEOLOGY

The Newfoundland Appalachians result from the closure of the Iapetus Ocean, which resulted in juxtaposition of Laurentia with several peri-Gondwanan continental blocks. Rocks formed within the oceanic realm of Iapetus are preserved in Newfoundland's Dunnage Zone (Williams, 1979). The Dunnage Zone has been subdivided into the peri-Laurentian Notre Dame and Dashwoods subzones, and the Exploits Subzone, which mainly has a peri-Gondwanan provenance (Williams et al., 1988; Williams, 1995; Fig. A3.1). The Notre Dame and Dashwoods subzones are separated from peri-Gondwanan rocks of the Exploits Subzone by the Red Indian Line (Williams et al., 1988; van Staal et al., 1998). Both the Notre Dame and Dashwoods subzones are dominated by granitoid arc plutons and associated volcanic rocks of the Notre Dame Arc (e.g., Whalen et al., 1987, 1997), ophiolites, and dominantly mafic arc-back arc complexes. Magmatism in the Notre Dame Arc was episodic, with major pulses in the Tremadoc, Llanvirn-Caradoc, and Ashgill-Wenlock (van Staal et al., 2003; Whalen et al., 2003). Ophiolites occur in three distinct belts: the Lushs Bight and Baie Verte oceanic tracts, which overlie metasedimentary rocks of the Notre Dame and Humber (sub)zones, respectively (e.g., Swinden et al., 1997), and the Annieopsquotch ophiolite belt (Annieopsquotch ophiolite belt; Appendix A1). The Annieopsquotch ophiolite belt, along with most mafic arc-back arc complexes, occurs in a linear belt along the eastern margin of the Notre Dame Subzone. Together, these rocks are referred to as the Annieopsquotch Accretionary Tract (van Staal et al., 1998). The Dashwoods Subzone generally exposes a deeper crustal level than the Notre Dame Subzone and has a larger sedimentary component (e.g., the amphibolite- to granulite-facies Cormacks Lake Complex; Pehrsson et al., 2003), but both share a common Ordovician tectonic history (Pehrsson et al., 2003).

It has been inferred on the basis of isotopic and geochronological studies (e.g., Swinden et al., 1997; Whalen et al., 1997), combined with tectonic relationships, that both subzones are underlain by thinned continental crust, which is interpreted as a ribbon-shaped microcontinent, referred to as Dashwoods, that rifted-off of the Laurentian margin during the Early Cambrian (Waldron and van Staal, 2001). During the Cambrian to Early Ordovician the Dashwoods microcontinent was separated from Laurentia by the Humber Seaway. The Humber Seaway was closed by east-directed subduction underneath the Dashwoods microcontinent in the Tremadoc, leading to the first magmatic phase of the Notre Dame Arc, and ended with the collision between Laurentia and the Dashwoods microcontinent by at least 475 Ma (Waldron and van Staal, 2001). This collision is thought to have resulted in slab break-off of the oceanic portion of the Laurentian slab, generating the second pulse of Notre Dame arc magmatism (van Staal et al., 2003; Whalen et al., 2003), and initiated convergence to the east (i.e. outboard) of the Dashwoods microcontinent, leading to the formation of a west-dipping subduction zone that was responsible for formation of the units now preserved within the Annieopquotch Accretionary Tract (Chapter 1; Appendix A1).

THE ANNIEOPSQUOTCH ACCRETIONARY TRACT

The Annieopsquotch Accretionary Tract is the easternmost unit of the Notre Dame Subzone, and is defined as a complex east-vergent thrust stack of ophiolites and arc-back arc complexes that is bounded by the Lloyds River Fault Zone (Lloyds River Fault Zone; Lissenberg 2005) and Hungry Mountain Thrust to the west and by the Red Indian Line to the east (Fig. A3.1; van Staal et al., 1998). Each thrust slice becomes progressively younger to the east (Thurlow et al., 1992; Chapter 2), suggesting sequential accretion to the Dashwoods microcontinent (van Staal et al., 1998). Sedimentary rocks are scarce within the Annieopsquotch Accretionary Tract, allowing detailed reconstruction of the relationships among the various mafic oceanic complexes. The different components of the Annieopsquotch Accretionary Tract are mainly separated by northwest-dipping, amphibolite- to sub-greenschist-grade shear zones, which in many places have been intruded by plutonic rocks during assembly of the tract. Most of these shear zones are thought to be Ordovician in age, although some of them accommodated out of sequence movement (e.g., Thurlow et al., 1992) or Silurian reactivation (Zagorevski and van Staal, 2002). The Annieopsquotch

Accretionary Tract has a structural thickness varying from 8 to 15 km, and comprises, from top to bottom, the Annieopsquotch ophiolite belt (Appendix A1), the younger Lloyds River Ophiolite Complex (Chapter 2), the mature arc volcanic sequence of the Buchans Group (Swinden et al., 1997), and the younger arc-back arc succession of the Red Indian Lake Group (Fig. A3.2; Chapter 2). In addition, the Annieopsquotch Accretionary Tract contains a suite of syn-kinematic plutonic and syn-orogenic volcanic and associated metasedimentary rocks, termed the Otter Pond Complex (Figs. A3.1 & A3.2; defined below). The limited structural thickness of the tract suggests parts of the units are currently missing. This likely resulted from strike slip movements that accompanied accretion of the Annieopsquotch Accretionary Tract (Chapter 4; Zagorevski and van Staal, 2002), and possibly from subduction of some elements or parts thereof.

The Annieopsquotch ophiolite belt (481-478 Ma; Dunning and Krogh, 1985) is defined as a band of ophiolite complexes and fragments that extends for c. 200 km along the eastern margin of the Notre Dame Subzone (Fig. A3.1; Appendix 1). Its main components are the Annieopsquotch, Star Lake and King George IV ophiolites, all of which lack the mantle section and lowermost crust, but are otherwise intact (Fig. A3.1). Correlative ophiolitic fragments occur along strike within the Hungry Mountain Complex (Whalen et al., 1997), and on the north coast of Newfoundland within the Hall Hill Complex (Bostock, 1988). The ophiolite belt records early boninitic magmatism followed by a tholeiitic phase, and is interpreted to have formed during initiation of west-directed subduction outboard of the Dashwoods microcontinent following the Dashwoods-Laurentia collision (Appendix 1). The Annieopsquotch ophiolite belt is separated from the Dashwoods microcontinent by the Lloyds River Fault Zone. The Lloyds River Fault Zone is marked by highly strained amphibolites, separated by lenticular bodies of less deformed plutonic rocks, and comprises three major northwest-dipping shear zones (the northwestern, central and southeastern shear zones; Figs. A3.2, A3.3a). The three shear zones are characterized by predominantly steeply northwest-dipping foliations with moderately (40-60°) north to northeast-dipping lineations, and record sinistral oblique underthrusting of the Annieopsquotch ophiolite belt beneath the Dashwoods microcontinent (Lissenberg 2005). This interpretation is consistent with the sense of motion observed in

amphibolite-facies mylonites that define the Hungry Mountain Thrust, the equivalent of the Lloyds River Fault Zone immediately north of the town of Buchans (e.g., Calon and Green, 1987).

The structurally underlying Lloyds River Complex is an ophiolitic sliver comprised of gabbro, anorthosite, sheeted dykes and pillow lava, which are geochemically distinct from the Annieopsquotch ophiolite belt, and yielded an age of 473 Ma (Chapter 2). It is interpreted to have originated in a back-arc basin to the Buchans arc (Chapter 2). The Lloyds River Complex is separated from the Annieopsquotch ophiolite belt by the Otter Brook Shear Zone (Fig. A3.1). The Otter Brook Shear Zone is a northwest-dipping amphibolite to greenschist facies shear zone characterized by mylonite, mica schist, and phyllonite with strong northeast-trending foliations and north-northeast-plunging lineations (Fig. A3.3b; Zagorevski and van Staal, 2002). It records an important phase of sinistral oblique underthusting of the Lloyds River Complex beneath the Annieopsquotch ophiolite belt (Zagorevski and van Staal, 2002).

The Otter Pond Complex is defined herein as a distinct suite of plutonic rocks and associated highly deformed felsic volcanic and metasedimentary rocks, which is spatially associated with the Otter Brook Shear Zone. The volcano-sedimentary rocks (rhyolite, amphibolite, garnet-mica schist, and graphitic schist) are contained within strands of the Otter Brook Shear Zone, whereas the plutonic rocks intrude both within the shear zone and within surrounding units (Fig. A3.1). The plutonic rocks of the Otter Pond Complex have been subdivided into a mafic suite, which comprises generally hornblende porphyritic to oikocrystic gabbros, diorites, and associated mafic dykes, and a granodiorite suite. The mafic suite predominantly intruded the Annieopsquotch ophiolite, both as a c. 2 by 2 km sized, medium-grained pluton (Fig. A3.1), and as metre wide, (very) fine-grained dykes. Otter Pond mafic dykes have also been observed to intrude sheeted dykes of the Star Lake and King George IV ophiolites (Fig. A3.1). The main body of the granodiorite suite intruded the southeastern margin of the Annieopsquotch ophiolite, forming an elongate body (c. 5 by 0.7 km) parallel to the Otter Brook Shear Zone (Fig. A3.1). In addition, the granodiorite suite occurs as metre-scale sheets intruding amphibolites of the Otter Brook Shear Zone and as subordinate aphanitic, locally flow-banded dykes that intrude the Annieopsquotch ophiolite and Lloyds River Complex. The granodiorite is chemically similar to the aphanitic dykes and rhyolite of

the volcano-sedimentary sequence (see below), suggesting that together they form part of a consanguineous suite of shallow plutonic-volcanic bodies. These relationships suggest that the Otter Pond Complex formed by intrusion and local extrusion and sedimentation along the Otter Brook Shear Zone during thrusting of the Lloyds River Complex underneath the Annieopsquotch ophiolite belt.

The Lloyds River Complex is separated from the structurally underlying Buchans Group (473 Ma; Dunning et al., 1987) and Red Indian Lake Group (464 Ma; Chapter 2) by a series of southeast-directed, ductile-brittle thrusts in the Buchans area (Calon and Green, 1987; Thurlow and Swanson, 1987; Thurlow et al., 1992); similar kinematic relationships have been found elsewhere along strike (Zagorevski et al., 2003). Geochemical and isotopic data suggest that the Buchans Group (and its northeastern equivalent, the Robert's Arm Group; Bostock, 1988) represents a volcanic arc that was formed on continental basement (Swinden et al., 1997; Chapter 2). It is postulated to have formed on a sliver of continental crust that rifted off of the Dashwoods microcontinent and was emplaced outboard of the Annieopsquotch ophiolite belt and Lloyds River Complex by trench-parallel strike-slip movement (Chapter 2). Rifting of the Buchans arc at 464 Ma produced an ensimatic back arc basin and younger arc phase, both preserved in the Red Indian Lake Group, which was subsequently thrust beneath the Buchans Group (Chapter 2). The Red Indian Lake Group is bounded to the southeast by the Red Indian Line, which separates it from the peri-Gondwanan arc-back arc complexes of the Exploits Subzone (Figs. A3.1, A3.2; van Staal et al., 1998; Chapter 2).

PLUTONIC ROCKS WITHIN THE ANNIEOPSQUOTCH ACCRETIONARY TRACT

Several units of plutonic rocks intrude into the Annieopsquotch Accretionary Tract and its boundaries, and are concentrated around the Lloyds River Fault Zone and the Otter Brook Shear Zone. In this section, we will discuss their geological relationships, whole-rock geochemistry and Nd-isotope geochemistry. Analytical techniques are described in Appendix 2, and detection limits and sample locations are given in Rogers (2004). Whole-rock geochemical data are listed in Table A3.1, and Nd-isotopic data in Table A3.2.

Pierre's Pond suite

Along the northwestern and southeastern shear zones of the Lloyds River Fault Zone, mylonitic amphibolites of ophiolitic origin are intimately interlayered with centimeter- to meter-wide veins and sheets of foliated diorite and subordinate tonalite. In general, the amphibolites and intrusive rocks are heavily deformed. However, near Star Lake (Fig. A3.1), such tonalite-diorite sheets have intruded outside of the Lloyds River Fault Zone, directly into ophiolitic gabbro of the Star Lake ophiolite (Fig. A3.4). The diorite is composed of aligned hornblende and plagioclase with accessory quartz, biotite, titanite, and oxides, whereas the tonalite is composed of plagioclase, quartz, biotite, hornblende with accessory titanite and oxides. There is a marked contrast in deformation between the narrow zones of sheared intrusive rocks, which have foliations striking predominantly parallel to the southeastern shear zone, and the largely unfoliated host ophiolitic gabbro, which displays a partial greenschist-facies metamorphic overprint (randomly oriented clinozoisite-actinolite-chlorite) of an earlier static amphibolite-facies metamorphism. The amphibolite-facies assemblage in turn largely replaced the original igneous assemblage of clinopyroxene and plagioclase. These relationships suggest that the diorite and tonalite sheets localized deformation during intrusion, the heat of the intrusions and associated fluids producing a contact greenschist-facies metamorphism in the surrounding host gabbro (Lissenberg 2005). Given that the diorites and tonalites also intrude Lloyds River Fault Zone amphibolites, this interpretation suggests that they intruded the Lloyds River Fault Zone syn-kinematically. We interpret these sheets as well-exposed, small-scale examples of less well-exposed larger bodies of mixed diorite and tonalite that have intruded the northwestern portion of the Lloyds River Fault Zone and the Star Lake ophiolite at Star Lake (Fig. A3.1), and were defined as the Pierre's Pond suite by Whalen et al. (1997).

Geochemically, the Pierre's Pond suite is composed of both arc rocks, characterized by enrichment in LILE and Th over Nb, and non-arc rocks, which lack Th enrichment with respect to Nb (Whalen et al., 1997). The arc-like rocks were further subdivided into La-rich and La-poor groups. We analyzed several small-scale, syn-kinematic diorite and tonalite sheets on Star Lake. The tonalite analyses are similar to equivalent rocks of the Pierre's Pond suite of Whalen et al.

(1997; Fig. A3.5a), with the exception of the higher K_2O content in samples VL01J225A and 238C (see Table A3.1). This is likely related to alkali metasomatism, expressed by replacement of plagioclase by irregular patches of muscovite. The large negative Nb and Ti anomalies, and the enrichment in Th and LILE (Cs, Rb, Ba) relative to the REE of the tonalites are typical of arc tonalite (Fig. A3.5a). La/YbN (chondrite normalized) spans a large range (8 – 71), suggesting the tonalites in the Lloyds River Fault Zone resemble both the La-rich and La-poor arc-like groups of Whalen et al. (1997). The diorites show depletion in Nb, Zr and Ti, albeit less than the analysed tonalites, and enrichment in LILE and Th. La/Yb_N ranges from 3 to 7, typical of the La-poor arc-like group of the Pierre's Pond suite (Fig. A3.5b). Sample VL01J210B deviates from this pattern by its low Th/Nb ratio (Fig. A3.5b), indicative of a non-arc setting, similar to the non-arc group defined in the Pierre's Pond suite by Whalen et al. (1997). A dominantly arc origin for the tonalites and diorites is consistent with the La-Y-Nb (diorites; Cabanis and Lecolle, 1989) and Rb vs Y+Nb (tonalites; Pearce et al., 1984) tectonic discrimination diagrams (Fig. A3.6). One diorite sample was analyzed for Nd-isotopes, and yielded an ε_{Nd} value of –5.1 (Table A3.2), similar to values previously obtained for the Pierre's Pond suite (average –5.0; Whalen et al., 1997, and unpublished data). Both geochemical and isotopic data thus support the interpretation that the syn-kinematic sheets belong to the Pierre's Pond suite.

Portage Lake monzogabbro

The Portage Lake monzogabbro is herein defined as a large sheet (~30 by 5 km) of foliated, generally medium-grained, K-feldspar porphyritic, hornblende monzogabbro to monzonite, which occupies a central position within the Lloyds River Fault Zone, between the central and southeastern shear zones (Fig. A3.1). Accessory phases include biotite, epidote, and titanite. K-feldspar phenocrysts typically have large aspect ratios (up to ~10), giving the Portage Lake monzogabbro a very distinct character (Fig. A3.7). It comprises an early, fine-grained facies, which is generally equigranular, and occurs as decimeter-sized enclaves in the later coarser grained porphyritic facies. In general, the Portage lake monzogabbro has a solid-state fabric parallel to the foliations of Lloyds River Fault Zone amphibolites. In low strain zones, however, a foliation subparallel to the Lloyds River Fault Zone is defined by the K-feldspar phenocrysts, which are

locally tiled (Fig. A3.7). The phenocrysts are enclosed in a low strain matrix and lack pressure shadows or deformed tails, suggesting the K-feldspar foliation originated by flow in the magmatic state. A magmatic fabric parallel to the Lloyds River Fault Zone, along with age constraints (see below), implies the Portage Lake monzogabbro intruded syn-kinematically into the Lloyds River Fault Zone. This is consistent with the presence of foliated amphibolite enclaves in a correlative monzodiorite immediately west of the Annieopsquotch ophiolite (Fig. A3.1). This pluton is generally highly deformed with foliation parallel to the Lloyds River Fault Zone amphibolites, and has a flaser gabbro-like appearance with hornblende augen up to 1 cm in length within a plagioclase-K-feldspar-quartz matrix.

The Portage Lake monzogabbro is primitive, with low SiO_2 (44.6-53.5%), high $MgO+Fe_2O_3$* (11.7-19.6%), and has a remarkably high alkali content (3.9-7.0%), with the majority of the alkalis being K_2O (average K_2O / Na_2O = 1.6). The abundance of K-feldspar within the monzogabbro indicates these high K_2O contents are a primary feature. The high K_2O defines the Portage Lake monzogabbro as absarokite (SiO_2 <52%) to shoshonite (SiO_2 >52%) (cf. Morrison, 1980). Such compositions are extremely rare within the Appalachians; to our knowledge, only one other shoshonitic pluton has been reported (Pavlides et al., 1994). Harker diagrams show well-defined trends suggestive of fractionation of olivine, clinopyroxene, plagioclase, ilmenite, and apatite. The Portage Lake monzogabbro is LREE-rich, with somewhat depleted HREE, leading to high La/Yb_N (19-24). Its trace element patterns reveal depletion in Nb, Ti, and Zr, and marked enrichment in LILE (Cs, Rb, Ba, Th, K, Pb), indicating a strong subduction component in their petrogenesis (Fig. A3.5c). This is consistent with the La-Y-Nb discrimination diagram (Fig. A3.6a). ε_{Nd} values of the Portage Lake monzogabbro range from –3.4 to –4.9 (Table A3.2), suggesting crustal assimilation or recycling of an old crustal component into the mantle source. Its primitive composition, combined with an incompatible element content higher than average upper continental crust and fractionation trends, suggest limited crustal assimilation. We therefore interpret the Portage Lake monzogabbro to be derived from a mantle source strongly enriched in alkalis and LREE by hydrous fluids and/or melts derived from a subducted slab and overlying sediments. This is in keeping with petrogenetic models for shoshonites elsewhere (e.g., Sun and Stern 2001; Chung et al., 2001).

Otter Pond Complex

Otter Pond mafic suite

The Otter Pond mafic suite comprises variably deformed predominantly gabbroic-dioritic bodies that occur along the Otter Brook Shear Zone and intrude the Annieopsquotch, Star Lake, and King George IV ophiolites, as well as the Lloyds River Complex (Fig. A3.1). The suite is generally distinct because of its hornblende porphyritic to oikocrystic nature, with the oikocrysts locally having a diameter of 1 cm. In thin section, brown, igneous, tschermakitic amphibole oikocrysts enclose crystals of calcic plagioclase, pyroxene, and oxides. Deformed equivalents along the Otter Brook Shear Zone locally preserve the igneous poikilitic to porphyritic texture as porphyroclastic hornblende aggregates in schists and mylonites.

Non-cumulate mafic bodies of this suite have basaltic to andesitic compositions (SiO_2 = 47.1-56.3 wt%, MgO+ Fe_2O_3* =14.2-21.1%), with moderate LREE enrichment (La/Yb_N = 2-8, average 5). LILE were likely remobilized in a post-magmatic stage, but they are consistently enriched. Nb is strongly depleted (average Nb/Th =0.8), while Zr, Hf, and Ti are slightly depleted (Fig. A3.5d). The presence of amphibole oiko- and phenocrysts, calcic plagioclase, and oxides in associated cumulates indicate high water activity and oxygen fugacity. Chemistry and mineralogy of the Otter Pond mafic suite thus indicate formation in an arc environment, supported by their position in the La-Y-Nb diagram (Fig. A3.6). ε_{Nd} values of –0.9 and –1.8 for a gabbro and a mafic dyke, respectively (Table A3.2), indicate assimilation or recycling of an old crustal component into the mantle source of the suite.

Otter Pond granodiorite suite

The Otter pond granodiorite suite comprises several granodioritic to tonalitic bodies that intrude the Annieopsquotch ophiolite and Lloyds River Complex, as well as subordinate rhyolites. Accessory mineral phases include chloritized hornblende, chloritized biotite and titanite. Several smaller, highly deformed, fine-grained granodioritic intrusions locally cut Otter Brook Shear Zone mylonites, and have a strong foliation parallel to those within the surrounding Otter Brook Shear Zone tectonites (Fig. A3.8). The dykes cut the Lloyds River Complex, Annieopsquotch ophiolite, and Otter Pond mafic suite, and hence also stitch the boundary between Annieopsquotch ophiolite

belt and Lloyds River Complex (Otter Brook Shear Zone). These relationships suggest the Otter Pond granodiorite suite intruded the Otter Brook Shear Zone syn-kinematically (Fig. A3.8). The suite must also postdate intrusion of the Otter Pond mafic suite. The felsic intrusions likely intruded at very shallow levels, as evidenced by the generally fine-grained nature of the larger bodies and flow-banding in the associated aphanitic dykes. Chemically similar rhyolitic tuff and flows (Fig. A3.5e), interlayered with graphitic sediment and mica schist, occur along the Otter Brook Shear Zone and are interpreted to represent the extrusive equivalents of the shallow level intrusions.

The Otter Pond granodiorite suite is characterized by high SiO_2 (68.0-73.2%) and alkali (3.7-6.2%) content, and low to moderate $MgO+Fe_2O_3^*$ (3.0-10.1%). LREE and LILE are enriched (La/Yb_N=6-9, average 7), while HFSE (Nb, Ti) are depleted (Fig. A3.5e). These features suggest formation in an arc environment, consistent with their position in the Rb vs Y+Nb discrimination diagram (Fig. A3.6b). The rhyolite has a similar composition (Fig. A3.5e), and yielded an ε_{Nd} value of –6.8 (Table A3.2).

GEOCHRONOLOGY

Analytical procedures

Laser $^{40}Ar/^{39}Ar$ step-heating analysis was carried out at the Geological Survey of Canada, with data collection protocols after Villeneuve and MacIntyre (1997) and Villeneuve et al. (2000) and error analysis following Scaillet (2000) and Roddick (1983). Analytical data are presented in Table A3.3 and plotted in Fig A3.9. U-Pb TIMS and SHRIMP II analyses were conducted at the GSC. U-Pb TIMS analytical methods are outlined in Parrish et al. (1987) and Davis et al. (1997), with treatment of analytical errors after Roddick et al. (1987). SHRIMP II analyses were conducted using analytical procedures described by Stern (1997), with standards and U-Pb calibration methods following Stern and Amelin (2003). U-Pb TIMS and SHRIMP analyses are presented in Tables A3.4 and A3.5, respectively, and are plotted in concordia diagrams with errors at the 2s level (Fig. A3.10). Further details on the U-Pb TIMS and SHRIMP analytical techniques are presented in Appendix 4. All of the geochronology sample locations are indicated in Fig. A3.1 and Tables A3.3, A3.4, and A3.5.

$^{40}Ar/^{39}Ar$ geochronology

$^{40}Ar/^{39}Ar$ analyses were carried out on hornblende separates from two amphibolites that mark the Lloyds River Fault Zone (sample # 1 and 2 in Fig. A3.1) to provide a minimum age of deformation along the Lloyds River Fault Zone. Sample VL01J261A is a strongly foliated amphibolite taken from a zone of amphibolites that defines the southeastern shear zone along the northwestern margin of the Annieopsquotch ophiolite (Fig. A3.1). Both aliquots of sample VL01J261A (z7152; #1) have fairly consistent Ca/K ratios, and yield a well-defined plateau, comprising 97.4% of the total gas and defining the age of the sample to be 468±6 Ma (Table A3.3, Fig. A3.9a). Sample VL02J368A (z7586; #2) was taken from a foliated amphibolite that marks the southeastern shear zone along the northwestern margin of the Star Lake ophiolite (Fig. A3.1). It has a nearly constant Ca/K ratio throughout most of the heating process, with the exception of the last steps of the two aliquots, which may indicate degassing of a second, contaminating phase. The two aliquots yield a plateau region, comprising 98.2% of the gas, which defines the age of the sample to be 471±5 (Table A3.3, Fig. A3.9b), in agreement with the age of VL01J261A. We therefore conclude that the age of c. 470 Ma is geologically significant, and represents the age at which the amphibolites cooled below the hornblende closure temperature for argon (c. 550°; Harrison, 1981), providing a minimum age for ductile deformation of the Lloyds River Fault Zone.

U/Pb geochronology

VL01J120 (z7508) – Portage Lake monzogabbro

A sample was collected from the main body of the Portage Lake monzogabbro, north of Lloyds Lake (#3 in Fig. A3.1). It contained abundant high-quality zircons, which were grouped into different fractions based on size and morphology (Table A3.4). Three of the analyzed fractions are near-concordant (-0.1% to 0.5 % discordant), while fraction 5 is slightly discordant (0.8%), suggesting it has been affected by minor lead loss (Fig. A3.10a). There is no evidence for inheritance in the sample. A weighted average of the $^{207}Pb/^{206}Pb$ ages of all four analyses is 462±2 Ma (MSWD = 0.9, probability = 0.45). This date is interpreted to be the crystallization age of the Portage Lake monzogabbro, and provides an age for syn-kinematic intrusion within the Lloyds River Fault Zone.

VL01J016 (z7153) – Portage Lake monzodiorite

A sample of the highly strained monzodiorite immediately west of the Annieopsquotch ophiolite, immediately south of the northwestern shear zone (#4 in Fig. A3.1), contains abundant zircon ranging in morphology from euhedral stubby prismatic grains to anhedral fragments (Table A3.4). All of the zircon fractions analyzed are somewhat discordant (0.5%-1.2%), and define a discordia, interpreted to result from recent lead loss (Fig. A3.10b). No cores have been observed, and there is no isotopic evidence for inheritance. A weighted average of the $^{207}Pb/^{206}Pb$ ages of all four analyses is 464±2 Ma (MSWD=0.5, probability=0.68; Fig. A3.10b), which is interpreted to be the crystallization age of the monzodiorite. This age provides a maximum age for the deformation of the monzodiorite within the Lloyds River Fault Zone.

Four titanite fractions are 0.4% to 3.8% discordant, and one fraction is slightly reversely discordant (-1.9%; Fig. A3.10b). The titanite analyses, which have large associated errors, define an array with $^{207}Pb/^{206}Pb$ ages ranging between 465 Ma and 426 Ma. This range could indicate the presence of distinct age populations within the multi-grain fractions, lead loss during a younger event, or a combination thereof. Given that the host rock crystallized at 464 Ma (see above), and that the adjacent amphibolite to granulite-facies Cormacks Lake Complex was juxtaposed along the Lloyds River Fault Zone during rapid Early Silurian exhumation (Pehrsson et al., 2003), we postulate that the titanite population reflects a mixture of titanite formed during initial cooling of the host rock following crystallization, and grains that were reset or crystallized during the c. 430 Ma uplift of the adjacent Cormacks Lake Complex.

VL02J238D (z7524) – Pierre's Pond suite diorite

A sample from a highly strained syn-kinematic diorite sheet intruding ophiolitic cumulates on the shore of Star Lake (#5 in Fig. 1) yielded small (50-100 μm), colorless to light brown zircons, which range from subhedral prismatic crystals to anhedral grain fragments with concoidal fractures. Cracks and inclusions are common, as are dark blurry cores, which likely represent inherited material. SEM imaging of the grains showed bright domains in the cores of many grains, with rims characterized by oscillatory zoning, suggesting magmatic overgrowth of inherited zircons. Some zircons are core-free, however, and are interpreted as entirely magmatic grains. A Concordia age,

calculated from the SHRIMP analyses of magmatic grains (n=18), is 458.6±3.2 Ma (MSWD of concordance and equivalence = 1.6, probability = 0.014) (Fig. A3.10c, Table A3.5). This age of 459±3 Ma is interpreted as the crystallization age of the diorite, and marks the age of syn-kinematic intrusion of the Pierre's Pond suite within the Lloyds River Fault Zone. One inherited core was analyzed and yielded an age of 1961 Ma (Table A3.5, not plotted).

VL01A258 – Otter Pond Granodiorite suite

A sample was collected from an elongate (500 by 70 m), sheared, fine-grained granodiorite intrusion that stitches the Otter Brook Shear Zone southeast of the Annieopsquotch ophiolite (#6 in Fig. A3.1). Two fractions of small, euhedral, prismatic zircons and two fractions of small, euhedral, equant zircons were analyzed. Fraction A1 is concordant and fractions A2 and B1 are slightly discordant (0.9 and –2.0%, respectively) (Table A3.4). A weighted average of the $^{206}Pb/^{238}U$ ages of these three analyses is 468±2 (MSWD = 2.1, probability = 0.11), which is interpreted to be the crystallization age of the granodiorite (Fig. A3.10d). This age provides a minimum age of juxtaposition of the Annieopsquotch ophiolite belt and the Lloyds River Complex, and hence a minimum age of formation of the Otter Brook Shear Zone. Zircon fraction B2 (n=74) is concordant at 473±1 Ma ($^{206}Pb/^{238}U$). This fraction has a distinct morphology, and its age is statistically distinct from the 468±2 Ma crystallization age of the rock (MSWD=26, probability=0.000). Since the sample is from a narrow intrusive sheet (~2 x 0.15 km) that intruded at shallow levels, the granodiorite probably crystallized over a short time perdiod. In addition, the four fractions do not define a linear trend, indicating the two populations cannot be explained by Pb-loss. Therefore, fraction B2 is interpreted to comprise inherited zircons.

DISCUSSION

Assembly of the Annieopsquotch Accretionary Tract

The data presented above impose strong time and dynamic constraints on the evolution of the Annieopsquotch Accretionary Tract. The earliest tectonic activity related to assembly of the Annieopsquotch Accretionary Tract is recorded by c. 470 Ma cooling ages of hornblende from amphibolites deformed within the Lloyds River Fault Zone. This provides a minimum age on ductile deformation related to accretion of the Annieopsquotch ophiolite belt to the Dashwoods

microcontinent, and suggests the belt was accreted to the Dashwoods microcontinent within 10 Ma after its formation (480 Ma; Dunning and Krogh, 1985). The Otter Pond granodiorite suite intruded both the Annieopsquotch ophiolite belt and the structurally underlying Lloyds River Complex, and hence its age of 468±2 Ma represents a minimum age for emplacement of the Annieopsquotch ophiolite belt above the Lloyds River Complex. The Lloyds River Complex was thus accreted within 5 Ma of its formation (473 Ma; Chapter 2). The overlap in ages of thrusting on the Lloyds River Fault Zone (bracketed between ~480-470 Ma) and Otter Brook Shear Zone (~473-468 Ma) suggests that both shear zones were active around the same time, and may have been genetically related, implying that that ophiolites of both the Annieopsquotch ophiolite belt and Lloyds River Complex were accreted to the Dashwoods microcontinent simultaneously. This is consistent with the similar kinematic histories recorded in the Lloyds River Fault Zone and Otter Brook Shear Zone (Lissenberg 2005; Zagorevski and van Staal, 2002).

The 473±1 Ma inherited zircon fraction in the Otter Pond granodiorite is the same age as the Lloyds River Complex (473Ma; Chapter 2), which it cuts, and the structurally underlying Buchans Group (473 Ma; Dunning et al., 1987). Zircons are rare within the ophiolitic Lloyds River Complex, and it is isotopically juvenile. In contrast, the ensialic Buchans contains abundant felsic volcanic rocks and has a non-juvenile ε_{Nd} signature typical of crustal contamination (e.g., Swinden et al., 1997). The Buchans group is thus a more likely source for the inherited zircon, and can in part account for the markedly negative ε_{Nd} of the Otter Pond granodiorite suite (-6.8). We thus infer that the granodiorite assimilated rocks of the Buchans Group during its ascent, and/or was in part generated by partial melting of the Buchans Group and its basement. If correct, this implies that the Buchans Group was also juxtaposed with the Lloyds River Complex by 468 Ma. This is consistent with structural relationships west of the town of Buchans, where the Buchans Group is interpreted to have been overthrust by a hot thrust sheet comprising c. 467 Ma plutonic rocks of the Notre Dame Arc along the Hungry Mountain Thrust (Thurlow, 1981; Whalen et al., 1987). Geochronological and structural data thus indicate a significant part of the Annieopsquotch Accretionary Tract was assembled and accreted to the Dashwoods by 468 Ma, within 10 Ma

(Annieopsquotch ophiolite belt) and 5 Ma (Lloyds River Complex, Buchans Group) after their intra-oceanic generation.

Convergence between intra-oceanic components of the Annieopsquotch Accretionary Tract and the Dashwoods microcontinent likely resulted from continued collision between Laurentia and the Dashwoods microcontinent with its Notre Dame Arc. This collision had started by at least 475 Ma (Waldron and van Staal, 2001), probably initially along promontories, propagating compression to the eastern side of the Dashwoods microcontinent, initiating west-directed subduction (Appendix A1; Chapter 1). Extension in the upper plate resulted in retreat of the subduction zone to form the progressively eastward younging units of the Annieopsquotch Accretionary Tract. However, continued Dashwoods-Laurentia collision caused the newly formed basins to collapse, and led to underthrusting of the Annieopsquotch ophiolite belt, Lloyds River Complex and Buchans Group underneath Dashwoods.

The subsequent tectonic history of the Annieopsquotch Accretionary Tract is recorded by formation of the arc-back arc complexes of the Red Indian Lake Group at 464 Ma, which must have occupied a position somewhat outboard of the composite Dashwoods microcontinent (Chapter 2). The Lloyds River Fault Zone was still active during this time, marked by the syn-kinematic intrusion of the Portage Lake monzogabbro (464-462 Ma) and Pierre's Pond suite diorite (459 Ma). Final assembly of the Annieopsquotch Accretionary Tract occurred when the Red Indian Lake Group was accreted to composite Dashwoods microcontinent as a result of the collision with the peri-Gondwanan Victoria arc (van Staal et al., 1998; Zagorevski et al., 2004). The age of this collision is constrained to lie between 454 Ma (the age of the latest volcanism of the Victoria arc; Zagorevski et al., 2004) and 450 Ma (presence of Laurentia-derived detritus in Upper Caradoc-Ashgill sedimentary cover of the Victoria arc; e.g., McNicoll et al., 2001). Accretion-related ductile motion on the Lloyds River Fault Zone and Otter Brook Shear Zone had ceased by the Early Silurian, indicated by the little-deformed Lloyds Lake granite (427±3 Ma, Whalen et al., submitted) and Boogie Lake suite (435 +6/-3 Ma; Dunning et al., 1990), which stitch the Lloyds River Fault Zone and Otter Brook Shear Zone, respectively.

Source of magmatism in the Annieopsquotch Accretionary Tract: Link with the Notre Dame Arc?

The plutonic rocks that intrude into the Lloyds River Fault Zone and Otter Brook Shear Zone have dominantly arc signatures, and show Nd-isotopic compositions indicative of involvement of an old crustal component in their petrogenesis. The plutons within the Annieopsquotch Accretionary Tract share these characteristics with and are coeval with plutons of the second, slab break-off related phase of the adjacent Notre Dame Arc (469-458 Ma; Whalen et al., 2003; van Staal et al., 2003). Notre Dame Arc pluton ε_{Nd} values range from 2.5 to –13.5 (Whalen et al., 1997), and, like the Pierre's Pond suite, they contain inherited Proterozoic zircon (Whalen et al., 1987; Dunning et al., 1989; McNicoll, unpublished data). This suggests an overall consanguineous relationship between magmatism in the Annieopsquotch Accretionary Tract and the Notre Dame Arc. This is consistent with the geochronological data presented above, which indicate that the Annieopsquotch ophiolite belt, Lloyds River Complex and Buchans Group were already accreted to the Dashwoods microcontinent prior to this magmatic phase.

The role of crustal assimilation

Despite the overall similarities, several notable differences exist between the plutons within the Annieopsquotch Accretionary Tract and the Notre Dame Arc. First, the absarokitic to shoshonitic composition of the Portage Lake monzogabbro is unique. Only one other occurrence has been reported within the Appalachians, suggesting conditions required for shoshonite generation (highly metasomatized mantle source) and preservation (limited crustal assimilation) were met only within the Annieopsquotch Accretionary Tract. Second, the plutonic rocks within the Annieopsquotch Accretionary Tract are volumetrically dominated by mafic compositions, with subordinate intermediate-felsic rocks (average Mg# 56), which contrasts with the dominantly evolved nature of the Notre Dame Arc (average Mg# 45; Fig. A3.11). In addition, the Otter Pond mafic suite and Portage Lake monzogabbro are as primitive or more primitive than the most primitive Notre Dame Arc suites. The cause of the more mafic nature of the plutons within the Annieopsquotch Accretionary Tract is unlikely to be source-related, as they are thought to be consanguineous with the Notre Dame Arc plutons, and the Portage Lake monzogabbro was likely

sourced by mantle of, or mantle derived from, the Dashwoods microcontinent (i.e., the same mantle source by which the Notre Dame Arc was underlain; see below). In contrast, we suggest the dominantly mafic character of the Portage Lake monzogabbro, Otter Pond mafic suite and part of the Pierre's Pond suite is caused by the tectonic environment in which they were emplaced. First, the Annieopsquotch Accretionary Tract likely formed thin crust that was dominantly composed of ophiolites. Second, the close spatial association between the plutons and the Lloyds River Fault Zone plus Otter Brook Shear Zone indicates the plutons ascended along active large-scale shear zones, significantly facilitating transport, thereby limiting crustal assimilation.

The bimodal distribution of plutons within the Annieopsquotch Accretionary Tract, with dominant mafic and subordinate evolved phases, reflects different petrogenetic processes between the Portage Lake monzogabbro and the Otter Pond mafic suite on the one hand, and the Otter Pond granodiorite and Pierre's Pond suite tonalites on the other. The Pierre's Pond diorites appear to have characteristics of both groups. The Otter Pond mafic suite and Portage Lake monzogabbro have high compatible element contents (MgO, Cr, Ni: up to 9.9%, 413 ppm, and 102 ppm, and 8.5%, 201 ppm, and 65 ppm for both suites, respectively), suggesting limited crustal assimilation and preservation of a significant mantle-derived component. In contrast, the magnitude of the negative ε_{Nd} values (up to –6.8) and the evolved nature of the Otter Pond granodiorite suite and Pierre's Pond suite tonalites, as well as the presence of inherited Paleoproterozoic zircons in the Pierre's Pond Suite diorite, suggest that partial melting and assimilation of continental crust was a major process in formation of these plutons. However, the crustal component of the plutons within the Annieopsquotch Accretionary Tract cannot be the derived from crust of the Dashwoods microcontinent, as both field- and seismic data indicate that the Annieopsquotch Accretionary Tract structurally underlies Dashwoods (Fig. A3.2). The 473 Ma inherited zircons in the Otter Pond granodiorite and structural relationships in the Buchans area are consistent with accretion of the Buchans Group, and by inference, its continental basement, to the Dashwoods microcontinent prior to magmatism in the Annieopsquotch Accretionary Tract. We thus infer that the Annieopsquotch Accretionary Tract was underlain by the continental basement of the Buchans Group during generation of the plutonic rocks in the Annieopsquotch Accretionary Tract. This is consistent with

seismic interpretations, which suggest that the thrust slices that contain the Buchans Group are present underneath the entire Annieopsquotch Accretionary Tract, and cut-out the Annieopsquotch ophiolite belt at depth (Fig. A3.2; van der Velden et al., 2004).

The source of the Portage Lake monzogabbro

The strong enrichment in LREE and LILE and negative ε_{Nd} of the Portage Lake monzogabbro, combined with its primitive nature, require a mantle source extensively enriched by an old crustal component. Given the marked absence of sediments within the Annieopsquotch Accretionary Tract, it is unlikely that the enrichment is caused solely by subduction of continent-derived material. In contrast, we propose that the Portage Lake monzogabbro taps old subcontinental lithospheric mantle of the Dashwoods microcontinent or its derivative, the basement to the Buchans arc. This is analogous to recent shoshonites and associated high-K magmas in the eastern Sunda arc and Taiwan, which were produced by melting of enriched subcontinental lithosphere following arc-continent collision (Varne, 1985; Wang et al., 2004). In the Sunda arc, there is a spatial relationship between K-enrichment, concurrent with decreasing ε_{Nd}, and proximity to the advancing Australian plate. Arc-continent collision has caused the arc to tap a dominantly subcontinental Australian mantle source in the east, yielding shoshonites, whereas to the west, where the collision has not yet occurred, the high-K signature decreases and calc-alkaline and transitional arc tholeiites erupt (Varne, 1985). The intrusion of the Portage Lake monzogabbro occurred c. 5 Ma after the Buchans arc-Dashwoods microcontinent collision, suggesting it was generated in a tectonic setting very similar to the Sunda and Taiwan shoshonites. Limited crustal assimilation within the Annieopsquotch Accretionary Tract allowed the lithospheric mantle signature to be largely retained, leading to the unique geochemical character of the Portage Lake monzogabbro.

Accretionary tectonics

The Annieopsquotch Accretionary Tract records a complicated history of generation and accretion of several intra-oceanic elements within a short time span. Two geochemically and geochronologically distinct suprasubduction zone ophiolites, the Annieopsquotch ophiolite belt and the Lloyds River Complex, were formed within a time span of 7 Ma (Chapter 2) above a west-

dipping subduction zone. The formation of the Lloyds River Complex was related to rifting of the coeval Buchans arc off of the Dashwoods microcontinent (Chapter 2). The Buchans arc in turn rifted shortly (9 Ma) after its formation to yield the Red Indian Lake arc and associated back arc (Chapter 2). The Red Indian Lake arc retained its intra-oceanic position for c. 10 Ma, when it collided with the Peri-Gondwanan Victoria Lake arc along the Red Indian Line. The accretion of the units to the Dashwoods microcontinent was coeval with the intrusion of several plutons. The observed complexities, notably the rapid generation and migration of arc-back arc igneous complexes and the intrusion of plutons into accretionary complexes, are reminiscent of the current southwest Pacific (e.g., Hall 2002) as well as other Paleozoic (e.g., Kunlun; Xiao et al., 2003) and Meso-Cenozoic orogens (e.g., Kamchatka; Konstantinovskaia, 2001), and illustrate the dynamic nature of accretionary margins.

However, the virtual absence of sediments and the importance of recycled continental basement of the Annieopsquotch Accretionary Tract (basement of Buchans and Red Indian Lake arcs) contrast with other major accretionary orogens, which are dominated by large, dominantly sedimentary accretionary complexes, intruded by arc plutons as a result of progressive retreat of the subducting slab (e.g., Sengör and Natal'in, 1996). These arc plutons are generally isotopically juvenile, signaling an important depleted mantle component in their petrogenesis (Chen et al., 2000, and references therein). Such accretionary orogens show little evidence of arc rifting or presence of rifted continental slivers, and are characterized by long-lived subduction-accretion in the fore-arc, leading to the formation of large sedimentary prisms (Sengör and Natal'in, 1996), similar to the Aleutian accretionary complex (Moore et al., 1991). In contrast, the Annieopsquotch Accretionary Tract results from repeated rifting and rapid accretion of slivers of the Dashwoods microcontinent, their overlying arcs and intervening basins. The short life span of these basins, as well as the submarine nature of the Buchans and Red Indian Lake arcs, limited sediment influx, and hence fore-arc accretion. Plutons intruding the Annieopsquotch Accretionary Tract formed in response to slab break-off, and tapped not only a sub-arc mantle source, but also an enriched lithospheric mantle and crustal source, leading to isotopically evolved signatures. The Annieopsquotch

Accretionary Tract thus records a greater ratio of recycled crustal material over newly added mantle-derived material than most other accretionary orogens.

CONCLUSIONS

The Annieopsquotch Accretionary Tract in Newfoundland is a well-preserved example of an Early Paleozoic accretionary complex, which formed by the accretion of several arc sequences and oceanic crust to the composite Laurentian margin. It preserves the record of circa 30 million years of west-directed subduction beneath Laurentia, providing a unique view of the tectonic proceses during the Early-Middle Ordovician closure of Iapetus. This record is poorly preserved esewhere in the Northern Appalachians, maily due to the presence of extensive Siluro-Devonian cover sequences (van Staal et al., 1998). Assembly of the Annieopsquotch Accretionary Tract is recorded by shear zones that separate distinct units, and syn-kinematic plutonic suites within those shear zones. Age constraints suggest that the various units of the Annieopsquotch Accretionary Tract formed and were accreted to the Laurentian margin within 5 to 10 million years of their formation.

Growth of the Appalachian Laurentian margin occurred maily due to the repeated accretion of oceanic crust and the addition of melts generated in both lithospheric and sub-arc mantle. However, recycling of continental crust, in the form of continental slivers that formed basement to the arc sequences, was an important process within the Annieopsquotch Accretionary Tract. The involvement of this basement, combined with an enriched lithospheric mantle, caused the syn-kinematic plutons in the Annieopsquotch Accretionary Tract to be isotopically evolved. Sediment influx during formation of the Annieopsquotch Accretionary Tract was apparently minor, significantly limiting the role of fore-arc accretion.

The data presented in this paper indicate that tectono-magmatic processes in Iapetus operated over very short time scales. In addition, it presents a record of dynamic interaction between extension due to subduction rollback and evidenced by the formation of marginal basins and arc-trench migration, and episodic compression in the abandoned back-arc region, leading to the rapid closure and accretion of the remnant arc phases and marginal basins.

The role of strike-slip tectonics, particularly the movement of fore-arc continental slivers, was probably significant during the tectonic evolution of the Annieopsquotch Accretionary Tract, although its exact role in the development of the Annieopsquotch Accretionary Tract remains to be established. The tectonic complexities along the Early Paleozoic Laurentian margin were thus similar to those operating at present in the Southwest Pacific. In general, the nature of accretionary tectonics thus appears to have remained unchanged throughout the Phanerozoic.

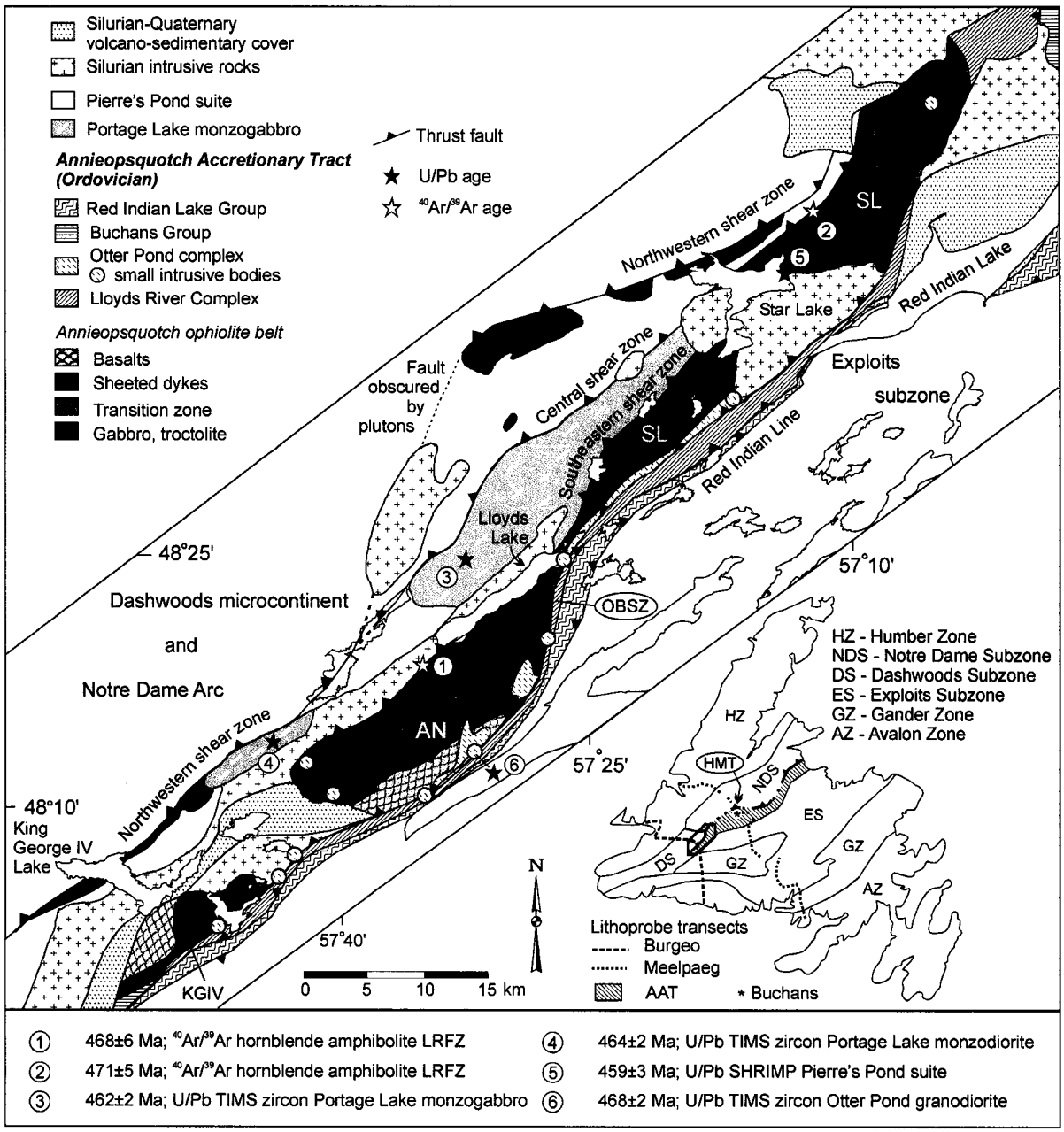

Figure A3.1: Simplified geological map of the Annieopsquotch Accretionary Tract, with approximate locations of samples dated in this study indicated by numbered filled stars (U/Pb) and open stars ($^{40}Ar/^{39}Ar$). Inset shows tectonostratigraphic zones of the Newfoundland Appalachians, extent of the Annieopsquotch Accretionary Tract (AAT), and the locations of the study area, Lithoprobe seismic transects and town of Buchans. AN=Annieopsquotch ophiolite; HMT=Hungry Mountain Thrust; KGIV=King George IV ophiolite; OBSZ=Otter Brook shear zone; SL=Star Lake ophiolite. Modified from Lissenberg et al. (in press) and van Staal et al. (in press a,b,c).

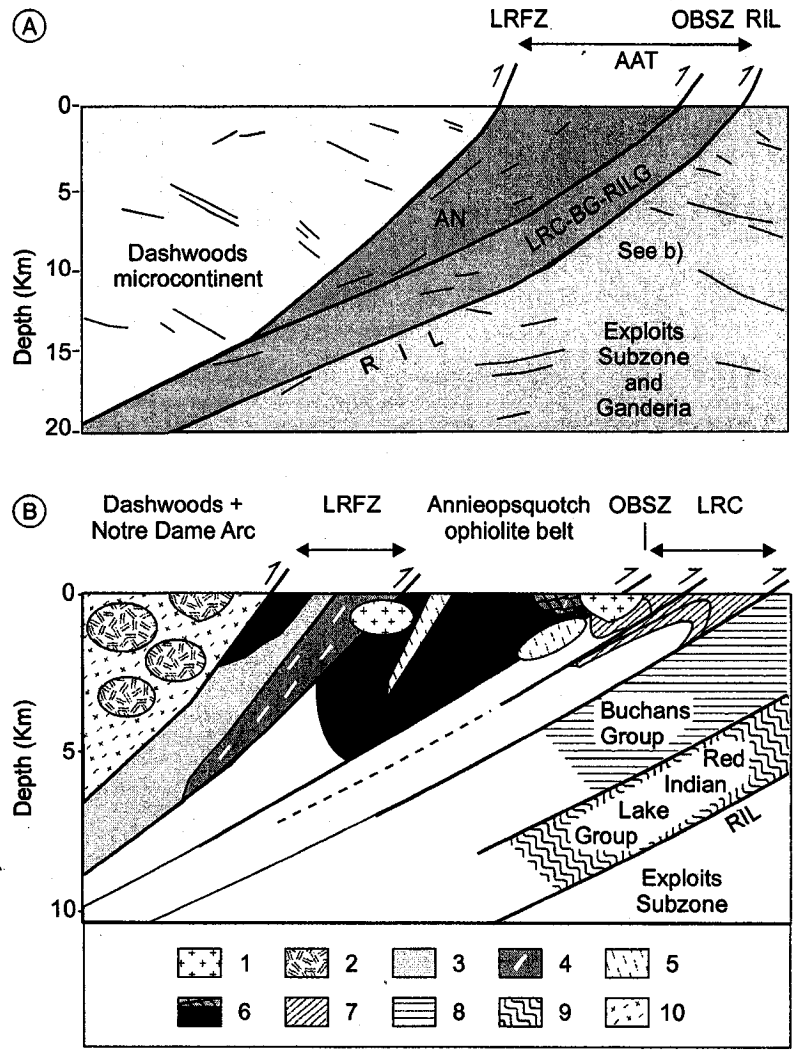

Figure A3.2: Schematic cross-sections of the study area (no vertical exaggeration). a) Cross-section based on Lithoprobe seismic reflection profile along the Burgeo transect, modified from van der Velden et al. (2004). b) Schematic composite cross-section interpolated between Burgeo and Meelpaeg transects showing structural relationships and stratigraphy of different components of the Annieopsquotch Accretionary Tract, as well as plutonic rocks described in this chapter (see text for discussion). 1=Silurian plutons (Lloyds Lake granite & Boogie Lake suite); 2=Notre Dame Arc plutons; 3= Pierre's Pond suite; 4= Portage Lake monzogabbro; 5=Otter Pond Complex; 6=Annieopsquotch ophiolite; 7=Lloyds River Complex; 8=Buchans Group; 9=Red Indian Lake Group; 10=Dashwoods. AAT=Annieopsquotch Accretionaty Tract; AN=Annieopsquotch ophiolite; LRC-BG-RILG=Lloyds River Complex + Buchans Group + Red Indian Lake Group; LRFZ=Lloyds River Fault zone; OBSZ=Otter Brook shear zone; RIL=Red Indian Line.

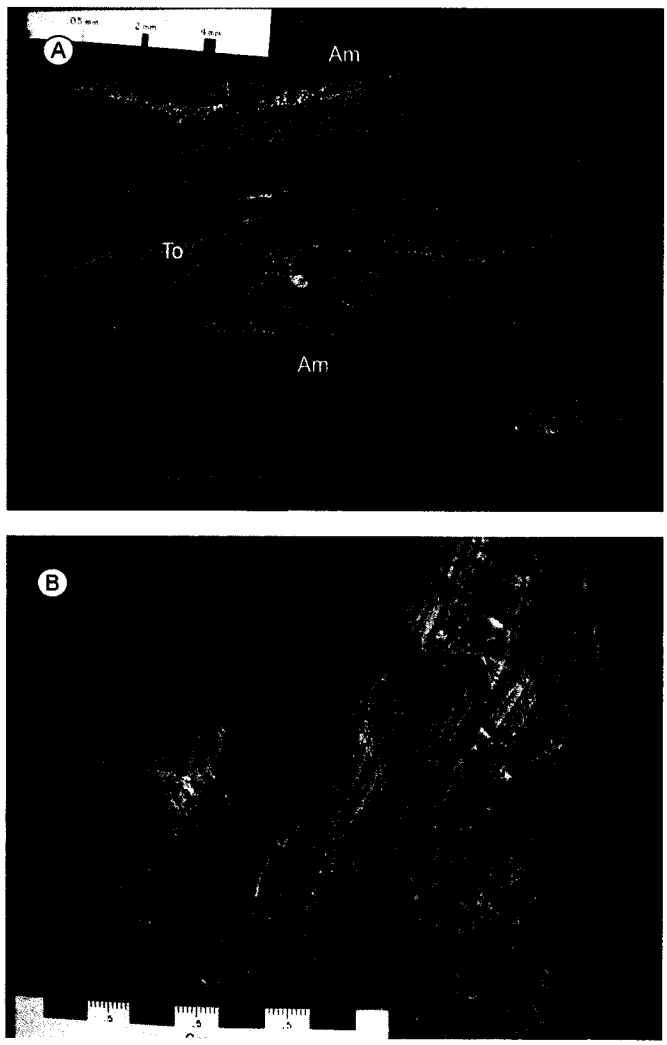

Figure A3.3: Field photographs illustrating the Lloyds River Fault Zone and Otter Brook Shear Zone. a) Highly strained tectonites of the Lloyds River Fault Zone composed of amphibolites (Am) and intrusive sheets of tonalite (To). b) Highly strained volcanic rocks of the Otter Pond Complex that mark the Otter Brook Shear Zone. View towards NE. Scale card divisions are 1 cm.

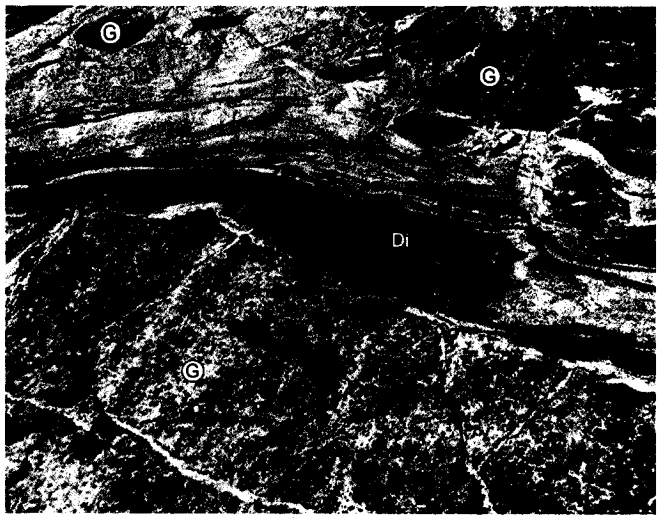

Figure A3.4: Sheet of highly deformed diorite (Di) and tonalite (To), correlated with the Pierre's Pond Suite, intrude unfoliated gabbros (G) of the Star Lake ophiolite on an island in Star Lake. Note gabbro enclaves in tonalite and large deformation contrast between host gabbro and intrusive rocks. Pen is 15 cm long.

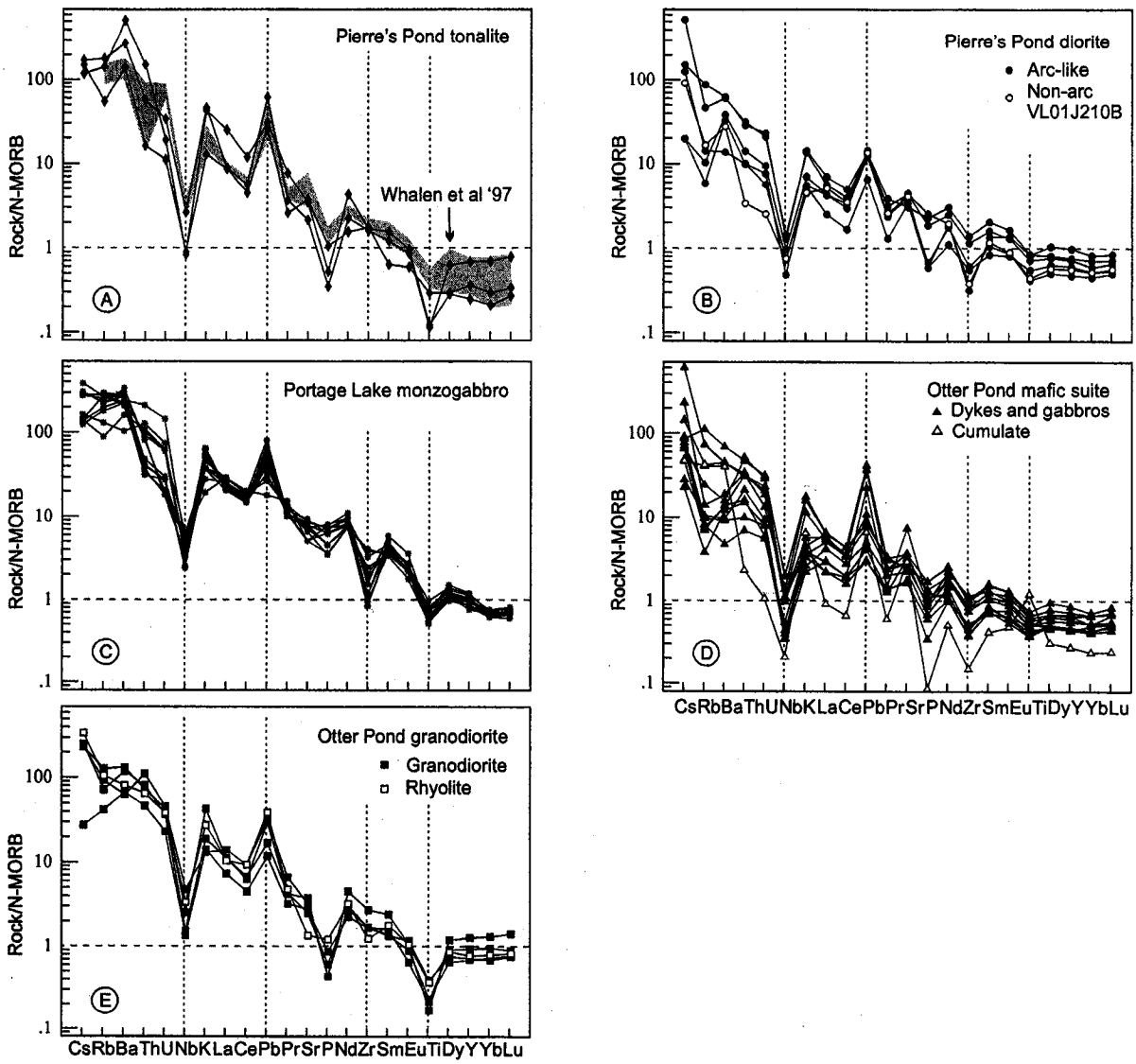

Figure A3.5: Trace element patterns of syn-kinematic plutonic rocks in the Annieopsquotch Accretionary Tract. a) Pierre's Pond Suite tonalites. b) Pierre's Pond Suite diorites. c) Portage Lake monzogabbro; d) Otter Pond mafic suite and associated cumulate. e) Otter Pond granodiorite and associated rhyolite. Normalizing values from Sun and McDonough (1989).

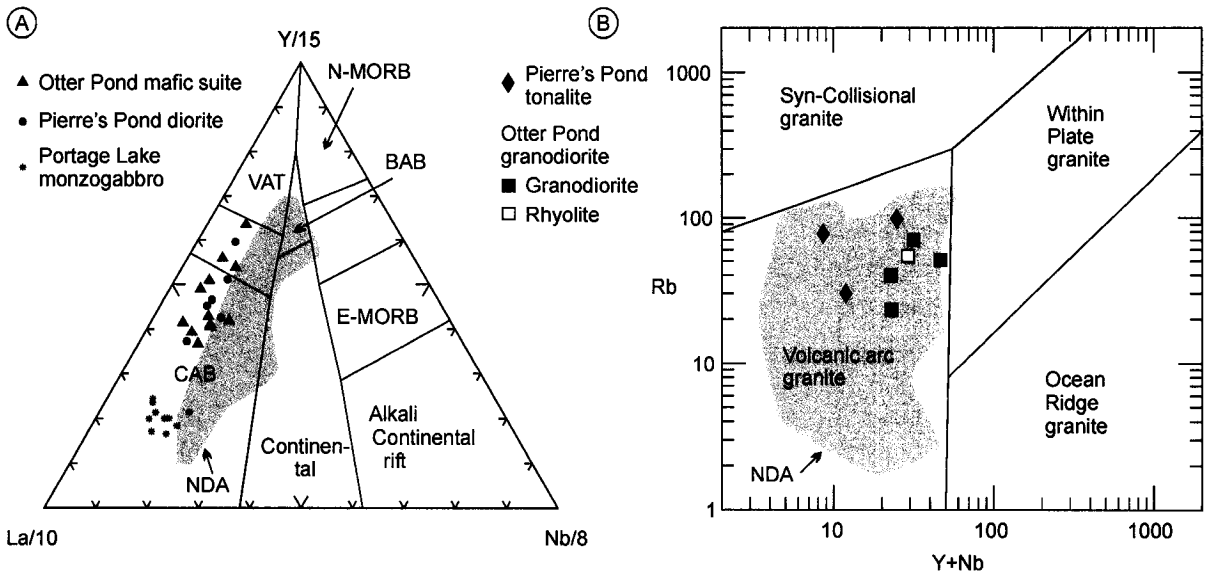

Figure A3.6: Tectonic discrimination diagrams for plutons within the Annieopsquotch Accretionary Tract compared with plutons of the Notre Dame Arc (shaded area; NDA). a) La-Y-Nb diagram of Cabanis and Lecolle (1989) illustrating the arc affinity of the mafic plutons (Portage Lake monzogabbro, Pierre's Pond suite diorites, Otter Pond mafic suite). BAB=back-arc basin basalt; CAB=calc-alkaline basalt; E-MORB=enriched mid-ocean ridge basalt; N-MORB=normal mid-ocean ridge basalt; VAT=volcanic arc tholeiite; b) Rb vs Nb+Y diagram of Pearce et al. (1984) indicating the granitoid plutons in the (Pierre's Pond suite tonalites, Otter Pond granodiorites and rhyolite) are of arc affinity. NDA data from Whalen et al. (1997) and unpublished data.

Figure A3.7: K-feldspar phenocrysts define a foliation in the Portage Lake monzogabbro. Low strain in the matrix suggests the monzogabbro was deformed in part in the magmatic state.

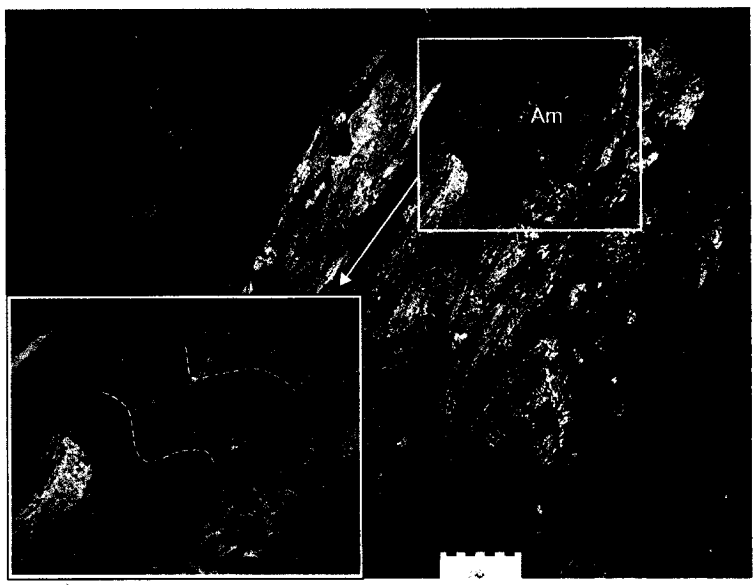

Figure A3.8: Small plug of Otter Pond granodiorite (Gd) contains enclaves of folded mylonitic amphibolite (Am) of the Otter Brook Shear Zone, and is itself highly deformed, suggesting it intruded the Otter Brook Shear Zone syn-kinematically. View towards NE. Scale card divisions are 1 cm.

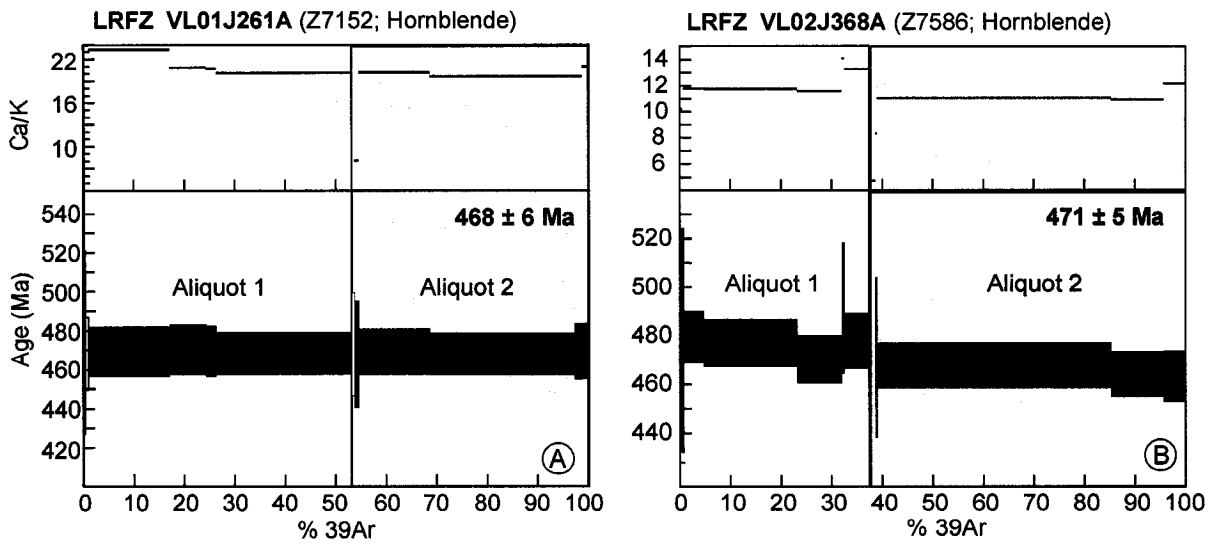

Figure A3.9: Results of $^{40}Ar/^{39}Ar$ hornblende geochronology. a) Age spectrum of ophiolite-derived amphibolite VL01J261A in the Lloyds River Fault Zone near the Annieopsquotch ophiolite. b) Age spectrum of ophiolite-derived amphibolite VL02J368 in the Lloyds River Fault Zone near the Star Lake ophiolite.

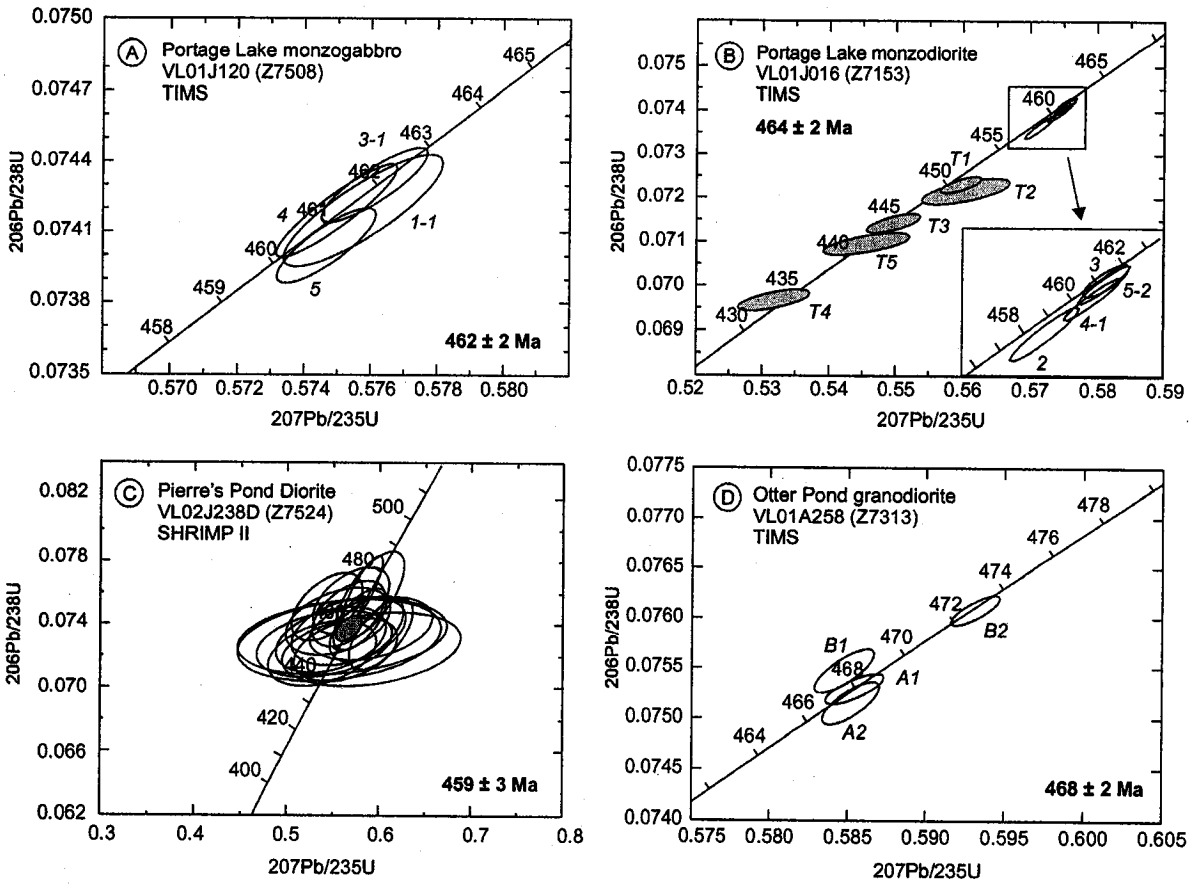

Figure A3.10: Concordia diagrams and ages of the Portage Lake monzogabbro (a; #3 in Fig. 1), Portage Lake monzodiorite (b; #4 in Fig. 1), Pierre's Pond suite (c; #5 in Fig. 1) and Otter Pond granodiorite (d; #6 in Fig. 1). Italic numbers refer to fraction numbers listed in Table 5.4. Grey ellipse in diagram of VL02J238D is calculated Concordia age following the method of Ludwig (1998).

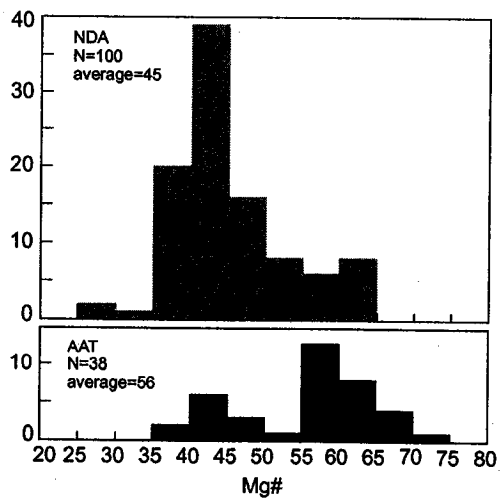

Figure A3.11: Histograms comparing the Mg# of plutonic rocks of the Notre Dame Arc (NDA) and plutonic rocks within the Annieopsquotch Accretionary Tract. Cumulates have been omitted. Mg#=100*Mg/Mg+Fe^{2+}, assuming Fe^{3+}/Fe^{2+}=0.1. NDA data from Whalen et al. (1997) and unpublished data.

Table A3.1: Whole-rock geochemical data from syn-kinematic plutonic rocks

sample	VL01 084	VL01A 050	VL01A 051	VL01A 349b	VL01J 035c	VL01J 036b	VL01J 209b	VL02A 193b	VL02J 307	VL02J 323a	VL02J 339c	VL02J 400	VL02A 278d
Unit	OPm	OPm	OPm	OPm	OPm	OPm	OPm	OPm	OPm	OPm	OPm	OPm	OPm
SiO_2	56.28	55.45	40.00	51.94	51.94	48.90	48.97	47.09	48.75	52.33	53.56	51.91	50.34
TiO_2	0.62	0.53	1.52	0.84	0.63	0.73	0.56	0.64	0.94	0.49	0.47	0.79	0.80
Al_2O_3	15.75	9.88	18.10	16.27	15.51	16.37	17.51	15.56	16.93	13.95	14.32	14.70	17.87
Fe_2O_3*	8.50	9.25	16.20	9.94	9.72	9.75	8.88	12.01	9.43	10.40	8.98	9.25	11.80
MnO	0.16	0.22	0.18	0.17	0.18	0.19	0.15	0.20	0.15	0.17	0.15	0.16	0.21
MgO	5.67	9.91	6.07	6.01	7.75	8.16	8.62	9.11	6.40	7.72	8.01	8.35	5.27
CaO	5.96	12.52	12.70	8.64	9.67	12.18	10.67	12.10	10.31	10.67	11.74	8.58	9.45
Na_2O	3.91	1.83	0.92	4.09	2.84	2.39	2.87	2.10	2.48	3.25	2.36	2.31	3.47
K_2O	0.33	0.28	0.47	1.16	0.41	0.26	0.24	0.29	1.28	0.19	0.16	0.83	0.30
P_2O_5	0.11	0.04	0.01	0.20	0.10	0.12	0.15	0.13	0.20	0.08	0.07	0.16	0.23
LOI	3.40	1.18	5.19	1.24	1.62	1.15	1.80	0.72	2.80	0.81	0.91	2.70	0.87
Total	100.68	101.09	98.60	100.51	100.39	100.19	100.42	100.02	99.76	100.10	100.80	99.85	100.64
Trace elements (ppm)													
Ba	119	88	256	282	100	87	58	30	435	61	77	286	43
Cr	121	413	31	117	328	299	315	304	171	145	338	397	52
Cs	1.61	0.34	0.33	4.18	0.49	0.46	0.54	0.63	0.60	0.20	0.16	1.00	0.94
Cu	43.8	19.0	55.0	105.4	79.2	150.1	25.5	27.5	63.6	5.7	10.0	11.3	18.1
Hf	2.26	1.25	0.37	1.94	1.67	1.44	0.84	0.90	2.20	1.00	0.90	2.30	1.90
Nb	2.27	0.93	0.48	3.20	2.59	2.58	0.82	1.28	4.60	1.02	0.80	2.50	3.64
Ni	45	102	10	64	100	96	141	66	31	42	69	93	14
Pb	2.6	1.3	2.0	2.5	3.3	2.3	0.9	6.8	12.6	1.5	0.9	11.3	9
Rb	7.9	3.9	23.0	40.9	13.7	4.2	5.5	4.6	62.6	5.9	2.1	23.9	5
Sc	32.1	59.2	42.0	34.6	38.4	41.5	34.4	48.0	32.0	52.5	41.3	29.0	43
Sr	232	159	273	217	268	332	292	669	328	203	148	253	863
Th	4.20	1.96	0.28	4.02	6.22	3.90	1.21	0.84	5.70	2.58	1.83	3.80	3.11
V	202	252	639	299	238	253	230	318	287	315	240	228	297
U	0.89	0.28	0.05	0.63	1.40	1.10	0.37	0.26	1.50	0.44	0.38	1.00	1.34
Y	18.4	13.1	7.6	20.2	15.4	16.7	12.6	12.4	23.9	12.5	12.2	18.9	16.0
Zn	67.1	59.2	97.0	65.3	74.4	67.4	56.6	72.3	273.0	55.0	48.5	69.0	89.0
Zr	85.1	39.3	11.0	71.6	62.3	55.4	27.6	32.8	76.5	34.5	28.8	62.6	69.6
La	16.1	7.3	2.3	15.8	14.4	12.8	5.6	5.5	16.4	10.5	7.5	13.7	16.8
Ce	32.3	14.6	5.0	33.0	26.8	25.5	12.1	14.3	32.7	21.0	14.6	26.9	33.4
Pr	4.13	1.80	0.80	4.49	3.25	3.21	1.68	1.97	4.28	2.67	1.87	3.17	4.18
Nd	16.1	7.2	3.7	18.3	12.8	13.0	7.9	9.0	18.7	10.7	7.6	14.4	17.5
Sm	3.48	1.86	1.10	4.00	2.74	2.94	2.00	2.13	4.20	2.25	1.98	3.30	3.79
Eu	1.02	0.65	0.49	1.31	0.89	1	0.77	0.64	1.32	0.62	0.55	1.16	1.03
Gd	3.18	2.22	1.3	3.76	2.84	2.97	2.16	2.37	4.5	2.19	1.98	3.59	3.57
Tb	0.50	0.35	0.22	0.59	0.44	0.46	0.34	0.37	0.6	0.38	0.33	0.50	0.54
Dy	3.13	2.27	1.4	3.53	2.62	2.93	2.08	2.27	4.33	2.21	2.27	3.11	2.94
Ho	0.66	0.48	0.3	0.76	0.59	0.6	0.46	0.48	0.81	0.49	0.51	0.65	0.58
Er	2.02	1.38	0.81	2.08	1.62	1.66	1.42	1.46	2.03	1.45	1.47	1.84	1.69
Tm	0.3	0.22	0.11	0.33	0.25	0.25	0.2	0.22	0.38	0.24	0.23	0.27	0.24
Yb	2.04	1.32	0.72	2.01	1.63	1.61	1.26	1.25	2.17	1.31	1.5	1.55	1.56
Lu	0.32	0.22	0.11	0.33	0.25	0.24	0.2	0.2	0.38	0.23	0.24	0.31	0.24
Mg#	59	70	45	57	63	65	68	62	60	62	66	66	49
La/Yb_N	5.7	4.0	2.3	5.6	6.3	5.7	3.2	3.2	5.4	5.7	3.6	6.3	7.7

Notes: OPm=Otter Pond mafic suite; Mg#=Mg/(Mg+Fe^{2+}), assuming Fe^{3+}/Fe^{2+}=0.1; b.d.=below detection limit

Table A3.1 (continued)

sample	VL01A 118	VL01A 258b	VL01A 267	VL01A 354b	VL01A 081	VL01J 225a	VL01J 229a	VL01J 238c	VL01J 227b	VL01J 231a	VL01J 229b	VL01J 232	VL01J 238b
Unit	OPgd	OPgd	OPgd	OPgd	OPr	PPSt	PPSt	PPSt	PPSd	PPSd	PPSd	PPSd	PPSd
SiO_2	72.06	72.75	68.04	73.20	70.18	72.25	67.03	74.62	50.08	48.90	48.54	52.07	48.98
TiO_2	0.29	0.27	0.49	0.21	0.46	0.15	0.36	0.14	1.07	0.57	0.93	0.54	1.08
Al_2O_3	14.11	13.76	15.24	14.02	11.76	14.38	16.60	13.84	18.48	17.61	16.74	17.36	16.24
Fe2O3*	2.65	2.47	4.21	2.09	7.40	1.58	3.63	1.47	11.22	10.92	10.50	9.85	10.18
MnO	0.09	0.09	0.08	0.03	0.32	0.02	0.04	0.05	0.24	0.18	0.18	0.18	0.18
MgO	0.80	0.90	1.23	0.91	2.76	0.58	1.22	0.52	3.69	7.06	7.30	6.10	8.11
CaO	1.95	1.65	3.94	2.73	1.98	3.12	5.25	1.75	9.13	11.84	11.53	10.70	10.74
Na_2O	4.69	3.13	4.39	4.51	1.68	3.10	3.61	3.89	4.18	1.59	2.49	2.38	2.77
K_2O	1.35	3.07	1.01	0.94	1.97	3.02	0.91	3.24	0.51	0.40	0.99	0.33	1.04
P_2O_5	0.07	0.05	0.10	0.05	0.14	0.06	0.12	0.04	0.30	0.07	0.22	0.08	0.27
LOI	2.49	1.60	1.64	1.14	1.35	0.83	0.91	0.64	0.54	0.86	1.03	0.74	1.02
Total	100.54	99.83	100.37	99.83	100.02	99.10	99.68	100.21	99.44	99.99	100.44	100.33	100.62
Trace elements (ppm)													
Ba	735	818	419	392	503	3185	864	1686	242	176	384	210	395
Cr	1	21	1	34	98	7	8	7	11	67	124	63	308
Cs	1.74	1.60	0.19	1.64	2.35	0.81	1.03	1.18	0.14	0.64	3.69	0.14	1.06
Cu	7.9	3.8	9.2	33.3	67.9	27.4	11.7	21.8	48.9	82.7	75.4	58.3	74.7
Hf	3.30	3.40	2.99	5.00	2.50	2.85	2.73	3.34	0.75	1.08	1.98	1.38	2.58
Nb	3.55	5.80	3.12	10.89	7.72	1.89	2.04	6.02	2.27	1.71	3.35	1.77	3.02
Ni	b.d.	b.d.	b.d.	5	51	b.d.	5	b.d.	6	37	73	30	101
Pb	5.0	8.8	3.5	9.5	11.6	9.0	7.8	18.0	3.7	3.7	4.0	4.4	4.1
Rb	39.8	69.9	23.2	50.8	58.0	77.7	30.1	99.0	5.8	9.4	26.2	3.3	49.2
Sc	7.5	7.0	10.7	5.3	16.7	2.1	5.3	3.7	37.9	43.0	38.8	36.5	36.2
Sr	221	334	244	285	120	304	329	188	406	377	402	347	279
Th	9.56	8.60	5.50	13.06	7.73	17.69	1.92	6.64	1.71	0.41	3.79	1.20	3.48
V	27	15	55	24	89	24	45	16	195	286	268	243	221
U	1.70	2.00	1.07	2.13	1.79	0.88	0.51	1.56	0.45	0.12	0.99	0.27	1.10
Y	19.2	25.8	19.9	35.6	21.5	6.7	9.9	18.7	21.4	15.9	20.2	13.4	27.8
Zn	62.5	36.0	32.3	25.8	57.2	11.2	27.7	18.3	96.0	60.7	67.0	59.6	69.8
Zr	124.6	122.9	122.2	198.5	90.7	120.7	126.2	115.8	23.8	28.5	85.6	45.2	103.6
La	27.6	27.5	18.0	34.5	25.9	61.0	21.1	21.9	10.8	10.7	14.0	12.9	17.5
Ce	49.5	46.6	33.2	69.2	69.2	87.3	32.9	40.8	22.4	25.3	30.1	26.5	37.4
Pr	5.58	5.48	4.18	8.60	6.22	9.88	3.34	4.74	3.14	3.47	4.20	3.33	5.17
Nd	19.7	21.8	16.3	32.4	23.3	30.7	11.1	16.0	14.3	14.3	18.3	13.1	22.4
Sm	3.54	4.20	3.48	6.25	4.64	3.98	1.63	3.08	3.62	3.11	4.24	2.79	5.42
Eu	0.91	0.65	1.19	1.07	1.06	0.95	0.59	0.85	1.41	0.92	1.34	0.89	1.69
Gd	3.12	3.95	3.35	5.67	4.19	2.4	1.47	2.51	3.83	2.8	3.95	2.5	5.4
Tb	0.48	0.6	0.54	0.9	0.65	0.27	0.21	0.41	0.6	0.42	0.59	0.40	0.84
Dy	2.91	4.09	3.38	5.4	3.87	1.25	1.31	2.79	3.74	2.65	3.52	2.32	4.82
Ho	0.65	0.82	0.76	1.14	0.81	0.23	0.3	0.62	0.82	0.58	0.73	0.48	1.00
Er	1.97	2.47	2.11	3.55	2.51	0.61	0.89	1.84	2.28	1.6	2.02	1.45	2.76
Tm	0.31	0.42	0.33	0.58	0.35	0.09	0.14	0.3	0.34	0.25	0.31	0.22	0.41
Yb	2.2	2.86	2.06	3.96	2.40	0.62	0.88	2.08	2.18	1.61	1.84	1.39	2.53
Lu	0.35	0.4	0.34	0.64	0.37	0.12	0.15	0.35	0.33	0.25	0.3	0.23	0.39
Mg#	40	44	39	49	45	44	42	44	42	58	60	57	63
La/Yb_N	9.0	6.9	6.3	6.3	7.7	70.6	17.2	7.6	3.6	4.8	5.4	6.7	5.0

Notes: OPgd=Otter Pond granodiorite; OPr=Otter Pond rhyolite; PPSt=Pierre's Pond Suite tonalite; PPSd= Piere's Pond Suite diorite

Table A3.1 (continued)

sample	VL01J 260b	VL01J 118	VL01J 120	VL01J 016A	WXNF 108	WXNF 117	WXNF 199	WXNF 216	WXNF 222	WXNF 223	WXNF 224	WXNF 225	WXNF 227
Unit	PPSd	PLM	PLM	PLM	PLM	PLM	PLM	PLM	PLM	PLM	PLM	PLM	PLM
SiO_2	49.17	44.60	49.82	51.74	49.06	53.46	50.00	53.30	48.90	48.00	53.10	47.40	43.95
TiO_2	0.71	0.86	0.76	0.70	0.80	0.64	0.91	0.78	0.94	1.03	0.67	1.01	1.22
Al_2O_3	15.85	16.88	16.28	16.93	16.50	16.70	15.50	16.30	16.30	16.00	16.70	15.60	15.25
Fe2O3*	9.69	10.52	9.16	10.53	9.60	7.84	8.78	7.51	9.40	10.01	7.48	9.91	11.15
MnO	0.17	0.19	0.16	0.19	0.17	0.17	0.16	0.15	0.17	0.17	0.15	0.17	0.19
MgO	8.91	7.71	5.83	4.61	5.49	4.11	5.82	4.25	6.29	6.21	4.26	6.36	8.47
CaO	12.87	12.05	9.76	8.64	9.28	7.76	9.68	7.71	10.47	10.79	7.87	10.83	12.57
Na_2O	2.08	1.49	1.98	2.98	2.08	2.39	1.90	2.40	2.50	3.00	2.60	1.70	1.10
K_2O	0.39	2.73	3.83	2.03	3.69	4.49	3.99	4.64	2.67	1.39	4.34	3.55	2.76
P_2O_5	0.07	0.90	0.74	0.42	0.71	0.52	0.73	0.53	0.84	0.83	0.53	0.82	0.93
LOI	0.85	1.56	0.99	1.18	0.90	1.10	0.60	0.50	0.40	0.60	0.80	0.40	0.60
Total	100.76	99.49	99.31	99.94	98.62	99.95	97.49	97.56	98.18	97.32	98.02	97.14	97.43
Trace elements (ppm)													
Ba	87	1690	1782	646	2092	1720	1900	1700	1400	1000	1400	1600	1300
Cr	342	167	117	73	103	61	105	81	116	116	80	125	201
Cs	0.88	2.10	1.95	1.13	0.00	0.00	1.90	1.90	0.86	0.98	1.00	2.00	2.65
Cu	83.1	94.2	86.3	85.7	75.5	59.5	99.0	49.0	32.0	48.0	51.0	108.0	165.0
Hf	1.19	2.76	1.86	1.89	3.12	4.53	1.80	7.20	2.20	6.30	4.10	3.30	2.45
Nb	1.14	11.88	5.90	7.73	11.42	8.15	5.70	9.60	5.50	15.00	7.40	11.00	14.00
Ni	89	80	42	20	33	22	39	28	41	41	29	42	65
Pb	2.0	5.4	12.2	16.5	14.3	19.5	14	17	10	9	15	12	8
Rb	8.1	123.8	136.4	72.2	121.0	163.9	140	160	100	49	150	150	150
Sc	44.2	41.3	32.3	30.0	36.7	25.1	32	22	32	33	23	33	45
Sr	307	450	450	450	829	710	701	642	759	768	671	788	644
Th	1.22	4.45	5.72	15.14	9.63	10.44	4.8	11.0	3.8	13.0	12.0	4.9	4.1
V	253	324	290	217	295	224	259	193	278	276	197	280	332
U	0.36	0.85	1.41	3.45	0.00	0.00	1.30	2.80	1.30	2.90	2.90	1.30	0.95
Y	17.1	33.1	28.0	27.6	22.9	21.1	27.0	26.0	28.0	31.0	27.0	29.0	32.0
Zn	50.3	70.1	62.8	85.0	63	59	70	65	77	80	68	79	95
Zr	41.5	112.8	61.2	69.4	86	137	62	280	85	240	180	150	84
La	6.3	73.4	53.0	64.4	62.7	58.4	51.0	57.0	51.0	73.0	57.0	63.0	61.0
Ce	12.6	149.6	110.4	118.1	127.0	120.0	109.0	116.0	109.0	143.0	115.0	132.0	135.5
Pr	1.74	20.12	14.72	14.24	15.55	14.14	14.00	13.00	14.00	18.00	14.00	16.00	17.00
Nd	8.1	79.9	59.4	53.2	59.9	56.9	56.0	54.0	58.0	70.0	53.0	66.0	69.5
Sm	2.23	15.21	11.23	9.33	10.77	10.23	10.00	9.50	11.00	12.00	9.30	12.00	13.00
Eu	0.83	3.62	2.78	2.24	2.62	2.40	2.40	2.30	2.70	2.70	2.20	2.70	2.60
Gd	2.66	11.11	8.36	7.51	8.37	7.56	8.00	7.20	8.50	9.50	7.30	9.10	10.00
Tb	0.45	1.38	1.03	0.99	0.99	0.93	1.00	0.97	1.10	1.30	0.96	1.20	1.30
Dy	2.9	6.8	5.33	5.29	5.29	5.12	5.10	4.80	5.20	5.90	4.80	5.50	6.30
Ho	0.61	1.19	0.99	1.03	0.88	0.96	0.92	0.89	0.96	1.10	0.89	1.00	1.10
Er	1.82	2.83	2.44	2.71	2.34	2.50	2.10	2.10	2.20	2.50	2.20	2.40	2.60
Tm	0.27	0.38	0.34	0.35	0.30	0.35	0.30	0.31	0.31	0.36	0.31	0.33	0.35
Yb	1.61	2.16	1.98	2.26	1.86	2.06	1.90	2.10	2.00	2.30	2.10	2.10	2.20
Lu	0.26	0.319	0.327	0.348	0.27	0.31	0.30	0.33	0.31	0.37	0.33	0.32	0.35
Mg#	67	61	58	49	55	53	59	55	59	57	55	58	62
La/Yb_N	2.8	24.4	19.2	20.4	24.1	20.3	19.3	19.5	18.3	22.8	19.5	21.5	19.9

Notes: PPSd= Piere's Pond Suite diorite; PLM=Portage Lake monzogabbro

Table A3.2: Nd isotopic data of syn-kinematic plutonic rocks

Sample	Unit	Nd	Sm	(143/144)m	(147/144)m	(143/144)i	CHURi	Age	$(\varepsilon_{Nd})t$
VL010084	Opm	15.59	3.35	0.512389 ±17	0.1299	0.5120	0.512035	468 Ma	-0.9
VL01J036b	Opm	12.79	2.96	0.512371 ±9	0.1399	0.5119	0.512035	468 Ma	-1.8
VL01A081	OPr	20.83	4.21	0.512063 ±20	0.1222	0.5117	0.512035	468 Ma	-6.8
VL01J232	PPSd	12.89	2.67	0.512163 ±10	0.1254	0.5118	0.512050	457 Ma	-5.1
VL01J118	PLM	76.07	14.52	0.512145 ±9	0.1154	0.5118	0.512043	462 Ma	-4.8
WXNF117	PLM	50.34	9.25	0.512191 ±17	0.1111	0.5119	0.512043	462 Ma	-3.7
WXNF216	PLM	48.37	8.82	0.512127 ±6	0.1102	0.5118	0.512043	462 Ma	-4.9
WXNF227	PLM	64.94	12.41	0.512190 ±16	0.1155	0.5118	0.512043	462 Ma	-4.0
VL01J016a	PLM	50.35	9.21	0.512204 ±9	0.1106	0.5119	0.512041	464 Ma	-3.4

Note: Abbreviations as in Table 1

Table A3.3: Ar/Ar data of Lloyds River Fault Zone amphibolites

#[1]	Power[2]	Vol. ^{39}Ar $x10^{-11}$ cc	$^{36}Ar/^{39}Ar$	$^{37}Ar/^{39}Ar$	$^{38}Ar/^{39}Ar$	$^{40}Ar/^{39}Ar$	$\%^{40}Ar$ ATM	$^{*40}Ar/^{39}Ar$	f_{39}[3] (%)	Apparent Age Ma[4]
1	VL01J261A Hornblende; J[5]=.01475990 (Z7152; UTM[6] 21456448/5355510)									
	Aliquot A									
	2.4	0.0302	0.2626 ± 0.0409	3.431 ± 0.305	3.117 ± 0.156	98.109 ± 8.397	79.2	20.406 ± 12.397	0.1	474.98 ± 253.96
	3.0	0.1817	0.0695 ± 0.0076	4.184 ± 0.124	0.789 ± 0.034	40.890 ± 1.485	50.3	20.319 ± 2.258	0.3	473.20 ± 46.26
	3.9	0.3846	0.0183 ± 0.0026	4.007 ± 0.109	0.246 ± 0.014	25.460 ± 0.760	21.3	20.040 ± 0.892	0.7	467.48 ± 18.32
	4.6	9.4429	0.0017 ± 0.0002	12.122 ± 0.101	0.811 ± 0.012	20.596 ± 0.108	2.4	20.095 ± 0.611	16.1	468.60 ± 12.55
	5.5	4.2294	0.0000 ± 0.0008	10.835 ± 0.089	0.674 ± 0.013	20.143 ± 0.117	0	20.133 ± 0.615	7.2	469.39 ± 12.63
	6.5	1.1513	0.0023 ± 0.0009	10.766 ± 0.127	0.699 ± 0.015	20.772 ± 0.268	3.2	20.098 ± 0.627	2	468.66 ± 12.87
	12.0	15.7649	0.0004 ± 0.0002	10.450 ± 0.068	0.703 ± 0.011	20.183 ± 0.049	0.7	20.048 ± 0.521	26.8	467.63 ± 10.72
	Aliquot B									
	2.4	0.0444	0.1593 ± 0.0376	2.713 ± 0.249	2.498 ± 0.221	66.774 ± 7.281	70.6	19.614 ± 10.358	0.1	458.70 ± 214.13
	3.0	0.3066	0.0593 ± 0.0042	2.738 ± 0.081	0.528 ± 0.021	37.793 ± 0.902	46.4	20.268 ± 1.275	0.5	472.14 ± 26.13
	3.9	0.5000	0.0148 ± 0.0039	4.185 ± 0.157	0.264 ± 0.015	24.419 ± 0.824	18	20.024 ± 1.315	0.9	467.15 ± 27.02
	4.6	8.2369	0.0021 ± 0.0002	10.501 ± 0.127	0.788 ± 0.014	20.706 ± 0.209	3	20.087 ± 0.561	14	468.43 ± 11.52
	5.5	16.8504	0.0009 ± 0.0001	10.210 ± 0.071	0.644 ± 0.011	20.289 ± 0.048	1.3	20.028 ± 0.509	28.7	467.22 ± 10.46
	6.5	0.8522	0.0014 ± 0.0012	10.212 ± 0.170	0.635 ± 0.020	20.520 ± 0.378	2.1	20.092 ± 0.687	1.5	468.54 ± 14.12
	12.0	0.7505	0.0020 ± 0.0012	10.912 ± 0.174	0.676 ± 0.015	20.688 ± 0.343	2.8	20.100 ± 0.684	1.3	468.71 ± 14.05
2	VL02J368A Hornblende; J=.02315970 (Z7586; UTM 21485040/5386911)									
	Aliquot A									
	3.0	0.6315	0.0292 ± 0.0039	5.318 ± 0.262	0.575 ± 0.018	27.344 ± 0.585	32.0	18.592 ± 0.810	0.4	646.01 ± 23.65
	3.5	0.3993	0.0187 ± 0.0066	2.549 ± 0.145	0.180 ± 0.015	18.590 ± 0.766	29.5	13.106 ± 1.433	0.3	478.20 ± 45.93
	4.2	6.1586	0.0020 ± 0.0005	6.141 ± 0.112	0.687 ± 0.013	13.728 ± 0.069	4.2	13.151 ± 0.331	4	479.67 ± 10.62
	4.6	28.9861	0.0014 ± 0.0001	6.112 ± 0.102	0.740 ± 0.011	13.491 ± 0.028	3.1	13.077 ± 0.305	18.6	477.28 ± 9.79
	5.0	13.6688	0.0008 ± 0.0002	6.032 ± 0.103	0.731 ± 0.011	13.105 ± 0.046	1.8	12.865 ± 0.304	8.8	470.46 ± 9.78
	6.0	0.8274	0.0015 ± 0.0035	7.339 ± 0.262	0.739 ± 0.023	13.782 ± 0.297	1.9	13.527 ± 0.844	0.5	491.66 ± 26.85
	12.0	8.0812	0.0010 ± 0.0004	6.913 ± 0.128	0.732 ± 0.012	13.373 ± 0.060	2.0	13.101 ± 0.355	5.2	478.06 ± 11.39
	Aliquot B									
	3.9	1.4655	0.0264 ± 0.0020	2.459 ± 0.125	0.412 ± 0.016	25.172 ± 0.353	31.1	17.334 ± 0.469	0.9	608.89 ± 13.99
	4.6	0.5851	0.0017 ± 0.0048	4.325 ± 0.166	0.420 ± 0.019	12.991 ± 0.469	0.8	12.890 ± 1.022	0.4	471.28 ± 32.88
	5.0	72.2574	0.0012 ± 0.0001	5.758 ± 0.101	0.727 ± 0.011	13.154 ± 0.025	2.8	12.785 ± 0.287	46.3	467.90 ± 9.24
	6.0	16.1870	0.0000 ± 0.0002	5.689 ± 0.103	0.722 ± 0.011	12.652 ± 0.039	-0.1	12.671 ± 0.289	10.4	464.21 ± 9.33
	12.0	6.7885	0.0006 ± 0.0004	6.326 ± 0.119	0.703 ± 0.012	12.800 ± 0.055	1.2	12.644 ± 0.326	4.4	463.34 ± 10.54

[1] Number refers to text and Figure 5.1
[2] As measured by laser in % of full nominal power (10W)
[3] Fraction 39Ar as percent of total run
[4] Errors are analytical only and do not reflect error in irradiation parameter.
[5] Nominal J, referenced to PP-20=1072 Ma (Roddick, 1983)
[6] UTM in NAD83
All uncertainties quoted at 2s level

Table A3.4: U-Pb TIMS analytical data of syn-kinematic plutons

#[1]	Fraction[2]	Description[3]	Wt. ug	U ppm	Pb[4] ppm	206Pb[5] 204Pb	Pb[6] pg	Isotopic Ratios[7] 208Pb 206Pb	207Pb 235U	±1SE Abs	206Pb 238U	±1SE Abs	Corr.[8] Coeff.	207Pb 206Pb	±1SE Abs	Ages (Ma)[9] 206Pb 238U	±2SE	207Pb 235U	±2SE	207Pb 206Pb	±2SE	% Disc
3	VL01J120 (Z7508; UTM[10] 21458004/5362821); Portage Lake monzogabbro																					
	1-1(Z;5)	Co, Clr, An, Frag, Dia, 250	33	251	21	5398	7	0.27	0.57578	0.00120	0.07419	0.00012	0.847	0.05628	0.00006	461.4	1.4	461.7	1.5	463.6	5.0	0.5
	3-1(Z;2)	Clr, El, Pr, Dia, 300	35	270	23	6599	7	0.27	0.57612	0.00080	0.07430	0.00008	0.857	0.05623	0.00004	462.0	1.0	462.0	1.0	461.6	3.2	-0.1
	4(Z;12)	Clr, El, Pr, Dia, 150	30	280	23	7031	5	0.26	0.57498	0.00091	0.07419	0.00010	0.914	0.05621	0.00004	461.3	1.2	461.2	1.2	460.8	2.9	-0.1
	5(Z;2)	Co, Clr, Mf, Dia, 300	29	178	15	6677	3	0.26	0.57467	0.00074	0.07404	0.00008	0.830	0.05629	0.00004	460.4	0.9	461.0	1.0	464.0	3.2	0.8
4	VL01J016 (Z7153; UTM 21446038/5349989); Monzodiorite																					
	2(Z;21)	Co, Clr, Eu, St, Dia, 150	34	689	52	8442	13	0.13	0.57143	0.00111	0.07364	0.00013	0.947	0.05628	0.00004	458.1	1.5	458.9	1.4	463.3	2.8	1.2
	3(Z;34)	Co, Clr, Eu, St, Dia, 100	27	486	38	5842	10	0.18	0.57538	0.00075	0.07416	0.00008	0.828	0.05627	0.00004	461.1	1.0	461.5	1.0	463.2	3.2	0.5
	4-1(Z;1)	Br, An, Frag, Dia, 75	17	2303	157	76503	2	0.02	0.57450	0.00093	0.07398	0.00011	0.960	0.05632	0.00003	460.1	1.3	460.9	1.2	465.0	2.0	1.1
	5-2(Z;10)	Co, Clr, An, Frag, Dia, 100	76	271	22	16974	6	0.21	0.57524	0.00083	0.07412	0.00009	0.946	0.05629	0.00003	460.9	1.1	461.4	1.1	463.8	2.1	0.7
	T1(T;11)	Br, Sh, Tab, fln, M75, 350	187	748	53	785	821	0.07	0.55973	0.00154	0.07231	0.00010	0.746	0.05614	0.00011	450.1	1.2	451.3	2.0	458.0	8.7	1.8
	T2(T;18)	Br, An, fln, M75, 200	131	650	45	403	989	0.06	0.56048	0.00329	0.07216	0.00015	0.677	0.05633	0.00027	449.2	1.8	451.8	4.3	465.4	20.8	3.6
	T3(T;26)	Br, Sh, fln, M75, 200	111	453	31	612	374	0.07	0.54962	0.00203	0.07142	0.00011	0.709	0.05581	0.00016	444.7	1.3	444.7	2.7	444.9	12.5	0.1
	T4(T;16)	Br, Sh, Mf, fln, M75, 200	47	432	32	381	244	0.16	0.53173	0.00268	0.06967	0.00012	0.662	0.05535	0.00023	434.2	1.4	433.0	3.6	426.4	18.3	-1.9
	T5(T;24)	Co, An, fln, M75, 200	68	285	20	358	250	0.10	0.54559	0.00325	0.07095	0.00012	0.666	0.05577	0.00028	441.9	1.5	442.1	4.3	443.4	21.9	0.4
6	VL01A258 (Z7313; UTM 21458607/5348154); Otter Pond granodiorite																					
	A1(Z;59)	Co, Clr, rln, St, NM0, 75	22	223	18	5266	4	0.19	0.58544	0.00094	0.07529	0.00007	0.771	0.05640	0.00006	467.9	0.9	468.0	1.2	468.0	4.7	0.0
	A2(Z;65)	Co, Clr, rln, St, NM0, 75	26	199	16	3385	7	0.19	0.58521	0.00092	0.07515	0.00011	0.761	0.05648	0.00006	467.1	1.3	467.8	1.2	471.3	4.6	0.9
	B1(Z;75)	Co, Clr, rln, Eq, NM0, 70	26	261	21	5627	4	0.18	0.58479	0.00096	0.07547	0.00011	0.786	0.05620	0.00006	469.0	1.3	467.5	1.2	460.2	4.5	-2.0
	B2(Z;74)	Co, Clr, fln, Eq, NM0, 70	33	125	10	3966	5	0.18	0.59314	0.00078	0.07608	0.00008	0.808	0.05655	0.00004	472.7	0.9	472.9	1.0	473.9	3.4	0.3

Notes:

[1] Number refers to text and Figure 5.1

[2] Z=zircon fraction; T=titanite fraction. All zircon fractions are abraded following the method of Krogh (1982). Number in brackets refers to the number of grains in the analysis.

[3] Zircon descriptions: Co=Colorless, Br=brown, Clr=Clear, fln=Few Inclusions, rln=Rare Inclusions, Eu=Euhedral, Sh=Subhedral, An=Anhedral, Pr=Prismatic, St=Stubby Prism Mf=multifaceted, Tab=Tabular, Fr=Fragments, Dia=Diamagnetic, NM0=NonMag @1.8A 0°SS, M75=Magnetic @ 0.75A 10°SS; Number refers to average size of zircons in um.

[4] Radiogenic Pb

[5] Measured ratio, corrected for spike and fractionation

[6] Total common Pb in analysis corrected for fractionation and spike

[7] Corrected for blank Pb and U and common Pb, errors quoted are 1 sigma absolute; procedural blank values for this study ranged from 0.1- 0.2 pg U and 2-4 pg Pb for zircon analyses and 1-2 pg U and 8-9 pg Pb for titanite analyses; Pb blank isotopic composition is based on the analysis of procedural blanks; corrections for common Pb were made using Stacey-Kramers compositions.

[8] Correlation Coefficient

[9] Corrected for blank and common Pb, errors quoted are 2 sigma in Ma

[10] UTM in NAD83

Table A3.5: U-Pb SHRIMP analytical data of Pierre's Pond suite diorite

#[1]	Spot name[2]	U (ppm)	Th (ppm)	Th/U	Pb* (ppm)	^{204}Pb (ppb)	$^{204}Pb/^{206}Pb$	$\pm ^{204}Pb/^{206}Pb$	$f(206)^{204}$	$^{208}Pb/^{206}Pb$	$\pm ^{208}Pb/^{206}Pb$	$^{207}Pb/^{235}U$	$\pm ^{207}Pb/^{235}U$	$^{206}Pb/^{238}U$	$\pm ^{206}Pb/^{238}U$	Corr Coeff	$^{207}Pb/^{206}Pb$	$\pm ^{207}Pb/^{206}Pb$	Ages (Ma)[3] $^{206}Pb/^{238}U$	$\pm ^{206}Pb/^{238}U$	$^{207}Pb/^{206}Pb$	$\pm ^{207}Pb/^{206}Pb$	Ages (Ma)[4] $^{206}Pb/^{238}U$	$\pm ^{206}Pb/^{238}U$
5	VL02J238D (Z7524; UTM[5] 21481714/5381618): Diorite Star Lake																								
	7524-18.1	333	237	0.734	27	7	0.000352	0.000135	0.0061	0.2288	0.0071	0.5419	0.0241	0.0722	0.0008	0.378	0.0545	0.0023	449	5	390	96	449	5
	7524-4.1	292	156	0.551	23	7	0.000362	0.000111	0.0063	0.1897	0.0061	0.5674	0.0231	0.0724	0.0008	0.394	0.0569	0.0022	451	5	486	86	450	5
	7524-3.1	171	52	0.314	12	7	0.000612	0.000227	0.0106	0.1115	0.0096	0.5953	0.0398	0.0724	0.0010	0.315	0.0596	0.0038	451	6	589	145	450	5
	7524-8.1*	138	59	0.440	10	3	0.000291	0.000161	0.0050	0.1304	0.0068	0.5443	0.0302	0.0728	0.0009	0.332	0.0543	0.0029	453	5	382	123	454	5
	7524-5.1	180	64	0.367	13	9	0.000766	0.000266	0.0133	0.1267	0.0112	0.5606	0.0454	0.0730	0.0011	0.300	0.0557	0.0043	454	6	440	183	455	6
	7524-26.1	451	199	0.455	34	9	0.000331	0.000134	0.0057	0.1344	0.0058	0.5512	0.0245	0.0730	0.0009	0.379	0.0548	0.0023	454	5	402	96	455	5
	7524-12.1	114	42	0.375	9	6	0.000845	0.000270	0.0146	0.1272	0.0123	0.5637	0.0467	0.0732	0.0010	0.283	0.0558	0.0045	455	6	446	189	455	6
	7524-28.1*	104	46	0.451	8	0	0.000010	0.000010	0.0002	0.1420	0.0072	0.6058	0.0143	0.0734	0.0009	0.629	0.0599	0.0011	457	6	598	40	455	6
	7524-16.1*	155	53	0.351	11	2	0.000198	0.000137	0.0034	0.1104	0.0100	0.5708	0.0254	0.0736	0.0009	0.389	0.0563	0.0023	458	5	463	94	457	5
	7524-6.1	358	266	0.769	30	5	0.000239	0.000155	0.0041	0.2538	0.0127	0.5948	0.0273	0.0737	0.0008	0.361	0.0585	0.0025	459	5	549	97	457	5
	7524-9.1	365	31	0.087	25	2	0.000081	0.000076	0.0014	0.0311	0.0033	0.5902	0.0165	0.0737	0.0009	0.521	0.0581	0.0014	459	5	532	53	458	5
	7524-27.1	417	199	0.494	32	10	0.000367	0.000096	0.0064	0.1458	0.0064	0.5589	0.0233	0.0742	0.0009	0.397	0.0546	0.0021	461	5	397	89	462	5
	7524-14.1*	530	317	0.619	42	1	0.000038	0.000048	0.0007	0.1885	0.0031	0.5828	0.0119	0.0743	0.0008	0.624	0.0569	0.0009	462	5	486	36	462	5
	7524-17.1	414	234	0.583	33	7	0.000275	0.000076	0.0048	0.1805	0.0057	0.5704	0.0162	0.0747	0.0009	0.516	0.0554	0.0014	464	5	428	56	465	5
	7524-2.1*	577	435	0.779	48	10	0.000264	0.000074	0.0046	0.2417	0.0043	0.5470	0.0158	0.0751	0.0009	0.512	0.0528	0.0013	467	5	321	58	469	5
	7524-1.1	884	61	0.072	62	6	0.000097	0.000054	0.0017	0.0234	0.0022	0.5732	0.0171	0.0755	0.0009	0.492	0.0551	0.0014	469	5	415	60	470	5
	7524-20.1*	488	403	0.853	42	2	0.000064	0.000044	0.0011	0.2679	0.0039	0.5938	0.0152	0.0758	0.0011	0.675	0.0568	0.0011	471	7	483	43	471	7
	7524-21.1*	743	544	0.757	63	2	0.000048	0.000021	0.0008	0.2401	0.0021	0.5846	0.0094	0.0760	0.0009	0.844	0.0558	0.0005	472	6	443	19	473	6
	7524-27.1*	29	20	0.699	11	1	0.000089	0.000164	0.0015	0.2057	0.0074	5.7170	0.1636	0.3445	0.0047	0.580	0.1204	0.0028	1908	23	1961	43	1902	22

Notes (see Stern, 1997):

Uncertainties reported at 1s (absolute) and are calculated by numerical propagation of all known sources of error

$f206^{204}$ refers to mole fraction of total ^{206}Pb that is due to common Pb, calculated using the ^{204}Pb-method; common Pb composition used is the surface blank

[1] Number refers to text and Figure 5.1

[2] analyses marked by asterisk on GSC mount# 295, unmarked analyses from mount #312

[3] 204-corrected ages

[4] 207-corrected ages (Stern, 1997)

[5] UTM in NAD83

APPENDIX 4: ANALYTICAL PROCEDURES

U/PB ANALYTICAL PROCEDURES

U-Pb TIMS analytical methods utilized in this study are outlined in Parrish et al. (1987). Heavy mineral concentrates were prepared using standard crushing, grinding, Wilfley™ table, and heavy liquid techniques. Mineral separates were sorted by magnetic susceptibility using a Frantz™ isodynamic separator. Single and multigrain zircon fractions analyzed were very strongly air abraded following the method of Krogh (1982). Treatment of analytical errors follows Roddick (1987) with errors on the ages reported at the 2σ level (Table 2). U-Pb TIMS concordia diagrams are presented in Fig. 7.

SHRIMP II analyses were conducted at the Geological Survey of Canada (GSC) using analytical procedures described by Stern (1997), with standards and U-Pb calibration methods following Stern and Amelin (2003). Zircons from the samples were cast in 2.5 cm diameter epoxy mounts (GSC mount #284 for samples VLA02178 (z7518) and VL02294 (z7522), GSC mount #254 for sample RAX01-908 (z7097), GSC mount #257 for sample VLA01-067 (z7630), and GSC mount #295 for sample VLA01-314 (z7630)) along with fragments of the GSC laboratory standard zircon (z6266, with $^{206}Pb/^{238}U$ age = 559 Ma).

The mid-sections of the zircons were exposed using 9, 6, and 1 μm diamond compound, and the internal features of the zircons were characterized with backscatter electrons (BSE) utilizing a Cambridge Instruments scanning electron microscope (SEM). Mount surfaces were evaporatively coated with 10 nm of high purity Au. Analyses were conducted using an $^{16}O^-$ primary beam, projected onto the zircons at 10 kV. The sputtered area used for analysis was ca. 25 μm in diameter with a beam current of ca. 6 nA for z7518 and z7522, ca. 13 nA for z7097 and z7252, and c. 5 nA for z7630. The count rates of ten isotopes of Zr^+, U^+, Th^+, and Pb^+ in zircon were sequentially measured over 6 scans for all samples except z7630 (4 scans) with a single electron multiplier and a pulse counting system with dead time of 35 ns. Off-line data processing was accomplished using customized in-house software. The 1σ external errors of $^{206}Pb/^{238}U$ ratios reported in Table 1 incorporate a ±1.0 % error in calibrating the standard zircon (see Stern and Amelin, 2003). No fractionation correction was applied to the Pb-isotope data; common Pb correction utilized the

measured $^{204}Pb/^{206}Pb$ and compositions modeled after Cumming and Richards (1975). The $^{206}Pb/^{238}U$ ages for the analyses have been corrected for common Pb using both the 204- and 207-methods (Stern, 1997), but there is generally no significant difference in the results (Table 2). Isoplot v. 2.49 (Ludwig, 2001) was used to generate concordia plots and calculate weighted means. The data are plotted in concordia diagrams with errors at the 2σ level (Fig. 7). A Concordia age (Ludwig, 1998) is calculated for some of the samples presented in this paper. A Concordia age incorporates errors on the decay constants and includes both an evaluation of concordance and an evaluation of equivalence of the data (how well the data fit the assumption that they are repeated measurements of the same point). The calculated Concordia ages and errors quoted in the text are at 2σ with decay constant errors included.

SM/ND ANALYTICAL PROCEDURES

Samples VL01A057, RAX01047, RAX01049, RAX01051, and RAX01059 were analyzed at Geospec (Edmonton Canada). The isotopic composition of Nd was determined in multi-dynamic mode by Thermal Ionization Mass Spectrometry (TIMS). The $^{143}Nd/^{144}Nd$ ratio of samples, normalized for variable mass fractionation, is presented relative to a value of 0.512107 for the Geological Survey of Japan Nd isotopic standard JNdi-1 (Tanaka et al., 2000), which is equivalent to a value of 0.511850 for the La Jolla Nd isotopic standard. Sm isotopic abundances were measured in static mode by TIMS and were normalized for variable mass fractionation. For Nd, the long-term average value for JNdi-1 is 0.512110 ± 0.000012 (1sd), equivalent to a value of 0.511853 for the La Jolla Nd isotopic standard, and within the generally accepted window of La Jolla values (0.511850 ± 0.000010). For Sm, the long-term average value for $^{149}Sm / ^{154}Sm$ determined from a Sm standard solution was 0.60759 ± 0.00009 (1sd), identical within quoted uncertainty to the value determined by Wasserburg et al. (1981) of 0.60750 ± 0.00002.

Samples VL01A097a, VL01A097a, VL01A360, VL02A283, VL02A295 were analyzed at Ottawa-Carleton Geoscience Centre Radiogenic Isotope Research Laboratory (Ottawa, Canada) using a Finnigan MAT261 multicollector mass spectrometer equipped with an electron multiplier. Samples were spiked with a mixed ^{148}Nd-^{149}Sm spike prior to dissolution. Concentrations were precise to + 1%, but $^{147}Sm/^{144}Nd$ ratios were reproducible to 0.5%. Samples were loaded with 0.25N

HCl on one side of a Re double filament, and run at temperatures of 1780-1820°C. Isotope ratios were normalized to $^{146}Nd/^{144}Nd = 0.72190$. Analyses of the USGS standard BCR-1 yield Nd = 29.02 ppm, Sm = 6.68 ppm, and $^{143}Nd/^{144}Nd = 0.512668$ +/- 20 (n=4). 32 runs of the La Jolla standard average $^{143}Nd/^{144}Nd = 0.511875$ +/- 18 (Sept. 1992-Sept. 1994).

WHOLE ROCK GEOCHEMISTRY ANALYTICAL PROCEDURES

Multiple laboratories, listed in Table DR1, were employed for analysis of samples. Detailed information on sample preparation and analytical procedures is available in Rogers (2004). Detection limits for all laboratories are listed in Table DR1. McGill University Geochemical Laboratories (Montreal, Canada) were utilized for XRF determination of major and select trace elements on glass pellets using PHILIPS PW2440 4kW automated XRF spectrometer, with accuracy within 1%. Ontario Geological Survey Laboratories (Sudbury, Canada) determined major and select trace elements on the Rigaku RIX-3000 WD-XRF; trace elements were analyzed on the Perkin-Elmer ELAN 5000 ICP-MS. Precision and accuracy are described in Richardson et al. (1996). Geological Survey of Canada Analytical Chemistry Laboratory (Ottawa, Canada) was utilized for both XRF (major elements) and ICP-MS (trace elements). The precision for trace elements is generally better than 10%. X-Ray Laboratories (XRAL, Toronto, Canada) determined major elements in duplicate on fused glass discs. Pressed powder pellets were utilized for select trace elements. Analysis of trace elements at Memorial University of Newfoundland (St. John's, Canada) followed the methods and had accuracy and precision outlined in Jenner et al. (1990).

ELECTRON MICROPROBE ANALYTICAL PROCEDURES

Mineral compositions were analyzed by electron microprobe at the Geological Survey of Canada (Ottawa) using a wavelength-dispersive Cameca SX-50, a mixture of natural and synthetic standards, and ZAF matrix correction procedures described by Armstrong (1988). Accelerating voltage and beam current were 20 kV and 10nA, respectively, and counting time was 15 seconds.

REFERENCES

Abbott, L.D., Silver, E.A., Galewsky, J., 1994, Structural evolution of a modern arc-continent collision in Papua New Guinea. Tectonics, v. 12 (5), p. 1007-1034.

Alvarez-Marron, J., Brown, D., Perez-Estaun, A., Puchkov, V., Gorozhanina, Y., 2000, Accretionary complex structure and kinematics during Paleozoic arc-continent collision in the southern Urals. Tectonophysics, v. 325, p. 175-191.

Apted, M.J., Liou, J.G, 1983; Phase relations among greenschist, epidote-amphibolite, and amphibolite in a basaltic system. American Journal of Science, v. 283a, p. 328-354.

Armstrong, H.A., Owen, A.W., 2001. Terrane evolution of the paratectonic Caledonides of northern Britain. Journal of the Geological Society of London, 158, 475-486.

Arnott, R.J., McKerrow, W.S., Cocks, L.R.M., 1985, The tectonics and depositional history of the Ordovician and Silurian rocks of the Notre Dame Bay, Newfoundland. Canadian Journal of Earth Sciences, v. 22, p. 607-618.

Barnes, S.J., 1986, The effect of trapped liquid crystallization on cumulus mineral compositions in layered intrusions. Contributions to Mineralogy and Petrology, v. 93, p. 524-531.

Barr, S.M., Kerr, A., 1997. Late Precambrian plutons in the Avalon Terrane of New Brunswick, Nova Scotia, and Newfoundland. In: Sinha, A.K., Whalen, J.B., Hogan, J.P. (Eds), The nature of magmatism in the Appalachian Orogen. Memoir – Geological Society of America, 191, 45-74.

Barr, S.M., Raeside, R.P., White, C.E., 1998. Geological correlations between Cape Breton Island and Newfoundland, northern Appalachian Orogen. In: Quinlan, G. (Ed.), Lithoprobe East transect. Canadian Journal of Earth Sciences, 35, 1252-1270.

Barr, S.M., White, C.E., 1996. Contrasts in late Precambrian – early Paleozoic tectonothermal history between Avalon composite terrane sensu stricto and other possible per-Gondwanan terranes in southern New Brunswick and Cape Breton Island, Canada. In: Nance, R.D., Thompson, M.D. (Eds.), Avalonian and related peri-Gondwanan terranes of the Circum-North Atlantic. Special Paper – Geological Society of America, 304, 95-108.

Barr, S.M., White, C.E., Miller, B.V., 2003. Age and geochemistry of Late Neoproterozoic and Early Cambrian igneous rocks in southern New Brunswick: similarities and contrasts. Atlantic Geology, 39, 55-73.

Bédard, J.H., 1994, A procedure for calculating the equilibrium distribution of trace elements among the minerals of cumulate rocks, and the concentration of trace elements in the coexisting liquids. Chemical Geology, v. 118, p.143-153.

Bédard, J.H., 1999, Petrogenesis of boninites from the Betts Cove ophiolite, Newfoundland, Canada: Identification of subducted source components. Journal of Petrology, v. 40, p. 1853-1889.

Bédard, J.H., in press, Partitioning coefficients between olivine and silicate melts. Lithos.

Bédard, J.H., Lauzière, K., Tremblay, A., and Sangster, A., 1998, Evidence for forearc seafloor spreading from the Betts Cove ophiolite, Newfoundland: oceanic crust of boninitic affinity. Tectonophysics, v. 284, p. 233-245.

Berman, R.G., 1988, Internally-consistent thermodynamic data for stoichiometric minerals in the system Na2O-K2O-CaO-MgO-FeO-Fe2O3-Al2O3-SiO2-TiO2-H2O-CO2. Journal of Petrology, v. 29, p. 445-522.

Bostock, H.H., 1988, Geology and petrochemistry of the Ordovician volcano-plutonic Robert's Arm group, Notre Dame Bay, Newfoundland. Geological Survey of Canada Bulletin 369, 84 p.

Boucot, A.J., 1962, Appalachian Siluro-Devonian, Some aspects of the Variscan fold belt. Inter-Univ. Geol. Cong., 9th, Exeter.

Brace, T.D., Squires, G.C., Hussey, A.M., 2001. 2000 impost report for Reid Lot 234 and A.N.D. Charter (pionjar till survey, re-logging diamond drill core, geological and lithogeochemical re-interpretations, diamond drilling), Tally Pond area, central Newfoundland (NTS 12A/9, 10). Unpublished assessment report, Thundermin Resources Inc., 70 p.

Bradley, D. C., 1983, Tectonics of the Acadian Orogeny in New England and adjacent Canada: Journal of Geology, v. 91, no. 4, p. 381-400.

Cabanis, B., Lecolle, M., 1989. Le diagramme La/10 – Y/15 – Nb/8: un outil pour la discrimination des series volcaniques et la mise en evidence des processus de mélange et/ou de

contamination crustal. Comptes Rendus de l'Academie des Sciences, Series II, 309, 2023-2029.

Calon, T.J., and Green, F.K., 1987, Preliminary results of a detailed structural analysis of the Buchans Mine area. In Kirkham, R.V., ed., Buchans Geology, Newfoundland. Geological Survey of Canada, Paper 86-24, p. 273-288.

Cann, J.R . 1970, Rb, Sr, Y, Zr, and Nb in some ocean floor basaltic rocks. Earth and Planetary Science Letters, vol. 58, p. 7-11.

Cawood, P.A., Dunning, G.R., Lux, D., van Gool, J.A.M., 1994, Timing of peak metamorphism and deformation along the Appalachian margin of Laurentia in Newfoundland: Silurian not Ordovician. Geology, v. 22, p. 399-402.

Cawood, P.A., McCausland, P.J.A., and Dunning, G.R., 2001, Opening Iapetus; constraints from the Laurentian margin in Newfoundland. Geological Society of America Bulletin, v. 113, p. 443-453.

Cawood, P.A., Nemchin, A.A., 2001, Paleogeographic development of the east Laurentian margin: Constraints from U-Pb dating of detrital zircons in the Newfoundland Appalachians. Geological Society of America Bulletin, v. 113 (9), p. 1234-1246.

Cawood, P.A., van Gool, J.A.M., and Dunning, G.R., 1996, Geological development of eastern Humber and western Dunnage zone: Corner Brook – Glover Island region. Canadian Journal of Earth Sciences, v. 33, p.182-198.

Chandler, F.W., Sullivan, R.W., Currie, K.L., 1987, The age of the Spingdale Group, western Newfoundland, and correlative rocks – evidence for a Llandovery overlap assemblage in the Canadian Appalachians. Transaction of the Royal Society of Edingburgh: Earth Sciences, v. 78, p. 41-49.

Chen, B., Jahn, B, Wilde, S., and Xu, B., 2000, Two contrasting Paleozoic magmatic belts in northern Inner Mongolia, China: petrogenesis and tectonic implications. Tectonophysics, v. 328, p. 57-182.

Chung, S.-L., Wang, K-L., Crawford, A.J., Kamenetsky, V.S., Chen, H.-H., Lan, C.-Y., and Chen, C.H., 2001, High-Mg potassic rocks from Taiwan. implications for the genesis of orogenic potassic lavas: Lithos, v. 59, p. 153-170.

Cocks, L.R.M., Trosvik, T.H., 2002, Earth geography from 500 to 400 million years ago: a faunal and palaeomagnetic review. Journal of the Geological Society, London, v. 159, p. 631-644.

Coish, R.A., Rogers, N.W., 1987, Geochemistry of the Boil Mountain ophiolitic complex, northwest Maine, and tectonic implications. Contributions to Mineralogy and Petrology, v. 97, p. 51-65.

Colman-Sadd, S.P., Dunning, G.R., Dec, T., 1992. Dunnage – Gander relationships and Ordovician orogeny in central Newfoundland: A sediment provenance and U/Pb age study. American Journal of Science, 292, 317-355.

Compston, W., Wright, A.E., Toghill, P., 2002. Dating the late Precambrian volcanicity of England and Wales. Journal of the Geological Society of London, 159, 323-339.

Crawford, A.J., Falloon, T.J., Green, D.H., 1989, Classification, petrogenesis and tectonic setting of boninites, *in* Crawford, A.J., ed., Boninites and related rocks: London, Unwin Hyman, p. 1-49.

Cumming, G.L . Richards, J.R . 1975. Ore lead in a continuously changing Earth. Earth and Planetary Science Letters, v. 28, p. 55-171.

Currie, K.I., van Breeme, O., Hunt, P.A., van Berkel, J.T., 1991, Age of high-grade gneisses south of Grand Lake, Newfoundland. Atlantic Geology, v. 28, p. 153-161.

Davis, W.J., McNicoll, V.J., Bellerive, D.R., Santowski, K., and Scott, D.J., 1997, Modified chemical procedures for the extraction and purification of uranium from titanite, allanite and rutile in the Geochronology Laboratory, Geological Survey of Canada. Radiogenic Age and Isotopic Studies, Report 10, Geological Survey of Canada, Current Research, v. 1997-F, p. 33-35.

D'Lemos, R.S. and Holdsworth, R.A . 1995, Samarium-neodymium isotopic characteristics of the northeastern Gander Zone, Newfoundland Appalachians. In Hibbard, J.P. et al. (eds), Current Perspectives in the Appalachian-Caledonian Orogen, Geological Association of Canada, Special Paper 41, p. 239-252.

Davenport, P.H., Honarvar, P., Hogan, A., Kilfoil, G., King, D., Nolan, L.W., Ash, J.S., Colman-Sadd, S.P., Hayes, J.P., Liverman, D.G.E., Kerr, A., and Evans, D.T.W., 1996, Digital

geoscience atlas of the Buchans-Robert's Arm belt: Newfoundland Newfoundland Department of Mines and Energy, Geological Survey, Open File NFLD/2611, CD-ROM.

Dean, P.L., Strong, D.F., 1977, Folded thrust faults in Notre Dame Bay, central Newfoundland. American Journal of Science, v. 277(2), p. 97-108.

Dec, T., Swinden, H.S., 1994, Lithostratigraphic model, geochemistry and sedementology of the Cottrels Cove Group, Buchans-Roberts Arm vocanic belt, Notre Dame Subzone, *in* Current Research, Newfoundland Department of Mines and Energy, Geological Survey Branch, report 94-1, p. 77-100.

Dec, T., Swinden, H.S., and Dunning, G.R., 1997, Lithostratigraphy and geochemistry of the Cottrell's Cove Group, Buchans – Roberts Arm volcanic belt: new constraints for the paleotectonic setting of the Notre Dame Subzone, Newfoundland Appalachians. Canadian Journal of Earth Sciences, v. 34, p. 86-103.

DePaolo, D.J., 1981. Neodymium isotopes in the Colorado Front Range and implications for crust formation and mantle evolution in the Proterozoic. Nature, 291, 193-197.

Desnoyers, D., 1990a. Victoria Mine prospect. In: Swinden, H.S., Evans, D.T.W., Kean, B.F. (Eds.), Metallogenic framework of base and precious metal deposits, central and western Newfoundland. Eighth IAGOD Symposium Field Trip Guidebook. Geological Survey of Canada, Open File 2156, 65-67.

Desnoyers, D., 1990b. Bobby's Pond alteration zone. In: Swinden, H.S., Evans, D.T.W., Kean, B.F. (Eds.), Metallogenic framework of base and precious metal deposits, central and western Newfoundland. Eighth IAGOD Symposium Field Trip Guidebook. Geological Survey of Canada, Open File 2156, p. 68-69.

Dewey, J.F., Shackleton, R.S., 1984, A model for the Evolution of the Grampian tract in the early Calledonides and Appalachians. Nature, v. 312, p. 115-121.

Dubé, B., Dunning, G.R., Lauziere, K., 1998. Geology of the Hope Brook Mine, Newfoundland, Canada; a preserved late Proterozoic high-sulfidation epithermal gold deposit and its implications for exploration. Economic Geology and the Bulletin of the Society of Economic Geologists, 93, 405-436.

Dunning, G.R., 1984, The geology, geochemistry, geochronology and regional setting of the Annieopsquotch Complex and related rocks of southwest Newfoundland. Memorial University of Newfoundland [Ph.D. thesis]: Memorial University of Newfoundland, 423 p.

Dunning, G.R., 1987, Geology of the Annieopsquotch Complex, southwest Newfoundland. Canadian Journal of Earth Sciences, v. 24, p. 1162-1174.

Dunning, G.R., Chorlton, L.B., 1985, The Annieopsquotch ophiolite belt of southwest Newfoundland: Geology and tectonic significance. Geological Society of America Bulletin, v. 96, p. 1466-1476.

Dunning, G.R., Kean, B.F., Thurlow, J.G., Swinden, H.S., 1987. Geochronology of the Buchans, Roberts Arm and Victoria Lake Groups and Mansfield Cove Complex, Newfoundland. Canadian Journal of Earth Sciences, 22, 1175-1184.

Dunning, G.R., Krogh, T.E., 1985, Geochronology of ophiolites of Newfoundland Appalachians. Canadian Journal of Earth Sciences, v. 22, p. 1659-1670.

Dunning, G.R., O'Brien, S.J., 1989, Late Proterozoinc – early Paleozoic crust in the Hermitage Flexure, Newfoundland Appalachians: U – Pb ages and tectonic significance. Geology, v. 17, p. 548-551.

Dunning, G.R., O'Brien, S.J., Colman-Sadd, S.P., Blackwood, R.F., Dickson, W.L., O'Neill, P.P., Krogh, T.E., 1990, Silurian orogeny in the Newfoundland Appalachians. Journal of Geology, 1990, v. 98, p. 895-913.

Dunning, G.R., Swinden, H.S. Kean, B.F., Evans, D.T.W., Jenner, G.A., 1991. A Cambrian island arc in Iapetus: geochronology and geochemistry of the Lake Ambrose volcanic belt, Newfoundland Appalachians. Geological Magazine, 128, 1-17.

Elders, C.F., 1987, The provenance of granite boulders in conglomerates of the Northern and Central Belts of the Southern Uplands of Scotland. Journal of the Geological Society, London, v. 144, p. 853-863.

Elliot, C.G., Dunning, G.R., Williams, P.F., 1991, New U/Pb zircon age constraints on the timing of deformation in north-central Newfoundland and implications for early Paleozoic Appalachian orogenesis. Geological Society of America Bulletin, v. 103, p.125-135.

Ernst, W.G., Liu. J., 1998, Experimental phase-equilibrium study of Al and Ti-contents of calcic amphibole in MORB – A semiquantitative thermobarometer. American Mineralogist, v. 83, p. 952-969.

Evans, D.T.W . Kean, B.F. and Dunning, G.R . 1990, Geological Studies, Victoria Lake Group, central Newfoundland. Current Research, Newfoundland Department of Energy and Mines, Geological Survey Report, 90-1, p. 131-144.

Evans, D.T.W., Kean, B.F., 2002, The Victoria Lake supergroup, central Newfoundland - its definition, setting and volcanogenic massive sulphide mineralization: Newfoundland Department of Mines and Energy, Geological Survey, Open File NFLD/2790, 68 p.

Evans, D.T.W., Kean, B.F., Dunning, G.R., 1990. Geological Studies, Victoria Lake Group, Central Newfoundland. Current Research, Newfoundland Department of Mines and Energy, Geological Survey Branch, Report 90-1, 131-144.

Evans, D.T.W., Kean, B.F., Jayasinghe, N.R., 1994a. Geology and mineral occurrences of Noel Paul's Brook. Map 94-222. Scale 1:50,000. Government of Newfoundland and Labrador, Department of Mines and Energy, Geological Survey Branch, Open File 012A/09/0685.

Evans, D.T.W., Kean, B.F., Jayasinghe, N.R., 1994b. Geology and mineral occurrences of Badger. Map 94-224. Scale 1:50,000. Government of Newfoundland and Labrador, Department of Mines and Energy, Geological Survey Branch, Open File 012A/16/0687.

Evans, D.T.W., Kean, B.F., Mercer, N.L., 1994. Geology and mineral occurrences of Lake Ambrose. Map 94-223. Scale 1:50,000. Government of Newfoundland and Labrador, Department of Mines and Energy, Geological Survey Branch, Open File 012A/10/0686.

Ewart, A., Bryan, W.B., Chappell, B.W., and Rudnick, R.L., 1994, Regional geochemistry of the Lau-Tonga arc and backarc systems, *in* Hawkins, J., et al., eds., Proceedings of the Ocean Drilling Program Scientific Results, v. 135, College Station, TX, p. 385-425.

Falloon, T.J. and Crawford, A.J . 1991, The petrogenesis of high-calcium boninite lavas dredged from the northern Tonga ridge. Earth and Planetary Science Letters, vol. 102, 375-394.

Freidrich, A.M., Hodges, K.V., Bowring, S.A., Martin, M.W., 1999, Geochronological constraints on the magmatic, metamorphic and thermal evolution of the Connemara Caledonides, western Ireland. Journal of the Geological Society, London, v. 156, p. 1217-1230.

Fretzdorff, S., Livermore, R.A., Devey, C.W., Leat, P.T., Stoffers, P., 2002, Petrogenesis of the back-arc East Scotia Ridge, South Atlantic Ocean. Journal of Petrology, v. 43, no. 8., p. 1435-1467.

Frost, B.R., Chamberlain, K.R., Schumacher, J.C., 2000, Sphene (titanite): phase relations and role as a geochronometer: Chemical Geology, v. 172, p. 131-148.

Fryer, P. and Pearce, J.A . 1992, Introduction to the scientific results of Leg 125. in Fryer, P. et al. (eds.), Proceedings of the Ocean Drilling Program, Scientific Results, vol. 125, p. 3-11.

Fyffe, L.R., Pickerill, R.K., 1993. Geochemistry of Upper Cambrian and Lower Ordovician black shale along a northeastern Appalachian transect. Geological Society of America, 105, 897-910.

Gamble, J.A . Wright, I.C . Woodhead, J.D. and McCulloch, M.T . 1995, Arc and back-arc geochemistry in the southern Kermadec arc – Ngatoro Basin and offshore Taupo Volcanic Zone, SW Pacific. In Smellie, J.L . ed . Volcanism associated with extension at consuming plate margins. Geological Society Special Publication, v. 81, p. 193-212

Gibbons, W., Horak, J.M., 1996. The evolution of the Neoproterozoic Avalonian subduction system; evidence from the British Isles. In: Nance, R.D., Thompson, M.D. (Eds.), Avalonian and related peri-Gondwanan terranes of the Circum-North Atlantic. Special Paper – Geological Society of America, 304, 269-280.

Girby, C., Johnson, S.E., Aleinikoff, J., 2005, The Chain Lakes massif: Laurentian source and anatectic history: Geological Society of America Abstracts with Programs, v. 37, no. 1, p. 31.

Grimes-Graeme, R., 1934. Report on a geological reconnaissance survey for Terra Nova properties Lloyds and Victoria Lake, Newfoundland. Hans Lundberg Ltd., Montreal, Buchans Mining Company Ltd., unpublished report, 32 p.

Hall, R., 2002, Cenozoic geological and plate tectonic evolution of SE Asia and the SW Pacific: computer-based reconstructions, model and animations. Journal of Asian Earth Sciences, v. 20, p. 353-431.

Hall, C.E., Gurnis, M., Sdrolias, M., Lavier, L.L., and Müller, R.D., 2003, Catastrophic initiation of subduction following forced convergence across fracture zones. Earth Planetary Science Letters, v. 212, p. 15-30.

Harrison, T.M., 1981, Diffusion of ^{40}Ar in Hornblende. Contributions to Mineralogy and Petrology 78, p.324-331.

Hartz, E.,H., Torsvik, T.H., 2002. Baltica upside down: A new plate tectonic model for Rodinia and the Iapetus Ocean. Geology, 30, 255-258.

Hawkins, J.W., Allan, J.F, 1994, Petrologic evolution of Lau Basin Sites 834 through 839, *in*, Hawkins, J., et al., eds., Proceedings of the Ocean Drilling Program, Scientific Results, V. 135, p. 427-470.

Herd, R.K., Dunning, G.R., 1979. Geology of the Puddle Pond map area, south-western Newfoundland. In Current Research. Geological Survey of Canada, Paper 79-1A, 305-310.

Hibbard, J., 1983, Geology of the Baie Verte Peninsula, Newfoundland: Memoir - Government of Newfoundland and Labrador, Department of Mines and Energy, Mineral Development Division, v. 2, 279 p.

Hibbard, J.P., Stoddard, E.F., Secor, D.T., Dennis, A.J., 2002. The Carolina Zone; overview of Neoproterozoic to early Paleozoic peri-Gondwanan terranes along the eastern flank of the Southern Appalachians. Earth-Science Reviews, 57, 299-339.

Hickey, R.L., and Frey, F.A., 1982, Geochemical characteristics of boninite series volcanics: implications for their source. Geochimica et Cosmochimica Acta, v. 46, p. 2099-2115.

Holland, T., Blundy, J., 1994, Non-ideal interactions in calcic amphiboles and their bearing on amphibole-plagioclase thermometry. Contributions to Mineralogy and Petrology, v. 116, p. 433-447.Karlstrom et al. 1983

Hsü, K.J., Guitang, P. Sengör, A.M.C., Briegel, U., Haihong, C., Changhua, C., Harris, N., Hsü, P., Jiliang, L., Jianning, L., Lee, T., Li, Z.X., Lu, C., Powell, C., Qingchen, W., and Winterer, E.L.,

1995. Tectonic evolution of the Tibetan Plateau: A working hypothesis based on the archipelago model of orogenesis. International Geology Review, v. 37, p. 473-508.

Ingle, S., Mueller, P.A., Heatherington, A.L., Kozuch, M., 2003. Isotopic evidence for the magmatic and tectonic histories of the Carolina terrane: implications for stratigraphy and terrane affiliation. Tectonophysics, 371, 187-211.

Jacobi, R.D. and Wasowski, J.J . 1985, Geochemistry and plate-tectonic setting of the volcanic rocks of the Summerford Group. Geology, v. 13, p. 126-130.

Jenner, G.A. and Swinden, H.S . 1993, The Pipestone Pond Complex, central Newfoundland: complex magmatism in an eastern Dunnage Zone ophiolite. Canadian Journal of Earth Sciences, v. 30, p. 434-448

Jenner, G.A., Longerich, H.P., Jackson, S.E., and Fryer, B.J., 1990, ICP-MS- a powerful new tool for high precision trace element analysis in earth sciences: Evidence from analysis of USGS standards. Chemical Geology, v. 83, p. 133-148.

Johnson, S.C., 2001. Contrasting geology in the Pocologan River and Long Reach areas: implications for the New River belt and correlations in southern New Brunswick and Maine. Atlantic Geology, v. 37, 61-79.

Johnson, S.C., McLeod, M.J., 1996. The New River Belt: A unique segment along the western margin of the Avalon composite terrane, southern New Brunswick, Canada. In: Nance, R.D., Thompson, M.D. (Eds.), Avalonian and related peri-Gondwanan terranes of the circum-North Atlantic. Geological Society of America Special Paper, 304, 149-164.

Karabinos, P., Samson, S.D., Hepburn, J.C., Stoll, H.M., 1998, Taconian orogeny in the New England Appalachians: Collision between Laurentia and the Shelburne Falls arc. Geology, v. 26(3), p. 215-218.

Karson, J.A., 1999, Geological investigation of a lineated massif at the Kane Transform Fault: implications for oceanic core complexes. Philosophical Transactions of the Royal Society of London, v.357, p. 713-740.

Kean, B.F., 1977. Geology of the Victoria Lake map area (12-A/06), Newfoundland. Government of Newfoundland and Labrador Department of Mines and Energy, Mineral Development Division. Report 77-4, 11 p.

Kean, B.F., 1978. Geology of the Star Lake east half sheet (12A/11E), Newfoundland. Report of Activities for 1977, Newfoundland Department of Mines and Energy, Mineral Development Division, Report 78-1, 129-134.

Kean, B.F., 1979a. Star Lake, Newfoundland. Map 79-001. Scale 1:50,000. Government of Newfoundland and Labrador, Department of Mines and Energy, Mineral Development Division.

Kean, B.F., 1979b. Buchans, Newfoundland. Map 79-125. Scale: 1:50,000. Government of Newfoundland and Labrador, Department of Mines and Energy, Mineral Development Division.

Kean, B.F., 1982, Victoria Lake, Newfoundland. Map 87-087: Government of Newfoundland and Labrador, Department of Mines and Energy, Mineral Development Division, scale 1:50,000, 1 sheet.

Kean, B.F., 1983, King George IV Lake, Grand Falls district, Newfoundland. Map 82-051, scale 1:50,000, 1 sheet, in Geology of the King George IV Lake map area (12-A/4). Government of Newfoundland and Labrador, Department of Mines and Energy, Mineral Development Division, Report 83-04, 74 p.

Kean, B.F., Dean, P.L., Strong, D.F., 1981. Regional geology of the Central Volcanic Belt of Newfoundland. Geological Association of Canada, Special Paper 22, 65-78.

Kean, B.F., Evans, D.T.W., 1988a. Regional metallogeny of the Victoria Lake Group. Current Research, Newfoundland Department of Mines, Mineral Developments Division, Report 88-1, 319-330.

Kean, B.F., Evans, D.T.W., 1988b., Geology and mineral deposits of the Victoria Lake Group. In: Swinden, H.S., Kean, B.F. (Eds.), The Volcanogenic Sulphide Districts of Central Newfoundland. Geological Association of Canada, Mineral Development Division, 144-156.

Kean, B.F., Jayasinghe, N.R., 1980, Geology of the Lake Ambrose (12-A/10) - Noel Pauls Brook (12-A/9) map areas, central Newfoundland: Government of Newfoundland and Labrador, Department of Mines and Energy, Mineral Development Division. Report 80-02, 33 p., scale 1:50,000, 2 sheets.

Kean, B.F., Jayasinghe, N.R., 1982. Geology of the Badger map area (12-A/16), Newfoundland. Government of Newfoundland and Labrador, Department of Mines and Energy, Mineral Development Division, Report 81-02, 42 p.

Kean, B.F., Mercer, N.L., 1981. Grand Falls map area (2D/13), Newfoundland. Newfoundland Department of Mines and Energy, Mineral Development Division, Map 8199 (with descriptive notes).

Kelemen, P.B., Johnson, K.T.M., Kinzler, R.J., and Irving, A.J., 1990, High-field-strength element depletions in arc basalts due to mantle-magma interaction. Nature, v. 345, p. 521-524.

Keppler, H., 1996, Constraints from partitioning experiments on the composition of subduction-zone fluids. Nature, v. 380, p. 237-240.

Keller, R.A., Fisk, M.R. Smellie, J.L., Strelin, J.A., and Lawver, L.A., 2002, Geochemistry of back arc basin volcanism in Bransfield Strait, Antarctica; subducted contributions and along-axis variations. Journal of Geophysical Research, v. 107, no. 8, 10.1029/2001JB000444.

Kerr, A . Jenner, G.A. and Fryer, B.J . 1995, Sm-Nd isotopic geochemistry of Precambrian to Paleozoic granitoid suites and the deep-crustal structure of the southeast margin of the Newfoundland Appalachians. Canadian Journal of Earth Sciences, vol. 32, p. 224-245.

Kerr, A., 1996, New perspectives on the stratigraphy, volcanology, and structure of island-arc volcanic rocks in the Ordovician Roberts Arm Group, Notre Dame Bay. Current Research, Newfoundland Department of Energy and Mines, Geological Survey Report, 96-1, p. 283-310.

Kerr, A., Dunning, G.R., 2003, A note of the U/Pb zircon age of the Woodford Arm granite, and its relationship to the Roberts Arm Group, central Newfoundland (NTS 2E/12). Current Research, Newfoundland Department of Energy and Mines, Geological Survey Report, 03-1, p. 47-50.

Kerr, A., Jenner, G.A., Fryer, B.J., 1995. Sm-Nd isotopic geochemistry of Precambrian to Paleozoic granitoid suites and the deep-crustal structure of the southeast margin of the Newfoundland Appalachians. Canadian Journal of Earth Sciences, 32, 224-245.

Kim, J. and Jacobi, R.D., 2002, Boninites: characteristics and tectonic constraints, northeastern Appalachians. Physics and chemistry of the Earth, vol. 27, p. 109-147.

Kim, J., Coish, R., Evans, M., Dick, G., 2003, Supra-subduction zone extensional magmatism in Vermont and adjacent Quebec: Implications for early Paleozoic Appalachian tectonics. Geological Society of America Bulletin, v. 115 (12), p. 1552-1569.

Kokelaar, P., 1986. Petrology and geochemistry of the Rhobell volcanic complex; amphibolite-dominated fractionation at an Early Ordovician arc volcano in North Wales. Journal of Petrology, 27, 887-914.

Konstantinovskaia, E.A., 2001, Arc-continent collision and subduction reversal in the Cenozoic evolution of the Northwest Pacific: an example from Kamchatka (NE Russia). Tectonophysics, v. 333, p.75-94.

Krogh, T.E., 1982, Improved accuracy of U-Pb ages by creation of more concordant systems using an air abrasion technique. Geochimica et Cosmochimica Acta, v. 46, p. 637-649.

Krough, T.E., Strong, D.F., O'Brien, S.J., Papezik, V.S., 1988. Precise U-Pb zircon dates from the Avalon Terrane in Newfoundland Appalachians. Canadian Journal of Earth Sciences, v. 25, 442-453.

Kurth, M., Sassen, A., Suhr, G., and Mezger, K., 1998, Precise ages and isotopic constraints for the Lewis Hills (Bay of Island Ophiolite). Preservation of an arc-spreading ridge intersection: Geology, v. 26, p. 1127-1130.

Kusky, T.M., Chow, J.S., Bowring, S.A., 1997, Age and origin of the Boil Mountain Ophiolite and Chain Lakes Masif, Maine: implications for the Penobscotian Orogeny. Canadian Journal of Earth Sciences, v. 34, p. 646-654.

Lafrance, B., Williams, P.F., 1992, Silurian deformation in eastern Notre Dame Bay, Newfoundland. Canadian Journal of Earth Sciences, v. 29, p. 1899-1914.

Leake, B.E., et al., 1997, Nomenclature of the amphiboles: report of the subcommittee on amphiboles of the international mineralogical association, commission on new minerals and mineral names. Canadian Mineralogist, v. 35, p. 219-246.

Leat, P. T., Livermore, R. A., Millar I. L., Pearce, J. A., 2000, Magma supply in back-arc spreading centre segment E2, East Scotia Ridge. Journal of Petrology, v. 41, p. 845-866

LeBas, M.J., LeMaitre, R.W., Streckeisen, A., Zanettin, B., 1986. A chemical classification of volcanic rocks based on the total alkali silica diagram. Journal of Petrology, 27, 745-750.

Liou, J.G., 1973, Synthesis and stability relations of epidote, $Ca_2Al_2FeSi_8O_{12}(OH)$. Journal of Petrology, v. 14. p. 381-413.

Liou, J.G., Kuniyoshi, S., Ito, K., 1974, Experimental studies of phase relations between greenschist and amphibolite in a basaltic system. American Journal of Science, v. 274, p. 613-632.

Liss, M.J., van der Pluijm, B.A., van der Voo, R., 1993. Avalonian proximity of the Ordovician Miramichi terrane, northern New Brunswick, northern Appalachians: Palaeomagnetic evidence for rifting and back-arc basin formation at the southern margin of Iapetus. Tectonophysics, v. 227, 17-30.

Lissenberg, C.J., 2005, Origin and evolution of the Annieopsquotch Ophiolite Belt, Newfoundland Appalachians. Ph. D. thesis, Univeristy of Ottawa, Ottawa, Canada, 130 p.

Lissenberg, C.J., van Staal, C.R., 2002, The relationships between the Annieopsquotch ophiolite belt, the Dashwoods block and the Notre Dame arc in southwestern Newfoundland. Current Research, Newfoundland Department of Energy and Mines, Geological Survey Report 02-1, p. 145-153.

Lissenberg, C.J., van Staal, C.R., Bédard, J.H., Zagorevski, A., 2005a, Geochemical constraints on the origin of the Annieopsquotch ophiolite belt, southwest Newfoundland. Geological Society of America Bulletin, v. 117 (11), p. 1413-1426.

Lissenberg, C.J., Zagorevski, A., McNicoll, V.J., van Staal, C.R., Whalen, J.B., 2005b, Assembly of the Annieopsquotch Accretionary Tract, Newfoundland Appalachians: Age- and geodynamic constraints from syn-kinematic intrusions. Journal of Geology, v. 113, p. 553-571

Lissenberg, C.J., Zagorevski, A., Rogers, N., van Staal, C.R., Whalen, J., McNicoll, V., 2005c: Geology, Star Lake, Newfoundland (NTS 12-A/11): Geological Survey of Canada Open File OF1669, scale 1:50,000, 1 sheet.

Ludwig, K.R . 2001. User's manual for Isoplot/Ex rev. 2.49: a Geochronological Toolkit for Microsoft Excel. Special Publication, 1a, Berkeley Geochronology Center, Berkeley, 55 p.

Ludwig, K.R. 1998. On the treatment of concordant uranium-lead ages. Geochimica et Cosmchimica Acta, v. 62, p. 665-676.

MacKenzie, A.C., Desnoyers, D., Barbour, D., Graves, M., 1990. Contrasting VMS styles in the Tulks Belt, central Newfoundland. Canadian Institute of Mining , District 1 Annual Meeting, St. John's, Newfoundland, Program with Abstracts, p. 10.

MacKenzie, A.C., Squires, G., MacInnis, D., 1988. The geology of the Duck Pond deposit, central Newfoundland. Geological Association of Canada – Canadian Society of Petroleum Geologists, Joint Annual Meeting, Program with Abstracts, 13, A77.

MacLachlan, K . O'Brien, B.H. and Dunning, G.R . 2001, Redefinition of the Wild Bight Group, Newfoundland: implications for models of island arc evolution in the Exploits Subzone. Canadian Journal of Earth Sciences, v. 38, p. 889-907.

MacLachlan, K. and Dunning, G.R . 1998a, U-Pb ages and tectonomagmatic relationships of early Ordovician low-Ti tholeiites, boninites and related plutonic rocks in central Newfoundland, Canada. Contributions to Mineralogy and Petrology, v. 133, p. 235-258.

MacLachlan, K. and Dunning, G.R . 1998b, U-Pb ages and tectono-magmatic evolution of Middle Ordovician volcanic rocks of the Wild Bight Group, Newfoundland Appalachians. Canadian Journal of Earth Sciences, v. 35, 998-1017.

Macpherson, C.G., and Hall, R., 2001, Tectonic setting of Eocene boninite magmatism in the Izu-Bonin-Mariana forearc. Earth and Planetary Science Letters, v. 186, p. 215-230.

Mallard, L.D., Rogers, J.J., 1997. Relationships of Avalonian and Cadomian terranes to Genville and Pan-African events. Journal of Geodynamics, 23, 197-221.

Massone, H.-J., Szpruka, Z., 1997, Thermodynamic properties of white micas on the basis of high-pressure experiments in the systems K_2O-MgO-Al_2O_3-SiO_2-H_2O and K_2O-FeO-Al_2O_3-SiO_2-H_2O. Lithos, v. 41, p. 229-250.

Massone, H.-J.,Schreyer, 1987, Phengite geobarometry based on the limiting assemblage with K-feldspar, phlogopite and quartz. Contributions to Mineralogy and Petrology, v. 96, p. 212-224.

Max, M.D., Barber. A.J., Martinez, J., 1990. Terrane assemblage of the Leinster Massif, SE Ireland, during the lower Palaeozoic. Journal of the Geological Society of London, 147, 1035-1050.

Max, M.D., Roddick, J.C., 1989. Age of Metamorphism in the Rosslare Complex, S.E. Ireland. Proceedings of the Geologists' Association, v. 100, p. 113-121.

McLeod, M.J., Johnson, S.C., Krogh, T.E., 2003, Archived U-Pb (zircon) dates from southern New Brunswick. Atlantic Geology, v. 39 (3), p. 209-226.

McNicoll, V.J., van Staal, C.R., Waldron, J.W.F., 2001, Accretionary history of the northern Appalachians: SHRIMP study of Ordovician-Silurian syn-tectonic sediments in the Canadian Appalachians. Geological Association of Canada – Mineralogical Association of Canada Joint Annual Meeting, Abstracts Volume, v. 26, p. 100-101.

Meyer, A., 1980, Primitive arc volcanism and a boninite series: examples from western pacific island arcs, *in* Hayes, D.E., ed., The tectonic and geological evolution of South Asian seas and islands, Washington, AGU Geophysical Monograph, p. 269-282.

Moench, R.H., Aleinikof, J.N., 2003, Stratigraphy, geochronology, and accretionary terrane setting of two Bronson Hill arc sequences, northern New England. Physics and Chemistry of the Earth, v. 28, p. 113-160.

Moench, R.H., Aleinikoff, J.N., Boudette, E.L., 2000, Revised Early Ordovician age for the ophiolitic Jim Pond Formation, NW Main: Tectonic history reappraised. Geological Society of America Abstracts with Programs, v. 32 (1), A-60.

Monzier, M., Danyushevsky, L.V., Crawford, A.J., Bellon, H., and Cotton, J., 1993, High-Mg andesites from the southern termination of the New Hebrides island arc (SW Pacific). Journal of Volcanology and Geothermal Research, v. 57, p. 193-217.

Moore, P.J., 2003. Stratigraphic implications for mineralization: Preliminary findings of a metallogenic investigation of the Tally Pond volcanics, central Newfoundland. Current Research. Newfoundland Department of Mines and Energy, Geological Survey, Report 03-1, 241-257.

Moore, J.C., Diebold, J., Fisher, M.A., Sample, J., Brocher, T., Talwani, M., Ewing, J., von Huene, R., Rowe, C., Stone, D., Stevens, C., and Sawyer, D., 1991, EDGE deep seismic reflection transect of the eastern Aleutian arc-trench layered lower crust reveals underplating and continental growth. Geology, v. 19, p. 420-424.

Morrison, G.W., 1980, Characteristics and tectonic setting of the shoshonite rock association. Lithos, v. 13, p. 97-108.

Mueller, P.A., Kozuch, M., Heatherington, A.L., Wooden, J., Offield, T., Koeppen, R., Klein, T., 1996. Evidence for Mesoproterozoic basement in the Carolina terrane and speculations on its origin. In: Nance, R.D., Thompson, M.D. (Eds), Avalonian and related peri-Gondwanan terranes of the circum-North Atlantic. Geological Society of America Special Paper, v. 304, p. 207-217.

Müller, R.D., Gaina, C., Roest, W.R., and Lundbek Hansen, D., 2001 A recipe for microcontinent formation. Geology, v. 29, p. 203–206.

Murphy, J.B., Nance, R.D., 2002. Sm-Nd isotopic systematics as tectonic tracers: an example from West Avalonia in the Canadian Appalachians. Earth Science Reviews, v. 59, 77-100.

Nance, R.D., Murphy, J.B., 1994. Contrasting basement isotopic signatures and palinspatic restoration of peripheral orogens: example from the Neoproterozoic Avalonian – Cadomian belt. Geology, v. 22, p. 617-620.

Nance, R.D., Murphy, J.B., Keppie, J.D., 2002. A Cordilleran model for the evolution of Avalonia. Tectonophysics, v. 352, p. 11-31.

Nowlan G. S., Thurlow J.G., 1984, Middle Ordovician conodonts from the Buchans Group, central Newfoundland, and their significance for regional stratigraphy of the Central Volcanic Belt. Canadian Journal of Earth Sciences, v. 21, p. 284-296.

Nowlan, G., 2004, Report on one sample from Ordovician strata in the Victoria Lake area, Newfoundland (NTS 12A/4). Report 008-GSN-2004, Paleontology Subdivision, Geological Survey of Canada, Calgary.

O'Brien, B.H . 1992, Internal and external relationships of the South Lake Igneous Complex, north-central Newfoundland (NTS 2E/5, 6): Ordovician and later tectonism in the Exploits Subzone? Current Research, Newfoundland Department of Energy and Mines, Geological Survey Report, 92-1, p. 159-169.

O'Brien, B.H . Swinden, H.S . Dunning, G.R . Williams, S.H . and O'Brien, F.H.C . 1997, A peri-Gondwanan arc-backarc complex in Iapetus: Early-mid Ordovician evolution of the Exploits Group, Newfoundland. American Journal of Science, v. 297, p. 220-272.

O'Brien, B.H., 2003, Geology of the central Notre Dame Bay region (parts of NTS areas 2E/3,6,11), northeastern Newfoundland: Newfoundland Department of Energy and Mines, Geological Survey Report 03-03, 147 p.

O'Brien, S.J., O'Brien, B.H., Dunning, G.R., Tucker, R.D., 1996. Late Neoproterozoic Avalonian and related peri-Gondwanan rocks of the Newfoundland Appalachians. In: Nance, R.D., Thompson, M.D. (Eds), Avalonian and related peri-Gondwanan terranes of the circum-North Atlantic. Geological Society of America Special Paper, v. 304, p. 9-28.

Oneschuk, D., Tod, J., Kilfoil, G., 2001, Red Indian Line Airborne Geophysics Compilation (Part 1), Central Newfoundland. Geological Survey of Canada Open File 3923, Government of Newfoundland and Labrador, Department of Mines and Energy, Geological Survey Open File 12A/0911. CD-ROM.

Oneschuk, D., Tod, J., Kilfoil, G., 2002, Red Indian Line Airborne Geophysics Compilation (Part 2), Central Newfoundland. Geological Survey of Canada Open File 4254, Government of Newfoundland and Labrador, Department of Mines and Energy, Geological Survey Open File NFLD/2773. CD-ROM.

Parrish, R.R., Roddick, J.C., Loveridge, W.D., Sullivan, R.W. 1987. Uranium-lead analytical techniques at the Geochronology Laboratory, Geological Survey of Canada. Radiogenic age and isotope studies, Report 1: Geological Survey of Canada, Paper 87-2, p. 3-7.

Parrish, R.R., Roddick, J.C., Loveridge, W.D., Sullivan, R.W. 1987. Uranium-lead analytical techniques at the Geochronology Laboratory, Geological Survey of Canada. Radiogenic age and isotope studies, Report 1: Geological Survey of Canada, Paper 87-2, p. 3-7.

Passchier, C.W., Trow, R.A.J., 1998, Microtectonics. Springer-Verlag, Berlin Heidelberg. 290p.

Pavlides, L., Arth, J.G., Sutter, J.F., Stern, T.W., and Cortesini, H., 1994, Early Paleozoic alkalic and calc-alkalic plutonism and associated contact metamorphism, central Virginia Piedmont: U. S. Geological Survey Professional Paper. U. S. Geological Survey. Reston, VA, United States, 147 pp.

Pearce, J.A . Harris, N.B.W . and Tindle, A.G . 1994, Trace element discrimination diagram for tectonic interpretation of granitic rocks. Journal of Petrology, v. 25, p. 956-983.

Pearce, J.A., 1982. The role of subcontinental lithosphere in magma genesis at destructive plate margins. In: Hawksworth, C.J. Norry, M.J. (Eds.), Continental basalts and mantle xenoliths. Shiva. p. 230-249.

Pearce, J.A., 1996, A user's guide to basalt discrimination diagrams, in Wyman, D.A., ed., Trace element geochemistry of volcanic rocks: application for massive sulphide exploration. Geological Association of Canada, Short Course Notes, v. 12, p. 79-113.

Pearce, J.A., Cann, J.R., 1973. Tectonic setting of basic volcanic rocks determined using trace element analysis. Earth and Planetary Science Letters, 19, 290-300.

Pearce, J.A., Parkinson, I.J, 1993, Trace element models for mantle melting: Application to volcanic arc petrogenesis, *in* Prichard, H.M., et al., eds., Magmatic Processes and Plate Tectonics. Geological Society of London Special Publication, v. 76, p. 373-403.

Pearce, J.A., van der Laan, S.R., Arculus, R.J., Murton, B.J., Ishii, T., Peate, D.W., and Parkinson, I.J., 1992, Boninite and Harzburgite from leg 125 (Bonin-Mariana forearc): A case study of magma genesis during the initial stages of subduction, *in* Fryer, P., et al., eds., Proceedings of the ODP, Scientific results, v. 125, p. 623-659.

Pearce, J.A., Ernewein, M., Bloomer, S.H., Parson, L.M., Murton, B.J., Johnson, L.E., 1995, Geochemistry of Lau Basin volcanic rocks: influence of ridge segmentation and arc proximity,

in, Smellie, J.L., ed., Volcanism associated with extension at consuming plate margins, Geological Society Special Publication No. 81, p. 53-75

Pearce, J.A., Harris, N.B.W., Tindle, A.G., 1994, Trace element discrimination diagram for tectonic interpretation of granitic rocks. Journal of Petrology, v. 25, p. 956-983.

Pehrsson, S.J., van Staal, C.R., Herd, R.K., McNicoll, V., 2003, The Cormacks Lake complex, Dashwoods Subzone: A window into the deeper levels of the Notre Dame arc. Current Research, Newfoundland Department of energy and Mines, Geological Survey Report, v. 03-1, p. 115-125.

Phillips, E.R., Evans, J.A., Stone, P., Horstwood, M.S.A., Floyd, J.D., Smith, R.A., Akhurst, M.C., Barron, H.F., 2003, Detrital Avalonian zircons in the Laurentian Southern Uplands terrane. Scotland: Geology, v. 31(7), p. 625-628.

Phillips, E.R., Evans, J.A., Stone, P., Horstwood, M.S.A., Floyd, J.D., Smith, R.A., Akhurst, M.C., Barron, H.F., 2003. Detrital Avalonian zircons in the Laurentian Southern Uplands terrane, Scotland. Geology, v. 31, p. 625-628.

Pickett, J.W. 1987: Geology and geochemistry of the Skidder Basalt, in Buchans Geology Newfoundland, in Kirkham, R.V., ed., Geological Survey of Canada, Paper 86-24, p. 195-218.

Pollock, J.C. and Wilton, D.H.C . 2001, Metallogenic studies of the Tally Pond Belt, Victoria Lake Group: Trace-element geochemistry and lead-isotope data from the Exploits Subzone, Newfoundland. Current Research, Newfoundland Department of Energy and Mines, Geological Survey Report, 02-1, p. 197-209

Pollock, J.C., Wilton, D.H.C., van Staal, C.R., Turbrett, M.N., 2002. Laser ablation ICP-MS geochronology and provenance of detrital zircons from the Rogerson Lake Conglomerate, Botwood Belt, Newfoundland. Current Research. Newfoundland Department of Mines and Energy, Geological Survey, Report 02-1, 169-183.

Pope, A.J., Calon, T.J., Swinden, S.H., 1991, Stratigraphy, structural geology and mineralization in the Gullbridge area, central Newfoundland: in Swinden, H.S. et al., eds., Metallogenic

framework of base and precious metal deposits, central and western Newfoundland (Fieldtrip 1): Open File Report, Geological Survey of Canada, p. 93-100.

Pubellier, M., Bader, A.G., Rangin, C., Deffonaines, B., Quebra, R., 1999, Upper Plate deformation induced by subduction of a volcanic arc: The Snellius Plateau (Molucca Sea, Indonesia and Mindanao, Philippines). Tectonophysics, v. 304, pp. 345-368.

Rejebian, V.A., Harris, A.G., Huebner, J.S., 1987, Conodont color and textural alteration: An index to regional metamorphism, contact metamorphism, and hydrothermal alteration. Geological Society of America Bulletin, v. 99, p. 471-479

Reynolds, J.R., and Langmuir, C.H., 2000, Identification and implications of off-axis lava flows around the East Pacific Rise. Geochemistry, Geophysics, Geosystems, v. 1, paper number 1999GC000033.

Richardson, W.P., Stein, S., Stein, C.A., and Zuber, M.T., 1995, Geoid data and thermal structure of the oceanic lithosphere. Geophysical Research Letters, v. 22, p. 1913-1916.

Richardson, J.M., Lightfoot, P.C. and de Souza, H., 1996, Current Geoscience Laboratories geoanalytical programs and their quality Assurance underpinnings. Geostandards Newsletter, vol. 20 (1), p. 141-156

Riley, G.C., 1957. Red Indian Lake (west half), Newfoundland. Geological Survey of Canada, Map 8-1957 (with descriptive notes).

Robinson, P., Tucker, R.D., Bradley, D., Berry IV, H.N., Osberg, P.H., 1998, Paleozoic orogens in New England, USA. GFF, v. 120, p. 119-148.

Roddick, J.C . Loveridge, W.D.,Parrish, R.R . 1987, Precise U-Pb dating of zircon at the sub-nanogram Pb level. Chemical Geology, v. 66, p. 111-121.

Roddick, J.C., 1983, High-precision intercalibration of ^{40}Ar-^{39}Ar standards. Geochimica et Cosmochimica Acta, v. 47, p. 887-898.

Roeder, P.L., and Emslie, R.F., 1970, Olivine-liquid equilibrium. Contributions to Mineralogy and Petrology, v. 29, p. 275-289.

Rogers, N., van Staal, C.R., 2002, Toward a Victoria Lake Supergroup: a provisional stratigraphic revision of the Red Indian to Victoria lakes area, central Newfoundland. *in* Current Research

(2002) Newfoundland Department of Mines and Energy, Geological Survey, Report 02-1, pages 185-195

Rogers, N., van Staal, C.R . McNicoll, V . Pollock, J . Zagorevski, A . Whalen, J. and Kean, B., in press, Neoproterozoic and Cambrian arc magmatism along the eastern margin of the Victoria Lake Supergroup: a remnant of Ganderian basement in central Newfoundland? Precambrian Geology

Rogers, N. and van Staal, C.R., in press, Geology, Grand Falls, Newfoundland (NTS 02-D/13). Geological Survey of Canada Open File OF4545, scale 1:50,000, 1 sheet.

Rogers, N., 2004. Geochemical Database, Red Indian Line Project, Central Newfoundland. Geological Survey of Canada, Open File 4605, 1 CD-ROM.

Rogers, N., van Staal, C.R., 2002. Toward a Victoria Lake supergroup: a provisional stratigraphic revision of the Red Indian to Victoria Lakes area, central Newfoundland. Current Research. Newfoundland Department of Mines and Energy, Geological Survey, Report 02-1, 185-195.

Rogers, N., van Staal, C.R., 2005. Geology, Grand Falls, Newfoundland (NTS 02-D/13). Geological Survey of Canada Open File 4545. Map. Scale 1:50,000.

Rogers, N., van Staal, C.R., Pollock, J., Zagorevski, A., McNicoll, V., Squires, G.C., 2005a. Geology, Lake Ambrose and part of Buchans, Newfoundland (NTS 12-A/10 and part of 12-A/15). Geological Survey of Canada Open File 4544. Map. Scale 1:50,000.

Rogers, N., van Staal, C.R., Valverde-Vaquero, P., Squires, G., Pollock, J., McNicoll, V., 2005b. Geology, Noel Paul's Brook, Newfoundland (NTS 12-A/09). Geological Survey of Canada Open File 4547. Map. Scale 1:50,000.

Ryan, P.D., Dewey, J. F., 2004, The South Connemara Group reinterpreted: a subduction-accretion complex in the Caledonites of Galway Bay, western Ireland. Journal of Geodynamics, v. 37, p. 513-529.

Saunders, A.D., Fornari, D.J., and Morrison, M.A., 1982, The composition and emplacement of basaltic magmas produced during the development of continental-margin basins: the Gulf of California, Mexico. Journal of the Geological Society of London, v. 139, p. 335-346.

Scaillet, S., 2000, Numerical error analysis in $^{40}Ar/^{39}Ar$ dating: Chemical Geology, v. 162, p. 269–298.

Schofield, D.I., D'Lemos, R.S., 2000. Granite petrogenesis in the Gander Zone, NE Newfoundland: mixing of melts from multiple sources and the role of lithospheric delamination. Canadian Journal of Earth Sciences, v. 37, p. 535-547.

Şengör, A.M.C., Natal'in, B.A., 1996, Turkik-type orogeny and its role in the making of the continental crust: Annual Review of Earth and Planetary Science, v. 24, p. 263-337.

Squires, G.C., MacKenzie, A.C., MacInnis, D., 1990. Geology and genesis of the Duck Pond volcanogenic massive sulphide deposit. In: Swinden, H.S., Evans, D.T.W., Kean, B.F. (Eds), Metallogenic framework of base and precious metal deposits, central and western Newfoundland. Eighth IAGOD Symposium Field Trip Guidebook. Geological Survey of Canada, Open File 2156, 56-64.

Squires, G.C., Moore, P.J., 2004. Volcanogenic massive sulphide environments of the Tally Pond volcanics and adjacent area: Geological, lithogeochemical and geochronological results. Current Research. Newfoundland Department of Mines and Energy, Geological Survey, Report 04-1, 63-91.

Solobev, A.V., and Danyushevsky, L.V., 1994, Petrology and geochemistry of boninites from the northern termination of the Tonga trench: Constraints on the generation conditions of primary high-Ca boninite magmas, Journal of Petrology, v. 35, no. 5, p. 1183-1211.

Stampfli, G.M., Borel, G.D., 2002. A plate tectonic model for the Paleozoic and Mesozoic constrained by dynamic plate boundaries and restored synthetic oceanic isochrones. Earth and Planetary Science Letters, v. 196, p. 17-33.

Stern, R. A., 1997. The GSC Sensitive High Resolution Ion Microprobe (SHRIMP): analytical techniques of zircon U-Th-Pb age determinations and performance evaluation. In: Radiogenic age and Isotopic Studies, Report 10: Geological Survey of Canada Current Research 1997-F, 1-31.

Stern, R.A . 1999. In situ zircon trace element analysis by high mass-resolution SIMS; Ninth Annual V.M. Goldschmidt Conference, p. 284-285.

Stern, R.A., Amelin, Y., 2003, Assessment of errors in SIMS zircon U-Pb geochronology using a natural zircon standard and NIST SRM 610 glass; Chemical Geology, v. 197, p. 111-146.

Stern, R.J., Bloomer, S.H., 1992, Subduction zone infancy: examples from the Eocene Izu-Bonin Mariana and Jurassic California arcs. Geological Society of America Bulletin, v. 104, p.1621-1636.

Sun, C-H., Stern, R.J., 2001, Genesis of Mariana shoshonites: Contribution of the subduction component: Journal of Geophysical Research, v. 106-B1, p. 589-608.

Sun, S-S., McDonough, W.F., 1989, Chemical and isotopic systematics of oceanic basalts: implications for mantle compositions and processes, *in*, Saunders, A.D. and Norry, M.J. eds., Magmatism in the ocean basins, Geological Society of London Special Publication, v. 42, p. 313–345.

Swinden H.S., Jenner, G.A., Kean, B.F., Evans, D.T.W., 1989. Volcanic rocks geochemistry and a guide for massive sulphide exploration in central Newfoundland. Current Research, Newfoundland Department of Mines and Energy, Geological Survey Branch, Report 89-1, 201-219.

Swinden, H.S. and Jenner, G.A . 1992, Volcaninc stratigraphy of the New Bay Pond, central Newfoundland, and the strike-extent of the Point Leamington massive sulphide horizon, Current Research, Newfoundland Department of Energy and Mines, Geological Survey Report, 92-1, p. 267-279.

Swinden, H.S., Jenner, G.A., Szybinski, Z.A., 1997, Magmatic and tectonic evolution of the Cambrian-Ordovician Laurentian margin of the Iapetus: Geochemical and isotopic constraints from the Notre Dame Subzone, Newfoundland, in Sinha, A.K., et al., eds., The Nature of magmatism in the Appalachian Orogen: Boulder, Colorado, Geological Society of America Memoir 191, p. 337-364

Swinden, H.S., Sacks, P.E., 1986, Stratigraphy and economic geology of the southern part of the Roberts Arm Group, central Newfoundland, Current Research, Newfoundland Department of Energy and Mines, Geological Survey Report, 86-1A, p. 213-220.

Swinden, H.S., Thorpe, R.I., 1984. Variations in style of volcanism and massive sulphide deposition in Early – Middle Ordovician island arc sequences of the New Brunswick Mobile Belt. Economic Geology, 79, 1569-1619.

Swinden, S.H., Jenner, G.A . Fryer, B.J., Hertogen, J., and Roddick, J.C . 1990, Petrogenesis and paleotectonic history of the Wild Bight Group, an Ordovician rifted island arc in central Newfoundland. Contributions to Mineralogy and Petrology, vol. 105, p. 219-241.

Swinden, S.H., 1996, Geochemistry of volcanic rocks in the Moreton's Harbour-Twillingate area, Notre Dame Bay: Current Research, Newfoundland Department of Energy and Mines, Geological Survey Report, 96-1, p. 207-226.

Szybinski, Z.A., 1995, Paleotectonic and structural setting of the western Notre Dame Bay area, Newfoundland Appalachians, unpublished Ph. D. thesis, Memorial University of Newfoundland. St. John's, NF, Canada, 493 p.

Tanaka, T., Togashi, S., Kamioka, H., Amakawa, H., Kagami, H., Hamamoto, T., Yuhara, M., Orihashi, Y., Yoneda, S., Shimizu, H., Kunimaru, T., Takahashi, K., Yanagi, T., Nakano, T., Fujimaki, K., Shinjo, R., Asahara, Y., Tanimizu, M., and Dragusanu, C., 2000, JNdi-1: A neodymium isotopic reference in consistency with La Jolla neodymium. Chemical Geology, v. 168, p. 279–281.

Thorogood, E.J., 1990. Provenance of the pre-Devonian sediments of England and Wales: Sm- Nd isotopic evidence. Journal of the Geological Society, London, v. 147, p. 591-594.

Thurlow, J.G., 1981, The Buchans Group: its stratigraphic and structural setting, in Swanson, E.A. et al., eds., The Buchans orebodies: Fifty years of geology and mining. Geological Association of Canada Special Paper, v. 22, p. 79-89.

Thurlow, J.G., 1991, Geology of the Buchans orebodies – a 1990 summary, in Swinden, H.S. et al., eds., Metallogenic framework of base and precious metal deposits, central and western Newfoundland (Fieldtrip 1). Open File Report, Geological Survey of Canada, p. 84-91.

Thurlow, J.G., Spencer, C.P., Boerner, D.E., Reed, L.E., Wright, J.A., 1992, Geological interpretation of a high resolution seismic survey at the Buchans mine, Newfoundland. Canadian Journal of Earth Sciences, v. 9, p. 2022-2037.

Thurlow, J.G., Swanson, E.A., 1987, Stratigraphy and structure of the Buchans Group, *in* Kirkham, R.V., ed., Geological Survey of Canada, Paper 86-24, p. 35-46.

Tucker, R.D . O'Brien, S.J . and O'Brien, B.H . 1994, Age and implications of Early Ordovician (Arenig) plutonism in the type area of the Bay du Nord Group, Dunnage Zone, Southern Newfoundland Appalachians. Canadian Journal of Earth Sciences, v. 31, p. 351-357.

Tucker, R.D., Pharaoh, T.C., 1991. U-Pb zircon ages for Late Precambrian igneous rocks in southern Britain. Journal of the Geological Society of London, v. 148, p. 435-443.

Valverde-Vaquero, P. and van Staal, C.R . 2002, Geology and magnetic anomalies of the Exploits – Meelpaeg boundary zone in the Victoria Lake area (central Newfoundland): Regional implications. Current Research, Newfoundland Department of Energy and Mines, Geological Survey Report, 02-1, p. 197-209.

Valverde-Vaquero, P. and van Staal, C.R., 2001, Relationships between the Dunnage-Gander zones in the Victoria Lake-Peter Strides Pond area, Current Research (2001) Newfoundland Department of Mines and Energy Geological Survey, Report 2001-1, p. 1-9.

Valverde-Vaquero, P., van Staal, C.R., McNicoll, V., Dunning, G., in press. Middle Ordovician magmatism and metamorphism along the Gander margin in Central Newfoundland. Journal of the Geological Society London.

van der Pluijm B.A., Johnson, R.J.E., van der Voo, R., 1993, Paleogeography, accretionary history, and tectonic scenario; a working hypothesis for the Ordovician and Silurian evolution of the Northern Appalachians, *in* Roy, D.C., Skehan, J.W. (eds.), The Acadian Orogeny; recent studies in New England, Maritime Canada, and the autochthonous foreland, Geological Society of America, Special Paper 275, p. 27-40.

van der Pluijm, B.A.,1986, Geology of eastern New World island, Newfoundland: An accretionary terrane in the northeastern Appalachians. Geological Society of America Bulletin, v. 97, p. 932-945.

van der Velden, A.J., van Staal, C.R., and Cook, F.A., 2004, Paleosubduction of Ganderia beneath Laurentia: a reprocessed Lithoprobe seismic reflection survey of the Newfoundland Appalachians. Geological Society of America Bulletin, v. 116, n. 11, p. 1485–1498.

van Staal, C.R., 2005, North America; Northern Appalachians, *in* Selley, R.C. et al., eds., Encyclopedia of Geology: Oxford, Elsevier Academic Press, v. 4, p. 81-92.

van Staal, C.R., Dewey, J.F., MacNiocaill, C., McKerrow, W.S., 1998, The Cambrian-Silurian tectonic evolution of the northern Appalachians and British Caledonides: history of complex, west and southwest Pacific-type segment of Iapetus, in Blundell, D.J., and Scott, A.C., eds., Lyell: the Past is the Key to the Present, Geological Society, London, Special Publication, v. 143, p. 199-242

van Staal, C.R., Fyffe, L.R., 1991. Dunnage and Gander Zones, New Brunswick; Canadian Appalachian Region. New Brunswick Department of Natural Resources and Energy, Mineral Resources Branch, Geoscience Report 91-2, 39p.

van Staal, C.R., Lissenberg, J., Pehrsson, S, Zagorevski, A., Valverde-Vaquero, P., Herd, R.K., McNicoll, V., Whalen, J., 2005a, Geology, Puddle Pond, Newfoundland (NTS 12-A/05): Geological Survey of Canada Open File OF1664, scale 1:50,000, 1 sheet.

van Staal, C.R., Sullivan, R.W., and Whalen, J.B., 1996, Provenance and tectonic history of the Gander Zone in the Caledonian/Appalachian orogen: Implications for the origin and assembly of Avalon. In Nance, R.D. et al. (eds.), Avalonian and Related Peri-Gondwanan Terranes of the circum-North Atlantic, Geological Society of America Special Paper 304, p. 347-367.

van Staal, C.R., Valverde-Vaquero, P., Zagorevski, A., Boutsma, S., Pehrsson, S., van Noorden, M., and McNicoll, V., 2005b, Geology, King George IV Lake, Newfoundland (NTS 12-A/04); Geological Survey of Canada, Open File OF1665, scale 1:50,000, 1 sheet.

van Staal, C.R., Valverde-Vaquero, P., Zagorevski, A., Rogers, N., Lissenberg, J., and McNicoll, V., 2005c, Geology, Victoria Lake, Newfoundland (NTS 12-A/06); Geological Survey of Canada Open File OF1667, scale 1:50,000, 1 sheet.

van Staal, C.R., Whalen, J.B. Pehrsson, S.J., and McNicoll, V.J., 2003a, Tectonic evolution of the Notre Dame magmatic arc, Newfoundland Appalachians, Eos Transactions of the American Geophysical Union, v. 84, no. 46, Fall Meeting Supplement, Abstract V41A-06.

Van Staal, C. R., Whalen, J. B., McNicoll, V.J., Pehrsson, S. J., Lissenberg, C.J., Zagorevski, A., van Breemen, O. and Jenner, G.A., in press, The Notre Dame arc and the Taconic Orogeny

in Newfoundland. In: Hatcher, Jr., Carlson, M.P., McBride, J.H. and Martínez Catalán, J.R. (editors), The 4D Framework of Continental Crust, Geological Society of America Special Paper.

van Staal, C.R., Wilson, R.A., Rogers, N., Fyffe, L.R., Langton, J.P., McCutcheon, S.R., McNicoll, V., and Ravenhurst, C.E., 2003b, Geology and tectonic history of the Bathurst Supergroup, Bathurst mining camp, and its relationships to coeval rocks in southwestern New Brunswick and adjacent Maine – a synthesis, Economic Geology, Monograph 11, p. 37-60.

van Staal, C.R., Winchester, J.A., and Bédard, J.H., 2001, Geochemical variations in Middle Ordovician volcanic rocks of the northern Miramichi Highlands and their tectonic significance, Canadian Journal of Earth Sciences, v. 28, p. 1031-1049.

Varne, R., 1985, Ancient subcontinental mantle: a source for K-rich orogenic volcanics: Geology, v. 13, p. 405-408.

Villeneuve, M.E., and MacIntyre, D.G., 1997, Laser $^{40}Ar/^{39}Ar$ ages of the Babine porphyries and Newman Volcanics, Fulton Lake map area, west-central British Columbia: Radiogenic Age and Isotopic Studies, Report 10, Geological Survey of Canada, Current Research, v. 1997-F, p.131–139.

Villeneuve, M.E., Sandeman, H.A., and Davis, W.J., 2000, A method for the intercalibration of U-Th-Pb and $^{40}Ar/^{39}Ar$ ages in the Phanerozoic: Geochimica et Cosmochimica Acta, v. 64, p. 4017-4030.

Wang, K.-L., Chung, S.-L., O'Reilly, S.Y., Sun, S.-S., Shinjo, R., and Chen, C.-H., 2004, Geochemical constraints for the genesis of post-collisional magmatism and the geodynamic evolution of the northern Taiwan region: Journal of Petrology,v. 45, p. 975-1011.

Wager, L.R., Brown, G.M., and Wadsworth, W.J., 1960, Types of igneous cumulates, Journal of Petrology, v. 1, p. 73-85.

Waldron, J.W.F., van Staal, C.R., 2001, Taconian orogeny and the accretion of the Dashwoods block: a peri-Laurentian microcontinent in the Iapetus Ocean: Geology, vol. 29 p. 811-814.

Wasserburg, G.J., Jacobsen, S.B., DePaolo, D.J., McCulloch, M.T., and Wen, T., 1981, Precise determination of Sm/Nd ratio, Sm, Nd isotopic abundances in standard solutions: Geochimica et Cosmochimica Acta, vol. 45, p. 2311-2323.

Whalen, J.B., 1993, Geology, Star Lake, Newfoundland (NTS 12A/11), Geological Survey of Canada Open File 2735, scale 1:50.000.

Whalen, J.B., Currie, K.L., and van Breemen, O., 1987, Episodic Ordovician-Silurian plutonism in the Topsails igneous terrane, western Newfoundland: Transactions of the Royal Society of Edinburgh, v. 78, p. 17-28.

Whalen, J.B., Jenner, G.A., Longstaffe, F. J., Gariepy, C., Fryer, B.J., 1997, Implications of granitoid geochemical and isotopic (Nd, O, Pb) data from the Cambrian-Ordovician Notre Dame Arc for the evolution of the central mobile belt, Newfoundland Appalachians, in Sinha, A.K., et al., eds., The nature of magmatism in the Appalachian Orogen, Geological Society of America Memoir, v. 191; p. 367-395.

Whalen, J.B., McNicoll, V., van Staal, C.R., Pehrsson, S., 2003, Plutonic rock geochemical and isotopic evidence for a transition from arc (c. 489-435 ma) to within-plate (c. 430 ma) magmatism within the Notre Dame arc, Geological Society of America Abstracts with Programs, v. 35(3), p. 33-34.

Whalen, J.B., McNicoll, V.J., van Staal, C.R., Lissenberg, C.J., Longstaffe, F.J., Jenner, G.A., and van Breemen, O. in press. Spatial, temporal and geochemical characteristics of Silurian collision-zone magmatism: an example of a rapidly evolving magmatic system related to slab break-off, Lithos.

Whitmore, G.P., Crook, K.A.W., Johnson, D.P., 1999, Sedimentation in a complex convergent margin: the Papua New Guinea collision zon of the western Solomon Sea. Marine Geology, v. 157, p. 19-45.

Williams, H., Hatcher, R.D., 1983, Appalachian suspect terranes, *in* Hatcher, R.D., Williams, H., and Zietz, I., eds., The tectonics and geophysics of mountain chains, Geological Society of America Memoir, v. 158, p. 33-53.

Williams, H., 1995, Temporal and spatial divisions; Chapter 2, in Williams, H. ed . Geological Survey of Canada, Geology of Canada, no. 6, p. 21-44.

Williams, H., Currie, K.L., and Piasecki, M.A.J., 1993, The Dog Bay Line: a major Silurian tectonic boundary in northeast Newfoundland. Canadian Journal of Earth Sciences, v. 30, p. 2481-2494

Williams, H., 1979: Appalachian Orogen in Canada: Canadian Journal of Earth Sciences, v. 16, p. 792-807.

Williams, H., 1970. Red Indian Lake (east half), Newfoundland. Geological Survey of Canada, Map 1196A.

Williams, H., Colman-Sadd, S.P., O'Neill, P.P., 1995. Gander Zone – Newfoundland. In: Williams, H. (Ed.), Chaper 3, geology of the Canadian Appalachian – Caledonian Orogen in Canada and Greenland, Geological Survey of Canada, Geology of Canada no. 6, 199-212.

Williams, H., Colman-Sadd, S.P., Swinden, H.S., 1988, Tectonic-Stratigraphic subdivisions of central Newfoundland, in Current Research, Part B. Geological Survey of Canada, Paper 88-1B, p. 91-98.

Williams, H., Currie, K.L., Piasecki, M.A.J., 1993: The Dog Bay Line: a major Silurian tectonic boundary in northeast Newfoundland: Canadian Journal of Earth Sciences, v. 30, p. 2481-2494.

Williams, H., Piasecki, M.A.J., 1990. The Cold Spring Mélange and a possible model for Dunnage – Gander Zone interaction in central Newfoundland. Canadian Journal of Earth Sciences, 27, 1126-1134.

Williams, S.H., 1989. New graptolite discoveries from the Ordovician of central Newfoundland. Current Research, Newfoundland Department of Mines and Energy, Geological Survey Branch, Report 89-1, 201-219.

Williams, S.H., Harper, D.A.T., Neuman, R.B., Boyce, W.D., Mac Niocaill, C., 1995. Lower Paleozoic fossils from Newfoundland and their importance in understanding the history of the Iapetus Ocean. In: Hibbard, J., van Staal, C.R., Cawood, P. (Eds.), Current Persectives in the

Appalachian – Calidonian Orogen. Geological Association of Canada, Special Paper, 41, 115-126.

Wilson, R., 2003, Geochemistry and Petrogenesis of Ordovician arc-related mafic volcanic rocks in the Popelogan Inlier, northern New Brunswick. Canadian Journal of Earth Sciences, v. 40, p. 1171-1189.

Winchester, J.A. and Floyd, P.A . 1977, Geochemical discrimination of different magma series and their differentiation products using immobile elements. Chemical Geology, v. 20, p. 325-343.

Wood, D.A., 1980. The application of a Th – Ha – Ta diagram to problems of tectonomagmatic classification and to establishing the nature of crustal contamination of basaltic lavas of the British Tertiary volcanic province. Earth and Planetary Science Letters, 50, 11-30.

Xiao, W.-J., Han, F., Windley, B.F., Yuan, C., Zhou, H., and Li, J., 2003, Multiple accretionary orogenesis and episodic continental growth of continents: Insights from the western Kunlun range, central Asia: International Geology Review, v. 45, p. 303-328.

Zagorevski, A. Rogers, N. McNicoll, V. Lisseneberg, C.J. van Staal, C.R . Valverde-Vaquero, P. 2006, Lower to Middle Ordovician evolution of peri-Laurentian arc and back-arc complexes in the Iapetus: Constrains from the Annieopsquotch Accretionary Tract, central Newfoundland,. Geological Society of America Bulletin.

Zagorevski, A., Lissenberg, C.J., van Staal, C.R., McNicoll, V., Rogers, N. 2003a. Tectonic history of the Annieopsquotch accretionary tract: Geological Society of America Abstracts with Programs, v. 35 (3), p. 34.

Zagorevski, A., N. Rogers, N., van Staal, C.R. 2003b. Tectonostratigraphic relationships in the Lloyds River and Tulks Brook region of central Newfoundland: A geological link between Red Indian and King George IV lakes: Current Research, Newfoundland Department of Energy and Mines, Geological Survey Report, 03-1, p. 167-178.

Zagorevski, A., van Staal, C. R., McNicoll, V., Rogers, N., 2004, Pats Pond and Wigwam Brook groups: record of episodic per-Gondwanan Upper Cambrian-Caradoc island arc activity in the Exploits Subzone of central Newfoundland: Geological Society of America Abstracts with Programs, vol. 36 (2), p. 129.

Zagorevski, A., van Staal, C.R. 2002. Structures associated with the Red Indian Line in southwestern Newfoundland: Current Research, Newfoundland Department of Energy and Mines, Geological Survey Report, 02-1, p. 211-218.